SAND2015-6693 R

MELCOR Computer Code Manuals

Vol. 3: MELCOR Assessment Problems
Version 2.1.7347 2015

Date Published: August 2015

Prepared by: L L. Humphries, D. L.Y. Louie, V. G. Figueroa, M. F. Young, S. Weber, K. Ross, J. Phillips, and R. J. Jun*

Sandia National Laboratories
Operated for the U.S. Department of Energy
Albuquerque, New Mexico 87185

H. Esmaili, Nuclear Regulatory Commission Project Manager

Prepared for Division of System Analysis
Office of Nuclear Regulatory Research
U.S. Nuclear Regulatory Commission
Washington, DC 20555-0001
NRC Job Code V6343

* Currently employed at the Federal Authority for Nuclear Regulation in the United Arab Emirates

Acknowledgments

We would like to thank the following individuals contributed and reviewed this document.

Matthew R. Denman

Fred Gelbard

Salvador B. Rodriguez

Bradley A. Beeny, Graduate Intern, Texas A&M University

We also acknowledge Mr. Hitoshi Tamaki, a visiting scientist from the Japan Atomic Energy Agency, who participated in the review of this report.

Abstract

MELCOR is a fully integrated, engineering-level computer code that models the progression of severe accidents in light-water reactor nuclear power plants. MELCOR is being developed at Sandia National Laboratories (SNL) for the U.S. Nuclear Regulatory Commission (NRC) as a second-generation plant risk assessment tool and the successor to the Source Term Code package. A broad spectrum of severe accident phenomena in both boiling and pressurized water reactors is treated in MELCOR in a unified framework. These include thermal-hydraulic response in the reactor coolant system (RCS), reactor cavity, containment, and confinement buildings; core heatup, degradation, and relocation; core-concrete attack; hydrogen production, transport, and combustion; and fission product release and transport behavior. Current uses of MELCOR include estimation of severe accident source terms and their sensitivities and uncertainties in a variety of applications.

This publication of the MELCOR computer code manuals corresponds to MELCOR 2.0, released to users in September 2008. Volume 1 contains a primer that describes MELCOR's phenomenological scope, organization (by package), and documentation. The remainder of Volume 1 contains the MELCOR User's Guides, which provide the input instructions and guidelines for each package. Volume 2 contains the MELCOR Reference Manuals, which describe the phenomenological models that have been implemented in each package. Volume 3, MELCOR Assessment Problems, presents a portfolio of test and sample problems consisting of both analyses of experiments and of full plant problems. These analyses will be repeated with future releases of MELCOR in order to provide a metric on code predictions as new versions are released.

Table of Contents

Acronyms

ACE Advanced Containment Experiments
ADS automatic depressurization system
B&W Babcock and Wilcox
BMC Battelle Model Containment
BST blowdown suppression tank
BWR boiling water reactor
CF control function
CFD computational fluid dynamics
CFM central fuel module
CMMI capability maturity model integration
CND condenser
COR core package
CRGTs control rod guide tubes
CSE Containment Systems Experiment
CSP core support plate
CSTF Containment Systems Test Facility
CV control volume
CVH control volume hydrodynamics package
CVTR Carolinas-Virgina Tube Reactor
CWTI corium-water thermal interactions
DBA design basis accident
DCH direct containment heating
DEC Digital Equipment Corporation
DF damaged fuel
DF decontamination factor
ECC emergency core coolant
ECCS emergency core cooling system
EDF external data file
EPRI Electric Power Research Institute
FCL fan cooler
FL flow path
FP fission product
FPMS fission product measurement system
HBTF High Bay Test Facility
HEDL Hanford Engineering and Development Laboratory
HPCS high-pressure core spray system
HPI high-pressure injection
HPME high pressure melt ejection
HS heat structure
HTGR high temperature gas reactor
ILCL intact loop cold leg
INEL Idaho National Laboratory
IPSN Nuclear Safety and Protection Institute
ISP International Standard Problem
LB large-break
LOCA loss-of-coolant accident
LOFT Loss-of-Field Test
LPCI low-pressure coolant injection
LPCS low-pressure core spray system
LPSI low pressure safety injection
LPIS low-pressure injection system
LWR light water reactor
MCCI molten core concrete interactions
MP materials properties
MSIV main steam isolation valve
MSLB main steam-line break
NRC Nuclear Regulatory Commission
NS non-supporting structure
NUPEC Nuclear Power Engineering Corporation
ORNL Oak Ridge National Laboratory
OS other structures
PAR passive autocatalytic recombiner
PBR Power Burst Facility
PCS primary coolant system
PFM peripheral fuel assembly module
PNL Pacific Northwest Laboratory
PORV power-operated relief valve
PRA probabilistic risk assessment
PWR pressurized water reactor
RCP reactor coolant pump
RCS reactor coolant system
RN radionuclide
RWST refueling water storage tank
SFD severe fuel damage
SNL Sandia National Laboratories
SPR containment sprays
SQA software quality assurance
SRVs safety relief valves
SS supporting structures
SURC sustained urania-concrete
TAF top of active fuel
TMI Three-Mile Island
UF under-prediction factor
USDOE United States Department of Energy
USNRC United States Nuclear Regulatory Commission

List of Figures

Figure **Page**

List of Tables

Table **Page**

1. INTRODUCTION

Code verification and validation are important elements of the MELCOR software quality assurance (SQA) program. These two code-testing elements are completely independent processes for assuring the verification and validation of the code. Verification is needed to ensure the MELCOR SQA program is coded to properly reproduce the model that is intended by the developer; validation is needed for assuring that the model envisioned by the developer is appropriate for simulating the physical processes involved in a severe accident. Verification is performed by the code developer throughout the development cycle and involves unit testing, integral testing, regression testing, stress testing, and code reviews. Validation can take place prior to code implementation in the form of peer reviews of models; but it usually takes place formally by testing the models through simulation of experiments and then, comparison to test data or the results of analytic test cases. Proper validation of physical models encoded into analytical tools is essential to provide developers the necessary guidance in developing and improving algorithms and numerical methods for describing physical processes. It is an important SQA requirement for USNRC code development [1.1] as well as a requirement for Capability Maturity Model Integration (CMMI) level 3. Moreover, validation results are essential for code users in order to gain confidence and guidance in applying the code to real-world applications. It is important that such validation exercises be performed objectively by both developers, who may better understand the nuances of particular models, as well as users, who may have a more distant knowledge of the internal models but may have a greater knowledge of real-world applications.

Validation should be performed using conventional modeling best practices. For MELCOR, this means that default values for input should be used. However, there are justifiable reasons for using non-default values that may relate to experimental scale or otherwise non-prototypic experimental conditions. Use of non-default parameters in a simulation should be justified by the modeler and documented in the validation report. In general, users should use non-default parameters only when they are able to justify the use of another value. However, sensitivity runs performed as part of these assessments may be used to justify improvements to default values in future code versions.

Many validation studies have been performed and documented for historical versions of the MELCOR code (see references [1.1] - [1.14]).This report provides a current update to these reports, reflecting code corrections, code enhancements, new modeling approaches, and updated best practices. This report is a synthesis of many assessments into a document which can be referenced by code users. For each major code release, Sandia National Laboratories publishes three reports documenting the code. Volume 1 is the User Guide and provides information regarding code input and syntax. Volume 2 is the Reference Manual which discusses the various code models and numerics. Volume 3 is a code assessment report meant to quantify the correctness and judge the appropriateness of MELCOR models for simulating various experiments. The validation performed in this report is for MELCOR version 2.1. Most of the

assessments were performed with revision 6110, though a few were performed with revision 6061. The difference between these code versions is insignificant since it represents only 3 changes to the source code, two of which involved non-physics issues. However, even though this validation report is intended for the purpose of assessing the MELCOR 2.1 code version, most assessments were also performed for the MELCOR 1.8.6 code version and therefore, this documentation serves as validation for both code versions.

In addition to nuclear reactor applications, MELCOR is also used for non-reactor safety analysis applications, such as estimating the amount of radioactive or toxic airborne materials emitted from a facility, building, or a confined space structure. Appendix C describes the verification of MELCOR 2.1 usage for Department of Energy facility safety analysis applications.

This report is not a final MELCOR validation test report as code validation is an ongoing practice, and the assessment document should be viewed as a living document where additional assessments will be added, and existing assessments may be improved. Furthermore, these test cases have become a part of the ongoing regression testing performed for the code to identify issues that may arise during the code development life cycle. The development team will continue to review and improve the validation cases as model improvement goes forward.

1.1 Selection of Validation Test Cases

It is an objective of the MELCOR development team to assess all new code models against available test data, where that data exists. However, this objective is often limited by the availability of useful data, that is, data for which the conditions are specified in enough detail to create a model. Code assessment and qualification testing can be accomplished by comparing MELCOR results to results or data obtained from various methods, such as:

1. Comparison with analytic results.
2. Code-to-code comparison with other validated computer programs.
3. Validation against experimental results.
4. Comparison to published data from real-life accidents or events.

Each method has advantages and disadvantages associated with the quality of benchmarking data that is available. Analytical results provide ideal data quality, though the data may be severely limited to very specific phenomena and conditions. Code-to-code comparison provides an excellent source of repeatable data, though the comparison is dependent on the assumed accuracy of the code used for validation. Experiments provide real data obtained under controlled boundary conditions but with data limitations arising from the accuracy of the measurement capability, as well as the extent of instrumentation, which is often constrained by budget or the foresight of the experimenters. Often the experiment is designed to study a particular phenomenon and may miss important coupling to other phenomena. Published data from real-life events

provides integrated, system data that includes all important physics, though the quality of the data may be undesirable.

Experiments can be classified as either separate effects tests or integral tests. Both separate effects tests, as well as integral tests, are required for valid code assessment. Separate effects tests are designed to focus on a specific physical process; the goal of the design is to eliminate the combined effects of multiple physical processes, which may complicate the validation of a model for that physical process. However, it may be impossible to design a single test that isolates a single process; further, separate effects tests often ignore the important coupling between processes that are inherent in real world applications. Integral tests, on the other hand, are valuable for examining the relationship between such coupled processes. Overall, tests should be selected that are applicable to the calculation domain of the code and this domain should be clear to code users. Often, this requires significant analytical experience in applying the code to real-world problems in order to understand the calculation domain.

MELCOR has been assessed against numerous severe accident experiments performed by the USNRC, EPRI, USDOE, as well as many international research programs. Often, International Standard Problems (ISPs) are used as reference validation cases because they are “standard” problems that are assessed against other codes, which may have alternate modeling capabilities. These ISPs are generally well documented, and may enable code-to-code comparisons to compare modeling approaches.

An important aspect of validation is that of coverage. Ideally, it is desirable to target each physics model available in the code with one or more validation test cases that can reveal the capabilities of the model in simulating test conditions and responses. However, limited resources and limited availability of data requires some prioritization of effort in determining those processes that are most uncertain and contribute most to the sensitivity of results.

More than 50 such validation tests have been proposed for the MELCOR 2.1 assessment document. Figure 1-1 shows a summary of severe accident validation experiments (many used in this report) categorized by physics examined by the test, i.e., RN transport, core (COR) heat-up and degradation, containment, ex-vessel corium, and integral tests. Important physics assessed in this study includes, but is not limited to, heat-up/heat transfer, oxidation of materials, re-flood cooling, core degradation, molten pool modeling, fission product release, vessel failure, critical flow, molten core concrete interactions (MCCI), direct containment heating (DCH), condensation, containment stratification, hydrogen burn, hygroscopic effects, aerosol deposition, radionuclide transport, iodine pool chemistry, suppression pool scrubbing, vent cleaning, and engineering safety features such as sprays (washing of radionuclides and cooling of atmosphere) and ice condensers. These validation tests exercise all the MELCOR physics packages to at least some degree, with the exception of the Condenser (CND), Fan Cooler (FCL), and Passive Autocatalytic Recombiner (PAR) packages. Furthermore, specific models such as the point kinetics model, high temperature gas reactor (HTGR) models, spent fuel pool models, lower head

penetration models, mechanical model, integral heat exchanger model, flashing models, and the counter-current stratified flow model are not assessed in the current set of validation tests.

There is a significant amount of effort involved in developing an input model, and in understanding the results in light of the uncertainties inherent in the experiment design. This effort involves comparison of important measurements to calculated results, interpretation of discrepancies, and variation of model parameters and nodalization to best describe the particular case. Often, analysts are tempted to manipulate input variables to get the 'best' results compared to data. However, it is more desirable to focus on what can be learned from the analysis in terms of exposing specific modeling adequacies or deficiencies. For all assessments included in this report, default values are typically used and any non-default parameters are discussed or justified. Sometimes this may mean running sensitivity studies to assess the importance of particular input parameters. Finally, it is desirable to understand the numerical convergence of such calculations by examining both spatial and temporal nodalization of the model.

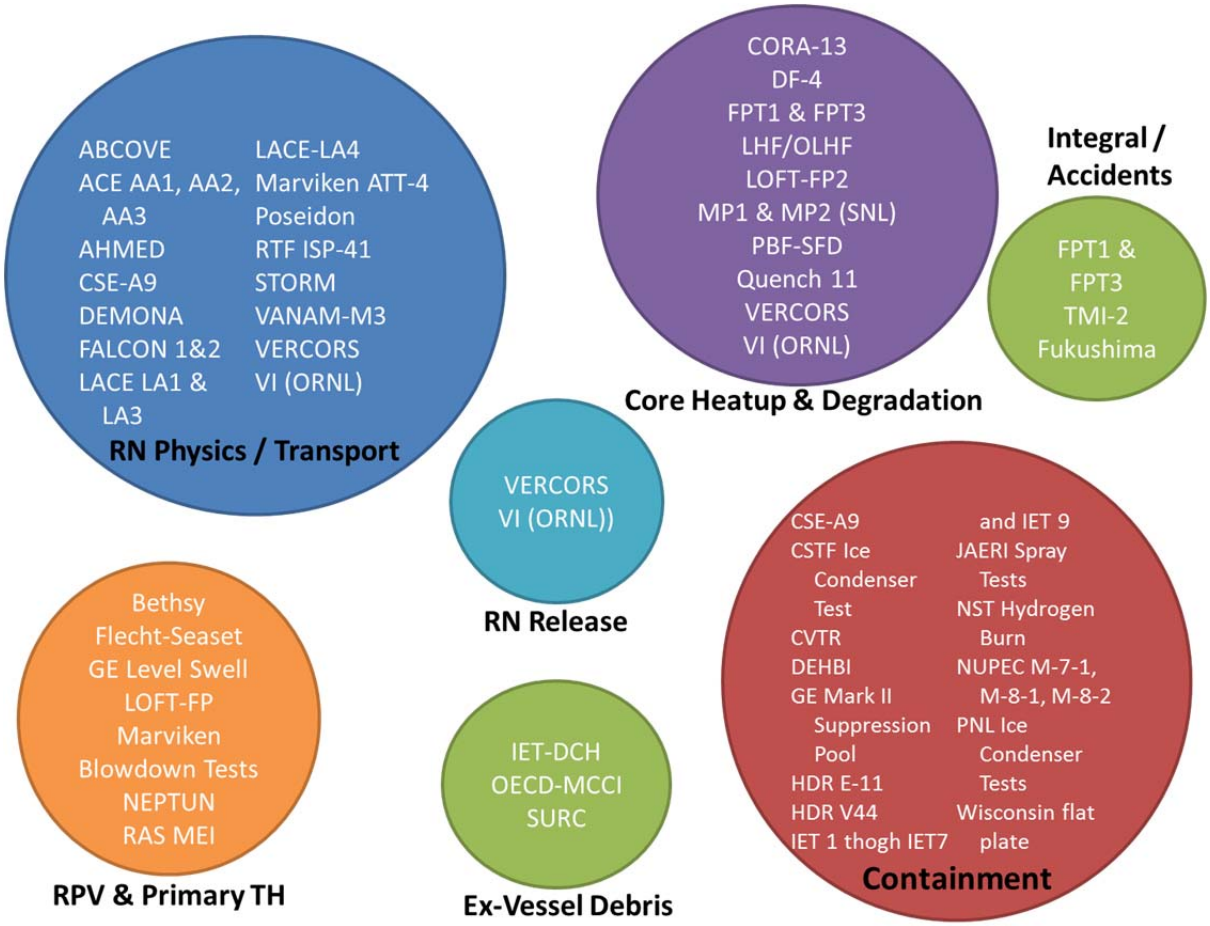

Figure 1-1.Experiments/accidents used for validation of MELCOR.

1.2 Discussion of MELCOR Validation Tests

Assessment analyses have been performed historically as part of the MELCOR code development process. Table 1-1 summarizes the validation test matrix for various versions of MELCOR and the plans for future validation. It is desirable to perform an assessment analysis with each new model added to the code. For example, aerosol mechanics for nonhygroscopic aerosols is modeled using the MAEROS code (analogous to the NAUA code) where good verification of aerosol agglomeration physics and gravitational depletion was demonstrated in early versions of MELCOR based on MARVEKIN, ABCOVE and LACE testing. MELCOR Version 1.8.5 introduced extensions to treat hygroscopic aerosol effects where good validation against the VANAM M3 test (similar to DEMONA), as well as the AHMED experiments, was demonstrated. The Containment Systems Experiment (CSE) A9 test, in the CONTAIN-MELCOR parity assessment study, was used to validate the containment spray scrubbing modeling in MELCOR on code Version 1.8.5. The CONTAIN-MELCOR parity study introduced numerous other containment behavior assessments including the NUPEC mixing tests, the Nevada Test Site hydrogen burn tests, and the IET DCH containment heating experiments. Fission product release from fuel, including MOX and High Burnup, were assessed against ORNL HI/VI tests and against more recent VERCORS experiments using MELCOR Version 1.8.5. In Version 1.8.5 fission product release models were adjusted using sensitivity coefficient over-rides to the Version 1.8.5 models. These were formalized as code options and defaults for code Version 1.8.6. MELCOR Version 1.8.6 also introduced expanded modeling detail for core melt progression processes, including molten pool convection treatments. These extensions provided improved prediction of the TMI-2 accident, some of which are still currently under assessment. The Phebus FPT-1 test stands as the most comprehensive integral assessment of core damage progression, hydrogen generation, fission product release, reactor cooling system (RCS) deposition, and containment natural depletion processes. The Phebus FPT-1 test provides an excellent assessment database for key deposition behavior in the RCS and for containment depletion.

In addition to experimental validation tests, a series of simple test cases were developed with analytical solutions available to benchmark the following phenomena:

1. Saturated liquid depressurization,
2. Adiabatic flow of hydrogen,
3. Transient heat flow in a semi-infinite solid with convective boundary conditions,
4. Cooling of rectangular and annular heat structures in a fluid,
5. Self-initialization of steady-state radial temperature distributions in annular structures, and
6. Establishment of flow in a pipe.

These are very simple, fast-running test cases that provide an excellent test of nodalization and time-step dependence.

Table 1-1. Historical review of MELCOR assessment studies.

Assessment	Category[1]	2.1[2]	1.8.5	1.8.4	1.8.3	1.8.2	1.8.1
ABCOVE: AB5 &AB6	A	1					
ACE Pool Scrubbing	A	1				x	
AHMED:RH=22,28,96,98	A	1	x				
BCL Pool scrubbing	A	2					
BETHSY-6.9C(ISP-38)	D	1					
CCI:1,2 and 3	E	1					
Containment Spray CSE-A9	A	1	x		x		
CORA-13	C	1					x
CVTR: Test 3,4 and 5	B	2					
DEMONA:B3	A	1				x	
DF: DF4	C	2				x	
FALCON: 1 & 2	A	1					
Fan Cooler Tests	B	2					
FLECHT_SEASET	D	2					x
GE Level Swell	D	1			x		
GE Mark I Suppression Pool	B	2					
HDR-T31.5		2					
HDR-V44	B	2	x				
JAERI Spray Tests: PHS 1,6	B	1					
LACE LA4	A	1					
LACE Turbulent Dep (LA1 & LA3)	A	2					
LHF/OLHF(OLHF-1)	C	2					
LOFT:LP-FP-2	C	1					x
Marviken ATT-4	A	1					
Marviken: CFT-21 & JIT-11	B	1					
MeltSpread Model Tests	E	2					
NEPTUN: 5006 & 5007	D	2					
NTS Burn: P01,P12,P15,P20	B	1	x				
NUPEC: M-8-1, M-8-2	B	1	x				
PBF SFD:1-4	C	2					
PHEBUS B9 (ISP 28)	C	2	x				
PHEBUS: FPT1 &FPT3	C	1	x				
PNL ICE Condenser:11-6 &16-11	B	2	x				x
POSEIDON: PA16,17,20	C	1					
QUENCH (ISP45 or Quench-6)	C	2					
RAS MEI		2					
RTF: ISP41	A	2	x				
SNL Melt Progression: MP1 & MP2	C	2				x	
SNL/IET (DCH Tests): IET-1,3,6	B	2	x				
STORM: SR-11 (ISP 40)	A	1					
SURC: 1 & 2	E	2					
TMI-2 Accident	D	1	x				
VANAM: M3 (ISP37)	A	1	x				
VERCORS	A	2	x				
VI	A	2	x				
Vulcano (VE-U7)	E	2					

[1] A – Aerosols & vapors, B – Containment TH, C – Core Heat-up & degradation, D – RCS thermal hydraulics and Integral Tests, E – Ex-vessel MCCI

[2]Publication release (1 indicates assessment will be in this first release of the validation document, 2 will be published in a subsequent release). This prioritization is somewhat subjective, based on assumed importance of the validation or ability to complete within schedule.

1.3 Brief Description of Experimental Validation Tests and Important Physics Modeled

This section provides a brief description for most of the experiments that make up the validation test matrix. This description also provides a list of key physics that is observed for each experiment, and hence points to MELCOR models that can be validated.

ABCOVE: AB5 and AB6

General Description:

Simulation of the dry atmosphere conditions of an LMFBR-containment with a sodium fire, i.e., sodium combustion product aerosols. AB6 modeled fission product aerosols, sodium iodide (NaI), in the presence of sodium combustion product aerosol.

Important Physics:

Agglomeration behavior of two aerosol species (hygroscopic and non-hygroscopic) and condensation of water vapor.

ACRR: MP1 and MP2

General Description:

Investigation of late-phase, core-melt progression. Examined material interactions and rod degradation for an intact rod / dense Zr-UO2 crust / rubblized debris bed geometry.

Important Physics:

Heat transfer in a degraded core geometry, core degradation, and material interactions.

AHMED: AMMD

General Description:

A series of hygroscopic aerosol experiments were conducted at the AHMED Test Facility by injecting NaOH in aerosol form into an atmosphere with controlled humidity.

Important Physics:

Hygroscopic effects under differing humidity conditions and the impact on aerosol masses available for release.

Bethsy-6.9c (ISP-38)

General Description:

The purpose of the Bethsy test was to study the accident transient following the loss of the Residual Heat Removal System during mid-loop operation with the primary circuit open at the pressurizer and steam generator outlet plenum manways. The Bethsy facility is a three-loop pressurized water reactor (PWR) core and primary circuit, with the elevations scaled 1/1, and the volume scaled to 1/100.

Important Physics:

Entrainment and retention of water in the pressurizer caused by steam flow through the pressurizer manway, low pressure pool boiling, level swell in the upper head, expulsion of water through the steam generator manway, level of pressurization, and re-flooding of the core from the gravity and forced emergency core cooling water injection.

CORA-13 (ISP-31)

General Description:

Analysis of the heat-up and meltdown phases of a PWR-type fuel element in the CORA test facility. The CORA facility consists of a fuel rod bundle with heated and unheated rods under controlled thermal-hydraulic boundary conditions with a steam supply to provide superheated steam and a quench capability

Important Physics:

Oxidation/hydrogen generation, fragmentation of rods, relocation of core materials, formation of blockages, forced convection, conduction, radiation, and fluid-structure heat transfer.

CSE-A9

General Description:

Eight experiments have been performed in the CSE containment vessel to evaluate the performance of aqueous sprays as a means of decontaminating containment atmospheres.

Important Physics:

Cesium and uranium aerosol and iodine vapor washout by sprays. Aerosol depletion by gravity and thermal-hydraulic response to containment sprays.

CVTR: Test 3, 4, and 5

General Description:

Design basis simulation of a postulated main steam-line break (MSLB) inside a large dry PWR containment. The Carolinas-Virginia Tube Reactor (CVTR) facility is a decommissioned reactor containment building.

Important Physics:

Multi-component gas compression/expansion, thermal-hydraulic response to containment sprays, atmosphere cooling by fan cooler, jet-plume gas interaction, buoyancy/stratification, 1-D heat transfer to heat structures, free convection, and forced convection.

DEMONA: B3

General Description:

Investigation of the transport and deposition behavior of aerosols in the containment. Performed in the Battelle model containment (total volume 640 m^3), using an open (quasi one-room) geometry and condensation aerosols from a plasma torch generator.

Important Physics:

Effects of steam condensation on aerosol settling.

DF: DF4

General Description:

The purpose of the damaged fuel (DF) series of experiments was to investigate core melt progression. This experiment investigated the behavior of BWR-type fuel materials and configurations in a high-temperature oxidizing environment typical of the conditions during a Loss Of Coolant Accident (LOCA).

Important Physics:

Eutectic interaction between the control poison material (B_4C) and the stainless steel control blade sheath and tubes, and the oxidation of zircaloy in the cladding and canister.

FALCON: 1 & 2 (ISP 34)

General Description:

Heating of a bundle of six fuel specimens and six absorber specimens in steam-helium environment containing boric acid. Deposition along a controlled thermal gradient tube and containment structure.

Important Physics:

Physical and chemical behavior of fission products under simulated severe accident conditions and multi-component aerosol effects, vapor-aerosol interactions, and thermophoretic deposition.

FLECHT-SEASET (Natural Circulation)

General Description:

The facility design is scaled to a typical Westinghouse PWR on a 1:307 volume basis, with prototypic full-lengths and full-heights. The loop piping consists of two

flow paths representing the unbroken, or intact, three loops and the broken loop of a 4-loop PWR. However, for the natural circulation tests, the broken loop is not connected to a containment tank, simulating a break, but is connected to the downcomer extension to provide a normal, uninterrupted, flow path from the upper plenum, through the steam generator, through the loop pump seal, and through the cold leg to the downcomer.

Important Physics:

Pool boiling in core, natural circulation, steam condensation, and reflux.

FPT1 (ISP 46)

General Description:

The FPT-1 system consisted of an in-pile fuel bundle assembly and upper plenum region, an external circuit including a steam generator U-tube and connecting lines, and a containment section. The objective of the fuel bundle assembly was to assess fuel degradation and fission product release from a degraded fuel assembly. In the circuit, the objective was to determine fission product transport and deposition in steam generator tubes.

Important Physics:

- Thermal modeling was assessed from thermocouple responses and temperature profiles.
- Oxidation (thermocouple responses and measurements of hydrogen generation).
- Material relocation (thermocouple and radiography and transmission tomography for the end state).
- Fission product release, transport, and deposition (emission tomography of the fuel bundle and steam generator, as well as, measurements of activity along the external line to the containment).

GE Mark III Suppression pool

General Description:

Purpose is to obtain validation data for Mark II suppression pool vents during design basis accident (DBA) conditions.

Important Physics:

Vent clearing times, pressures in drywell/wetwell, DBA conditions.

GE Level Swell

General Description:

A number of blowdown tests were conducted, some with blowdown occurring near the top of the vessel (vapor blowdown) and others with blowdown occurring

near the bottom of the vessel (liquid, two-phase, vapor transient). These experiments were conducted in the “large blowdown vessel” (4.5 m^3).

Important Physics:

Vessel blowdown, level swell, critical flow.

SNL/IET: IET-1, 3, 6

General Description:

Series of experiments done at 1:10 linear scale in the Surtsey test facility at Sandia, and at 1:40 linear scale in the corium-water thermal interactions (CWTI) test facility at ANL; experiments were performed to evaluate the effects of high pressure melt ejection (HPME) on DCH.

Important Physics:

High-pressure melt ejection, direct containment heating, oxidation and hydrogen generation, and hydrogen combustion

RTF (ISP41)

General Description:

Objective was to develop data on the behavior of iodine in reactor containment pools. The experiment consisted of a pool in a stainless steel vessel with a radioisotope dose source and aqueous iodine provided by adding CsI to the pool. The pool pH was controlled during the experiment by adding acid and base chemicals to the pool.

Important Physics:

Speciation of iodine in the aqueous and gaseous phases, effect of radiation on H_2O_2 and H_2 concentrations, and adsorption/desorption of iodine on surfaces.

Quench-6 (ISP45)

General Description:

The objective of the Quench-6 test was to assess the capability of severe accident codes to simulate delayed reflood situations in which a pre-oxidized light water reactor (LWR) fuel rod bundle is quenched by water inserted from the bottom.

Important Physics:

Oxidation of metallic and bottom reflood cooling.

JAERI Spray Tests: PHS-1, 6

General Description:

Pressure suppression spray tests were conducted in Japan during the late 1970s in a 700 m^3 steel vessel (20 m high, 7 m in diameter). PHS-6 was a single nozzle test whereas PHS-1 was a 6 nozzle test. Vessel walls are hot so that droplets contacting walls are vaporized degrading spray effectiveness.

Important Physics:

Containment pressure reduction by sprays.

LACE Turbulent Deposition: LA1 & LA3

General Description:

The LACE LA1 and LA3 tests examined the transport and retention of aerosols (typical of LWRs) through pipes with high-speed flow and in containment volumes during rapid depressurization. Specific objectives of these tests were to provide validation data that would demonstrate important dependencies in modeling deposition. The effects of gas velocity, aerosol composition and aerosol size were considered.

Important Physics:

Turbulent deposition of aerosols in pipes and in pipe bends.

LACE: LA4

General Description:

The purpose of the experiment was to determine the disposition of aerosols in the containment building under conditions of high-steam concentrations. Of particular interest was the difference in aerosol disposition between hygroscopic (watersoluble) aerosols such as CsOH and nonhygroscopic aerosols such as MnO in a high-steam concentration.

Important Physics:

Hygroscopic effects, deposition of water-soluble aerosols on surfaces, heat transfer to surfaces and steam condensation on surfaces

LOFT: LP-FP-2

General Description:

Experiment LP-FP-2 models the V-sequence accident and is defined as a rupture in a low-pressure injection system (LPIS) line outside the containment, with simultaneous failure to isolate the system. The experimental subsystems include the reactor vessel, the intact loop, the broken loop, the blowdown suppression tank (BST) system, and the ECCS.

Important Physics:

Heat conduction/convection (temperatures and pressures measured), hydrogen generation (hydrogen mass measured), fission product release, flow blockage in degraded core, and choked flow.

MARVIKEN: ATT-4

General Description:

Test ATT-4 studied fission product transport in the presence of a structural aerosol simulant; in addition to the fissium aerosol, a “corium” aerosol was produced that was composed of Ag and Mn. Corium vapors were mixed with vaporized fissium and steam in the lowest portion of the reactor vessel to form aerosols that were transported through the simulated large-scale primary piping.

Important Physics:

Thermal hydraulics of a PWR, aerosol and vapor transport and deposition.

MARVIKEN Blowdown Tests: CFT-21 & JIT-11

General Description:

Large-scale tests intended to provide data for analysis of critical flow from vessel blow-down were performed at the Marviken facility. The CFT-221 test was designed for validation of subcooled and two-phase flow through a discharge nozzle, whereas JIT-11 tested a saturated steam flow.

Important Physics:

Vessel blowdown, critical flow of vapor, subcooled liquid, and two-phase flow

NEPTUN – 5006 & 5007

General Description:

The NEPTUN experiments were designed to measure the rate of boil-off and additionally, the heat up of fuel rods during two-phase uncovery of the core in a severe accident.

Important Physics:

Boil-off, fuel rod heat up, and level swell.

NTS Burn: NTSP01, NTSP12, NTSP15, NTSP20

General Description:

Premixed hydrogen combustion experiments with hydrogen concentrations ranging from 5 to 13% (by volume) and steam concentrations from 4 to 30%.

Important Physics:

Combustion burn completeness, burn time, and vessel pressurization.

NUPEC: M-7-1, M-8-1, M-8-2

General Description:

Explored the response of a ¼ scale containment with steam and helium injection and containment spray actuation (M-7-1 and M-8-2) with helium serving as a surrogate for hydrogen gas.

Important Physics:

Pressure response, temperature distribution and stratification, and hydrogen mixing.

PBF SFD: 1-4

General Description:

The Severe Fuel Damage (SFD) tests were performed at the Power Burst Facility (PBF) to investigate fuel rod and core response, and the release of fission products and hydrogen during degraded core accidents.

Important Physics:

Fission product release, oxidation and hydrogen generation.

PHEBUS: B9+ (ISP 28)

General Description:

The B9+ test was designed to provide data principally on fuel degradation. It consists of a driver reactor core to provide neutronic heating to the test bundle, a fluid supply system to inject steam and helium into the test bundle, and associated cooling systems for the bundle and driver core.

Important Physics:

Heat conduction/convection (temperatures measured), hydrogen generation (hydrogen mass measured), and fuel degradation (no direct measurement).

PNL Ice Condenser: 11-6 & 16-11

General Description:

A series of large-scale experiments conducted at the High Bay Test Facility (HBTF) at Pacific Northwest Laboratory (PNL) to investigate the extent to which an ice condenser may capture and retain air-borne particles. In Experiment 11-6, the low-flow rate induced a natural circulation flow between the diffuser outlet and the ice condenser. Experiment 16-11 was performed with every compartment full of ice and was a high-flow test with no recirculation.

Important Physics:

Aerosol deposition, heat transfer in ice condenser containment, natural circulation, and ice phase transition.

STORM: SR-11 (ISP 40)

General Description:

The STORM test SR-11, was intended for examining aerosol deposition and resuspension in pipes and included two distinct phases: (1) the aerosol deposition by thermophoresis and eddy impaction, and (2) aerosol resuspension under a stepwise increasing gas flow. MELCOR does not have a resuspension model and the second phase was not modeled.

Important Physics:

Aerosol deposition from thermophoresis and eddy impaction and resuspension (not modeled in MELCOR).

SURC: SURC-1 & SURC-2

General Description:

The sustained urania-concrete (SURC) experiments were designed to measure and assess releases due to interactions between core materials and concrete in containment structures.

Important Physics:

Ablation of concrete, release of reactant gases, temperature response.

MCCI: CCI-1 & CCI-2

General Description:

The CCI Phase 1 experiments were designed to measure concrete ablation with different types of concrete.

Important Physics:

Ablation of concrete, release of reactant gases, and temperature response.

TMI-2

General Description:

Though not an experiment, the Three Mile Island Unit 2 (TMI-2) accident serves as an excellent resource for code validation.

Important Physics:

The accident conditions stress the capabilities of the code for predicting core degradation, formation of a debris bed in the upper core, formation of a molten pool in the core, relocation of molten corium to the lower plenum, the response of the lower head, and reflood and quench of the degraded core.

VANAM: M3 (ISP 37)

General Description:

The objectives of the VANAM-M3 test were to provide data on containment-building response to severe accident conditions with particular emphasis on characterizing the depletion rate of hygroscopic aerosol under varying humidity and thermal-hydraulic conditions.

Important Physics:

Multi-compartment geometry, stratified atmosphere, atmosphere mixing by forced convection loops, thermal energy balance, structural heat transfer, steam condensation effects, and aerosol behavior.

1.4 References

[1.1] "Software Quality Assurance Program and Guidelines," NUREG/BR-0167, February 1993.

[1.2] Gauntt, R. O., Cash, J.E., Cole, R. K., Erickson, C. M, Humphries, L.L., Rodriguez, S. B., Young, M. F., 2005, "MELCOR Computer Code Manuals, Vol. 1: Primer and User's Guide, Version 1.8.6," NUREG/CR 6119, Vol. 1, Rev. 3, U.S. Nuclear Regulatory Commission, Washington, DC (2005).

[1.3] Souto, F.J., Haskin, F.E., Kmetyk, L.N., "MELCOR 1.8.2 Assessment: Aerosol Experiments ABCOVE AB5, AB6, AB7, and LACE LA2," SAND94-2166 (1994).

[1.4] Tautges, T.J., "MELCOR 1.8.2 Assessment: The MP-1 and MP-2 Late Phase Melt Progression Experiments," SAND94-0133 (1994).

[1.5] Kmetyk, L.N., "MELCOR 1.8.3 Assessment: CSE Containment Spray Experiments," SAND94-2316 (1994)

[1.6] Kmetyk, L.N., "MELCOR 1.8.3 Assessment: CSE Containment Spray Experiments," SAND94-2316 (1994).

[1.7] Tills, J., Notafrancesco, A, Longmire, P., "An Assessment of MELCOR 1.8.6: Design Basis Accident Tests of the Carolinas Virginia Tube Reactor (CVTR) Containment (Including Selected Separate Effects Tests)," SAND2008-1224 (2008).

[1.8] Tautges, T., "MELCOR 1.8.2 Assessment: The DFI-4 BWR Damaged Fuel Experiment," SAND93-1377 (1993).

[1.9] Tautges, T., "MELCOR 1.8.3 Assessment: GE Large Vessel Blowdown and Level Swell Experiments," SAND94-0361 (1994).

[1.10] Kmetyk, L.N., “MELCOR 1.8.2 Assessment: IET Direct Containment Heating Tests,” SAND93–1475 (1993).

[1.11] Kmetyk, L.N., “MELCOR 1.8.1 Assessment: LACE Aerosol Experiment LA4,” SAND91–1532 (1991).

[1.12] Kmetyk, L.N., “MELCOR 1.8.1 Assessment: LOFT Integral Experiment LP-FP-2,” SAND92–1373 (1992).

[1.13] Kmetyk, L.N., “MELCOR 1.8.1 Assessment: Marviken-V Aerosol Transport Tests ATT-2b/ATT-4,” SAND92–2243 (1993).

[1.14] Kmetyk, L.N., “MELCOR 1.8.1 Assessment: ACRR Source Term Experiments ST-1/ST- 2", SAND91-2833 (1992).

2. MELCOR ANALYTIC ASSESSMENT

As part of the MELCOR assessment effort, MELCOR is validated against small problems for which an analytical solution is available. These problems were first published as an assessment for the MELCOR 1.8.1 code 31 [2.1]. Problems included in this assessment are:

1. Saturated liquid depressurization,
2. Adiabatic flow of hydrogen,
3. Transient heat flow in a semi-infinite solid with convective boundary conditions,
4. Cooling of rectangular and annular heat structures in a fluid,
5. Self-initialization of steady-state radial temperature distributions in annular structures, and
6. Establishment of flow in a pipe.

2.1 Saturated Liquid Depressurization

The analysis of severe accidents involves predicting the depressurization of the reactor vessel into its containment. For some accident sequences, the reactor vessel contains significant quantities of high-pressure, high-temperature water, which will undergo rapid flashing during depressurization. The ability of MELCOR to adequately represent the outcome of such a depressurization has been tested using a simple model that allows comparison to an exact analytic solution.

This problem tests the CVH/FL/CVT packages and the HS package. It was originally run and documented as part of the 1986 MELCOR V&V effort for MELCOR 1.6.0 [2.2]. The final results given here are for MELCOR 2.1 (revision 6061) but results for MELCOR 1.8.6 YT (revision 1010) and 1.8.5 (RL) are also provided.

2.1.1 Problem Description

A volume containing saturated water at high pressure is connected to another volume containing only a low-pressure, steam atmosphere by a flow path and a heat structure. The flow path is opened at time zero and the system is allowed to come into pressure and thermal equilibrium. The heat structure, which thermally equilibrates the two volumes, is thin enough to be negligible in the energy balances. The initial conditions are listed in Table 2-1, and the system is shown schematically in Figure 2-1.

Table 2-1. Initial Conditions for the Saturated Liquid Depressurization Problem

Parameter	Volume 1	Volume 2
Pressure (MPa)	7.999	0. 01
Temperature (K)	568.23	568.23
Water Mass (kg)	72240	0. 0
Steam Mass (kg)	0. 0	152.57
Void Fraction	0. 0	1. 0

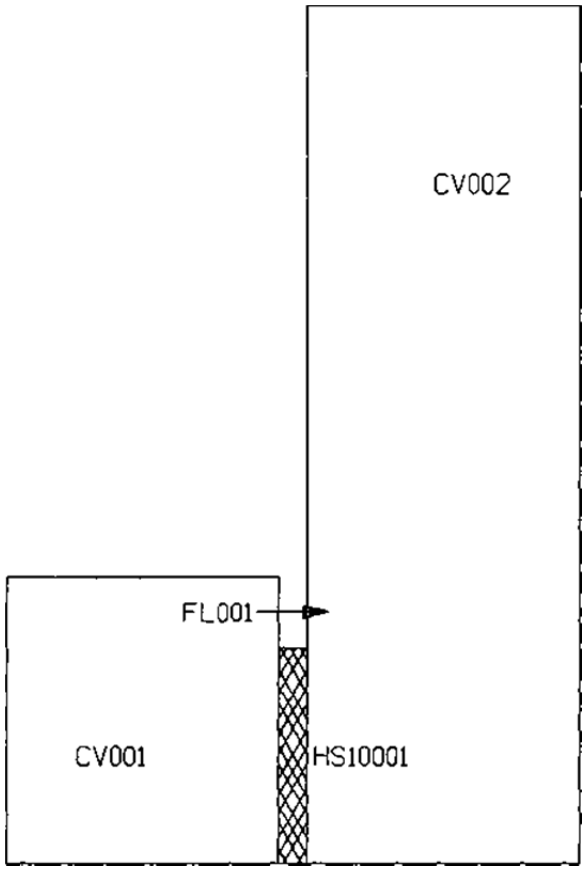

Figure 2-1. Saturated Liquid Depressurization Problem Model

2.1.2 Analytical Solution

The analytical solution for the final system state is obtained from mass and energy balances:

$$u_f + x u_{fg} = (U_o + E_s)/M_t \quad \text{(Equation 2-1)}$$

$$v_f + x v_{fg} = V/M_t \quad \text{(Equation 2-2)}$$

$$U_o = M_{1o}u_{1o} + M_{2o}u_{2o} \quad \text{(Equation 2-3)}$$

$$E_S = M_S C_p (T_i - T_f) \quad \text{(Equation 2-4)}$$

where

u_f= specific internal energy [J/kg] of liquid,
u_{fg} = specific internal energy [J/kg] of evaporation,
v_f = specific volume [m^3/kg] of liquid,
v_{fg} = specific volume [m^3/kg] of evaporation,
x = steam quality at equilibrium,
M_t = total mass [kg],
V = total volume [m^3],
M_{1o} = initial mass [kg] in volume 1,
M_{2o} = initial mass [kg] in volume 2,
u_{1o} = initial specific internal energy [J/kg] in volume 1,
u_{2o} = initial specific internal energy [J/kg] in volume 2,
M_s= mass of structure [kg],
C_p = structure specific heat [J/K],
T_i = initial structure temperature [K], and
T_f = final structure temperature [K]

This test was designed with E_s about six orders of magnitude smaller than U_Q so the structure term can be removed from the energy balance equation.

Using the Keenan and Keyes steam tables [2.3] and the initial conditions given in Table 2-1, the above equations reduce to:

$$u_j + x u_{fg} = 1.30886 \times 10^{v}\ J/kg \quad \text{(Equation 2-5)}$$

$$v_j + x\ v_{fg} = 0.0566356\ m^3/kg \quad \text{(Equation 2-6)}$$

These two equations can be solved for the steam quality by iterating on pressure. The final values are 1.037MPa with a saturation temperature of 454.7K and a steam quality of 0.297.

2.1.3 Results

Results from MELCOR 2.1 are compared to this analytical solution in Table 2-2 along with results calculated from previous code versions. The MELCOR results given were taken from

the larger volume (volume 2) at the end of the calculations (3,000s); the pressures and temperatures of the two volumes differed by only 0.0003MPa and 0.013K. The pressure and temperature equilibrations predicted for these two volumes are illustrated in Figure 2-2 and Figure 2-3; aside for the case run with the MELCOR 2.1 defaults, the results from the different code versions are indistinguishable.

Table 2-2. Results Comparison for the Saturated Liquid Depressurization Problem

Parameter	Analytic	MELCOR Version				
		1.60	1.81	1.85	1.86	2.1
Pressure (MPa)	1.037	1.034	1.0373	1.03724	1.0373	1.0576
Temperature (K)	454.7	454.8	454.6935	454.6943	454.6954	455.5453
Quality	0.297	0.2964	0.29736	.29735	0.29734	0.29753

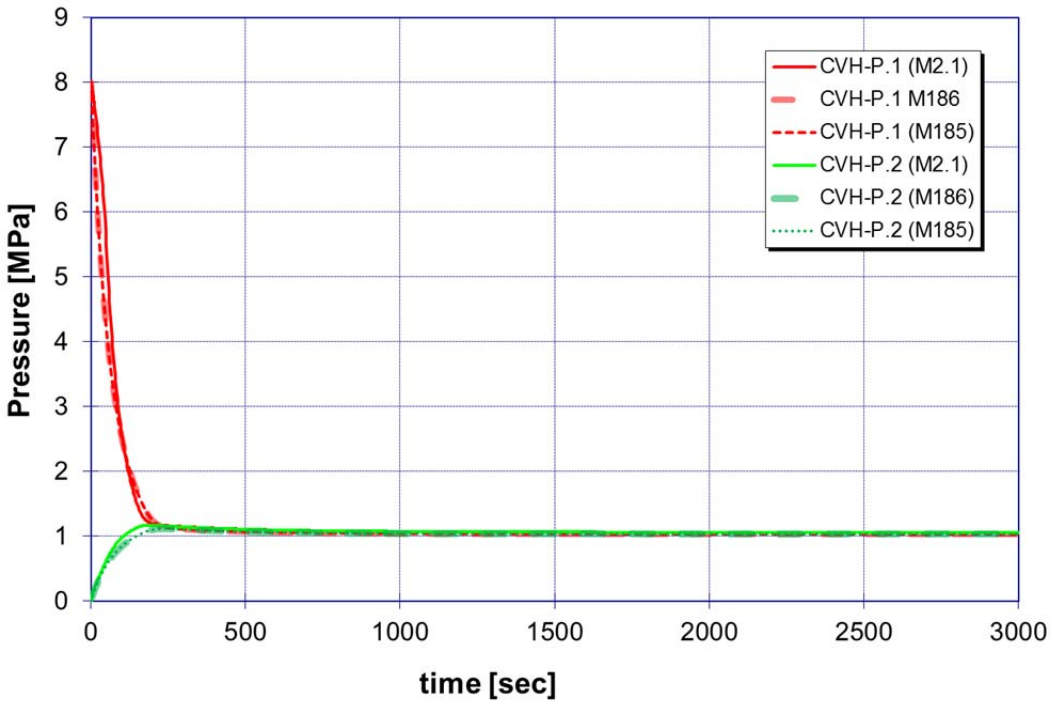

Figure 2-2. Calculated Pressure Equilibration for Saturated Liquid Depressurization Problem Model

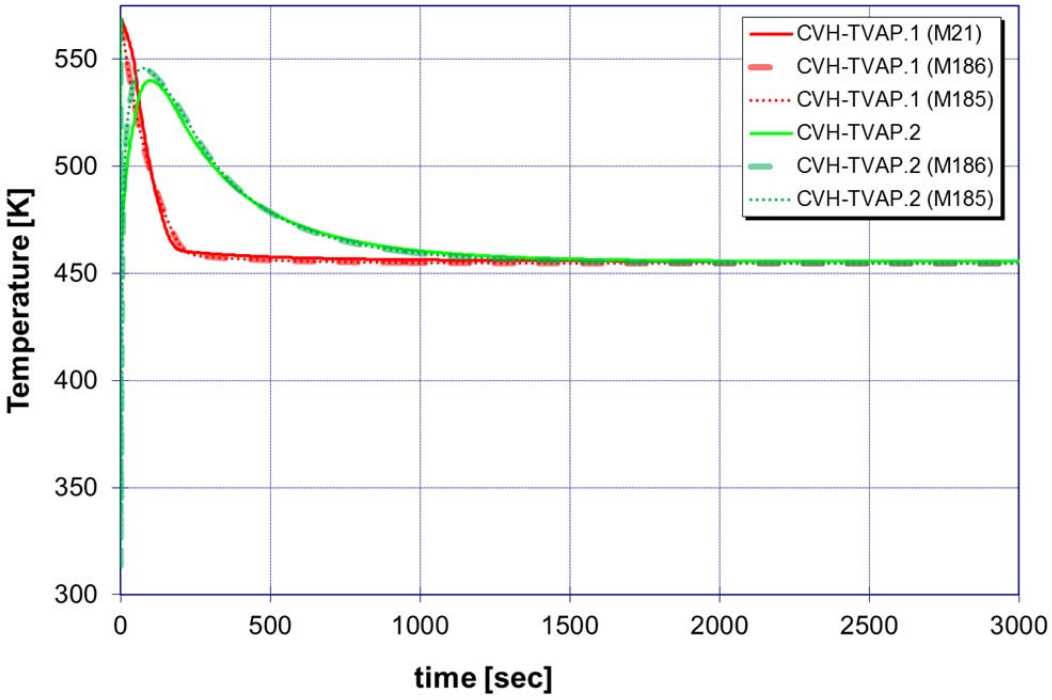

Figure 2-3. Calculated Temperature Equilibration for Saturated Liquid Depressurization Problem Model

2.2 Adiabatic Expansion of Hydrogen

MELCOR calculations for the adiabatic flow of hydrogen between two control volumes have been run, and are compared to a closed-form analytical solution. This problem tests the CVH/FL/CVT packages and the NCG package. It was originally run and documented as part of the 1986 MELCOR V&V effort for MELCOR 1.6.0 [2.2]. The final results given here are for MELCOR 2.1 (revision 6061), although results for MELCOR 1.8.6 YT (revision 1010) and 1.8.5 (RL) are also provided.

2.2.1 Problem Description

The problem consists of two control volumes that are pressurized with hydrogen such that the pressure in volume 1 is greater than that in volume 2. At time zero, a flow path is opened between the two control volumes, and hydrogen from the higher-pressure control volume expands into the lower-pressure control volume until the two pressures equilibrate.

For the original publication of these analytical assessment problems [2.1], the initial conditions, control volume sizes, and flow path parameters were varied over a wide range to provide a thorough test of the MELCOR packages. Six cases were analyzed, according to the specifications given in Table 2-3. For this report we have presented full results for the first case (Case 1) only, though the adiabatic pressure response is shown for all cases.

Table 2-3. Initial Conditions for the Hydrogen Adiabatic Expansion Problem

Case No.	Volume 1 (m^3)	Volume 2 (m^3)	T(l=2) (K)	P(1) (Pa)	P(2) (Pa)	Flow Area (m^2)	Loss Coeff.
1	1000.	1000.	300.	2.0e5	1.0e5	0.05	2.0
2	1000.	1000.	300.	5 0e5	1.0e5	0.05	2.0
3	100.	1000.	300.	2.0e5	1.0e5	0.05	2.0
4	10000.	1000.	300.	2.0e5	1.0e5	0.05	2.0
5	1000.	1000.	300.	2.0e5	1.0e5	50.0	2.0
6	1000.	1000.	300.	2.0e5	1.0e5	0.05	0.1

2.2.2 Analytical Solution

Assuming adiabatic flow and treating hydrogen as an ideal gas, analytic expressions for the control-volume temperatures and pressures, as transient functions of the mass transferred, are:

$$T_1 = T_{10}\left(\frac{m_1}{m_{1o}}\right)^{\gamma-1} \qquad \text{(Equation 2-7)}$$

$$P_1 = P_{1o}\left(\frac{m_1}{m_{1o}}\right)^{\gamma} \qquad \text{(Equation 2-8)}$$

$$T_2 = \frac{m_{2o}T_{2o}}{m_2} + \frac{m_{1o}T_{1o}}{m_1}\left[1-\left(\frac{m_1}{m_{1o}}\right)^{\gamma}\right] \qquad \text{(Equation 2-9)}$$

$$P_2 = P_{2o} + \frac{V_1}{V_2}\left[1-\left(\frac{m_1}{m_{1o}}\right)^{\gamma}\right] \qquad \text{(Equation 2-10)}$$

where

T_N = temperature [K] in volume N,
T_{No} = initial temperature [K] in volume,
P_N =pressure [Pa] in volume N,
P_{N0} = initial pressure [Pa] in volume N,
m_N mass [kg] of hydrogen in volume N,
m_{No} = initial mass [kg] of hydrogen in volume N,
V_N = volume [m^3] of volume N, and
γ = the ratio of specific heats for hydrogen (taken to be 1.4).

2.2.3 Results

Results from M2.1, M1.8.6, and M1.8.5 for the pressures and temperatures in both control volumes, as a function of the mass remaining in the donor cell, are compared to the analytical solution in Figure 2-4 and Figure 2-5. For all code versions, the agreement is very good. The slight differences sometimes visible are in part due to using temperature-dependent heat capacities in MELCOR, which introduces some minor deviations from the ideal gas assumption in the analytical solution, and partly due to the time-step selection.

Plots of the time-dependent temperatures, pressures, and control volume masses are presented in Figure 2-6 through Figure 2-9; all the figures show good agreement between all code versions.

2.2.4 Conclusions

These results show good agreement between MELCOR predictions and analytical solution, demonstrating MELCOR's ability to predict the adiabatic expansion of a noncondensable gas. The slight differences sometimes visible are in part due to using temperature-dependent heat capacities in MELCOR, which introduces some minor deviations from the ideal gas assumption in the analytical solution, and partly due to the time-step selection. No significant differences were found between these MELCOR 2.1 results and the earlier, MELCOR 1.8.6 and MELCOR 1.8.5, results.

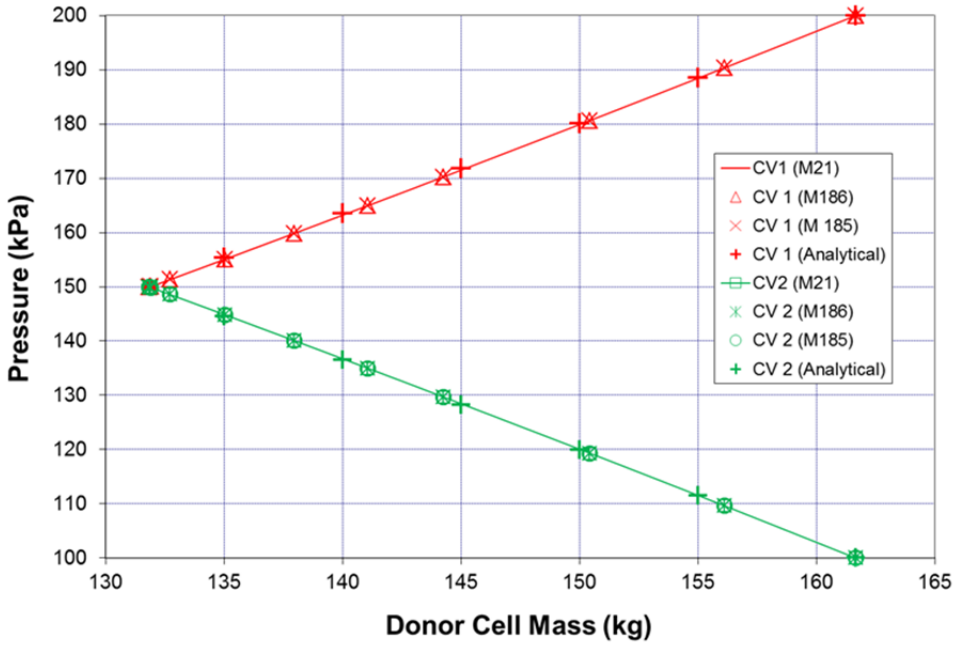

Figure 2-4. Pressure vs. Donor Cell Mass for Hydrogen Adiabatic Expansion

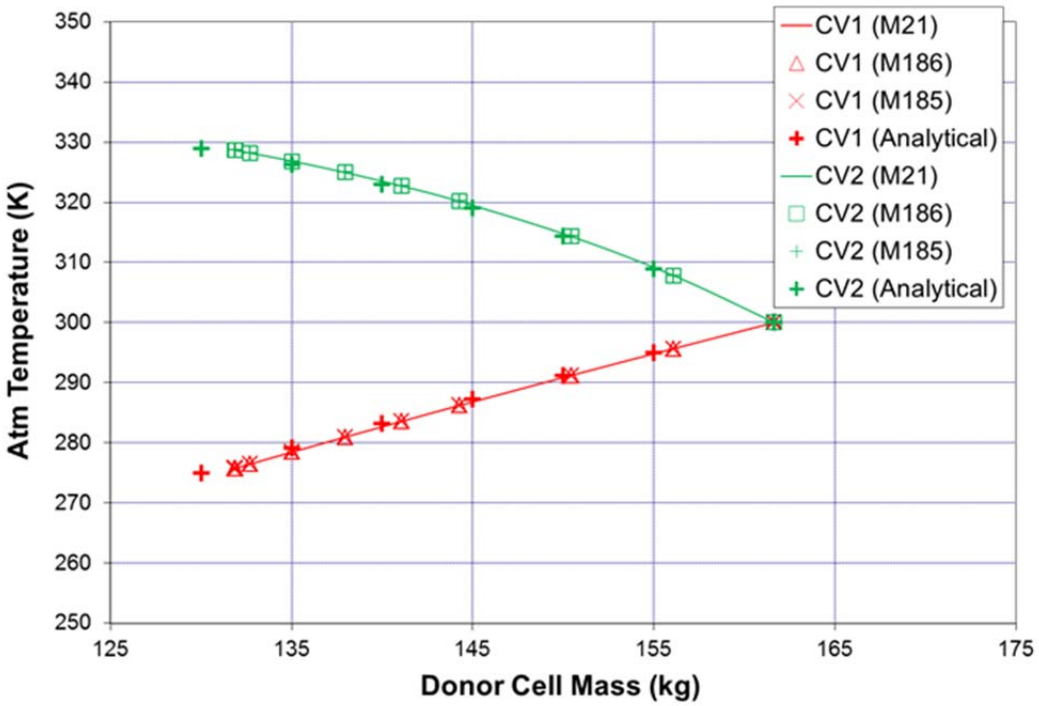

Figure 2-5. Temperature vs. Donor Cell Mass for Hydrogen Adiabatic Expansion

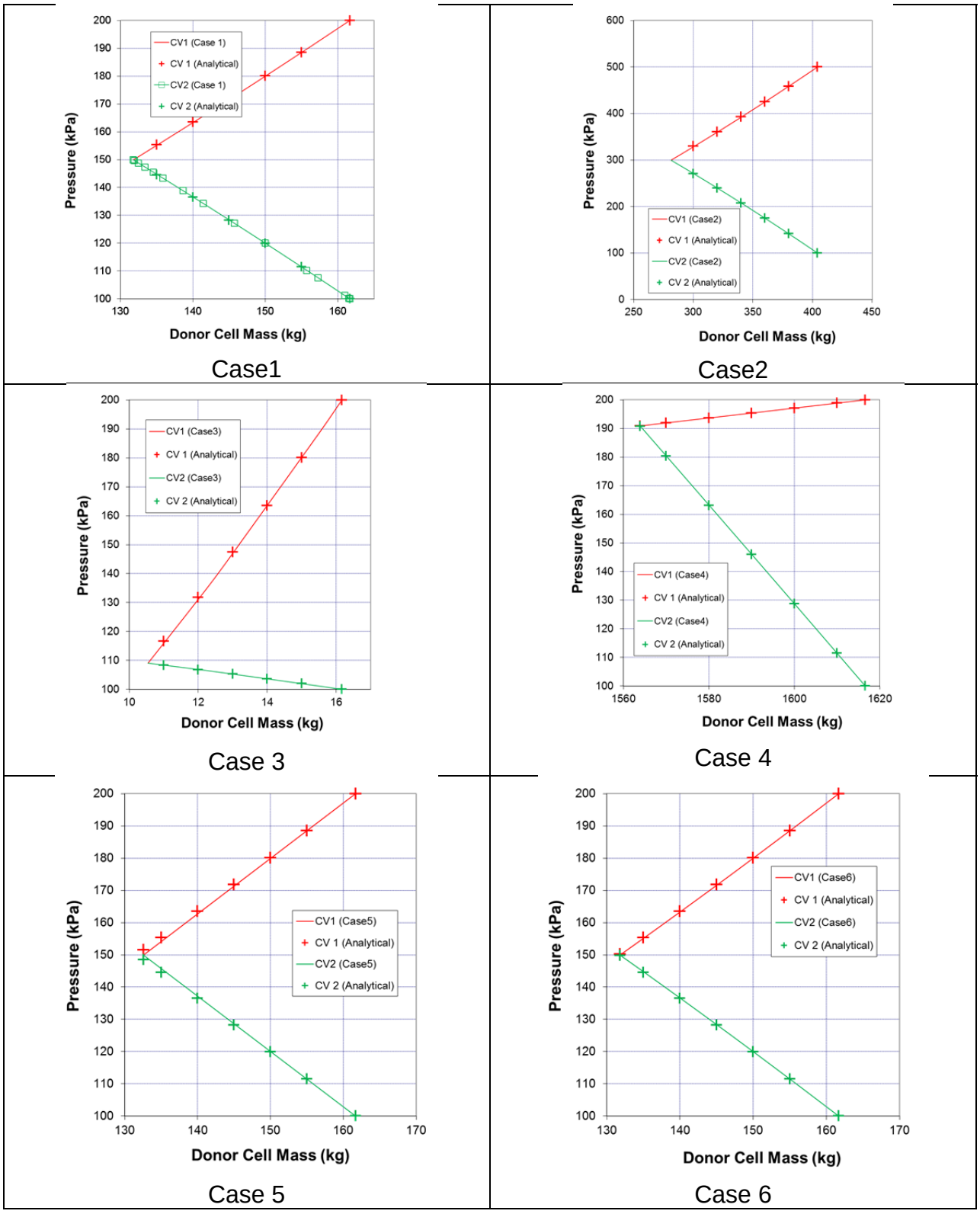

Figure 2-6. Pressure vs. Donor Cell Mass for Hydrogen Adiabatic Expansion – All Cases

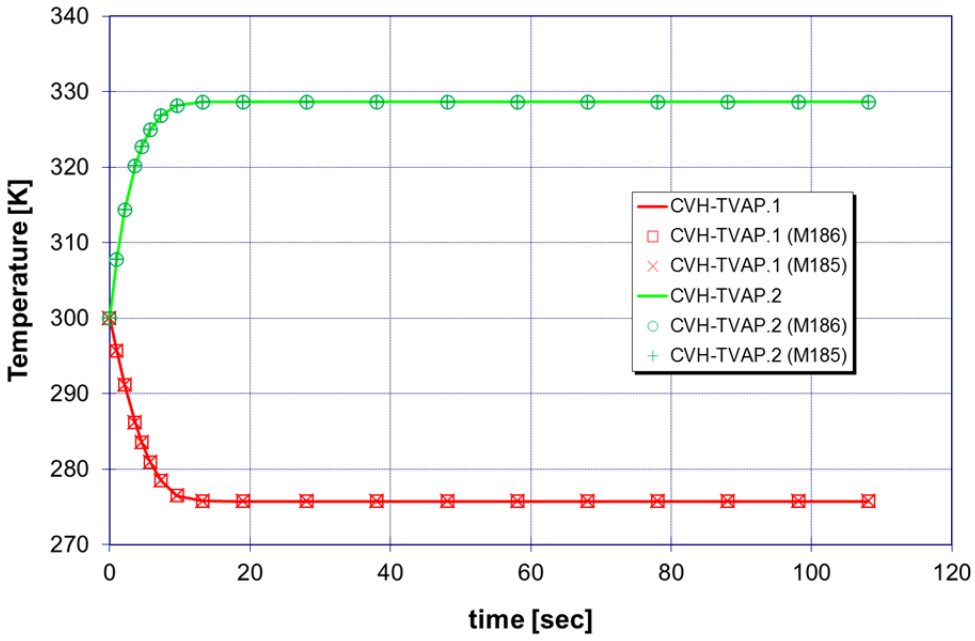

Figure 2-7. MELCOR Calculated Temperatures vs Time for Hydrogen Adiabatic Expansion Problem

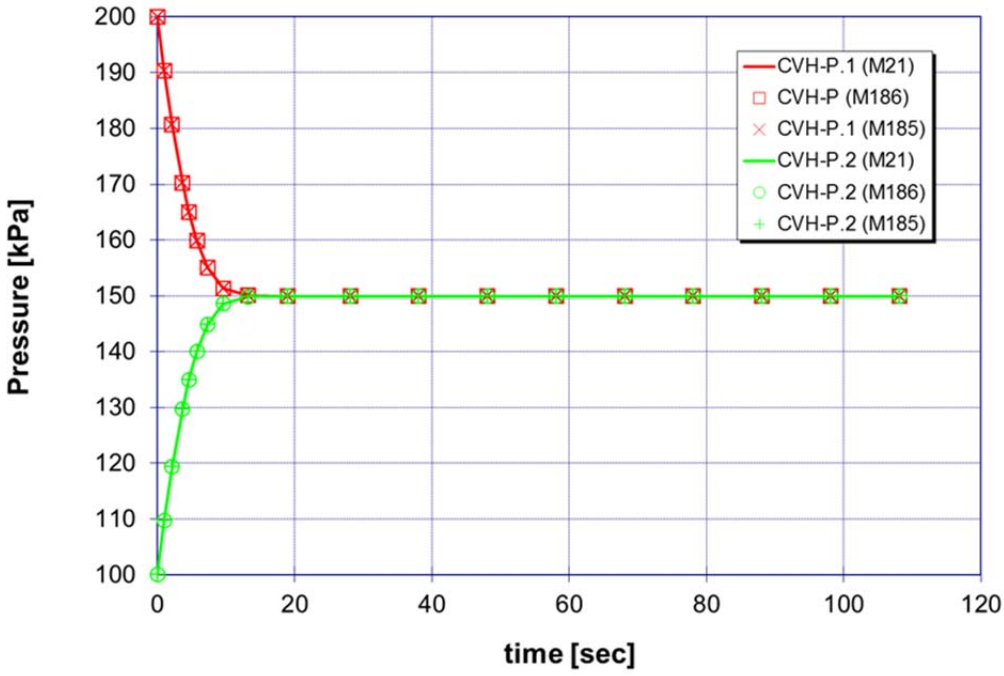

Figure 2-8. MELCOR Calculated Pressure vs Time for Hydrogen Adiabatic Expansion Problem

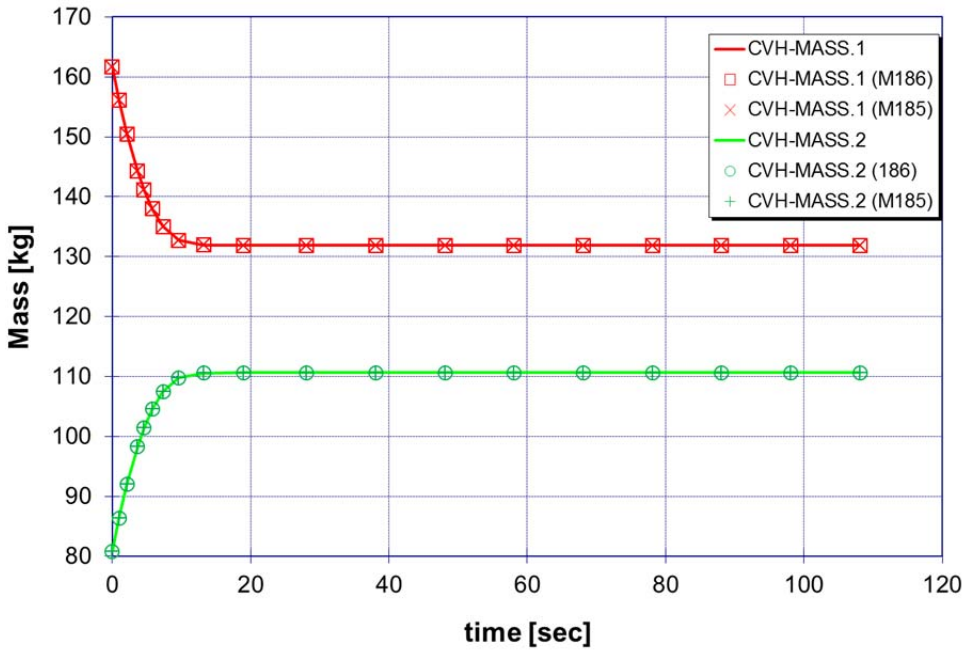

Figure 2-9. MELCOR Calculated Mass vs Time for Hydrogen Adiabatic Expansion Problem

2.3 Transient Heat Flow in a Semi-Infinite Heat Slab

In order to test the MELCOR heat conduction models, MELCOR predictions for heat conduction in a solid are compared to the corresponding exact analytical solution for transient heat flow in a semi-infinite solid with convective boundary conditions. This problem simulates the conduction heat transfer in thick walls, in particular, the concrete containment walls of a nuclear plant during a severe accident. This analysis demonstrates the accuracy of the MELCOR heat conduction models, and provides guidelines for node spacing and time step sizes for concrete containment walls.

This problem primarily tests the HS package, although a control volume is used to set the boundary temperature; the test was originally run and documented as part of the 1986 V&V effort [2.2]. Those results were for the MELCOR 1.1 code; two of the cases were later run with MELCOR 1.6.0 with no significant differences from the MELCOR 1.1 results presented in [2.2]. The results provided here are for MELCOR 2.1 (revision 6061), although results for MELCOR 1.8.6 YT (revision 1010) and 1.8.5 (RL) are also provided.

2.3.1 Problem Description

Transient heat flow in a semi-infinite solid with convective boundary conditions is modeled in MELCOR using a finite slab heat structure of sufficient thickness to approximate a semi-infinite solid. In the MELCOR calculations for this problem, a 10m-thick heat structure with

logarithmic node spacing was assumed. The smallest node spacing was on the left side of the heat structure, which is adjacent to a very large control volume. On the left side of the heat structure, a convective heat transfer boundary condition was specified with a heat transfer coefficient of 10W/m^2-K. An adiabatic boundary condition was specified for the right side of the heat slab.

MELCOR calculations were performed for two different materials (steel and concrete) and two different fluid temperatures to verify MELCOR's ability to predict the analytical solution. Table 2-4 summarizes the specifications for the first three tests. These cases were run with 69 nodes within the first meter of thickness and with 10s time steps. Case 1 is considered the base case for this analysis. The parameters for this case simulate the concrete wall of a containment building during a severe accident. Then, the number of nodes used and the time-step sizes were varied to examine the effects on the accuracy of the results and to recommend node spacing and time-step sizes for severe accident analyses.

Table 2-4. Specifications for Semi-Infinite Heat Conduction Analyses

Case	Initial Temp (K)	Fluid Temp (K)	Material	Density (kg/m^3)	Specific Heat (J/kg-K)	Thermal Conductivity (W/m-K)	Thermal Diffusivity (m^2/s)
1	300.0	450.0	concrete	2300.0	650.0	1.6	1.07×10^{-6}
2	300.0	450.0	steel	7850.0	500.0	47.0	1.20×10^{-5}
3	300.0	600.0	concrete	2300.0	650.0	1.6	1.07×10^{-6}

Six different node structures were analyzed to survey the effect of the node spacing on calculation results. These node structures were designed to include 69, 35, 18, 11, 8, and 5 nodes in the first meter. Nodes between 0.0 and 0.001m were equally spaced, while nodes between 0.001 and 10m were logarithmically spaced according to:

$$\frac{X_i}{X_{i-1}} = (10)^{1/N} \qquad \text{(Equation 2-11)}$$

where X_i/X_{i-1} is the ratio of adjacent node positions and N is the number of nodes desired per order of magnitude (i.e., between 1mm and 1cm). A graphical representation of the node locations for the six cases is given in Table 2-5.

2.3.2 Analytical Solution

The analytical solution for transient heat flow in a semi-infinite slab is given in Holman [2.4] as a function of the time and the position from the surface given the initial slab temperature, the fluid temperature, the convective heat transfer coefficient, and the thermal properties of

the solid (i.e., thermal conductivity, specific heat and density), which are all assumed constant. The solution is given by the following:

$$\frac{T-T_i}{T_o-T_i}=1-erf\left[\frac{x}{2\sqrt{\alpha t}}\right]-\exp\left[\frac{hx}{k}+\frac{h^2\alpha t}{k^2}\right]\left[1-erf\left(\frac{x}{2\sqrt{\alpha t}}+\frac{h\sqrt{\alpha t}}{k}\right)\right] \quad \text{(Equation 2-12)}$$

where

T = temperature at time t and position x (in K),
T_i = initial temperature of solid (in K),
T_o = fluid temperature (in K),
h = convective heat transfer coefficient (in W/m^2-K),
k = thermal conductivity (in W/m-K), and
α = thermal diffusivity (in m^2/s).

Table 2-5.Node Locations for Semi-Infinite Heat Conduction Analysis

Node Number	Location (m)	Number of Nodes in First Meter					
		69	35	18	11	8	5
Equally-spaced surface nodes							
1	0.0	*	*	*	*	*	*
2	0.000125	*					
3	0.000250	*	*				
4	0.000375	*					
5	0.000500	*	*	*			
6	0.000625	*					
7	0.000750	*	*				
8	0.000875	*					
9	0.001000	*	*	*	*	*	*
Logarithmic-spaced Interior Nodes							
10	0.01122	*					
11	0.001259	*	*				
12	0.001413	*					
13	0.00155	*	*				
14	0.001778	*					
15	0.001995	*	*				
16	0.002239	*					
17	0.002519	*	*	*	*	*	
18	0.002818	*					
19	0.003162	*	*				
20	0.003548	*					

21	0.003981	*	*	*			
22	0.004467	*					
23	0.005012	*	*				
24	0.005623	*					
25	0.006310	*	*	*	*		
26	0.007079	*					
27	0.007943	*	*				
28	0.008913	*					
29	0.01	*	*	*	*	*	*
49	0.1	*	*	*	*	*	*
69	1.0	*	*	*	*	*	*
89	10.0	*	*	*	*	*	*

The time-integrated surface heat flux, Q, is obtained from solving this equation and numerically integrating:

$$Q = \int_0^{100,000} h\left(T_o - T_s\right)dt \qquad \text{(Equation 2-13)}$$

where T_s is the temperature of the surface, T_0 is the fluid temperature, and h is the heat transfer coefficient.

2.3.3 Results

MELCOR results are compared to the exact solution as plots of temperature vs time. All MELCOR variations were run to 100,000s.

Temperature comparison plots are shown in Figure 2-10 for the base case (i.e., case 1 in Table 2-4). The temperatures predicted by MELCOR are virtually indistinguishable from those given by the analytical solution. The MELCOR surface temperatures lag the analytical temperatures by ~0.06K at 1,000 seconds, which diminishes to ~0.02 K by the end of the calculation. The error in the calculated surface temperature for all test cases is plotted in Figure 2-11. Overall, the MELCOR and analytical results compare extremely well.

An otherwise-identical test problem was run with steel thermal properties in place of the concrete properties. The results of this variation are shown in Figure 2-12, for three nodes. The MELCOR surface temperature lags the analytical temperature by 0.01–0.05K. The MELCOR results for this case were not as accurate as for the base case with concrete properties used; the accuracy of the current results with MELCOR 2.1 is very similar to that obtained in the base case, concrete analysis.

The base case was rerun with a fluid temperature of 600K, increased from 450K. Temperature vs time results for this case are given in Figure 2-13. The MELCOR surface temperature lags the analytical temperature by ~0.04-0.12K.

Case 1 was repeated with MELCOR version 1.8.6 and 1.8.5 (Figure 2-14 and Figure 2-15 respectively). There were no significant differences observed for these code versions.

The surface temperature results obtained for Case 3 using different nodalizations within the heat structure are shown in Figure 2-16. All nodalizations performed provided nearly identical surface temperatures and hence the integrated surface heat flux is well produced for all nodalizations.

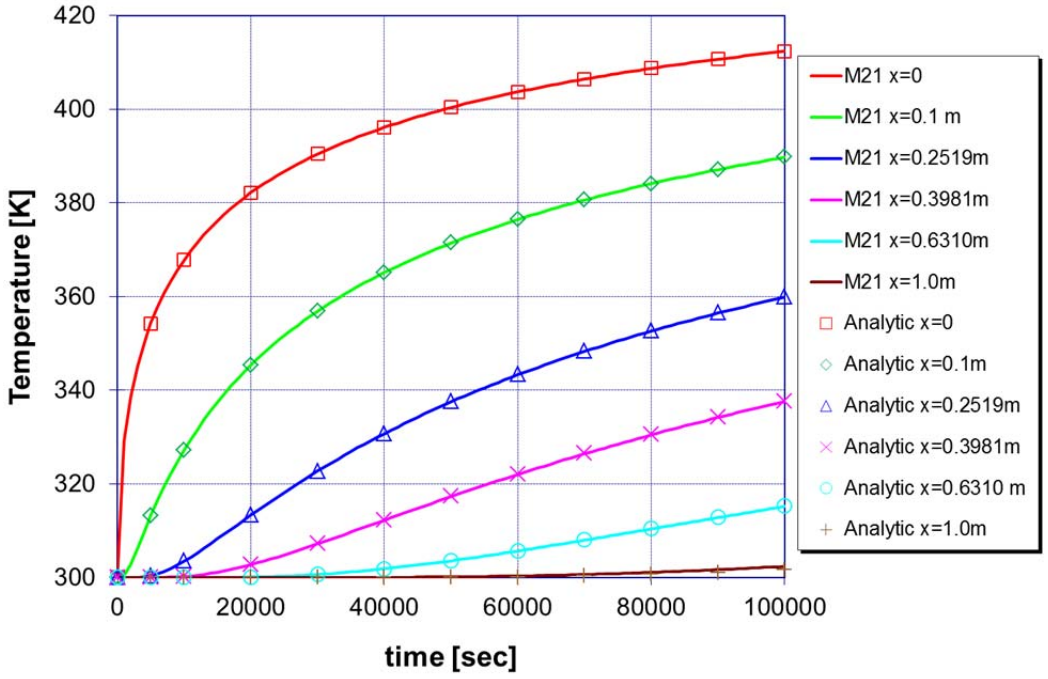

Figure 2-10. Temperature vs Time at Six Positions within a Thick Slab (Case 1)

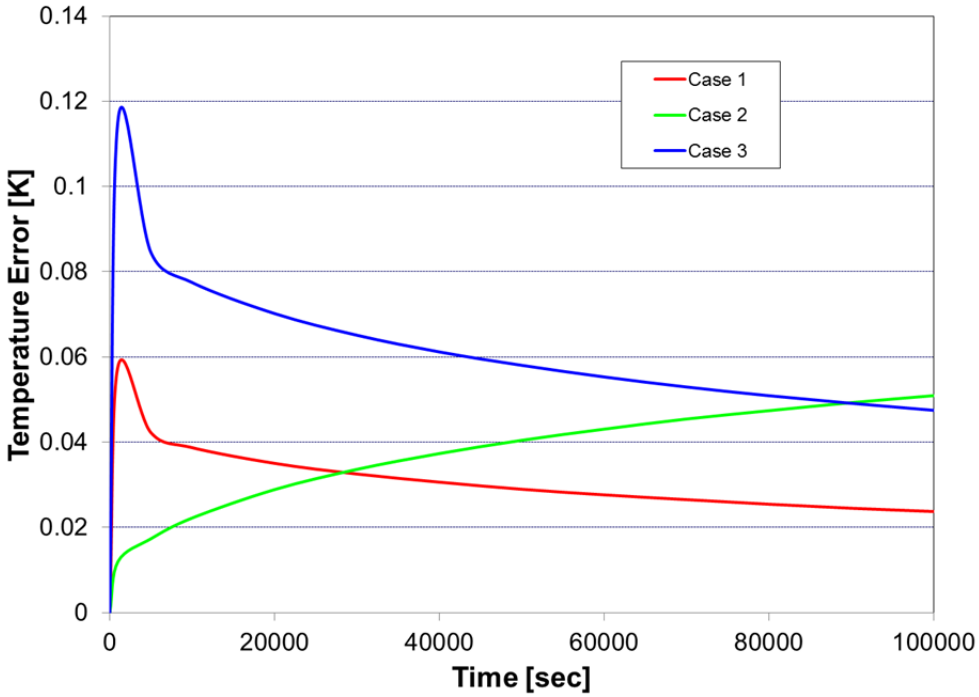

Figure 2-11. Error in Surface Temperature – all cases.

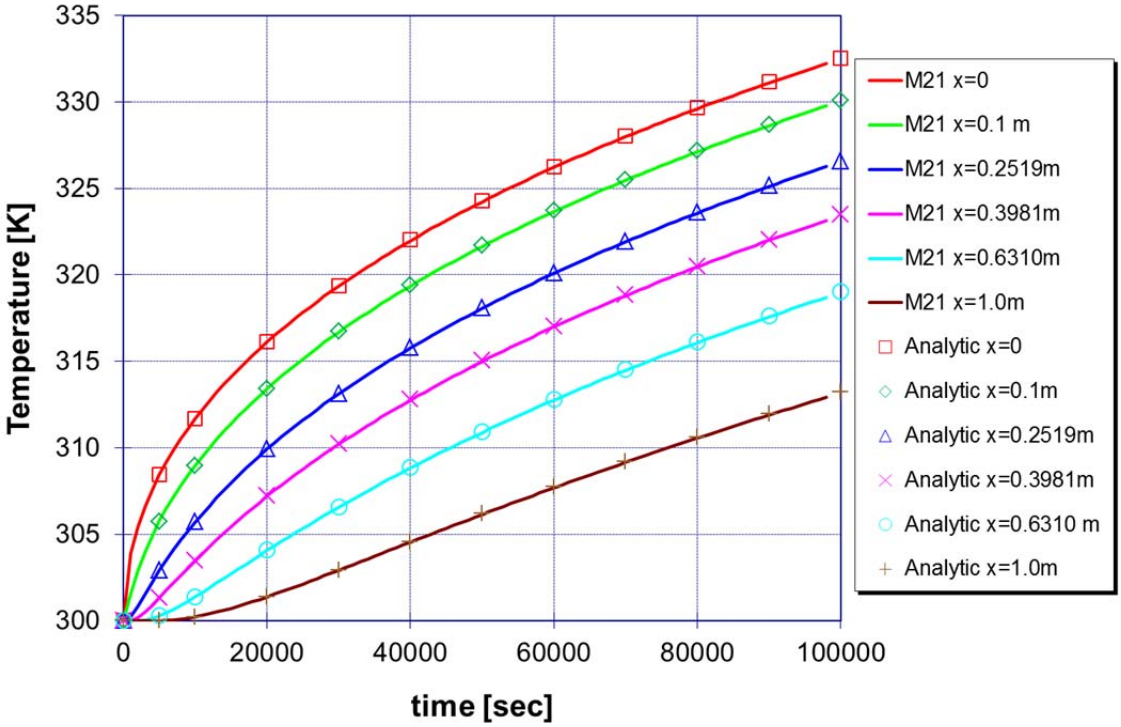

Figure 2-12. Temperature vs Time at Six Positions within a Thick Slab (Case 2)

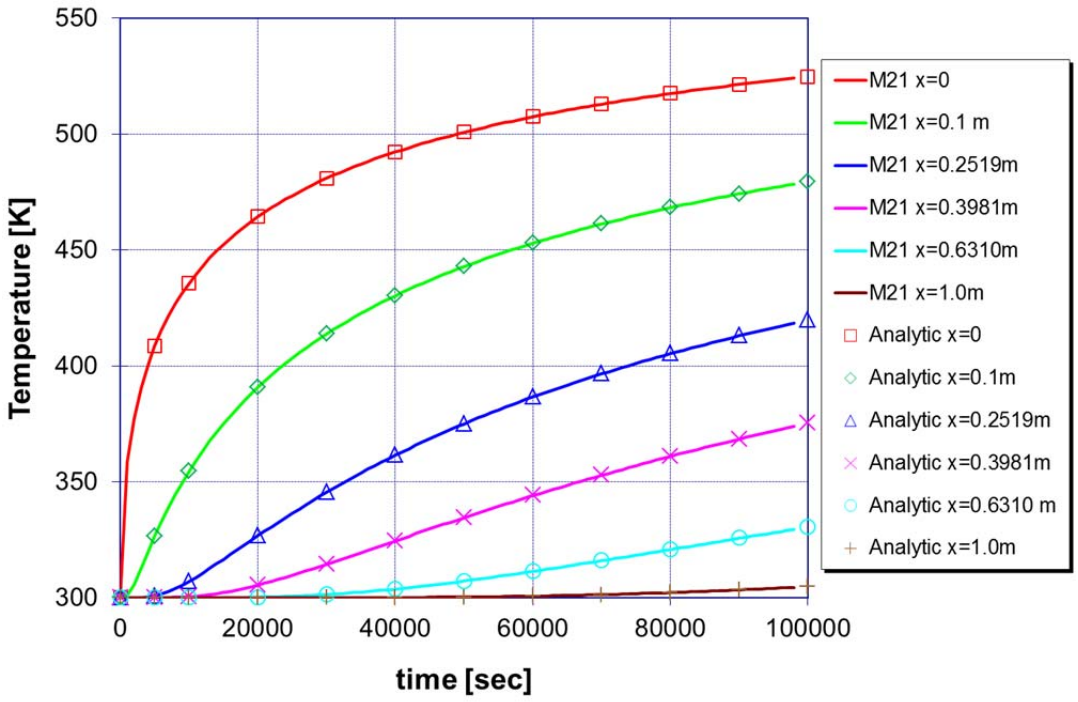

Figure 2-13. Temperature vs Time at Six Positions within a Thick Slab (Case 3)

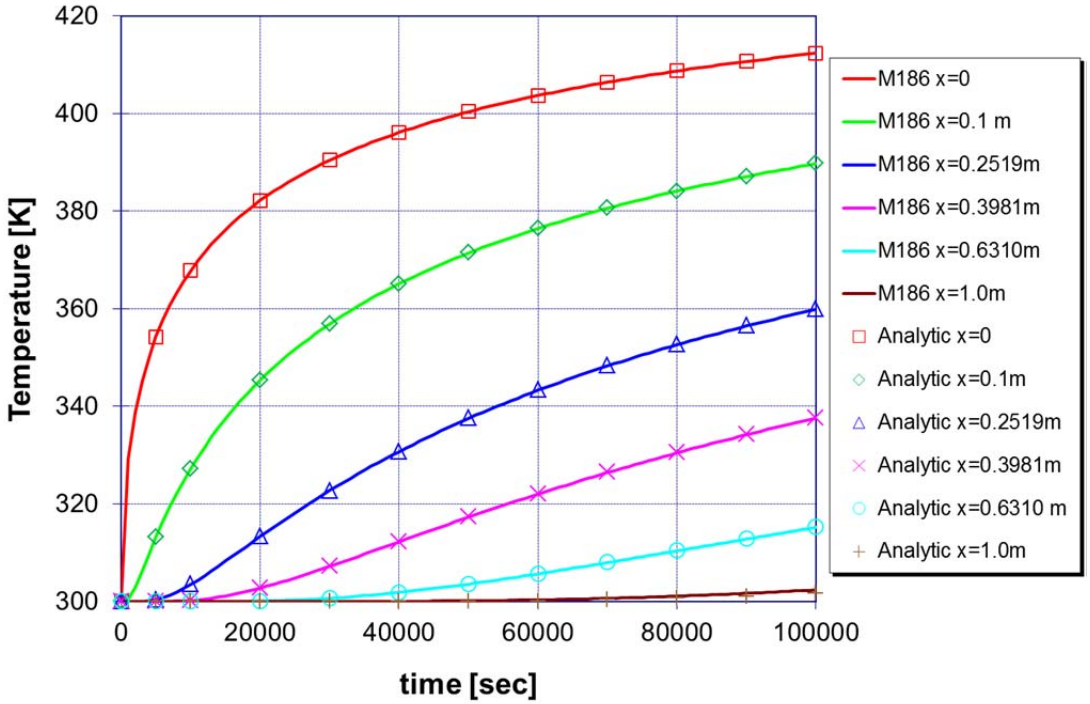

Figure 2-14. Temperature vs Time at Six Positions within a Thick Slab (MELCOR 1.8.6)

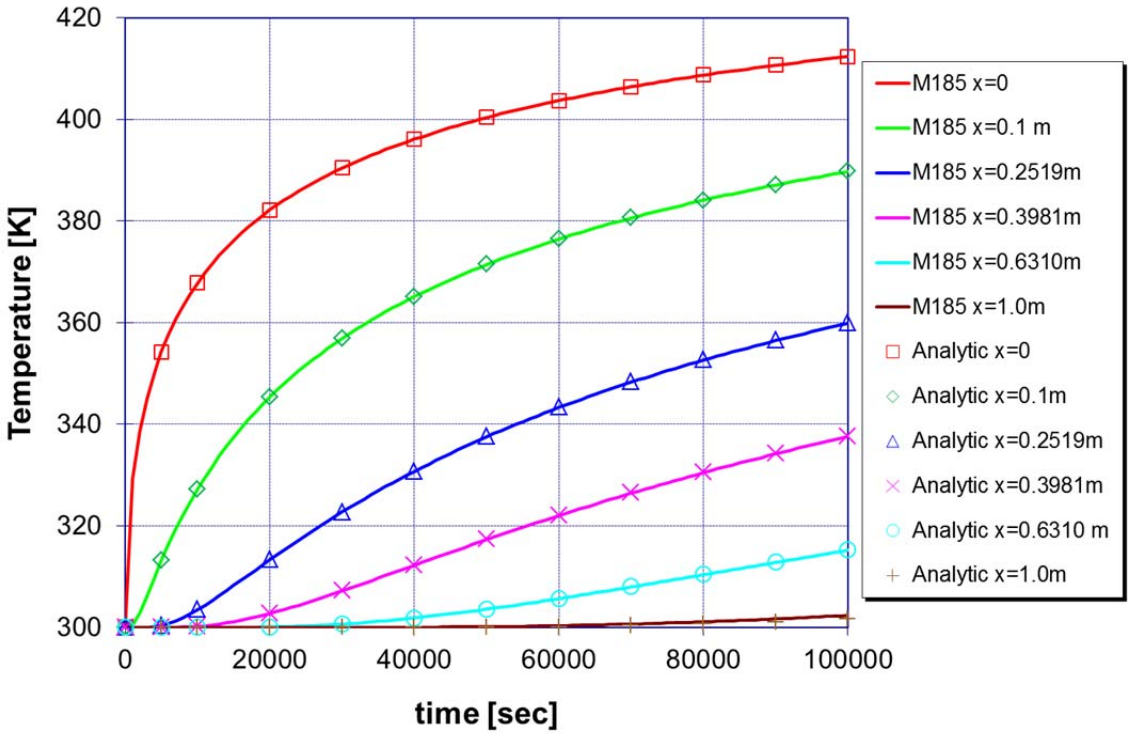

Figure 2-15. Temperature vs Time at Six Positions within a Thick Slab (MELCOR 1.8.5)

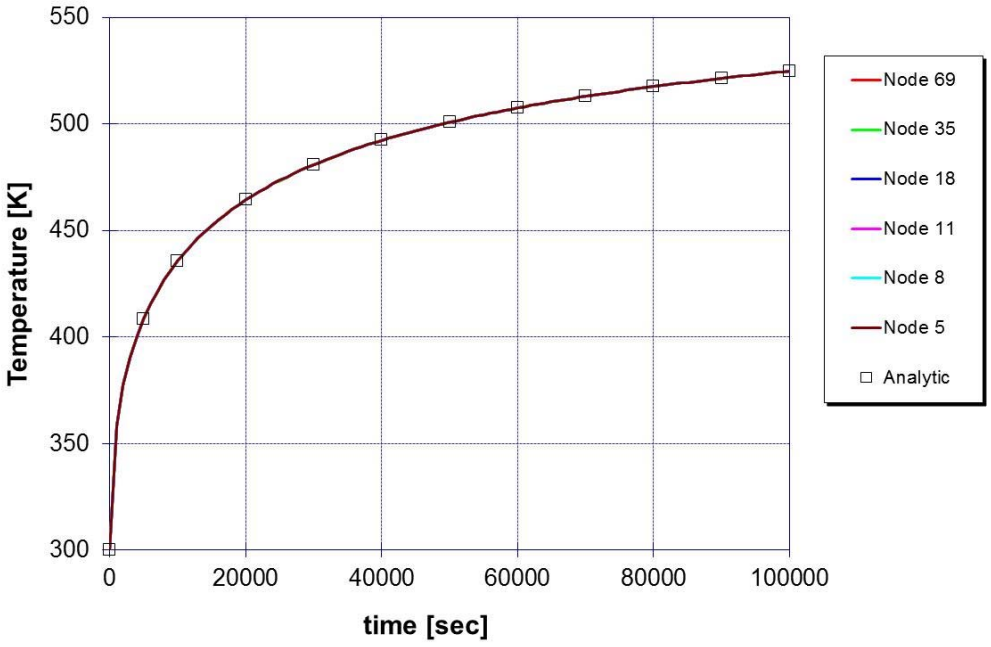

Figure 2-16. Surface Temperature vs Time for various nodalizations (Case 3)

2.3.4 Conclusions

Predictions of the heat conduction models in the MELCOR heat structures package have been compared to exact analytical solutions for transient heat flow in a semi-infinite solid with convective boundary conditions. The accuracy of the heat conduction models is demonstrated and the effects of various node spacings are investigated.

2.4 Cooling of Heat Structures in a Fluid

This section presents MELCOR 2.1 calculations for the cooling of two heat structures in a fluid, and compares the results to an exact, analytic solution, though MELCOR 1.8.6 YT (revision 1010) and 1.8.5 (RL) are also presented for comparison. Both rectangular and cylindrical geometries were tested. This problem primarily tests the implementation of the internal heat conduction methodology in the absence of internal or surface power sources.

This problem primarily tests the HS package, although a control volume is used to set the boundary conditions, and was originally run and documented as part of the 1986 MELCOR V&.V effort [2.2], those results were for MELCOR 1.6.0. The results provided here are for MELCOR 2.1 (revision 6061), although results for MELCOR 1.8.6 YT (revision 1010) and 1.8.5 (RL) are also provided.

2.4.1 Problem Description

MELCOR calculations were performed for two uniform, solid heat structures (one rectangular and one cylindrical) with constant thermal properties and constant surface heat transfer coefficients. These structures, initially at 1,000K, were immersed in a fluid at 500K. Table 2-6 gives values of the various thermal properties of the material in these structures, as well as other parameters used in these calculations. (The material in these structures does not correspond to any common material, but was chosen to permit easy comparison of the MELCOR results with an exact analytic solution.)

Table 2-6 Specifications for Heat Structure Cooling Analyses

Parameter	Value
Thermal Conductivity	50.0 W/m-k
Density	1.0 kg/m^3
Specific Heat Capacity	1500.0 J/kg-K
Surface heat transfer coefficient	50.0W/m^2-K
Structure initial temperature	1000.0 K
Fluid temperature	500.0 K
Rectangular slab thickness	0.1 m
Rectangular slab surface area	1.0m^2
Cylindrical slab radius	0.1m
Cylindrical slab height	1.0m

2.4.2 Analytic Solution

It is well documented in heat transfer texts that lumped-heat-capacity (LHC) methods are adequate for transient heat conduction calculations for a structure if its Biot number is <0.1 [2.4]. The Biot number for a structure is defined as:

$$Bi = \frac{h\left(\frac{V}{A}\right)}{k} \qquad \text{(Equation 2-14)}$$

where

Bi = Biot number (dimensionless),
h = heat transfer coefficient (W/m^2-K),
V = volume of structure (m^3),
A = surface area of structure (m^2), and
k = thermal conductivity of structure material (W/m-K).

A low Biot number implies that the transfer of energy within the structure is rapid relative to the transfer of energy from the structure to the fluid. The temperature within a structure with a low Biot number therefore can be assumed to be uniform.

The analytic solution for the temperature of a lumped-heat-capacity structure that is immersed in a fluid is given by [2.4] as:

$$T = T_f + \left(T_i - T_f\right)\left[\exp\left(\frac{-hAt}{\alpha V}\right)\right] \qquad \text{(Equation 2-15)}$$

where

T = uniform temperature [K] of structure,
T_f = temperature [K] of fluid,
T, = initial temperature [K] of structure,
h = heat transfer coefficient [w/m^2-K],
α = volumetric heat capacity [J/m^3-K],
V = volume [m^3] of the structure,
A = surface area [m^2] of the structure, and
t = time [s].

This solution is obtained by solving the first order linear differential equation that follows from the global energy balance between the structure and the fluid under the assumption of a uniform temperature throughout the solid.

The Biot number is Bi=0.05 for both the rectangular and cylindrical structures whose parameters were given in Table 2-6. The temperature histories calculated by MELCOR therefore should be close to the temperatures given by this analytic solution.

2.4.3 Results

Figure 2-17 compares the temperature histories predicted by MELCOR 2.1 for both rectangular and cylindrical structures, to each other and to the analytic solution. This figure illustrates excellent agreement between the MELCOR results and the analytic solution. Both structures are cooled as expected and have surface temperatures at the end of the 10s period calculated that are nearly equal to the fluid temperature, held fixed at 500.0K.

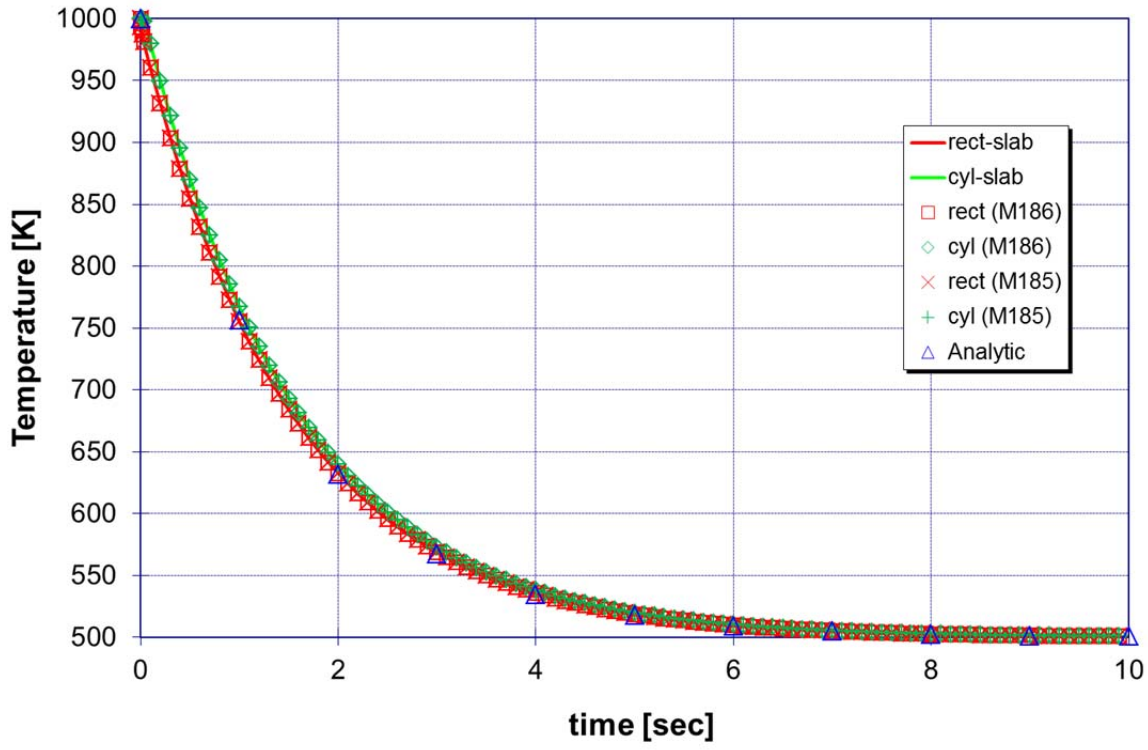

Figure 2-17. Temperature Histories for Cooling of a Heat Structure in a Fluid.

2.5 Radial Heat Conduction in Annular Structures

This section compares MELCOR 2.1 predictions of the steady-state temperature distributions resulting from radial heat conduction in annular structures to results obtained from exact analytic solutions. This steady-state temperature profile can be calculated by MELGEN as a steady-state initialization option. In addition, a transient calculation was performed with an initially uniform temperature profile to test whether MELCOR can achieve the correct steady-state temperature profile.

This problem primarily tests the HS package, although tabular functions are used to set the boundary conditions, and was originally run and documented as part of the 1986 MELCOR V&V effort [2.2]. Those results were for MELCOR 1.6.0; the results given here are for MELCOR 2.1 (revision 6061).

2.5.1 Problem Description

The MELCOR model consists of a hollow, cylindrical heat structure, with assorted boundary conditions specified on the inside and outside surfaces. Two cases were considered, with dimensions and initial and boundary conditions as specified in Table 2-7. The first case tests the heat structure temperature self-initialization logic in MELCOR where the second case test is initialized with a uniform temperature across the annulus that is then driven by heat transfer to the steady-state temperature profile.

Table 2-7 Specifications for Annular, Radial Heat Conduction Analyses

Case No.	Type	Left/Inside		Right/Outside		Radius	
		T (K)	h (W/m^2-K)	T(K)	h (W/m^2-K)	Inner (m)	Outer (m)
1	Steady	600.0	1000.0	550.0	5.0	3.1856	3.3412
2	Transient	600.0	1000.0	550.0	5.0	3.1856	3.3412

2.5.2 Analytic Solution

The analytic solution for the temperature profile resulting from radial, steady-state heat conduction in an annular structure, given the inner and outer surface temperatures, is given by [2.4]:

$$T = T_i - \ln\left(r/r_i\right)\left[\frac{T_i - T_o}{\ln\left(r_o/r_i\right)}\right] \qquad \text{(Equation 2-16)}$$

where

T = the temperature [K], at radius r
T_i = inner annular surface temperature [K],
T_o = outer annular surface temperature [K],
r_i = inner annular radius [m], and
r_o = outer annular radius [m].

Given specified heat transfer coefficients and fluid temperatures at the inner and outer surfaces, the analytic solution becomes [2.4]:

$$T = T_{env,i} - \left(\frac{\ln\left(r_i / r_o\right)}{k} + \frac{1}{h_i r_i} \right) \left(\frac{\left(T_{env,i} - T_{env,o}\right)}{\frac{\ln\left(r_o / r_i\right)}{k} + \frac{1}{h_i r_i} + \frac{1}{h_o r_o}} \right) \quad \text{(Equation 2-17)}$$

where

k = thermal conductivity (W/m-K),
h_i = heat transfer coefficient [W/m^2-K] at inner surface,
h_o = heat transfer coefficient [W/m^2-K] at outer surface,
$T_{env,i}$ = fluid temperature adjacent to the inner surface (K), and
$T_{env,o}$ = fluid temperature adjacent to the outer surface (K).

2.5.3 Results

The analytic solutions and the MELGEN/MELCOR results for both cases are shown in **Figure 2-18**. The agreement between the MELGEN/MELCOR results and the analytic solutions is very good. The MELGEN steady state option leads to an identical temperature profile through the heat structure. As shown in Figure 2-19, this profile is identical to those results obtained with MELCOR 1.8.6, MELCOR 1.8.5, and previous code versions.

2.5.4 Conclusions

MELCOR predictions of the steady-state temperature distributions resulting from radial heat conduction in annular structures have been compared to the exact analytical solutions for both the HS steady state initialization option as well as a transient calculation that was run to steady state. The agreement between MELCOR results and the analytic solution is excellent in both cases. No significant differences were found between these MELCOR 2.1, 1.8.6, and 1.8.5 results and earlier MELCOR 1.6.0 results.

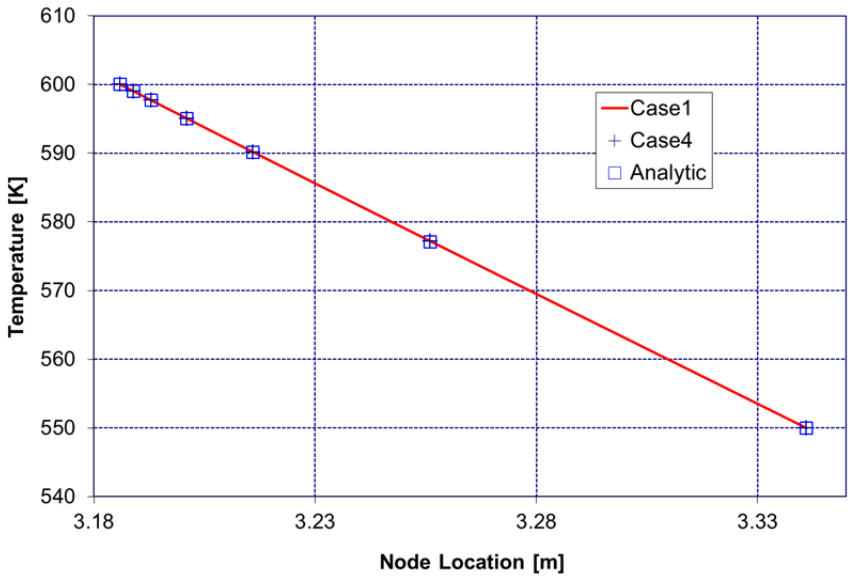

Figure 2-18. Temperature profile for radial heat conduction in annular structures (Case 1 and case 4)

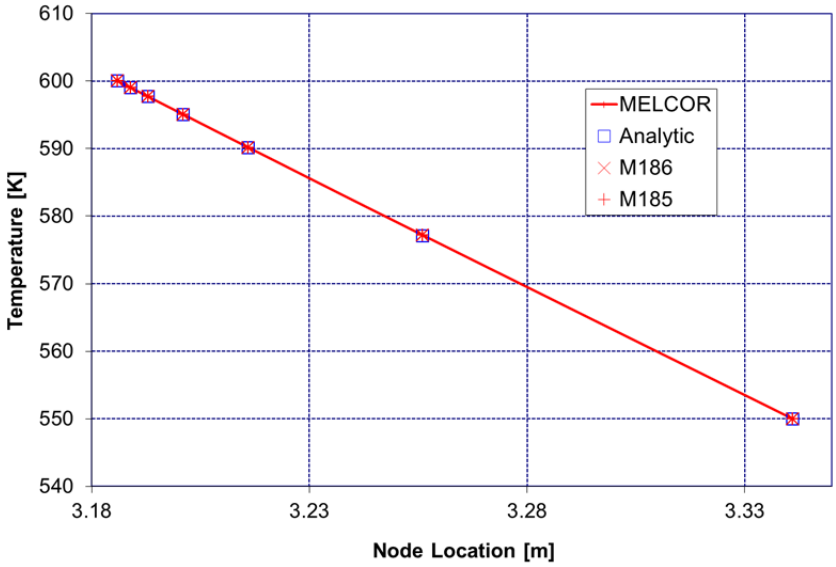

Figure 2-19. Temperature profile for radial heat conduction in annular structures (Case 1 for various code versions)

2.6 Establishment of Flow

This section compares MELCOR 2.1 predictions for the establishment of flow in a pipe connected to a large reservoir after a valve is suddenly opened to results obtained from exact analytic solutions, for both the final, asymptotic velocity attained and for the time required to establish this flow. Several variations in controlling parameters were considered.

This problem primarily tests the CVH/FL package. The results provided here are for MELCOR 2.1 (revision 6061), although results for MELCOR 1.8.6 YT (revision 1010) and 1.8.5 (RL) are also provided.

2.6.1 Problem Description

The MELCOR model, shown in Figure 2-20 consists of two control volumes and one flow path. One control volume represents a reservoir 75% full of liquid water, while the other control volume models the surrounding environment; both volumes are specified to be time-independent, to keep conditions constant. The flow path represents the pipe in which the flow is being established. The problem is initialized with zero flow, but with an open flow area at t=0 seconds. A total of twenty cases were considered, with dimensions and initial conditions as specified in Table 2-8. The minimum flow for choking was set arbitrarily high to avoid choking in the calculation. This was the only non-default parameter used in the calculation.

2.6.2 Analytic Solution

The asymptotic flow velocity established in the pipe is given by [2.5]:

$$V_\infty = \sqrt{\frac{2gDH}{fL}} = \sqrt{\frac{2gH}{fL/D}} \qquad \text{(Equation 2-18)}$$

where

D = pipe diameter (m),
L = pipe length (m),
f = pipe friction factor (m),
g = gravity (9.8 m/s^2) and
H = head of liquid in the reservoir (m).

The actual velocity V approaches the asymptotic velocity according to:

$$\frac{V_\infty + V}{V_\infty - V} = \exp\left\{\frac{2gH}{LV_\infty}t\right\} \qquad \text{(Equation 2-19)}$$

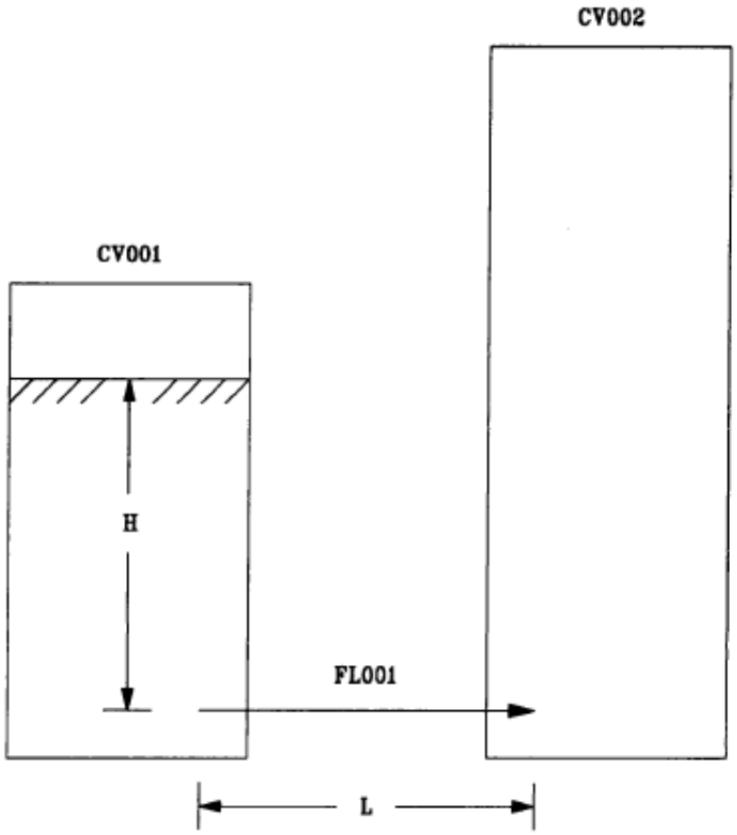

Figure 2-20. MELCOR Model for Establishment of Flow

Table 2-8. Specifications for Flow Establishment Analyses

Case	T (K)	Head (m)	K (m)	D (m)	L (m)
A	370	20	5.0×10^{-5}	1.0	50
B	370	100	1.0×10^{-6}	2.0	10
C	300	5	1.0×10^{-3}	0.1	5000
D	300	1000	3.0×10^{-2}	2.0	50
E	300	5	1.0×10^{-6}	0.2	5000
F	300	5	1.0×10^{-6}	0.2	3000
G	300	5	1.0×10^{-6}	0.2	1000
H	300	5	1.0×10^{-6}	0.2	100
I	300	5	1.0×10^{-6}	0.2	10
J	300	5	1.0×10^{-6}	0.2	2.5
K	300	20	5.0×10^{-4}	1.0	5000
L	300	20	5.0×10^{-4}	0.2	5000
M	300	5	5.0×10^{-4}	1.0	50
N	300	5	5.0×10^{-4}	1.0	5000
O	300	5	5.0×10^{-4}	0.6	50
P	300	5	5.0×10^{-4}	0.4	50
Q	300	500	1.0×10^{-4}	0.01	10
R	300	100	1.0×10^{-4}	0.01	10
S	300	20	1.0×10^{-4}	0.01	10
T	300	5	1.0×10^{-4}	0.01	10

This relation assumes a constant friction factor; if the friction factor, k, is a function of velocity, V, an exact analytic solution is not possible and instead one must numerically integrate

$$\int_0^t dt = 2D\int \frac{dv}{f_\infty V_\infty^2 - fv^2} \qquad \text{(Equation 2-20)}$$

2.6.3 Results

Table 2-9 presents the asymptotic flows calculated by MELCOR and from the analytic expression using the parameter sets listed in Table 2-8. These results indicate that the results calculated by MELCOR are within 1% of the analytic solution.

Figure 2-21 through Figure 2-24 show the comparison of the time-dependent velocity predicted to those obtained from the analytic solution for four of the cases investigated

(A, C, E, and S). Each of these cases demonstrate the ability of MELCOR to predict the time dependence of the establishment of flow conditions when the time-step is chosen sufficiently small relative to the relaxation for the analytical solution. In Figure 2-25, the dependence of the solution on time step is shown for Case S. This sensitivity calculation shows that when the time step is on the order of the relaxation time, the error is small. Even when the time step is large, the asymptotic velocity is well calculated.

2.6.4 Conclusions

The results of this problem show that the flow-solution algorithm in MELCOR can correctly calculate both the flow startup and subsequent steady-state flow in a pipe fed from a liquid reservoir.

Table 2-9. Asymptotic Velocities for Flow Establishment.

Case	Analytic Solution	MELCOR 2.1	MELCOR 1.8.1
A	27.231	27.266	27.27
B	269.80	269.86	269.9
C	0.2211	0.2218	0.221
D	134.04	134.05	134.1
E	0.4707	0.4691	0.467
F	0.6254	0.6234	0.621
G	1.1492	1.1462	1.141
H	4.0630	4.0566	4.039
I	14.119	14.114	14.05
J	29.588	29.604	29.48
K	2.6176	2.6139	2.614
L	0.9550	0.9514	0.950
M	13.508	13.567	13.57
N	1.2709	1.2725	1.273
O	9.9540	9.9956	9.976
P	7.7934	7.8243	7.801
Q	16.020	16.016	16.02
R	7.1274	7.1240	7.122
S	3.1521	3.1512	3.147
T	1.5467	1.5504	1.542

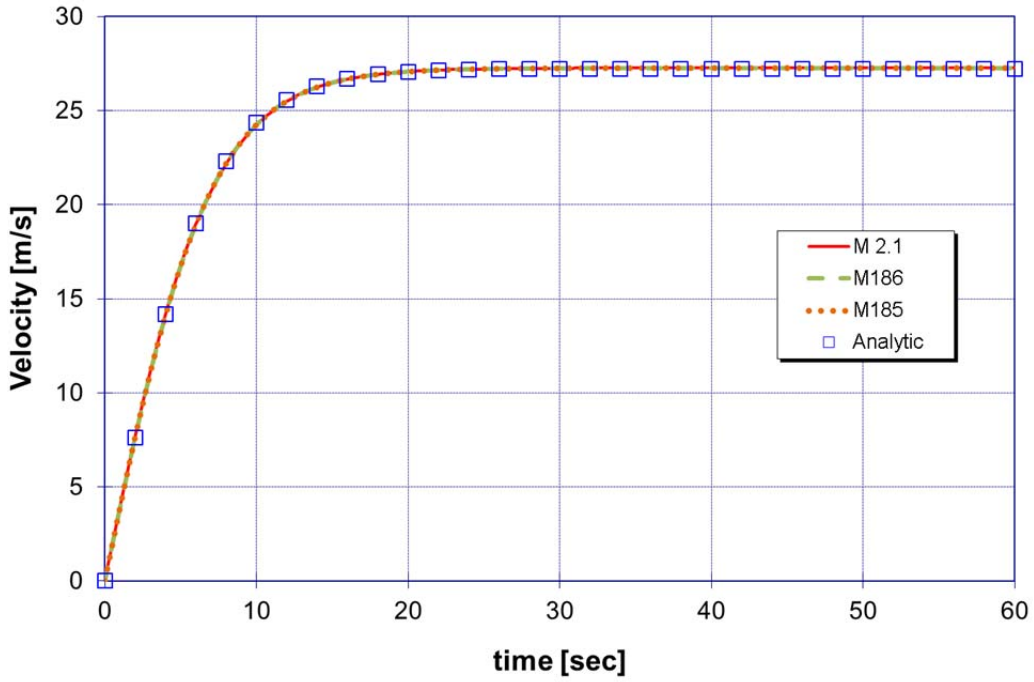

Figure 2-21. Velocity History for Flow Establishment Calculation - Case A.

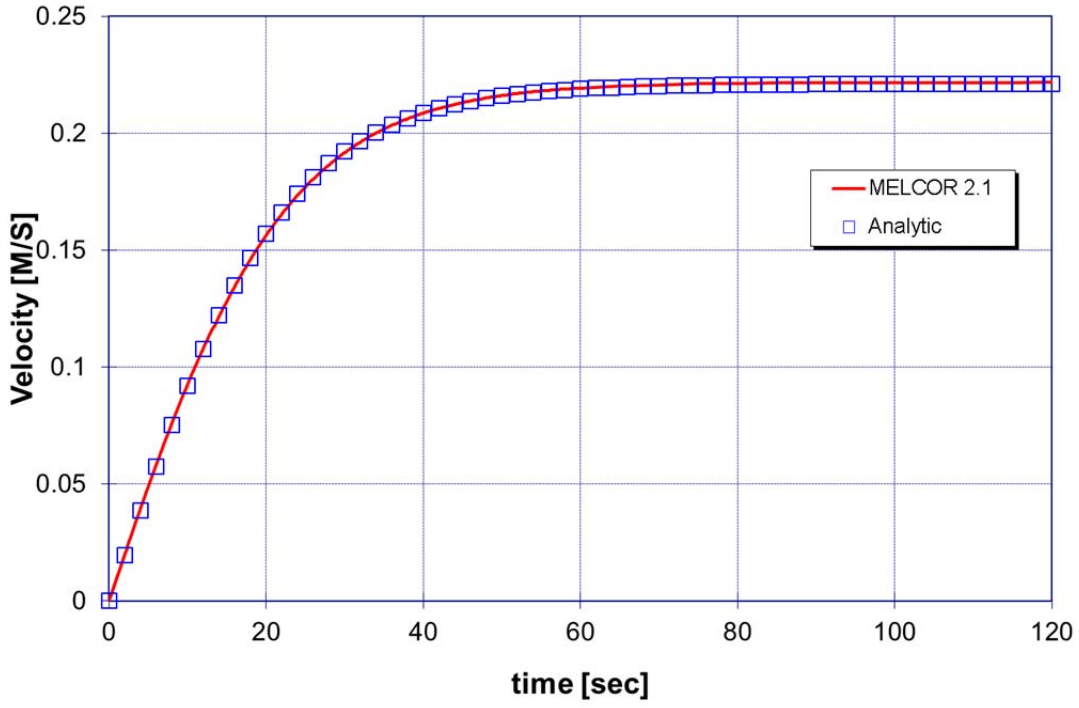

Figure 2-22. Velocity History for Flow Establishment Calculation - Case C.

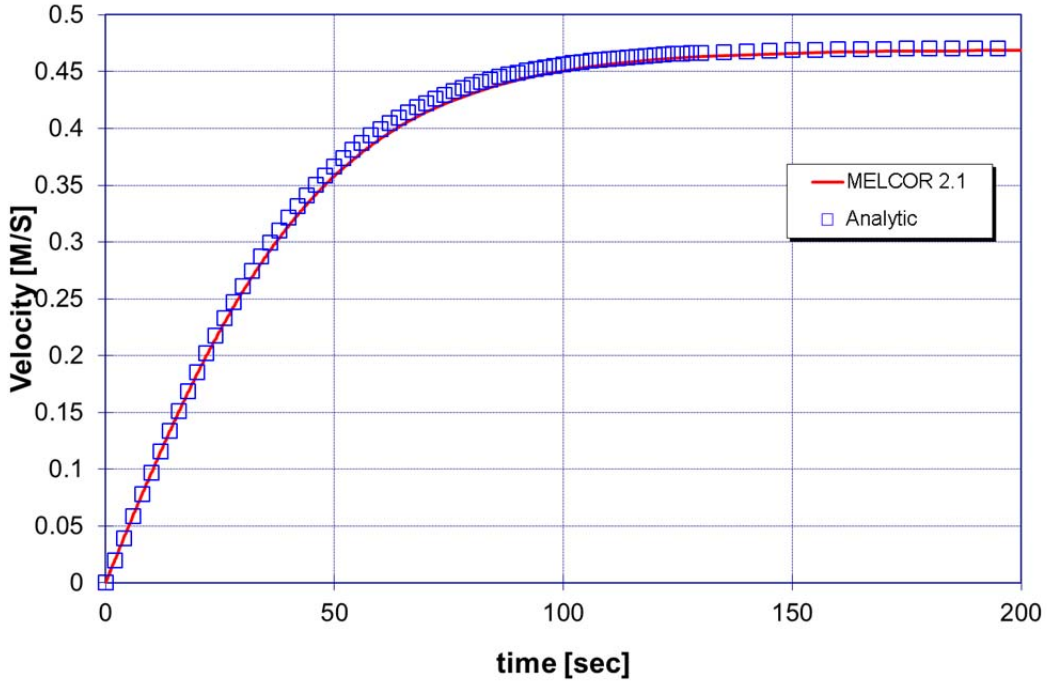

Figure 2-23. Velocity History for Flow Establishment Calculation - Case E.

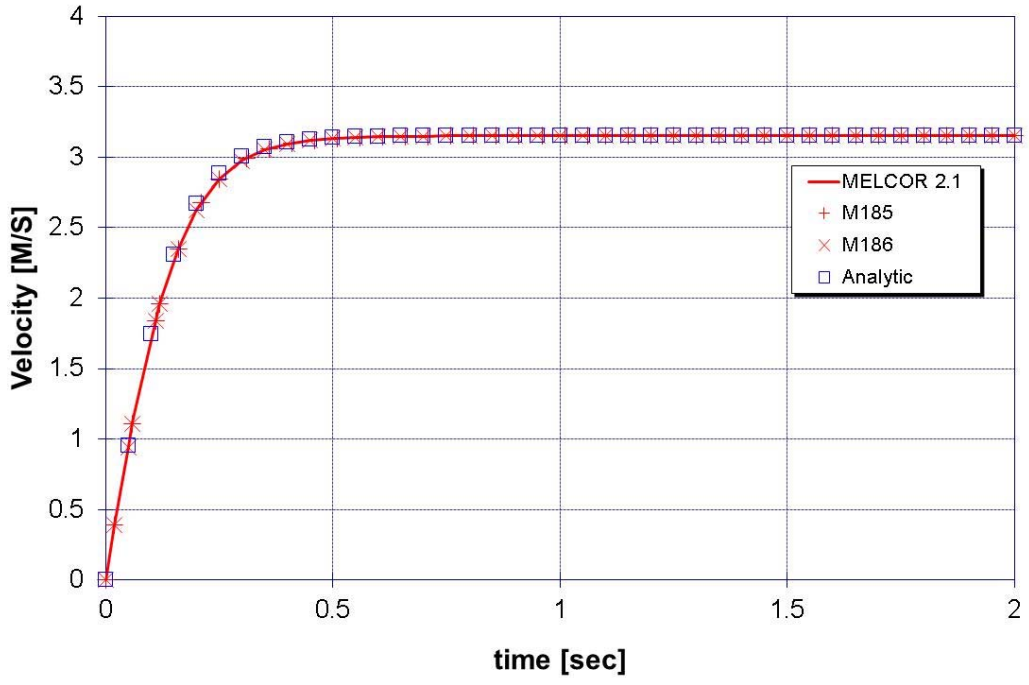

Figure 2-24. Velocity History for Flow Establishment Calculation - Case S.

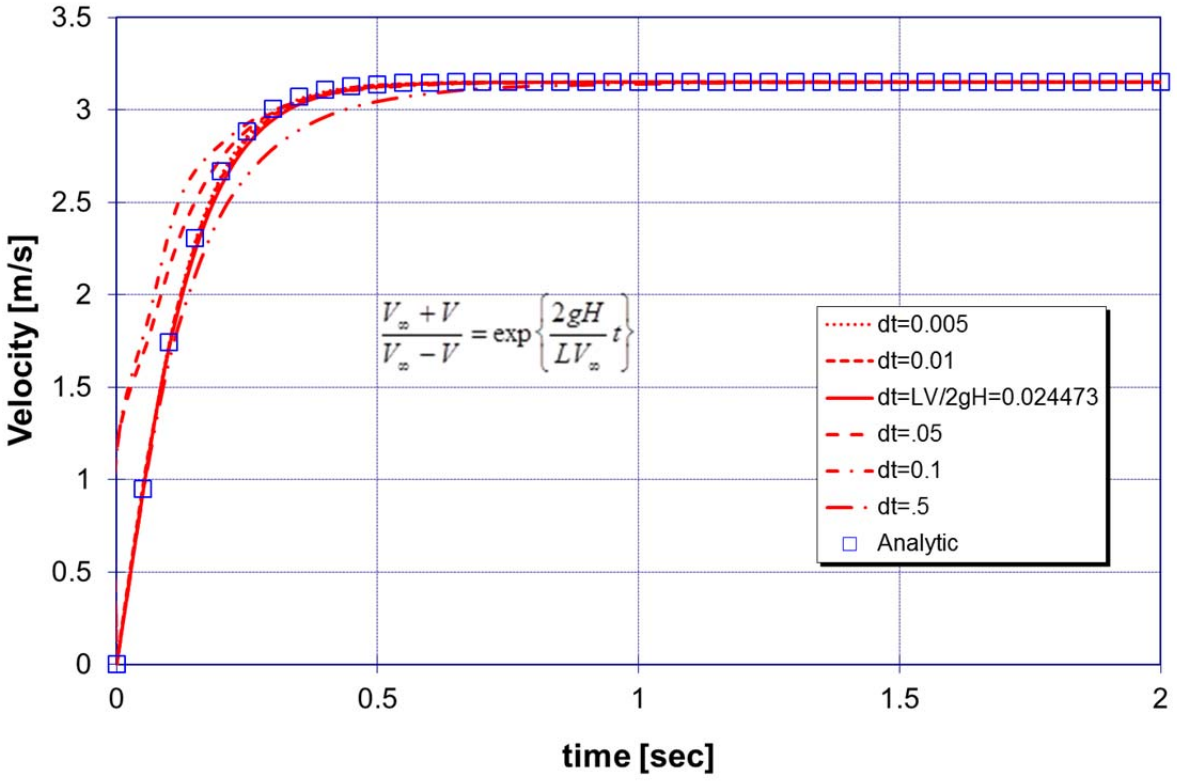

Figure 2-25. Velocity History for Flow Establishment Calculation - Case S. Time step dependence of solution.

2.7 References

[2.1] L.N. Kmetyk, "MELCOR Assessment: Gedanken Problems Volume 1", SAND92-0762, NPRW-SA92-22, Sandia National Laboratories, January 1993

[2.2] C. D. Leigh, ed.,"MELCOR Validation and Verification - 1986 Papers", NUREG/CR-4830, SAND86-2689, Sandia National Laboratories, March 1987.

[2.3] J. H. Keenan, F. G. Keyes, P. G. Hill, J. G. Moore, "Steam Tables: Thermodynamic Properties of Water Including Vapor, Liquid, and Solid Phases (International System of Units - S.I.)", John Wiley and Sons, 1969.

[2.4] J. P. Holman, Heat Transfer. 4nd Ed., McGraw-Hill Book Co., 1976

[2.5] V. L. Streeter, E. B. Wylie, Fluid Mechanics. McGraw-Hill Book Co., 1976

3. MELCOR ASSESSMENTS AGAINST EXPERIMENTS

3.1 Analysis of ABCOVE AB5 and AB6 Aerosol Experiments

3.1.1 Background

The Aerosol Behavior Code Validation and Evaluation (ABCOVE) experiments investigated nuclear aerosol behavior in liquid metal fast breeder reactors (LMFBRs). The experiments provide a basis for judging the adequacy of aerosol behavior codes in describing inherent aerosol attenuation in containment buildings during postulated accidents.

The ABCOVE experiments were performed in the Containment Systems Test Facility (CSTF) located at the Hanford Engineering Development Laboratory. In the AB-5 test, performed in 1982, a single-species aerosol was generated by spraying sodium at a high rate into an air atmosphere. In the AB6 test, performed in 1983, a sodium iodide (NaI) aerosol was released in the presence of a sodium spray fire. This study assesses the MELCOR models, such as the aerosol physics model (including agglomeration and settling) and thermal hydraulic models using the AB5 and AB6 experiments.

3.1.2 AB5 and AB6 Experiment

In this report, two of ABCOVE tests are discussed: AB5 and AB6 [3.1.1]. AB5 was performed with a single-component aerosol under conditions, which simulate LMFBR containment during a severe accident. The primary objective of test AB5 was to provide experimental data on aerosol behavior for use in validating computer codes for the case of a moderate duration which included a strong aerosol source generated by a sodium spray fire in air. On the other hand, the experimental conditions of AB-6 simulated an accident in which a fission product aerosol (sodium iodide [NaI]) was released in the presence of a sodium fire that released sodium combustion product aerosol. The release of the aerosol in terms of mass from the spray fire was approximately 500 times that of the NaI. This aerosol source was continued well past the NaI source cutoff to demonstrate the "washout" of the NaI. The primary objective of the AB6 test was to demonstrate co-agglomeration behavior of two aerosol species, and to validate the capabilities of aerosol behavior codes to simulate such conditions. Both tests were performed in the CSTF vessel.

The specification for the CSTF containment vessel used in these two experiments is tabulated in Table 3.1-1. The corresponding CSTF arrangement for these experiments is shown in Figure 3.1-1. As shown in Figure 3.1-1 the carbon steel vessel is installed in a concrete pit. All interior surfaces were coated with a modified phenolic paint, and exterior surfaces were covered with a 25.4 mm layer of fiberglass insulation with an outer aluminum vapor barrier. The only major difference between the experiments is the apparatus setup for the source injection as evidenced in Figure 3.1-1(b).

The test conditions for both AB-5 and AB-6 experiments are summarized in Table 3.1-2. As shown in Table 3.1-2, the AB-5 experiment consists of spraying 223 kg of sodium over a period of 872 s, with all the sodium being converted to 60% sodium peroxide

(Na_2O_2) and 40% sodium hydroxide (NaOH) aerosol. Compressed air (23.3% O_2) was injected at several times in the test to make up for sampling losses and to prevent the containment pressure from going negative. The containment vessel was kept sealed for 5.136×10^5 s (5.94 days), after which the access door was opened. The maximum containment pressure and mean atmospheric temperature attained were 214 kPa and 552.15 K, with local temperatures reaching 843.15 K. The maximum suspended mass concentration measured was 170 g/m^3, which was attained 383 s after the initiation of sodium spray. The suspended concentration then decreased to a steady-state value of 110±17 g/m^3 for the duration of the spray period.

For the AB6 experiment (see Table 3.1-2), the experimental conditions simulated an accident in which a fission product aerosol (NaI) was released in the presence of a sodium fire: this fire releases sodium combustion product aerosol. The test consisted of spraying 205 kg of sodium into the CSTF over a period of 4780 s. Oxygen was also injected so that the oxygen concentration remained relatively constant during the test. All sodium was converted to an aerosol consisting primarily of a mixture of Na_2O_2 and NaOH. To simplify discussion, the aerosol formed by burning sodium is referred to as NaOx. About 620 s before the sodium spraying, the NaI aerosol began to be injected into the containment vessel atmosphere. The NaI source was terminated at 3000 s, while the NaOx source continued for an additional 2400 s.

Table 3.1-1. CSTF Containment Vessel Properties [3.1.1]

Dimension/Mass/Weight		**Aerosol Surface Area (m^2)**	
Diameter (ID)	7.62 m	***For Heat Transfer***	
Total Height	20.3 m	Top Head	63.0
Cylinder Height	16.5 m	Bottom Head	63.0
Enclosed Volume	852 m^3	Cylinder	394
		Total CSTF Vessel Shell	*520*
		Internal Components	232
Top Head	8,753 kg	***For Aerosol Settling***	
Bottom Head	8,753 kg		36.7
Cylinder	69,390 kg	Bottom Head	11.1
Penetrations and Doubler Plates	10,295 kg	Catch Pan	4.2
Catch Pan	500 kg	Personnel Deck	36.2
Internal Components	5,580 kg	Internal Components	*88.2*
Total Weight	*103,260 kg*	*Total*	
Top Head	18.1 mm	***For Aerosol Plating***	
Bottom Head	18.1 mm		520
Cylinder	22.9 mm	Vessel Shell	232
Internal Components	3.4 mm	Internal Components	*752*
		Total	

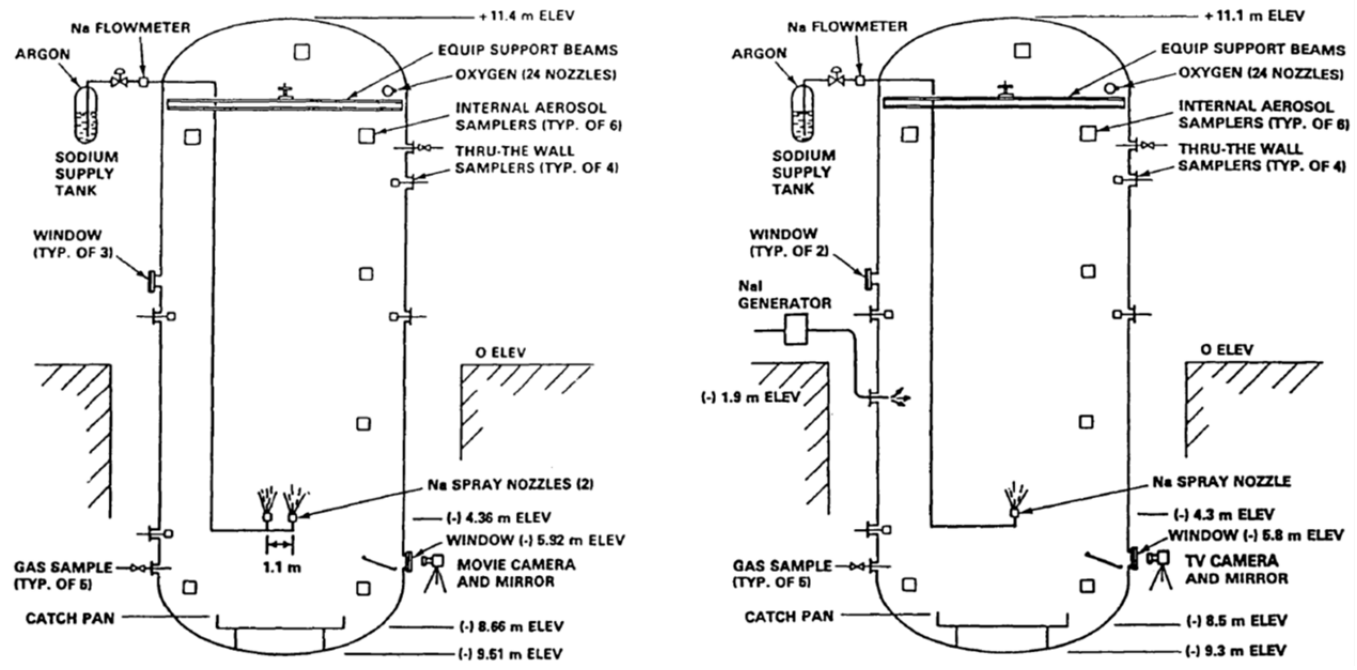

Figure 3.1-1. CSTF Arrangement for AB5 (a) and AB6 (b) [3.1.1]

Table 3.1-2. Summary of Test AB5 and AB6 Test Conditions [3.1.1]

AB5		AB6	
INITIAL CONTAINMENT ATMOSPHERE	***PARAMETER***	***INITIAL CONTAINMENT ATMOSPHERE***	***PARAMETER***
Oxygen Concentration	23.3±0.2%	Oxygen Concentration	23.9±0.2 %
Temperature (mean)	302.25K	Temperature (mean)	304.15 K
Pressure	0.122MPa	Pressure	114 kPa
Dew Point	289.15±2K	Dew Point	285.35±2 K
Nominal Leak Rate	1%/day at 68.9kPa		
Na SPRAY	***PARAMETER***	***Na SPRAY***	***PARAMETER***
Na Spray Rate	256±15g/s	Spray Rate	42.8±2.1 g/s
Spray Start Time	13s	Spray Start Time	620 s
Spray Stop Time	885 s	Spray Stop Time	5400 s
Total Na Sprayed	223±11 kg	Total Na Sprayed	204.7±4.1 kg
Na Temperature	836.15 K	Temperature	833.15 K
Spray Drop Size, MMD	1030±50 μm	Spray Drop Size, MMD	640±40 μm
Spray Size Geom. Std. Dev., GSD	1.4	Spray Size Geom. Std. Dev., GSD	1.4
OXYGEN CONCENTRATION	***PARAMETER***	***CONTAINMENT CONDITIONS DURING TESTS***	***PARAMETER***
Initial O_2 Concentration	23.3±0.2 vol %	Maximum Average Atmosphere Temperature	438.25 K
Final O_2 Concentration	19.4±0.2 vol %	Maximum Average Steel Vessel Temperature	352.05 K
Oxygen Injection Start	60 s	Maximum Pressure	169.5 kPa
Oxygen Injection Stop	840 s	Final Dew Point	268.95 K
Total O_2	47.6 m^3 (STD)		
CONTAINMENT CONDITIONS DURING	***PARAMETER***	***NaOx AEROSOL SOURCE***	***PARAMETER***

AB5		AB6	
TESTS			
Maximum Average Atmosphere Temperature	552.15 K	Release Rate	77.9±4 g/s
		Start Time	620 s
Maximum Average Steel Vessel Temperature	366.65 K	Stop Time	5400 s
		Total NaOx Released	372.4±10 kg
Maximum Pressure	213.9 kPa	Material Density	2.45 g/cm^3
Final Dew Point	271.65 K	Source 50% Radius	0.25 μm
		Source Sigma	2.0
		Mass Ratio, Total to Na	1.82
AEROSOL GENERATION	***PARAMETER***	***NaI AEROSOL SOURCE***	***PARAMETER***
Generation Rate	445 g/s	Release Rate	0.14 g/s
Mass Ratio, Total Na	1.74	Start Time	0 s
Material Density	2.50 g/cm^3	Stop Time	3000 s
Initial Suspended Concentration	0	Total NaI Released	420 g
		Material Density	3.67 g/cm^3
Source Mass Median Dia.	0.50 μm	Source 50% Radius	0.272 μm
Source Sigma, σ_g	1.5	Source Sigma	1.55
Maximum Suspended Mass Concentration	170 g/m^3		
Suspended Conc. Steady-State Value	110±17 g/m^3		

3.1.2.1 MELCOR Models and Nodalizations

To simulate the ABCOVE experiments, the MELCOR model was developed, but it was for MELCOR 1.8.2 [1]. The original MELCOR model for simulating these experiments for the CSTF includes two control volumes representing the containment vessel and an infinite environment outside the vessel; and, five heat structures representing the top and bottom heads, the cylindrical walls, and the internal components for aerosol plating and settling. For AB5 and AB6 experiments, the external energy source from the sodium spray fire was included, and the details of the calculation are given in Souto, et.al [3.1.1]. The specific data for the MELCOR Model of AB5 and AB6 are shown in Table 3.1-3. Note that many of the CSTF conditions are similar, which includes the surfaces and aerosol specific data. However, unlike AB5 which has a single Na source, AB6 contains two sodium sources as indicated in Table 3.1-3. The specific release of the sources is shown in Table 3.1-2. Thus, there are slight differences in the external chemical energy source for the two experiments. In addition to those parameters listed in Table 3.1-3, the MELCOR 2.1 model uses 10 aerosol sections as a “base case” and 20 sections as a sensitivity case. Note that the original 1.8.6 and 2.1 models utilized 20 aerosol sections. This difference was not expected to significantly impact results. The 20 section bin sensitivity study applies to MELCOR 2.1 only. The MELCOR 1.8.6 model had 20 sections only, and as such, this is the 1.8.6 “base case”.

Since the original assessment was done with an early version of MELCOR as shown in Souto et.al [1], the code version comparison between MELCOR 1.8.6 (v3964) and MELCOR 2.1 (v6110) will also be provided. Thus input deck conversion from MELCOR 1.8.6 to MELCOR 2.1 was done for both AB5 and AB6 input decks. Note that sodium is being represented by Class 2 (Cs). For AB6, component 2 of aerosol represents the NaO_x source as Class 2 (Cs) while CsI (Class 16) represents NaI. Also, the density of NaI is used for modeling the density of aerosol for AB6.

Table 3.1-3. Specific Data for MELCOR Model of AB5 and AB6 [3.1.1]

Parameter	AB5	AB6
Aerosol Constants		
Dynamic Shape Factor	1.5	
Agglomeration Shape Factor	2.25	
Slip Coefficient	1.37	
Sticking Coefficient	1.0	
Turbulence Dissipation	$0.001 m^2/s^3$	
Thermal Accommodation Coefficient	1.00	
Gas Thermal Conductivity/Particle Thermal Conductivity	0.05	
Diffusion Boundary Layer Thickness	1.0×10^{-5} m	
Aerosol Parameters		
Lower Bound Diameter	1×10^{-8} m	1×10^{-7} m
Upper Bound Diameter	1×10^{-5} m	1×10^{-4} m
Density	$2500 kg/m^3$	
MMD	5×10^{-5} m	
GSD	1.5	
NaI Density		$3670 kg/m^3$
NaI MMD		5.44×10^{-5} m
NaI GSD		1.55
NaO_x Density		$2450 kg/m^3$
NaO_x MMD		5.0×10^{-7} m
NaO_x GSD		2.0
Surface Areas		
Top Head	$63.0 m^2$	
Bottom Head	$45.6 m^2$	
Cylindrical Walls	$395.0 m^2$	
Int. Comp. (Plating)	$232.0 m^2$	
Int. Comp. (Settling)	$42.7 m^2$	
CSTF Initial Conditions		
Pressure	1.22×10^5 Pa	1.142×10^5 Pa
Temperature	302.25 K	304.15 K
Dew Point	289.15 K	285.35 K
External Energy Source (including both chemical and sensible heat)	2.89×10^9 J	3.0×10^9 J

3.1.3 Results of Analysis of AB5 and AB6

In this section, the results of the AB5 and AB6 MELCOR calculations are provided. The results from MELCOR 1.8.6 and 2.1 calculations will be reported and compared to experimental data.

3.1.3.1 AB5

The primary objective of the ABCOVE test AB5 was to provide experimental data for use in validating aerosol behavior computer codes for the case of a moderate-duration, strong, single-component aerosol source generated by a sodium spray in an air atmosphere. A secondary objective was to provide experimental data on the temperature and pressure in the containment vessel and its atmosphere, for use in validating containment response codes.

Comparison of measured and calculated pressures and temperatures in the containment vessel atmosphere are presented in Figure 3.1-2. The measured pressure increased to a maximum value of 213.9 kPa attained near the end of the sodium spray period (see Figure 3.1-2(a)). Thus, general behavior is simulated correctly by MELCOR, but the calculated pressure is significantly higher than the observed pressure most of the time. In particular, the predicted peak pressure of approximately 255 kPa overestimates the pressure in the containment vessel atmosphere by 20%. As indicated in this figure, the predicted peak pressure occurs at about 800s, slightly earlier than the measured peak. Figure 3.1-2(b) compares measured and calculated bulk temperatures in the containment vessel atmosphere. The measured average temperature increased at a rate of 1.58K/s during the initial minute of spraying. This rate slowed to 0.08 K/s near the end of the spray period, when a maximum temperature of 581 K was obtained. MELCOR calculations follow a similar trend, but over-predict the average temperature in the containment vessel atmosphere during the spray period. MELCOR calculates a maximum temperature of approximately 635 K at about 760 s. Following the sodium spray period, the MELCOR calculated temperatures agree well with the experimental results.

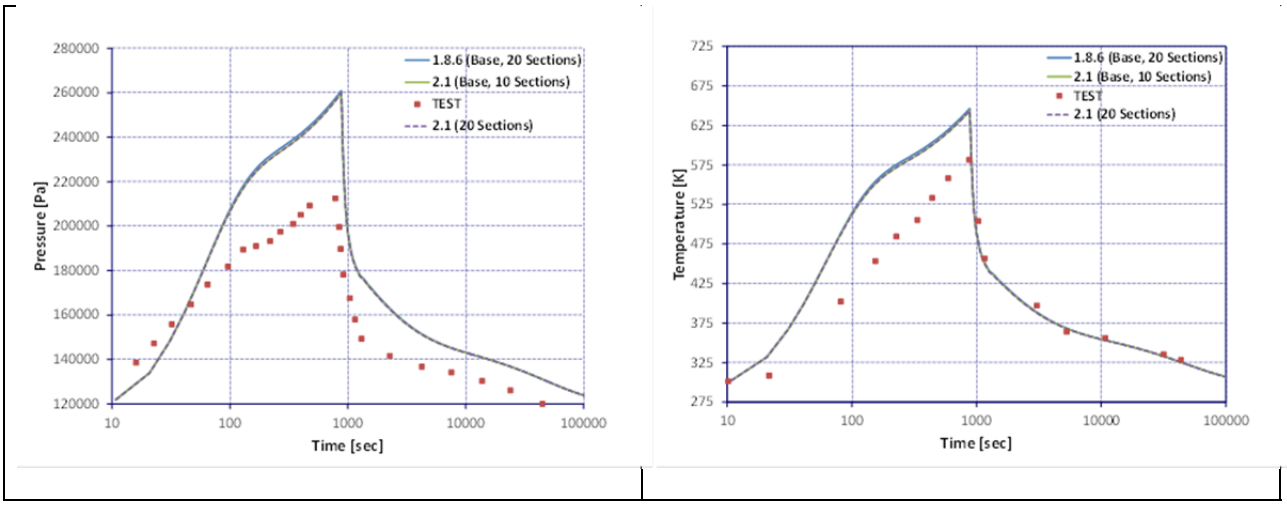

(a) (b)

Figure 3.1-2. CSTF Atmosphere Pressure (a) and Temperature (b) in AB5

The measured average temperature in the containment vessel internal steel shell is shown in Figure 3.1-3. Also shown in this figure are the MELCOR calculated temperatures for each of the structures in this shell, i.e., the top and bottom heads, and the cylindrical wall. The maximum value for the measured average steel shell temperature was 367 K, attained at 883 s. As indicated in Figure 3.1-3, the steel shell temperature is slightly under-predicted by MELCOR during the sodium spray period; and, although the general trend is similar, the calculated maximum occurs, for nearly each structure, at about 3000 s, i.e., 35 minutes later than the measured maximum.

Then at about 10,000 seconds and longer, the calculated value is within the range of the measured values.

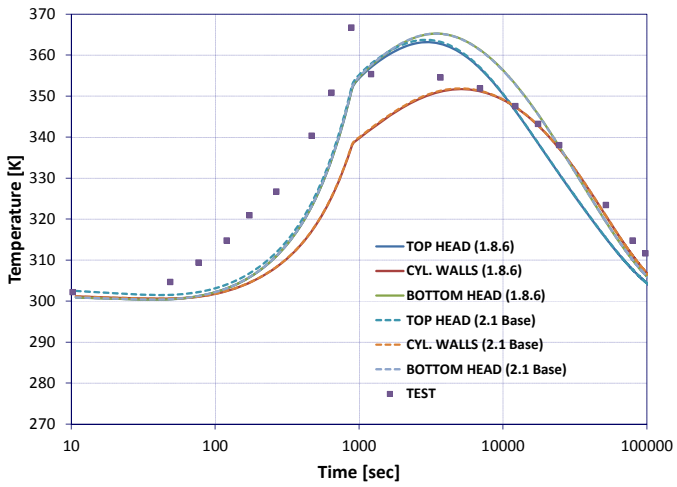

Figure 3.1-3. CSTF Shell Temperature in Test AB5 for Base Case

Calculated aerosol suspended and deposited masses in the containment atmosphere are plotted in Figure 3.1-4. The measured airborne mass varies slowly during the sodium spray period, and then decreases during the remainder of the experiment. No general aerosol re-suspension from the walls or floor was observed during the test. As indicated in Figure 3.1-4(a), the airborne mass predicted by MELCOR is in very good agreement with the experimental results. Slight differences are apparent about two hours after the spray period, when the airborne mass is less than 1% of the maximum mass of 145 kg attained at 383 s after initiation of sodium spray. Agreement with experimental data by the end of the test, when masses are reduced by a factor of 10^{-6}, is within a factor of two or three. The total calculated mass of aerosol deposited on the containment vessel shell is presented in Figure 3.1-4(b). Time dependent experimental data for this variable are not available, but the measured total of 402.8 kg is included in Figure 3.1-4(b) for comparison. A calculated uniform value of approximately 390 kg is attained at about 3000 s, and since it is within ±3% of the reported value, the agreement from this time, up to the end of the test, is considered excellent.

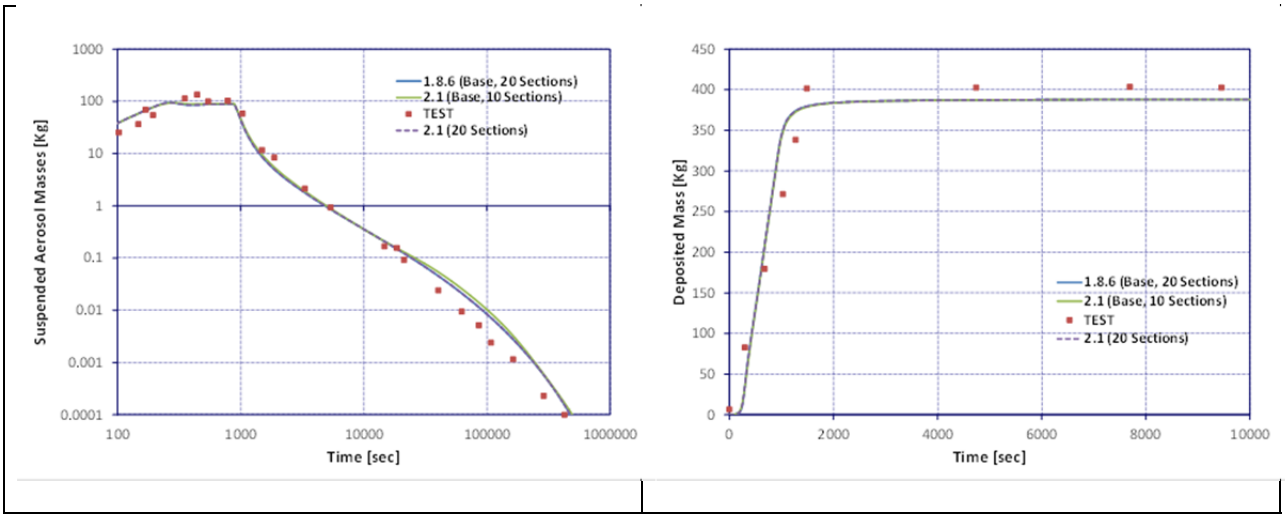

(a) (b)

Figure 3.1-4. CSTF Airborne (a) and Deposited (b) Masses in Test AB5

Figure 3.1-5 presents the calculated aerosol plated masses. For the purpose of making experimental measurements, plated mass is defined as the mass of aerosol deposited on the containment vessel vertical walls and top head. Although the time evolution of the experimental result for this variable is not available, the reported total of 0.959 kg is included in Figure 1-5(a). At l000 s, the mass of aerosol plated on the vessel's top head is 1.9 kg according to MELCOR, and represents an over-prediction of about 97% with respect to the reported value. Although the standard error associated with the reported value is around ±30% [1], the discrepancy between the calculated and measured values is apparent. However, the mass deposited in the containment vessel's top-head is less than 0.3% of the total deposited mass and, therefore, this discrepancy is not of great importance. The MELCOR calculated mass plated on the containment vessel's cylindrical walls is shown in Figure 1-5(b). As in the case of the other experimental measures for the deposited masses, for which the time dependencies of aerosol deposition are not available, the reported value of 17.75 kg for the total aerosol mass plated on the cylindrical walls is presented in this figure for comparison. MELCOR predicts an aerosol mass of approximately 20 kg plated on the walls by the end of the test. The difference between the experimental and the calculated values is about 12%.

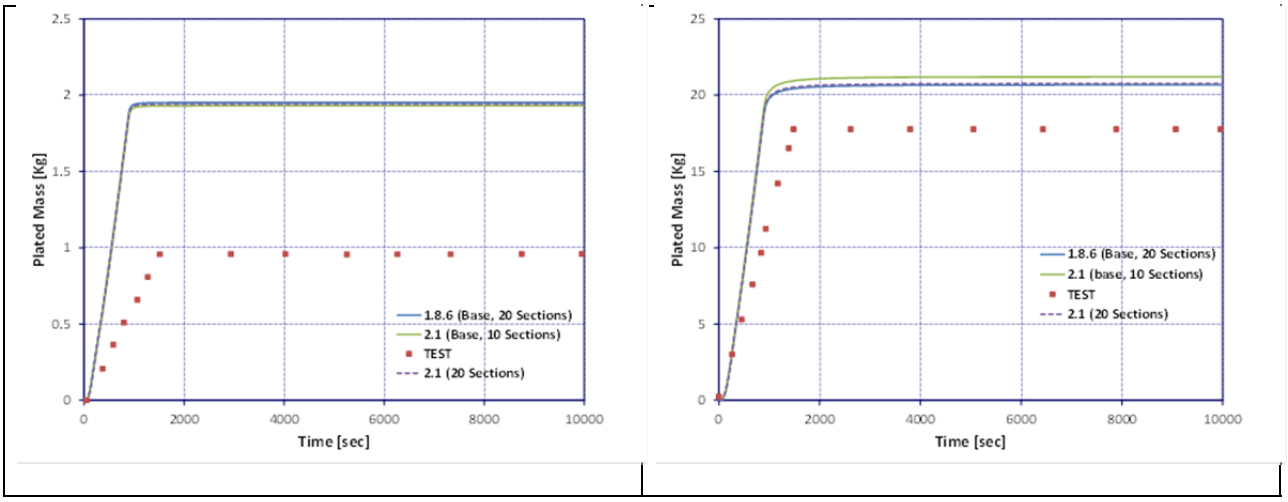

(a) (b)

Figure 3.1-5. Aerosol Plated Masses on the Top Head (a) and Walls (b) in Test AB5

Figure 3.1-6 gives the comparison of the measured and calculated aerosol settled masses. As shown in Figure 3.1-6(a), the calculated variable reaches a final value of approximately 187 kg at about 4000 s, giving a difference of 6% with respect to the experiment. Since the standard error of this measurement is within ±l0% [1], the MELCOR calculations for the mass of aerosol settled on the bottom head are in good agreement. The MELCOR prediction for the mass of aerosol collected on the horizontal surfaces of internal components is presented in Figure 3.1-6(b). This parameter was measured experimentally only at the end of the experiment; the reported value of 184 kg is also included in the figure. The calculated settled mass on internal components increases up to 173.4 kg at about 4000 s. The difference between this value and the measured one is around 6%.

Note that in all the MELCOR calculations, there are virtually identical results between MELCOR 1.8.6 and 2.1 for the base case. There is no noticeable difference between MELCOR 2.1 runs on the effect of section numbers for aerosol, except the plated masses in Figure 1-5(b).

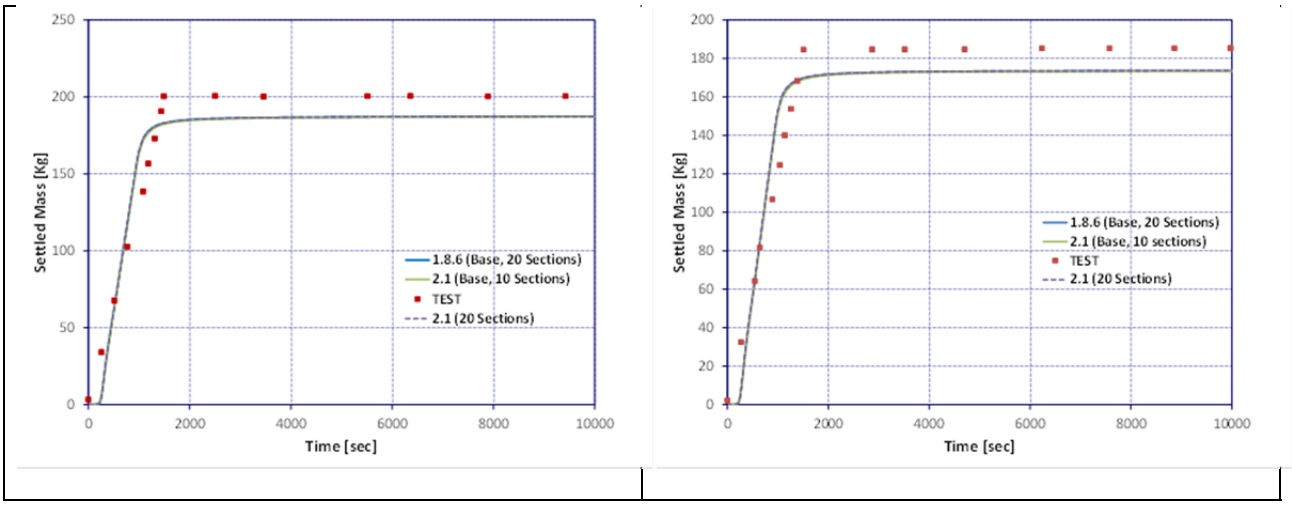

(a) (b)

Figure 3.1-6. Aerosol Settled Masses on the Bottom Head (a) and Internal Component (b) in Test AB5

3.1.3.2 AB6

The objective of the ABCOVE test AB6 was to provide experimental data to validate aerosol behavior codes for the case of a two-component aerosol simulating the release of a fission product in the presence of sodium spray fire. As in AB5, the pressure and temperatures in the containment vessel and its atmosphere are included to validate MELCOR predictions of the thermal-hydraulic behavior during the experiment.

A comparison of measured and calculated pressures and temperatures is presented in Figure 3.1-7. The measured pressure increased up to a maximum value of 170 kPa, at a time which coincides with the end of the sodium spray as shown in Figure 3.1-7(a). As in the case of test AB5, MELCOR slightly over-predicts the pressure during the sodium spray period, estimating a maximum pressure of 174.5 kPa attained at 5200 s, about 200 s earlier than the end of the sodium source. The over-prediction in the pressure represents an error of about 3% in the MELCOR calculation, so the agreement is considered to be excellent. Figure 1-7(b) shows that the measured average bulk temperature in the containment vessel atmosphere increased during the sodium spray period, reaching a maximum of 438 K near the end of this period. As also indicated in this figure, MELCOR once again slightly over-predicts the bulk temperature in the containment atmosphere during the sodium spray period, calculating a maximum temperature of 465K at 5300 s. This represents an over-prediction of about 6%; an error which is considered reasonable for this type of calculation.

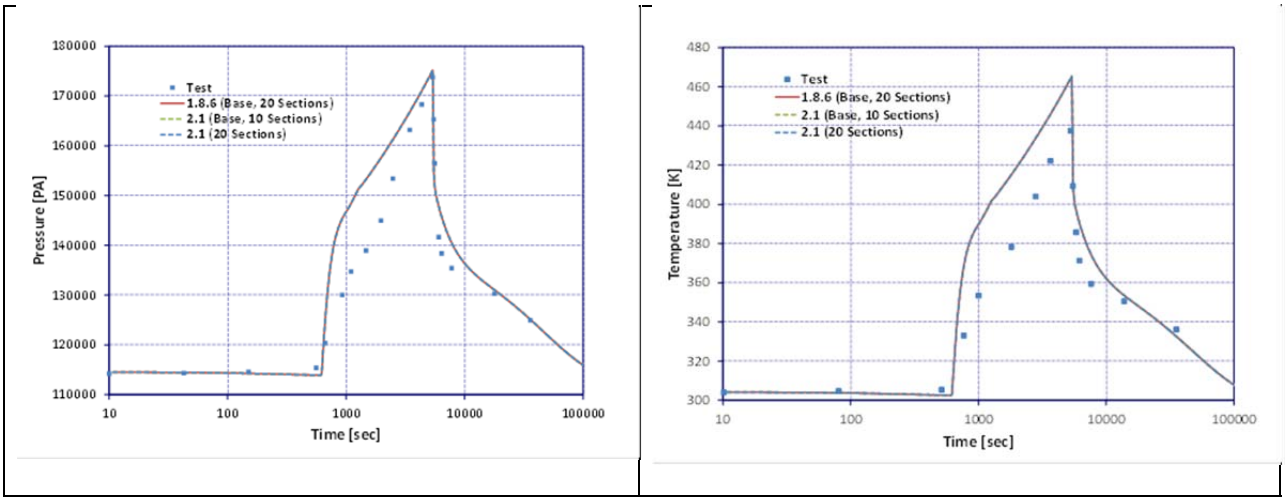

(a) (b)

Figure 3.1-7. CSTF Atmosphere Pressures (a) and Temperatures (b) in Test AB6

The measured average temperature in the containment vessel internal steel shell is shown in Figure 3.1-8. Also shown in this figure are the temperatures calculated by MELCOR for each of the structures in this shell. As indicated in this figure, the agreement between the calculated temperatures and the measured average temperatures is better at the containment vessel cylindrical walls than the calculated values for the top and bottom heads. This is expected because the vessel cylindrical walls represent most of the surface area. In this case, the general trend of the calculated results is very similar to that of the test measurements, but the maximum value calculated by MELCOR, 363 K, occurs at 6800 s, i.e., about 1200 s after the measured maximum of 352 K.

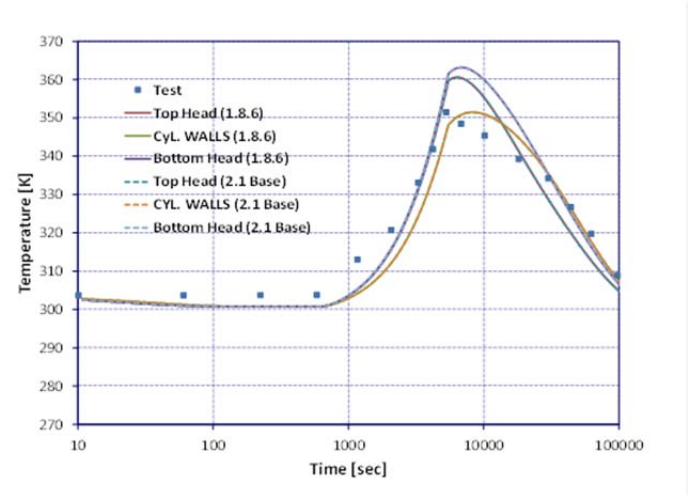

Figure 3.1-8. CSTF Steel Shell Temperature in Test AB6 for Base Case

Measurements of containment vessel atmosphere temperature and suspended aerosol concentration showed that the containment atmosphere during the early phase of the test was divided into two mixing cells. This two-cell effect was not observed in test AB5, and it is believed [3.1.1] that the energy release rate in test AB5 was sufficiently high to induce convection currents capable of entraining air from the lower region of the vessel, while the lower energy release rate in test AB6 was insufficient to mix the two cells. The MELCOR model assumes that the aerosol is instantaneously distributed homogeneously throughout the entire containment volume as it is released. The development of the two cells is not modeled. Because the upper cell occupied a large fraction (80%) of the total containment vessel volume, the lack of a model for the non-homogeneities in the atmosphere is not serious.

The suspended aerosols of both NaO_x and NaI are shown in Figure 3.1-9. As shown in Figure 1-9(a), NaO_x aerosol release period began at 620 s and ended at 5400 s. To compare the experimental results with code predictions for test AB-6, a weighted average NaO_x concentration is used to take into account the measured concentrations in the upper and lower cells formed in the containment vessel [3.1.1]. Figure 3.1-9(a) shows this average for the suspended mass of NaO_x and the corresponding MELCOR prediction. The measured NaO_x airborne mass rapidly increased to a maximum value of 28.l kg at about 1220 s. It then slowly decreased to a value of 19.6 kg, and at about the end of the NaI source release period (3000 s), as shown in Figure 3.1-9(b), increased again to a value of 23.9 kg. After the NaO_x source cutoff, the suspended mass decreased rapidly. The MELCOR results follow a similar trend, but slightly over-predict the NaO_x airborne mass during the NaO_x source release period. In fact, MELCOR estimates a maximum NaO_x airborne mass of 41 kg at 1170 s. About 10 minutes after the end of the sodium spray, MELCOR predictions are in good agreement with the experimental results.

As shown in Figure 3.1-9(b), the NaI source period started at time zero and ended 3,000 s later. Non-uniform mixing was observed for this aerosol as well as for NaO_x. For this reason, a weighted average concentration of NaI was also used to compare the experimental results with code predictions in test AB6. This weighted average, as well as the MELCOR predictions for the NaI airborne mass, are presented in Figure 3.1-9(b). The measured NaI airborne mass increased to a maximum of 0.23 kg, attained at about 900 s, and then decreased to 0.07 kg at the end of the NaI source period. Immediately after the NaI source cutoff, the airborne mass decreased rapidly. As shown in this figure, reasonably good agreement with experimental results is obtained by MELCOR during the NaI source release period. The calculated maximum is 0.15 kg at 1070 s. The predicted NaI mass decreases to 0.07 kg approximately 200 s before the end of the source period. The maximum value is under-predicted by approximately 35%. After the end of the NaI source, MELCOR greatly under-predicts the experimentally measured NaI mass.

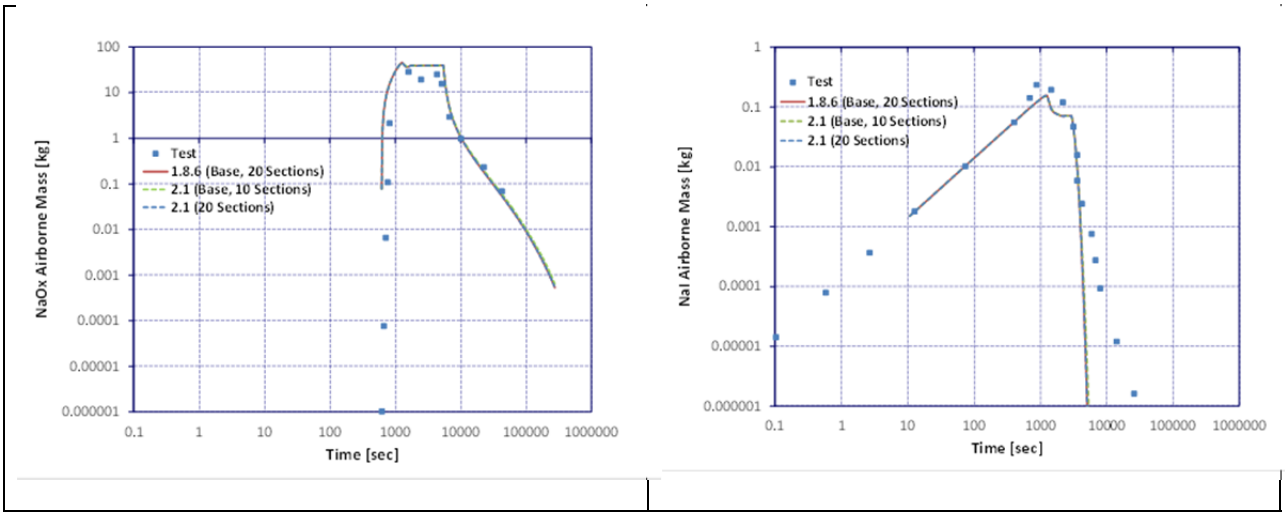

(a) (b)

Figure 3.1-9. Airborne Mass of NaO_x (a) and NaI (b) in Test AB6

Figure 3.1-10 presents the mass of the NaOx aerosol plated on the containment vessel top head calculated by MELCOR. The corresponding reported total value of 1.58 kg is also included in Figure 3.1-10 for comparison. The MELCOR result of 0.5 kg under-predicts the measured value by 68%, which represents a considerable error.

The MELCOR results for the NaI aerosol mass plated on the containment vessel top head and cylindrical walls are shown in Figure 3.1-10, which also includes the reported value of 1.68 g measured at the end of the test. In contrast with test AB5, MELCOR under-predicts the NaI and NaO_x masses plated on the top head (see Figure 3.1-10(a) and (b)). In this case, the MELCOR result calculated is 0.49 g, representing an error of approximately 71% with respect to the experimental value. Figure 3.1-10(c) shows results for the NaO_x aerosol plated mass on the containment vessel cylindrical walls calculated by MELCOR, as well as the corresponding measured value of 35.8 kg. As in the case of the containment vessel top head, the plated mass on the cylindrical walls is considerably under-predicted by MELCOR. In this case, MELCOR calculates a plated mass of 12.8 kg, which represents an error of about 64% with respect to the measured value. For the NaI aerosol mass plated on this structure, the MELCOR results and the reported value are shown in Figure 3.1-10(d). For the cylindrical walls, the NaI plated mass predicted by MELCOR is 13.9 g, an under prediction in this case of 70%. In summary, MELCOR is not able to adequately predict the aerosol-plated mass for AB-6 test. The experimenters concluded in Souto et.al [3.1.1] that the primary plating mechanism in this test was impaction; a phenomenon that MELCOR does not adequately model. There is no noticeable difference between MELCOR 2.1 runs on the effect of section numbers for aerosol, except the plated masses in Figure 3.1-10(a) and (b).

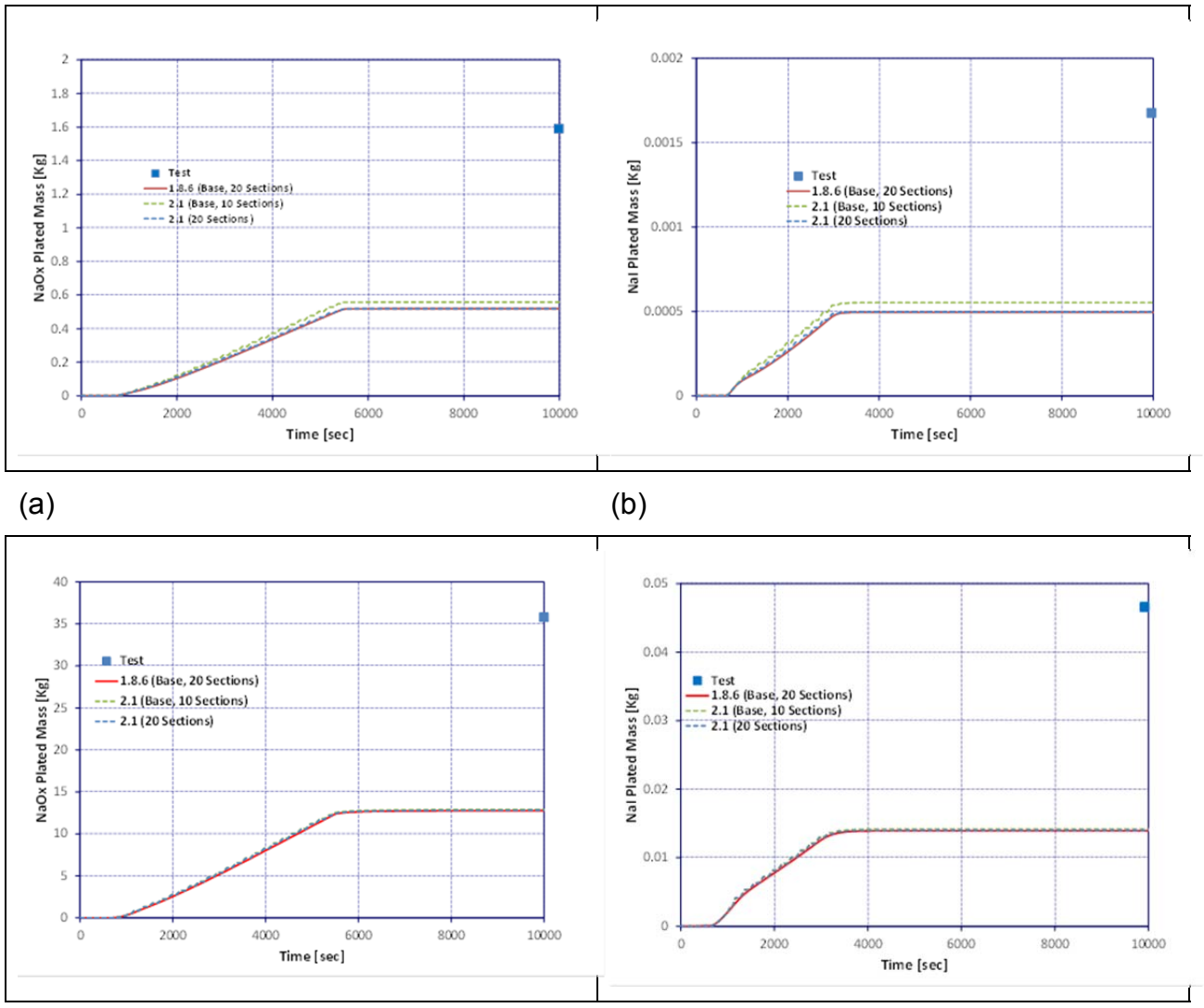

Figure 3.1-10. Plated Aerosol Mass on the Top Head for NaOx (a) and NaI (b) and on Internal Components (horizontal structures) for NaOx(c) and NaI(d) in Test AB6

The aerosol settled mass is the mass of aerosols deposited on the containment vessel's bottom head and the internal components as shown in Figure 3.1-11. Figure 3.1-11(a) shows the mass of the NaO_x aerosol settled on the bottom head as calculated by MELCOR. Also included in this figure is the corresponding value of 156.01 kg measured at the end of the test. The NaO_x aerosol mass settled on the bottom head as calculated by MELCOR is 184 kg, over-predicting measurements by about 18%. For the settled mass of NaI aerosol, Figure 3.1-11(b) shows the MELCOR results as well as the reported value of 195.6 g. MELCOR calculates a NaI settled mass on the bottom head of 200 g, over-predicting the measured values by only 2%.

The MELCOR calculations for the NaO_x mass settled on the internal components are presented in Figure 3.1-11(c). Also included in the figure is the reported 179 kg of NaO_x mass settled on this structure. MELCOR calculates a NaO_x mass of 173.7 kg settled on this structure, 3% less than the measured value. Figure 3.1-11(c) presents the MELCOR calculations and the reported value of 172.6 g. The MELCOR result for the NaI mass settled on internal components is calculated to be 195 g, 13% lower than the reported result (see Figure 3.1-11(d)).

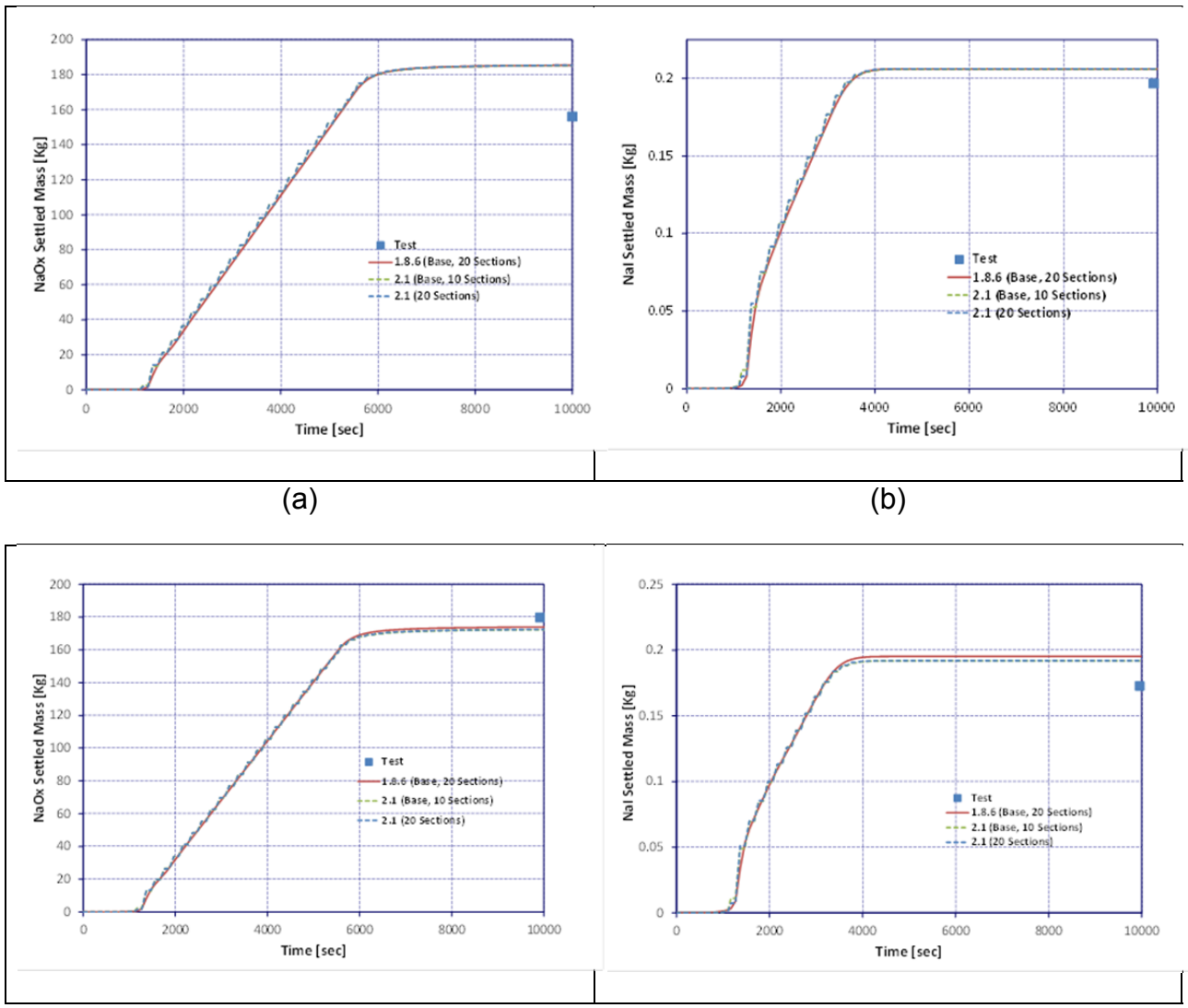

Figure 3.1-11. Aerosol Settled Mass on the Bottom Head for NaOx (a) and NaI(b), and on Internal Component for NaOx(c) and NaI (d) in Test AB6

In summary, MELCOR predictions are generally in good agreements with the settled and airborne masses with the AB5 and AB6 experimental results. However, MELCOR calculations generally under-predict plated masses for these experiments. The effect of

the number of aerosol sections used does not alter the results noticeably (see Table 3.1-4).

Table 3.1-4. Aerosol Summary at the End of Problem Time for MELCOR 2.1.

Test	10 Sections (kg)		20 Sections (kg)	
	Atmosphere	***Deposited***	***Atmosphere***	***Deposited***
AB5				
Cs	8.689E-05	3.884E+02	7.427E-05	3.884E+02
AB6				
Cs	6.230E-04	3.736E+02	5.330E-04	3.736E+02
CsI	3.260E-14	4.157E-01	1.938E-17	4.157E-01

3.1.4 References

[3.1.1] F.J. Souto, et.al, MELCOR 1.8.2. Assessment: Aerosol Experiments ABCOVE AB5, AB6, AB7, and LACE LA2, SAND94-2166, Sandia National Laboratories, Albuquerque, NM, October 1994.

3.2 Analysis of ACE Pool Scrubbing Experiments

3.2.1 Background

In most light water reactor core-degraded accident scenarios, the transport paths of fission product aerosols include passages through stagnant pools of water. In boiling water reactors for instance, the steam-gas-fission product mixture is directed towards the suppression pool where steam is condensed to prevent over-pressurization of containment. In pressurized water reactors, the mixture could pass through the pressurizer quench tank before reaching the containment. Fission product aerosols could be captured (scrubbed) in these pools and hence it is important to assess the realism of MELCOR's pool scrubbing model. Pool scrubbing tests were performed as part of the Advanced Containment Experiments (ACE) [3.2.1]. MELCOR simulations of the ACE tests are presented here.

Decontamination factor (DF) is the metric reported in the ACE tests and determined in the MELCOR calculations for comparing pool-scrubbing efficiency. A quantitative figure of merit is used to assess the aggregate values of DFs across multiple experiments/calculations. DF is determined as the ratio of the material introduced to the pool and the material escaping the pool. The figure of merit is the "under-prediction factor (UF)", as reported by Owczarski and Burk [3.2.2], i.e.,

$$\boldsymbol{UF = log_{10}^{-1}(MD)} \qquad \text{Equation 3.2-1}$$

where,

$$\boldsymbol{Mean\ difference\ (MD) = \frac{\sum_{j=1}^{n}[log_{10}DF_{measured} - log_{10}DF_{calculated}]_j}{n}} \qquad \text{Equation 3.2-2}$$

For any given calculation (i.e., where the number of calculations, n, is equal to 1), the UF provides a number, that when multiplied by the calculated DF, would yield the measured DF. For example, if MELCOR calculated a DF of 100 when the measured value was 10, the UF would be 0.1. Therefore, a UF of 1.0 would indicate exact agreement between calculated and measured data. UFs greater than 1.0 would indicate under-prediction of DF, and UFs less than 1.0 would indicate over-prediction of DF. When applying the UF over an entire data set (n>1), a general assessment can be made as to the quality of the model being assessed. For example, assume a UF for an entire data set was calculated to be 1/3. This would mean that, in general, the calculated values over-predict DF by a factor of 3. In the context of Probabilistic Risk Assessment (PRA), and considering the overall uncertainty in source term technology and predictive capability for a specific parameter (e.g., pool DF), a UF in the range of 0.1 to 10 (i.e., prediction of DF within a factor of 10 of measured values) is generally considered adequate. It should be noted here that this is a general rule of thumb. In fact, for low values of measured DF, the predictive capability of MELCOR should be more precise. For example, if a specific experimental case yielded a measured DF of 1.2, a UF of 0.1 (i.e., calculated DF of 12) would not be considered a good prediction.

3.2.2 Description of the ACE Pool Scrubbing Experiments

The ACE pool scrubbing experiments modeled were designed to evaluate the effectiveness of pool scrubbing on an aerosol/gas mixture entering a pool through a multi-hole sparger at various levels of submergence [3.2.1]. The sparger and experimental conditions were designed to simulate T- or X-quencher at the terminus of a safety/relief valve tailpipe in a BWR suppression pool or a PWR quench tank. A schematic of the experimental facility is shown in Figure 3.2-1, and the test apparatus geometry is given in Table 3.2-1.

.

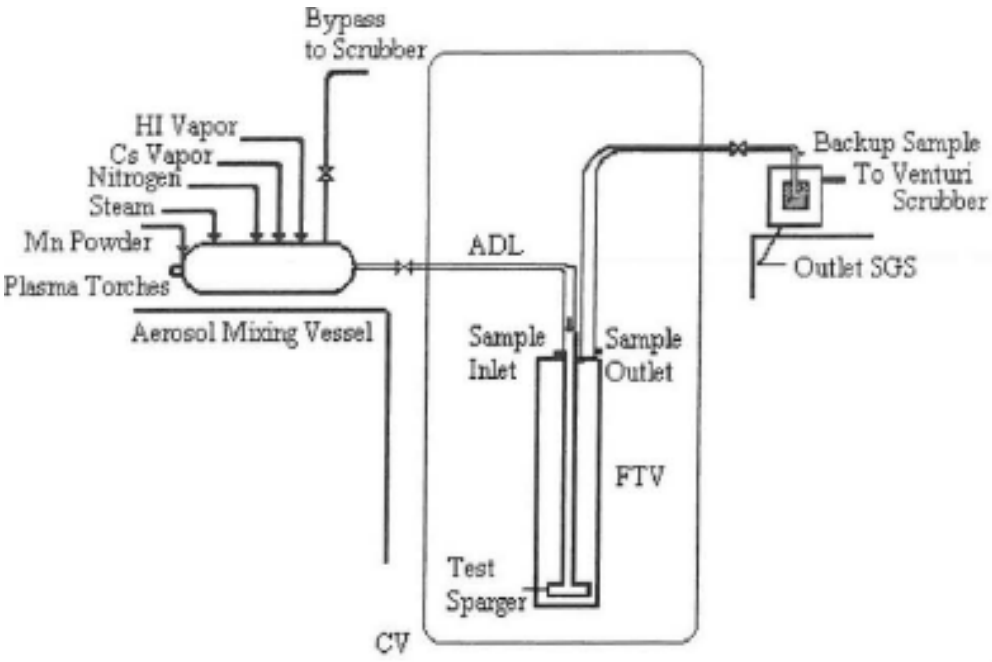

Figure 3.2-1 ACE Experimental Aerosol Pool Scrubbing Test Arrangement

Table 3.2-1 Fixed Geometric Parameters for the ACE Experimental System

Parameter	Value
Scrubbing Tank	
Height	6.1 m (20.01 ft)
Diameter	1.524 m (5.00 ft)
Aerosol Source Volume	
Centerline Elevation *	m (ft)
Length	Not specified (assumed to be 1 m, 3.281 ft)
Diameter	Assumed equal to sparger pipe (0.206 m, 8.1 in)
Sparger Pipe Volume	
Orientation	Vertical - Connects Source to Sparger
Length	~ 5.8 m (19 ft)
Diameter	0.206 m (8.1 in)
Sparger	
Number of Holes	51
Diameter of Holes	0.9525 cm (0.375 in)
Ht above Tank Bottom	~ 0.263 m (0.863 ft)

* Reference Elevation of 0.0 m corresponds to the elevation of sparger holes

A carrier gas of nitrogen and steam was mixed with Cs vapor, Mn powder and HI vapor to produce the aerosol/gas mixture prior to injection into the pool. Two samples of this aerosol/gas mixture were taken for each experiment at a point just upstream of the sparger to determine the properties of the mixture that enters the pool. The aerosol size distribution for each sample was measured using isokinetic-sample/cascade-impactors. These data, along with other initial experimental conditions, are listed in Table 3.2-2.

Table 3.2-2. ACE Test Conditions

Test	Gas Steam Fraction	Gas Flow Rate [g/s]	Gas Pressure [atm]	Gas Temp [°C]	Tank Pressure [atm]	Pool Temp [°C]	Submergence [m]
AA1	0.012	109.5	1.191	138.3	1.054	26	1.38
AA2	0.185	76.7	1.484	142.3	1.047	25	4.52
AA3	0.013	109.6	1.305	150	1.067	82	2.62
AA4	0.41	92.9	1.482	141.4	1.055	84	4.61

Test/Aerosol		Aerosol Size Distribution[2] AMMD [μm]	σ	Aerosol $\dot{m}$ [g/s]
AA1:	CsOH	2.43	1.75	0.663
	CsI	2.50	1.88	0.158
	MnO	2.08	1.90	0.668
AA2:	CsOH	1.58	2.12	0.840
	CsI	1.93	1.87	0.154
	MnO	1.49	2.13	0.362
AA3:	CsOH	1.90	2.89	0.675
	CsI	2.03	2.79	0.120
	MnO	2.27	2.18	1.780
AA4:	CsOH	2.34	2.17	0.707
	CsI	2.56	2.21	0.118
	MnO	2.11	2.33	1.010

Notes: 2. Two samples were taken for each experiment. Only the first was used for this analysis

3.2.3 Description of the ACE MELCOR Model

The MELCOR model of the ACE tests is a five-volume hydrodynamic model as illustrated in Figure 3.2-2. Modeling parameters reflect the information in Table 3.2-1 and Table 3.2-2.

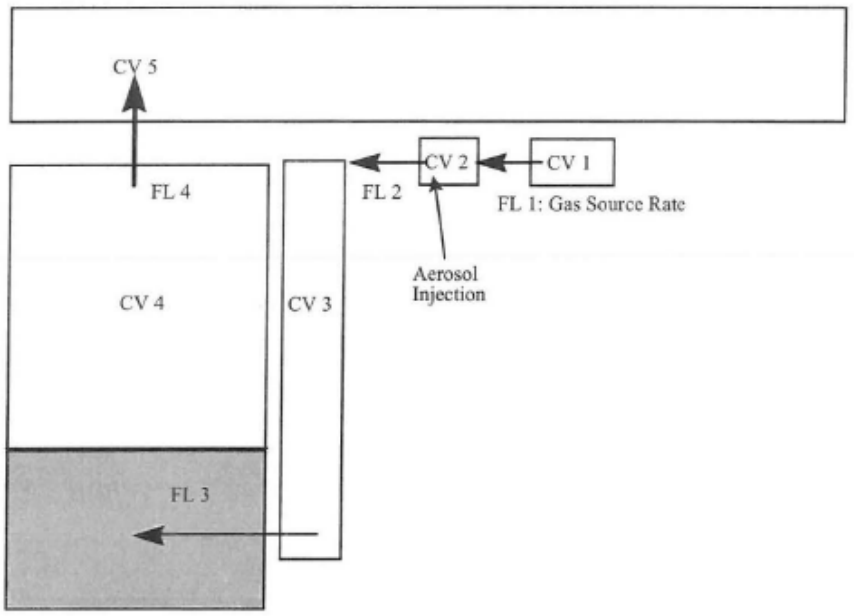

Figure 3.2-2.ACE MELCOR Model Nodalization

3.2.4 Results of the ACE MELCOR Analysis

Figure 3.2-3 and Table 3.2-3 present the results of the MELCOR ACE calculations. In Figure 3.2-3, points left of the dashed line reflect MELCOR underestimates of DF while points to the right of the line (of which there are none) reflect overestimates of DF. UFs in Table 3.2-3 were calculated from the relations presented in Section 3.2.1. The aggregate UFs from the MELCOR calculations lie outside the range 0.1 to 10 and thus fail to satisfy the acceptance criteria described in Section 3.2.1.

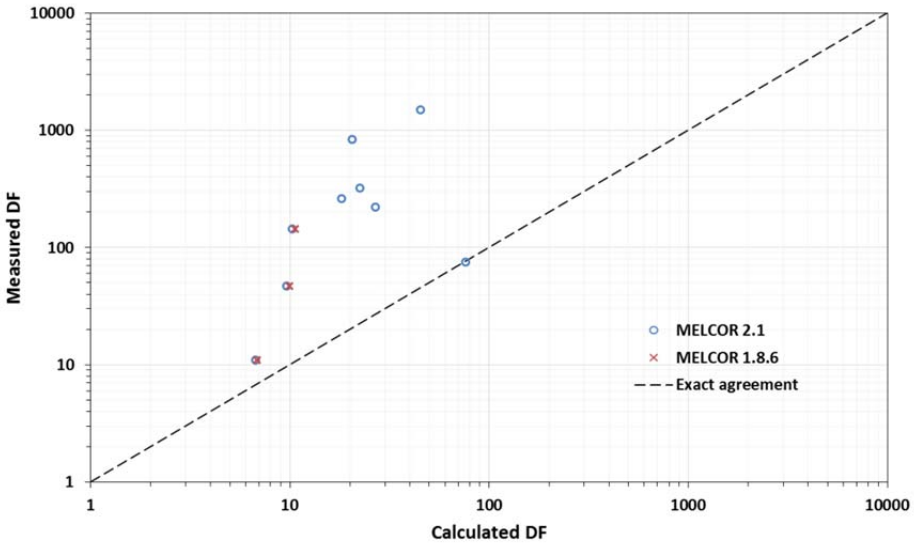

Figure 3.2-3. MELCOR DF Comparisons to ACE Tests

Table 3.2-3. MELCOR DF and UF Comparisons to ACE Tests

Case No.	MELCOR Version	Calculated DF	Measured DF	UF
AA1 - CsI	2.1	9.6	47.0	4.9
AA1 - CsOH	2.1	10.3	145	14.1
AA1 - MnO	2.1	6.7	11.0	1.6
AA1 - CsI	1.8.6	10.0	47.0	4.7
AA1 - CsOH	1.8.6	10.7	145	13.6
AA1 - MnO	1.8.6	6.9	11.0	1.6
AA2 - CsI	2.1	45.3	1500	33.1
AA2 - CsOH	2.1	20.5	840	41.0
AA2 - MnO	2.1	18.2	260	14.3
AA3 - CsI	2.1	26.9	220	8.2
AA3 - CsOH	2.1	22.5	320	14.2
AA3 - MnO	2.1	76.2	75.0	1.0
			Aggregate 2.1	8.6
			Aggregate 1.8.6	4.7

3.2.5 REFERENCES

[3.2.1] R.T.Allemann and J.A. Bamberger. Comparison of Code Results with ACE Pool Scrubbing Tests. Advanced Containment Experiments Technical Report ACE-TR-A13. Battelle, Pacific Northwest Laboratories. June 1990.

[3.2.2] P.C. Owczarski, et al. Technical Bases and User's Manual for the Prototype of a Suppression Pool Aerosol Removal Code (SPARC). NUREG/CR-3317, PNL-4742, Revision 1. Pacific Northwest Laboratory, Richland, WA. May 1985.

3.3 Analysis of AHMED 1993 NaOH Experiments

3.3.1 Background

The Aerosol and Heat Transfer Measurement Device (AHMED) facility was constructed in 1991 by VTT (Technical Research Center of Finland) Aerosol Technology Group [3.3.1]. A series of aerosol experiments were conducted at the AHMED Test Facility by injecting NaOH in aerosol form into an atmosphere. The experiments were designed to provide data for hygroscopic and non-hygroscopic aerosol behavior - single as well as multi-component - under controlled temperature and humidity conditions. Due to the simplicity of the facility and the relatively low-aerosol concentration, AHMED provided a wealth of hygroscopic aerosol data, free of integral effects.

CSNI PWG4 accepted the AHMED NaOH experiments from 1993 as the basis for a code comparison exercise designed to test aerosol codes in well-defined conditions [3.3.1]. For this assessment, MELCOR 2.1 and 1.86 were used to simulate the NaOH experiments for which the relative humidity (RH) was 22, 82, and 96%. Comparison of these cases with MELCOR provides assessment of the thermal-hydraulic and aerosol models in this code.

3.3.2 AHMED Experiment

The AHMED Test Facility was designed to provide aerosol data under conditions where the thermal-hydraulics were well-defined and not subject to coupled thermal-hydraulic phenomena associated with large, integral test facilities (see Figure 3.3-1).

Figure 3.3-1. Photograph of AHMED Facility [3.3.1]

The AHMED Facility consists of a cylindrical 1.81 m^3 vessel measuring 0.635 m in radius with a sedimentation area of 1.27 m^2. Wall temperatures were measured at thirteen locations, and internal and external ambient temperatures at fourteen locations using Pt100-type RTDs. The ambient temperatures were about 23 ˚C. For this test, the temperatures of the walls of the cylinder were controlled using heating cables. All vessel inner surfaces and gas temperatures were approximately equal. Vessel and input line pressures, and steam and air flow rates were monitored throughout the experiment. The pressure inside the vessel was kept at the same pressure as the ambient (1 atm). The relative humidity was measured at three locations using Vaisala Humicap detectors.

NaOH in an aerosol state was injected into a vessel at constant relative humidity. Mass and number concentrations measured from different heights were equal within the experiment accuracy. The aerosol concentration was diluted (no more than 0.7 g/m^3), so most aerosol deposition occurred mainly as a result of gravitational settling; the low concentration kept aerosol coagulation low. Thus, the primary phenomenon was the hygroscopic growth of aerosols, with the typical aerosol particle growing in mass as it absorbed water from the atmosphere due to hygroscopic effects such as the Kelvin effect and solubility. Hygroscopic growth continued until the particles were large enough that gravitational setting was significant.

3.3.2.1 MELCOR Nodalization

An input deck of MELCOR 1.8.3 initially developed by VTT was used in the analysis [3.3.1]. The input deck was relatively simple, as it consisted of a control volume (CV) that modeled the tank where the NaOH was injected, another CV that simulated the atmosphere surrounding the tank, and a heat structure (HS) that thermodynamically connected the two CVs (see Figure 3.3-2). The input deck did not have flow paths.

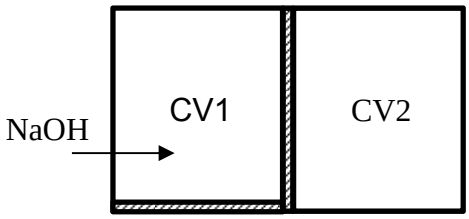

Figure 3.3-2. MELCOR Nodalization Modeled by VTT [3.3.1]

The VTT input deck was modified slightly by setting the hygroscopic aerosol flag to active (i.e. input variable ihygro = 1), specifying different relative humidity values in each test, and changing AMMD to 2.13 μm, the value shown in the figures of Ref. [3.3.1]. Simulations were then conducted for tests with relative humidity values of 22, 82, and 96%. These tests represented low, mid-range, and high relative humidity cases.

Because the NaOH is implemented into MELCOR as the Cs class (Class 2), VTT modified several sensitivity coefficients (SC) in the input deck to provide the appropriate elemental and compound molecular weights (C7120), solubility fractions (C7136) and hygroscopic properties (C7170) for NaOH. All other input was set to default. That is, no CV, HS, or Radionuclide (RN) Package input was modified to obtain output that more closely matched data.

The MELCOR input parameters used for this exercise are specified in Table 3.3-1 and Table 3.3-2. As shown in Table 3.3-1, the aerosol parameters, dimension of the vessel, and information pertaining to the experiment were incorporated into the MELCOR model. The information provided in Table 3.3-2 is used for each of the three cases that were run for MELCOR. The initial mass concentration as listed in Table 3.3-2 was used to adjust the multiplier in the aerosol source input record for each relative humidity case. Both MELCOR 1.8.6 and 2.1 calculations were performed for all three humidity cases.

Table 3.3-1. Facility and Experimental Conditions [3.3.1]

Vessel Effective Volume	1.81 m^3
Vessel Radius	0.635 m
Vessel Effective Height	1.425 m
Sedimentation Area	1.27 m^2
Approximate Diffusion Area	9.42 m^2
NaOH atomic weight	40 g/mol
Pressure	1.013×10^5 Pa
Leakage Rate (RH constant during test)	206% of volume/24h (~2.6 liters per minute)
NaOH density	2130.0 kg/m^3
Dry NaOH particle size (AMMD/GSD)	$2.4x10^{-6}$ m / 1.64

Table 3.3-2. MELCOR Run Description [3.3.1]

Run	Relative Humidity (%)	Temperature (K)	Initial Mass Concentration (mg/m^3)
RH22	22	323.15	112
RH82	82	300.15	208
RH96	96	296.15	218

3.3.2.2 Results of Analysis.

Both MELCOR 2.1 and 1.8.6 calculations were performed for various relative humidity values; their results were compared with experiment data. Figure 3.3-3 to Figure 3.3-5 show the measured and MELCOR normalized aerosol concentration for a relative humidity of 22, 82, and 96%, respectively. Table 3.3-3 shows the balance of the NaOH in the calculations. As shown in, for a relative humidity of 22%, the MELCOR results show very close agreement with the test data. In addition, the results from both

MELCOR versions are nearly identical. However, for a relative humidity of 86%, as shown in, the results from MELCOR 2.1 deviated further from the test data than those of MELCOR 1.8.6. This contributes to slightly high-settling or deposition at this humidity level, which reduces the amount of the NaOH in the atmosphere (see Table 3.3-3). For a 96% relative humidity as shown in, the results from MELCOR versions are very similar and they are in close agreement with the test data.

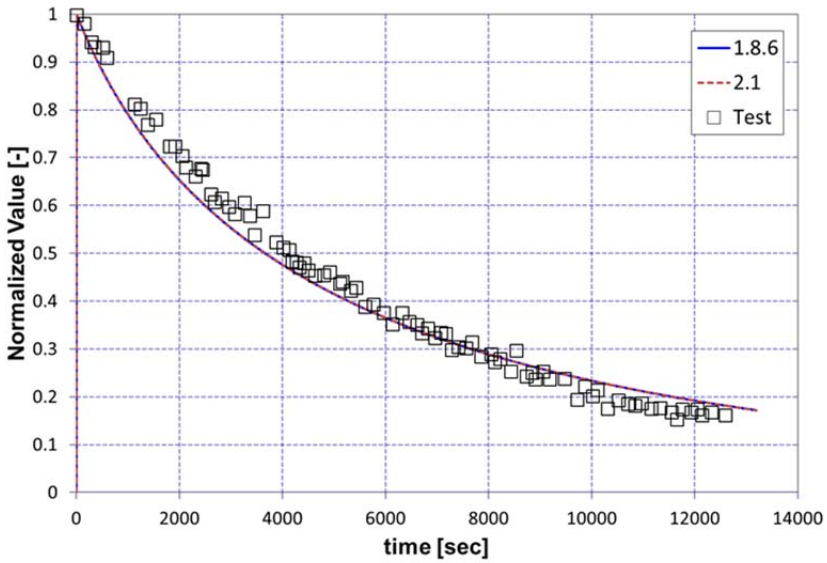

Figure 3.3-3. Normalized NaOH Concentrations at RH=22%.

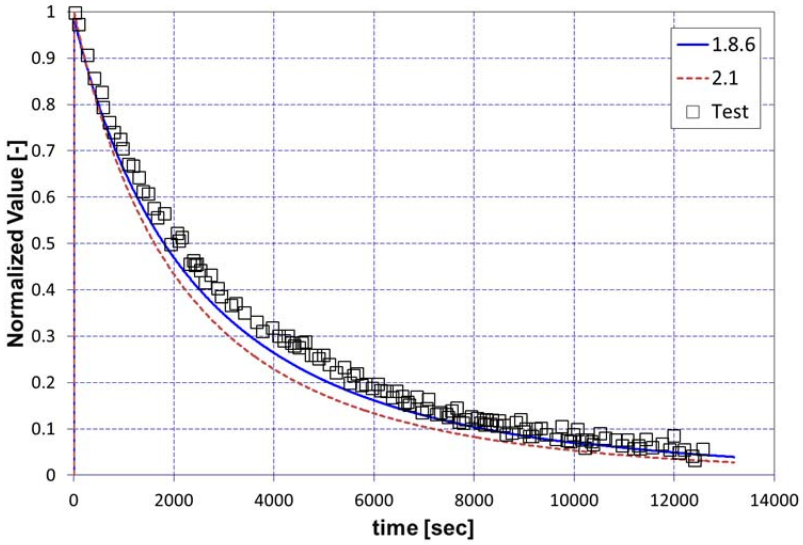

Figure 3.3-4. Normalized NaOH Concentrations at RH=82%.

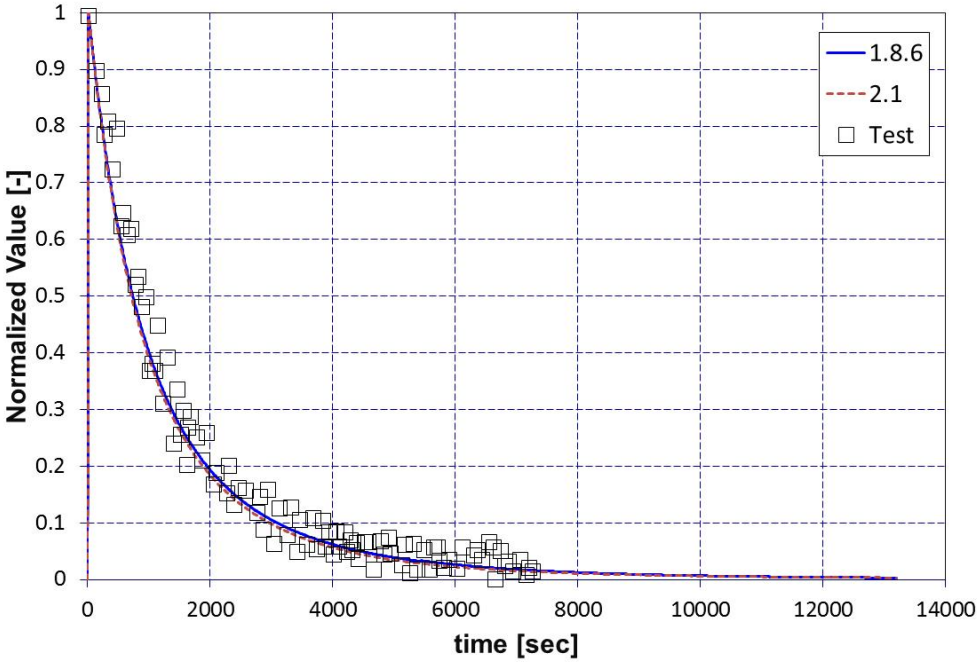

Figure 3.3-5. Normalized NaOH Concentrations at RH=96%.

Table 3.3-3. MELCOR Calculated NaOH Distribution

Run*	Mass Distribution (Kg)		
	Total	Atmosphere	Deposited
RH22 (1.8.6)	2.027E-04	3.479E-05	1.679E-04
RH22 (2.1)	2.027E-04	3.477E-05	1.679E-04
RH82 (1.8.6)	3.765E-04	1.454E-05	3.619E-04
RH82 (2.1)	3.765E-04	9.812E-06	3.667E-04
RH96 (1.8.6)	3.946E-04	1.157E-06	3.934E-04
RH96 (2.1)	3.946E-04	1.252E-06	3.933E-04

*Calculations were done using MELCOR 1.8.6 (rev.3964) and 2.1 (rev. 6110)

3.3.3 Discussions

This assessment indicates that MELCOR can be used for this type of experiment, particularly with a varying humidity level for aerosol depositions. Although there were some deviations between MELCOR 1.8.6 and 2.1 at relative humidity level of 82%, MELCOR 2.1 can generally model the hygroscopic phenomena.

3.3.4 References

[3.3.1] AHMED Code Comparison Exercise, CSNI/PWG4/FPC, Edited by J. Makynen and J. Jokiniemi, VTT Energy, Finland, October 1995.

3.4 Analysis of the Bethsy 6.9c Experiment (ISP-38)

3.4.1 Background

The Bethsy experimental facility is a model of a three-loop PWR core and primary circuit, with the elevations scaled 1/1 and the volume scaled to 1/100. The reactor core is simulated by 428 electrically heated rods arranged in prototypic 17x17 fuel bundles. A discussion of the facility and the 6.9c experiment can be found in Reference [3.4.1].

A view of the test facility is shown in Figure 3.4-1. Notice that the surge line (from hot leg 1 to the pressurizer) has a fairly long, almost horizontal section in it.

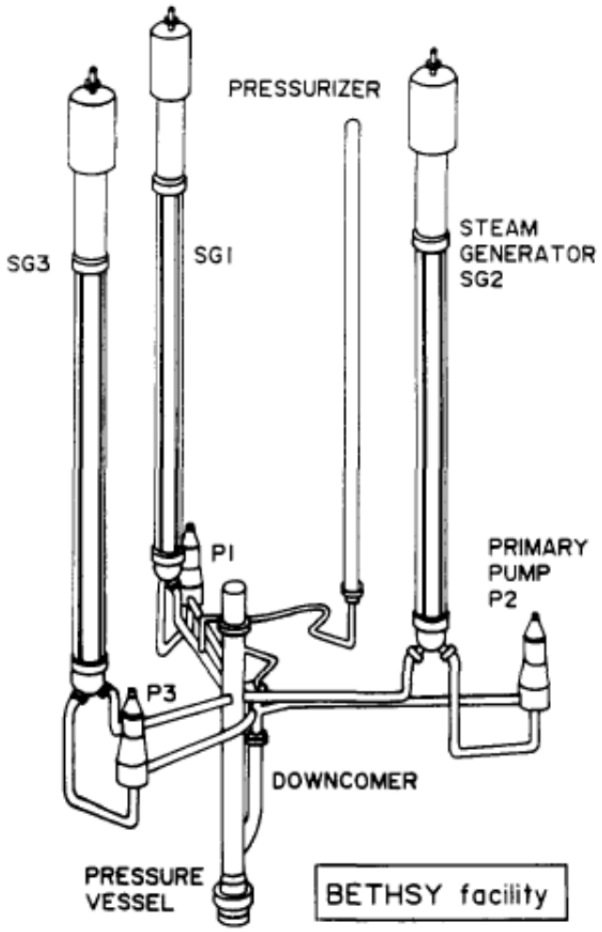

Figure 3.4-1. Rendition of Bethsy facility from reference [3.4.2]

3.4.2 Bethsy 6.9c Experiment

The Bethsy 6.9c experiment (ISP-38) [3.4.1] was intended to study the thermal hydraulics of the primary circuit and core under conditions of low pressure and partial draining (mid-loop operation) following the loss of the Residual Heat Removal System

with the primary system open at the pressurizer and steam generator outlet plenum manways.

The aims of the test were to study:

a. Entrainment and retention of water in the pressurizer caused by steam flow through the pressurizer manway.
b. Level swell in the upper head.
c. Expulsion of water through the steam generator manway.
d. Level of pressurization.
e. Reflooding of the core from the gravity and forced emergency core cooling water injection.

3.4.2.1 Experiment Setup

At the start of the experiment, (time = 0 sec), the power is off, the water level in the primary is at the centerline elevation of the hot leg, and the remainder of the primary is full of steam at saturation. The steam generator secondary sides were filled with air and isolated. Trace heating in the walls of the facility is used to balance heat losses to the environment. The trace heating power was left constant during the experiment. The surge line and pressurizer are on the hot leg of loop 1 (HL1), the manway valves are on loop 1, and the emergency water injection is on the loop 3 cold leg (CL3).

The test was conducted by raising the core power to 138kW and simultaneously opening the manway valves. Constant power was maintained during the experiment, and water injection was started when the clad temperature reached a maximum of 250 °C.

3.4.2.2 Nodalization

Information for setting up a Bethsy MELCOR assessment problem was taken from the IBRAE Final Report [3.4.2], ISP-38 Final Report [3.4.1] and the International Agreement Report.[3.4.3] A resultant historical input deck was produced. Figure 3.4-2 illustrates the configuration of Bethsy and key elevations within it. (Note: add 2164 mm to elevations in Figure 3.4-2 to get CV elevations in MELCOR model, which were referenced to the bottom of the test section rather than the bottom of the heated zone).

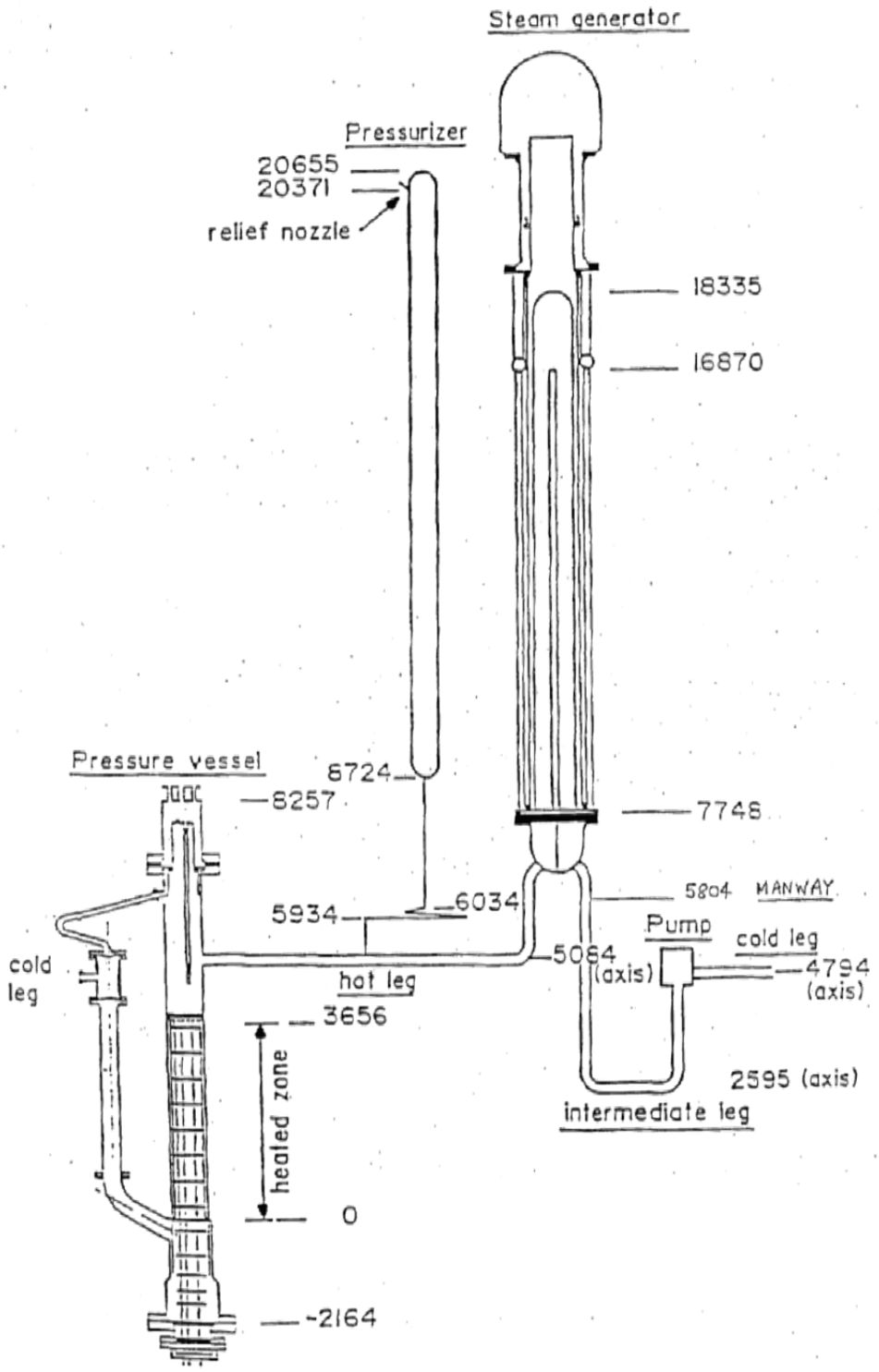

Figure 3.4-2. Bethsy Configuration and Elevations (mm)

The MELCOR nodalization is given in Figure 3.4-3 , which is the same as in the IBRAE Final Report [3.4.2] except that 1) the surge line CV is split into three CVs, representing

the two vertical portions and the long almost-horizontal section; 2) a correction has been made to inject to CL3 instead of CL1; and 3) the pressurizer is divided into 2 stacked volumes of equal height. The nodalization comprises the three primary loops and the reactor vessel (Loop 2 is not shown in the Figure). The core region consists of 13 axial levels by 2 rings. Levels 3-12 are in the fueled core region.

In the original deck [3.4.2], heat structures were not modeled except in the pressure vessel. If these were connected to the outside environment, the heat transfer to the air was represented as a convective HTC using a small value typical of air. This does not really simulate the actual BC using trace heaters in the structures, and, unless the heat structure (HS) is in contact with water on the internal side, the initial temperature will be set too low.

Some additional HSs were added later to the pressurizer and steam generators (SGs) to investigate the claim that HSs were not needed in this experiment.

Additional changes/enhancements made to the historical model used as base input for the subject assessment are itemized below:

1) A control-volume representation was added of the Steam Generator 1 Manway illustrated in Figure 3.4-4 to capture any influence of water filling the piping.
2) The bubble-rise model was enabled in the pressure vessel downcomer and the recirculation loop seals to allow the collapse of steam bubbling through pools if conditions warrant.
3) A common height was defined for 1) the “from” junction of the pressurizer surge line takeoff from Hot Leg 1 and 2) the transition from horizontal to vertical in the hot leg, to give both junctions a similar opportunity to draw (entrain) water.
4) Flow paths in the pressurizer surge line were defined with 1) junction heights subtending the full vertical extents of connected volumes and 2) momentum lengths equivalent to the full lengths of the flow paths, to closely couple water and steam phases flowing in the line.
5) The errant original shape of core axial power distribution was redefined to be cosine shaped as per the experiment.
6) Confusion between RPV wall and core shroud heat structures, wherein the inside surface of the wall was coupled to the core and the inside surface of the shroud was coupled to the bypass, was corrected.
7) MELCOR “dtdz” modeling associated with the shroud heat structures (at the core periphery) was enabled.
8) Large errors were corrected in the definition of core flow area (AFLOWC).
9) Unsubstantiated revisions to default values of sensitivity coefficients were removed.
10) The pressurizer was divided vertically into 2 control volumes to allow separation of flowing water and steam phases should it be indicated.

11) The CVH nodalization of the core was increased to match COR nodalization 1-to-1.
12) Junction opening heights were defaulted throughout the model but in the pressurizer surge line as described above and in the heated region of the vessel and the steam generator tubes bundles where they were defined to be 0.05 m.
13) Momentum lengths were defaulted throughout the model with the exception of in the pressurizer surge line.
14) Flow losses at the manways were defined anew based on Bethsy construction shown in Figure 3.4-4 and Figure 3.4-5.
15) The flow losses in the bypass between the vessel inlet plenum and the vessel head were defined anew per best interpretation of the confusing flow resistance information in Reference [3.4.1] p. 429.
16) The conditions at time 0 were reinitialized consistent with saturation at atmospheric pressure.
17) Unequal definitions of HS critical pool fraction were removed to stop artificial heat transfer between atmosphere and pool throughout the model.

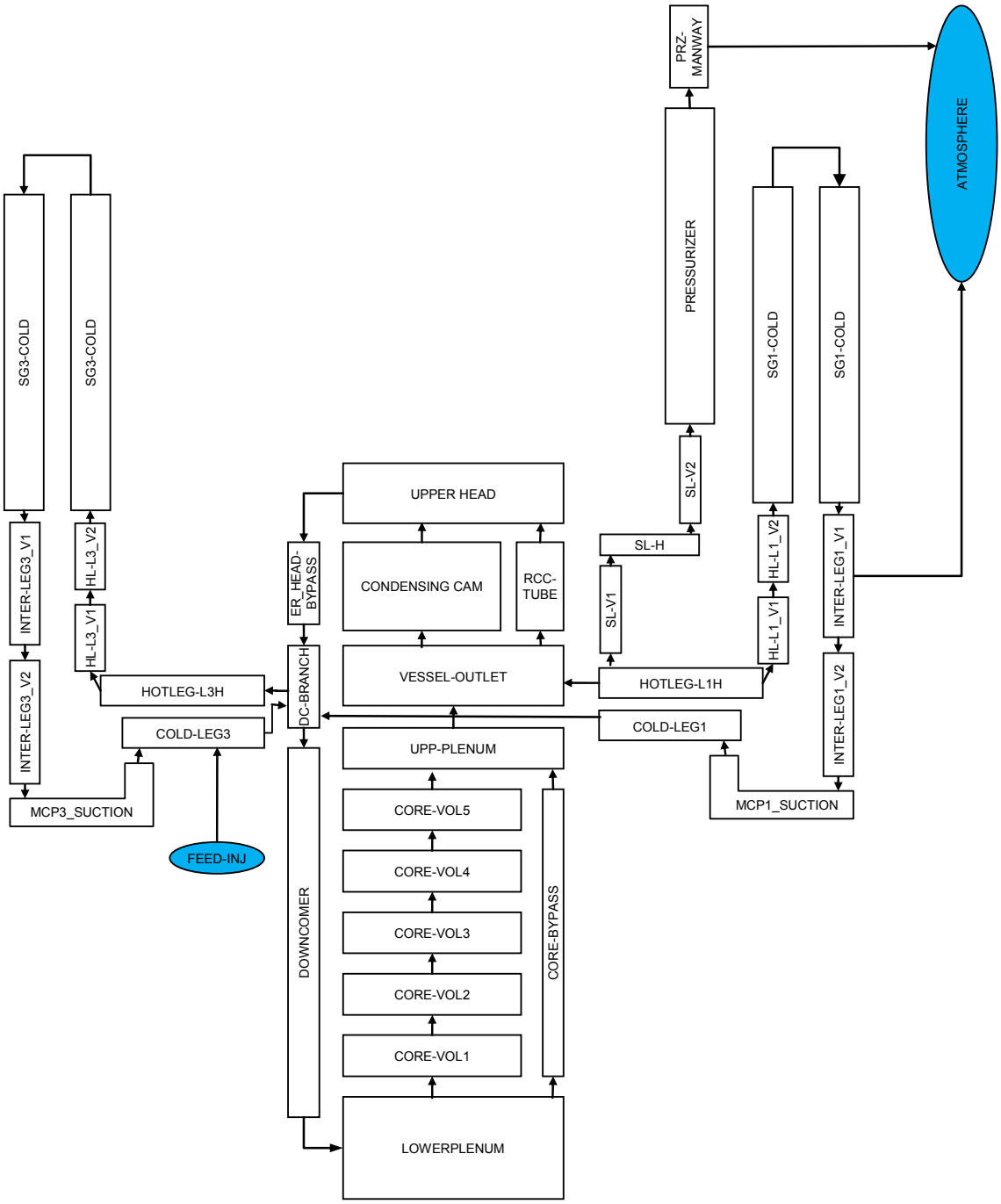

Figure 3.4-3. MELCOR Nodalization of Bethsy

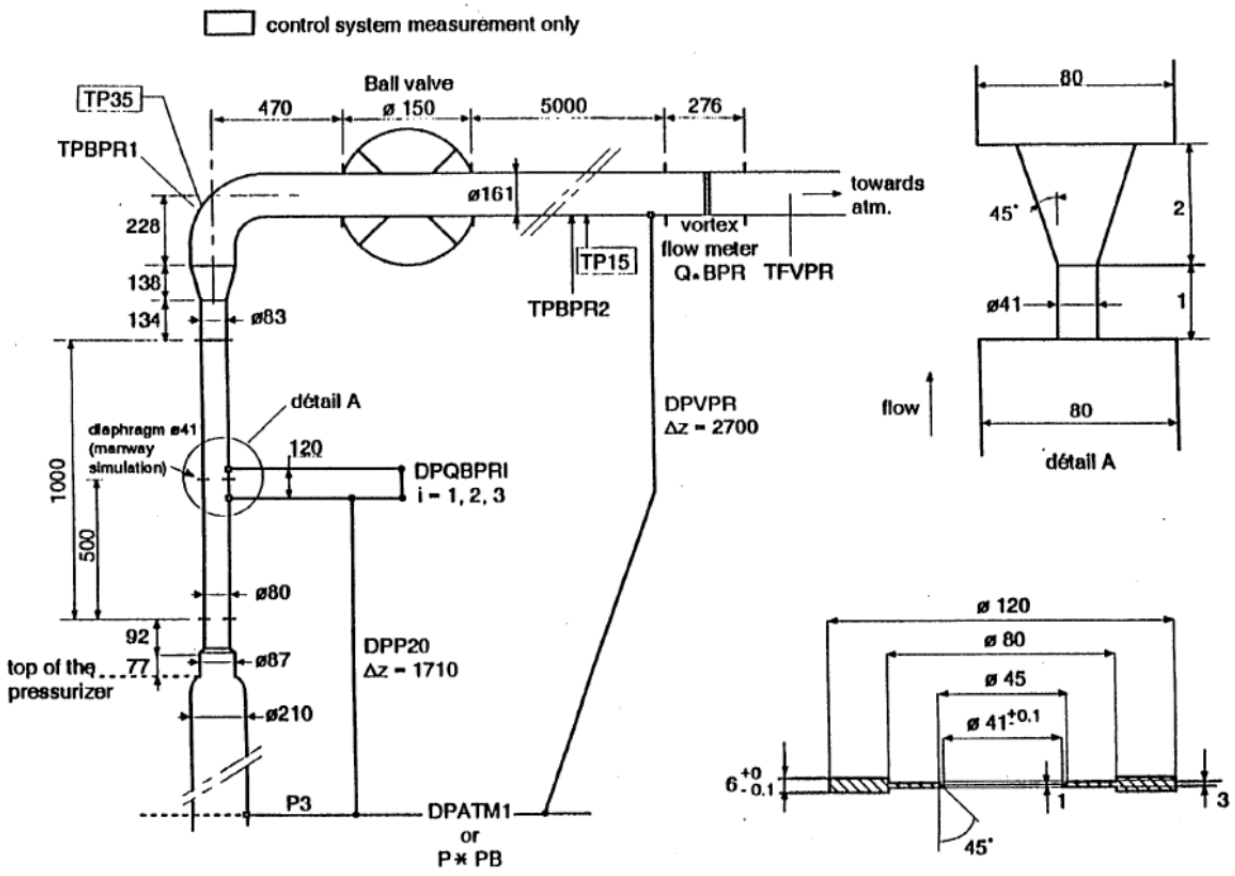

Figure 3.4-4. Bethsy Pressurizer Manway Configuration [3.4.3]

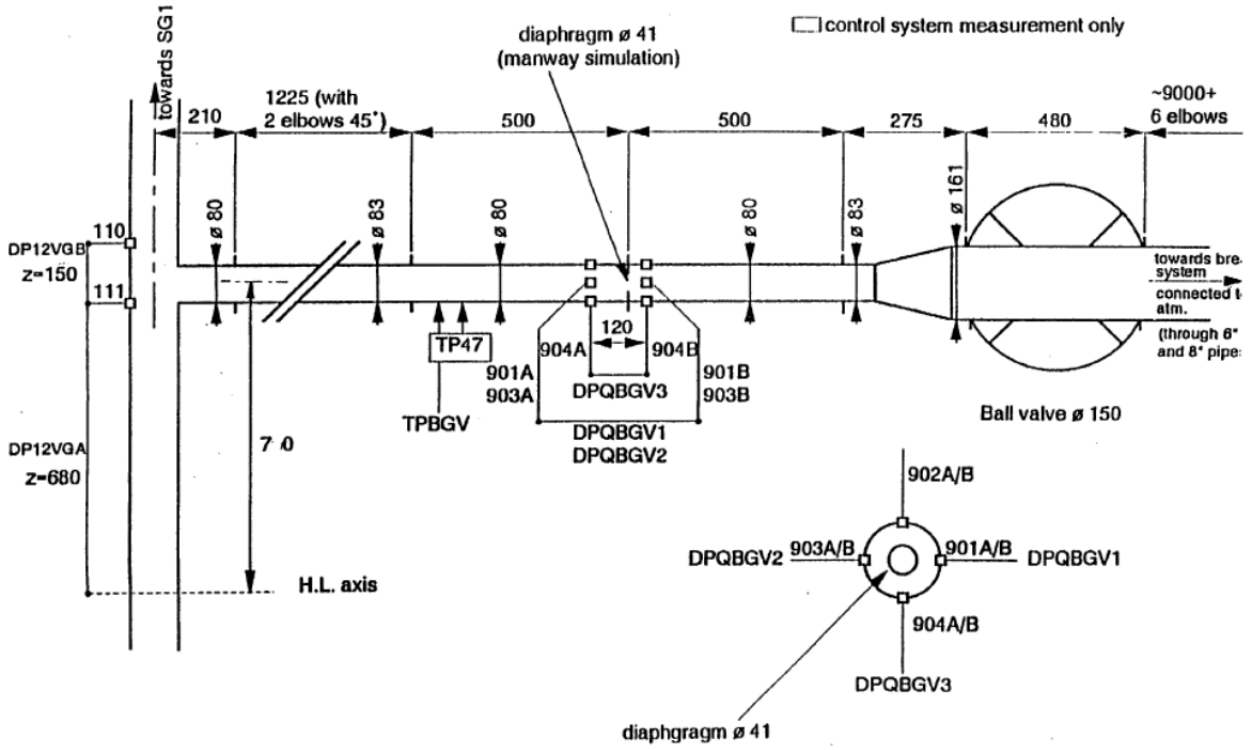

Figure 3.4-5. Bethsy Steam Generator Manway Configuration [3.4.3]

3.4.2.3 MELCOR Input Specifications

The simulation was started as per the experimental initial conditions. The cooling water injection into CL3 was simulated using a flow rate injection equation provided to the ISP-38 participants [3.4.3]:

$$\dot{m} = \left(\frac{1.5x10^5 - P}{2.4x10^5} \right)^{0.5} \frac{1}{3.6} \qquad \text{(Equation 3.4-1)}$$

where $\dot{m}$ is the water flow rate in kg/s and the pressure P is in Pa.

Problem end time was 9144 s.

3.4.2.4 Results of Analysis

Figure 3.4-6 to Figure 3.4-11 present results of the Bethsy MELCOR calculation alongside data from the experiment for comparison.

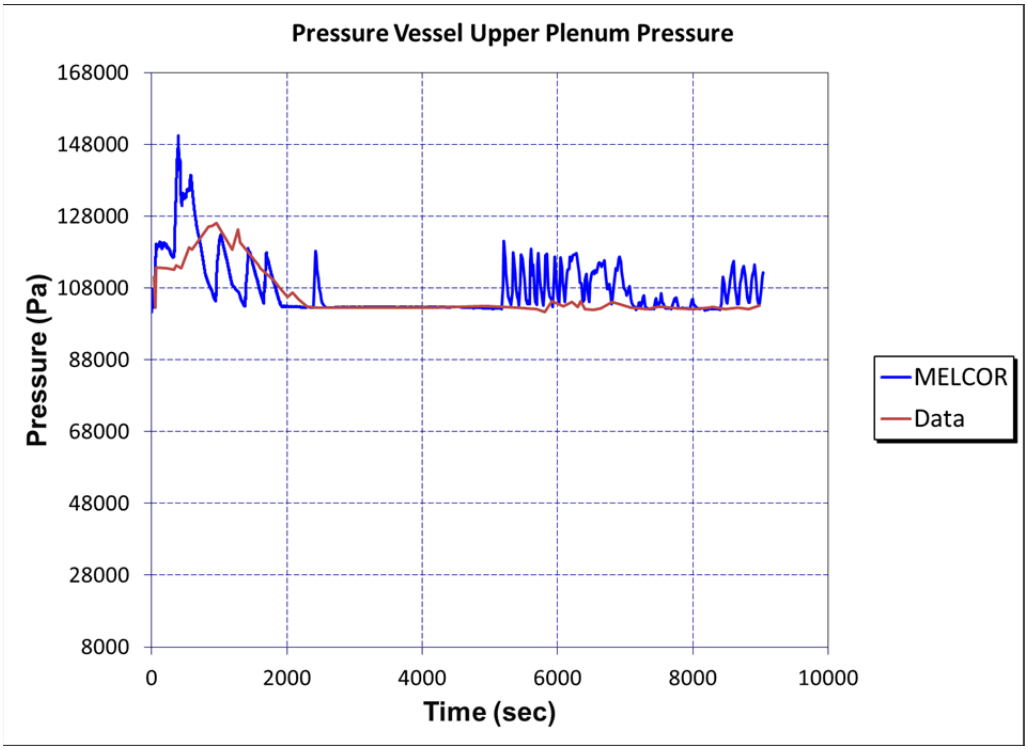

Figure 3.4-6: Pressure Vessel Upper Plenum Pressure

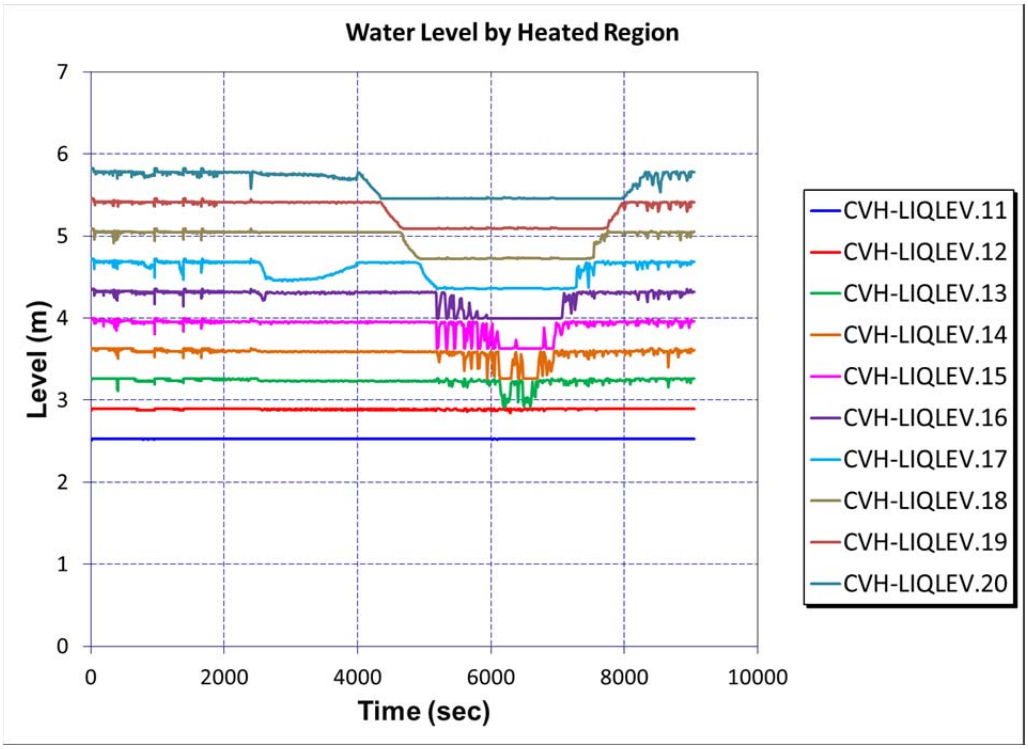

Figure 3.4-7: Water Level by Pressure Vessel Heated Region

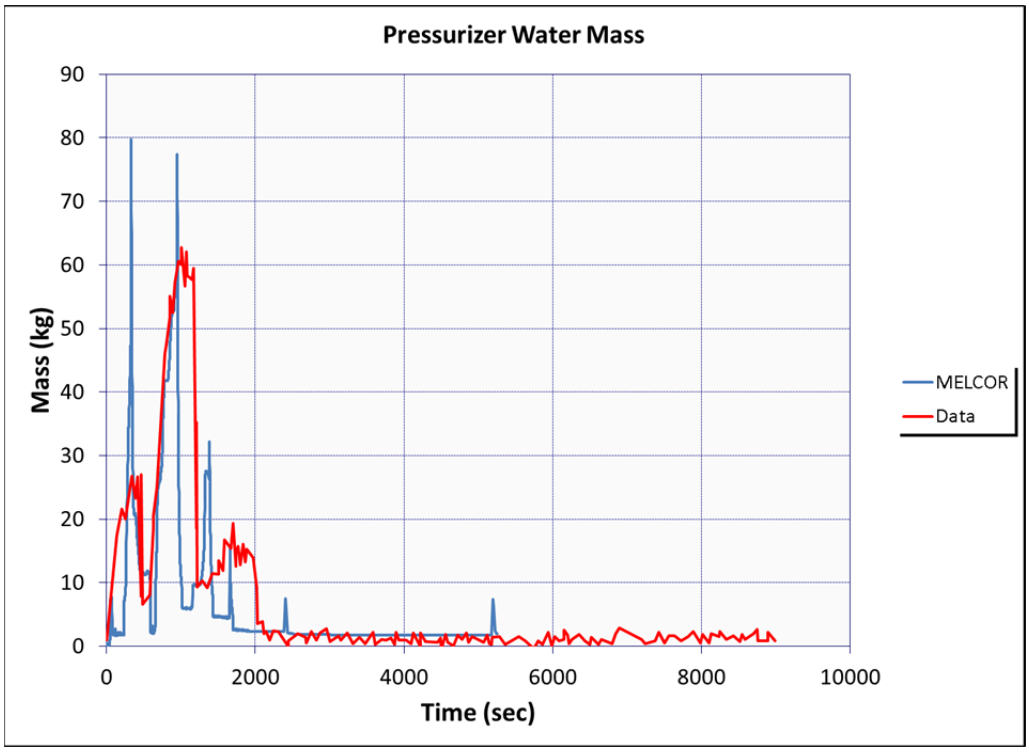

Figure 3.4-8: Pressurizer Water Mass

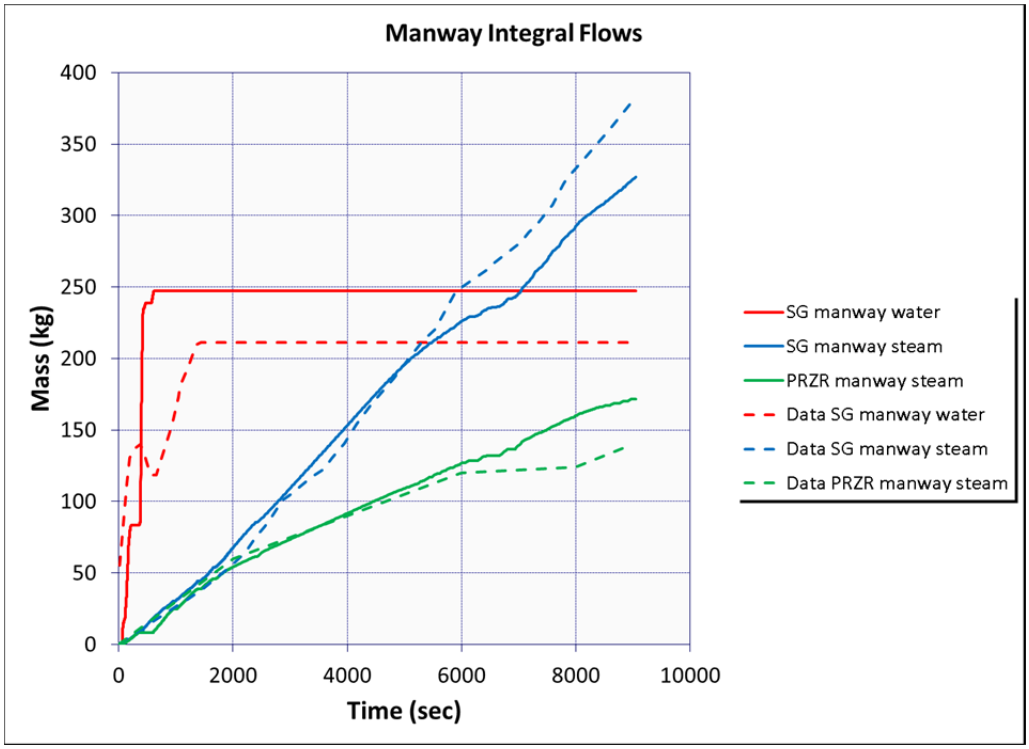

Figure 3.4-9: Manway Integral Flow

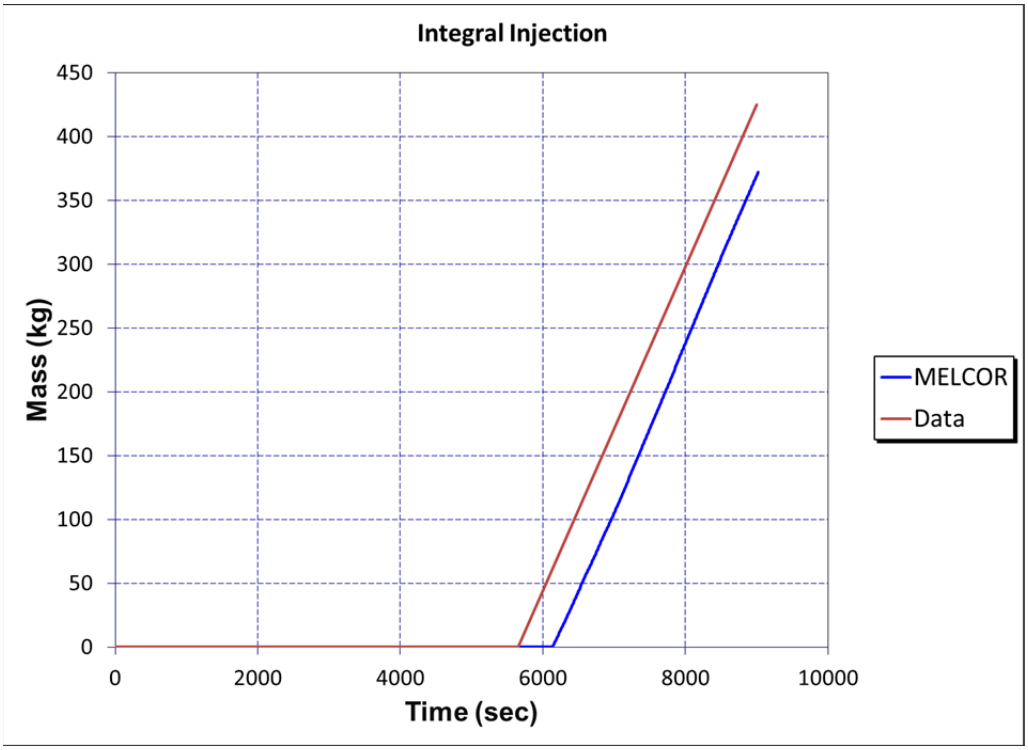

Figure 3.4-10: Integral Injection

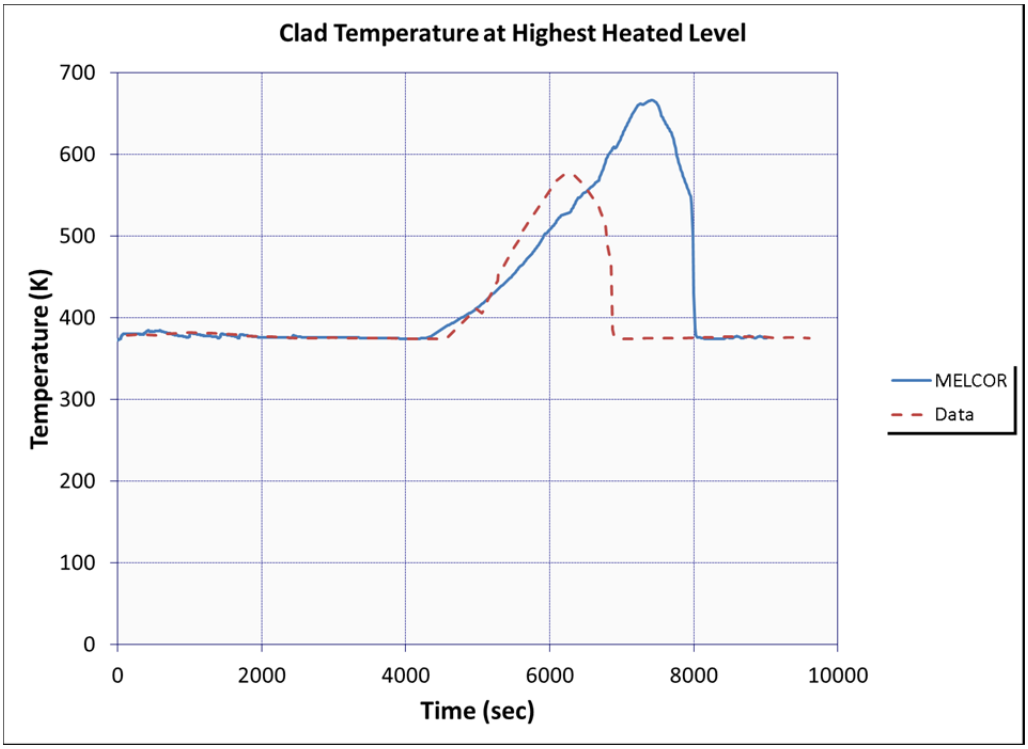

Figure 3.4-11: Clad Temperature at Highest Heated Level

3.4.3 Discussion

It was found that splitting the surge line into two vertical sections and a near-horizontal section, as in the experiment, gave a better simulation of the pressurizer draining behavior than using one surge line section.

Some experimentation was done adding HS's to the pressurizer and SGs. Heat transfer to the environment is supposed to be unimportant in this experiment, but in fact it was found that the added heat capacity of the HS's does affect the answers somewhat, particularly when the initial temperature is too low.

If the coupling between water and vapor flows is overly tight, the initial period of the calculation sees too much water pushed from the system out the open steam generator manway. Steam in this case is dragging an excessive amount of water with it as it moves towards the manway.

Steam condensation in the recirculation loop seals impacts the ability of steam to drag water to the open steam generator manway.

The problem was run using MELCOR 2.1 Revision 6616.

3.4.4 References

[3.4.1] G. Kimber, C. Leveque, G. Lavialle, "ISP-38 on Bethsy Test 6.9c Final report," NEA/CSNI/R(97)38, Volume I, OECD Nuclear Energy Agency (1998).

[3.4.2] V.F. Strizhov, N.A. Mosunova, "MELCOR 2.1 code verification: ISP-38 experiment at BETHSY facility," Russian Academy of Sciences, Moscow, Russia (2011).

[3.4.3] G.R. Kimber, M.A. George, "RELAP5/MOD3 Analysis of BETHSY Test 6.9c: Loss of RHRS: SG Manway Open," NUREG/IA-0187, U.S. Nuclear Regulatory Commission, Washington, DC (2000).

3.5 Analysis of Containment System Experiment for Spray- A9 Test

3.5.1 Background

A series of water spray experiments were conducted as parts of the Containment Systems Experiment (CSE) program at Pacific Northwest Laboratories in the 1970s [3.5.1] to [3.5.3]. The experiments were conducted to evaluate the performance of a containment spray engineered safety system as a means of removing fission products from the containment atmosphere. Measurements were obtained that provide a suitable basis for judging the ability of various mathematical models to predict spray performance in large nuclear power plants. This assessment documents the CSE A9 experiment, the last of the 9 spray experiments to benchmark the spray model and decontamination effect of the sprays in MELCOR [3.5.1].

3.5.2 A9 Experiment

The CSE experimental facility can be divided into 6 systems, which are briefly described (see Figure 3.5-1. CSE containment vessel with A9 experiment features) [3.5.2]:

- The containment vessel system, which consists of an outer containment vessel of 585.6 m^3 [30,680 ft^3] (7.62 m or 25 ft diameter by 20.33 m or 66.7 ft high), an inner drywell vessel, and a wetwell vessel occupying 4/5 of the annular space between the drywell and the containment vessel. All interior surfaces were coated with a modified phenolic paint. The wall thickness of the vessel is ranging from 1.63 cm (0.645") to 1.91 cm (0.75"). The exterior of the vessel is covered by a 0.254 cm (1") layer of fiberglass insulation. Note that there is a lid with a 3.35 m (11-ft) diameter that covered the drywell volume. For the sprays experiment, this lid remained open.
- The fission product simulant generation and injection system, which consists of a cave, standard radiochemical hoods, high frequency induction units, a heated transfer line, a steam jet, and a panel board.
- The gas and liquid sampling system, which consists mainly of the Maypack clusters located throughout the containment vessel volume. These clusters allow the sampling of gases and particulates. Other sampling includes rain collectors.
- The instrumentation system, which allows for monitoring the temperature, pressure, and liquid levels.
- The sample analysis system, and
- The containment sprays system, which consists of a solution storage tank, spray pump, recirculation piping and recirculation pump. The spray header/nozzles are located near the top of the containment vessel

A detailed description of these systems is given in the CSE experimental report [3.5.2]. A fresh, room-temperature spray solution was made up in an exterior, stainless steel storage tank. About 7,570 liters (2000 gal) were used in the experiment, which was about 1.3% of the gas volume in the main room. The spray manifold near the top of the

dome was arranged for 12 nozzles at a uniform spacing. About 80% of the gas space in the main room was washed by the spray. The physical and experimental conditions for this A9 test are given in Table 3.5-1.

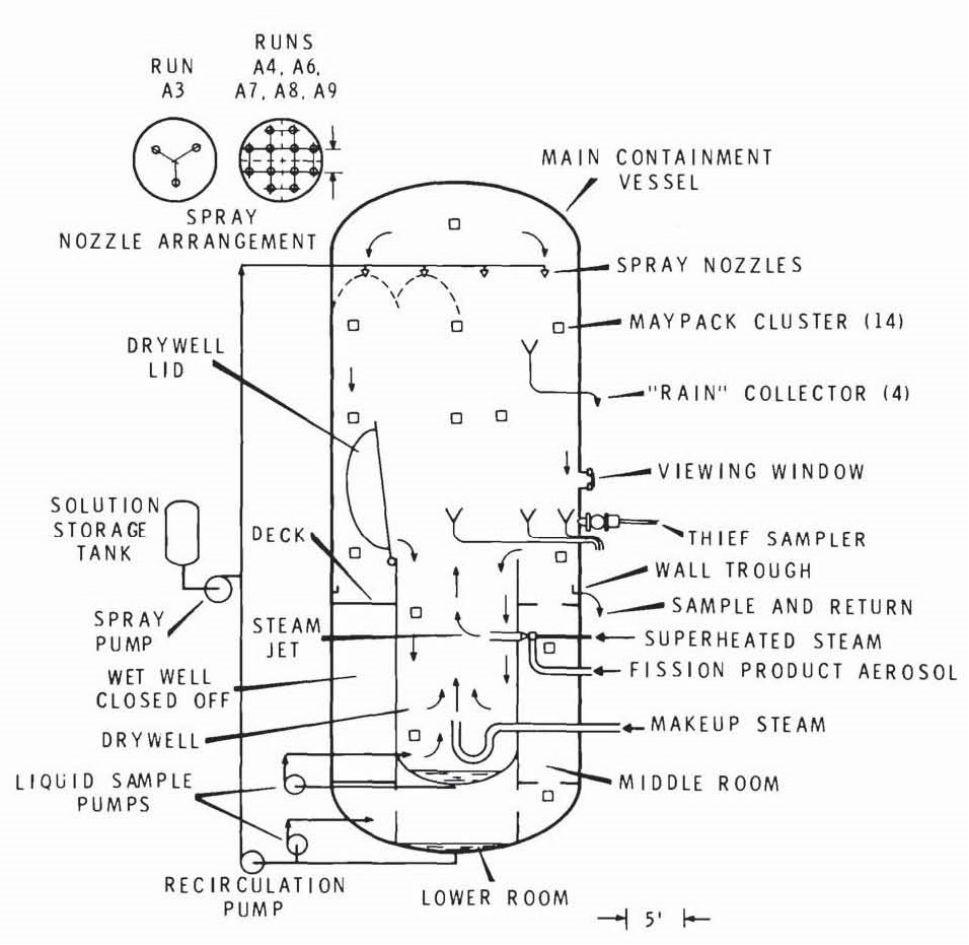

Figure 3.5-1. CSE containment vessel with A9 experiment features

Two kinds of materials were aerosolized in the CSE experiments to represent solids that could be released during postulated accidents. UO_2 fuel elements clad with stainless steel or zircaloy were heated inductively to temperatures high enough to form appreciable quantities of aerosol, likely converted to U_3O_8. Cesium carbonate volatilizes at a relatively low temperature and forms aerosols of cesium hydroxide, and possibly Cs_2CO_3, in humid atmospheres. Iodine was also injected in two forms: elemental iodine and methyl iodide [3.5.3].

The experimental procedure was to establish the desired atmospheric conditions in the containment vessel by using boiler house steam. The atmosphere initially was a saturated steam-air mixture at 3×10^5 Pa and 394 K (about 2/3 steam and 1/3 air). The steam feed rate was reduced to a point where thermal equilibrium was maintained. Then the fission product/fuel simulant was injected in a 10-minute period. After that, the simulants are allowed to mix for 30 minutes. The initial simulant concentration is given in Table 3.5-2. Time was referenced to the start of aerosol injection. The sprays were then operated intermittently (see Table 3.5-3). Fresh room-temperature water with

caustic (pH 9.4 to 9.5) boric acid was used. The spray system was operated for four spray periods as shown in Table 3.5-3. As shown in this table, the physical condition and composition of the sprays, including its origin are provided. In addition, the four spray periods include: the first period was operated for 180 s, the second was operated for 180 s, and the third was operated for 600 s. Then, the recirculation sump water was used for the remaining last spray period, as shown in this table.

Table 3.5-1. Physical and Experimental Conditions of A9 Test

Physical Condition*	Dimension
Volume above deck including drywell	595m^3
Surface area above deck including drywell	569m^2
Surface Area/Volume Ratio	0.958/m
Cross-sectional area in main vessel	45.5m^2
Cross-sectional area in drywell	8.8m^2
Volume in middle room Surface area in middle room	59m^3
Volume in lower room Surface area in lower room	96m^3
Total volume in all rooms Total surface area in all rooms	751m^3
Total surface area in all rooms	888 m^2
Drop fall height to deck Drop fall height to drywell bottom	10.3m
Drop fall height to drywell bottom	15.4m
Experimental Condition	Parameter
Atmosphere	Steam-air
Temperature (K)	394
Pressure (kPa)	303.36
Nozzle type	¾ A50, hollow cone
Droplet AMMD (μm)	1220

Droplet GSD	1.5
Number of nozzles	12
Spray rate (liters/s)	9.135
Total spray volume (liters)	8,694
Boron concentration (ppm)	3,000
Boron form	H_3BO_3
Boron carrier	NaOH
pH	9.4 to 9.5

*All interior surfaces coated with phenolic paint; Two coats phenolic 302 over one coat phenolic 300. In addition, all exterior surfaces covered with a 2.54 cm (1") fiberglass insulation (0.0467 W/m-K, 0.027 BTU-ft/hr-ft^2/°F).

Table 3.5-2. Typical Initial Fission Product Simulant Concentrations for A9 Test

Fission Product	Concentration (mg/m3)
Species Elemental iodine	100
Particulate-associated iodine	5
Methyl iodide	2
Cesium	5
Uranium	5

Table 3.5-3. Spray flow rates and Solutions used in A9 Test

Spray Characteristic and Period	Value
First Period	
Total flow rate	9.324 liters/s
Volume sprayed	1678 liters
Spraying pressure (differential)	352 kPa

Solution	Fresh, room temperature, 3000 ppm boron as H_3BO_3 in demineralized water, NaOH added to pH of 9.5
Start Time	1,800 s
Stop Time	1,980 s
Duration	180 s
Second Period	
Total flow rate (liters/s)	9.513 liters/s
Volume sprayed (liters)	1712 liters
Spraying pressure (differential)	359 kPa
Solution	Fresh, room temperature, 3000 ppm boron as H_3BO_3 in demineralized water, NaOH added to pH of 9.5
Start Time	3,300 s
Stop Time	3,480 s
Duration	180 s
Third Period	
Total flow rate	9.387 liters/s
Volume sprayed	5632 liters
Spraying pressure (differential)	352 kPa
Solution	Fresh, room temperature, 3000 ppm boron as H_3BO_3 in demineralized water, NaOH added to pH of 9.5
Start Time	5,400 s
Stop Time	6,000 s
Duration	600 s

Fourth Period	
Total flow rate	8.694 liters/s
Volume sprayed	31,298 liters
Spraying pressure (differential)	338 kPa
Solution	Solution in main vessel sump recirculated, no heat exchanger used
Start Time	12,600 s
Stop Time	16,200 s
Duration	3,600 s

3.5.3 MELCOR Input Model

This A9 test was modeled in MELCOR as six control volumes were specified to use non-equilibrium thermodynamics model. However, one control volume was a time-independent volume used to model a constant, ambient environment (see Figure 3.5-2). A recirculation flow path was provided; in the actual facility, there can be downward flow in some fraction of the dome with upflow in the remaining dome region. The area of that recirculation flow path was set to 1 m^2. All heat structures used the steady-state temperature-gradient self-initialization option. Radiation heat transfer was modeled with the emissivity set to 0.80.

The fission product simulants were specified to be class 2 (CsOH), class 4 (I_2), and class 10 (U), and the water droplets were in class 14 (H_2O). Three components (the default is 1 component) with 10 aerosol distribution size bins from 0.1 μm to 50 μm were specified. The aerosol density was set to 2,500 kg/m^3 (2.5 g/cm^3) and represents a compromise between the density of cesium particles and uranium oxide particles. These fission products were injected over a 10 min period at the start of the calculation. The cesium and uranium were injected as aerosols. The iodine was injected in vapor form.

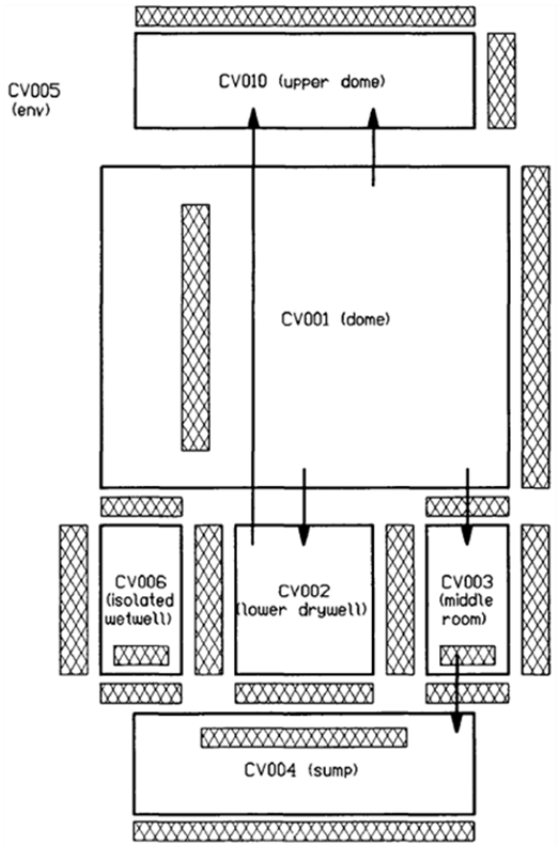

Figure 3.5-2. MELCOR Model A9 Experiment

Two sprays were defined, one for the (multiple) fresh sprays and one for the spray recirculating from the test vessel sump. Both spray sources were specified to have a five-size droplet distribution with equal numbers of droplets in each bin, and with the droplet AMMD of 1220 μm and GSD of 1.5 taken from Table 3.5-1. In these calculations, 70% of the spray flow rate was assumed to interact fully with the adjacent volume atmosphere. However, a MELCOR input parameter (iodine partition coefficient for spray) can be used to account for chemical interaction effects, as reagents such as water and/or borax solution react reversibly with iodine. This parameter was set to 3000 and 1 for the two spray types specified in the MELCOR model.

The calculations were begun at t = -18000 s (-5 hr), with t = 0 s taken as the start of the 10 min aerosol injection period. The user-specified, maximum time-step in these calculations was 2 s during the spray injection periods, and 20 s between the spray injection periods. A detailed discussion of the initial MELCOR model was given in SAND94-2316 [3.5.1].

3.5.4 Results of Analysis

Both MELCOR 1.8.6 (V3964) and 2.1 (v6110) were used to perform the calculations. The effect of the sprays on containment atmosphere pressure is shown in Figure 3.5-3, which compares calculated MELCOR results (both MELCOR 1.8.6 and 2.1) with test data for the test. The individual fresh spray periods (at 1,800 to 1,980 s, 3,300 to 3480 s, and 5,400 to 6,000 s) are predicted to cause rapid declines in the test vessel pressure, with the test vessel pressure recovering somewhat between sprays; this is in qualitative agreement with test data. The discrepancy is most noticeable after the second spray period because the spray period is longer than the first two, and because small changes in steam condensation have relatively larger effects at the lower pressures found later in this transient.

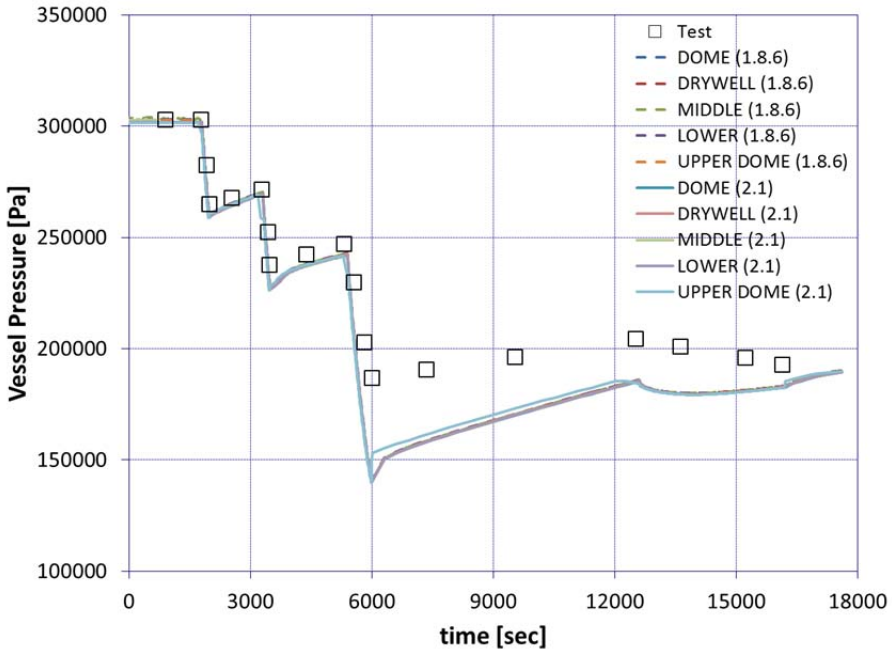

Figure 3.5-3. Calculated (MELCOR 1.8.6 and 2.1) Vessel Pressure for CSE A9 Test

The effect of the sprays on containment atmosphere temperature is shown in Figure 3.5-4, which shows calculated MELCOR results (1.8.6 and 2.1 versions) compared with test data. In this problem, liquid pools accumulate in the lower drywell and in the sump, with very small amounts in the dome and middle room volumes. As found for the vessel pressure, the three fresh spray periods are predicted to cause rapid declines in the test vessel temperature, with the test vessel temperature recovering somewhat between sprays; this is in qualitative agreement with test data. The recirculating spray was observed in the experiment to produce a small pressure increase and a temperature decline. The pressure increase is also found in the MELCOR results, but the calculated vessel temperatures remain nearly constant or increase slightly.

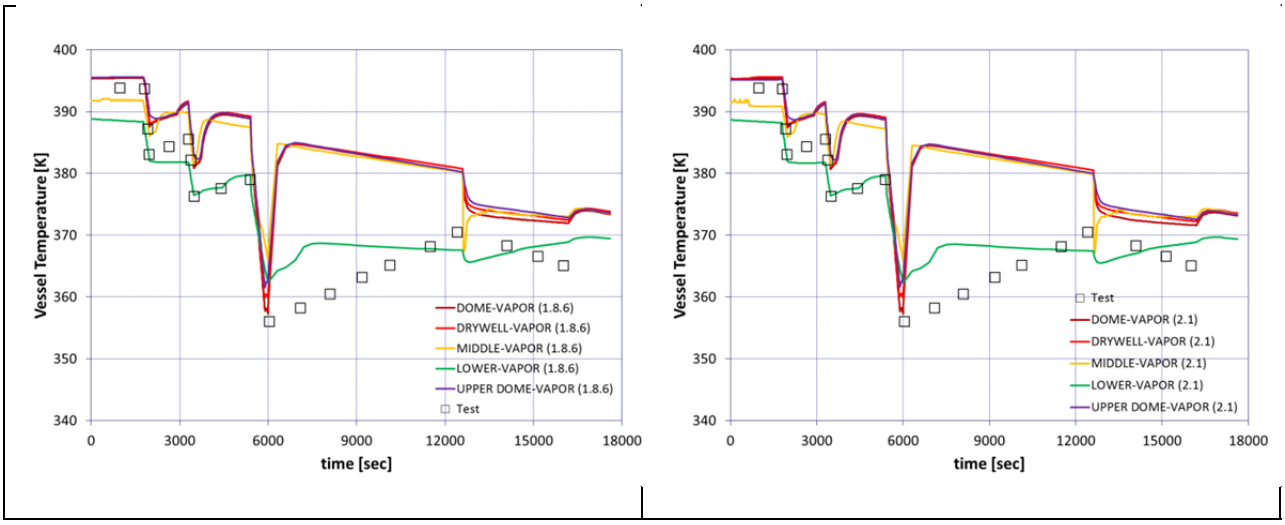

(a) (b)

Figure 3.5-4. Calculated Vessel (Heat Structure) Temperatures for CSE A9 Test (a) MELCOR 1.8.6 and (b) MELCOR 2.1

The test data included in Figure 3.5-4 represent the arithmetic average reading of five thermocouples located in the main room (dome) vapor space. The pressure measurement reflects global vessel conditions because pressure differentials between different parts of the vessel are very small; in contrast, the temperature measurement represents only localized conditions near the thermocouples and may not reflect the average response in either the dome or the remainder of the vessel.

Figure 3.5-5 presents the calculated concentrations of cesium aerosol in various regions in the test vessel atmosphere and compared with test data. The concentrations shown in this figure are the mass of airborne aerosol in the control volume atmosphere divided by the volume. The calculated concentrations of airborne cesium aerosols agree qualitatively with the measured concentrations. The code predicts stepwise decreases in concentration in the dome atmosphere during each of the three fresh spray periods, and a more gradual, linear decline during the longer, late-time recirculation period, as observed in the test. Also, the concentrations of airborne cesium aerosols in the middle room and lower room rise gradually during the first portion of the test until they approach the concentration in the dome, after which the concentrations throughout the vessel remain nearly equal as they drop uniformly.

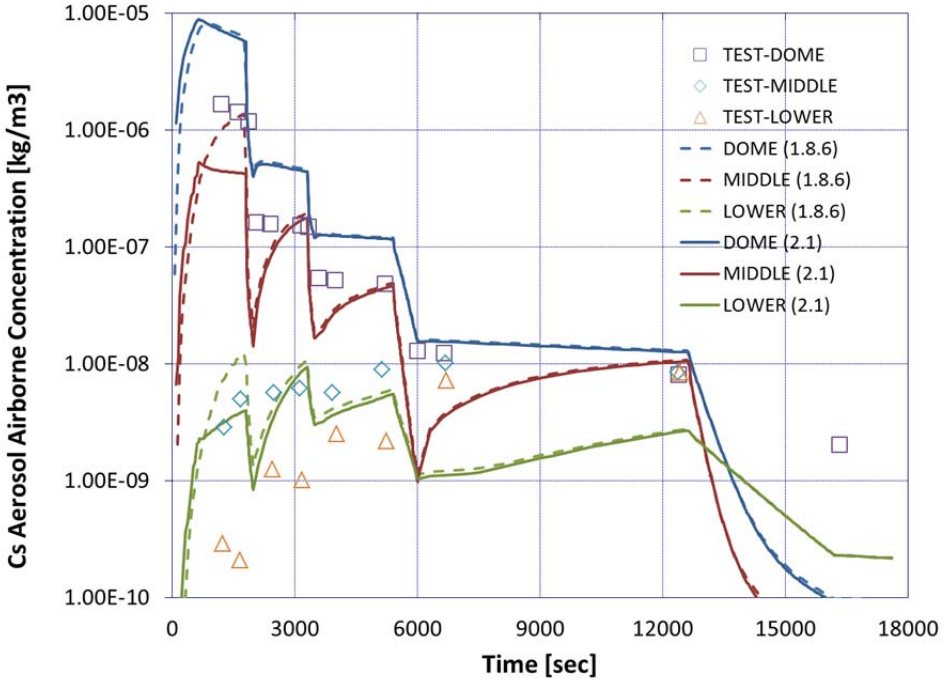

Figure 3.5-5. Calculated Aerosol Airborne Concentration for Cs

There are, however, a number of significant quantitative discrepancies in the calculated aerosol response compared with measured test data. The calculated concentration of airborne cesium aerosols in the dome remains very nearly constant between spray periods, while the test data show a substantial decline prior to the first spray period. Further, the stepwise decreases in concentration predicted in the dome atmosphere during each of the fresh spray periods are about equal, with slightly more aerosol removal occurring with each successive fresh spray, while the test data show much more aerosol removal during the first spray period than during subsequent sprays. Finally, the airborne concentrations in the middle and lower rooms equilibrate with the dome concentration at a much higher value in the calculation than was measured.

Figure 3.5-6 presents the calculated concentrations of uranium aerosol in the test vessel atmosphere, compared with experimental data for the same rooms. The predicted response of the uranium aerosol closely resembles the data already presented for the cesium aerosols. The calculated concentrations of airborne uranium aerosols agree qualitatively with the measured concentration, but there are a number of quantitative discrepancies. The calculated concentration of airborne uranium aerosols in the dome remains very nearly constant before the initial spray periods, while the test data show slow decreases in concentrations within each of the spray periods. Also, the test data show much more aerosol removal during the first spray period than predicted in the calculation. The initial concentration of uranium is given as 5 mg/m^3, which is equal to the initial cesium aerosol airborne concentration; however, the uranium aerosol airborne concentration measured prior to the first spray period is much lower than the

corresponding cesium aerosol airborne concentration given for the same test. The uranium aerosol airborne concentrations measured prior to the first spray period for the other CSE tests are generally at least an order of magnitude higher than the results given for this test, and are more similar to the corresponding cesium aerosol airborne concentrations given. Since the aerosol source was nominally the same in all the intermittent-spray tests, and since the only major difference between A9 test and other tests in the same series is the spray concentration, there is an inconsistency between the given initial concentrations in the early-time measurement. Also, note that samples were not analyzed for uranium after the first spray period.

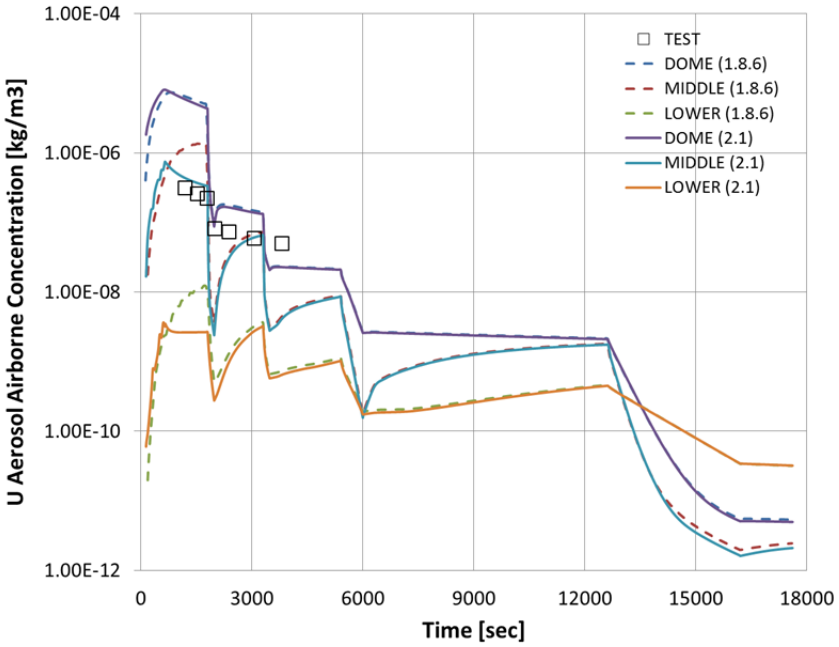

Figure 3.5-6. Calculated Aerosol Airborne Concentration for Uranium

Figure 3.5-7 presents the concentrations of iodine vapor in the test vessel atmosphere compared with test data. The default class description for iodine in MELCOR (i.e., class 4) includes a vapor pressure characteristic of iodine, so that iodine could potentially be present in either aerosol or vapor form, depending on other conditions such as volume pressure and temperature; in this problem, the conditions are such that iodine is predicted to be present only in vapor form. The calculated concentrations of airborne elemental iodine vapor show large stepwise decreases in concentration in the dome atmosphere during each of the three fresh spray periods, and during the fourth recirculating spray. The calculated washout rates during the three fresh spray periods are all nearly equal, and the calculated washout rate during the recirculating spray is only slightly slower than during the fresh sprays. The test data, in contrast, show significant iodine removal only during the first fresh spray period, with little or no further removal by the later sprays. The iodine removal measured during that first spray period is much greater than calculated, as was also the case for the cesium and uranium aerosol removal rates. However, owing to the continued removal of iodine in the

calculation, the predicted concentrations of airborne iodine vapor in the vessel are much lower than the measured airborne iodine concentrations late in the test; this is opposite to the case for aerosol behavior, where the code predicts higher, late-time airborne aerosol concentrations than measured.

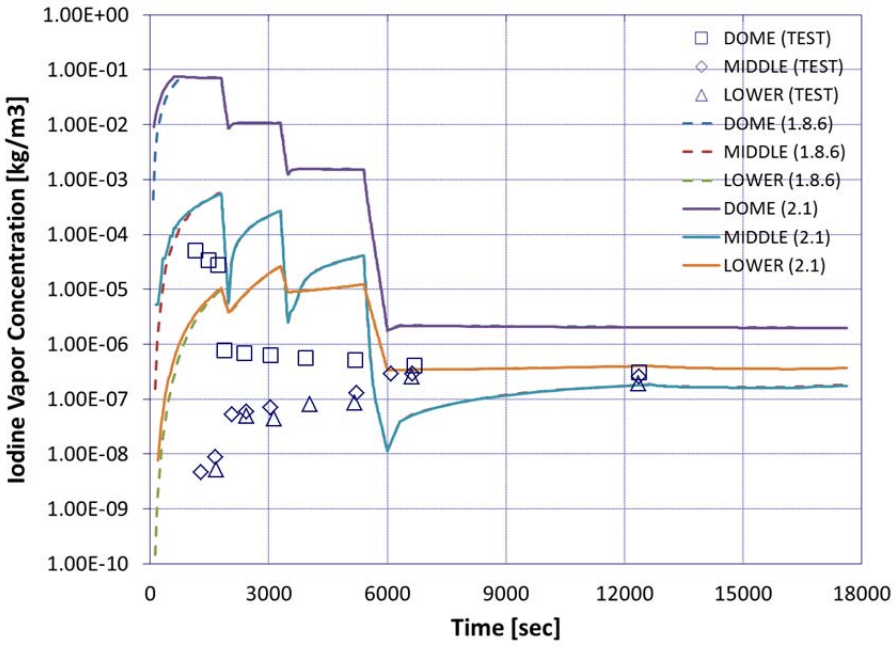

Figure 3.5-7. Calculated Aerosol Airborne Concentration for Iodine [3.5.1]

3.5.5 Discussion

The results for this A9 benchmark test show that the thermal-hydraulic responses calculated by MELCOR are in qualitative agreement with test data during the spray periods. However, during the recovery period, MELCOR shows a more rapid heat up than the experiment. The detail is not understood at this time. This discrepancy is explained by the inaccurate modeling of heat transfer between fluids and heat structures. This is most likely due to a deficiency in the input model. In terms of the suspended aerosol concentration, MELCOR agrees closely with the experimental results during the spray periods. However, MELCOR is lacking a detailed iodine chemistry model for this phenomenon in terms of the elemental iodine vapor removal. Thus, future improvement is necessary.

3.5.6 References

[3.5.1] L.N. Kmetyk, MELCOR 1.8.3 Assessment: CSE Containment Spray Experiments, SAND94-2316, Sandia National Laboratories, Albuquerque, New Mexico, December 1994.

[3.5.2] R.K. Hilliard, et.al, ”Removal of Iodine and Particles from Containment Atmospheres by Sprays – Containment Systems Experiment – Interim Report,

BNWL-1244, Pacific Northwest Laboratories, Richland, Washington, February 1970.

[3.5.3] R.K. Hilliard and A.K. Postma, Effect of Spray Flow Rate on Washout of Gases and Particles in the Containment System Experiment, Pacific Northwest Laboratories, Richland, Washington, July 1971.

3.6 Analysis of the Cora 13 (ISP 31) Experiment

3.6.1 Background

The CORA Facility was used to conduct ISP-31 [3.6.1]. The ISP-31 test bundle consisted of 16 heater rods, 7 unheated rods representing typical pressurized water reactor (PWR) fuel elements, and 2 absorber rods (Figure 3.6-1). The heater rods were 1.96 m long and made of tungsten, while the cladding was made of Zircaloy-4. The test bundle was cooled with an argon/steam mixture that entered at the bottom of the bundle.

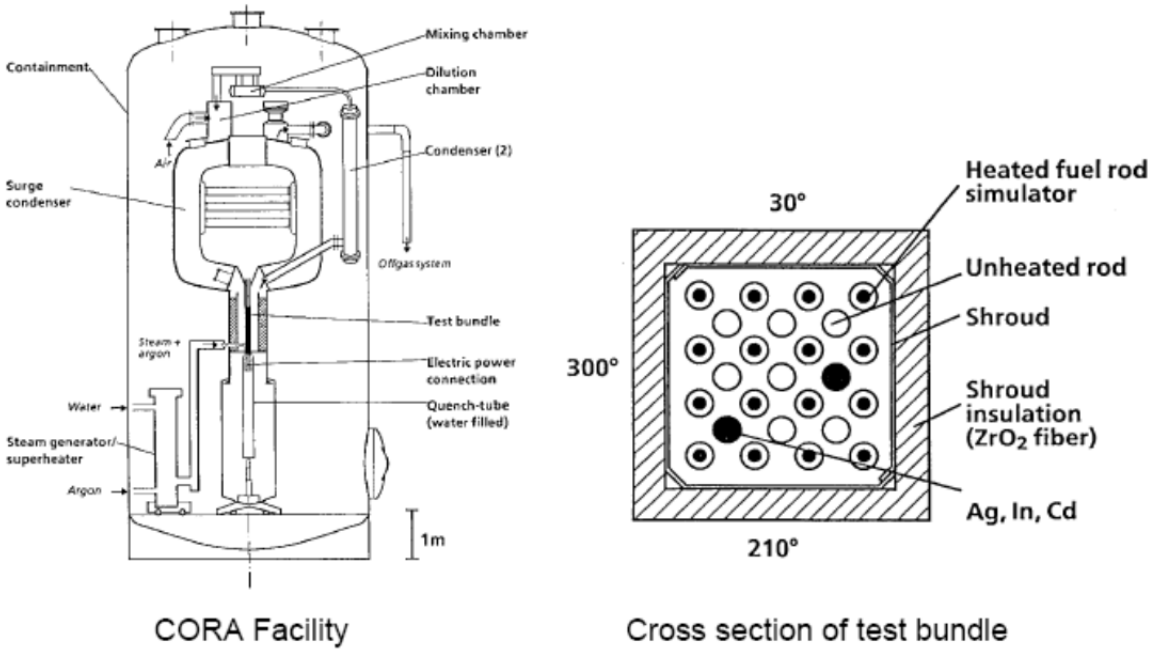

Figure 3.6-1. CORA Test Facility and Cross Section of Test Bundle

The experiment consisted of 3 phases: a preheat phase, a transient heat-up phase, and a cool-down phase. The preheat phase lasted from 0 to 3,000 s. During this time, the rods were heated at a low electric power input of 0.65 kW in preparation for the protracted heating phase - during which period the actual test is performed. During the transient heat-up phase, which lasted from 3,000 to 4,870 seconds, the heater rod power was increased linearly in time from 6 to 27 kW. Of course, the electrical heating produced an increase in the fuel rod temperatures. By 4,000 seconds, fuel-cladding temperatures were beginning to exceed 1,273 K, whereupon measurable hydrogen production was detected. After this point, oxidation energy became increasingly important as it accounted for nearly 50% of the total heat input during the experiment. Shortly after 4,200 seconds, cladding temperatures in the upper regions of the bundle were observed to increase very rapidly, exceeding the melting point of both the thermocouples in use, as well as the zircaloy cladding. The final phase was initiated at 4,870 seconds when the bundle was quenched by means of a water-filled quench

cylinder that rose directly into the test bundle. Finally, the rods were cooled for 180 seconds.

Key phenomena in the CORA-13 tests were oxidation/hydrogen generation, relocation of core materials, forced convection, conduction, radiation, and fluid-structure heat transfer.

3.6.2 Nodalization

The present MELCOR analysis is based on an earlier study performed with MELCOR 1.8.1 [3.6.2]. The MELCOR model for the fuel rod section split the test bundle into four radial rings. Referring to Figure 3.6-1, the first ring included a central unheated rod. The second ring had four heated rods, while the third ring had two absorber rods and six unheated rods. The last ring had twelve heated rods. The MELCOR CVH nodalization is shown in Figure 3.6-2. The fuel bundle is split into three control volumes: CV210, CV220, and CV230 using 6, 4 and 6 axial COR cells, respectively.

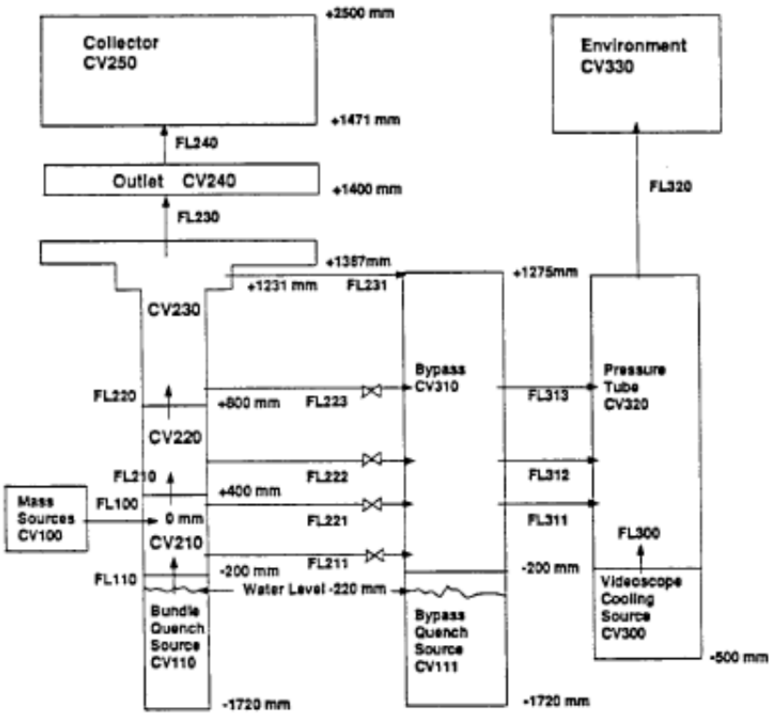

Figure 3.6-2 MELCOR CVH Nodalization of the CORA-13 Experiment Facililty

3.6.3 MELCOR Input Specifications

In the 185 deck, the control rods were modeled as SS (Supporting Structure), while the guide tubes were NS (Non-supporting Structure). This meant that the guide tubes and control rods were separate components and therefore, only connected for heat transfer purposes via the gas convection and radiation. In the 2.1 deck, the control rods and

guide tubes were modeled as NS, so that both are in the same component and have the same temperature.

Using NS instead of SS introduced some problems – the core requires SS in the lower cells for support. This was supplied by introducing fictitious SS (Zr) in the cells below the fuel rods.

A note on electrically heated rods: the code will allow heated fuel to stand on its own without support; however, the clad does not enjoy this benefit and will fall off without the SS.

For the most part, default parameter options were used in the present MELCOR model of CORA-13, with the following exceptions that were required primarily because of the specific nature of the CORA Facility:

```
COR_SC  8  ! N   SCnumber     Value       Index1 Index2
! SC1132 ROD FAILURE TEMPERATURE:
             1   1132        0.280000E+04   1
! SC1151 CONGLOMERATE DEBRIS SURFACE AREA COEFFS:
             2   1151        0.100000E+01   3      5  !FAMIN(CAN) = 1.0
             3   1151        0.000000E+00   3      6  !FBMAX(CAN) = 0.0
!SC1501 CANISTER MASS/SURFACE AREA SPLITS:
             4   1501        0.000000E+00   1
             5   1501        0.000000E+00   2
             6   1501        0.000000E+00   3
             7   1501        0.100000E+01   4
             8   1501        0.000000E+00   5
```

3.6.4 Results of Analysis

The CORA 13 experiment was simulated using MELCOR 2.1 Revision 4485 and the results are compared with data as well as calculations performed with previous versions of MELCOR. The problem was also rerun using MELCOR 2.1 Revision 6110.

Figure 3.6-3 through Figure 3.6-5 compare the calculated and measured first-ring axial fuel temperature at various levels. The figures show that the code was able to calculate the fuel temperature mostly to within 100 K, especially during the first 4,200 s of the transient.

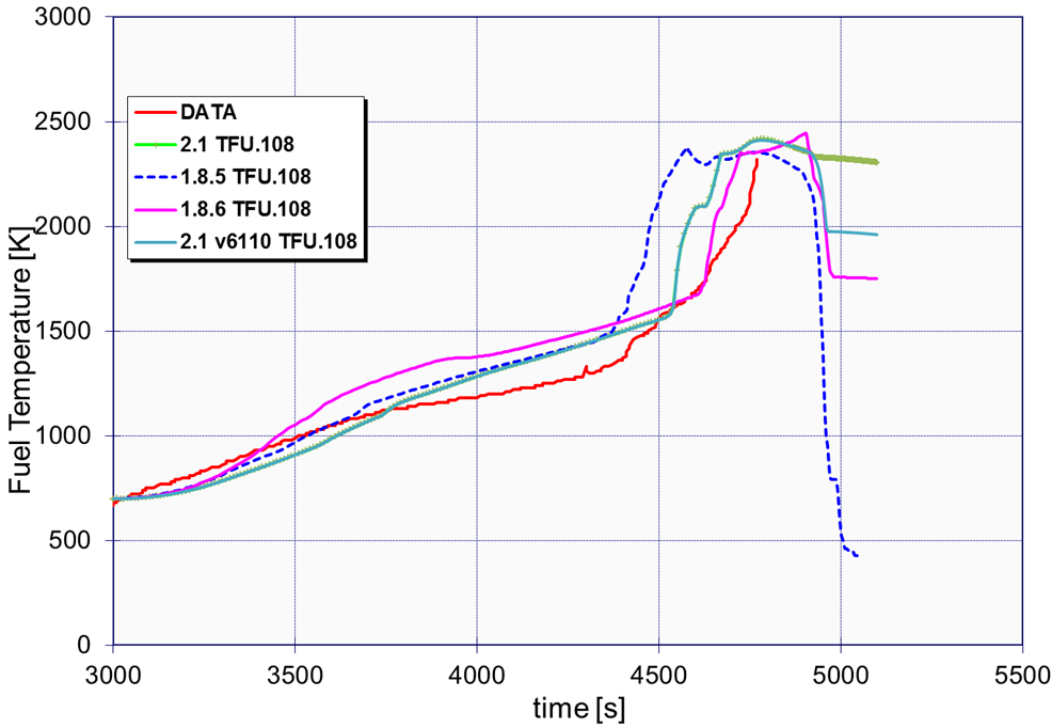

Figure 3.6-3 Measured and Calculated Fuel Temperature at 350 mm

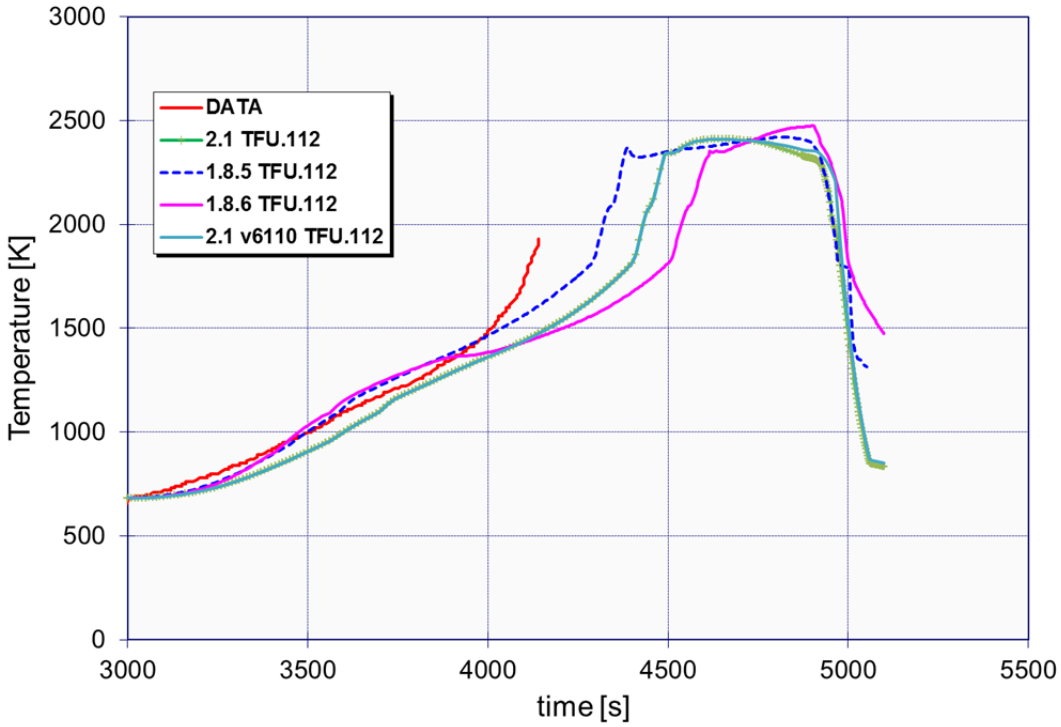

Figure 3.6-4 Measured and Calculated Fuel Temperature at 750 mm

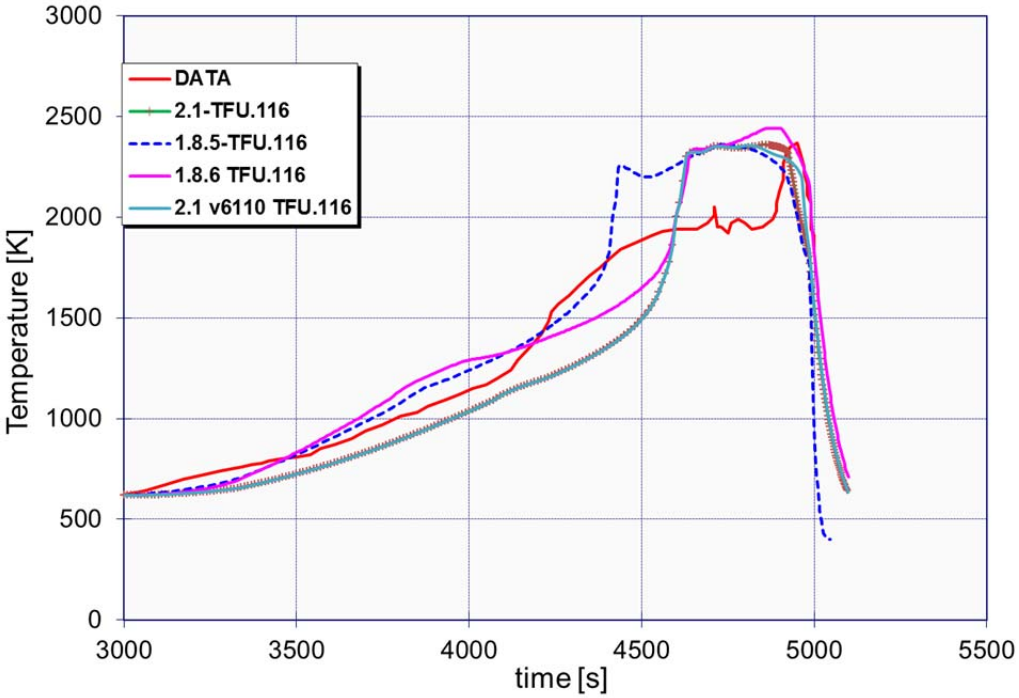

Figure 3.6-5 Measured and Calculated Fuel Temperature at 1150 mm

From 0 to 3,000 s, the experiment was being cooled by forced convection and the fuel temperature was predicted within 15 K or less. Radiation heat transfer was not important at this point as the fuel temperature was ~700 K. As a rule of thumb, radiation becomes important when the temperature exceeds about 1000 K. Furthermore, the amount of oxidation energy released from 0 to 3,000 s was negligible. The comparisons between MELCOR and the experiment during this time period are excellent, indicating that MELCOR's treatment of conduction and convection processes for this test are also reasonably good.

From 3,000 to 4,870 s, oxidation accounted for nearly 50% of the total heat input during the experiment. About 90% of the oxidation energy was released from 4300 to 4800 s, and that timeframe is also where the largest difference between the calculated and measured temperatures occurred. These differences were on the order of 200 to 400 K and are believed to have occurred more from the uncertainties in the modeling of heat losses from the test bundle than to deficiencies in the physics models themselves. In addition, the hydrogen production rate predicted by MELCOR differs somewhat from the measured value, especially with respect to the time signature (Figure 3.6-6). A large part of this discrepancy in the time signature is believed to be due to a delay in the response of the hydrogen measurement devices. The delay is due to the presence of long flow paths and volumes between the test bundle and the measurement sensor. These errors have been discussed in CORA and QUENCH workshops held annually at the Kernforschungszentrum Karlsruhe (KfK) facility but have never been published. The magnitude of the hydrogen produced up until the time of the quench compares fairly

well with the experiment; however, MELCOR versions 1.8.5, 1.8.6, and 2.1 fail to capture the burst of hydrogen produced when the reflooding action produces steam during the quench phase. The MELCOR 1.8.6 simulation produced 145 g, while the MELCOR 1.8.5 simulation generated 160 g. The experimental value, including the quench-phase hydrogen was 210 g. If we subtract the amount of hydrogen generated during the quench, roughly 170 g were generated during the experiment, well in line with the MELCOR 1.8.5 calculated results.

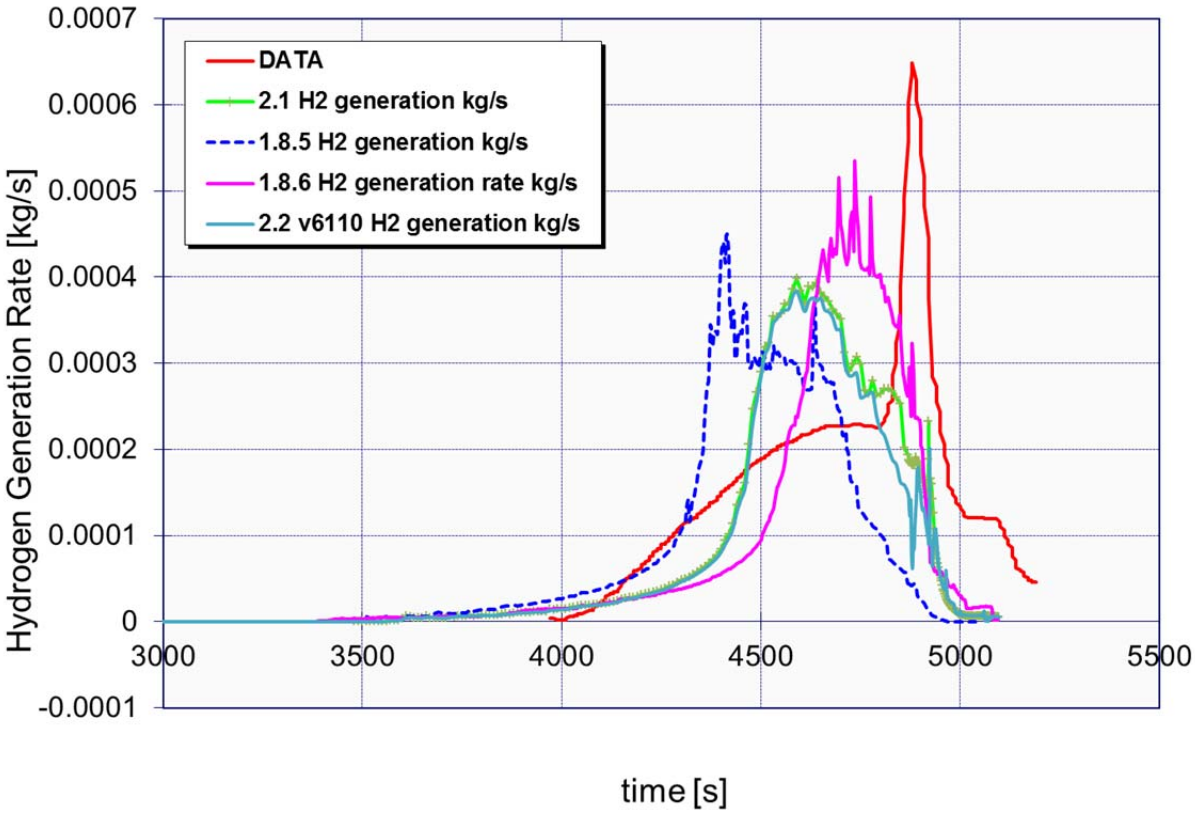

Figure 3.6-6 Measured and Calculated Hydrogen Generation Rate.

The causes of MELCOR's failure to predict significant hydrogen during the quench phase is attributable to two factors. One of these is that the reflooding procedure, by raising a cylinder of water over the bundle, probably caused an inverted annular flow situation, with film boiling on the clad. This was simulated in the problem by simply injecting water into the lower CVs; MELCOR is not going to simulate the inverted annular flow well with this model, reducing the possible oxidation of clad during reflood. Another factor not included in MELCOR is any quench-induced fracturing of the otherwise protective oxide layer on the cladding surface. Some experiments in the QUENCH facility suggest that such fracturing can result in high transient oxidation rates owing to the exposure of fresh metallic zircaloy following cool-down fracturing of the oxide layer. If needed, such features will be added to MELCOR following improvement to the quenching thermal-hydraulics modeling.

In the intermediate period where radiation was important (3,500 s and above) and the oxidation energy was relatively negligible (0 to 4,300 s), we have an overlapping period (3,500 to 4,300 s) where radiation was important and not overshadowed by oxidation. We note from the temperature figures that the calculated and measured temperatures were in good agreement, generally within 100 K in that regime. This shows the adequacy of the radiation model.

3.6.5 Summary

Overall, the MELCOR 2.1 component temperatures were about the same as those predicted using MELCOR 1.8.5 and 1.8.6. Calculated and experimental values for hydrogen generation are close if the quench period is not considered. Additionally, future assessment of MELCOR in this area is likely to come from more recent (and better-characterized) experiments from the QUENCH program.

3.6.6 References

[3.6.1] Hagen, S., et al., Results of SFD Experiment CORA-13 (OECD International Standard Problem 31) KfK 5054, February 1993.

[3.6.2] Gross, R.J. S.L. Thompson and G.M. Martinez, MELCOR 1.8.1 Calculations of ISP-31: The CORA-13 Experiment, SAND92-2863, June 1993.

3.7 Analysis of Aerosol Behavior from the Demona-B3 Experiment

3.7.1 Background

The DEMONA-B3 test emphasized phenomena associated with steam condensation effects on aerosol settling.

The DEMONA-B3 test was performed in the Battelle Model Containment (BMC) facility in Frankfurt, Germany, for the purpose of providing data on containment-building response to severe accident conditions with particular emphasis on characterizing the depletion rate of hygroscopic aerosol under varying humidity and thermal-hydraulic conditions. The DEMONA-B3 experiment has been widely studied by various aerosol and containment analysis codes in the context of a benchmark exercise. The results of the multi-code comparison are found in a report by Schock [3.7.1]. Details on the facility and the B3 experiment were taken principally from reference [3.7.1] with supplementary data from [3.7.3]. Later, the actual workshop report became available, which has more detail on the facility as configured for the DEMONA-B3 test [3.7.1].

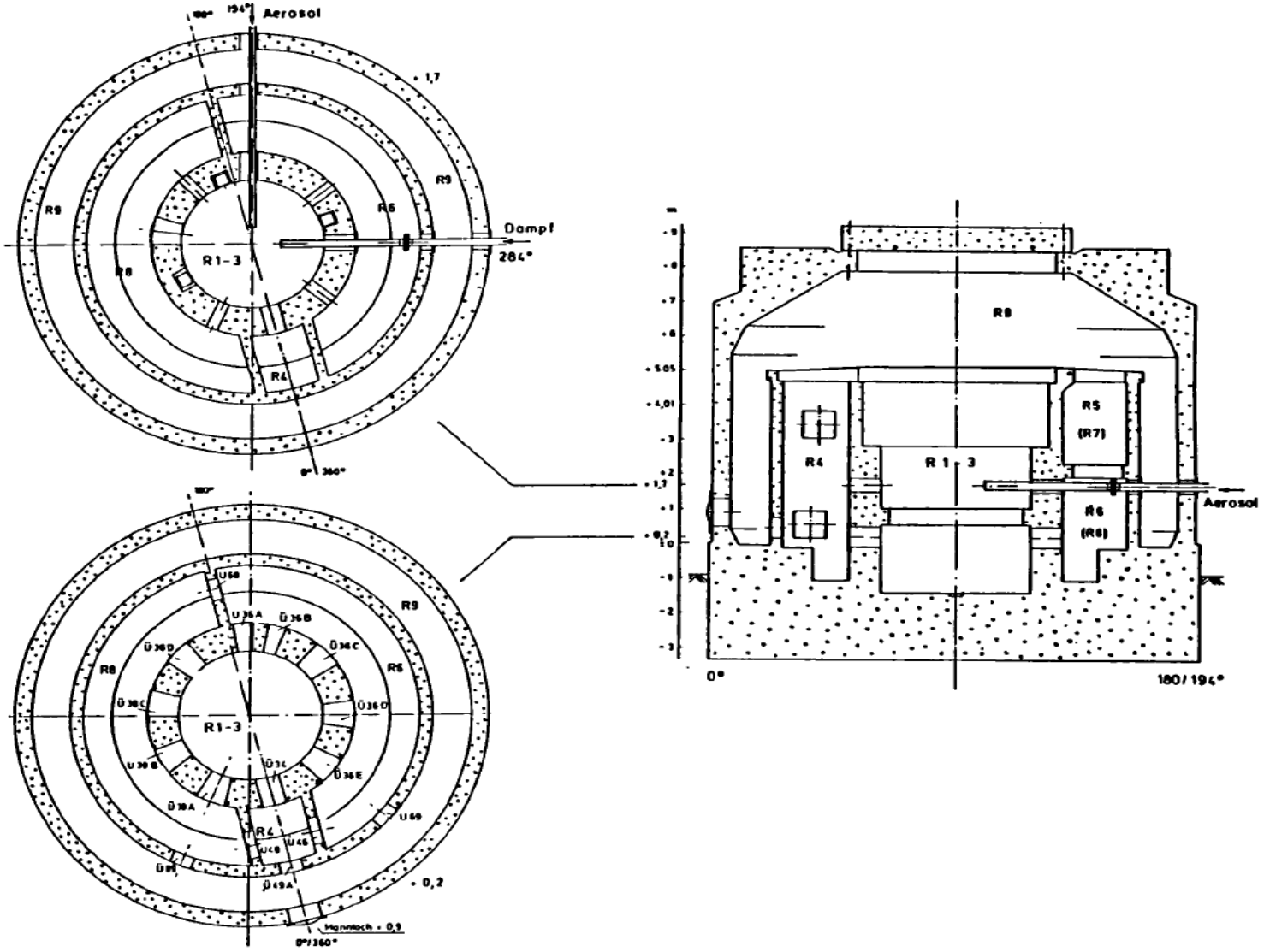

Figure 3.7-1. Schematic of BMC facility from Ref.[3.7.1]

A schematic of the test facility is shown in Figure 3.7-1. This figure shows the side view and top views at two elevations. The containment building was a mostly concrete construction with multiple connected rooms. The internal volume was 637 m^3 for this test. An artist's rendition of the facility is shown in Figure 3.7-2, which gives a better idea of the layout and also the dimensions and shape of the typical openings [3.7.4].

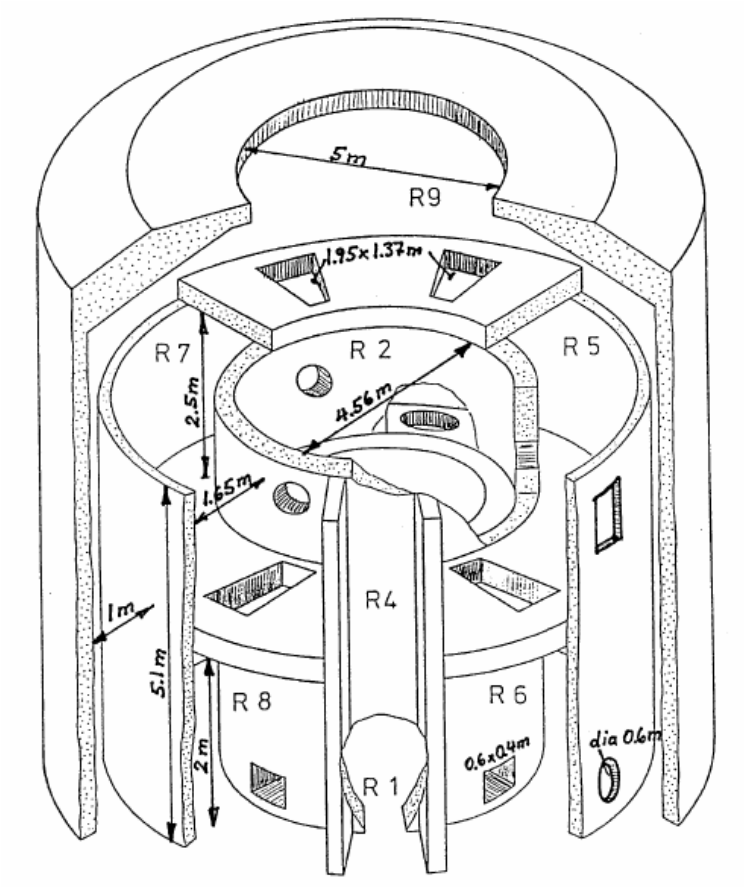

Figure 3.7-2. Artist's sketch of the BMC facility

3.7.2 B3 Experiment

The test was conducted over a period of 3 days in 1986. There were five phases:

a) Phase 1: The air was purged out of the containment to achieve a pure steam atmosphere (0.4-7.1 h).
b) Phase 2: Inject steam over 2 days to heat up BMC structure, at a constant pressure of 1.7 bar.
c) Phase 3: Hot air and aerosol were injected from 48.4 to 49.3 h, raising the pressure to 3 bar (partial pressures, air 1.3 bar, steam 1.7 bar). A small amount

of steam was also injected to maintain the 1.7 bar steam partial pressure. The measured peak aerosol concentration was 9 g/m^3.

d) Phase 4: Aerosol depletion 49.3-71.1 h. During this phase the pressure was kept constant at 3 bar by controlling the steam injection rate. Some air leakage occurs in the facility, so the air partial pressure slowly decreases and the steam pressure increases. The aerosol concentration was measured during this phase.
e) Phase 5: Cooldown (this was ignored in modeling).

Both the steam and the air/aerosol were injected into the central volume (air/aerosol into R1, steam into R3).

Figure 3.7-3 shows the aerosol (air) injection history. Figure 3.7-4 shows the steam injection history for the test. The air leakage rate from the facility was approximated in MELCOR as a constant rate of 3.6 g/s via a control function.

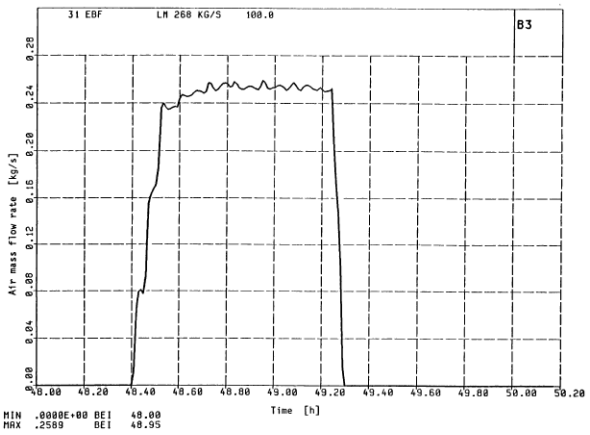

Figure 3.7-3. Aerosol air injection rate

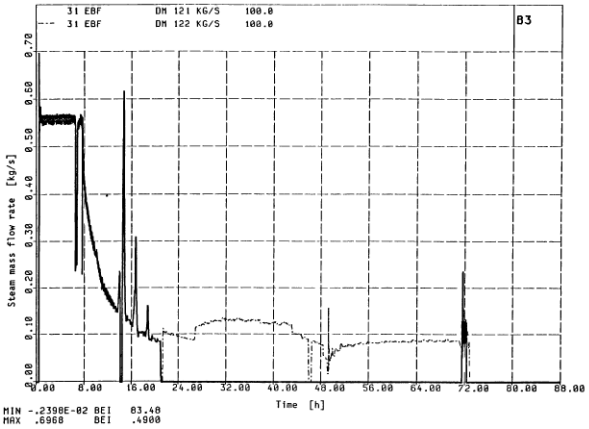

Figure 3.7-4. Steam injection rate

3.7.2.1 Nodalization

Since a description of the BMC facility as set up for DEMONA was not available initially, the nodalization was developed from a MELCOR deck used for the VANAM-M3 test and various references. The VANAM deck was modified by removing the floors in the central rooms to form one large volume, and adding openings between rooms to simulate what was known about the DEMONA configuration from Figure 3.7-1. This converts the CVs into essentially a large single volume, which was in fact the suggested modeling approach for the benchmark exercise; the VANAM multi-compartment description is probably overkill. The nodalization used is shown below in Figure 3.7-5. The diagram illustrates approximate elevations and volumes of the rooms in the facility as well as the flow paths between the rooms. The central volume is made up of rooms R1-R3. Heat structures, although modeled in the MELCOR input deck, are not shown in the nodalization diagram. Later, more information was obtained about the DEMONA test, and a few openings in the upper wall between R2 and R5/R7 were missed in the deck setup; it is thought that this has an insignificant effect on the results.

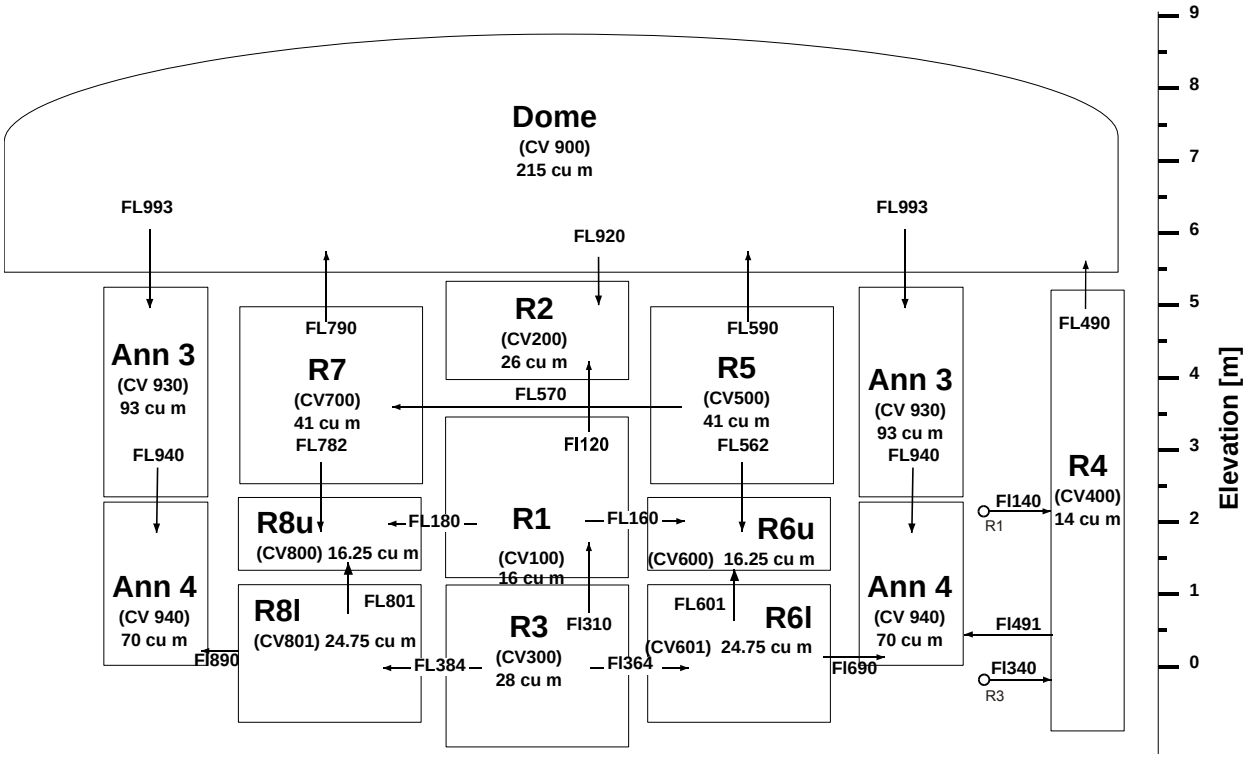

Figure 3.7-5. MELCOR node diagram for DEMONA experiment

3.7.2.2 MELCOR Input Specifications

The problem was run with MELCOR Revision 6110.

The aerosol was specified as a constant rate of 3.575 g/s (215 g/min) from the test description: peak tin feed rate of 211 g/min, generator efficiency of 0.8, and SnO_2/Sn molecular weight ratio of 1.27. Aerosol size, although not measured directly in the experiment, was taken from descriptions of the distribution used by most of the participants: log-normal distribution with 0.35 μm mass median diameter, standard deviation of 2.0. The aerosol was sourced into RN class 12, AG; despite the class name, the molecular weight of this group is actually that of Sn.

The air injection rate was approximated from Figure 3.7-3 as a table ramping up to 0.26 kg/s over 500s, then down to 0 over 500s at 49.28h; the SnO_2 aerosol injection was simulated using a similar table. The air injection temperature was taken as a constant 603K.

From Figure 3.7-4, the steam injection rate during the aerosol injection-depletion phases was taken as a constant 0.08 kg/s into R3. The air leakage during phase 4 was taken as a constant 3.6 g/s. Table 3.7-1 summarizes details of all injections/depletions.

Table 3.7-1. Injection rates during Aerosol injection/depletion phases

Material	Rate	Start time	End time	Duration	Location
SnO_2	215g/min	48.4h	49.3h	0.9h	R1
Aerosol Air	0.26kg/s	48.4h	49.3h	0.9h	R1
Steam	0.08kg/s	48.4h	71.1h	--	R3

Three approaches were taken in the course of modeling the DEMONA test. Initially, it was attempted to approximate the initial conditions at the start of the aerosol injection phase, using the specified atmosphere conditions and assumed temperature distributions in the heat structures; however, it was found that the results of the aerosol depletion phase are extremely sensitive to the atmospheric conditions, particularly the relative humidity, and the assumed initial conditions were not close enough, resulting in underprediction of the rate of aerosol depletion. The second and third attempt included the heatup phase, using a property-specified environment CV attached to the facility to set the correct atmosphere steam and air partial pressures and temperature, rather than attempting to control these with the steam injection rate.

In the second attempt, the atmosphere conditions in the attached large CV were changed during the aerosol injection/depletion phases to those measured during the depletion phase. The results from this problem were also not very close; it was thought that the relative humidity, maintained at 1 by the environment CV in MELCOR, was actually going higher in the experiment, causing fog to form and more steam to condense on the aerosol.

For the third attempt, the environment CV was valved off during the aerosol phases and only the steam/air injection sources were used. This resulted in excellent agreement with the test results.

3.7.2.3 Results of Analysis

Looking at Figure 3.7-6 and Figure 3.7-7, the relative humidity dips to 77% during the hot air/aerosol injection. Just afterwards, the aerosol mean diameter rises from 0.35 μm to 2.5 μm due to steam condensation on the aerosol.

Comparison of results with MELCOR 186 revealed no differences in results.

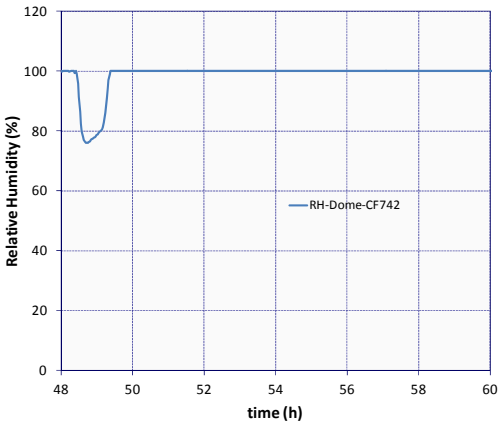

Figure 3.7-6. Relative humidity in central room

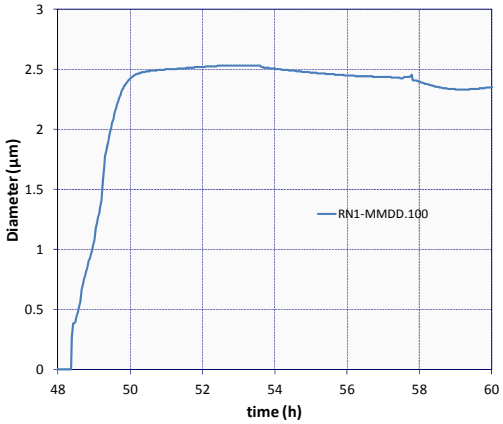

Figure 3.7-7. Mass mean diameter of aerosol

Figure 3.7-8 shows the fog formation immediately after the aerosol injection. The main result of the test, comparison of the aerosol depletion rate, is shown in Figure 3.7-9. The MELCOR result plotted, CF9001, is the mass of aerosol in the atmosphere divided by the facility volume, 637.3 m^3.

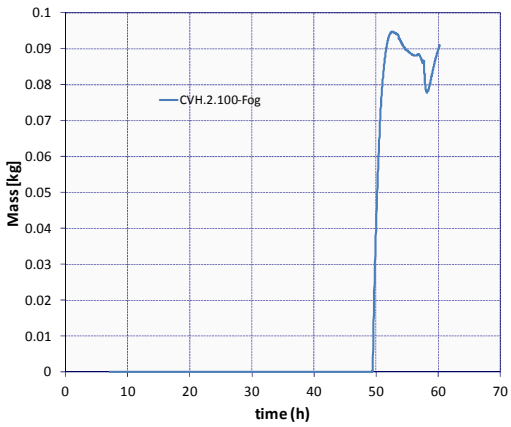

Figure 3.7-8. Fog formation after aerosol injection

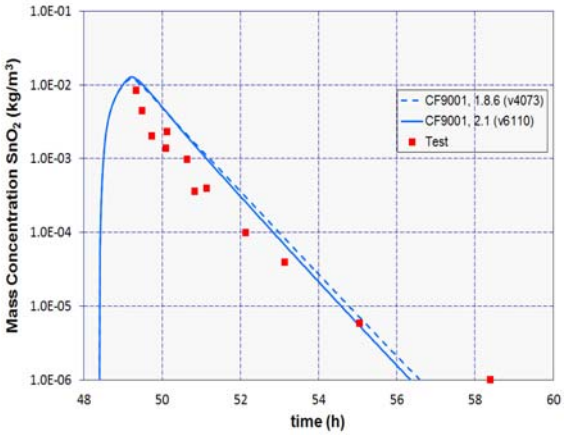

Figure 3.7-9. Aerosol depletion

3.7.3 Discussion

It was found that the result of this experiment was extremely dependent on the atmosphere and facility conditions during and after the aerosol injection phase. The MELCOR result matches the test result well for the depletion rate. The decrease in the air partial pressure during the depletion phase due to leakage from the facility also matched well; however, the increase in steam partial pressure during this phase was too high. It is unlikely that the injection rate could be too far off from the experiment, but

there was some question about whether to use the steam temperature upstream or downstream of the injection valve, which may make a difference.

3.7.4 References

[3.7.1] W. Schock, “Post-test Calculations of Aerosol Behavior in DEMONA Experiment B3 with Various Computer Codes Used in CEC Member States”, EUR-11374-EN, Commission of the European Communities (1988).

[3.7.2] J. Gauvain, “Post-test calculation of thermal-hydraulic behaviour in Demona experiment B3 with various computer codes used in EC Member States”, EUR-12197-EN, Commission of the European Communities (1989).

[3.7.3] W.O. Schikarski, “DEMONA – Research Program for the Demonstration of Nuclear Aerosol Behavior,” Kfk 3636, Kfk, Karlsruhe, Germany (1983).

[3.7.4] M. Heitsch, “Evaluation of Computational Fluid Dynamic Methods for Reactor Safety Analysis (ECORA)”, GRS (2004).

3.8 Analysis of Level Swell from the General Electric Large Vessel Blowdown and Level Swell Experiment – 5801-13.

3.8.1 Background

Rapid depressurization of a reactor vessel, due to either automatic depressurization system actuation or loss of the pressure boundary, may result in superheated liquid. Bubble generation in the liquid, usually nucleating at the wall, produces a swell in liquid level as the void fraction of the pool increases. The General Electric (GE) blowdown and level swell experiments [3.8.1] measured blowdown characteristics and level swell for two series of vessel experiments designated the “small blowdown vessel” and the “large blowdown vessel” tests. An assessment of the MELCOR code for the level swell of the large vessel experiment – 5801-13 – is presented.

A brief description of the large vessel test facility was given in reference [3.8.2] from which Figure 3.8-1 was adapted. Figure 3.8-1 shows the large blowdown vessel test apparatus including the vessel, the blowdown line, and instrumentation locations. The pressure vessel was 1.19 m (47 in) in diameter, 4.3 m (14 ft) long, and contained a volume of 4.5 m^3 (160 ft^3). The cylindrical body and hemispherical end caps of the vessel were 1 in-thick carbon steel and insulated on the outside. Initially saturated water at over 7.14 MPa (>1000 psia) partially filled the vessel; saturated steam filled the remainder of the tank. The vessel had a provision for a dip tube as part of the blowdown line. The dip tube had a 26.35 cm (10.374 in) inner diameter and was 0.4775 cm (0.188 in) thick. [3.8.2]

There were three basic types of measurements made during each test: pressures, pressure differences, and temperatures. Figure 3.8-1 includes the instrumentation arrangement used. Strain-gage pressure transducers were used for measuring vessel pressure and differential pressure. Iron-Constantan thermocouples were used for determining the fluid temperatures. Two-phase mixture densities in the measurement nodes were obtained from the measurements of the axial differential pressure, i.e., hydrostatic head of the fluid. [3.8.2]

The 5801-13 experiment employed a dip tube to depressurize the tank by evacuating the vapor space of the test vessel. A flow-limiting venturi nozzle within the blowdown line provided the characteristic “break size” of the experiment. The 5801-13 experiment simulated a 5.3975 cm (2-1/8 in) diameter break with a corresponding venturi throat size. The initial level of saturated water in the experiment was 1.6764 m (5.5 ft) from the base of the tank. The experiment was initiated by actuating a rupture disk in the blowdown line.

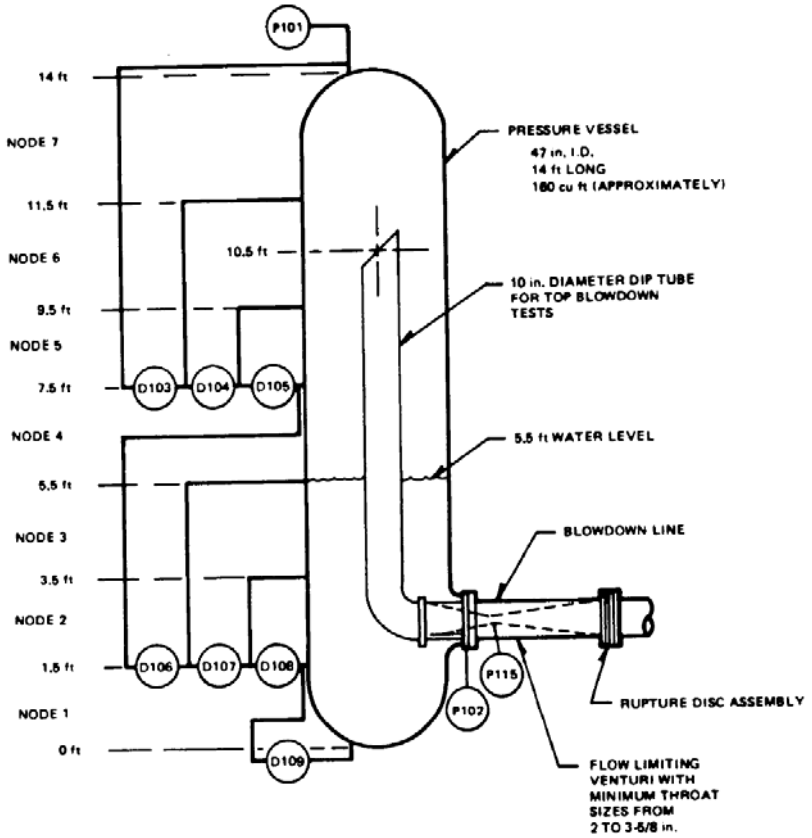

Figure 3.8-1. Schematic of GE Large Blowdown Vessel Test Facility

3.8.2 Analysis of the 5801-13 Experiment

3.8.2.1 Bubble Behavior in MELCOR

A simple discussion regarding bubble generation and transport is provided. A detailed description can be found in the MELCOR CVH/FL Reference Manual. This discussion is provided as background to the reader and is relevant to the analyses presented later.

During a blowdown where saturated water is present, superheating of the liquid results in bubble generation; however, MELCOR neither permits superheated liquid nor subcooled gas. An energy balance is employed to determine the mass of water which must change state to establish saturation; and in the case of superheated liquids, this mass corresponds to the mass of vapor bubbles generated. For stability reasons, a maximum void fraction of 0.4, which the user may adjust, is enforced as a MELCOR default. When the determined mass of vapor exceeds the void fraction limit, the excess mass and associated energy are placed directly into the atmosphere of the control volume, bypassing the bubble rise model.

To understand the relocation of vapor bubbles in this experiment, a familiarization with two fields utilized within MELCOR may be beneficial: the fields are the pool and atmosphere of a control volume. The atmosphere of a control volume is comprised of

the various user defined vapor species as well as liquid water drops referred to as fog. The pool is comprised only of water, either as liquid water or vapor bubbles. Transport of vapor bubbles is performed either due to transport of pool mass to another control volume or as bubble separation from the pool to the atmosphere of the control volume, i.e., bubbles rising to the surface of the pool. During the advection of mass associated with a control volume field, the receiving control volume field will be the same, i.e., pool mass is transferred to the pool of the receiving control volume pool and the atmosphere is transferred to the receiving control volume atmosphere. The bubble rise model in MELCOR assumes a bubble rise velocity of 0.3 m/s, an approximation of the gas bubble rise velocity in water near atmospheric pressure; this velocity is applied by default and can be adjusted by the user. In addition to the assumed bubble rise velocity, the distribution of the void fraction within the pool is assumed to be linear from 0.0 at the base of the control volume. The bubble rise velocity and assumed void distribution are combined to determine the volumetric release rate of vapor from the pool.

The advection for the atmosphere and pool is performed using flow paths, which connect control volumes to one another. A detailed discussion of flow paths may be found in the MELCOR CVH/FL Reference Manual. Relevant to the discussion concerning flow path connections are the junction opening heights and interface momentum length. Junction opening heights are used to determine the static head for the momentum equation and to determine which fields are available for advection: pool, atmosphere, or both. Adjusting the junction height can be used to exclude a field from being transported between control volumes. When both pool and atmosphere intersect the junction opening, the shear force between the pool and atmosphere is calculated, which occurs over a length known as the momentum exchange length. Reducing the momentum exchange length reduces shear between the two fields; while increasing the momentum exchange length will produce similar velocities for the two fields.

3.8.2.2 MELCOR Model Nodalizatio**n**

Two modeling nodalizations are presented for the 5801-13 experiment, as seen in Figure 3.8-2. The base model has a single volume representation of the tank. The heat structures associated with the tank are only modeled throughout the cylindrical portion of the tank. A single flow path represents the dip tube line. The surrounding reservoir is modeled at constant atmospheric conditions.

A higher-fidelity 13-control volume tank nodalization is also presented. The increase in control volume nodalization required a similar increase in the heat structure nodalization. The top and bottom control volumes represent the hemispherical caps of the tank. The flow path junctions and interface lengths of the connecting flow paths are default, i.e., defined by MELCOR.

The base model utilizes the MELCOR default value of 0.4 for the maximum permitted pool void fraction in any given control volume. This value is increased to 0.5 in a sensitivity study on the base model. For the 13-control volume model, the MELCOR default of 0.4 is always used.

Note that MELCOR 2.1 (v6110) and MELCOR 1.8.6 (v4073) were the code versions utilized. Only the single control volume base case was executed for MELCOR 1.8.6. For MELCOR 2.1, both the single and 13-control volume nodalizations were considered, along with the sensitivity of results to changes in maximum allowable pool void fraction.

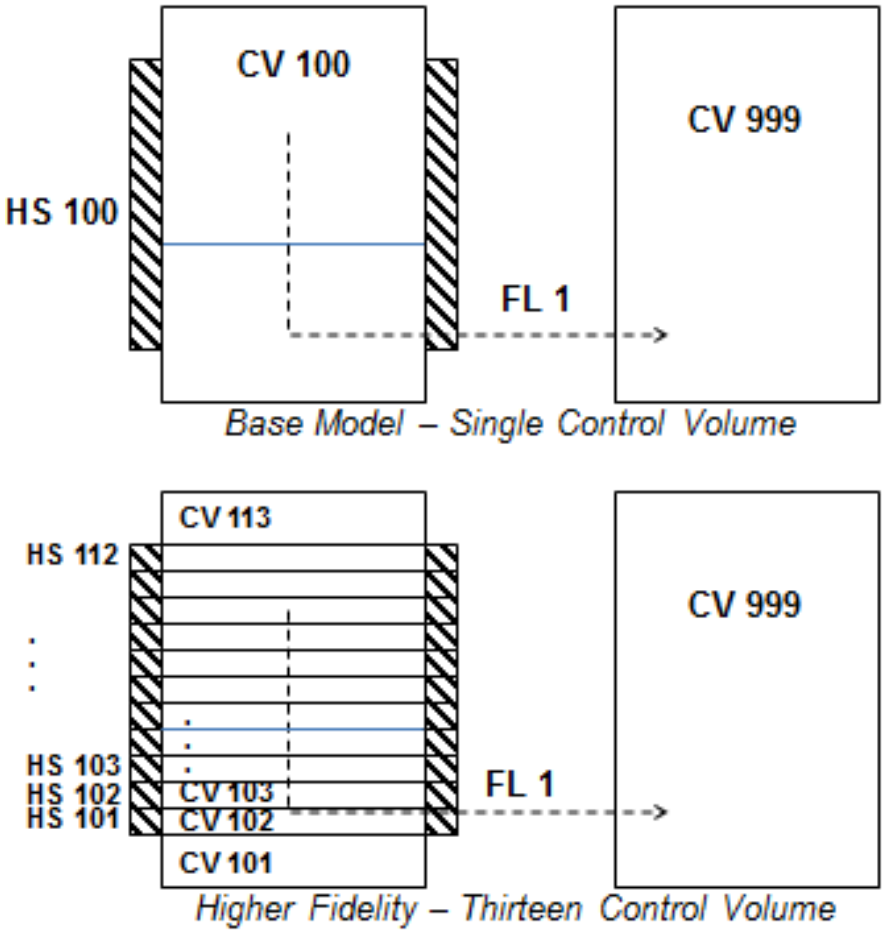

Figure 3.8-2. Nodalization of the Performed MELCOR Analyses

3.8.2.3 Results of Analysis

3.8.2.3.1 Case 1: Single Control Volume Representation (Base Case)

Available data recorded during the GE level swell test include the pressure response and liquid level, which are compared to the MELCOR analysis results in Figure 3.8-3 and Figure 3.8-4, respectively. Additionally, MELCOR 1.8.6 is included to demonstrate code agreement between both versions for the single control volume representation.

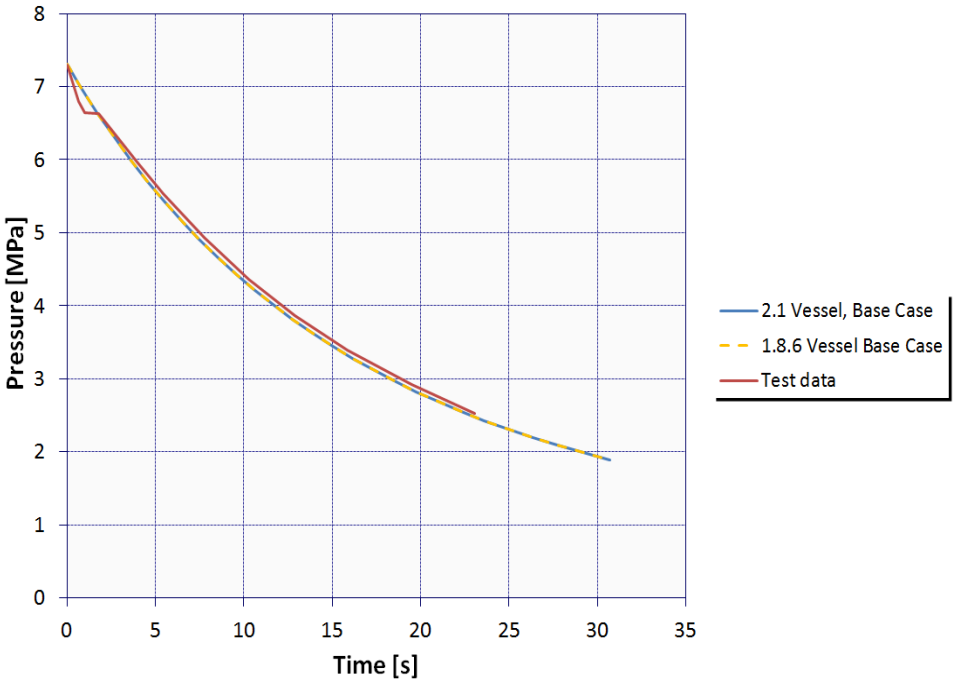

Figure 3.8-3. Base Case Pressure Response Comparison of Test Data

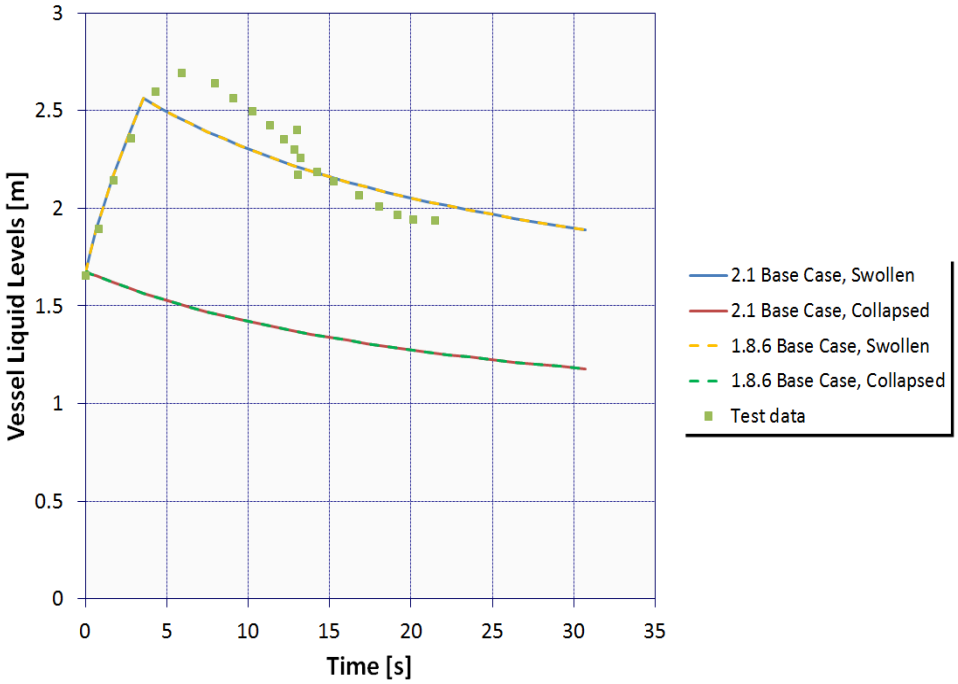

Figure 3.8-4. Base Case Level Swell Comparison of Test Data

The pressure comparison shows good agreement between the test data and the MELCOR calculations for the base case. However, a slight disparity is observed between the test data and the analyses during the first few seconds. The test data show a slightly faster depressurization than the MELCOR results; however, the discrepancy is short-lived as the analyses and available data nearly overlap for the remainder of the test. As expected, given a good approximation of the choked flow conditions, the pressure response is in relatively good agreement.

The disparity seen during the first couple of seconds may ultimately be the result of MELCOR predicting greater vapor transport to the atmosphere of the tank than produced in the experiment. Perhaps the critical flow rate through the venturi is being enhanced by condensation of the vapor passing through the exhaust piping during the beginning of the experiment, which the MELCOR model does not include. In any case, the good agreement observed for the swollen pool level during the first few seconds suggests that the hydraulic compression of the atmosphere by the pool level swell is similar, and therefore, not believed to be the direct cause of the observed disparity.

While good agreement is observed when comparing the swollen pool levels during the early phase of the experiment, the MELCOR calculated pool level deviates from the level swell data before 5 seconds, as seen in Figure 3.8-4. While the pool level appears to have good agreement during the first few seconds, this phase of the analysis corresponds with the initial vapor fraction of the pool increasing to the limiting maximum void fraction, 0.4, as seen in Figure 3.8-5. Nearly identical results are observed for MELCOR 1.8.6.

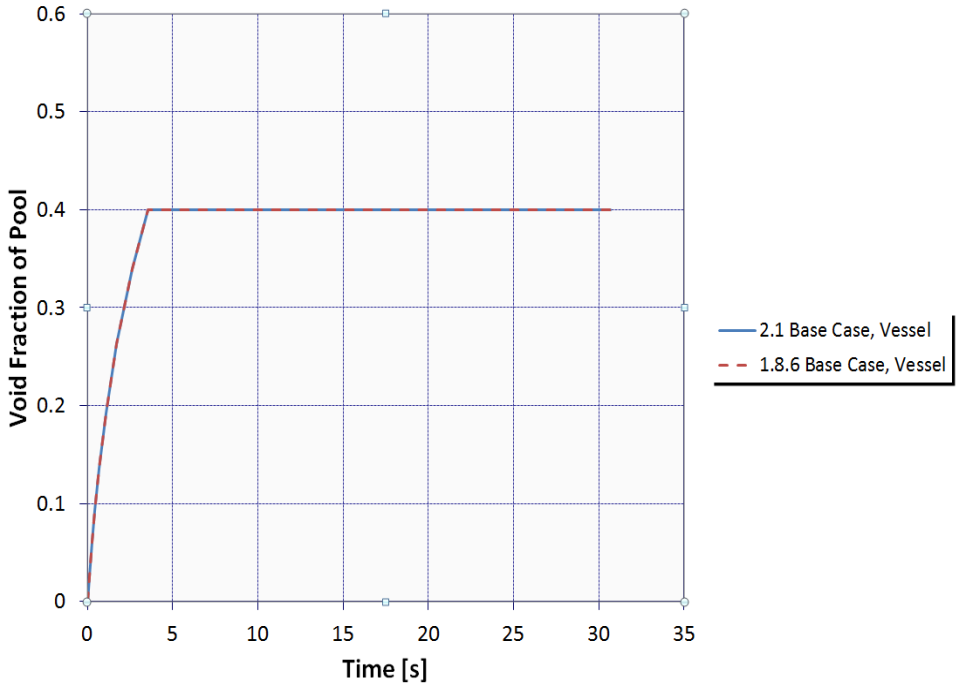

Figure 3.8-5. Maximum Void Fraction for Base Case

Once the maximum void fraction is established, the pool level observed in the MELCOR analyses departs from the experimental data. This is due to any vapor generated in excess of the maximum allowed void fraction is placed directly into the atmosphere of the control volume representing the tank, bypassing the bubble separation model in MELCOR. Sensitivity study on void fraction has demonstrated that increasing the void fraction simply permits the swollen pool level to increase further, until the newly defined maximum void fraction is achieved, and a similar level decrease trend is observed. This effect is evident in Figure 3.8-6 when a maximum void fraction of 0.5 is specified (as a sensitivity study on the base case). Further increases to the maximum void fraction can permit a pool level in excess of the dip tube opening, thus allowing liquid water to be released. Note that all sensitivities for the GE level swell test were performed only with MELCOR 2.1.

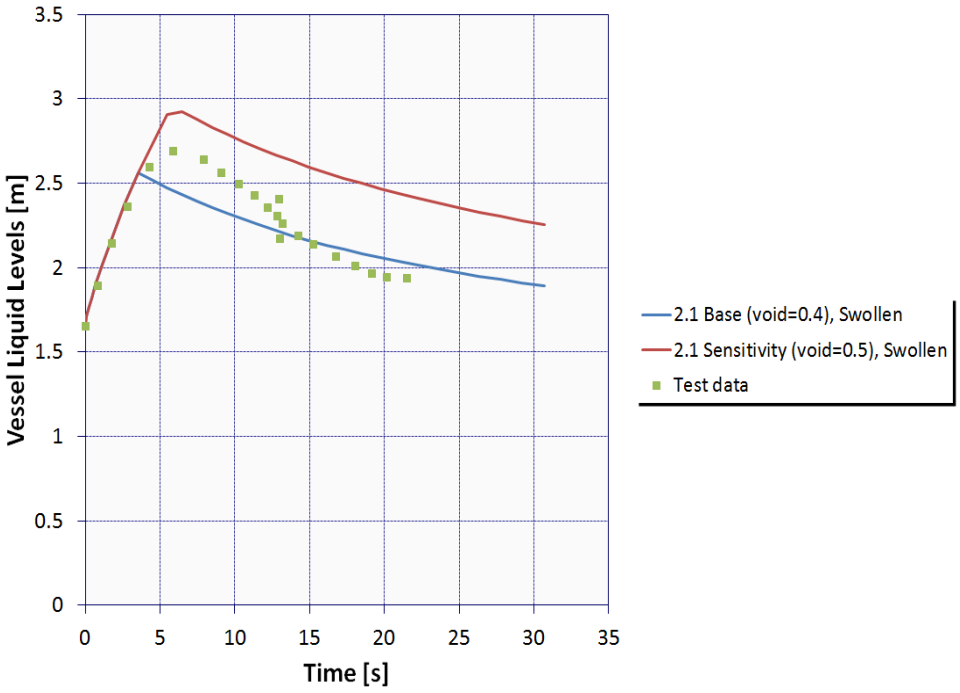

Figure 3.8-6. Maximum Void Fraction Sensitivity of Level Swell

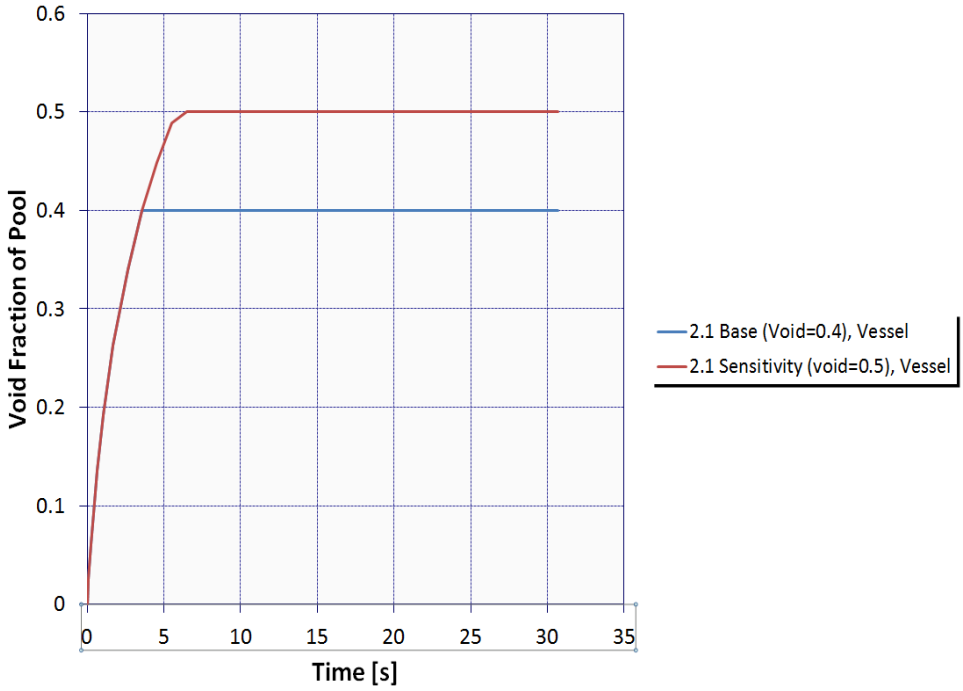

Figure 3.8-7. Maximum Void Fraction Increase Demonstrated

While increasing the void fraction does manage to produce an increase in the level, as is expected since the maximum void fraction was achieved and maintained for the duration of the analysis, the bubble rise velocity controls the rate of level swell (see Figure 3.8-7). The default constant bubble rise velocity of 0.3 m/s does produce good agreement for the level swell rate until the maximum void fraction is reached. Around 5 seconds, the bubble rise velocity may no longer be appropriate as the rate of the level swell changes and appears to vary throughout the remainder of the experiment. It should be noted that a constant bubble rise velocity cannot accommodate expected variations in rise velocity due to changing void fraction (impacting bubble agglomeration and size) or bubble shape variation (influencing drag and therefore terminal rise velocity).

The constant default values for the maximum void fraction (0.4) and bubble rise velocity 0.3 m/s) produce generally acceptable trends when compared to the GE level swell test. The onus is on the user to determine whether these values are appropriate for their analyses.

3.8.2.3.2 Case 2: Multiple Control Volume Representation

A multi-node representation, the 13-control volume nodalization of the tank is provided to gain insights into MELCOR calculations where multi-node geometries may be employed; this is often done to improve fidelity for reasons other than flashing induced void fraction distribution, such as core degradation, fission product release, or anticipated stratification. The nodalization applied is presented in Figure 3.8-2. Note the multiple control volume representation analyses for the GE level swell test are performed with MELCOR 2.1 and with default values of maximum pool void fraction and bubble rise velocity. As seen in Figure 3.8-8, the observed pressure response has remained very similar to the base case single control volume representation. The most notable deviation between the single control volume and multiple control volume representation concerns the pool behavior.

Pool levels for the various control volumes are presented in Figure 3.8-9. A commonly referred-to code behavior known as “floating pools” can be observed. With the reduction in pressure due to the opening of the rupture disc, bubble generation occurs in each of the control volumes containing pool mass. As the vapor separates from the pool, an atmosphere field develops within each of the control volumes. As long as the flow path junction heights include both fields, the shear between the two fields may prevent transport of the atmosphere field upward through the control volume stack, which is occurring in the provided analysis. Overall, the ultimate pool height achieved is greater than Case 1 and that observed in the GE level swell test data even though the total void fraction of the pools is less. This is caused in part by the atmosphere fields, which developed within the lower control volumes.

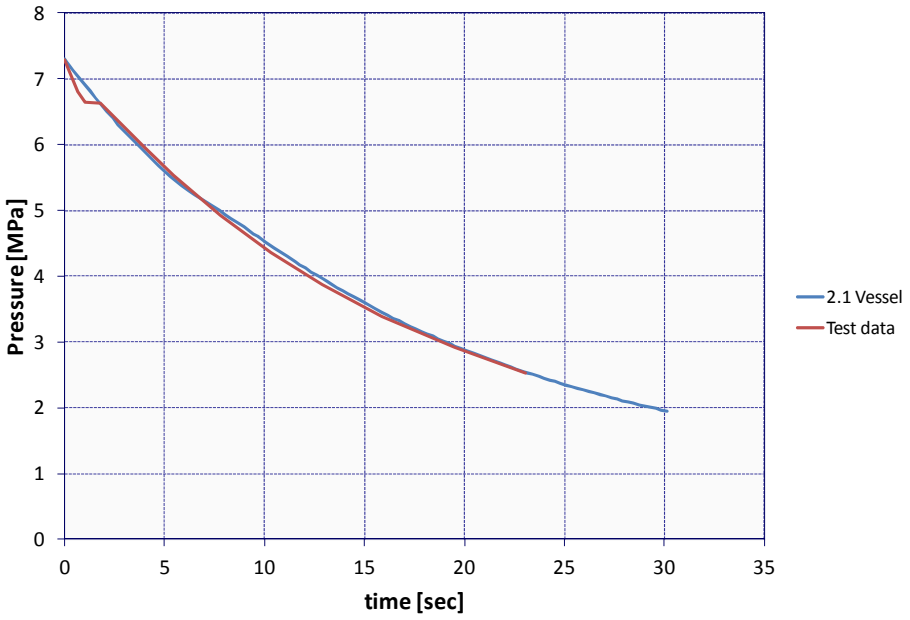

Figure 3.8-8. Pressure Results for 13-Control Volume Nodalization

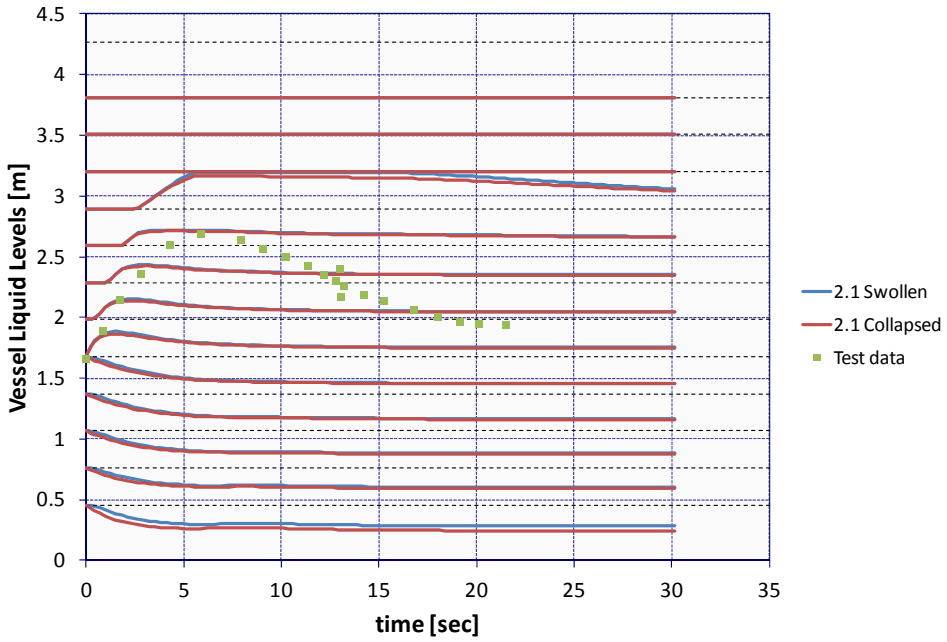

Figure 3.8-9. Results of 13-control Volume Nodalization on Liquid Level: Creation of Multiple Partially Liquid-Filled Control Volumes (i.e. Floating Pools). *Note: Dashed lines in figure represent control volume interfaces.*

A common practice to collapse the floating pools is to reduce the momentum exchange length between the pool and atmosphere fields within a flow path. Or a user may choose to tighten the junction heights to regions very close to the interfaces between control volumes, which will reduce the fraction of the control volume containing the atmosphere field observed. Either of these options, however, will not greatly impact the enhanced bubble separation beyond the effect of pool height modifications. Furthermore, atmosphere field material transported will bypass any interaction with the pool in the control volume located above (i.e., the atmospheric material does not "bubble up" through the pool). Atmospheric transfer between control volumes is directly to the donor control volume's atmosphere condition.

Limitations of the bubble separation model become transparent when multiple contiguously stacked control volumes are employed to represent a single pool. The bubble rise velocity along with the pool height, which in this case only spans a single control volume and not the actual pool, permits a more rapid release of vapor from the pool, since the residence time is reduced with smaller pool height. The increased bubble separation rates produce an overall reduction in void fractions as the maximum void fraction is not achieved throughout the pool regions.

If bubble separation is deemed relevant by the user, the prescribed practice is the application of a single control volume that spans the potential elevation range of the pool surface of interest. This will permit the bubble separation model to be applied

within the original design and formulation provided in the MELCOR CVH/FL Reference Manual. However, if the user finds that local effects throughout the pool are more relevant to the analysis, a multi-node approach may be preferable. Note that multi-node analyses were anticipated in MELCOR for core modeling, where the two fields are interpreted within the two-phase flow architecture in MELCOR. Both nodalization schemes should be considered.

3.8.3 Conclusion

The constraints on the maximum void fraction and the constant terminal rise velocity of the bubbles must be decided by the user. While maximum void fraction may be specified by the user, the prescribed value promotes code stability and was selected as the approximate upper limit of the bubbly flow regime. If the user determines that the maximum void fraction is achieved due to the maximum void fraction setpoint being too low, investigations into greater values may be warranted. However, if the user determines the maximum void fraction was reached due to improper bubble separation rates, the user may wish to modify the bubble rise velocity or inspect the nodalization employed. Evaluation of the anticipated bubble shape and size can permit a better estimate concerning the rise velocity; correlations may be found in the literature. The user should keep in mind that sensitivity coefficients are global controls and in the case of the maximum void fraction and bubble rise velocity will impact all pools that exist within the problem.

3.8.4 References

[3.8.1] G.L. Sozzi, Description of Void Fraction Distribution and Level Swell during Vessel Blowdown Transients, App. A-C in BWR Refill-Reflood Program Task 4.8 – Model Qualification Task Plan, NUREG/CR-1899, EPRI NP-1527, GEAP-24898, General Electric Co., August 1981

[3.8.2] L.N. Kmetyk, MELCOR 1.8.3 Assessment: GE Large Vessel Blowdown and Level Swell Experiments, Sandia National Laboratories, SAND94-0361, June 1994.References

3.9 Containment Analysis from the JAERI Spray Experiments

3.9.1 Background

Water spray tests were conducted at the Japan Atomic Energy Research Institute (JAERI) during the late 1970's [3.9.1]. These tests were conducted to confirm the effectiveness of pressure suppression through condensation by sprays that are often found in the containments of nuclear reactors. Following a postulated loss-of-coolant accident (LOCA), a large amount of high-pressure water will be released into containment, which quickly flashes into steam, thereby raising the pressure in the containment. Additionally, non-condensable gases can be created by fuel debris reactions with concrete if the lower head of the reactor pressure vessel (RPV) fails. The containment spray systems are designed to reduce these potential high-pressure excursions by cooling the atmosphere, thereby preventing over-pressurization failure of the containment. The containment sprays also have the secondary function of removing aerosolized fission products in the atmosphere by entraining them; this function was not included in the tests conducted at JAERI.

A large 700 m^3 steel vessel, simulating a containment structure, was initially filled with air at atmospheric pressure. Before the tests began, the vessel was pressurized to 3.5×10^5 Pa through the injection of steam. The vessel walls, which are insulated, are pre-heated by the steam to 395 K to preclude condensation on the walls; this process makes the tests a pure separate-effects test for pressure reduction by sprays. There is also a drain at the bottom of the vessel to prevent spray water in the vessel sump from effecting pressure by gas displacement. The entire experimental system can be seen in Figure 3.9-1. The testing matrix varied the number of sprays as well as their height and configuration. The two tests assessed in MELCOR [3.9.2] were PHS-1, which was a six spray test, and PHS-6, which was a single spray test.

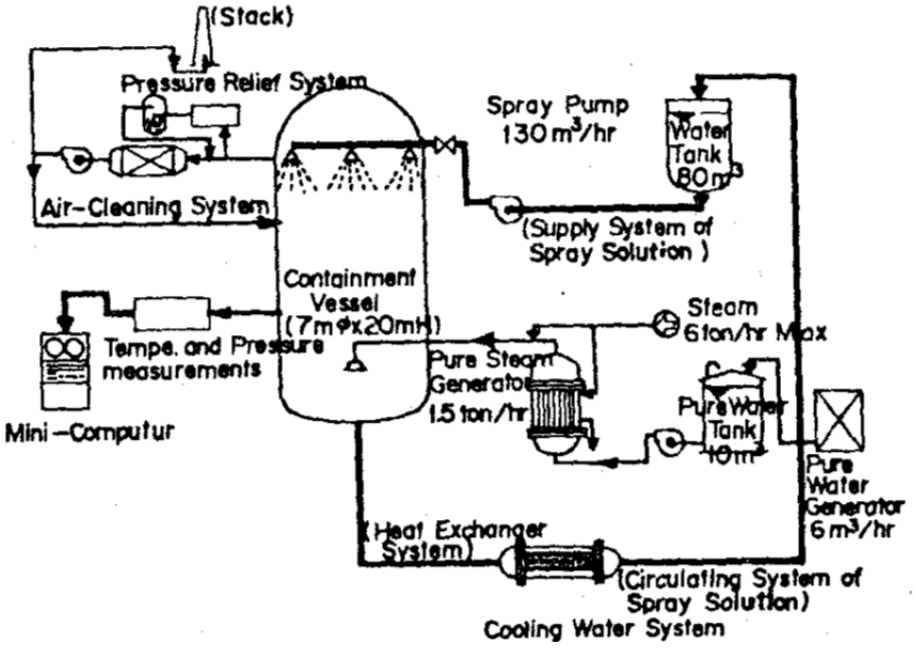

Figure 3.9-1 JAERI Experimental Spray System Set-Up

3.9.2 PHS-1 Experiment

3.9.2.1 Nodalization

The MELCOR input deck includes two nodalization options for the hydrodynamic volume in the steel vessel: 16 control volume (CV) and 1 CV. Figure 3.9-2 shows the 16-CV configuration (the 1 CV configuration is just a single lumped CV). The 16 CVs were chosen so that, with the exception of the upper head and the sump, the inner and outer CVs at each level (i.e. CVs 4 and 5) had the same total volume.

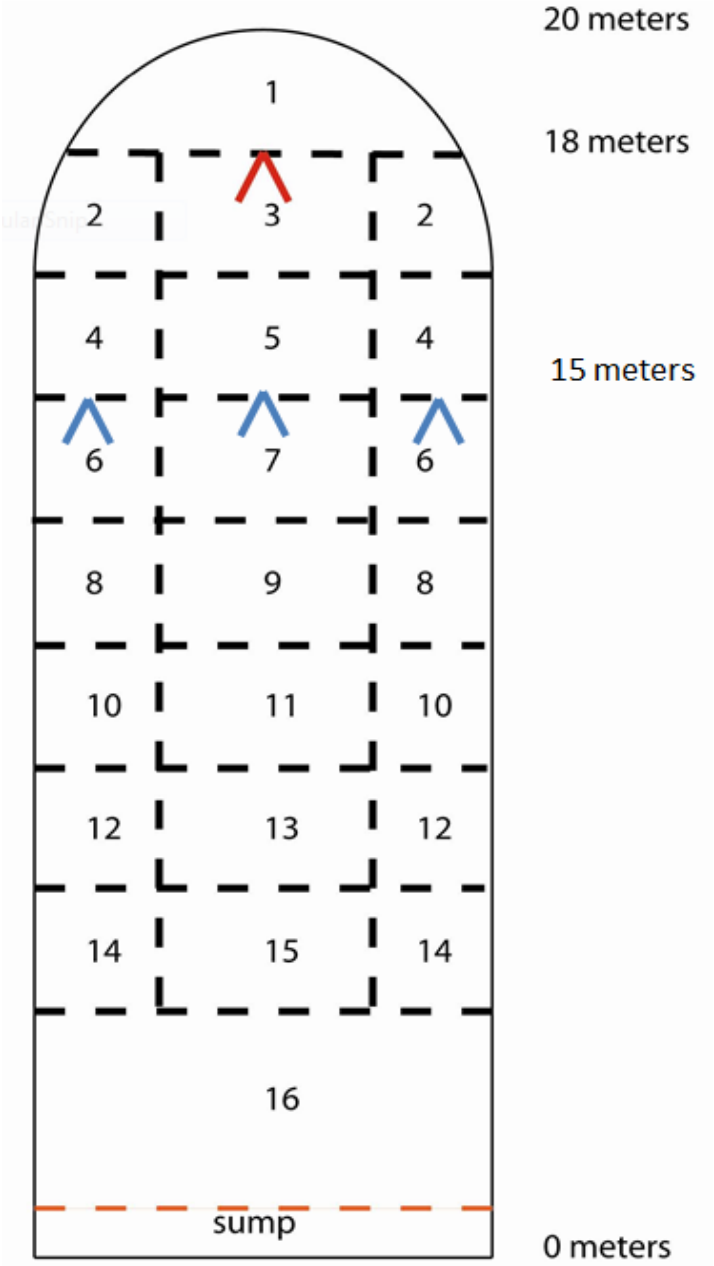

Figure 3.9-2 16 CV Nodalization Showing Sprays for PHS-1 (blue) and PHS-6 (red)

The PHS-1 Test used the same MELCOR nodalization options as the PHS-6 Test (discussed later), i.e. 1 and 16 CV. The only differences between PHS-1 and PHS-6 were the number, location, and volumetric flow rate of spray nozzles. In the PHS-1 Test, six sprays were attached to a ring-shaped header located at an elevation of 15 m. The combined flow rate for all sprays was 20.9 m^3/hr at a temperature of 40 ^oC. The radial location of the spray header was not given in the experiment report, so it was assumed that the location was at the interface between the inner and outer control volumes, which is a radius of about 2.43 m. Thus, half of the total spray mass flow was sourced into CV 6 and the other half into CV 7for the 16 CV model. For the 1 CV model, the two spray headers were both sourced into the single, large CV. Based on the assumed location and the given spray angle of 65-67^o, it is calculated that a certain fraction of the sprays will impact the hot vessel walls.

3.9.2.2 MELCOR Input Specifications

The PHS-1 simulation was run to 5,500 seconds (s), the experiment end time. Material properties were modified for insulation, carbon steel, and stainless steel in order to accurately simulate the steel vessel. The vessel was represented by 10 heat structures, eight in the wall, as well as a top and bottom heat structure. The wall sections were linked using MELCOR's film tracking model. This was maintained regardless of the CV nodalization. For the 16-CV nodalization, there were flow paths connecting each CV to its nearest neighbors, both axially and radially. Table 3.9-1 below outlines the several variations of PHS-1.

Table 3.9-1 PHS-1 Cases Executed in MELCOR 1.8.6 and 2.1

PHS-1 Variations	Code Version and Revision		Results shown in Assessment Document
	1.8.6 v4073	2.1 v6110	
1 CV,0% washout, dft SC4110	x	x	x
16 CV,0% washout, dft SC4110	x	x	
1 CV, 0% washout, mod SC4110	x	x	
16 CV, 0% washout, mod SC4110	x	x	
1 CV, 10% washout/90% spray, dft SC4110	x	x	x
16 CV, 10% washout/90% spray, dft SC4110	x	x	
1 CV, 90% spray, dft SC4110	x	x	x
16 CV, 90% spray, dft SC4110	x	x	
1 CV, 10% washout/90% spray, mod SC4110	x	x	
16 CV, 10% washout/90% spray, mod SC4110	x	x	
1 CV, 90% spray, mod SC4110	x	x	
16 CV, 90% spray, mod SC4110	x	x	

3.9.2.3 Results of Analysis

A set of calculations was conducted using MELCOR 1.8.6 (v4073) and 2.1 (v6110). The models included 1 and 16 CV nodalizations, as well as sensitivity studies related to run-off, spray percentage, and SC4110. All calculations were compared with the JAERI experimental data [3.9.1] when appropriate.

For Test PHS-1, six nozzles were used, and the height of the injection was 15 meters above the floor. Note that in MELCOR, there were only two lumped nozzles so as to allow for equal spray flow partitioning between CV 6 and CV 7 in the 16 CV model. The high spray rate (5.754×10^{-3} m^3/s) required that sump water be drained to avoid pressure effects from gas displacement. The single and multi-cell models included a sump flow path input that limited the sump to a maximum depth of 0.1 m.

Figure 3.9-3 and Figure 3.9-4 show the PHS-1 measured and calculated MELCOR pressure for the single CV model, respectively. Figure 3.9-3 also shows cases with 0% washdown, 10% washdown and 90% spray, and 90% spray. The figure shows that the case with 10% washdown and 90% spray compared favorably with the experimental data, while the case with 0% washdown had an error of up to 33% when compared with data. The calculations indicate that a small amount of spray contact with the hot vessel wall significantly reduced the rate of pressure decline. A washdown amount of 10% initial spray rate gave a very good estimate for the actual pressure reduction. Both the 1.8.6 and 2.1 simulations calculated the pressure transient reasonably well.

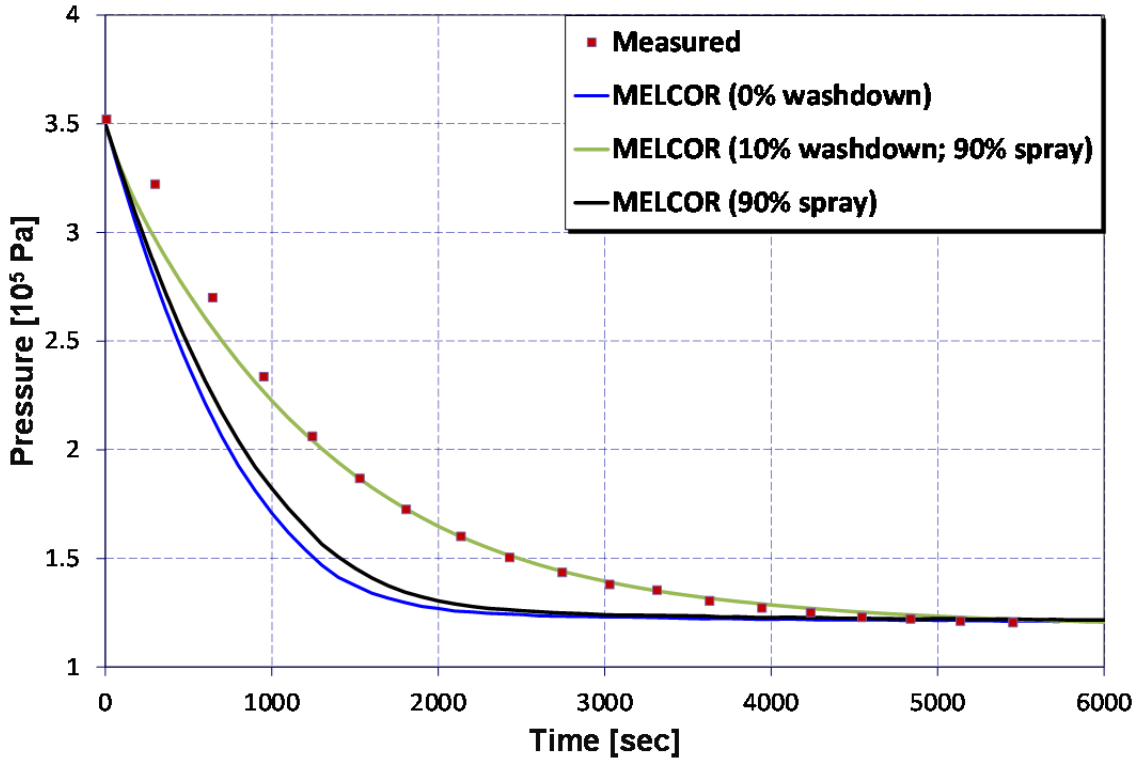

Figure 3.9-3. PHS-1 Test: 1 CV, Measured vs. Calculated MELCOR 1.8.6 Pressure

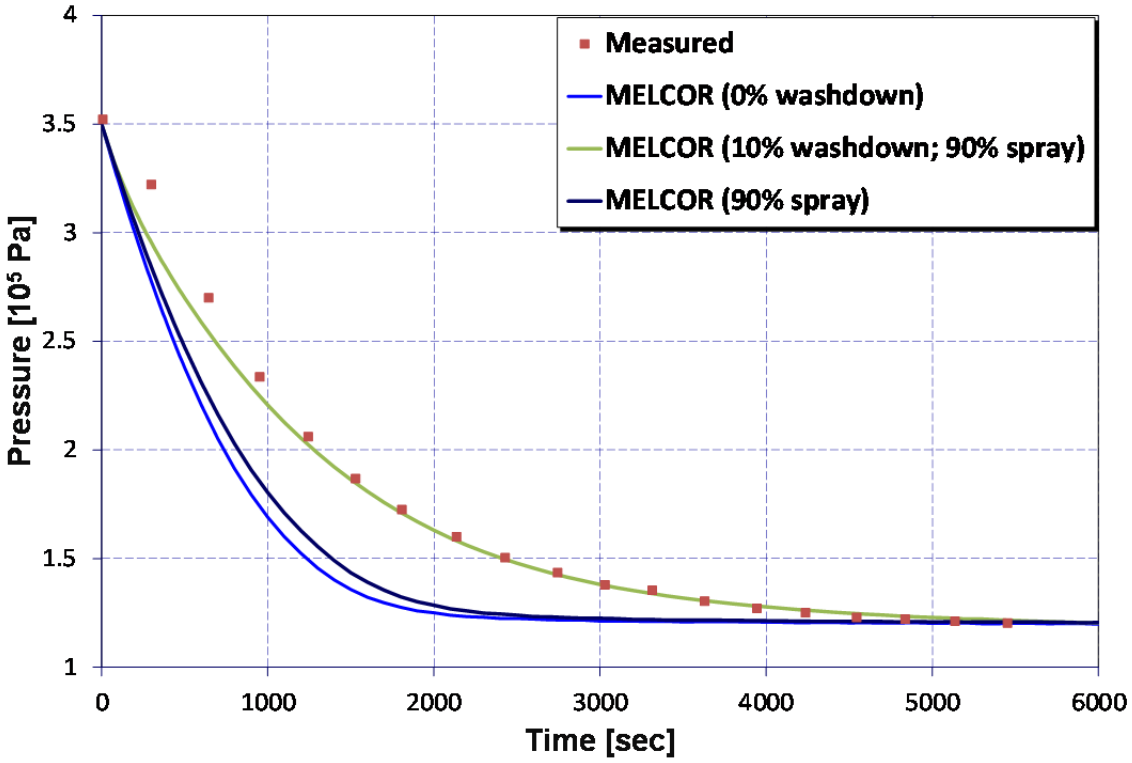

Figure 3.9-4. PHS-1 Test: 1 CV, Measured vs. Calculated MELCOR 2.1 Pressure

3.9.3 PHS-6 Experiment

3.9.3.1 Nodalization

The PHS-6 test used the same nodalization options as the PHS-1 test, i.e. 1 CV and 16 CV. Note that the difference in spray number and location is indicated on Figure 3.9-2.

3.9.3.1.1 MELCOR Input Specifications

MELCOR calculations for PHS-6 were run for 11,000 s, which is approximately the length of time experimental data were available for PHS-6. The single spray nozzle was located at a height of 18 meters and had a flow rate of 3.48 m^3/hr at a temperature of 40 ^oC. The vessel walls and top/bottom was modeled in the same way as for PHS-1; and again, the film-tracking model was active. Since the CV nodalization options remained the same as for PHS-1, so did the in-vessel flow path arrangement. Table 3.9-2 below outlines the variations of PHS-6.

Table 3.9-2. PHS-6 Cases Executed in MELCOR 1.8.6 and 2.1

PHS-6 Variations	Code Version and Revision		Results shown in Assessment Document?
	1.8.6 v4073	2.1 v6110	
1 CV,0% washout, dft SC4110	x	x	x
16 CV,0% washout, dft SC4110	x	x	x
1 CV, 0% washout, mod SC4110	x	x	x
16 CV, 0% washout, mod SC4110	x	x	

3.9.3.2 Results of Analysis

Figure 3.9-5and Figure 3.9-6 show the computed pressure for MELCOR 1.8.6 and 2.1, respectively, for PHS-6 with a 16 CV nodalization. They show the pressure decline due to the spray from a single nozzle (spray rate = 0.959×10^{-3} m^3/s). The agreement is very good for the "0% washdown" case; therefore, the calculation confirms the fidelity of MELCOR spray-atmosphere energy exchange models. Figure 3.9-7 and Figure 3.9-8 show the computed atmosphere temperatures for MELCOR 1.8.6 and 2.1, respectively, for the same instance of PHS-6 with a 16 CV nodalization. Note also that the experimental data points correspond to physical instrumentation locations (e.g. "19.5 Measured" for the instrument at height of 19.5 m in the experimental facility). A comparison shows that the 2.1 calculation was a few degrees closer to the experimental data than the 1.8.6 calculation.

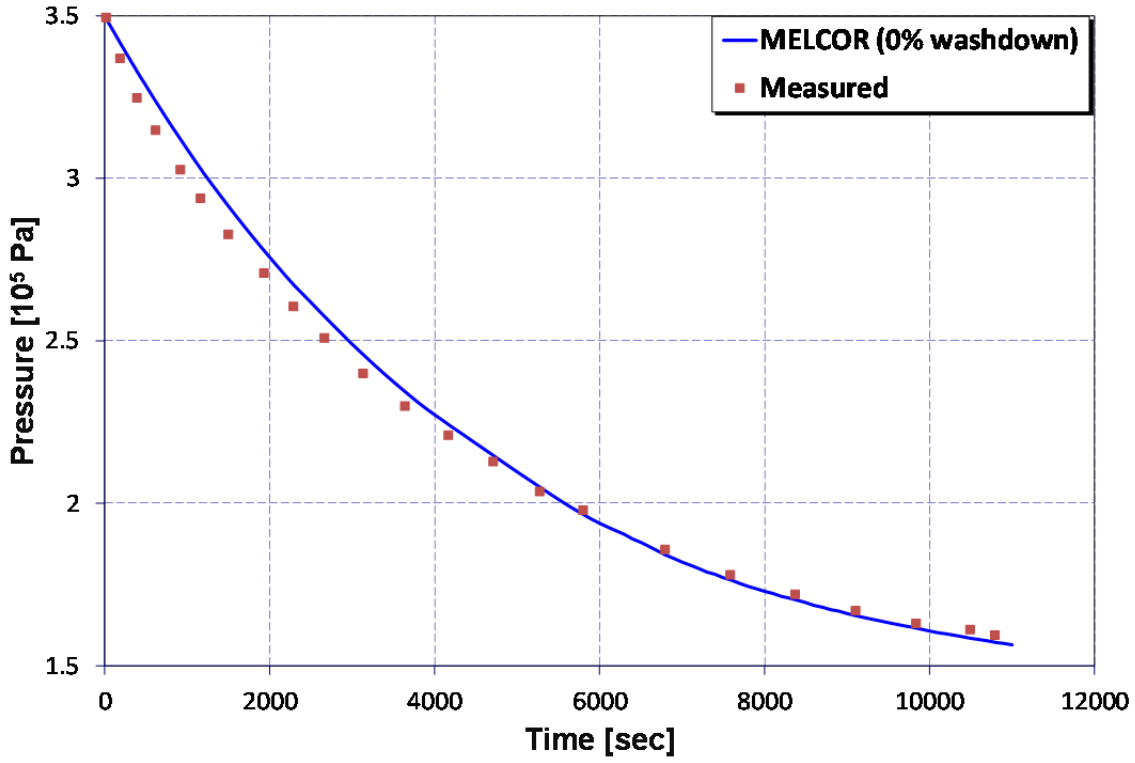

Figure 3.9-5 PHS-6 Test: 16 CV, Measured vs. Calculated MELCOR 1.8.6 Pressure

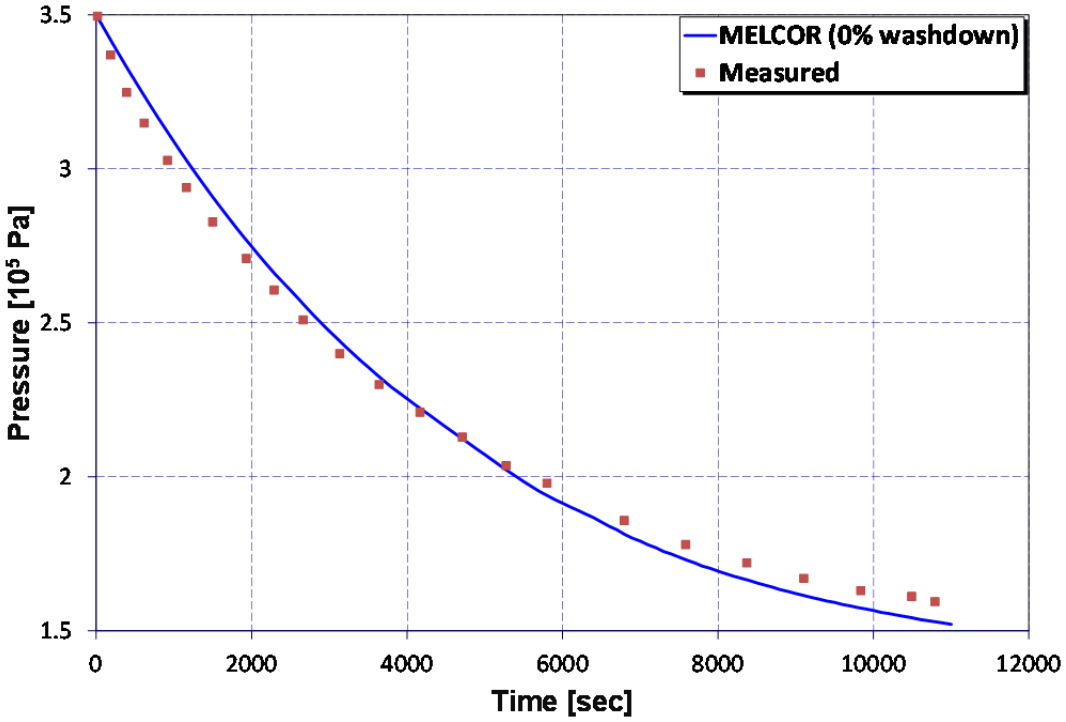

Figure 3.9-6 PHS-6 Test: 16 CV, Measured vs. Calculated MELCOR 2.1 Pressure

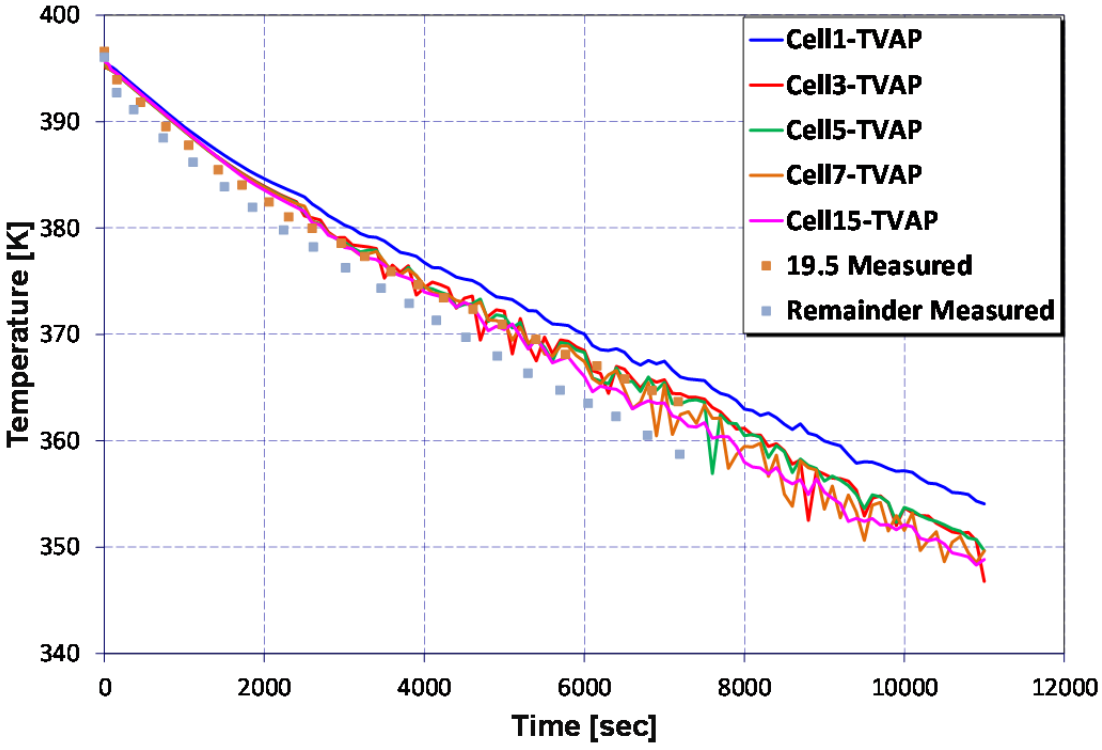

Figure 3.9-7 PHS-6 Test: 16 CV, Measured vs. Calculated MELCOR 1.8.6 Temperature

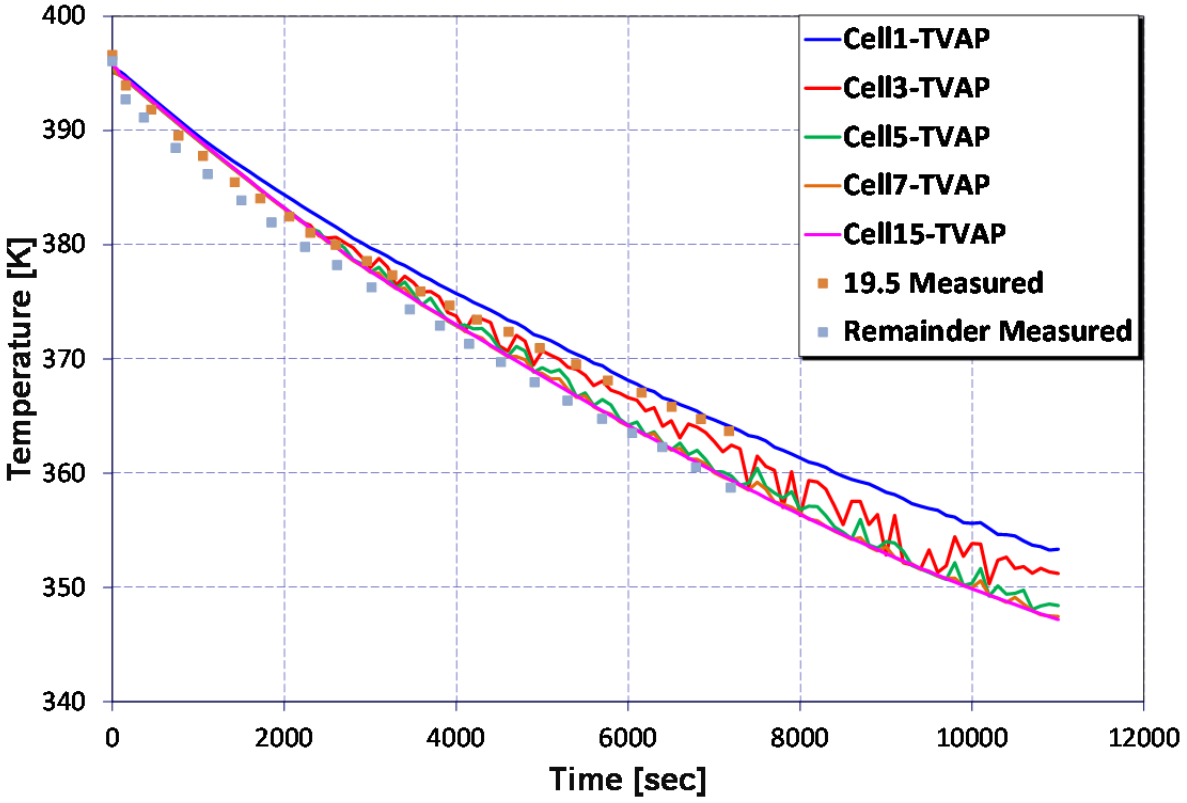

Figure 3.9-8 PHS-6 Test: 16 CV, Measured vs. Calculated MELCOR 2.1 Temperature

3.9.3.3 Sensitivity Study – Match to CONTAIN Code

Besides comparing MELCOR results to experimental data, it is beneficial to compare MELCOR to other codes. For this spray experiment, the most relevant comparison was to the CONTAIN code, licensed by the NRC for containment analyses. In order to make the comparison, one change was made in the input deck to ensure that the internal models of the two codes matched as closely as possible: sensitivity coefficient 4110. This is an array of coefficients, exponents, and additive constants for the natural convection Nusselt number (Nu) correlation formulated in terms of the Rayleigh number. It was changed from MELCOR defaults to more closely match CONTAIN defaults. The correlation in question [3.9.2] assumes the form:

$$\boldsymbol{Nu = C4110(1) * Ra^{C4110(2)} + C4110(3)} \qquad \text{Equation 3.9-1}$$

Where $C4110(j = 1 \ldots 3)$ are the first, second, and third members of the SC4110 array. The MELCOR defaults for these members are 0.1, 0.33, and 0.0, respectively. The values after augmentation for CONTAIN agreement were 0.14, 0.33, and 0.0. The net effect of changing SC4110 was to raise the CV vapor temperature by 3 to 5 K, as shown in Figure 3.9-9. Note that this figure shows vapor (noncondensible gas plus steam, fog) temperature (TVAP) and saturation temperature at the CV atmosphere pressure, TSAT(A), for the 1 CV case of PHS-6. PHS-6 conditions are described in the next section but are immaterial to the comparison made

here between results with and without default SC4110 values. Because the recorded measurements for PHS-6 at all instrumentation locations besides 19.5m are virtually identical, all are represented by the curve labeled “Remainder Measured”.

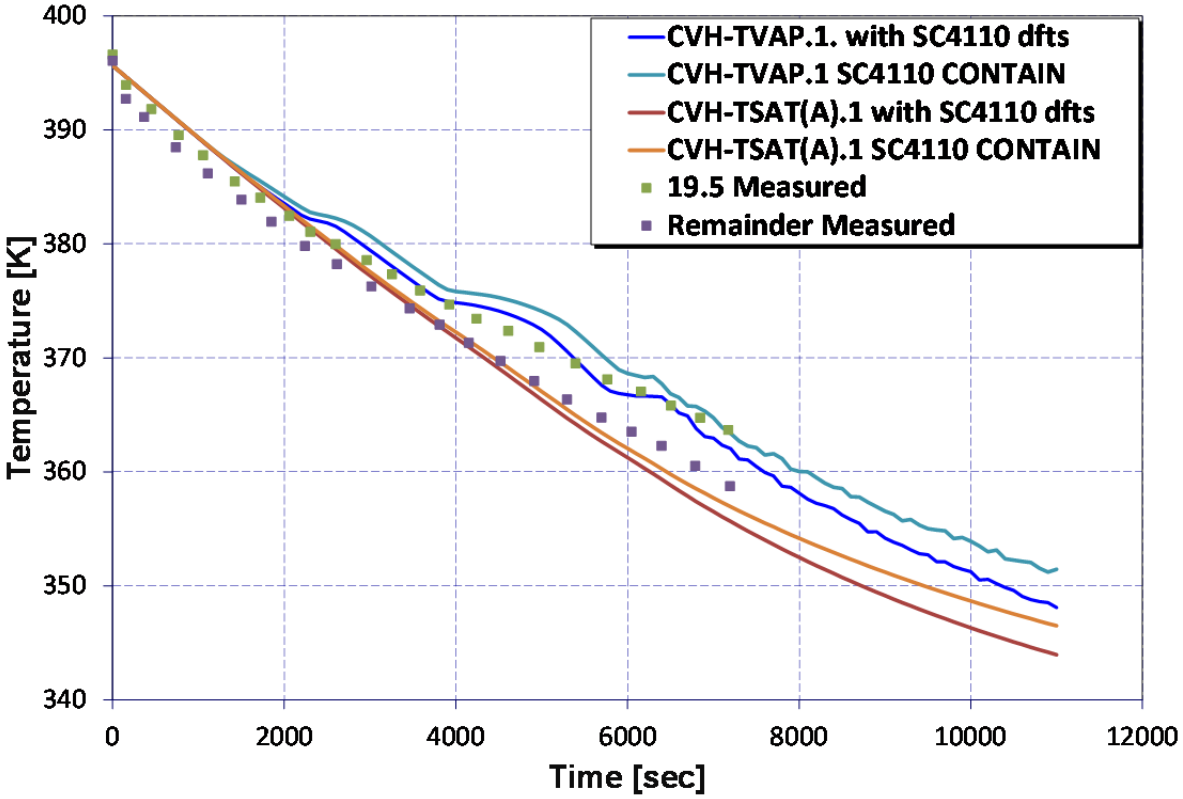

Figure 3.9-9 PHS-6 Test: 1 CV, Measured vs. Calculated MELCOR 2.1 Temperatures

3.9.4 References

[3.9.1] Kitani, S., “Containment spray experiments for pressure suppression,” presentation at 1st International Conference on Liquid Atomization and Spray Systems, Tokyo, Japan, August 27-31, 1978.

[3.9.2] Gauntt, R.O., et al., “MELCOR Computer Code Manuals: Vol. 1 Primer and User’s Guide, Version 1.8.6 September 2005,” NUREG/CR-6119, Vol. 1, Rev 3, SAND 2005-5713, Sandia National Laboratories, Albuquerque, New Mexico, September 2005.

3.10 Analysis of LACE LA-4 Experiment

3.10.1 Background

The LACE LA-4 experiment was conducted by the Westinghouse Hanford Company in the Containment Systems Test Facility (CSTF) [3.10.1]. The test, performed on August 21, 1986, was designed to simulate containment conditions in an LWR severe accident with late-containment failure. The purpose of the experiment was to determine the disposition of aerosols in the containment building under conditions of high steam concentrations. Of particular interest was the difference in aerosol disposition between hygroscopic (water-soluble) aerosols such as CsOH and non-hygroscopic aerosols in a high-steam concentration. CsOH is a highly hygroscopic material, while MnO is insoluble and essential non-hygroscopic.

3.10.2 Experiment

The experiment involved six separate phases. The initial phase was characterized by the introduction of steam into the CSTF vessel to preheat the atmosphere by about 70 K above ambient conditions and to establish the desired steam concentration. This period lasted about 3,000 seconds. Following the heat-up phase were three periods lasting 1,830, 1,200, and 1,782 seconds. These times were used in conjunction with sourcing the aerosols (see Table 3.10-1). The last two phases consisted of a long steady-state period that lasted about 12,000 seconds, and a venting and cooling phase lasting about 19,200 seconds.

Figure 3.10-1 shows the experiment apparatus. This figure shows the locations of the vent and aerosol injection lines as well as the locations where heat and mass transfer rates were measured. Steam was injected through the steam line near the bottom of the vessel during the heatup phase and continued at a reduced rate during the experiment phase to maintain a steady-state condition. The aerosol injection line was located at about the mid-plane of the vessel. Nitrogen gas and steam were used as the carrier medium for the aerosol injection through this line.

The atmospheric aerosol concentration was determined by taking filter samples at intervals during the test. These samples were later subjected to chemical analysis to determine quantity and composition. The samples were taken both by through-the-wall samplers and by samplers suspended at various locations within the vessel atmosphere.

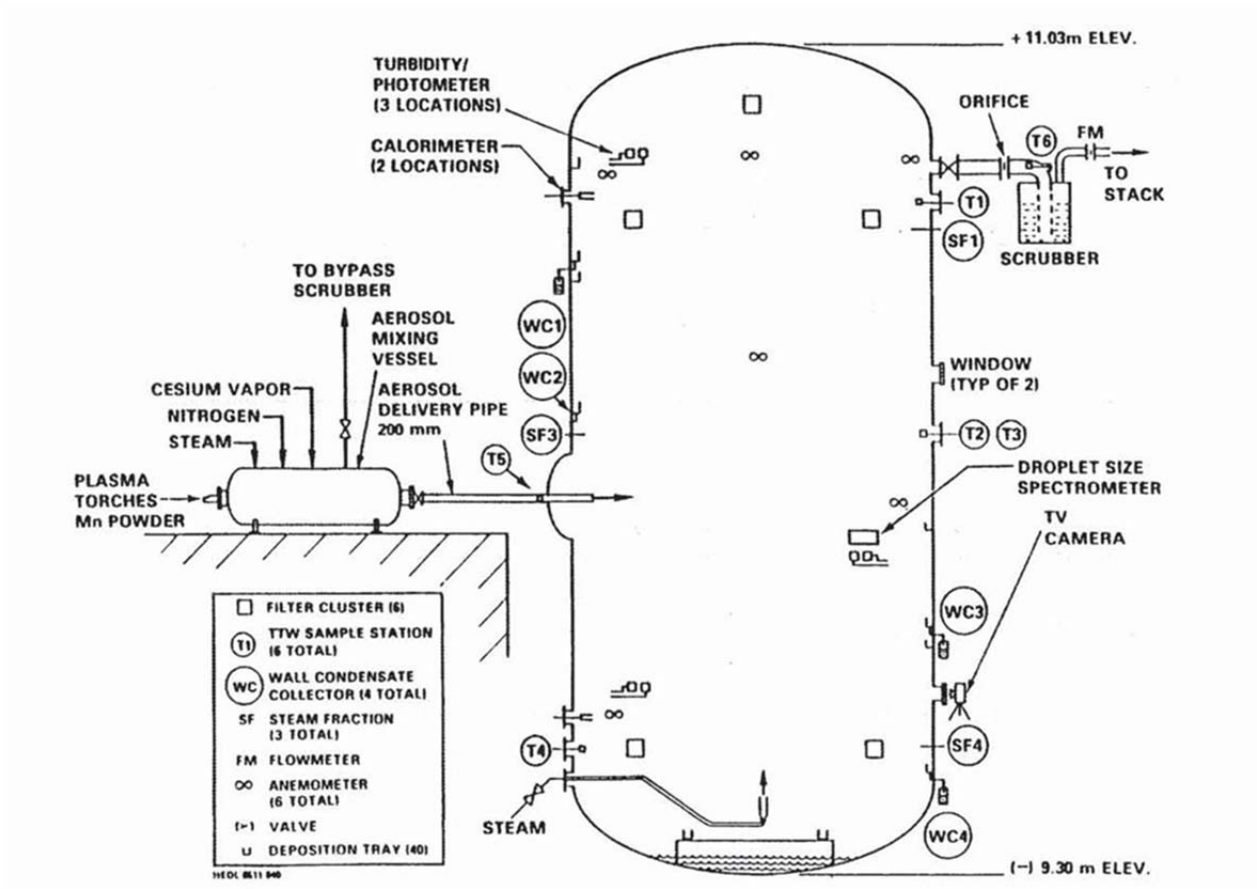

Figure 3.10-1 Experiment Apparatus [3.10.1]

3.10.3 MELCOR Model

The LA-4 experimental configuration was modeled with the MELCOR code using a single control volume for the vessel and two environment volumes, one to receive the vent discharge during the vent-down phase and the other to act as the sink for leakage. A previous MELCOR analysis of this experiment was used as a starting point for this analysis. (See Figure 3.10-2 for a diagram of the MELCOR nodalization.) Saturated steam sources were injected into the vessel at the lower steam line elevation in accordance with the measured data. The carrier gases (nitrogen and steam) were injected into the vessel at the elevation of the aerosol injection line as per the measured rates.

Appropriate enthalpy sources associated with the mass sources are applied as well as the enthalpy (energy) source associated with the lighting in the vessel. Note that the steam injection rate is provided in Figure 3.10-3. As shown in this figure, a mass flow rate of 0.45 kg/s was injected in the heatup phase of the experiment as devoted from -3,000 to 0 seconds. Also shown in this figure is the steam flow rate accompanying the aerosols starting from time zero. Aerosol sources were input at the times and rates

given in Table 3.10-1. The CsOH was sourced into Class 2 and the MnO was sourced into Class 7. Both the hygroscopic and non-hygroscopic aerosol classes and the water aerosol class were modeled as separate aerosol components. The important vessel structures (heat sinks) were modeled using six heat structures. Note that the default global of 2.0 is added in the input decks for 1.8.6 and 2.1. In addition, both deck versions use the maximum time-step of 10-second throughout the calculation.

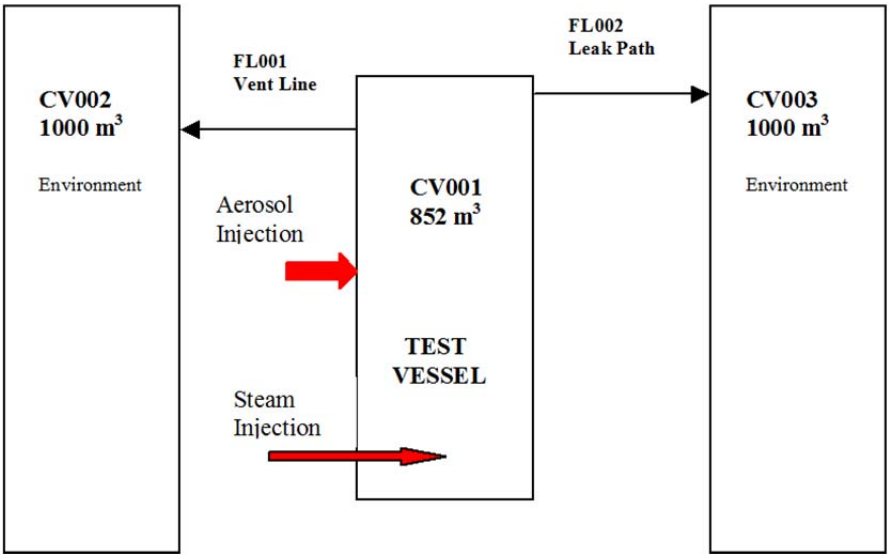

Figure 3.10-2 MELCOR Nodalization

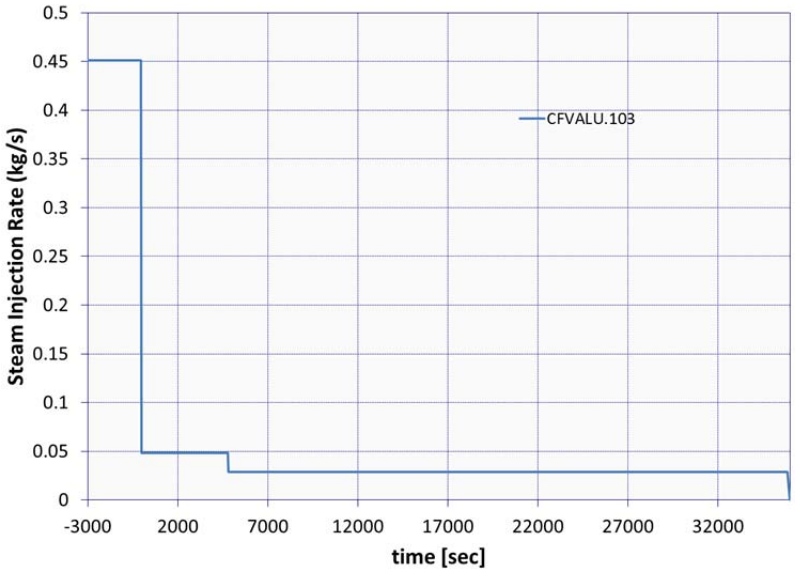

Figure 3.10-3 Steam Injection Rate

Table 3.10-1 Aerosol Sources

Period	Start (s)	End (s)	Aerosol	Rate (g/s)	AMMD** (μm)	GSD**
2–CsOH Only	0	1830	CsOH	0.949[1]	1.35	1.81
3–CsOH + MnO	1830	3030	CsOH MnO	0.949[1] 0.757[1]	2.22 2.43	1.80 1.70
4–MnO Only	3030	4812	MnO	0.757[1]	1.82	2.56

**AMMD – aerodynamic mass mean diameter, GSD – geometric standard deviation

[1]During aerosol sourcing, N_2 /steam are also injected. There are also small rate of N_2 injection before and after the aerosol sourcing. In addition, steam was first injected to vessel as a part of pre-heat condition for the experiment (see Figure 3.10-3 as modeled in MELCOR).

A number of cases were simulated, particularly for the condensation and liquid film drainage phenomena based on the humidity level in the problem. Table 3.10-2 shows the sensitivity case conducted for the MELCOR calculations. Case 1 is the default case. Case 2 approximates what was in MELCOR 1.8.5. Cases 3 and 4 are similar to Case 2, except the minimum film thickness increases to 0.1 mm and 0.5 mm, respectively, from the default value (0.00001 mm). Case 5 is similar to Case 1, except the minimum film thickness is set to 0.5 mm. All five cases are simulated in MELCOR 2.1 (rev 6110). For MELCOR 1.8.6, only Case 1 and Case 2 are simulated for purposes of code version comparison and provide results for upward compatible since MELCOR 1.8.5.

Table 3.10-2. MELCOR Sensitivity Cases

Case	MELCOR 2.1	MELCOR 1.8.6
Case 1 – default C4252(1) = 0.0, C4252(2) = 0.0, C4251(1) = $1x10^{-9}$ m	X	X
Case 2* – Same as Case 1, except C4252(2) = 0.70 (similar to 1.8.5)	X	X
Case 3 – Same as Case 2, except C4251(1) = $0.1x10^{-3}$ m	X	
Case 4 – Same as Case 2, except C4251(1) = $0.5x10^{-3}$ m	X	
Case 5 – Same as Case 1, except C4251(1) = $0.5x10^{-3}$ m	X	

*Additional cases were conducted in terms of sensitivity to the time-step used in the calculations. Case 2a assumes a constant Δt=1 s, Case 2b uses Δt=2 s, and Case 2c uses Δt=10s for MELCOR 2.1.

3.10.4 Discussions and Results

Results of an earlier MELCOR assessment of the LA-4 experiment using code version 1.8.1 were published in 1991 [3.10.2]. MELCOR 1.8.1 did not have a model for the hygroscopic process. Identical input decks were created for MELCOR 1.8.6 and 2.1, though these included hygroscopic models not found in MELCOR 1.8.1. Only the

compound density value of 5430 kg/m^3 was modified in the specific hygroscopic aerosol parameters for MnO.

In this section, the results for MELCOR 2.1 are presented followed by the code version comparison between MELCOR 1.8.6 and 2.1. Finally, the effect of the timestep to the results is discussed for MELCOR 2.1.

For MELCOR 2.1, the pressure response of the test vessel is shown in Figure 3.10-4 for all five cases. The comparisons of total and steam partial pressures with measured data agree well for these calculations. Thus this is essentially no difference among cases simulated for the sensitivity coefficients related to film tracking. Similarly, the vessel atmospheric temperatures agree very well with the measured data as seen in Figure 3.10-5. This figure also shows the measured and calculated pool temperatures, which do not agree quite as well. Here, MELCOR 2.1 appears to overestimate the pool temperature during injection.

To demonstrate the mass balance on the steam and water sources in the test vessel, Figure 3.10-6 presents the calculated pool mass over the duration of the experiment as compared to actual measured water mass for all five cases using MELCOR 2.1. As shown in this figure, MELCOR 2.1 over-predicts the pool mass in comparison with the experimental data to about 12%. With Case 5 matches closer to the experimental data than other cases within 5%.

In terms of aerosol mass, Figure 3.10-7 and Figure 3.10-8 shows the suspended aerosols for CsOH and MnO results. As shown in these figures, all cases compare well with experimental data before 30,000 s. Beyond this time, agreement with experimental data is reasonable at best, and the higher values of the cases for suspended CsOH were predicted for all cases in compared with the experimental data (see Figure 3.10-7). On the other hand, the experimental data for suspended MnO fall between the predicted values of the cases simulated (see Figure 3.10-8).

In terms of the code version comparison, the relative humidity or steam saturation ratio (P_{steam}/P_{sat}) in the test vessel is plotted in Figure 3.10-9 for both Case 1 and Case 2. The humidity was not available as a measured parameter, but Figure 3.10-9 shows the calculated relative humidity for MELCOR 1.8.6 and 2.1. As shown in this figure, the versions are in good agreement with one another though version 2.1 yields a slightly higher value below 10,000 s. Note that Figure 3.10-10 demonstrates excellent code version agreement between 1.8.6 and 2.1 for pool mass calculations of cases 1 and 2. In terms of aerosol behavior, Figure 3.10-11 plots the results of MELCOR 1.8.6 and 2.1 for both Case 1 and Case 2. As shown in this figure, MELCOR 2.1 compares more favorably than does MELCOR 1.8.6.

To identify if time-step size could affect the calculated suspended aerosol calculations in MELCOR a timestep sensitivity study was conducted for MELCOR 2.1. Figure 3.10-12 and Figure 3.10-13 show the calculated suspended CsOH and MnO aerosols, respectively. Decreasing the timestep only slightly improves predictions with respect to data. As shown in these figures, MELCOR still over-predicts the suspended aerosols

near the end phase of the experiment, particularly to the hydroscopic aerosol such as CsOH. Thus a further investigation with the effect of aerosol density may be needed.

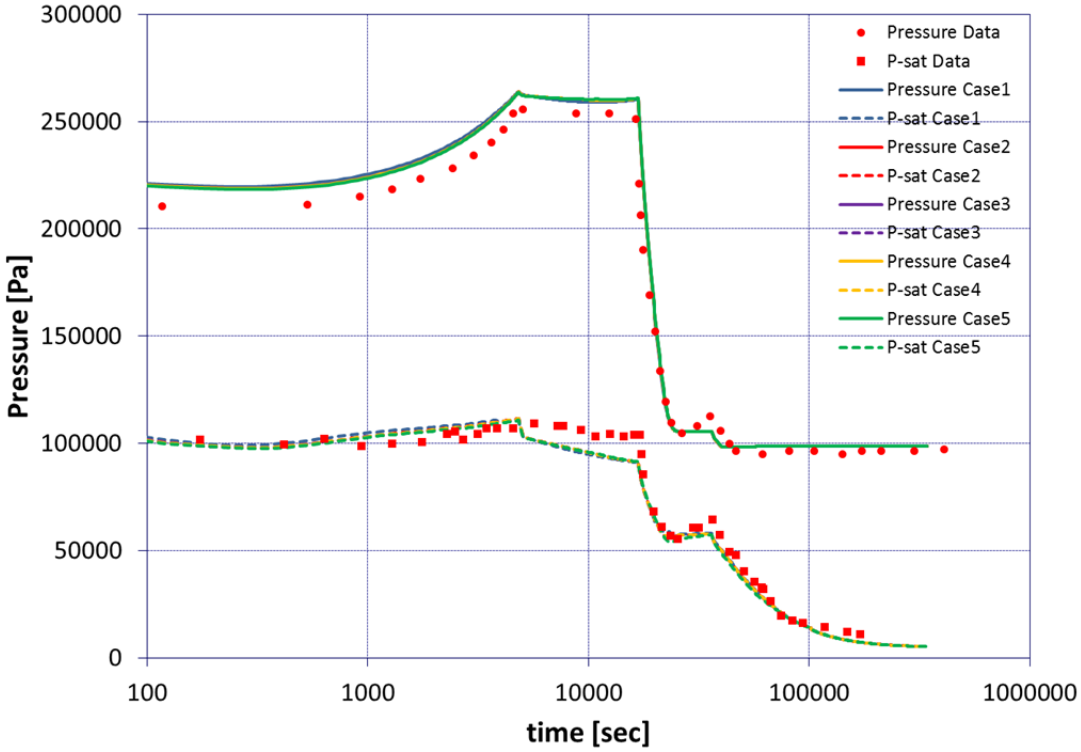

Figure 3.10-4. MELCOR 2.1 Calculated and Measured Vessel Pressures

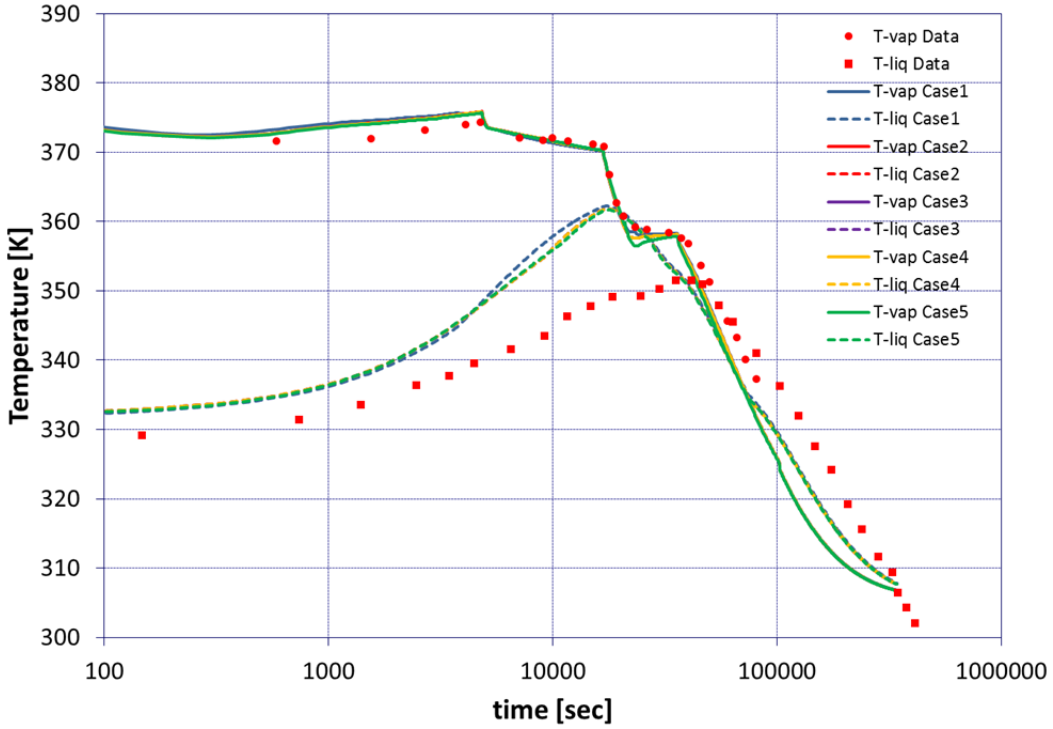

Figure 3.10-5. MELCOR 2.1 Calculated and Measured Vessel Gas/Pool Temperatures

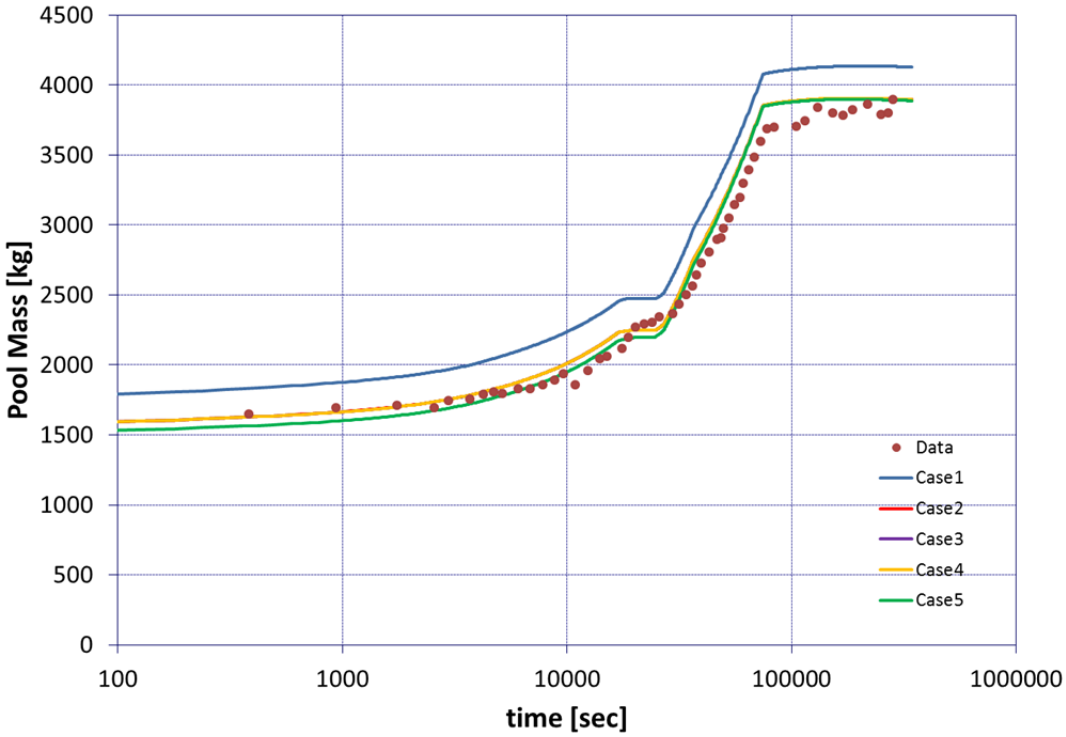

Figure 3.10-6. MELCOR 2.1 Calculated and Measured Pool Mass

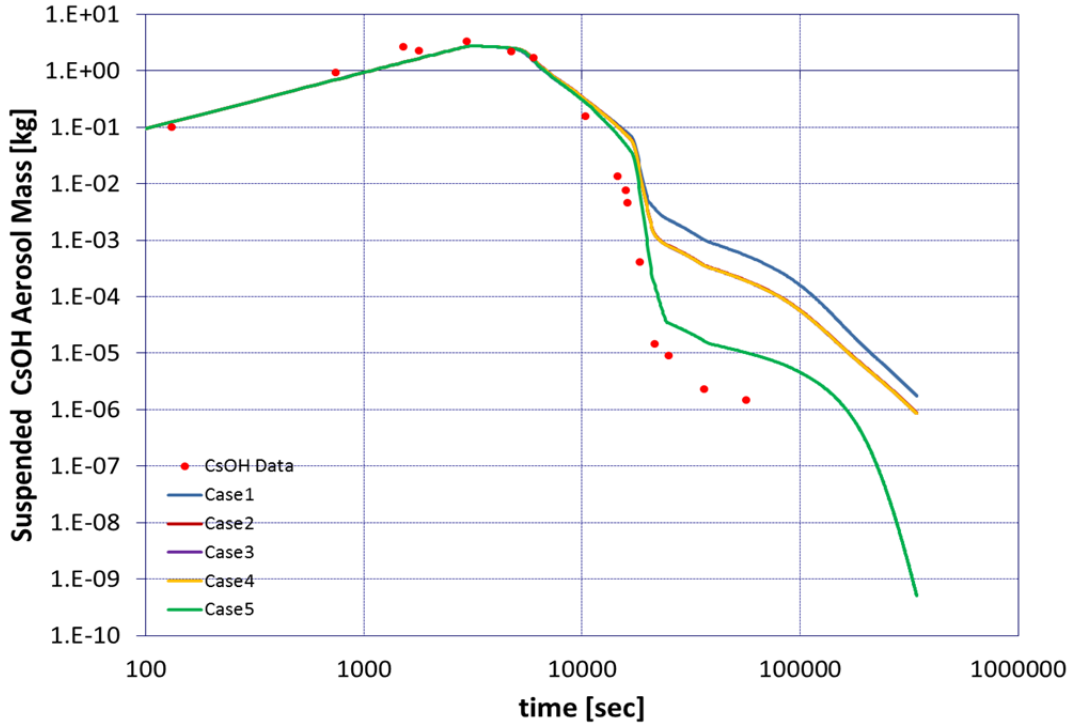

Figure 3.10-7. MELCOR 2.1 Calculated and Measured Suspended CsOH Mass

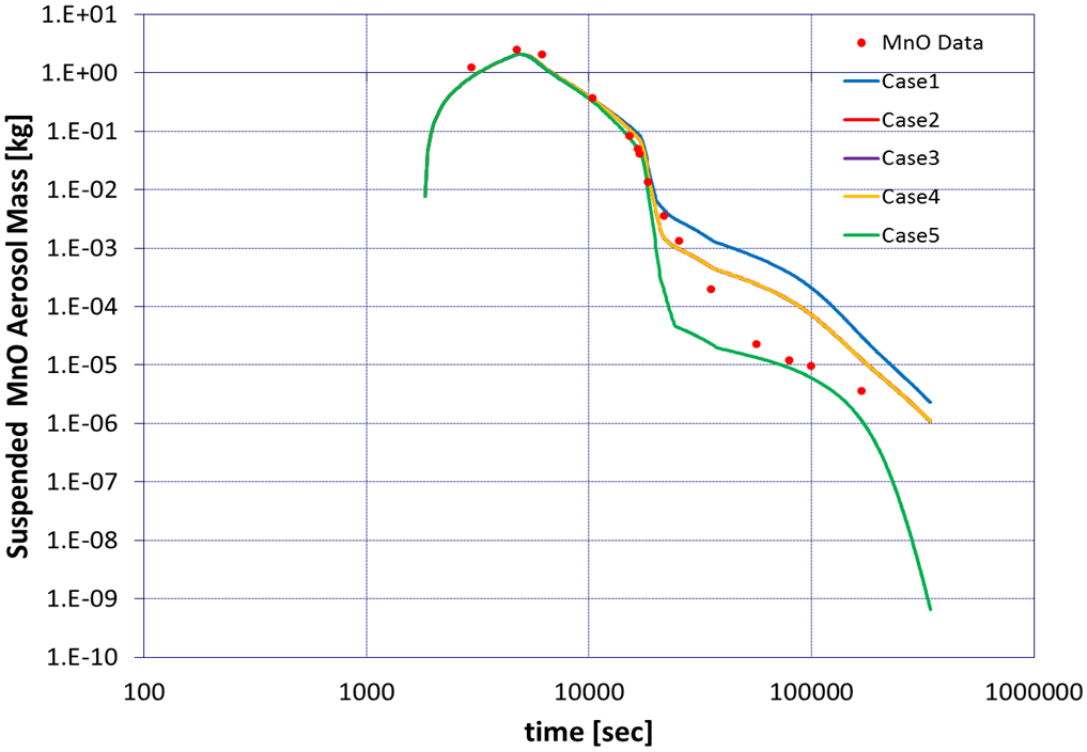

Figure 3.10-8. MELCOR 2.1 Calculated and Measured Suspended MnO Mass

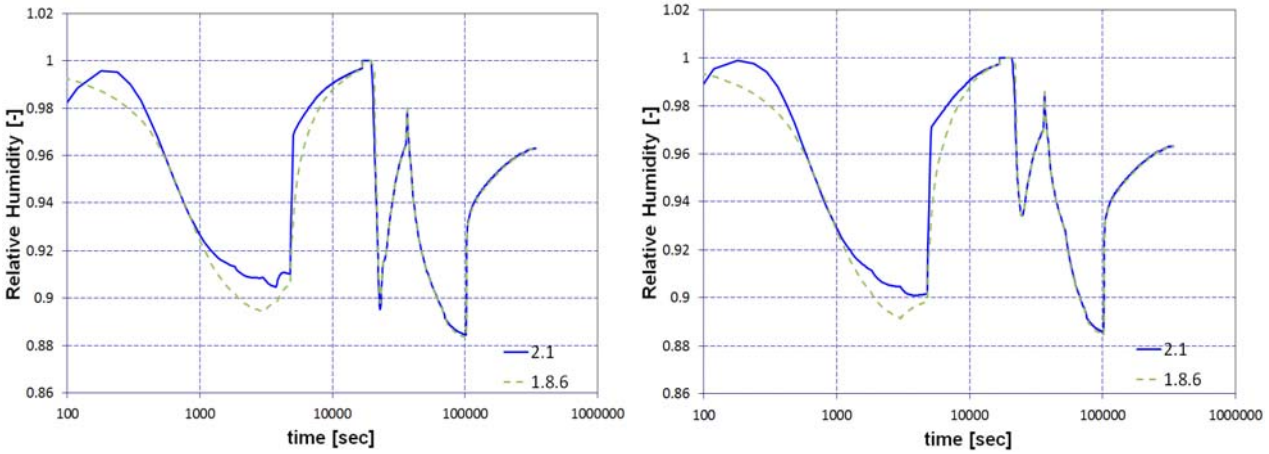

Figure 3.10-9. MELCOR Calculated Relative Humidity (a: Case 1, b: Case 2)

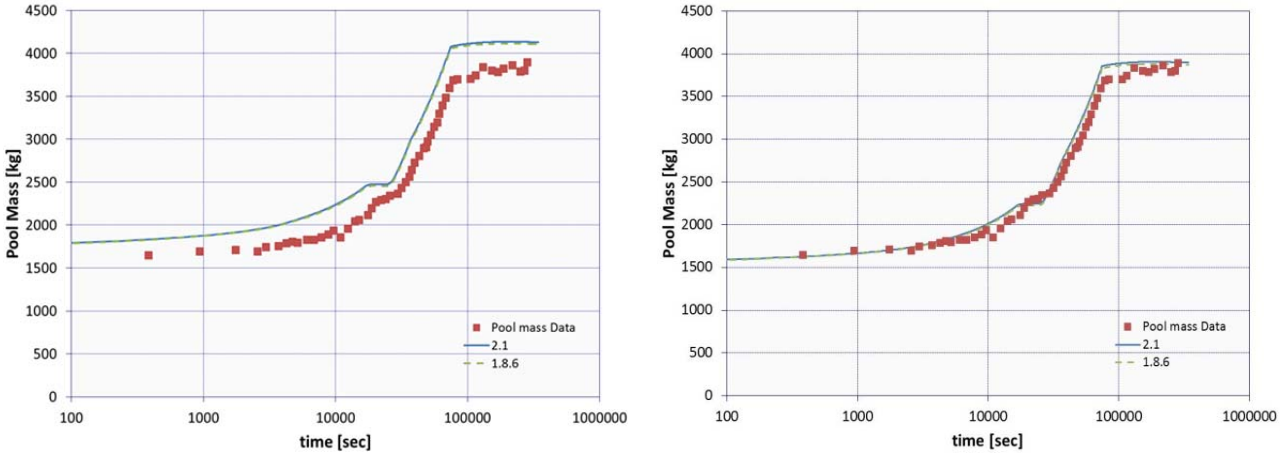

Figure 3.10-10. MELCOR Calculated Vessel Pool Mass (a: Case 1, b: Case 2)

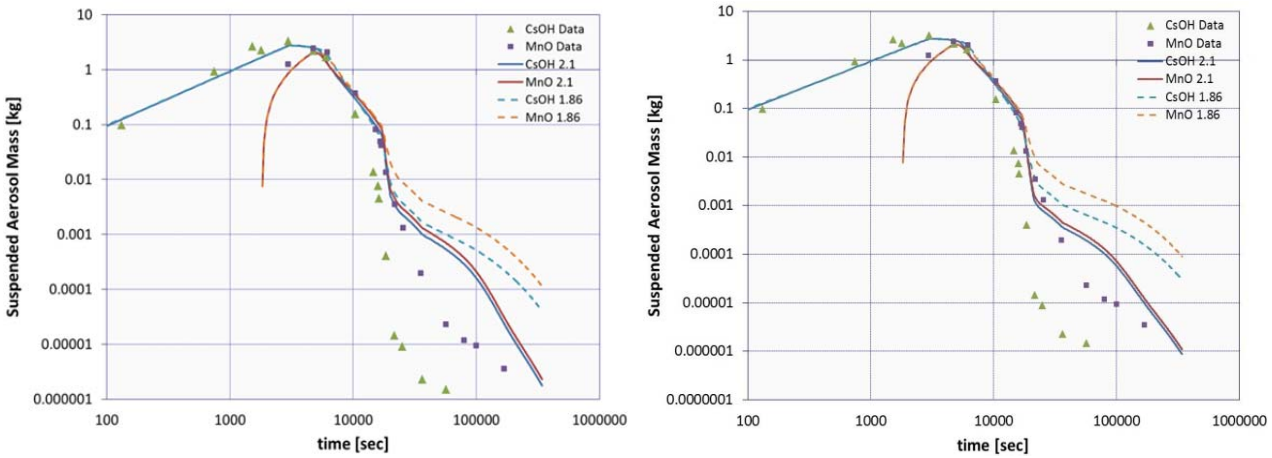

Figure 3.10-11. MELCOR Calculated Vessel Suspended Aerosols (a:Case 1, b:Case 2)

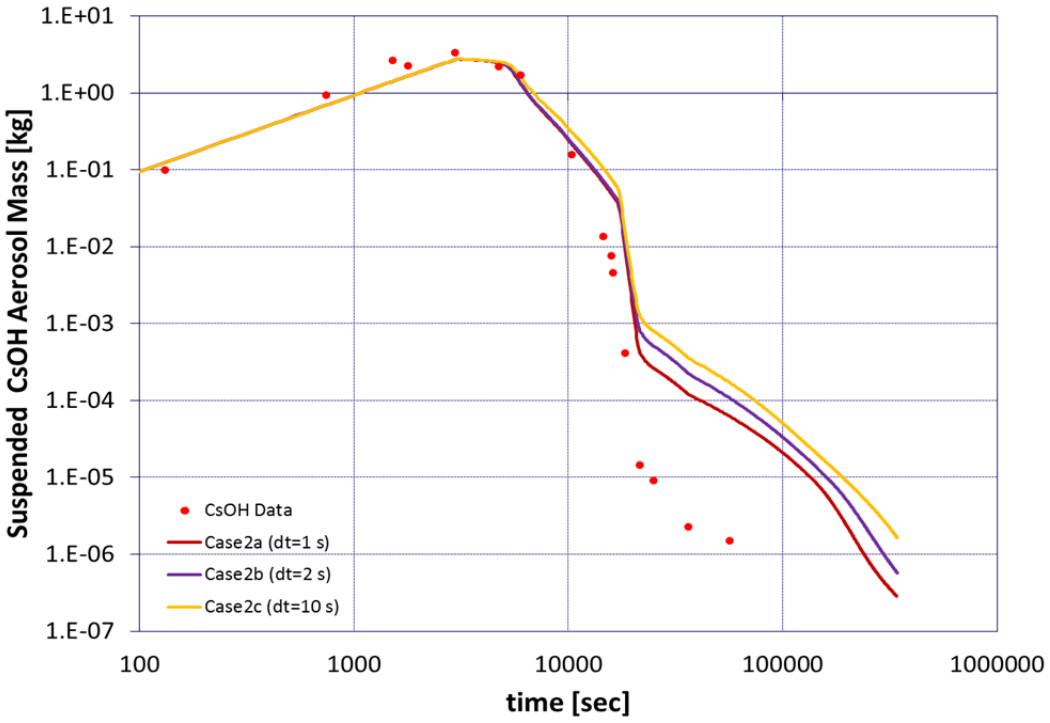

Figure 3.10-12. Timestep Sensitivity for CsOH Aerosol Mass (MELCOR 2.1)

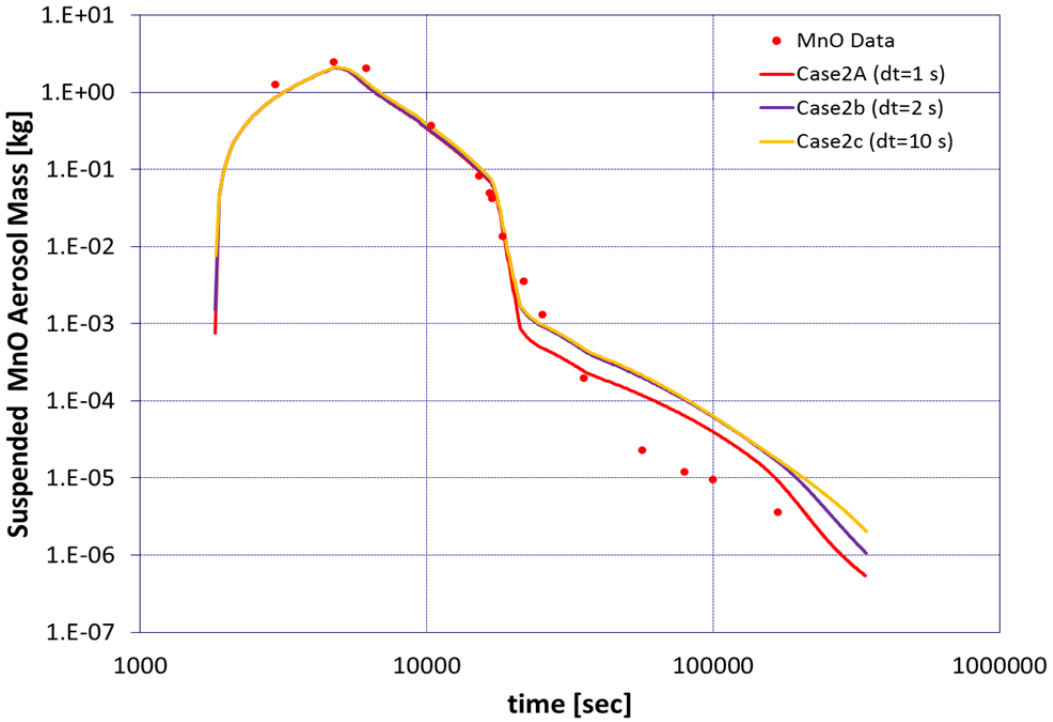

Figure 3.10-13. Timestep Sensitivity for MnO Aerosol Mass (MELCOR 2.1)

3.10.5 References

[3.10.1] McCormack, et al., “Final Report of Experimental Results of LACE Test LA-4,” LACE TR-025, Westinghouse Hanford Co., October 1987.

[3.10.2] Kmetyk, L.N., MELCOR 1.8.1 Assessment of LACE Aerosol Experiment LA-4, SAND91-1532, September 1991.

3.11 Analysis of LOFT LP-FP-2 Experiment

3.11.1 Background

The Loss-of-Fluid Test (LOFT) experimental facility [3.11.1] - [3.11.13] at the Idaho National Engineering Laboratory (INEL) was a 50 MW(t), volumetrically scaled, pressurized water reactor (PWR) system. It simulated a typical, current-generation, commercial 4-loop PWR reactor core, primary coolant system and emergency core cooling system (ECCS), and also included a secondary coolant heat removal circuit and a blowdown suppression system. Much of the background and experimental information for this experiment was adapted from SAND92-1373 [3.11.1].

Experiment LP-FP-2 [3.11.3] - [3.11.13], performed on July 9, 1985, was the second fission product (FP) release and transport experiment of the Organization for Economic Cooperation and Development LOFT Project, and the last experiment conducted in the LOFT facility. This FP test was the largest severe fuel damage experiment ever conducted, and serves as an important data point midway in size between smaller-scale tests and the TMI-2 accident. Many similarities have been identified in the materials behavior observed in the LP-FP-2 test and those reported for both smaller experiments and the TMI-2 accident.

The V-sequence accident, a hypothetical event first postulated in the Reactor Safety Study [3.11.14], is defined as a rupture in a low pressure injection system (LPIS) line outside the containment with simultaneous failure to isolate the system. The V-sequence was also identified as a major risk contributor for both Surry and Sequoyah in the more recent, more detailed NUREG-1150 PRA study [3.11.15].

3.11.2 Experiment

The LOFT experimental facility [3.11.2] was designed to simulate the major components and system response of a current-generation PWR during a LOCA. The experimental subsystems include the reactor vessel, the intact loop, the broken loop, the blowdown suppression tank (BST) system, and the ECCS. The arrangement of the major LOFT components for test LP-FP-2 is shown in Figure 3.11-1.

The objectives for this experiment include:

- Obtain FP release, transport and deposition data during the early phase of a risk dominant reactor transient
    - Assess the understanding of the physical phenomena controlling reactor system FP behavior
    - Assess the capability of computer models to predict this behavior, including release and transport

    - Observe the transport of these FPs in a vapor/aerosol dominated environment from the primary coolant system (PCS), through a simulated low pressure injection system line to a BST and determine
        - The fraction of volatiles (such as Cs, I, Te, Xe and Kr) and aerosol released to and from the upper plenum region of the core
        - The fraction of volatiles and aerosols out of PCS
        - The retention of volatiles on representative PCS surfaces in the plenum and piping
        - The general mass balance of volatiles in the fuel, PCS and BST
- Obtain information on the FP releases from fuel rods at temperature excessing 2100 K
- Use thermal hydraulic conditions similar to the V-sequence accident scenario (such as interfacing system LOCA)

The intact loop simulated three loops of a commercial 4-loop PWR and contains a U-tube steam generator, two primary coolant pumps in parallel, a pressurizer and surge line, a Venturi flowmeter and connecting piping. The LOFT intact loop steam generator was a vertical shell and U-tube recirculation-type heat exchanger. A spool piece was connected from the intact loop cold leg (ILCL) downstream of the pump discharge to the BST, providing the initial break path during the blowdown while the core was still covered with coolant. The pipe for this break path was 1.25-in Schedule 160 piping with an inner diameter of 0.0295 m (1.16 in); the full flow area was used to vent PCS coolant. This ILCL break was closed prior to fission product release so that the fission product transport would be solely through the simulated LPIS line as described below.

The broken loop consisted of a hot leg and a cold leg. For this experiment, the broken loop cold leg was flanged off, and the broken loop pump and steam generator simulators were removed. The simulated LPIS line is depicted in Figure 3.11-2. It contained an aerosol filter, gamma spectrometer and deposition coupons to measure aerosol and fission product release from the primary system. The LPIS line was connected to the end of the broken loop hot leg and provided the path for fission product transport from the primary system to the BST. The pipe size selected for the LPIS line was 1.25-in Schedule 160, identical to the ILCL break piping, with a total length of 21.34 m. A line also ran from the pressurizer power-operated relief valve (PORV) to the suppression tank, so all the coolant and effluent leaving the primary system was collected in a single vessel.

The LOFT reactor vessel, shown in Figure 3.11-3, has an annular downcomer, a bypass region, a lower plenum, lower core support plates, a nuclear core, and an upper plenum. The downcomer is connected to the cold legs of the intact and broken loops, and the upper plenum to the hot legs. The main flow path is around the distribution annulus, down the downcomer into the lower plenum, through the core and out the outlet nozzles; however, there are several alternate (core bypass) flow paths available which do not direct coolant through the core, and which can act as steam vent paths during a transient.

The core consists of approximately 1,200 enriched uranium fuel rods arranged in five square and four triangular (corner) fuel assemblies. The fuel rods were designed to commercial PWR specifications, except that they were only 1.68 m (5.5 ft) long and several fuel rods had special instrumentation. The central fuel module (CFM) contained 100 fuel rods and 21 control rod guide tubes in an 11 x 11 square array; 11 Ag-In-Cd control rods were inserted into selected guide tubes in the CFM during the LP-FP-2 experiment. (The main purpose of the CFM control rods was to provide Ag-In-Cd material for aerosol generation and deposition sites for fission products during the high-temperature portion of the experiment, as would be present in a PWR during a V-sequence.) All fuel rods in the CFM were pressurized to 2.41 MPa; all fuel rods in the peripheral fuel assemblies were unpressurized. An insulating flow shroud took the place of the outer two rows of fuel rods in the CFM, and protected the peripheral fuel assembly module (PFM) from excessive temperatures while allowing the central fuel assembly to reach requisite temperatures for fuel rod failure and fission product release.

The two LOFT ECCS trains are capable of simulating the emergency coolant injection of a commercial PWR. Each consists of an accumulator, a high-pressure injection system, and a low-pressure injection system. Because there were no programmatic considerations inherent in emergency core coolant (ECC) operation during test LP-FP-2, the ECC injection was not scaled to represent commercial PWR operations.

A complete Fission Product Measurement System (FPMS) was designed and fabricated for the detection, identification and collection of radioactive isotopes in the primary coolant system, LPIS piping, and suppression tank (see Figure 3.11-4).

Experiment LP-FP-2 consisted of four distinct phases: fuel pre-conditioning, pre-transient, transient and post-transient. These four phases were contiguous; however, each phase had a specifically designed beginning and end. The fuel pre-conditioning and post-transient phases were relatively long compared with the much shorter pre-transient and transient phases. The purpose of the fuel pre-conditioning phase was to build sufficient fission product inventory in the fuel. This was achieved in two steps of high power operation followed by an equally long shutdown period. During the second phase, a fuel exposure of 430 MWd/MTU was reached and the design steady-state full-power initial conditions were established; the initial condition requirements included a core decay heat of between 675 kW and 695 kW at 200 s following reactor scram, as well as typical pressure, temperature and flow conditions that would simulate a commercial PWR. The steady-state initial conditions specified and achieved are listed in Table 3.11-1. Table 3.11-2 summarizes the chronology of events for LP-FP-2. The measured pressure and corresponding major events in this experiment are shown in Figure 3.11-5. The major events shown in this figure reflects in events summarized in Table 3.11-2.

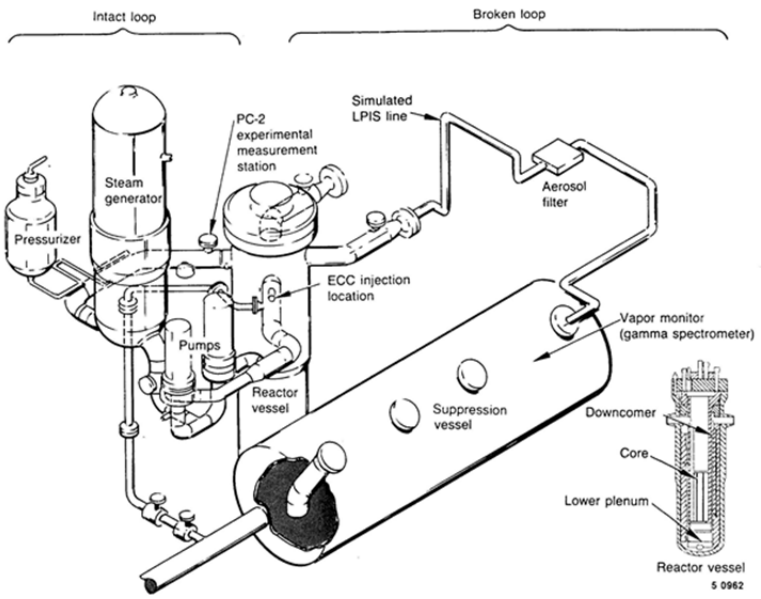

Figure 3.11-1 Experiment Apparatus [3.11.6]

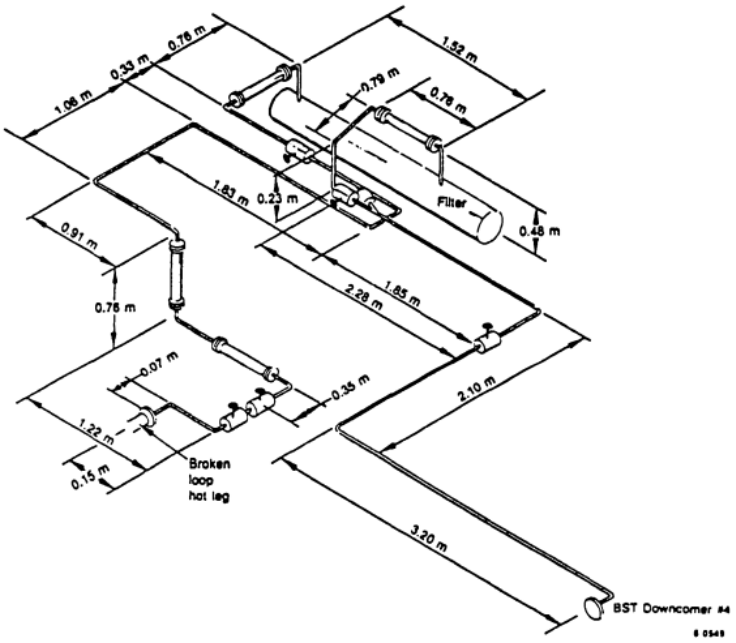

Figure 3.11-2 Schematic of Simulated LPIS Line for LOFT LP-FP-2 [3.11.16]

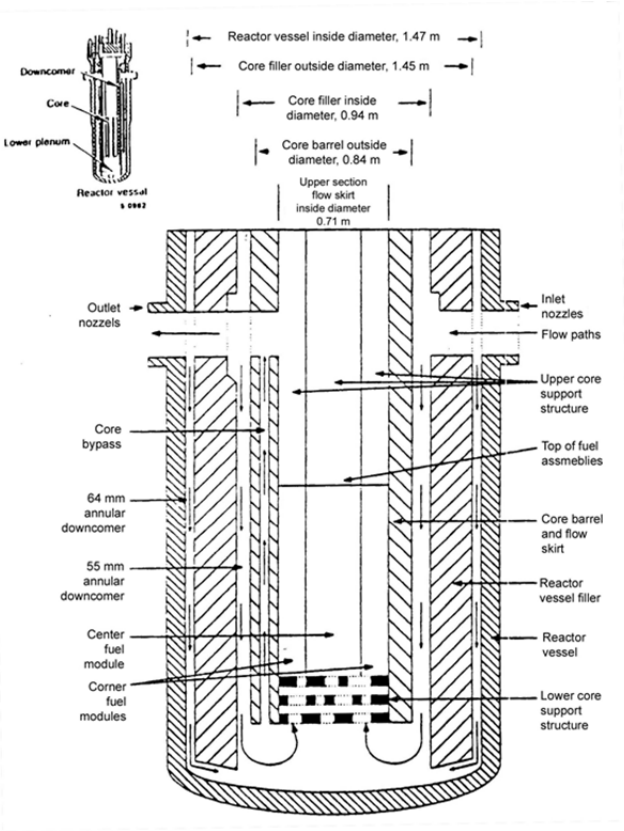

Figure 3.11-3 Schematic of Reactor Vessel for LOFT LP-FP-2 Experiment [3.11.17]

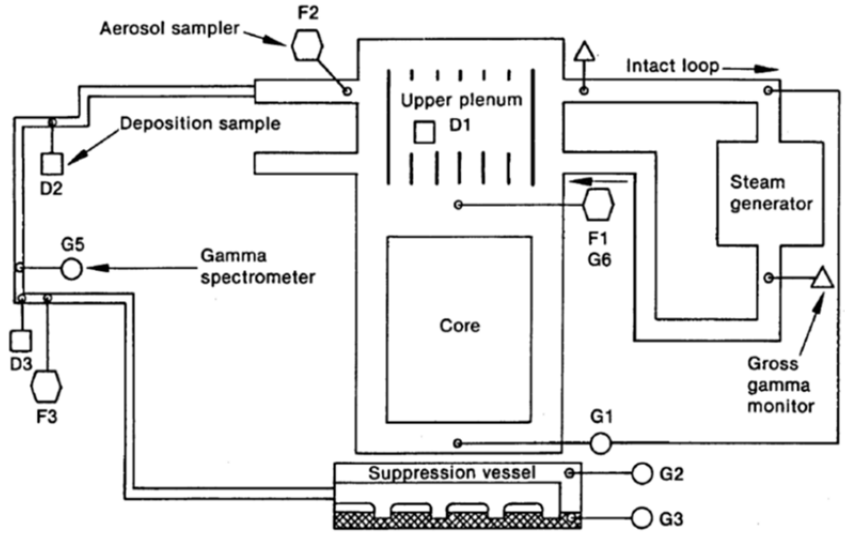

Figure 3.11-4 Fission Product Measurement System [3.11.16]

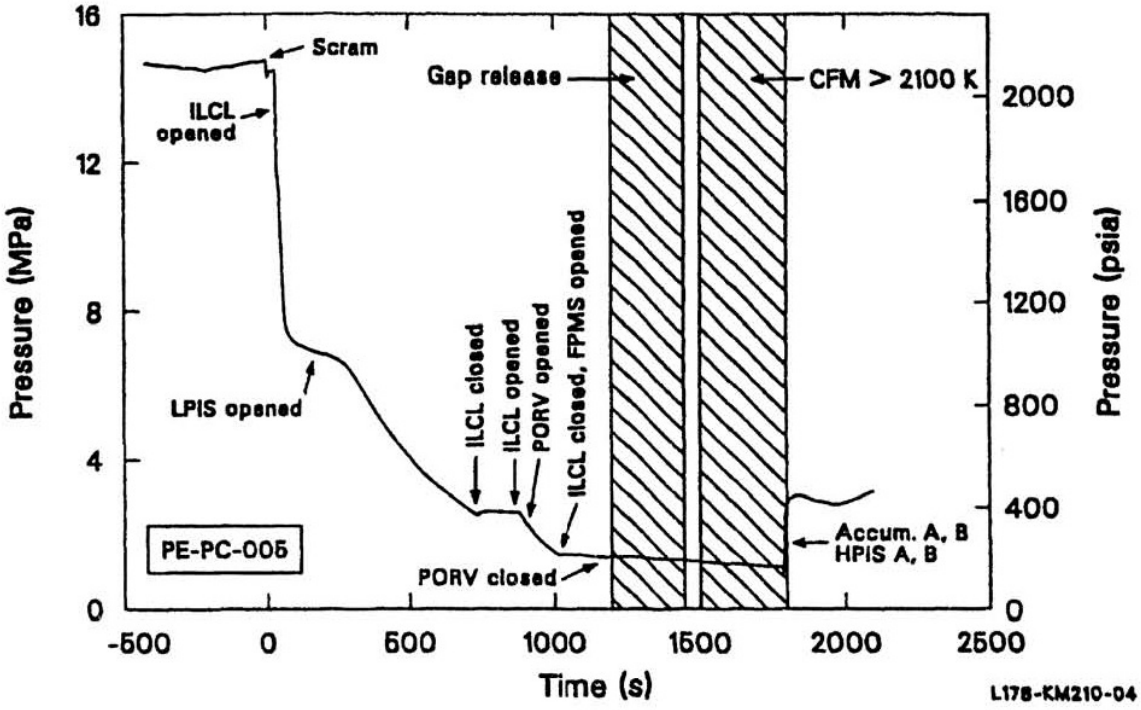

Figure 3.11-5 Measured Primary System Pressure and Corresponding Major Events [3.11.16]

Table 3.11-1 LOFT LP-FP-2 Experiment Steady-State Conditions [3.11.6]

Parameter	Specified [A]	Measured
Primary Coolant System		
Core ΔT (K)		11.7 ± 1.4
Pressure (MPa)	14.95 ± 0.1	14.98 ± 0.1
Hot leg temperature (K)	571 ± 1.1	571.6 ± 0.8
Cold leg temperature (K)		559.9 ± 0.8
Loop mass flow (kg/s)	479 ± 19	475 ± 2.5
Boron concentration (ppm)		499 ± 15
Pump injection (liter/s)	0.127 ± 0.016	0.128 ± 0.003
Reactor Vessel		
Power level (MW)	26.5 ± 0.5	26.8 ± 1.4
Decay heat @ 200 s (kW)	685 ± 10	684.8
Max linear heat generation rate (kW/m)	~40	42.6 ± 3.6
Control rod position (m)	1.37 ± 0.01	1.38 ± 0.01
Steam Generator Secondary		
Pressure (MPa)		6.38 ± 0.08
Water level [B] (m)		3.12+0.06
Pressurizer		
Liquid volume (m^3)		0.57 ± 0.03
Steam volume (m^3)		0.37 ± 0.03
Water temperature (K)		616.9 ± 2. 1
Pressure (MPa)		15.1 ± 0.1
Water level (m)	1.12 ± 0.1	1.06 ± 0.06
Suppression Tank		
Liquid level (m)	1.19 ± 0.051	1.18 ± 0.06 [C]
Gas volume (m^3)		59.11 ± 2.02
Water temperature (K)	<311	295.6 ± 0.5

Gas pressure (kPa)	100 ± 20	95 ± 3
Boron concentration (ppm)		3710 ± 15
ECCS		
Borated water storage tank temperature (K)	303 ± 3	301.3 ± 3
Accumulator A		
Liquid level (m)	<2.17	1.81 ± 0.02
Pressure (MPa)	>4.21	5.1 ± 0.06
Liquid temperature (K)	303 ± 3	303.1 ± 0.7
Accumulator B		
Liquid level (m)	<2.16	1.81 ± 0.02
Pressure (MPa)	>4.21	4.95 ± 0.06
Liquid temperature (K)	303 ± 3	305.6 ± 0.7

[A] If no value is listed, none was specified

[B] Steam generator liquid level referenced to 2.95 m above the top of the tube sheet

[C] This value is out of specification

Table 3.11-2 Operational Sequence of Events for LOFT LP-FP-2 Experiment [3.11.6]

Event	Time* (s)
Scram	0.0
Control rods fully inserted	2.4 ± 0.1
Pump coast-down initiated	9.7 ± 0.1
CFM control rods fully inserted	23.4 ± 0.5
ILCL break initiated	32.9 ± 0.1
Pump coast-down complete [A]	25.1 ± 0.1
End of subcooled blowdown [B]	53 ± 1
Secondary relief valve cycle	56 ± 1
Pressurizer empty	60 ± 5
LPIS break initiated	221.6 ± 0.1
$P_{sec} > P_{pri}$	260 ± 10
Earliest TC variation from saturation	-----
upper plenum	300 ± 10
hot leg piping	390 ± 10
downcomer	730 ± 10
lower plenum	800 ± 20
Fuel rod heat-up started in periphery	662 ± 2
Fuel rod heat-up started in CFM	689 ± 2
ILCL break closed	735.5 ± 0.1
ILCL break reopened	877.6 ± 0.1
PORV opened	882.0 ± 0.l
F3 filter online	950.8 ± 0.1
LPIS bypass closed	951.9 ± 0.1
FPMS lines opened	1013.0 ± 0.1
ILCL break closed	1021.5 ± 0.1
PORV closed	1162.0 ± 0.1
First (gap) fission products at F1	1200 ± 20

First (gap) fission products at F2	1200 ± 20
First (gap) fission products at F3	1249 ± 60
Max UP coolant temperature	1495 ± 5
First (fuel) fission products at F1,F2,F3	1500 ± 10
Clad temperatures reach 2100K	1504 ± 1
Shroud temperatures reached trip set point	-----
1st TC	1743 ± 1
2nd TC	1766 ± 1
LPIS break closed	1777.6 ± 0.1
FPMS lines closed	1778.1 ± 0.1
Max UP metal temperature	1780 ± 5
Deposition coupons isolated	1780.6 ± 0.1
ECCS initiated	1782.6 ± 0.1
Accumulator flow stopped	1795 ± 2
Max LPIS line coolant temperature reached [C]	1800 ± 5
Core quenched	1795 ± 5

*Measured data

[A]Pumps were allowed to coastdown under the influence of the motor generator flywheel until the pump speed reached 750 rpm. At that time, the flywheel was disconnected from the motor generator and the pumps quickly stopped adding energy to the fluid. The time at which the flywheel was disconnected is defined for this time.

[B] End of subcooled blowdown is defined as the time when the first measured fluid temperature outside of the pressurizer reaches saturation conditions.

[C] These temperatures represent the maximum measured temperatures prior to reflood at these locations.

3.11.3 MELCOR Model

The original development of the MELCOR 1.8.1 model [3.11.1] for LOFT LP-FP-2 experiment was derived from the RELAP5/MOD1 independent assessment analyses [3.11.18], [3.11.19], [3.11.20], [3.11.21], [3.11.22]. The latest MELCOR model for MELCOR 1.8.6 and MELCOR 2.1 includes a more refined nodalization of the core and loop with 24 control volumes (CVs), 37 flow paths (FLs) and 71 heat structures (HSs). This refined nodalization is presented in Figure 3.11-6. As shown in Figure 3.11-6, 12 CVs for the reactor vessel are numbered in 100s, the 7 primary loop CVs in 200s and 3 secondary loop CVs in 300s. The break flows from the primary loop are to the BST as represented as CV400, and the containment is represented as CV500. As shown in this figure, the COR nodalization for the core is also given. The reactor vessel was modeled – a downcomer (CV100), bypass (CV105), lower plenum (CV110) and upper plenum (CV130), and 8 core CVs. The core region contains 4 axial CVs for CFM (CV111 to CV114), and PFM (CV121 to CV124). In addition, the core includes 19 internal FPs and 54 internal and coupled HSs. Among the internal FPs, a cross flow from CFM to PFM CVs was added. A single containment volume for any flow out for the secondary loop and a single CV for the BST where the PORV, broken loop and intact cold leg (ILCL) flows can be directed. CV320 as shown in Figure 3.11-6presents the normal flow out of the steam in the secondary side of the steam generator via FL215. CV500 represents the containment for the flow (FL225) from the safety relief valve from the secondary side of the steam generator after the MSIV (FL215) is closed. Excluding the core HSs, there

are a total of 13 HSs for the loops, including those in the secondary sides of the heat exchanger. Also shown in this figure is the assignment of CVH volumes to the core cells and their corresponding height level (the lowest point is referenced to the bottom of the lower plenum).

Efforts have been made to minimize the use of the high loss coefficients in the FL inputs to benchmark the thermal-hydraulics conditions of the experiment by increasing the number of the CVs in the model. These efforts were done in the core region by increasing the number of the volumes in the core, which allows the loss coefficients to reduce from the order of hundreds down to the order of tens or smaller. Other regions of the models, such as the primary and secondary loops, have not been done. The loss coefficients are in the order of tens or smaller.

In addition, similar to the previous calculation done with MELCOR 1.8.1 [1], SC1502(1) and SC1502(2) for the COR-package sensitivity coefficients are set to 1x10-7 kg and 0.167 kg, respectively; however, SC1502(2) was deviated slightly from 0.001 kg. This deviation was due to the ratio recalculated for a 50MW versus 3000 MW reactor sizes between the LOFT and the typical commercial plant. As the previous calculation [3.11.1], the original MELCOR 1.8.1 model predicted the timing of the first gap release between 1285 to 1333 seconds as results of the computer platform dependency. Nonetheless, this model reported herein predicted the similar timing, which is consistent with the previous calculation [3.11.1]. Similarly, the SCDAP/RELAP calculation [3.11.17] showed the similar predicted timing of the first gap release at 1358 seconds. This similar timing in MELCOR may have been caused by the adaptation of the RELAP model into MELCOR. As a sensitivity study, aerosol section size was increased from 5 to 10. Both MELCOR 1.8.6 and MELCOR 2.1 cases have the same run cases (see Table 3.11-3), except those cases involved with turbulent deposition as described below.

Table 3.11-3 MELCOR Sensitivity Cases

Test Case	2.1	1.8.6
Base case*	X	X
Same as Base case, except increase aerosol section to 10 (default).	X	X

*Aerosol section was chosen to be 5, deviated from default of 10

PULSE computer code predicted that turbulent deposition in the LPIS piping is dominated for the aerosol deposition because of the high gas velocity which yields high Reynolds number (> 300,000) [3.11.23]. This deposition would reduce the amount of FPs into the BST. Base on this, and given that a new turbulent deposition has been implemented into MELCOR 2.1, additional runs were conducted for MELCOR 2.1. This turbulent deposition model requires heat structures to be specified and the orientation of

the heat structures to be specified. No turbulent deposition occurs when the heat structure is submerged. In MELCOR, the horizontal surfaces, regardless if it is a slab, a pipe or sphere, will always be submerged if the volume void fraction is not unity. In this case, there would be no turbulent deposition. To overcome this, the horizontal surfaces must be modified to include a vertical wall heat structure, so that any portion of the vertical surface that is not submerged can be used to calculate the amount of FPs deposited. To simplify the heat structure modeling for the cylindrical piping, a floor and a vertical wall with the same surface area in a rectangular geometry are assumed. As shown in Figure 3.11-6, the LPIS piping is included in CV290 and the flow path representing the flow from LPIS to the BST is FL415. In addition to CV290, CV210 has a flow path, FL405 which represents ILCP flow to the BST. FL405 may For CV290, HS41501 represents the LPIS piping. For CV210, there are two heat structures, representing the ILCL piping (HS40501 and HS40502). Additionally, the number of bends was also added for the turbulent model, but they were estimated. Using the information from these heat structures, the heat structures are modeled as floors with additional three, new vertical heat structures matching the inner surface area of the piping. Thus, a modified input deck (V0) was created.

3.11.4 Results and Discussions

In terms of MELCOR calculations, the cases identified in Table 3.11-3 were run using MELCOR 1.8.6 revision 3964, and MELCOR 2.1, revision 6450. All plots presented in this section are for the base case using both MELCOR 1.8.6 and 2.1. As shown in Figure 3.11-7 and Figure 3.11-8, respectively, the primary pressure and secondary pressure calculated by MELCOR are in close agreement with the experimental data [3.11.1]. As shown in Figure 3.11-7, MELCOR predicted slightly higher values than that of the experiment at the beginning of the experiment, then matches very closely with the experiment. Finally, after the ILCL opened and PORV opened, MELCOR predicted lower values than the experiment as shown in Figure 3.11-7. The timings of the events denoted in this figure are those provided in Figure 3.11-5, except the first gap release timing (2.1 predicted at 1319 s), which is calculated by MELCOR. This timing is consistent with the previous MELCOR calculation and the RELAP calculation as described above. For the secondary pressure prediction, MELCOR predicted more oscillatory and slightly higher pressures than the experiment as shown in Figure 3.11-8. MELCOR 2.1 predicted slightly secondary pressure than that of MELCOR 1.8.6 as shown in this figure. In terms of core data validation, Figure 3.11-9 shows the predicted MELCOR cladding temperatures for Core cell 106 in the CFM near the bottom of the active fuel region. As shown in this figure, MELCOR predictions closely follow the experimental data up to about 1,650 s, then MELCOR 2.1 exhibits early heat up of the cladding than that of MELCOR 1.8.6, which may be due to the early cladding oxidation (see Figure 3.11-10). Note that the MELCOR model is intended to validate the aerosol deposition and is not to validate the thermal-hydraulic response. Consequently, the loss coefficients were chosen to match the thermal-hydraulic response to provide the appropriate boundary conditions for the calculation of the aerosol deposition as given below.

In terms of the aerosol physics, Table 3.11-4 shows the comparison between MELCOR and experimental data. As shown in this table, columns 5 and 6 are the lower and upper bound of the measuring and calculated data from the experiment. In terms of MELCOR calculations, both MELCOR 2.1 and 1.8.6 predicted the aerosol release within the experimental bound as shown in this table, except I_2, Ba and Te, which is below the lower bound of the experiment.

As previously discussed, the turbulent deposition may further reduce the amount of the aerosol release. In order for the turbulent deposition to occur, the gas or vapor velocity must be sufficiently high. Figure 3.11-11 shows the vapor velocities of the two flow paths (FL405 and FL415) that lead to the BST. As shown in this figure, the velocity for FL415 is about 250 m/s for most the time, which FL405 only occurs prior to the gap release. As previously described, the original MELCOR model in the control volumes of concern for the turbulent deposition must be modified. This modified input (V0) was used for both the base case and for aerosol section of 10. The results for MELCOR 2.1 are given in Table 3.11-5. As shown in this table, the turbulent deposition, particularly for the Cs group is significantly increased in the RCS piping, thus reducing the amount released to BST. The turbulent deposition effect was also evidenced for other fission product groups as well, but not significant. For I_2, only a slight reduction in the release to the BST is shown when turbulent deposition is turned on.

In closing, the detailed nodalization of the MELCOR model for this experiment seems to work well, without using extensive friction and loss coefficients to match the experimental thermal-hydraulics at power. In terms of radionuclide releases, MELCOR generally predicts well for most of the aerosol classes. The use of the turbulent deposition in the modeling will increase the amount of the deposition in the piping prior to the release to the BST. The gap release timing calculated by MELCOR is later than that of the experiment to about 100 s may underestimate the gap release. Since this MELCOR model was adapted from the RELAP calculation, this model is known to be off about 100 s as previously described. This difference in the gap release timing may contribute to the lower aerosol release calculated for some of the classes in comparison to the experiment. Thus, a refined MELCOR model may be required to better predict the gap release. It should be noted that the use of any friction and loss coefficients as stated above, other than reflecting the actual geometry may be due to some model inconsistencies which may be dated back to the original MELCOR model development. Thus, it is recommended that this model may be only used as the intent described here. Further review of the MELCOR model against the actual experiment may be required to ensure the thermal-hydraulic condition is modeled correctly.

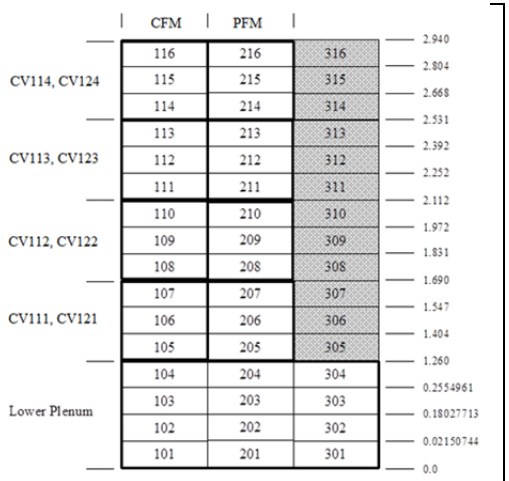

Figure 3.11-6 MELCOR CVH/FL and COR Nodalizations for LOFT LP-FP-2 Experiment

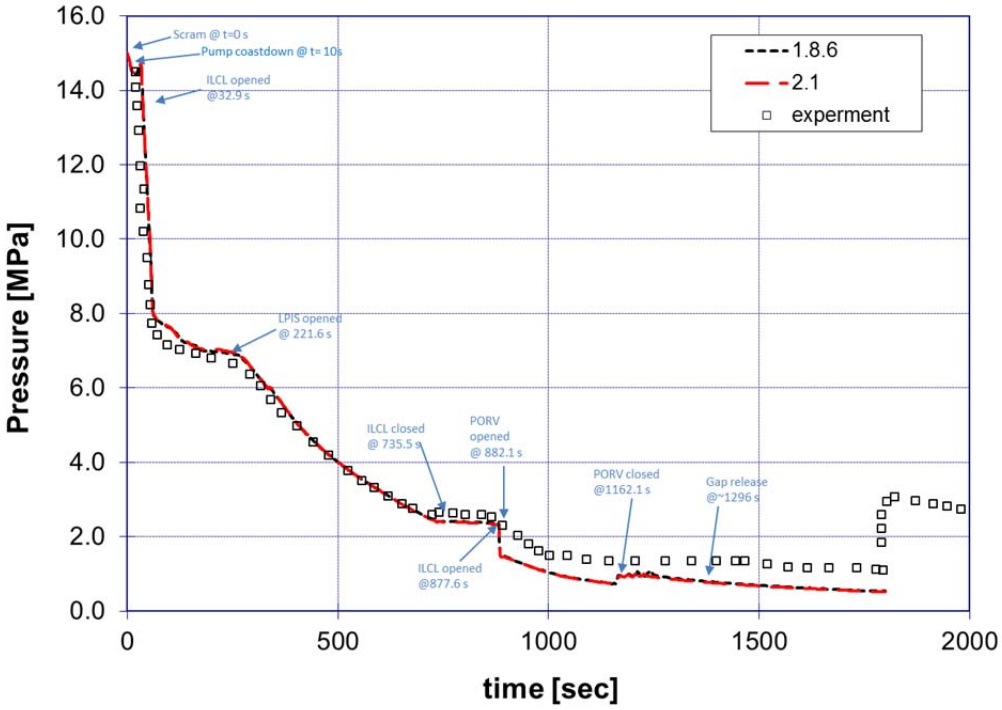

Figure 3.11-7 Primary Pressure Results

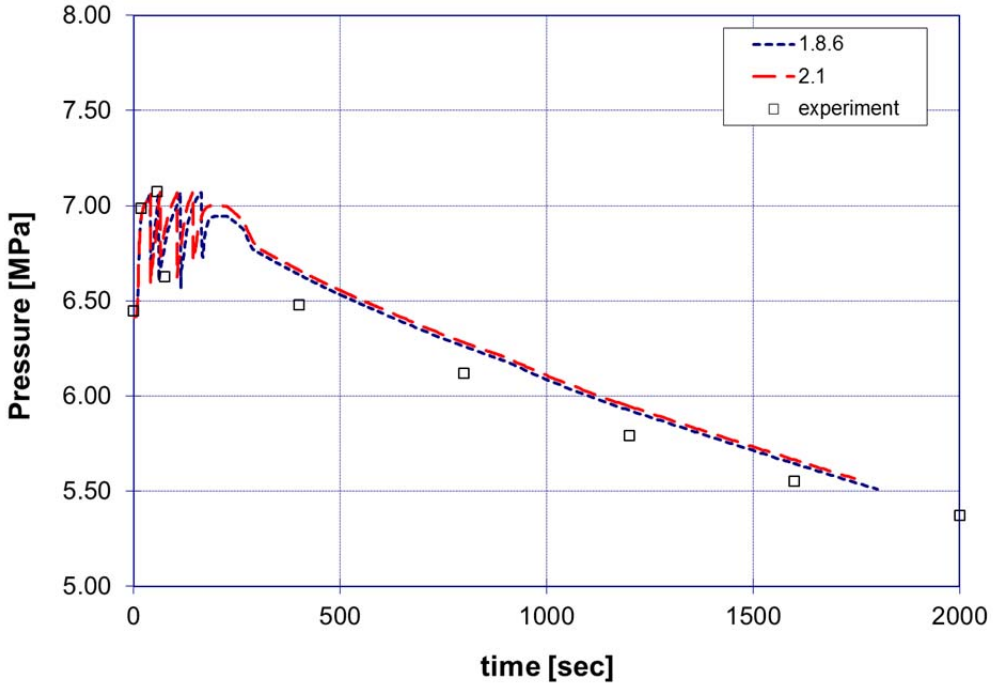

Figure 3.11-8 Secondary Pressure Results

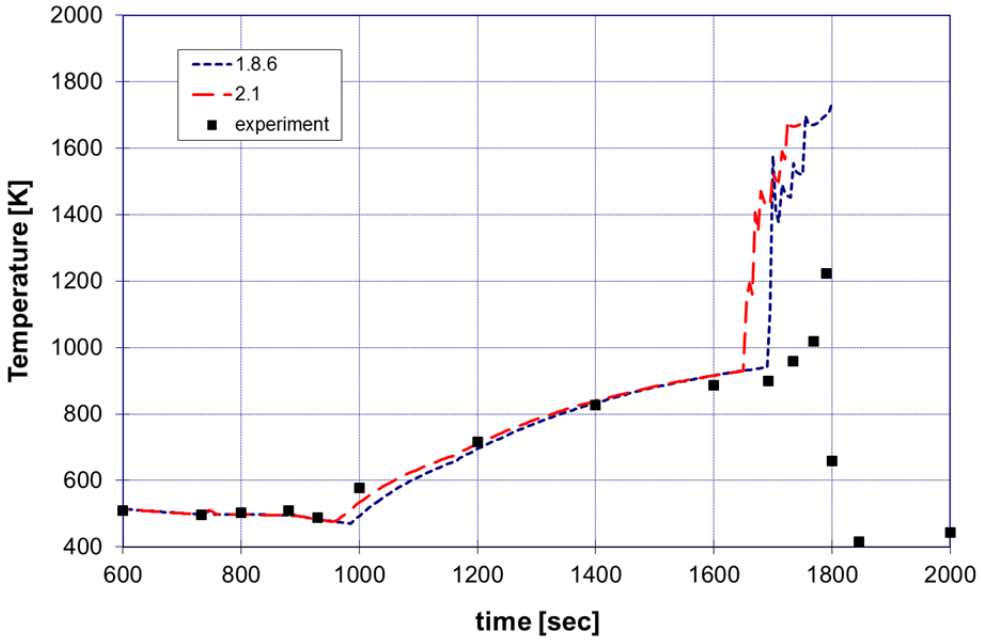

Figure 3.11-9 Cladding Temperature Results for Core Cell 106

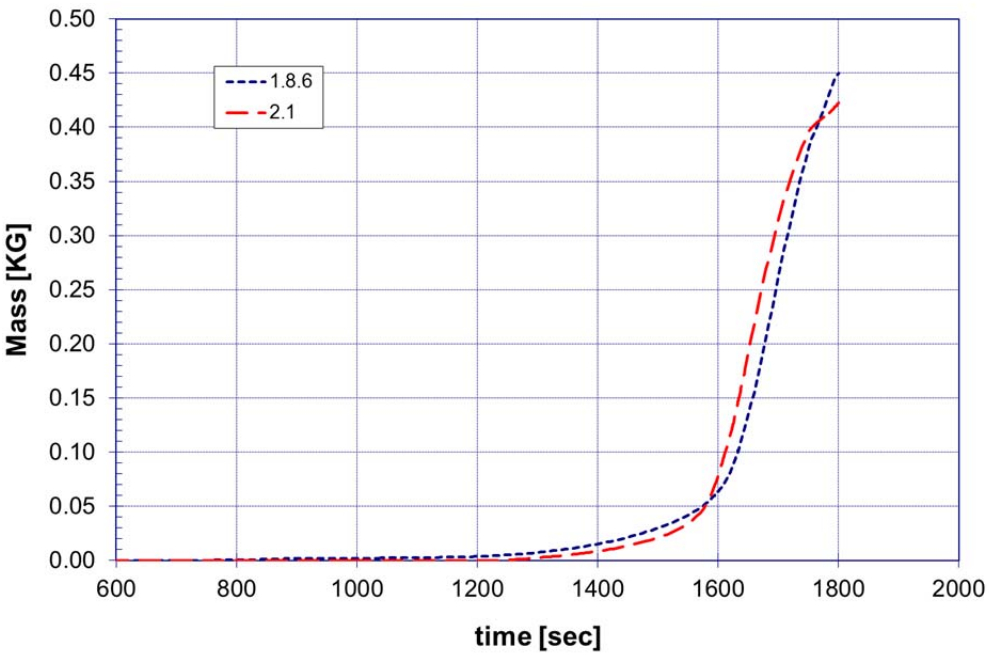

Figure 3.11-10 MELCOR Predicted Hydrogen Production Mass Results

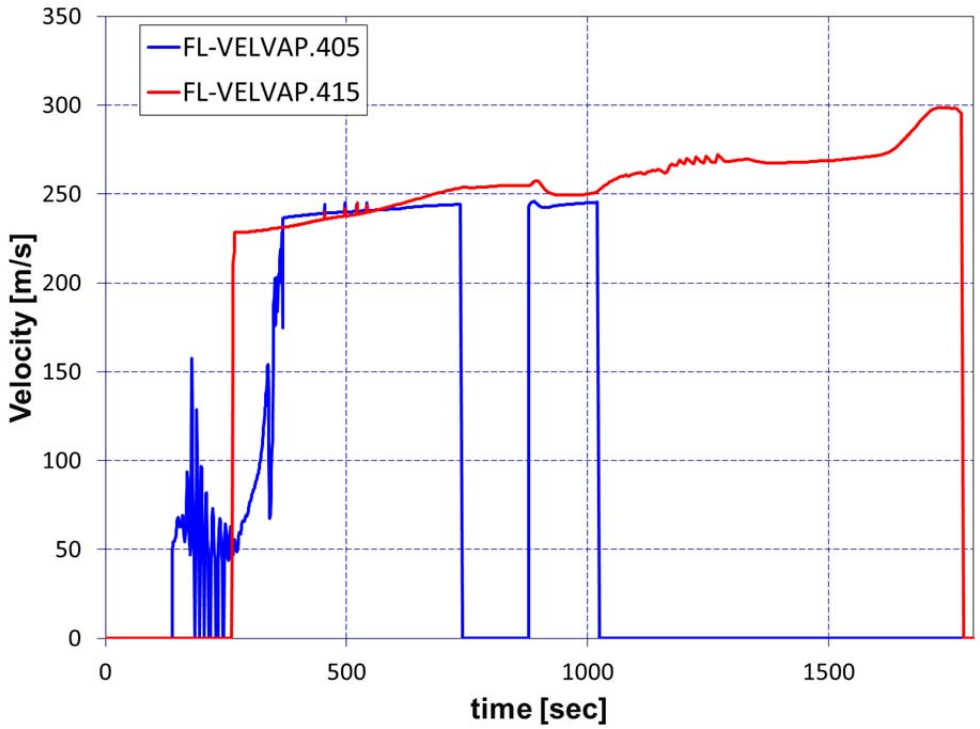

Figure 3.11-11 Calculated Vapor Velocity at ILCL (FL405) and LPIS (FL415) Lines in MELCOR 2.1

Table 3.11-4 Aerosol Calculated Release Fraction Results in BST

Aerosol Class	Estimated on Deposited or DST Data**	Calculated from F1 Sample Line**	Measured Values for PCS**	Experimental Range		MELCOR 2.1 (v6450)***		MELCOR 1.8.6 (v3964)***	
				Low	High	Base Case	10 Section	Base Case	10 Sections
Xe+Kr	3.70E-02	1.01E-01	9.00E-02	3.70E-02	1.01E-01	4.21E-02	4.06E-02	3.43E-02	4.14E-02
Cs	8.00E-03	2.90E-02	1.56E-01	8.00E-03	1.56E-01	3.33E-02	3.21E-02	2.84E-02	3.39E-02
I2	3.00E-02	5.20E-02	1.35E-01	3.00E-02	1.35E-01	2.92E-02	2.81E-02	2.35E-02	2.87E-02
Ba	8.40E-03	2.20E-03	8.20E-02	2.20E-03	8.20E-02	5.36E-05	5.21E-05	4.65E-05	5.10E-05
Te	5.40E-03	2.50E-04	2.90E-02	2.50E-04	2.90E-02	2.26E-02	2.18E-02	1.83E-02	2.23E-02

**The experimental data were obtained from NUREG/CR-6160 [3.11.16]

***Gap release predicted: 2.1-base (1296s), 10 Section (1292s); 1.8.6-base (1329s), 10 section (1320s)

Table 3.11-5 Aerosol Calculated Release Fraction Results for Input Deck (V0) using MELCOR 2.1 (v6450)

Aerosol Class	Base Case (5 Sections)				10 Sections			
	No Turbulent		Turbulent Enabled		No Turbulent		Turbulent Enabled	
	RCS Piping	BST	RCS Piping	BST	RCS Piping	BST	RCS Piping	BST
Xe+Kr	6.32E-03	4.99E-02	6.75E-03	4.14E-02	6.25E-03	4.77E-02	6.67E-03	4.27E-02
Cs	6.21E-03	3.21E-02	2.41E-02	1.42E-02	5.93E-03	3.86E-02	2.50E-02	1.46E-02
I2	4.72E-03	3.49E-02	4.92E-03	2.86E-02	4.64E-03	3.32E-02	4.88E-03	2.96E-02
Ba	5.50E-06	5.93E-05	3.68E-05	2.14E-05	5.29E-06	5.49E-05	3.70E-05	2.21E-05
Te	3.83E-03	2.67E-02	1.62E-02	9.65E-03	3.77E-03	2.55E-02	1.67E-02	9.85E-03

3.11.5 References

[3.11.1] Kmetyk, L. N., “MELCOR 1.8.1 Assessment: LOFT Integral Experiment LP-FP-2”, SAND92-1373, Sandia National Laboratories, December 1992.

[3.11.2] Reeder, D. L., “LOFT System and Test Description”, NUREG/CR-0247, TREE-1208, EG&G Idaho, Idaho National Engineering Laboratory, July 1978.

[3.11.3] Berta, V. T., “Experiment Specification Summary for OECD LOFT Experiment LP-FP-2”, OECD LOFT-T-3801, EG&G Idaho, Idaho National Engineering Laboratory, February 1984 (Rev. 1, June 1985).

[3.11.4] Berta, V. T., “OECD LOFT Project Experiment Specification Document, Fission Product Experiment LP-FP-2, OECD LOFT-T-3802, EG&G Idaho, Idaho National Engineering Laboratory, June 1984 (Rev. 1, May 1985).

[3.11.5] Guntay, S., M. Carboneau, and Y. Anoda, “Best Estimate Prediction for OECD LOFT Project Fission Product Experiment LP-FP-2”, OECD LOFT-T-3803, EG&G Idaho, Idaho National Engineering Laboratory, June 1985.

[3.11.6] Adams, J. P., and J.C. Birchley, N. Newman, E.W. Coryell, M.L. Carboneau, S. Guntay, L.J. Siefken, “Quick-Look Report on OECD LOFT Experiment LP-FP-2, OECD LOFT-T-3804, EG&G Idaho, Idaho National Engineering Laboratory, September 1985.

[3.11.7] Carboneau, M.L., R.L. Nitschke, D.C. Mecham, E.W. Coryell, and J.A. Bagues, “OECD LOFT Fission Product Product Experiment LP-FP-2: Fission

Product Data Report", OECD LOFT-T-3805, EG&G Idaho, Idaho National Engineering Laboratory, May 1987.

[3.11.8] Carboneau, M.L., V.T. Berta, S.M. Modro, "Experiment Analysis and Summary Report for OECD LOFT Fission Product Experiment LP-FP-2, OECD LOFT-T-3806, EG&G Idaho, Idaho National Engineering Laboratory, June 1989.

[3.11.9] Pena, J.J., S. Enciso, F. Reventòs, "Thermal-Hydraulic Post-Test Analysis of OECD LPFT LP-FP-2 Experiment", OECD LOFT-T-3807, OECD LOFT Spanish Consortium (CIEMAT, CSN, EN RESA, ENUSA, UNESA, UP M), March 1988.

[3.11.10] Carboneau, M.L., "Containment Analysis Report for LOFT Experiment LP-FP-2", OECD LOFT-T-3808, EG&G Idaho, Idaho National Engineering Laboratory, January 1989.

[3.11.11] Blanco, J. et al., "OECD LOFT Experiment LP-FP-2 Fission Product Behavior Analysis", OECD LOFT-T-3809, EG&G Idaho, Idaho National Engineering Laboratory, September 1988.

[3.11.12] Jensen, S.M., D.W. Akers, and B.A. Pregger, "Postirradiation Examination Data and Analyses for OECD LOFT Fission Product Experiment LP-FP-2; Volumes 1 and 2", OECD LOFT-T-3810, EG&G Idaho, Idaho National Engineering Laboratory, December 1989.

[3.11.13] "OECD LOFT Code Comparison Report; Volume 1: Thermal-Hydraulic Comparisons; Volume 2: Fission Product Companions", OECD LOFT-T-3811, EG&G Idaho, Idaho National Engineering Laboratory, February 1990.

[3.11.14] "Reactor Safety Study - An Assessment of Accident Risks in U. S. Commercial Nuclear Power Plants", WASH-1400, U.S. Nuclear Regulatory Commission, October 1975.

[3.11.15] "Severe Accident Risks: An Assessment for Five U. S. Nuclear Power Plants", NUREG-1150, U.S. Nuclear Regulatory Commission, June 1989.

[3.11.16] Coryell, E.W., "Summary of Important Results and SCDAP/RELAP5 Analysis for OECD LOFT Experiment LP-FP-2," NUREG/CR-6160, EG&G Idaho, Inc., April 1994.

[3.11.17] Pena, J.J., S. Enciso, and F. Reventos, "Thermal-Hydraulic Post-Test Analysis of OECD LOFT LP-FP-2 Experiment," NUREG/IA-0049, U.S. Nuclear Regulatory Commission, April 1992.

[3.11.18] Thompson, S.L., and L.N. Kmetyk, "RELAP5 Assessment: LOFT Large Break L2-5, NUREG/CR-3608, SAND83-2549, Sandia National Laboratories, January 1984.

[3.11.19] Orman, J.L., L.N. Kmetyk, "RELAP5 Assessment: LOFT Intermediate Break L5-l/L8-2", NUREG/CR-3406, SAND83-1575, Sandia National Laboratories, August 1983.

[3.11.20] Byers, R.K., and L.N. Kmetyk, “RELAP5 Assessment: LOFT L9-1/L3-3 Anticipated Transient with Multiple Failures”, NUREG/CR-3337, SAND83-1245, Sandia National Laboratories, August 1983.

[3.11.21] Thompson, S.L., and L.N. Kmetyk, “RELAP5 Assessment: LOFT Turbine Trip L6-7/L9-2”, NUREG/CR-3257, SAND83-0832, Sandia National Laboratories, July 1983.

[3.11.22] Kmetyk, I.N., “RELAP5 Assessment: LOFT Small Break L3-6/L8-1”, NUREG/CR-3163, SAND83-0245, Sandia National Laboratories, March 1983.

[3.11.23] Fell, J., and S.M. Modro “An Account of the OECD LOFT Project”, OECD LOFT-T-3907, OCED LOFT Project, EG&G Idaho, Inc.,May 1990.

3.12 Analysis of Critical Flow from the Marviken CFT-21 and JIT-11 Experiments

3.12.1 Background

Critical flow is an important phenomenon in reactor safety analysis for both pressurized water and boiling water reactors. The ability to calculate discharge flow rates from pipes, nozzles, safety relief valves, and vessels is an important requirement in determining system boil-down and whether the core remains covered. However, critical flow is a complex phenomenon which is dependent on flow conditions, pressure loss in the flow channel, geometry of the discharge duct, and flow orientation. Both subcooled and two-phase flow is important in reactor safety analysis.

MELCOR's flow equation cannot predict choking (in part because it does not include the v^2 terms in the full momentum equation, where v is the velocity). Therefore, the limit on flow must be imposed externally, using correlations. This is common for control-volume/flow path codes. When only atmosphere is flowing through the flow path, MELCOR calculates the mass flux as the sonic flux at the minimum section in the flow path. When only pool is flowing, MELCOR uses the RETRAN model for the critical mass flux [3.12.1], based on pressure and specific enthalpy of the pool (see CVH-FL reference manual for more detail). When both are present MELCOR uses a weighted average for the two phases.

The RETRAN critical flow model consists of two 36-parameter, double-polynomial fits to extended Henry-Fauske critical flow for subcooled water (below and above 300 psia) and two 36-parameter fits to Moody critical flow for saturated (two-phase) water (below and above 200 psia), all as functions of stagnation pressure and enthalpy. It also includes a 9- parameter expression for a —transitional enthalpy as a function of pressure. A linear transition is constructed between the Henry-Fauske model at and below this enthalpy and the Moody model at and above saturation. Contour plots showing the flow rate calculated by both models are presented in Figure 3.12-1 and Figure 3.12-2 over the domain of the CFT-21 calculated transient where the dashed line roughly shows the path followed by the CFT-21 test during the blowdown. The reader is referred to RETRAN reference for a description of the basic models and the fitting procedure employed.

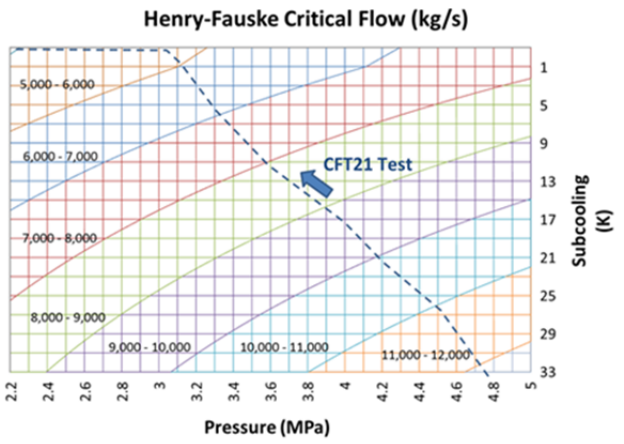

Figure 3.12-1. Henry-Fauske critical flow contours

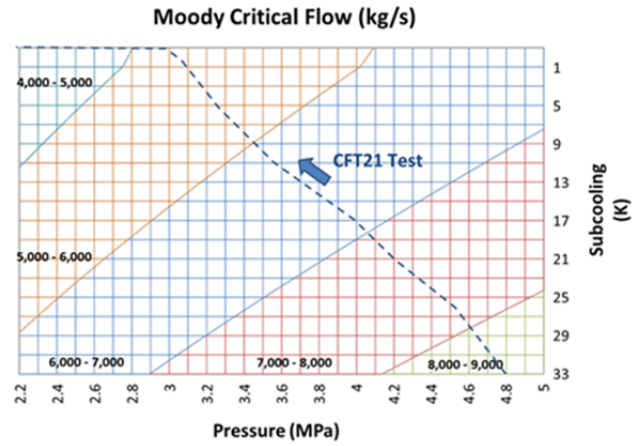

Figure 3.12-2. Moody critical flow contours

Large scale tests intended to provide data for analysis of critical flow from vessel blow-down were performed at the Marviken facility in Sweden between 1978 and 1979 [3.12.2]. A schematic showing the layout of the test facility is provided in Figure 3.12-3. Twenty-seven tests were performed in the facility, which were conducted for downward discharge of water/steam mixtures from a full-size reactor vessel (5.2 m diameter, 22 m high and volume of 425 m^3). The blowdown occurred through a vertical discharge pipe at the bottom of the vessel, which contained a valve, rupture discs and a nozzle. The CFT-21 test was designed for validation of models for subcooled and two-phase flow through a discharge nozzle whereas JIT-11 tested a saturated steam flow. For the CFT21 test, flow was taken directly from the bottom of the vessel so that liquid was discharged first. For the JIT 11 test, a 18-m tall standpipe was placed above the exit to prevent liquid from being discharged. Detailed schematics are included in subsequent descriptions of each test. Conditions and vessel dimensions for the two tests are summarized in Table 3.12-1. Note that the reported vessel volume in the table is 5 m^3 smaller than that reported elsewhere [3.12.3]. Another discrepancy is the L/D ratio of the nozzle for CFT-21. L is the length of the discharge pipe, and D is the diameter of the discharge nozzle. As reported in Table 3.12-1, the length is 1.5 m, but Ref. [3.12.3] reported a value of 0.73 m. According to Figure 3.12-3, the volume below the vessel is 1934 m^3 drywell. This volume receives vessel discharge.

Table 3.12-1. Comparison of test conditions [3.12.4].

Parameter	CFT-21	JIT-11
Vessel volume (m^3)	420	420
Vessel inside diameter (m)	5.22	5.22
Standpipe: height (m)	-	18
outside diameter (m)	-	1.04
wall thickness (m)	-	8.8
Discharge nozzle: diameter(m)	0.500	0.299
area (m^2)	0.1963	702 x 10^{-4}

length (m)	1.5	1.18
Initial Pressure (MPa)	4.9	5.0
Final pressure (MPa)	2.5	1.88
Initial water level (m)	19.9	10.2
Final water level (m)	<0.8	8.0
Initial inventory: water (kg)	330 x 10^3	145 x 10^3
Steam (kg)	6 x 10^2	5 x 10^3
Maximum subcooling (K)	33	< 3

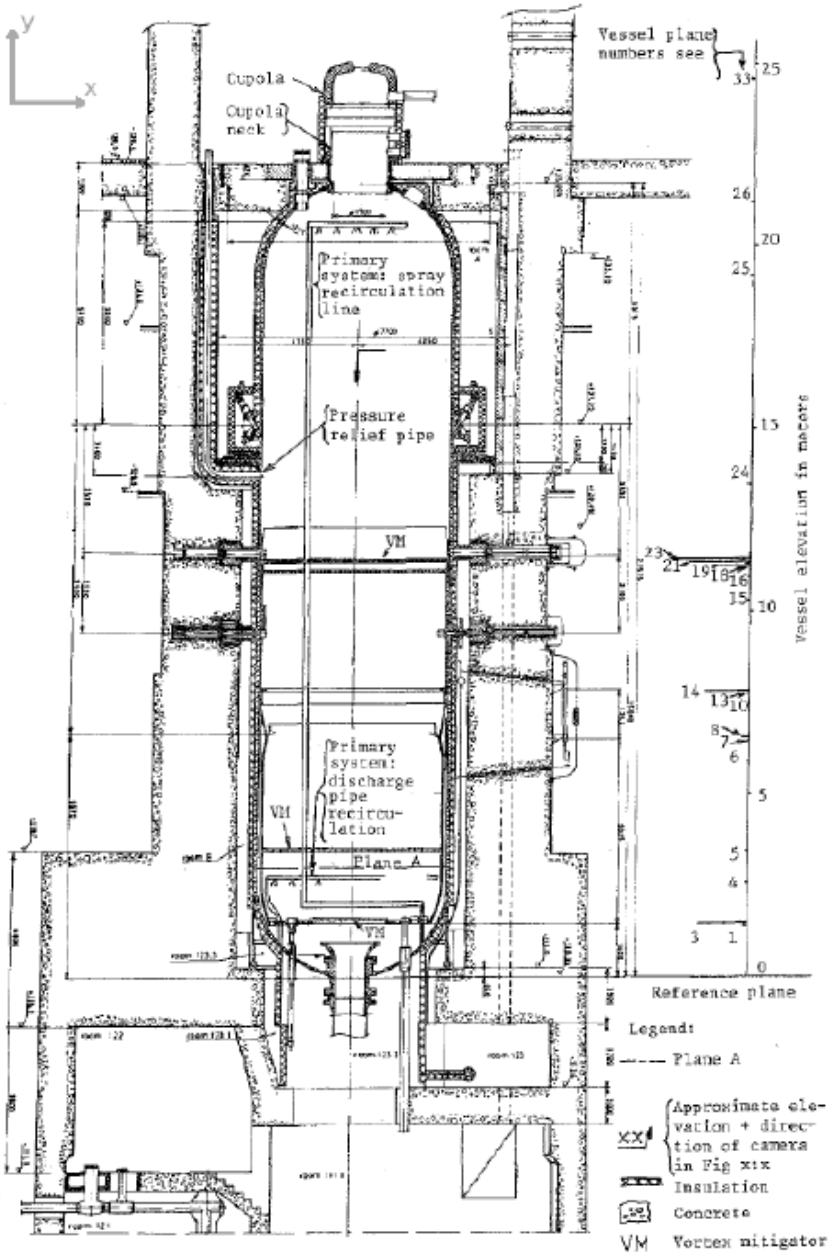

Figure 3.12-3. Marviken test facility [3.12.3]

3.12.2 CFT-21 Experiment

3.12.2.1 Nodalization

Two approaches were taken in modeling the CFT-21 experiment. The first approach was to not model the details of the vessel, but rather to impose the test conditions observed at the bottom of the vessel as boundary conditions on the calculation. This method tests only the critical flow models used in MELCOR and avoids the complications of modeling the vessel response. This case is modeled as two control volumes (CVs): the vessel and the containment. The vessel CV was a property-specified volume with properties specified as tabular functions, from test data. Pressure, quality, and pool temperature were all specified as boundary conditions to the calculation. The flow path was specified as having 3 segments, segment 1 (L=10.5584 m, A = 19.9794 m^2), segment 2 (L=6.31 m, A = 0.441 m2), and segment 3 (L=1.25 m, A = 0.1963 m2) which represented the flow through the vessel, the discharge pipe, and the nozzle, respectively.

In addition, a calculation was performed to model the details of the vessel during the blowdown. For this calculation, 2 cases were considered. For the first case, a detailed nodalization was performed for the vessel, which was subdivided into 21 CVs with a single volume representing both the discharge pipe and nozzle. A second calculation was performed in which the vessel was modeled with a single CV together with a single CV for the discharge pipe. As shown later in the results, the detailed nodalization was necessary to calculate the subcooling at the outlet. This is important because of the initial conditions in the test vessel prior to the start of the transient. Two zones existed at the onset of the test, with a subcooled zone at the bottom of the vessel and saturation conditions near the pool/atmosphere interface (see Figure 3.12-5). There was also a transition region between these two zones. When the ball valve is opened at the beginning of the transient, the subcooled zone moves out through the discharge pipe first and there is a traveling front as the water in the vessel is rapidly ejected through the pipe. It is impossible to capture this traveling front with a single CV modeling the vessel.

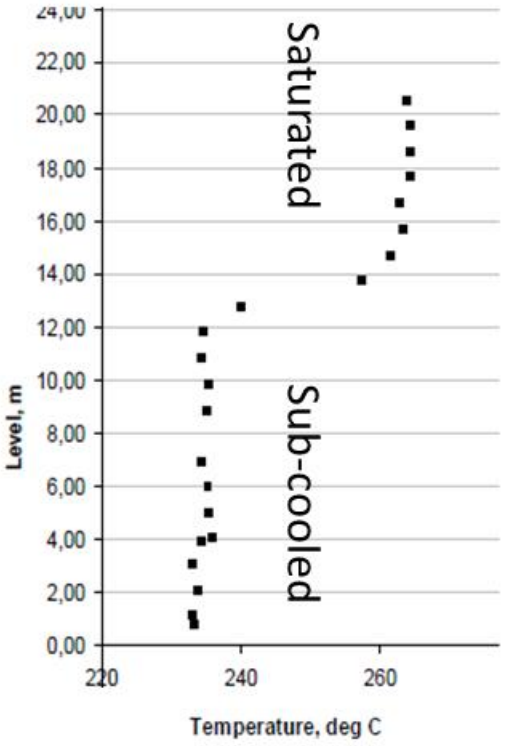

Figure 3.12-4 Vessel Temperature Profile at Start of Transient [3.12.31].

Vessel and discharge pipe walls were not modeled. Since both transients have such short durations, heat transfer to the walls would be small. Therefore, the MELCOR model does not have any heat structures.

3.12.2.2 MELCOR Input Specifications

For all calculations a discharge coefficient of 0.9 was applied for both the forward and reverse choked flow at the nozzle. This is a modest departure from the default value of 1.0 and led to only a modest improvement in the results. Note that MELCOR versions 1.8.6 (v3964) and 2.1 (v6110) are used in this calculation. Table 3.12-2 shows the calculation matrix of MELCOR used in this assessment.

An additional calculation was performed (case 3) using a modified solution strategy recently implemented into MELCOR 2.1. This strategy is intended to improve the efficiency of the solution and reduce CPU time. Internally, the code redefines the flow resistance to be very large for flows greater than critical, by extending the definition of the friction coefficient. This reduces the number of iterations required to solve the flow equations (discussed in more detail in the CVH-FL Reference Manual). This critical flow solution method is activated by modifying sensitivity coefficient 4450 (see CVH Users Guide).

Table 3.12-2. MELCOR Cases Conducted for CFT-21

Case	MELCOR 2.1	MELCOR 1.8.6
1 – Boundary Condition	×	
2a – 21 volumes of vessel and discharge pipe	×	×
2b – 1 volume vessel with 1 volume discharge pipe	×	×
3 – same as 2a, except SC4450 is set to 1	×	

3.12.2.3 Results of Analysis

3.12.2.3.1 Case 1: Vessel Specified by Boundary Condition

For this particular case, the vessel was not modeled directly by MELCOR 2.1, but rather test conditions at the bottom of the vessel were applied to the discharge pipe. The CVs modeled in this case are the vessel volume and the containment volume. Important parameters at the pipe exit included the vessel pressure and the water temperature (subcooling). These input conditions are plotted along with test data in Figure 3.12-5 and Figure 3.12-6, respectively. Notice that the pool temperature at the bottom of the vessel was the measured parameter and the subcooling was calculated from this temperature and the saturation conditions for the measured pressure. Only test data to 30 seconds were available but a 1 K subcooling was assumed beyond that. The resulting flow rate from the discharge pipe is plotted in Figure 3.12-7 which shows that the calculated flow rate closely tracks the measured values up to the point that two-phase flow exists at the nozzle, i.e., subcooling reaches zero. When two-phase flow

conditions dominate after 30 seconds, MELCOR 2.1 predicts a larger mass flow rate from the discharge pipe than was observed.

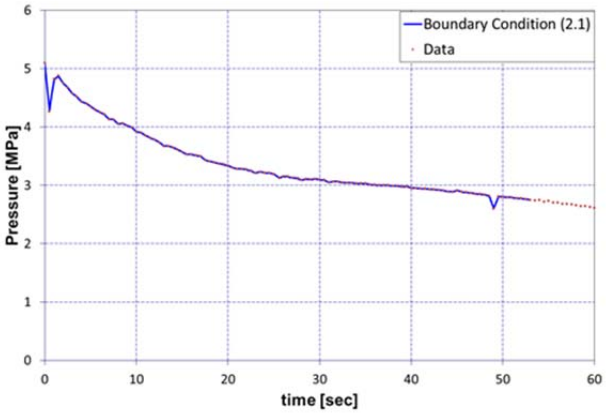

Figure 3.12-5. Pressure at Vessel Bottom for CFT-21 (MELCOR 2.1 – Case 1)

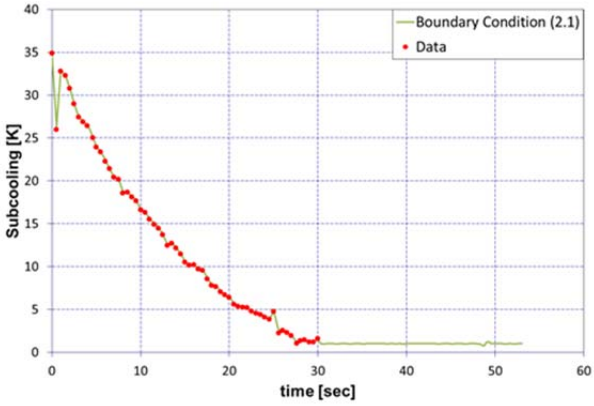

Figure 3.12-6. Subcooling of Water in Discharge Pipe for CFT-21 (MELCOR 2.1 – Case 1)

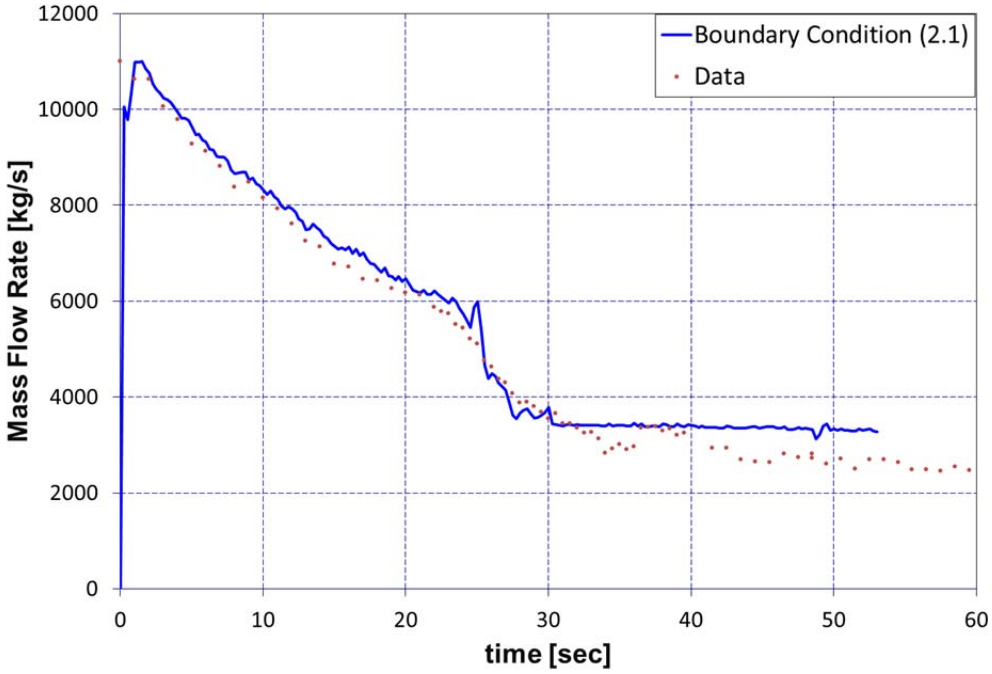

Figure 3.12-7 Mass flow rate calculated for CFT-21 (vessel specified as boundary condition for MELCOR 2.1)

3.12.2.3.2 Case 2: Nodalized Vessel Volume

The previous calculation demonstrates that when the boundary conditions are correctly applied to the discharge pipe/nozzle: (1) the critical mass flow rate is correctly calculated for subcooled liquid, and (2) a larger flow rate is predicted for the case of saturated two-phase flow. However, this calculation ignored the details of modeling the test vessel as water drains from the vessel during the depressurization. This section describes a more detailed modeling of the vessel and discharge pipe. As shown in Table 3.12-2, both MELCOR version 1.8.6 and 2.1 uses the vessel nodalization as discussed in this case. Figure 3.12-9 shows the two MELCOR nodalizations (a) 21 volumes and (b) a single volume cases. For the single volume case, a single control volume was used to model the vessel during the transient and another volume modeling the discharge pipe/nozzle. This calculation proved to greatly underestimate the flow rate, leading to a much longer blowdown time (90 sec as opposed to 60 sec). Because the single control volume necessitates a uniform mixed temperature, the control volume quickly becomes saturated as the pressure drops, leading to a greatly decreased flow rate for saturated two-phase flow. The single volume model is not able to track the advancing saturation/subcooled front as the vessel drains.

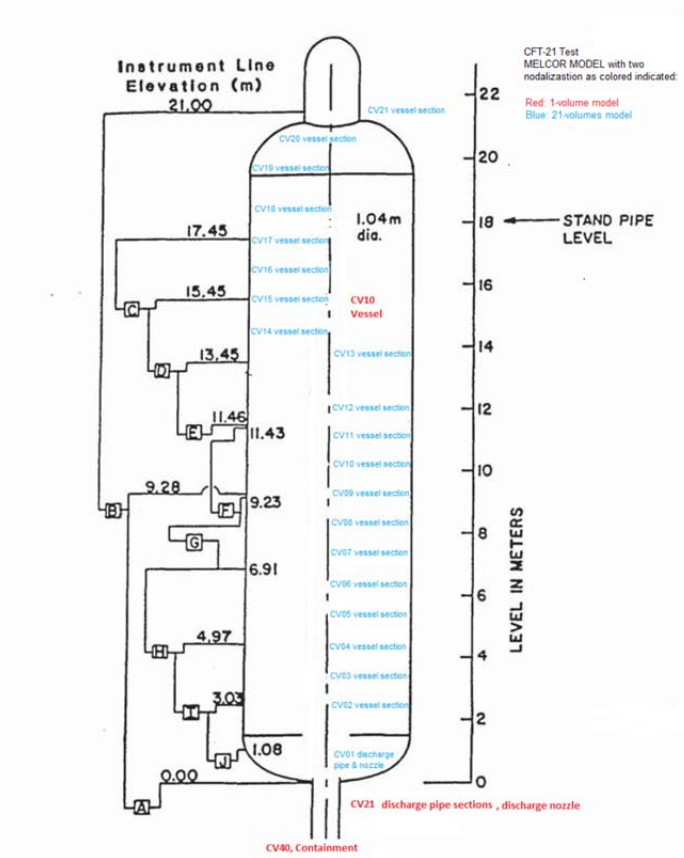

Figure 3.12-8. MELCOR Nodalization for CFT-21 Test (1-volume and 21-volumes Models)

A much improved result is obtained from the 21 volume representation. In this case, 1 volume models the discharge pipe and bottom part of the vessel (see Figure 3.12-8). As previously indicated, MELCOR utilizes both the Henry-Fauske and Moody critical flow models for the subcooled and saturated regions, respectively. In the saturated 2-phase region, the latter is used. As shown in Figure 3.12-9, the amount of subcooling in the MELCOR 2.1 calculations is well represented as the data and the input are in good agreement, except for the single volume case. The reason of the lumped parameter treatment in a single volume is that the subcooling is being averaged out for the entire vessel, which may not adequately predict the subcooling correctly. In terms of the mass flow rate calculated by MELCOR 2.1, the 21-volume model matches closely to the data for the first 30 seconds, since this is the time during subcooling (see Figure 3.12-10). Also shown in Figure 3.12-10 are the calculations from RELAP5 and TRACE [3.12.3]. RELAP5 employs two critical flow models (Henry-Fauske and Ransom-Trapp). Both RELAP5 Henry-Fauske and MELCOR 2.1 (21-volume) show similar trends in mass flow for much of the 60 seconds of time. MELCOR seems to be closer to data for the first 30 seconds when subcooling occurs, but deviates further than RELAP5 Henry-Fauske model. This could be due to the fact that MELCOR uses the Moody correlation at the saturated region. The RELAP5 Ransom-Trapp model demonstrates better agreement with data in the saturated region than does MELCOR 2.1 (21 volume) or the RELAP5 Henry-Fauske model. These results suggest that while the Henry-Fauske model yields excellent results for this test, the Moody model does not.

Figure 3.12-11 to Figure 3.12-13 show the calculated and experimental data of the mass flow rates, subcooling and pressures for this test. These results suggest that there is no difference between MELCOR code versions, though there is some deviation from the experimental data.

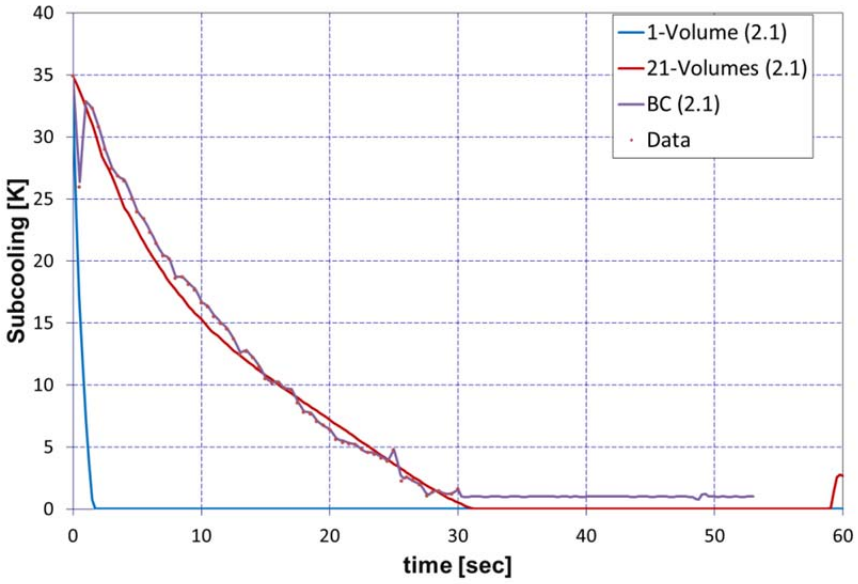

Figure 3.12-9. Subcooling MELCOR 2.1 Calculations for CFT-21

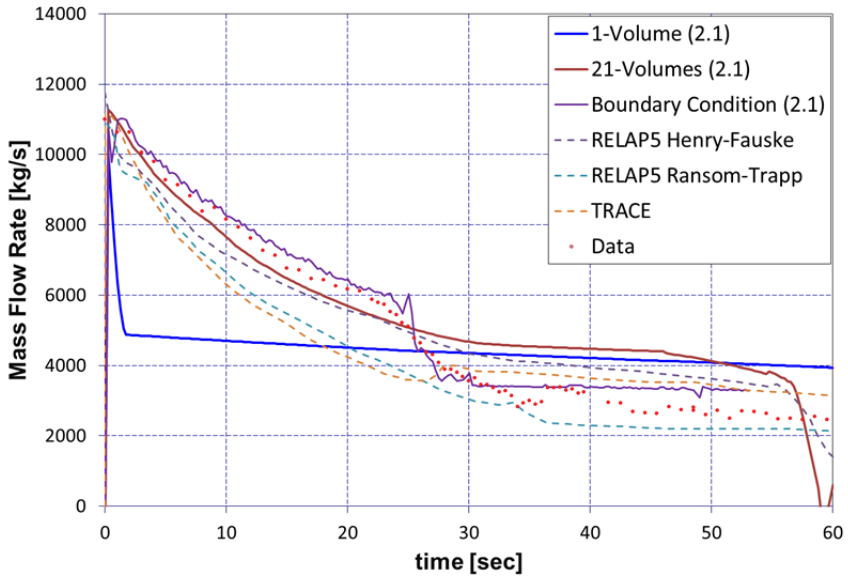

Figure 3.12-10. Mass Flow Rate MELCOR 2.1 Calculations for CFT-21 and Comparison with RELAP5 Models and TRACE [3.12.3]

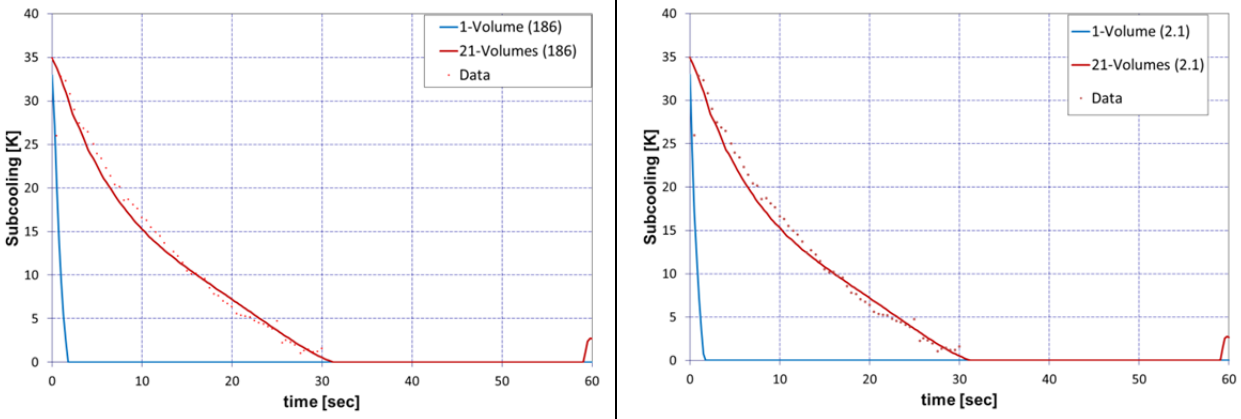

Figure 3.12-11. Subcooling Comparison of MELCOR Results for CFT-21 (a) 1.8.6 (b) 2.1

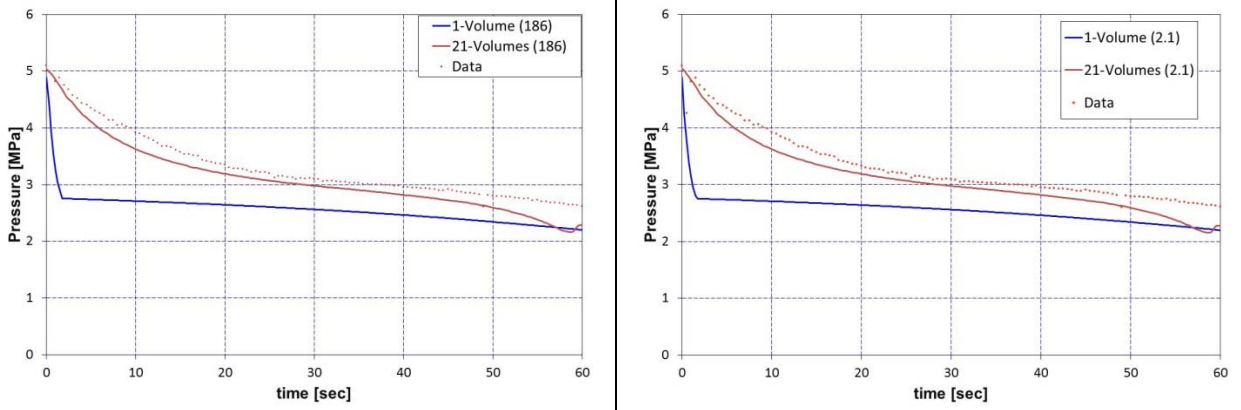

Figure 3.12-12. Pressure Comparison of MELCOR Results for CFT-21 (a) 1.8.6 (b) 2.1

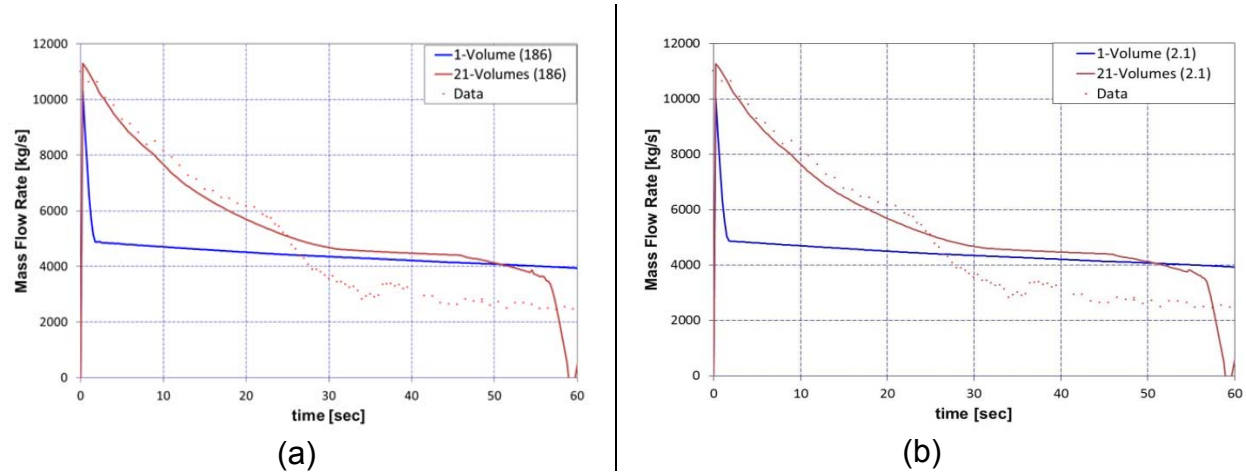

Figure 3.12-13. Mass Flow Comparison of MELCOR Results for CFT-21 (a) 1.8.6 (b) 2.1.

3.12.2.3.3 Case 3: Improved solution strategy

The new and improved critical flow solution strategy was tested with the 21 volume model, and the calculated flow rate is presented in Table 3.12-3. To invoke this model, the sensitivity coefficient 4450(1) is set to 1. For this test, the two methods gave nearly identical results. Unfortunately it is difficult to conclusively assess performance improvements for this test because of the simplicity of the MELCOR model with only 22 flow paths. Performance metrics are summarized in Table 3.12-3.

Table 3.12-3. Performance Metrics for Flow solution*

	Original (Default) Solution	Improved Solution
CPU for CVH & FL Packages	1.43521sec	7.80005E-01 sec
Matix Inversions	11602	6270
Flow Reversals	790	516
Choked Flows Identified	2222	38965

*PC used: Intel Core I7-3770 CPU@3.40GHz, MELCOR 2.1 release version of 6110.

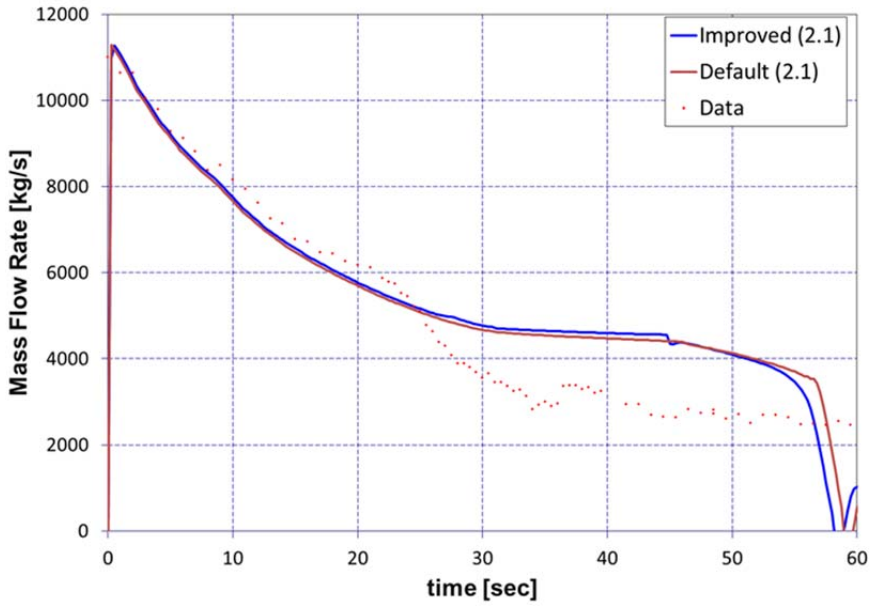

Figure 3.12-14. Mass Flow Rate MELCOR 2.1 Calculation for CFT-21 (21-Volume Model) Using Improved Solution Strategy.

3.12.3 JIT-11 Experiment

3.12.3.1 Nodalization

A single volume of 405.22 m^3 was used to model the net volume of the vessel (less the volume of the standpipe which was 14.78 m^3). This, together with the volume of the standpipe (modeled by a single CV) which was inserted in this test gives the total vessel volume of 420 m^3. A single CV with volume of 3.7685 m^3 was used to model the discharge pipe and nozzle. Details of the nodalization are provided in Figure 3.12-15.

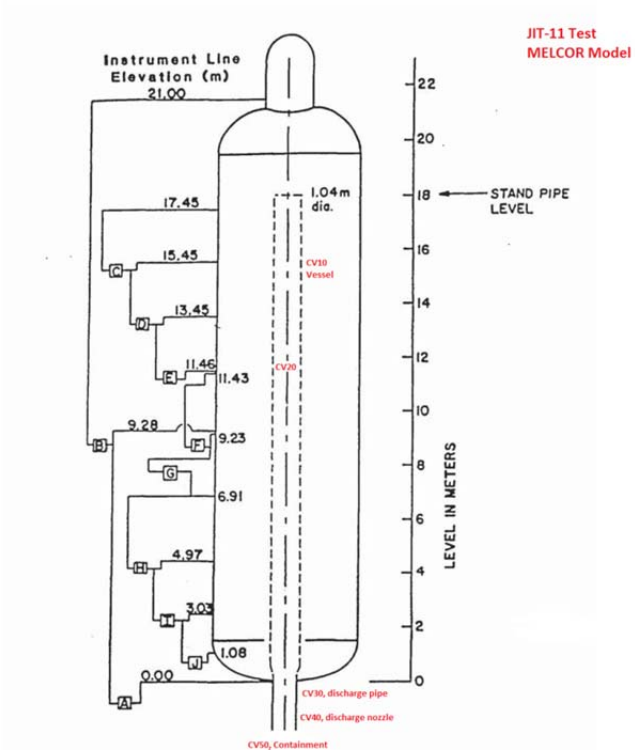

Figure 3.12-15. MELCOR Nodalization for JIT-11 Test

3.12.3.2 MELCOR Input Specifications

The default calculation uses a discharge coefficient (C_d) of 0.9 for both the forward and reverse choked flow at the nozzle which is consistently with the modeling assumption for the CFT-21 experiment. The pressure used for the containment volume on the downstream side of the nozzle was calculated as a function of time. Since the volume of this CV was unknown, it was varied until the final pressure reported for the vessel in the experiment was predicted. This volume was 3100 m^3. Additional variation is conducted by reducing this discharge coefficient to 0.8 (see Table 3.12-4 for the cases conducted).

Table 3.12-4. MELCOR Cases Conducted for JIT-11

Case	MELCOR 2.1	MELCOR 1.8.6
1 – Default	×	×
2 – Same as 1, except decreases C_d to 0.8	×	×

3.12.3.3 Results of Analysis

The calculated vessel pressure is plotted Figure 3.12-16. As shown in this figure, the MELCOR calculation is very close to the measured values, leading the measurement in time by about 5 seconds. Using a smaller C_d (0.8) yields a better agreement with the data as shown in this figure. Both versions of MELCOR calculate the identical pressure. For the mass flow rate, MELCOR results show a close agreement with the data as shown in Figure 3.12-17. The use of the smaller C_d (0.8) under-predicts the mass flow for the first 50 seconds, but then over-predicts the zero flow rate point. Use of the default Cd (0.9) leads to under-prediction of the zero flow rate point. For this calculation, MELCOR uses neither the Henry-Fauske nor Moody models, but rather a relationship for the sonic flux at the stagnation conditions. Figure 3.12-18 plots the mass flow versus pressure relationship for this test. Error bars are provided to indicate the 5% uncertainty inherent in the experiment. Also shown is a calculation that was performed with the equation which MELCOR uses for calculating flow rate as a function of steam density (ρ), sonic velocity C_s, and the ratio of the specific heat at constant pressure to that at constant volume (γ), evaluated at test conditions. The equation curve in Figure 3.12-18 is for the default case in MELCOR 2.1. MELCOR employs the following equation for estimating the exit mass flow through the nozzle:

$$\dot{m} = \frac{\rho}{A} \cdot C_s \cdot \left(\frac{2}{\gamma+1}\right)^{\left(\frac{\gamma+1}{2(\gamma-1)}\right)} \qquad \text{(Equation 3.12-1)}$$

Because the multiplier in (Equation 3.12-1) is a very weak function of γ, MELCOR does not calculate this parameter, but instead uses a nominal value of 1.4. Note that the equation data in this figure was calculated using a constant sound speed of 348.99 m/s for the containment with a minor adjustment of the discharge coefficient to 0.9. As described in the CVH-FL reference manual, this sound speed is further reduced because of cooling between stagnation conditions and the minimum section. Thus, the equation curve as shown in this figure is higher than that was calculated by MELCOR, but the profile is nearly identical to MELCOR.

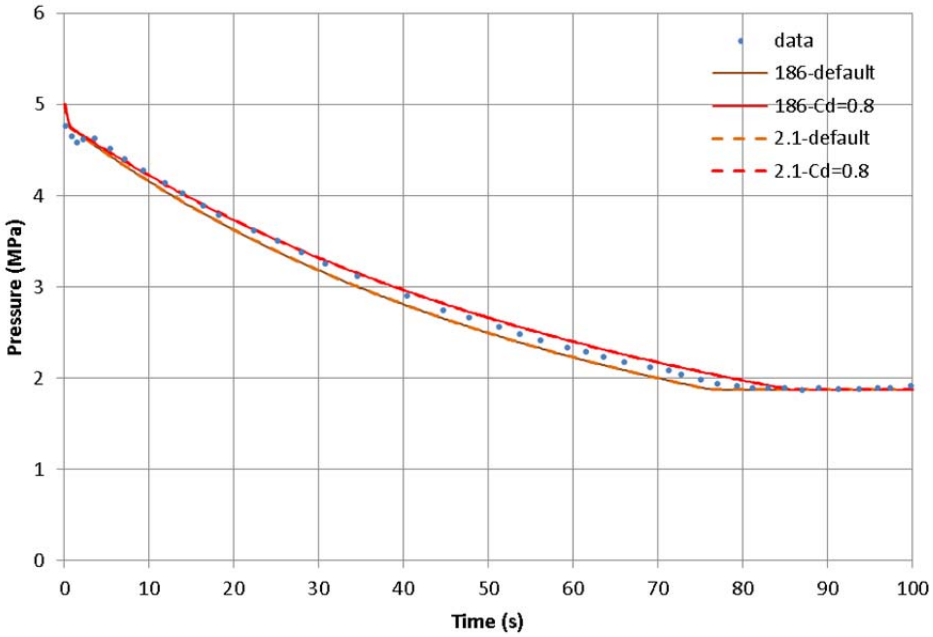

Figure 3.12-16. Vessel Pressure of MELCOR Calculation for JIT-11

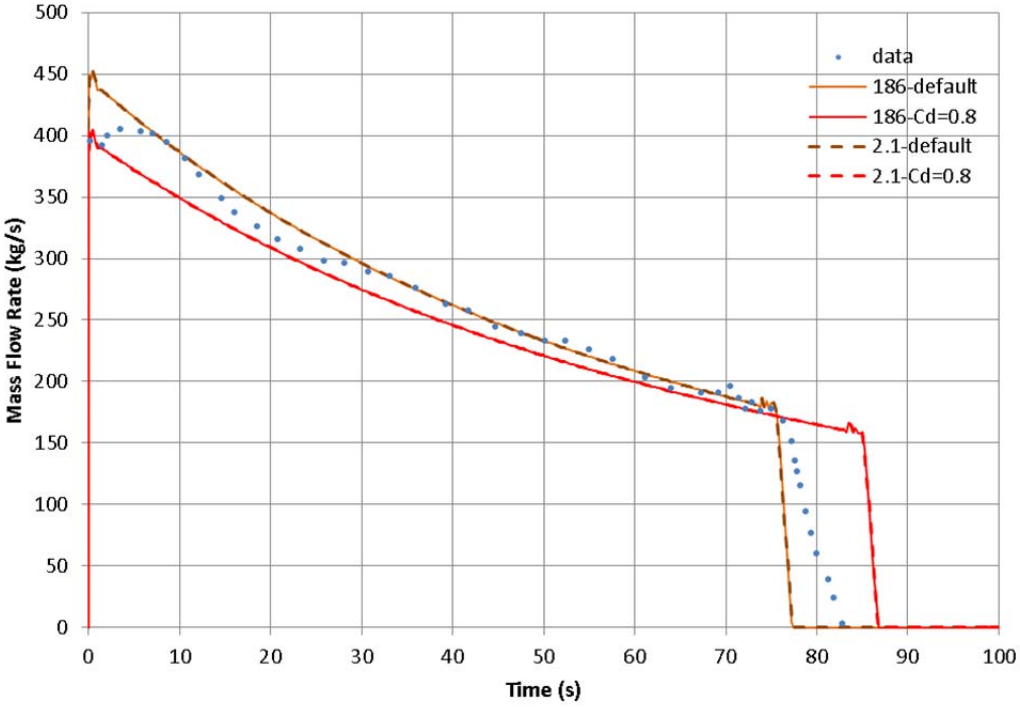

Figure 3.12-17. Mass Flow Rate of MELCOR Calculation for JIT-11

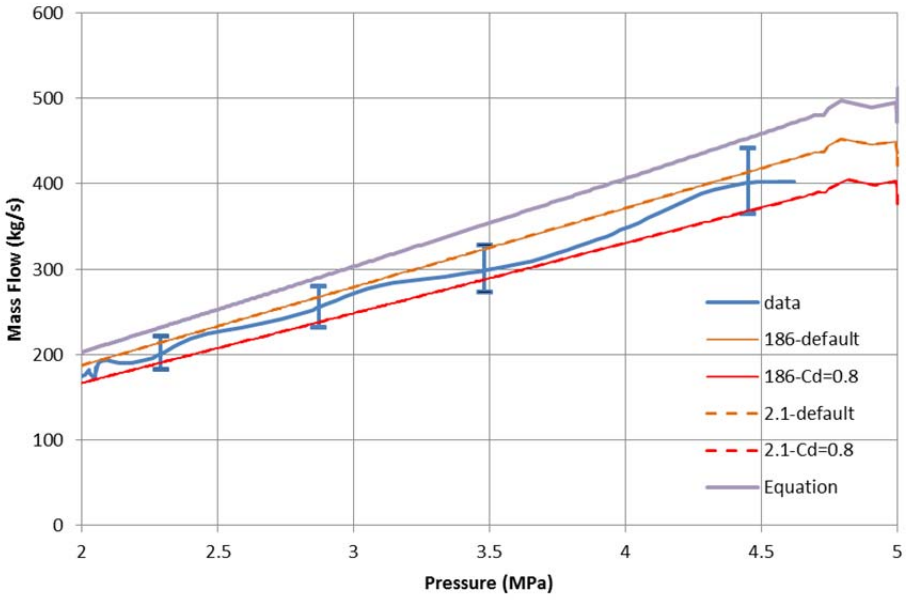

Figure 3.12-18. Mass Flow versus Pressure of MELCOR Calculations for JIT-11

3.12.4 Discussion

For the case of subcooled critical flow (CFT-21/Henry-Fauske) and single phase atmosphere (JIT-11) the MELCOR models predict the flow rate for subcooled conditions very well. However, for two-phase conditions (CFT-21/Moody), the Moody model tends to predict a larger flow rate than was observed in the experiment. For the JIT-11 test, MELCOR predicts a mass flow as a function of the pressure that is within the error bound of the experiment. Overall, MELCOR satisfactorily predicts the JIT-11 experiment in regards to critical flow.

A study by Ardron [3.12.5] argues that the Moody model always predicts larger flow rates than observed due to "formation of high vapor concentrations close to the inlet to the exit pipe, and a tendency of the Moody theory to over-estimate discharge flow rates for stagnation qualities greater than 1%". His analysis defines a Moody multiplier to be the "time-averaged ratio of experimental instantaneous blowdown flow rate to that given by the use of the Moody theory" and compares this calculated parameter for various experimental conditions. For an area ratio of 0.5, similar to conditions in these tests, the Moody multiplier is 0.6, which is consistent with the MELCOR calculations.

3.12.5 References

[3.12.1]RETRAN-02—A Program for Transient Thermal-Hydraulic Analysis of Complex Fluid Systems, Volumes 1-3, NP-1850-CCM, Electric Power Research Institute, Palo Alto, CA (May 1981).

[3.12.2]Schultz, R.R., Ericson, L., “The Marviken Critical Flow Test Program,”Nuclear Safety, 22(6), 712-724, 1981.

[3.12.3]Lukasz Sokolowski, Tomasz Kozlowski, "Assessment of Two-Phase Critical Flow Models Performance in RELAP5 and TRACE Against Marviken Critical Flow Tests", NUREG/IA-0401, U.S. Nuclear Regulatory Commission, February 2012.

[3.12.4]Rosdal, O., Caraher, D., “Assessment of RELAP5/MOD2 Against Critical Flow Data From Narviken Tests JIT11 and CFT 21,” NUREG/IA-0007, U.S. Nuclear Regulatory Commission, September 1986.

[3.12.5]Ardron, K.H. and Furness, R.A., “A Study of the Critical Flow Models Used in Reactor Blowdown Analysis,” Nuclear Engineering and Design 39, 257-266, 1976.

3.13 Analysis of Marviken-V Aerosol Transport Test (ATT-4)

3.13.1 Background

A series of large-scale aerosol transport tests (ATTs) was conducted at the Marviken research facility in Studsvik, Sweden. This facility provides a pressure vessel, which is connected to the pressurizer through piping and terminated in a closed, filtered relief tank simulating a containment suppression pool (see Figure 3.13-1) [3.13.1]. Figure 3.13-2 shows measurement locations throughout the experiment hardware. This ATT provides validation data for aerosol transport and attenuation of vapor aerosols and volatile fission products within a RCS (pressurizer hot loop with a relief tank) under severe fuel damage conditions for the pressurized water reactor (PWR) plants.

3.13.2 Experiment

The experiment described here is the ATT-4 test, which is used to study fission product transport. The description of this experiment and results are from the previous MELCOR report [3.13.1]. The corium vapors (Ag and Mn), vaporized fission products (I_2, CsI and CsOH, as fissium) and steam are mixed at the lowest portion of the reactor vessel to form aerosols (see 1 in Figure 3.13-1) [3.13.1]. Once the aerosols are generated in the corium and fissium chamber (see upper left diagram in Figure 3.13-2), they are transported through the reactor vessel (see 2 in Figure 3.13-1 and the reactor vessel in the upper right corner of Figure 3.13-2), including the simulated pressurized water reactor internals (which consist of a support plate simulating the upper core plate and vertical tubes simulating control rod guide tubes). As shown in Figure 3.13-2, the corium and fissium chambers are used to generate aerosols using a plasma arc heater. The inlet flow rates are steam at 36 g/s (at 384 K), water at 6.3 g/s, Ar at 15.3 g/s, N_2 at 81 g/s and H_2 at 0.3 g/s. A high-temperature stainless steel pipe from the reactor vessel connects to the pressurizer. This pipe has an inner diameter of 0.73 m inside the reactor vessel, and is reduced to a 0.35 inner diameter just after leaving the reactor vessel. This pipe rises vertically for ~10m then it runs horizontally for 6 m before connecting to the pressurizer inlet. The pressurizer is a stainless steel tank with an inside height of 10.5 m, an inside diameter of 2.49 m, and an overall volume of 49.5 m^3; this is similar to typical PWR pressurizers. A stainless-steel pipe with an inside diameter of 0.3 m runs vertically 3.45 m is connected from the pressurizer top; the pipe then continues horizontally for 10 m and then drops 19.6 m to the relief tank that has a volume of 20 m^3.

A summary of the aerosol injection rates and temperature distributions for various components in the experiment is presented in Table 3.13-1. As shown in this table, the duration of this experiment is about 80 minutes, during which time various aerosol sources are active. The CsI source, however, is active for only about 5 minutes. The range of expected temperatures at various component locations is also given in Table 3.13-1.

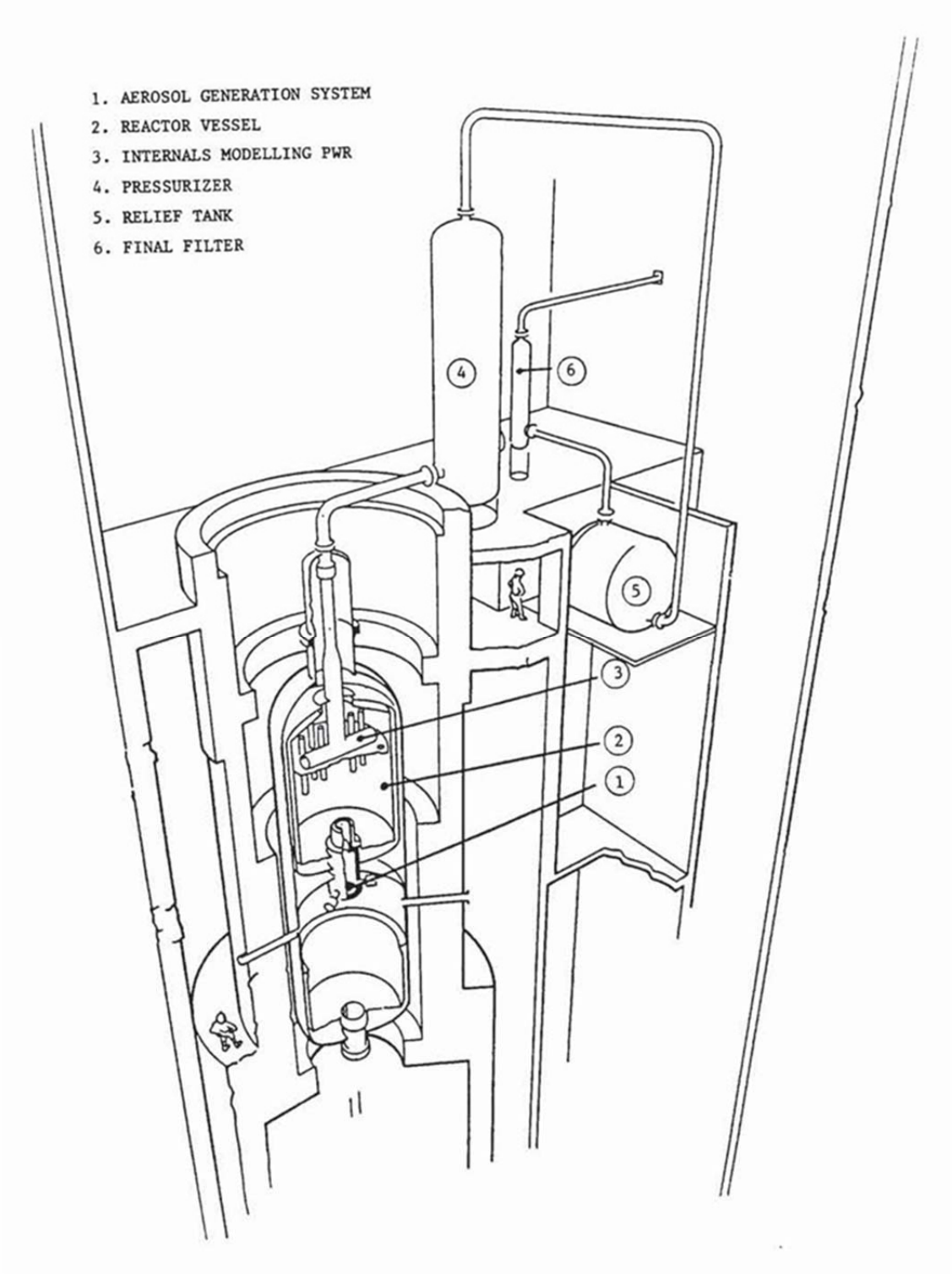

Figure 3.13-1 Marviken Test Facility Setup [3.13.1]

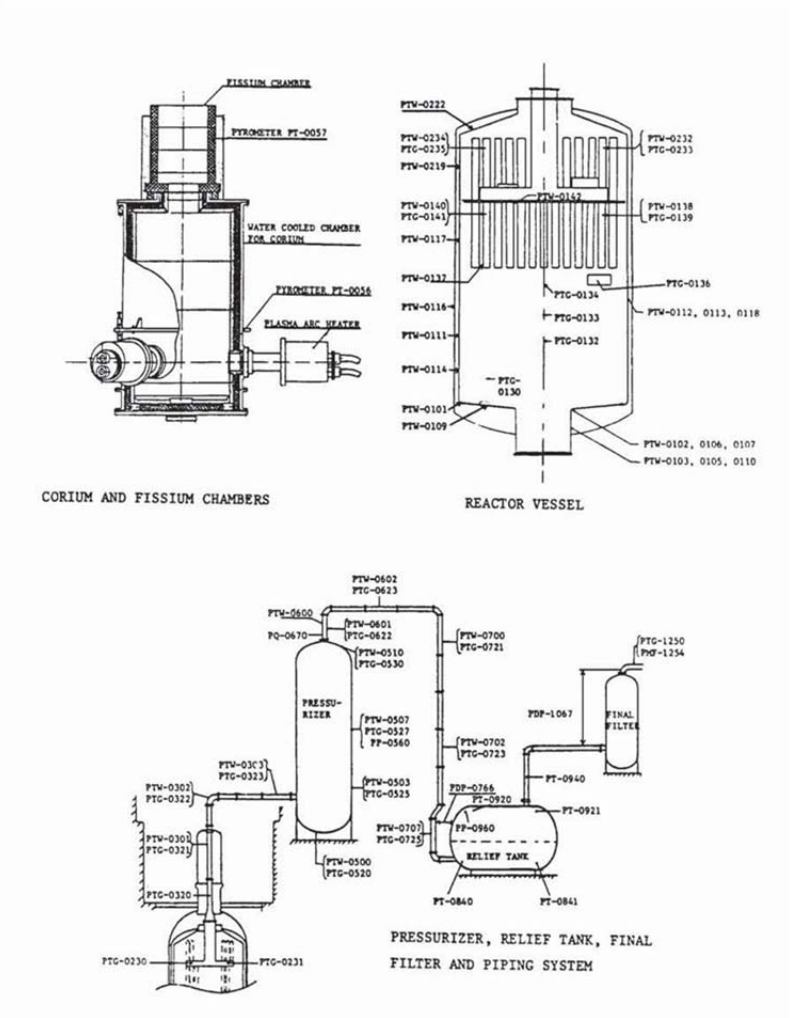

Figure 3.13-2 Measuring Locations of the Marviken Test Facility for the ATT-4 Test [3.13.1]

Table 3.13-1 Experimental Conditions for ATT-4 Test [3.13.1]

Parameter	Quantity	Parameter	Quantity
Test duration	79 minutes[1]		Temperatures (K)
Aerosol Feed Rate (g/s)		Reactor vessel wall	903-1123
CsI	4.19	Reactor vessel gas	1023-1473
CsOH	14.0	Piping to pressurizer wall	693-763
Te	2.3	Piping to pressurizer gas	753-873
Ag	52.5	Pressurizer wall	553-623

Mn	3.8	Pressurizer gas	563-623
Gross electrical power	1650 kW	Piping to relief tank wall	398-563
		Piping to relief tank[2] gas	473-573

[1]All aerosol injection starts at 2 minutes, and test completes at 81 minutes
[2]Relief tank has a 20 m^3 volume, and the fluid temperatures of 297-306 K, and wall temperatures of 297-305 K.

Table 3.13-2 shows the aerosol measurements for the experiment. As shown in this table, more than 60% of injected iodine was lost. This is a significant experimental error. The least aerosol mass lost is Ag, with about 8% lost. The mass listed in this table will be compared with the code calculations.

Table 3.13-2 Aerosol Experimental Results at Various Measured Locations

	Silver (Ag)		Manganese (Mo)		Cesium (Cs)		Iodine (CsI)		Tellurium (Te)	
Location	**kg**	**(% injected)**	**kg**	**(% injected)**	**kg**	**(% injected)**	**kg**	**(% injected)**	**kg**	**(% injected)**
Vaporization chamber	0.25	0.12	0.03	0.22	0.1	0.20	0	0.00	0.01	0.12
Reactor vessel										
Floor	19.2	9.40	1.27	9.22	4.56	9.33	0.01	1.96	0.62	7.14
Lower wall	8.6	4.21	0.63	4.58	1.16	2.37	0.01	0.01	0.21	2.42
Upper wall & internals	23.91	11.70	1.74	12.64	9.85	20.16	0.01	1.38	0.61	7.03
Center plate	4.12	2.02	0.32	2.32	0.47	0.96	0.01	0.01	0.13	1.50
Coarse Particles	5.28	2.58	0.34	2.47	0.03	0.06	0	0.00	0.09	1.04
Total	61.11	29.91	4.3	31.23	16.07	32.88	0.04	3.36	1.66	19.13
Piping										
Pipe LO1	1.4	0.69	0.23	1.67	1.16	2.37	0	0.00	0.04	0.46
Bend BO12	8.05	3.94	0.51	3.70	1.17	2.39	0.01	2.61	0.28	3.23
Pipe LO2	6.36	3.11	0.4	2.90	1.03	2.11	0.01	2.58	0.22	2.53
Total	15.81	7.74	1.14	8.27	3.36	6.87	0.02	5.19	0.54	6.22
Pressurizer										
Floor	45.31	22.17	2.87	20.84	7.59	15.53	0.05	20.44	1.87	21.54
Lower wall	6.37	3.12	0.4	2.90	1.08	2.21	0.01	3.32	0.27	3.11
Middle wall	0.76	0.37	0.06	0.44	0.18	0.37	0	0.19	0.04	0.46
Upper wall	0.52	0.25	0.04	0.29	0.12	0.25	0	0.18	0.03	0.35
Top	0.07	0.03	0.01	0.07	0.02	0.04	0	0.00	0	0.00
Total	53.03	25.94	3.38	24.54	8.99	18.40	0.06	24.13	2.21	25.46
Piping										
Pipe LO4	1.84	0.90	0.12	0.87	0.34	0.70	0	1.12	0.08	0.92
Pipe LO5	18.53	9.07	1.2	8.71	3.49	7.14	0.03	12.42	0.83	9.56

Pipe LO6	2.67	1.31	0.18	1.31	0.6	1.23	0	0.65	0.14	1.61
Total	23.04	11.28	1.5	10.89	4.43	9.07	0.03	14.19	1.05	12.09
Relief Tank	49.93	24.43	3.3	23.97	15.54	31.80	0.13	65.00	3.14	36.18
Grand TOTAL	204.36	92.03	13.77	86.22	48.87	81.63	0.2	40.00	8.68	80.52
Final filter	0.17	0.08	0.04	0.29	0.07	0.14	0	0.00	0.01	0.12
Miscellaneous	1.02	0.50	0.08	0.58	0.31	0.63	0	0.00	0.06	0.69
Mass lost	17.7	7.97	2.2	13.78	11	18.37	0.4	60.00	2.1	19.48

3.13.3 MELCOR Model

The original MELCOR model using MELCOR revision 1.8LO was developed when the MELCOR 1.8.1 assessment was performed (see SAND92-2243 [3.13.1]). The nodalization of the MELCOR model is shown in Figure 3.13-3. However, more recent coding enhancements can also be tested in this assessment. For example, SAND92-2243 indicated that the vessel temperature was sufficiently high that the volatile fission products would contain substantial vapor fractions, which would be a good test for the MELCOR RadioNuclide (RN) package physics model; however, MELCOR 1.8.1 lacked vapor chemisorption and turbulent deposition, which contributed to the underestimation of the aerosol settling in the reactor vessel.

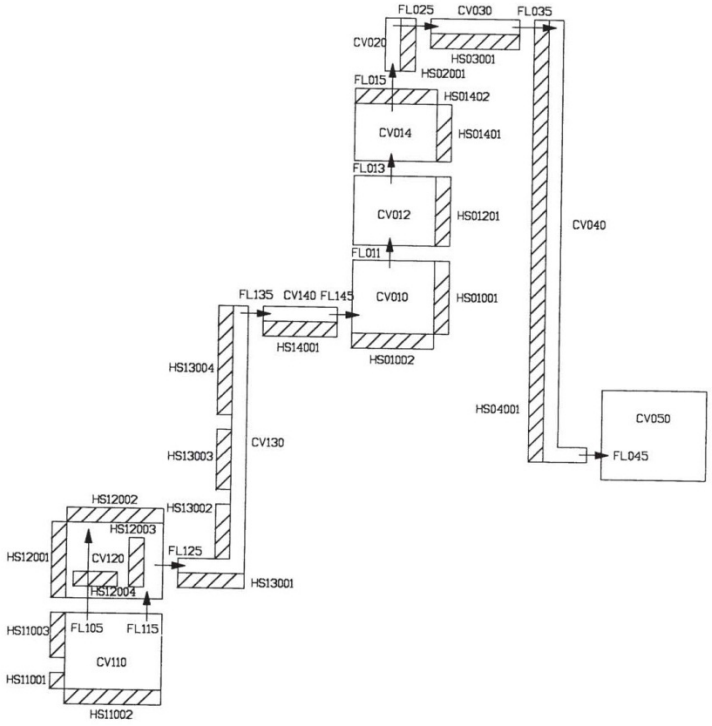

Figure 3.13-3 MELCOR Nodalization [3.13.1]

Also, the report [3.13.1] indicated that the initial and injected aerosol particle size distribution was not known. This is the major experimental uncertainty for the experiment. Based on these inputs, a sensitivity analysis on the chemisorption for iodine, turbulent deposition in the vessel, and the varying aerosol size was examined (see Table 3.13-3). As shown in this table, a base case with an aerosol size (AMMD – aerodynamic mass median diameter) of 5 μm and the global default of 2.0 is created for both 1.8.6 and 2.1. The aerosol feed rates, as shown in Table 3.13-3, are sourced in the CV110. All aerosol size distributions are discretized into 20 sections and only a single chemical component is used with a material density of 4,120 kg/m^3. Note that a sensitivity study was carried out previously to study the effect of the number of aerosol sections used [3.13.1]. The study concluded that decreasing the aerosol sections in the problem would decrease progressively the size of AMMD and the amount of the aerosol suspended, but the magnitude was not significant. However, the 20 sections were yielded closer to the experimental data [3.13.1]. Other variations in MELCOR 2.1 were simulated as shown in Table 3.13-3. For MELCOR 1.8.6, only the base case is simulated. In particular, the initial AMMD for each aerosol type was varied as either CsOH (2.5 μm), Ag/ Mn (3.5 μm), CsI (10 μm), or Te (5 μm) in Case "2.5Cs". For the case labelled "Turb" in the table, turbulent deposition is only applied to the vessel surfaces. For the case labelled "Chem" in the table, chemisorption of iodine was exercised.

Table 3.13-3 Sensitivity Runs* Conducted

Case #	1.8.6**	2.1**
Base	Default 2.0, Aerosol size (5 μm)	Default 2.0, Aerosol size (5 μm)
Chem	N/A	same as Base, except turns on chemisorption, and modified "steel" to "stainless steel"
2.5Cs	N/A	same as Base, except models initial AMMD for CsOH (2.5 μm), Ag/Mn (3.5 μm), CsI (10 μm), and Te (5 μm)
Turb	N/A	Same as Base, except turns on the turbulent deposition model to the heat structures associated with the upper wall and internals
Turb+2.5Cs	N/A	Same as Turb, except models the initial AMMD for CsOH (2.5 μm), Ag/Mn (3.5 μm), CsI (10 μm), and Te (5 μm)

*Actual injection rates for the aerosols modeled as shown in Table 3.13-4: CsOH starts at 2 minutes from the start of the experiment and lasts 79 minutes; CsI starts at 32 minutes and lasts 5 minutes; Te starts at 2 minutes and lasts 70 minutes; Mn starts at 7 minutes at ½ the injection rate in Table 3.13-1 for 7 minutes, and at the full rate for 67 minutes; and Ag starts at 7 minutes at ½ the injection rate in Table 3.13-1 for 7 minutes, and at the full rate for 67 minutes.

**Runs were conducted using MELCOR 1.8.6 (v3964) and MELCOR 2.1 (v6110)

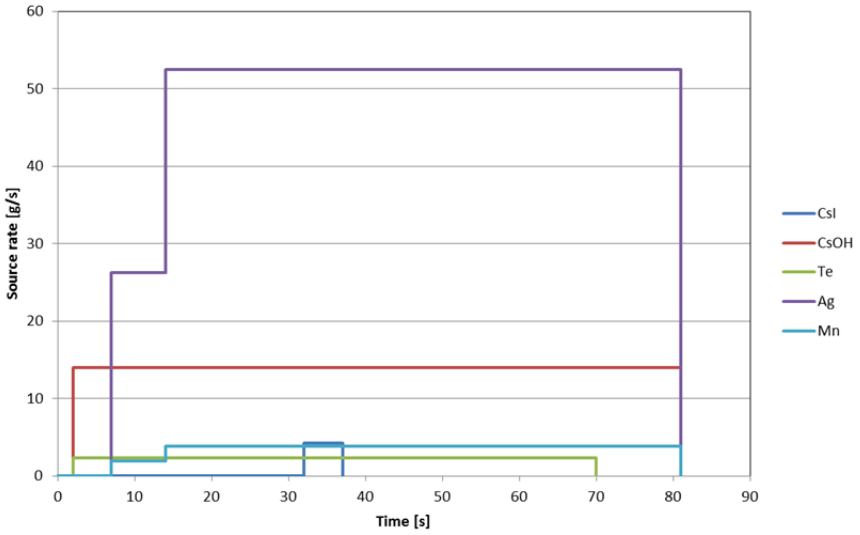

Figure 3.13-4. Aerosol Injection Rate Profile [3.13.1]

3.13.4 Discussions and Results

The thermal conditions calculated by MELCOR are compared with the experiment. The MELCOR calculated gas temperatures for the base case are compared to the experiment in Figure 3.13-5. In this figure, both MELCOR 2.1 and 1.8.6 calculated results and experimental data for the gas temperatures in the vessel at the upper plenum region, and in the pipe from the vessel to pressurizer are shown (see Table 3.13-3 for the base case). There was no difference in the calculated gas temperatures between MELCOR 2.1 and 1.8.6. In comparing to the experiment, the calculated vessel gas temperature is in the lower range of the data and decreases gradually in value with time. As given in Figure 1-5, MELCOR over-predicts the gas temperature in the piping to the pressurizer. The MELCOR calculated wall (structural surface) temperature for the vessel and the measured temperature for the upper plenum region are plotted in Figure 3.13-6. As shown in this figure, similar to the gas temperature plot, there is no difference between MELCOR 2.1 and 1.8.6, and MELCOR predictions are within bounds of the vessel and piping prior to the pressurizer of the experimental data. For the wall temperature in the piping before the pressurizer shown in Figure 3.13-6, MELCOR predictions are higher than the experiment data. The calculated gas and wall temperatures for the vessel are similar to that reported in Ref. [3.13.1]. Since the current focus of this assessment is toward the topic of aerosol transport, the disagreement on the thermal prediction by MELCOR may require future detailed assessment, including the refinement of the MELCOR volumes and heat structures to capture the details of the thermal behavior.

In terms of aerosol transport, the comparison between MELCOR and the experiment is done by integrating the deposited aerosol mass along the experimental line, and presenting the cumulative deposited mass starting from the bottom of the lower vessel. The distance and the referenced control volumes in the MELCOR nodalization are tabulated in Table 3.13-4. The cumulative mass of each of the five corium and fission

products for the distance measured from the bottom of the lower vessel can be seen in Figure 3.13-8 to Figure 3.13-12. This cumulative mass represents the total aerosol mass including deposited (which accounts for the majority of the aerosols), liquid (primarily for the aerosol mass in the relief tank) and gas in MELCOR. The inclusion of the gas phase values from MELCOR accounts for experimental uncertainty. Less than 1% of the total injected aerosol mass remains in the gas phase at the end of the MELCOR calculation. As shown in Figure 3.13-8 and Figure 3.13-9, the cumulative corium (Ag and Mn) calculated by MELCOR agrees well with the experiment. The use of the initial diameter of 3.5 μm for Ag (curves: "Turb+2.5Cs" for MELCOR 2.1and "2.5Cs" for MELCOR 1.8.6) agrees well with the experiment for the first 30 m of piping before the pressurizer. However, from the pressurizer and beyond, the use of this initial particle size under-predicts the mass accumulated. The use of the turbulent deposition model option in MELCOR 2.1 for the vessel structures does not impact the results significantly (see curves of MELCOR 2.1 "base" and MELCOR 2.1 "Turb" in Figure 3.13-8 and Figure 3.13-9). For Cs transport, only "Turb+2.5Cs" bounds the experiment data closely as shown in Figure 3.13-10. As shown in this figure, the initial size is 10 μm for "2.5Cs" case. Decreasing this size to 5 μm, as in the base case, would over-predict the mass as shown in this figure. In terms of the iodine transport, the use of chemisorption does not improve the results as shown in Figure 3.13-11. As shown in this figure, MELCOR over predicts the mass in the pressurizer and beyond. It is not certain how good the experiment data was collected, since more than 50% of the original mass was lost. In terms of Te transport, MELCOR in general over-predicts the mass as shown in Figure 3.13-12. Only near the lower vessel, does MELCOR under-predict the mass. Note that the results discussed in this section does not account for any effect of the aerosol density on deposition, particularly for the steam environment. The use of the representative density for the aerosol under this environment should be close to that of the water. Attachment ATT shows the results of the aerosol density for this experiment. Only the base case is being conducted for MELCOR 2.1.

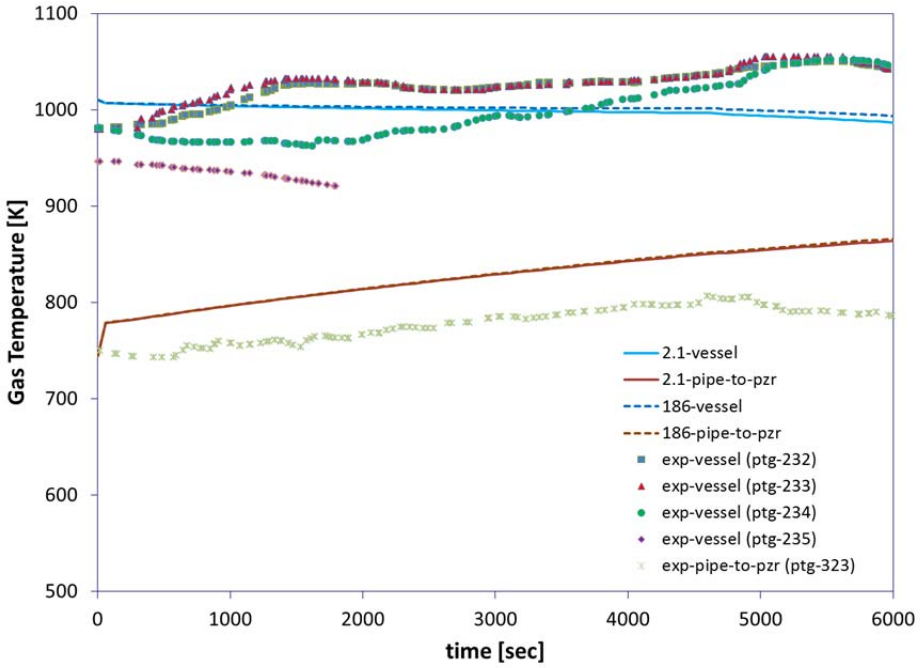

Figure 3.13-5 MELCOR and Measured Gas Temperatures for the Base Case (see Figure 3.13-2 for the measuring locations)

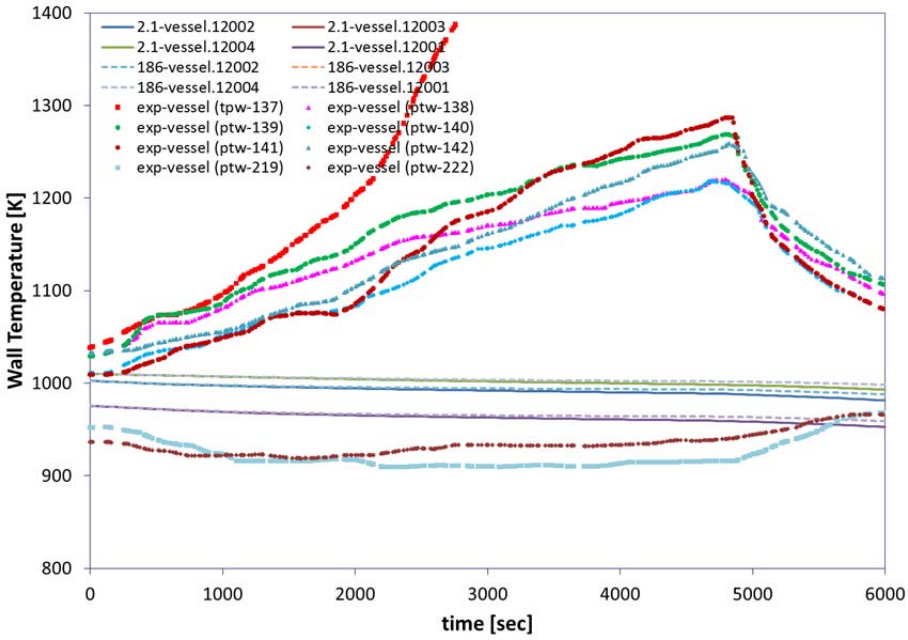

Figure 3.13-6 MELCOR and Measured Vessel Wall Temperatures for the Base Case (see Figure 3.13-2 for the measuring locations)

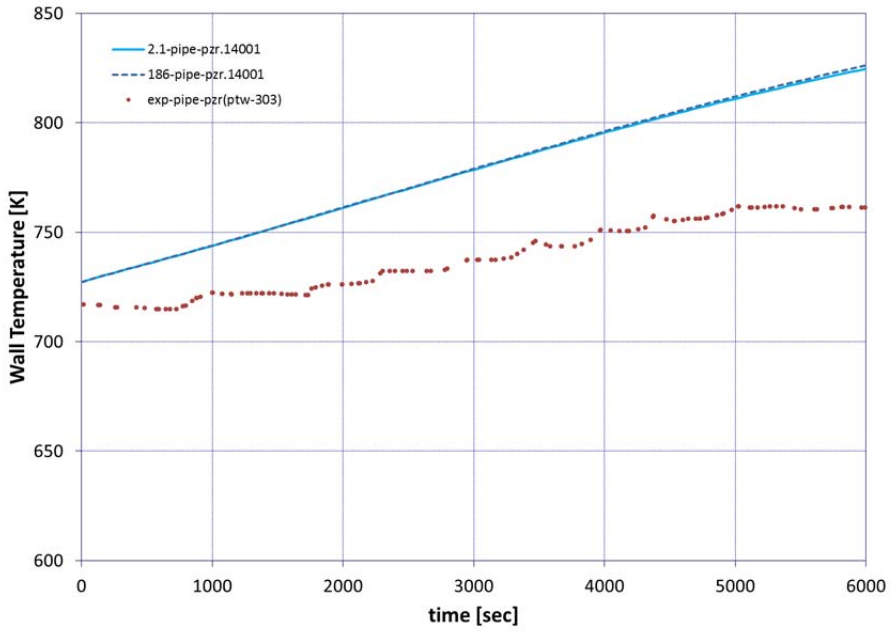

Figure 3.13-7 MELCOR and Measured Pipe Wall Temperatures for Piping from the Reactor Vessel for the Base Case (see Figure 3.13-2 for the measuring locations)

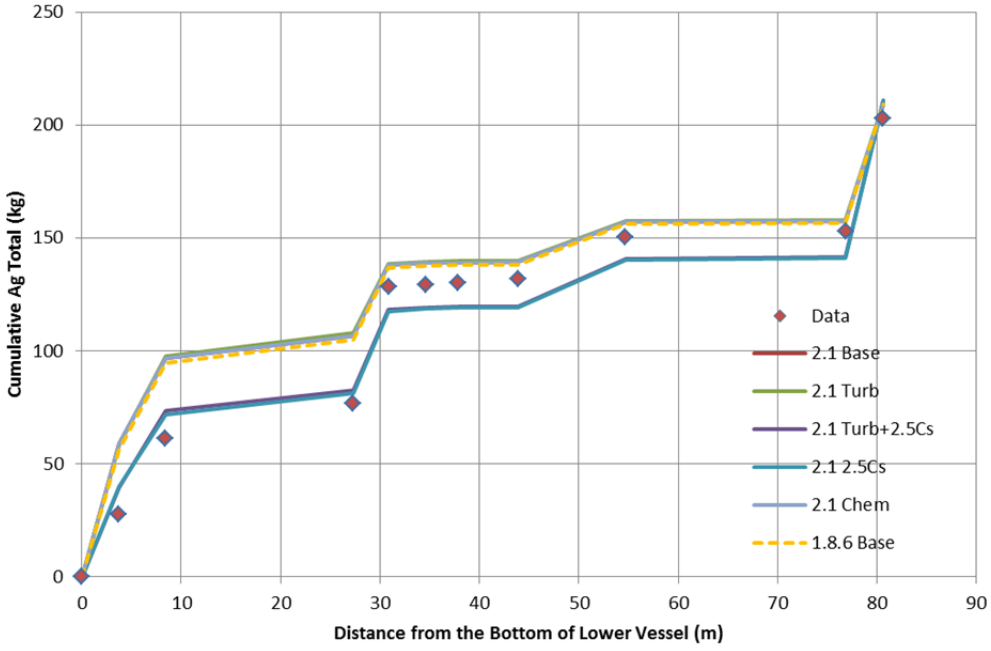

Figure 3.13-8 Cumulative Deposited Ag mass Along Circuit

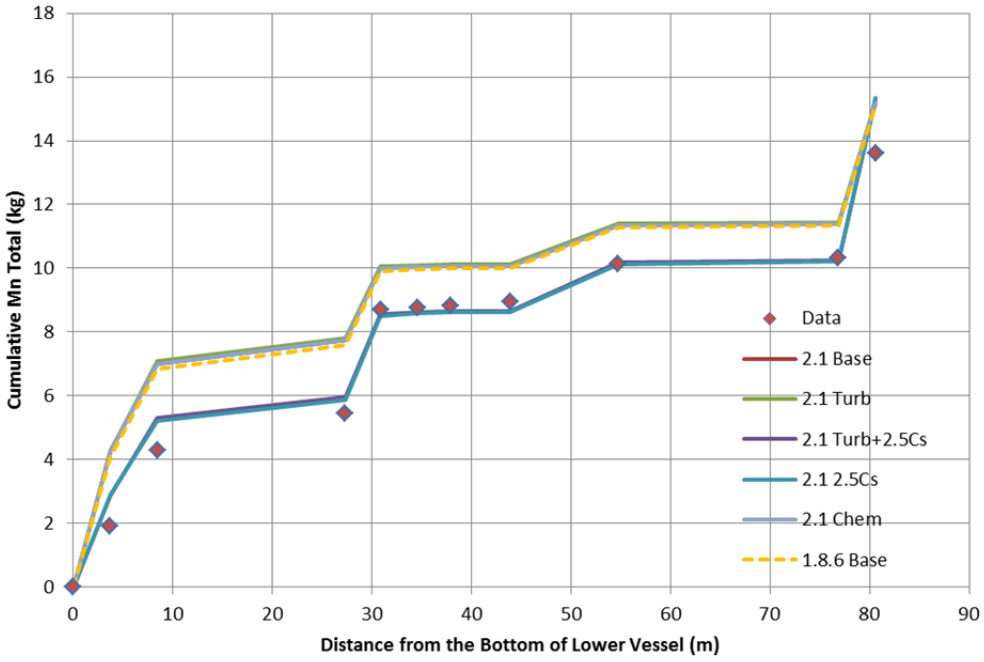

Figure 3.13-9 Cumulative Deposited Mn mass Along Circuit

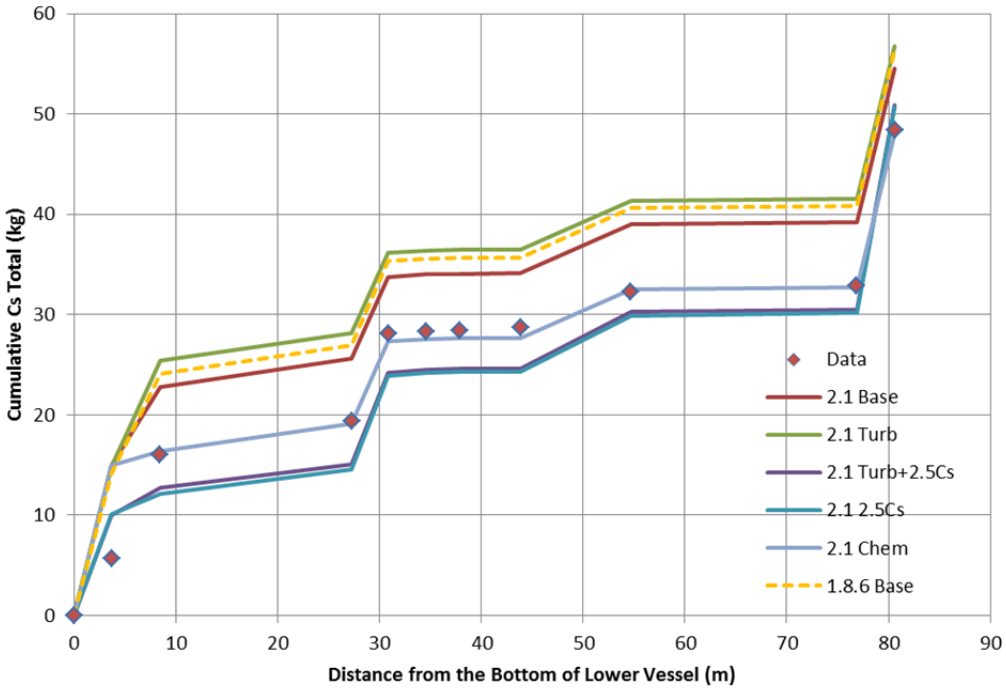

Figure 3.13-10 Cumulative Deposited Cs mass Along Circuit

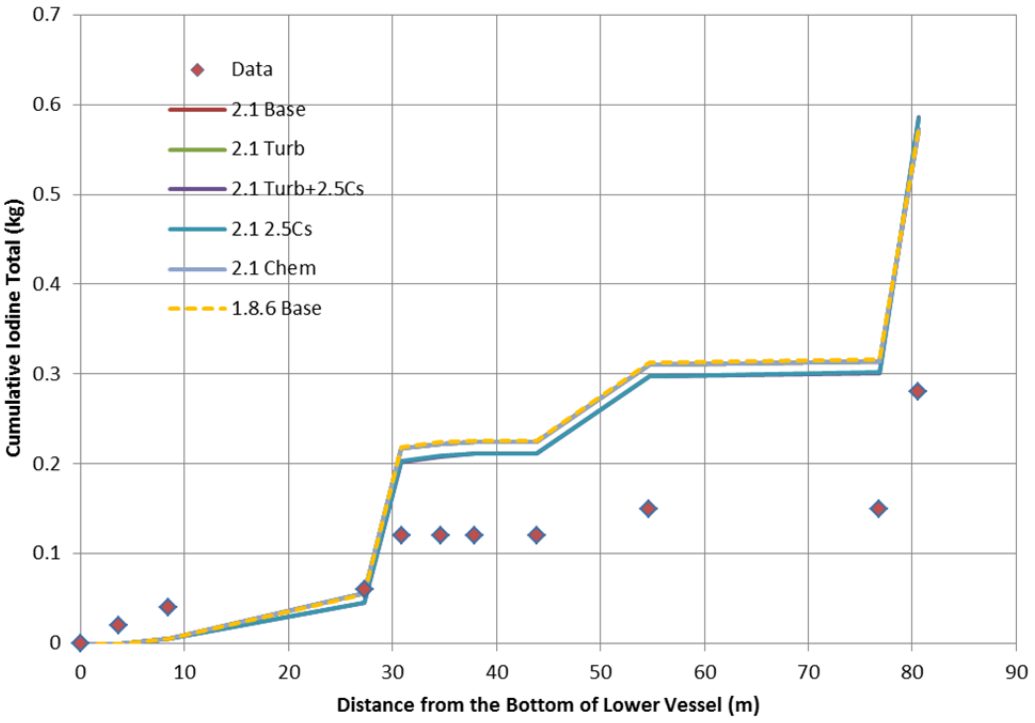

Figure 3.13-11 Cumulative Deposited Iodine mass Along Circuit

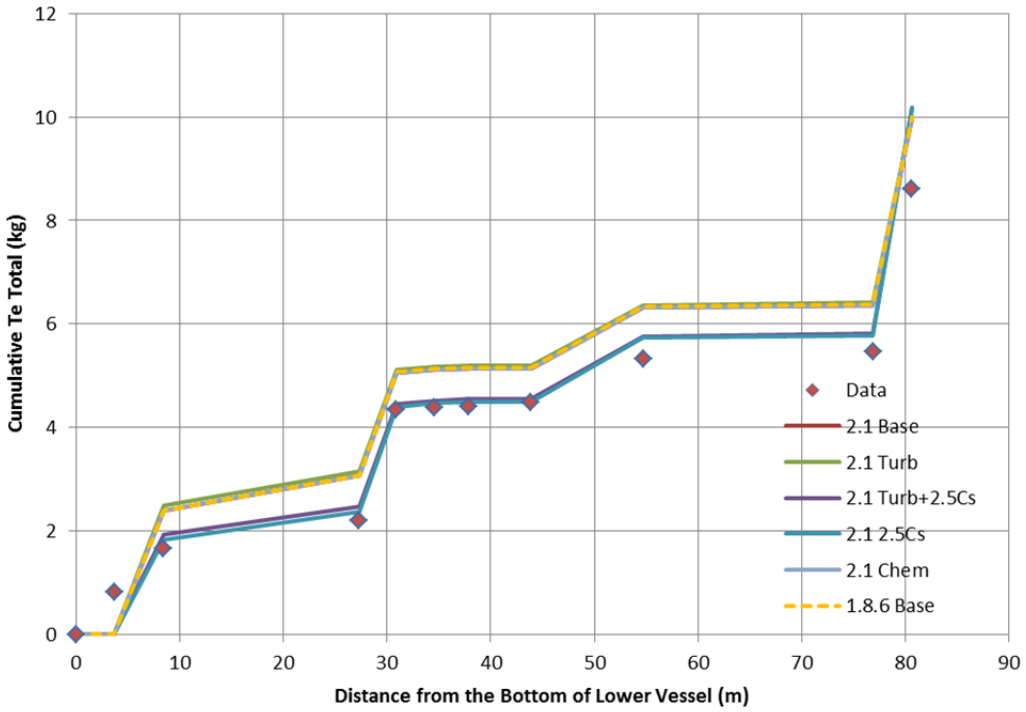

Figure 3.13-12 Cumulative Deposited Te mass Along Circuit

Table 3.13-4 Distance Reference to MELCOR Nodalization

Distance	(m)
Bottom Lower Vessel	0
CV110 (top lower vessel)	3.71
CV120 (top upper vessel)	8.44
CV130+140 (top LO2 Pipe)	27.3
CV010 (top przr lower)	30.88
CV012 (top przr middle)	34.62
CV014 (top przr upper)	37.88
CV020 (top LO4)	43.86
CV030 (top LO5)	54.71
CV040 (top LO6)	76.86
CV050 (tank)	80.62

3.13.5 Conclusions

There is a question about the aerosol mass lost in the experiment and the uncertainty about the initial size distribution of the aerosols in the experiment. Nonetheless, based on the results given in this document, MELCOR agrees well, within the uncertainty for this experiment, using the "2.5Cs" initial aerosol size distribution for all aerosol types, except for the iodine. It is unclear why there are significant differences between MELCOR calculations and the experimental data. Because the specific AMMD used in "2.5Cs" case is applied only for this test, it is not certained that using the AMMD for this case can be bounded most of the severe accident conditions of the accidents. It is noted that excessive mass lost in the experiment may explain the differences in the MELCOR calculated values for iodine.

As shown in Attachment ATT, the results are not significant different when using aerosol densities other than the default water density for wet environment. Future assessment may examine closely for the case of wet environment for aerosol deposition. In addition, it is necessary to explain the thermal prediction by MELCOR for this experiment. Future assessment should also examine this issue.

Attachment ATT

This attachment attempts to describe the effect of the aerosol density for this experiment, since steam does present in this experiment. Only the base case as shown in Table 3.13-3 is conducted for MELCOR 2.1. In MELCOR 2.1, the aerosol density input is included in the RN1_ASP record. In this record, there are two other inputs: DMIN, and DMAX, the minimum and maximum diameter of the aerosol, respectively. For the base case, DMAX is set at 2.5E-4 m, while default value is 5.0E-4 m. For the aerosol density, the base case uses 4120 kg/m^3, while default value is 1000 kg/m^3. For DMIN, the base case uses the default value of 1.0E-7 m. Table 3.13-5 to Table 3.13-9 show the comparison of the density from the base case to 1000 and 2500 kg/m^3,

including the effect of DMAX from 5.0E-4 to 2.5E-4 m, respectively for Ag, Mn, Cs, I, and Te. As shown in these tables, the effect of the aerosol density is not significant enough to warrant the use of the water density for wet aerosol. However, future assessment and future aerosol physics model improvement may be required.

Table 3.13-5 Effect of Aerosol Density for Base Case (Ag Aerosol)

Location	Data	Base case (4120 kg/m^3)	Default Values	Base with 1000 kg/m^3	Base with 2500 kg/m^3
Vaporization chamber					
Reactor vessel					
Floor	19.2	49.900	37.300	36.342	43.464
Lower wall	8.6	9.020	9.090	9.126	9.106
Upper wall & internals	23.91	5.130	5.350	5.368	5.290
Center plate	4.12	32.500	28.200	28.465	30.788
Coarse Particles	5.28				
Total	***61.11***	***96.550***	***79.940***	***79.301***	***88.648***
Piping					
Pipe LO1	1.4	0.001	0.001	0.001	0.001
Bend BO12	8.05				
Pipe LO2	6.36	10.300	8.170	8.609	9.706
Total	***15.81***	***10.301***	***8.171***	***8.610***	***9.707***
Pressurizer					
Floor	45.31	29.800	47.200	44.812	35.312
Lower wall	6.37	1.380	1.480	1.455	1.435
Middle wall	0.76	0.790	0.778	0.783	0.803
Upper wall	0.52	0.288	0.277	0.281	0.291
Top	0.07	0.002	0.002	0.001	0.002
Total	***53.03***	***32.260***	***49.737***	***47.332***	***37.843***
Piping					
Pipe LO4	1.84	0.058	0.055	0.056	0.059
Pipe LO5	18.53	17.700	15.100	16.584	17.696
Pipe LO6	2.67	0.663	0.662	0.668	0.678
Total	***23.04***	***18.421***	***15.817***	***17.308***	***18.433***

Relief Tank	49.93	51.800	58.200	58.393	55.284
Grand TOTAL	**202.92**	**209.332**	**211.865**	**210.944**	**209.915**

Table 3.13-6 Effect of Aerosol Density for Base Case (Mn Aerosol)

Location	Data	Base case (4120 kg/m^3)	Default Values	Base with 1000 kg/m^3	Base with 2500 kg/m^3
Vaporization chamber					
Reactor vessel					
Floor	1.27	3.610	2.700	2.631	3.146
Lower wall	0.63	0.653	0.658	0.661	0.659
Upper wall & internals	1.74	0.372	0.387	0.389	0.383
Center plate	0.32	2.350	2.040	2.060	2.228
Coarse Particles	0.34				
Total	***4.3***	***6.985***	***5.785***	***5.741***	***6.416***
Piping					
Pipe LO1	0.23	0.000	0.000	0.000	0.000
Bend BO12	0.51				
Pipe LO2	0.4	0.744	0.592	0.623	0.703
Total	***1.14***	***0.744***	***0.592***	***0.623***	***0.703***
Pressurizer					
Floor	2.87	2.160	3.420	3.244	2.556
Lower wall	0.4	0.100	0.107	0.105	0.104
Middle wall	0.06	0.057	0.056	0.057	0.058
Upper wall	0.04	0.021	0.020	0.020	0.021
Top	0.01	0.000	0.000	0.000	0.000
Total	***3.38***	***2.338***	***3.603***	***3.426***	***2.739***
Piping					
Pipe LO4	0.12	0.004	0.004	0.004	0.004
Pipe LO5	1.2	1.280	1.090	1.200	1.281
Pipe LO6	0.18	0.048	0.048	0.048	0.049
Total	1.5	1.332	1.142	1.252	1.334

Relief Tank	***3.3***	***3.750***	***4.210***	***4.001***	***4.001***
Grand TOTAL	**13.62**	**15.149**	**15.332**	**15.043**	**15.193**

Table 3.13-7. Effect of Aerosol Density for Base Case (Cs Aerosol)

Location	Data	Base case (4120 kg/m^3)	Default Values	Base with 1000 kg/m^3	Base with 2500 kg/m^3
Vaporization chamber					
Reactor vessel					
Floor	4.56	12.500	9.070	8.844	10.769
Lower wall	1.16	2.480	2.500	2.505	2.500
Upper wall & internals	9.85	1.420	1.490	1.491	1.465
Center plate	0.47	6.430	0.000	0.000	0.000
Coarse Particles	0.03				
Total	***16.07***	***22.830***	***13.060***	***12.840***	***14.734***
Piping					
Pipe LO1	1.16	0.003	0.003	0.003	0.003
Bend BO12	1.17				
Pipe LO2	1.03	2.770	2.150	2.262	2.593
Total	***3.36***	***2.773***	***2.153***	***2.265***	***2.596***
Pressurizer					
Floor	7.59	7.780	12.200	11.550	9.144
Lower wall	1.08	0.406	0.439	0.432	0.423
Middle wall	0.18	0.221	0.220	0.221	0.225
Upper wall	0.12	0.079	0.077	0.078	0.080
Top	0.02	0.000	0.000	0.000	0.000
Total	***8.99***	***8.486***	***12.936***	***12.281***	***9.872***
Piping					
Pipe LO4	0.34	0.018	0.017	0.017	0.018
Pipe LO5	3.49	4.890	4.180	4.591	4.898
Pipe LO6	0.6	0.193	0.197	0.199	0.199
Total	***4.43***	***5.101***	***4.394***	***4.807***	***5.115***

Relief Tank	15.54	15.300	17.600	17.631	16.468
Grand TOTAL	**48.39**	**54.490**	**50.143**	**49.824**	**48.785**

Table 3.13-8 Effect of Aerosol Density for Base Case (I Aerosol)

Location	Data	Base case (4120 kg/m^3)	Default Values	Base with 1000 kg/m^3	Base with 2500 kg/m^3
Vaporization chamber					
Reactor vessel					
Floor	0.01	0.000	0.000	0.000	0.000
Lower wall	0.01	0.000	0.000	0.000	0.000
Upper wall & internals	0.01	0.006	0.006	0.006	0.006
Center plate	0.01	0.000	0.000	0.000	0.000
Coarse Particles					
Total	***0.04***	***0.006***	***0.006***	***0.006***	***0.006***
Piping					
Pipe LO1	0	0.003	0.003	0.003	0.003
Bend BO12	0.01				
Pipe LO2	0.01	0.047	0.033	0.035	0.042
Total	***0.02***	***0.050***	***0.036***	***0.038***	***0.045***
Pressurizer					
Floor	0.05	0.153	0.212	0.201	0.170
Lower wall	0.01	0.008	0.008	0.008	0.008
Middle wall	0	0.005	0.005	0.005	0.005
Upper wall	0	0.002	0.002	0.002	0.002
Top	0	0.000	0.000	0.000	0.000
Total	***0.06***	***0.168***	***0.227***	***0.216***	***0.185***
Piping					
Pipe LO4	0	0.000	0.000	0.000	0.000
Pipe LO5	0.03	0.087	0.064	0.071	0.081
Pipe LO6	0	0.003	0.003	0.003	0.003
Total	***0.03***	***0.090***	***0.067***	***0.074***	***0.084***

Relief Tank	0.13	0.258	0.251	0.251	0.257
Grand TOTAL	**0.28**	**0.572**	**0.587**	**0.585**	***0.577***

Table 3.13-9. Effect of Aerosol Density for Base Case (Te Aerosol)

Location	Data	Base case (4120 kg/m^3)	Default Values	Base with 1000 kg/m^3	Base with 2500 kg/m^3
Vaporization chamber					
Reactor vessel					
Floor	0.62	0.000	0.000	0.000	0.000
Lower wall	0.21	0.000	0.000	0.000	0.000
Upper wall & internals	0.61	0.445	0.435	0.435	0.442
Center plate	0.13	1.950	1.540	1.545	1.766
Coarse Particles	0.09				
Total	***1.66***	***2.395***	***1.975***	***1.980***	***2.208***
Piping					
Pipe LO1	0.04	0.001	0.001	0.001	0.001
Bend BO12	0.28				
Pipe LO2	0.22	0.672	0.486	0.508	0.606
Total	***0.54***	***0.673***	***0.487***	***0.509***	***0.607***
Pressurizer					
Floor	1.87	1.890	2.750	2.594	2.142
Lower wall	0.27	0.097	0.097	0.095	0.097
Middle wall	0.04	0.054	0.050	0.050	0.053
Upper wall	0.03	0.020	0.018	0.018	0.020
Top	0	0.000	0.000	0.000	0.000
Total	***2.21***	***2.061***	***2.915***	***2.757***	***2.312***
Piping					
Pipe LO4	0.08	0.004	0.004	0.004	0.004
Pipe LO5	0.83	1.180	0.935	1.021	1.136
Pipe LO6	0.14	0.047	0.044	0.044	0.046
Total	***1.05***	***1.231***	***0.983***	***1.069***	***1.186***

Relief Tank	3.14	3.630	3.890	3.873	3.768
Grand TOTAL	**8.6**	**9.990**	**10.250**	**10.188**	***10.081***

3.13.6 References

[3.13.1]L.N. Kmetyk, MELCOR 1.8.1 Assessment: Marviken-V Aerosol Transport Tests ATT-2b/ATT-4, SAND92-2243, Sandia National Laboratories, January 1993.

3.14 Analysis of NTS Hydrogen Burn Combustion Tests

3.14.1 Background

Between July 1983 and January 1984, a series of premixed hydrogen combustion experiments were conducted in a hydrogen dewar located at Test Cell C, at the Nevada Test Site (NTS) Ref. [3.14.1]. A total of twenty-four combustion experiments were performed to examine the hydrogen behavior and the safety-related equipment response. Hydrogen concentrations for these tests ranged from 5 to 13% (by volume) and steam concentrations from 4 to 40%. Several tests also incorporated spray systems and/or fans, which enhanced the combustion rate and significantly affected the post-combustion gas cooling.

3.14.2 Experiment

A spherical test vessel, as shown in Figure 3.14-1, having an inner diameter of 15.85 m (2048 m^3 volume) and a design pressure of about 0.7 MPa was used to perform the premixed and continuous-injection combustion experiments. The dewar consists of two concentric stainless steel spheres, each 10 mm thick, with an intermediate layer of perlite insulation about 1 m thick. This facility contains the following modification:

1. A heated-water spray system containing 16 or 17 Sprayco model 1713 hollow cone nozzles.
2. A boiler to generate 2.1 kg/s steam at 1 MPa.
3. Two mixing fans to be used for pretest equilibration and other uses. Each fan is rated at 2.4 m^3/s (5000 CFM).
4. An air compressor (rated at 0.28 m^3/s or 600 CFM) to supply air to the mixing fans and primary spray pump air motors, and for post-test purge and refill operations.
5. A gas sampling system for pre- and post-test evaluations for gas uniformity and combustion completeness.

Hydrogen was supplied from gas cylinders in a tube trailer. Hydrogen, after mixing with steam, enters the dewar through a nozzle (about 2 m in diameter) located above the bottom, as a diffusive stream or as a jet, depending on the test configurations (see Figure 3.14-2). Once inside the vessel, the mixture is ignited by using typical hydrogen igniter sources; the igniters are installed in the existing reactor containment for burning any hydrogen, before a detonated mixture is reached. The igniters were positioned to allow for combustion initiated at various locations within the dewar, such as along the central vertical axis of the sphere at the top, bottom or center, and along the vessel walls. Each igniter was a hot surface at about 1000 to 1400 K, and each could be independently operated. For most cases, the igniter located at the bottom was utilized. There were a number of measurements performed to provide pertinent data to quantify combustion phenomena and equipment-specific response data in the combustion environments. Table 3.14-1 lists the types and locations of the instruments used in the

experiment (see Ref. [3.14.1] for details). Figure 3.14-3 shows the coordinate system in the dewar, which can locate a particular instrument as listed in Table 3.14-2. As shown in Table 3.14-3, both P101, P102 and P105 can measure up to 100 psi, while P103 can measure up to 50 psi; P104 can measure up to 200 psi. Also shown in Table 3.14-1 are the Gardon and Schmidt-Boelter gauges, which gauge the heat flux.

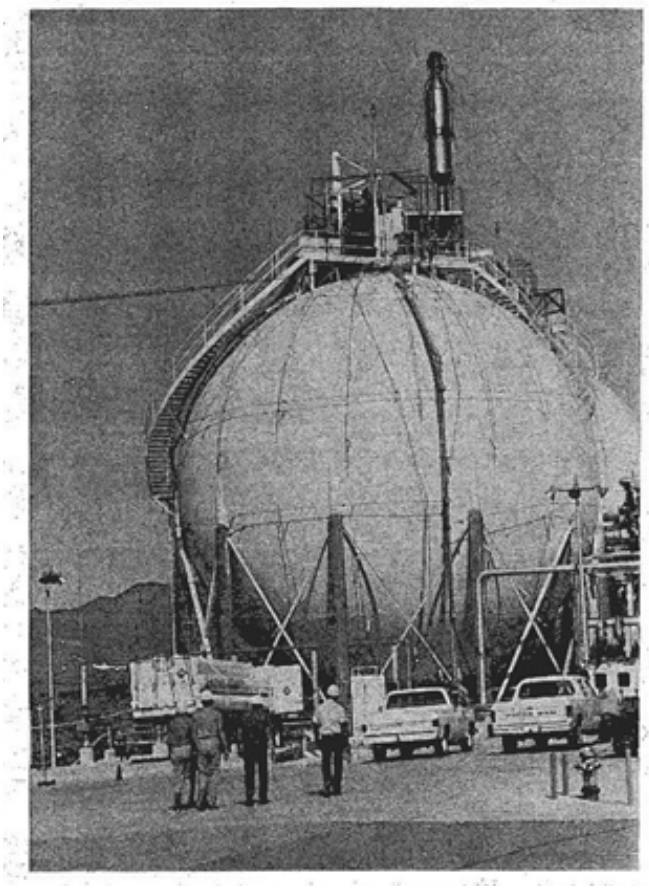

Figure 3.14-1 Hydrogen Dewar at NTS REF. [3.14.1]

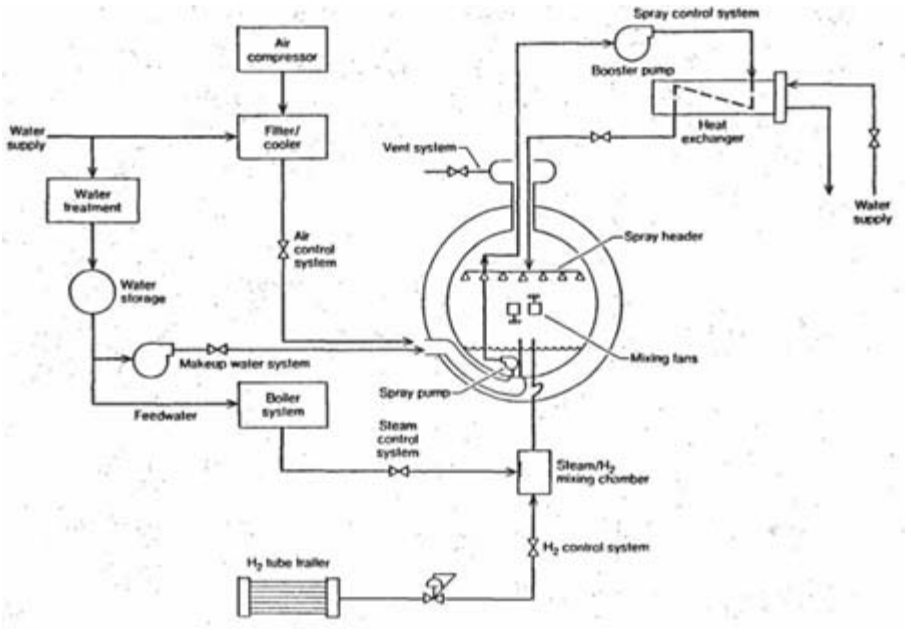

Figure 3.14-2 Schematic of the Test Ref. [3.14.1]

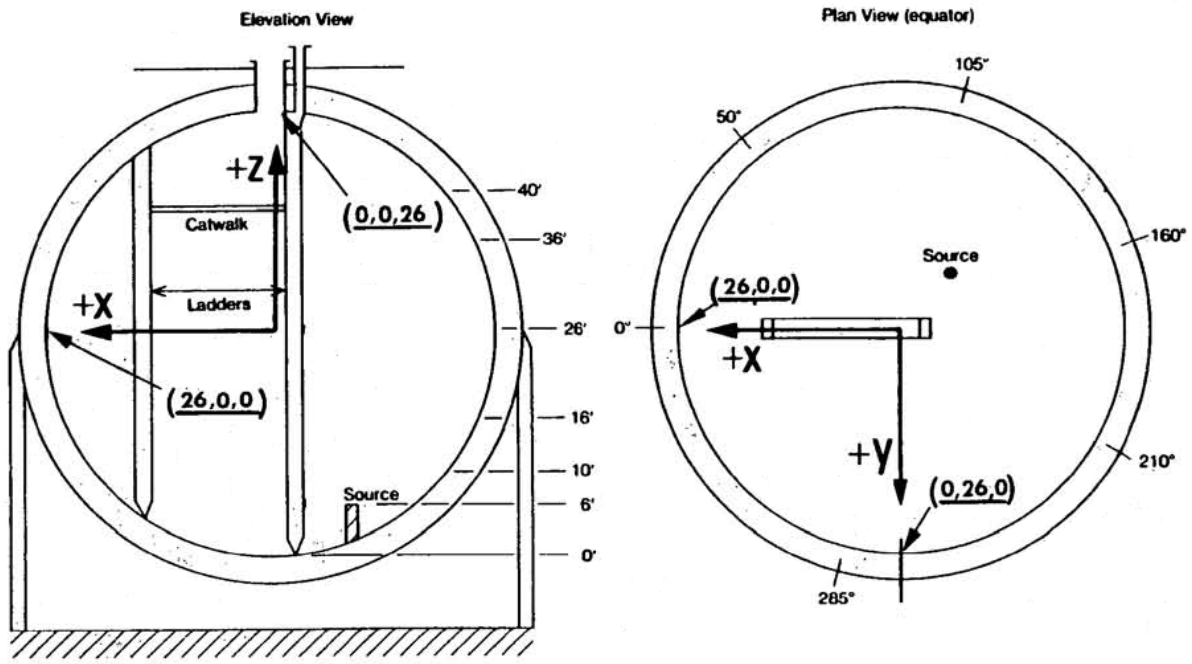

Figure 3.14-3 Coordinate System Used to Define Measuring Device Locations in the Dewar Ref. [3.14.1]

Table 3.14-1 Instruments Used

Instrument Name/Type	Coordinate in X,Y,Z (ft) Referenced to Figure x-3	Instrument Name/Type	Coordinate in X,Y,Z (ft) Referenced to Figure x-3
Pressure Sensors		Gardon Gauge[1]	
P101	0,0,21	H105(R)	1,3,25.5
P102	-5,-5,0	H106(T/R)[2]	0,3,25,5
P103	-5,-5,20	Schmidt-Boelter Gauge[1]	
P104	-1,-1,26	H501(R)	1,-2.5,2
P105	16,0,6	H502(T)	1,-2.5,2
Gas Temperature (thermocouple)		H503(T)	1,-2.5,2
T114	9,0,21	H504(T)	14.5,-2.5,2
T118	20,0,0	H505(R)	-4.5,-2.5,2
T151	-5,-5,6	H506(T)	-4.5,-2.5,2
Wall Temperature		H507(T)	-4.5,-2.5,2
T120	-2,-3,26		
T121	-18.4,1,18.4		

[1]Radiative(R) or Total (T) instrumentation
[2]Gauage H106 was re-configured from a total to a radiative gauge prior to NTSP08

3.14.3 MELCOR Model

Both the 1.8.6 and the 2.1 calculations were run using the MELCOR 2.0 default values. Revision 3964 of MELCOR 1.8.6 and revision 6110 of MELCOR 2.1 were used for assessment purposes. In addition, the input parameters for the hydrogen burn model are those in the default values, except the H2 model fraction limit for ignition with igniters was chosen to be 0.041 instead of 0.07 (default). A total of 4 premixed combustion experiments were simulated as shown in Table 3.14-2. Both Case NTSP01 and NTSP15 are the standard tests, while Cases NTSP12 and NTSP20 are the Steam-Laden tests, where the dewar was heated by high-temperature steam, resulting in a steam concentration greater than 10 volume %. Note that no water sprays or mixing fans were used in any of the NTS experiments simulated with MELCOR.

Table 3.14-2 Cases Simulated

Test	Conditions		
	Gas Mixture*	Temperature (K)	Pressure (kPa)

NTSP01	5.3% H2, 4.2% steam	302.7	97.4
NTSP12	6.9% H2, 28.3% steam	339.7	92.6
NTSP15	9.9% H2, 4.2% steam	304.4	109.3
NTSP20	12.9% H2, 27.8% steam	342.0	104.2

*Percentage reported is volume percent. Note that the mixing fan is off for all these tests.

3.14.4 Discussions and Results

Using the original MELCOR 1.8.5 decks developed for the 4 tests as shown in Table 3.14-2, the thermal conditions resulting from the hydrogen burn are given in Figure 3.14-4 to Figure 3.14-7. As shown in these figures, the test data were obtained from Ref. [3.14.2], which are different from Ref. [3.14.1] in terms of the combustion period. It seems that Ref. [3.14.2] shifted the test data to the same starting time of the MELCOR results. All temperature and pressure plots are in the ratio of the initial values or time-zero values. The test data for the temperature ratios is the maximum temperature measured in the experiment Ref. [3.14.1]. As shown in these figures, both versions of MELCOR yield the identical thermal results. For the exception of NTSP20, MELCOR results show a higher pressure ratio value than the test data. For the temperature ratios, the peak calculated by MELCOR is generally slightly higher than that of the test data maximum. For the heat flux to the heat structures, MELCOR results seem to be larger than the test data, especially the peak values; an exception for NTSP20 is noted, where the test data show a higher peak value than MELCOR. Some of these differences may be attributed to the burn completeness and burn time between the experiment and MELCOR. Table 3.14-3 shows burn characteristics between the experiment and the MELCOR results. For the oxygen limited cases: NTSP01 and NTSP12, MELCOR over predicts the burn completeness relative to the experiment as shown in Table 3.14-3. This may be due to the fact that MELCOR assumes a homogeneous mixture, whereas in reality, the hydrogen entering into the dewar may not fully mix, since mixing fans are not turned on for these cases. In terms of burn time, MELCOR under predicts it for the first three cases as shown in Table 3.14-3, and over predicts NTSP20. This may be due to the burn model parameters such as burn frame speed as reported in Ref. [3.14.2]. However, the burn time calculated by MELCOR in both versions of the code is similar to the reported MELCOR value in Ref. [3.14.2].

Table 3.14-3 Hydrogen Burn Characteristics from Experiment and MELCOR

Test	Burn Completeness (%)		Burn Time (s)	
	Experiment*	MELCOR***	Experiment**	MELCOR***
NTSP01	32.0	35.4	88.5	2.0
NTSP12	58.0	72.9	27.2	9.2

NTSP15	100.0	100.0	6.0	1.3
NTSP20	100.0	100.0	2.1	4.0

*Obtained from Table 6 of SAND report [3.14.1]

**Obtained from Δt_{qr}(s) of Table A.5 in the SAND report [3.14.1].

***Both versions of MELCOR (MELCOR 1.8.6, version 3964, and 2.1, version 6087) reported identical results.

3.14.5 Conclusions

This test indicates that the hydrogen burn model in MELCOR is consistent with what has been reported in Ref. [3.14.2]. Thus the burn model in MELCOR is good in terms of overall comparison with the test data [3.14.2]. There was no default improvement recommended [3.14.2].

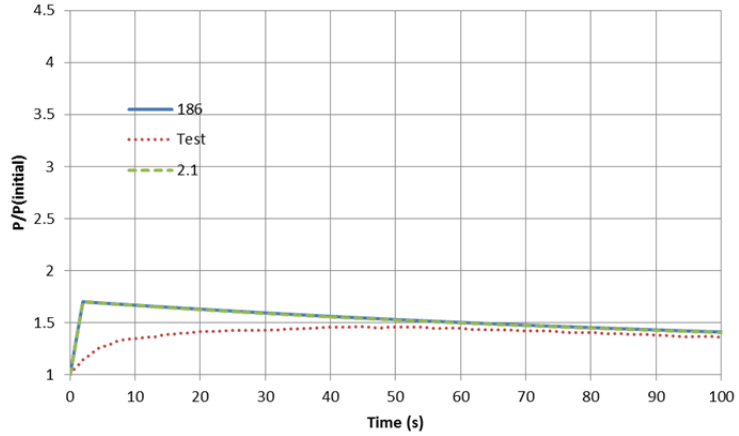

(a)

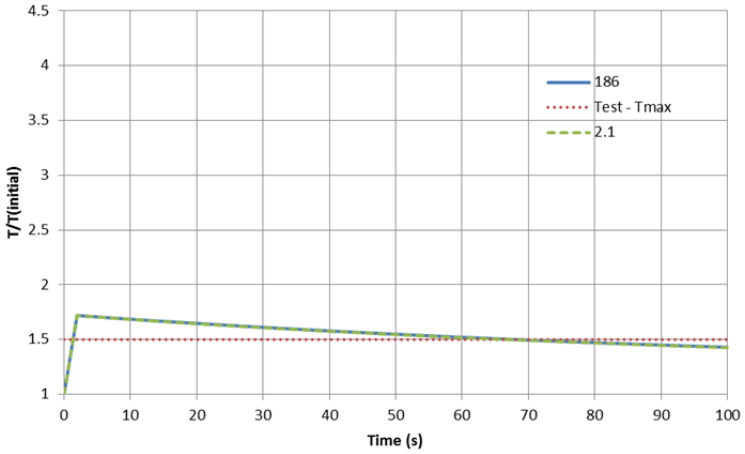

(b)

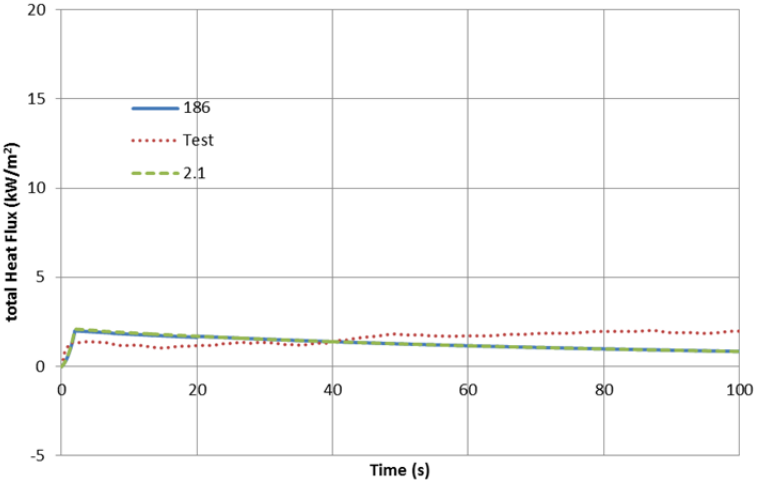

(c)

Figure 3.14-4 NTSP01 Results (a) Pressure ratio, (b) Temperature ratio, (c) Heat Flux

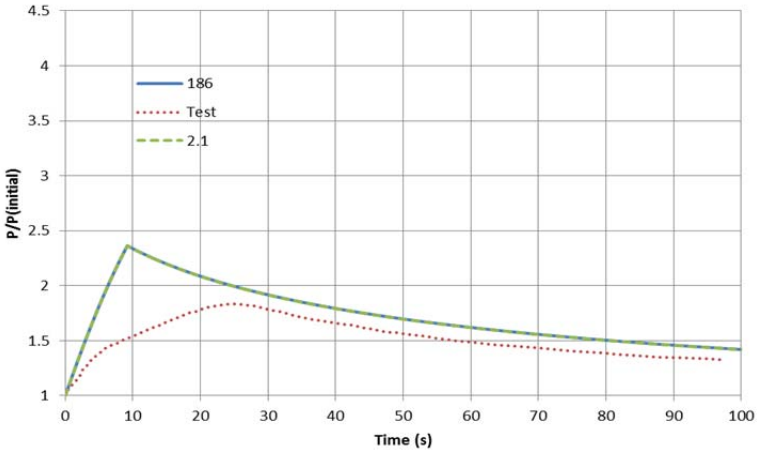

(a)

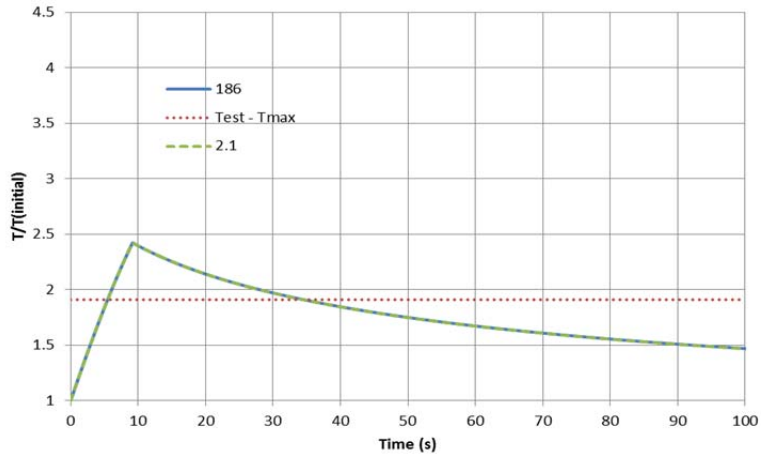

(b)

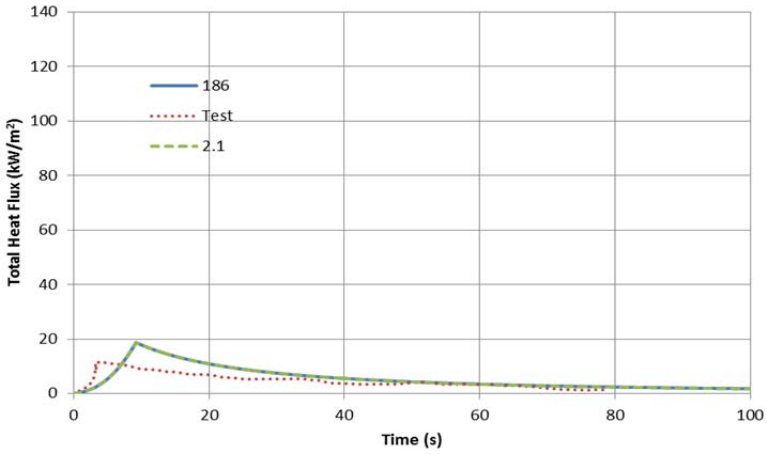

(c)

Figure 3.14-5 NTSP12 Results (a) Pressure ratio, (b) Temperature ratio, (c) Heat Flux

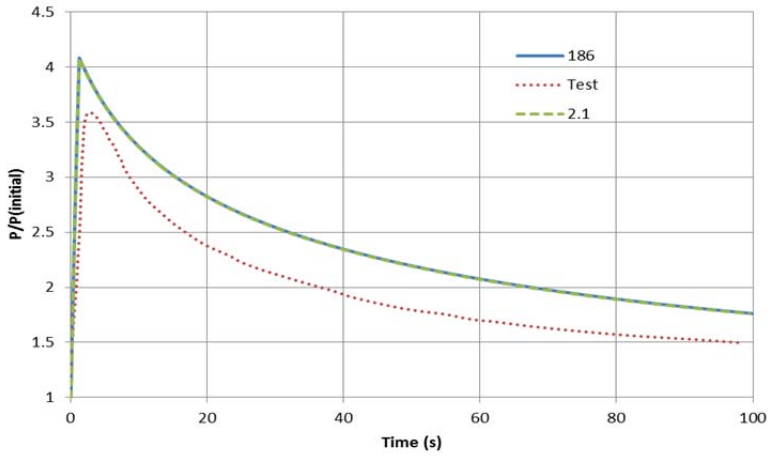

(a)

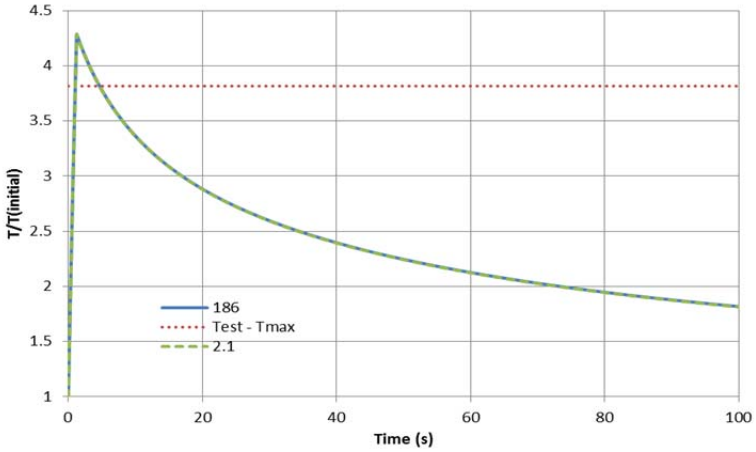

(b)

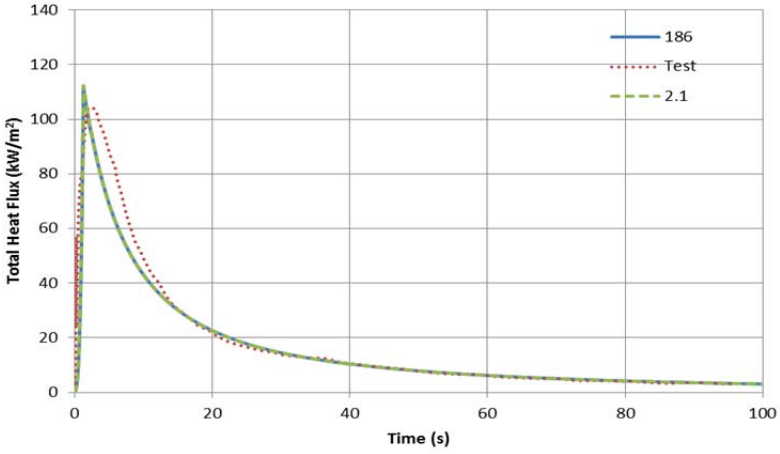

(c)

Figure 3.14-6 NTSP15 Results (a) Pressure ratio, (b) Temperature ratio, (c) Heat Flux

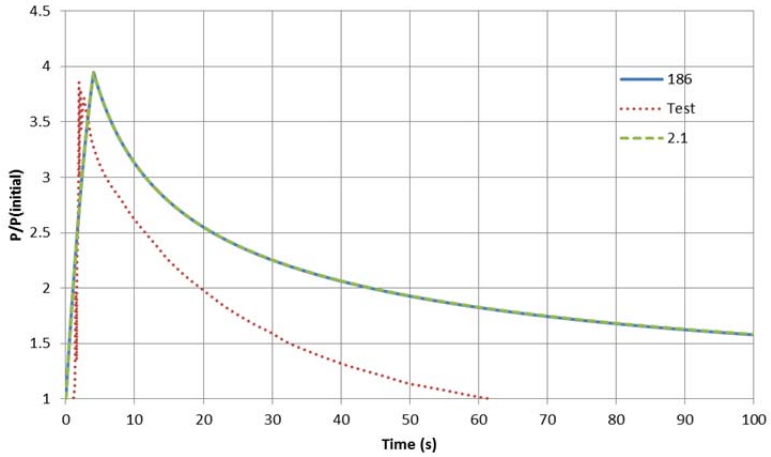

(a)

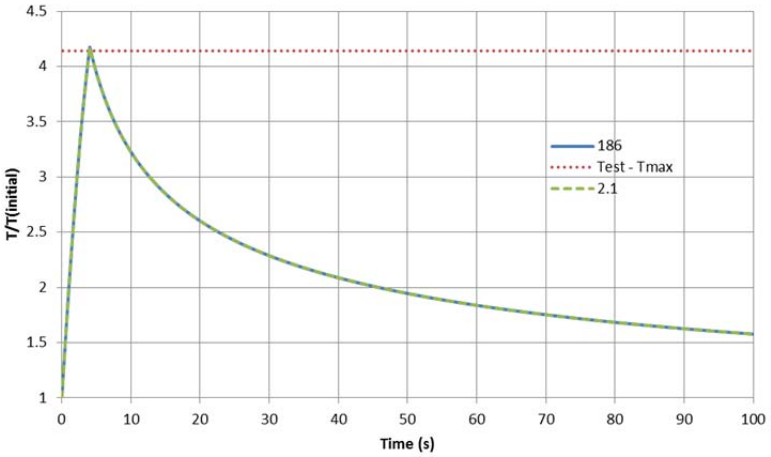

(b)

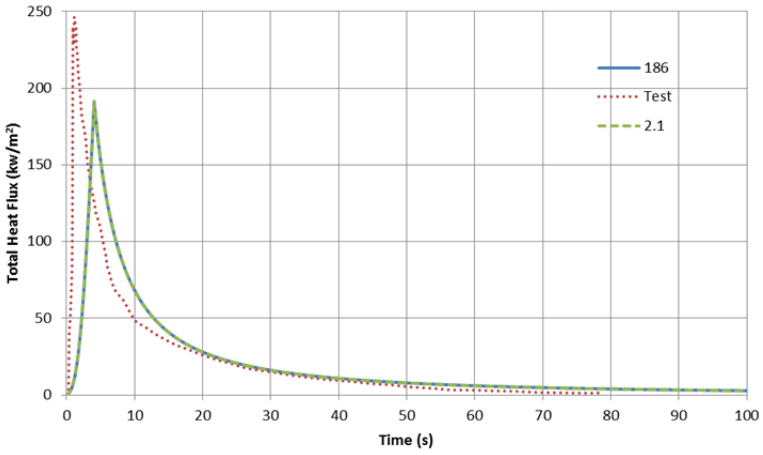

(c)

Figure 3.14-7 NTSP20 Results (a) Pressure ratio, (b) Temperature ratio, (c) Heat Flux

3.14.6 References

[3.14.1] A.C. Ratzel, Data Analyses for Nevada Test Site (NTS) Premixed Combustion Tests, NUREG/CR-4183 R3, Sandia National Laboratories, May 1985.

[3.14.2] D. Gido, Individual Parity Assessment Report – Hydrogen Premixed Single Burn Combustion, Sandia National Laboratories. Unpublished.

3.15 Analysis of the Nuclear Power Engineering Corporation (NUPEC) Mixing Tests

3.15.1 Background

The NUPEC mixing tests were conducted in a large, 1/4-scale simulated containment 3.15.7 [3.15.1] (See Figure 3.15-1). The tests explored the containment response to steam injection and containment spray actuation. This report discusses MELCOR 2.1 simulations for the M-7-1, M-8-1, and M-8-2 tests. These simulations were run with revision 6003, though results are identical to 6110 since only seven revisions were made to the source code (6004, 6019, 6027, 6061, 6087, 6106, and 6110), none of which had the potential to change results for these calculations. Helium gas was introduced into the containment as a surrogate for hydrogen. Test M-8-1 introduced a combined source of helium and steam into the lower portion of one of the steam generator compartments [3.15.1]. These tests are modeled to examine MELCOR's performance in three broad areas: (1) pressure response; (2) temperature distribution and stratification; and (3) hydrogen mixing and containment spray performance.

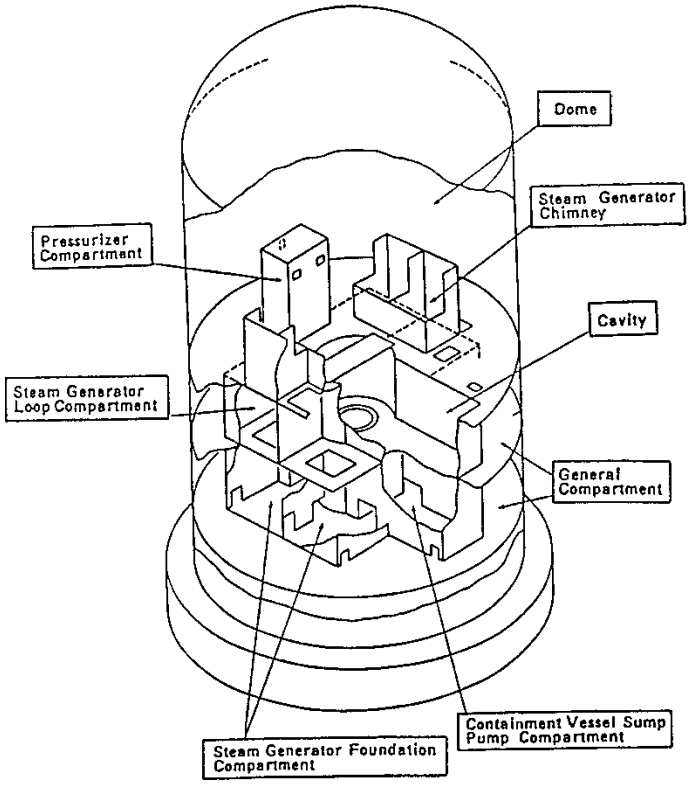

Figure 3.15-1. NUPEC 1/4-Scale Containment Mixing Facility [3.15.1]

The NUPEC facility is a domed cylinder, approximately 10.8 m in diameter, 17.4 m high, and 1310 m^3 in volume [3.15.1]]. The facility contains 28 compartments, of which only 25 are interconnected. The dome volume constitutes approximately 71% of the total containment volume. The containment is constructed entirely of carbon steel. The containment shell and floors are 12 mm thick, except for the first floor, which is 16 mm

thick. The compartment walls are 4.5 mm thick. The outside of the containment is covered with a layer of insulation, which is covered by a thin metal sheet to protect from weather damage. The insulation around the cylinder and hemisphere is 125 mm and 150 mm thick, respectively. A water storage tank is located below the first floor of the containment to collect draining condensate and spray water. The tank is separated from the rest of the containment by 100 mm of insulation. Water is pumped from the tank to 21 spray nozzles in the dome. The facility is equipped with a remote boiler for co-injecting steam and helium. The facility includes instrumentation for helium gas concentration at various locations, pressure, gas temperature, and wall temperatures.

3.15.2 Test Conditions

A summary of the conditions that were modeled in these three tests is provided in Table 3.15-1. Test M-7-1 is identical to Test M-8-2 except for the location of the steam and helium source, which are lower in the containment for M-7-1. Both of these tests were conducted with the containment sprays on. Note that M-8-1 and M-8-2 tests are similar, except that M-8-2 includes the effects of spray operation. The helium, steam, and containment spray source rates as a function of time are shown in Figure 3.15-2.

Table 3.15-1 Summary of Selected NUPEC Tests

Test	Injection Location	Initial Conditions	Relative Humidity	Helium Source	Steam Source	Containment Sprays
M-7-1	Bottom of SG Comp D (8)	343 K, 146 kPa	0.95	0→0.03 kg/s→0 283 K	0.08 kg/s→0.03 kg/s 383 K	19.4 m^3/s 313 K
M-8-1	Upper Pressurizer Comp (22)	303 K, 101 kPa	0.7	0.027 kg/s 283 K	0.33 kg/s, 388 K	*None*
M-8-2	Upper Pressurizer Comp (22)	343 K, 146 kPa	0.95	0→0.03 kg/s→0 283 K	0.08 kg/s→0.03 kg/s 363 K	19.4 m^3/s 313 K

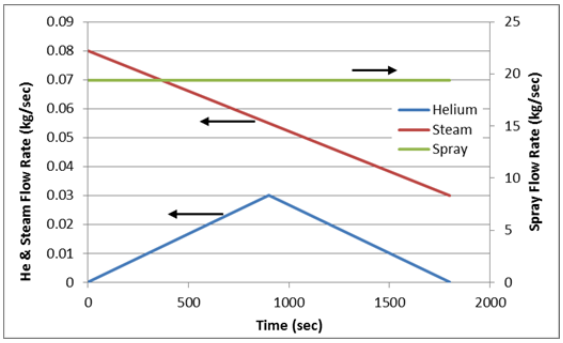

Figure 3.15-2. Mass Source Rates for Helium, Steam, and Spray Flow (M-7-1 & M-8-2)

3.15.3 Nodalization

The MELCOR nodalization of the NUPEC Mixing Facility is presented in Figure 3.15-3. The nodalization contains 35 control volumes (CVs), with a single control volume

modeling each room, except for the dome and the upper pressurizer compartment. The dome and the pressurizer compartment were further subdivided into seven and two volumes, respectively. The dome (in green) was subdivided into central volumes (CVs 30, 32, and 34), annular volumes (CVs 29, 31, and 33), and the top of the dome (CV 25). This nodalization allowed convection loops to form during the calculation. The upper pressurizer compartment (in red) was also subdivided (CVs 22 and 35) to allow circulation of gases from the upper pressurizer compartment to the lower pressurizer compartment (CV 16), which is a dead-end room. This was particularly important for M-8-1 and M-8-2 because the helium and steam were sourced into the upper pressurizer compartment. A detailed layout of the containment rooms and connectivity is given in Figure 3.15-4.

The reactor vessel and primary shield cells (CVs 27 and 28) were also explicitly included in the MELCOR model. Rather than modeling the drain tank explicitly, condensate and spray water were removed via CVH package mass and energy sinks. Two additional CVs were added (CVs 998 and 999) to represent ambient heat transfer boundary conditions. CV 998 represents the thermal conditions below the bottom of the primary shield, and CV 999 represents the outside environment.

A total of 124 MELCOR heat structures are included in the NUPEC model. The MELCOR film-tracking model is able to model the drainage of a condensed film from one heat structure onto other heat structures or into pools. The MELCOR model defines heat structure film drainage networks as described below.

3.15.4 MELCOR Input Specifications

In general, the NUPEC model was developed using standard, default MELCOR modeling parameters. A few exceptions are noted below. Also, since this calculation was performed strictly as an assessment of containment thermal-hydraulic modeling capabilities, the Radionuclide (RN) and Core (COR) packages were not activated.

3.15.4.1 Flow Paths

The flow path junction levels for vertical flows are specified at the interfaces between the two connected volumes rather than from the volume center to volume center.

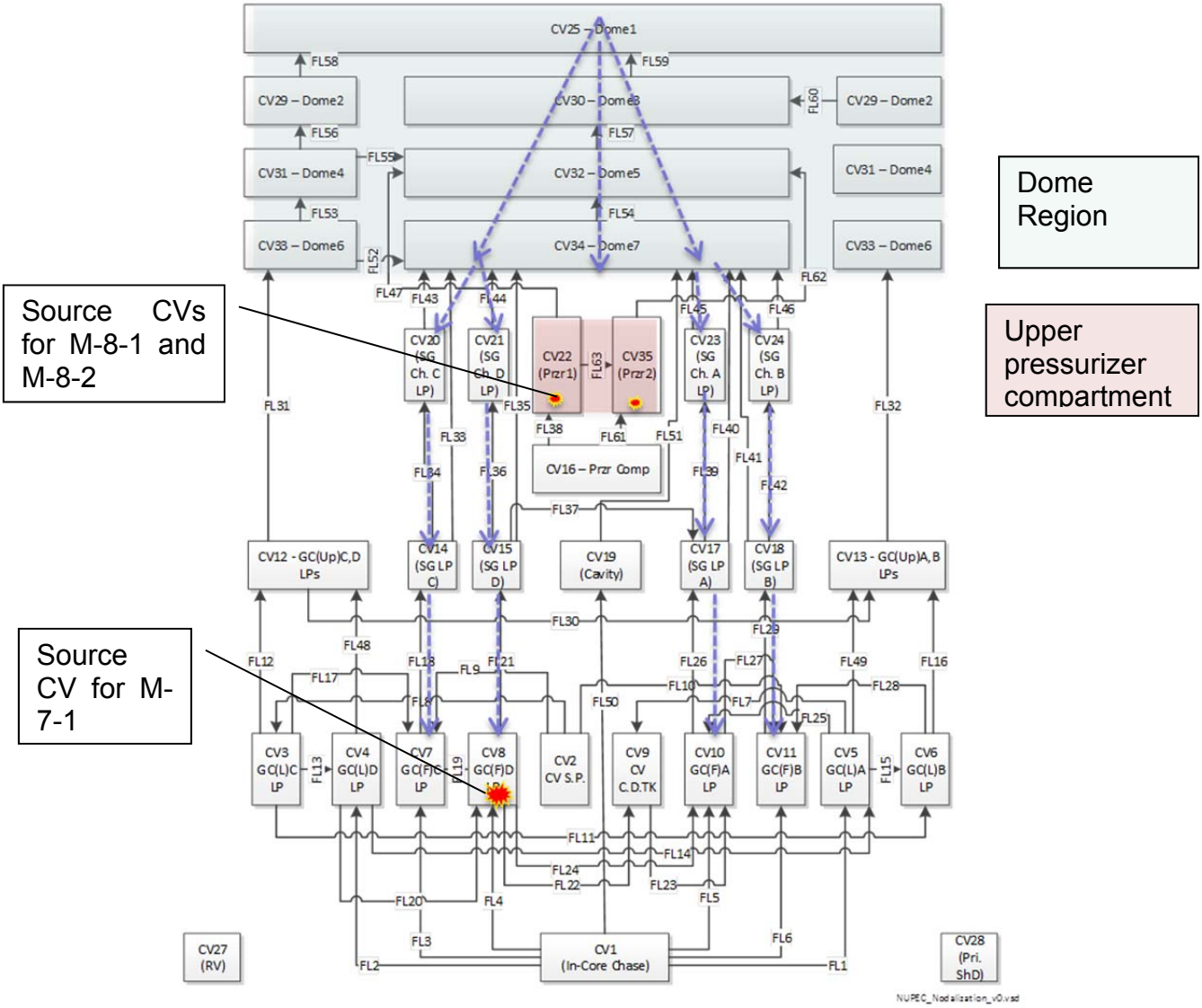

Figure 3.15-3. MELCOR NUPEC Nodalization (Dashed blue arrows indicate spray paths)

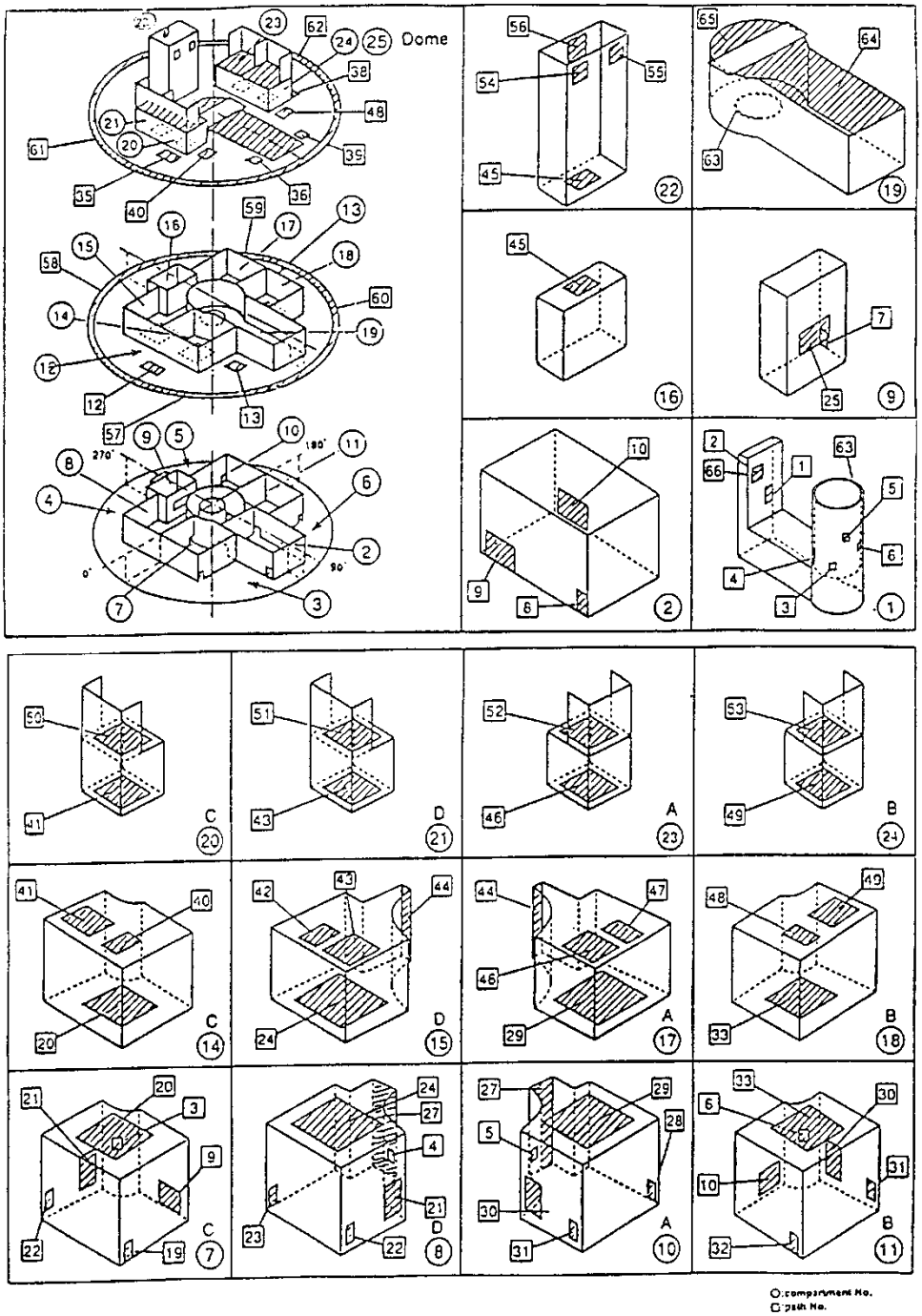

Figure 3.15-4. Detailed NUPEC Facility Layout [3.15.1]

3.15.4.2 Containment Sprays

The M-7-1 and M-8-2 tests both had sprays that were active in the test while there were no active sprays in M-8-1. The implementation of the containment spray modeling was accomplished using the following modeling assumptions:

(1) The MELCOR containment spray model can track the fraction of droplets that carry over into lower control volumes directly without having to use pumps to move the fluid. Sump directives were added to control volumes where spray water would collect to transfer the water droplets that are not carried over to a lower cell directly to the sump (e.g., bottom of the containment in the NUPEC model).

(2) MELCOR does not include a modeling option to augment the heat transfer coefficient for a user-specified forced flow condition. During preliminary calculations, the calculated heat transfer coefficients from MELCOR were reviewed. The dome heat transfer coefficients were calculated to be a natural convective coefficient of ~3–5 W/m^2–K. Spreadsheet calculations were performed assuming forced convection at 14 m/s using a Dittus-Boelter relationship [3.15.2]. The spreadsheet calculations suggested the forced flow condition would be ~25 W/m^2–K, or approximately five times the maximum natural convective value. Assuming heat and mass transfer were equally affected, scale multipliers that increased the heat and mass transfer coefficient by a factor of five were added to the dome heat structures.

(3) The MELCOR film-tracking models were activated to model the flow of condensed water between heat structures and to water pools.

(4) Mass and energy sinks were added to the MELCOR model to remove sump water from CVs 1 and 6.

3.15.4.3 Heat Structures

There were 124 heat structures included in the MELCOR nodalization scheme. Heat structures were modeled with the band radiation model activated. At containment temperatures during NUPEC Test M-8-1, radiative exchange is not expected to be important. However, for completeness, the models were activated.

Several heat transfer coefficients were augmented to reflect local conditions not directly simulated by the thermal-hydraulic models in MELCOR. These heat transfer coefficients were based on CONTAIN calculations of the M-8-1 test [3.15.3][3.15.4]. The modified heat transfer coefficient, for structures exposed to the environment, was augmented to 6.02 W/m^2–K with a 284 K outside temperature. The locations of the augmented heat transfer coefficients are summarized in Table 3.15-2.

Table 3.15-2. Locations of Augmented Heat Transfers

Location	Purpose	Value
Outer Wall	To simulate external environment conditions.	Similar to the CONTAIN deck, a specified value of heat transfer coefficient of 6.02 W/m^2–K was used.
Floor of Primary Shield	Room underneath the primary shield was not modeled.	T = 313 K

3.15.4.4 Film Flow Networks

The M-7-1 and M-8-2 tests both had sprays that were active in the test while there were no active sprays in M-8-1. Some of the spray water is diverted onto seven separate film flow networks to allow MELCOR's film flow model to transfer water to associated heat structures. Film flow systems are created to allow flow down each of the four steam generator compartments (CV20, CV21, CV23, and CV24) onto the refueling floor, into the refueling pool, and into the lower peripheral regions of the containment. In addition, there is a flow network for water draining down the containment walls from the dome.

With the exception of a fraction of the overall spray mass, which is sourced directly to heat structure surfaces, it was assumed that the containment sprays first interacted with the dome atmosphere and then impacted the dome wall, the refueling floor, the refueling pool, and the steam generator compartment walls above the refueling floor. The spray droplets are assumed to interact with the structures and drain down the seven film networks. In addition, some of the droplets fell downward through the gas space to lower control volumes as previously described. Since the heat structure film temperature and the spray temperature were close, it was expected that this model would better represent the uniform cooling of both structures and gases observed in the test. Film-tracking networks defined in the model are depicted in Figure 3.15-5 to Figure 3.15-11 below.

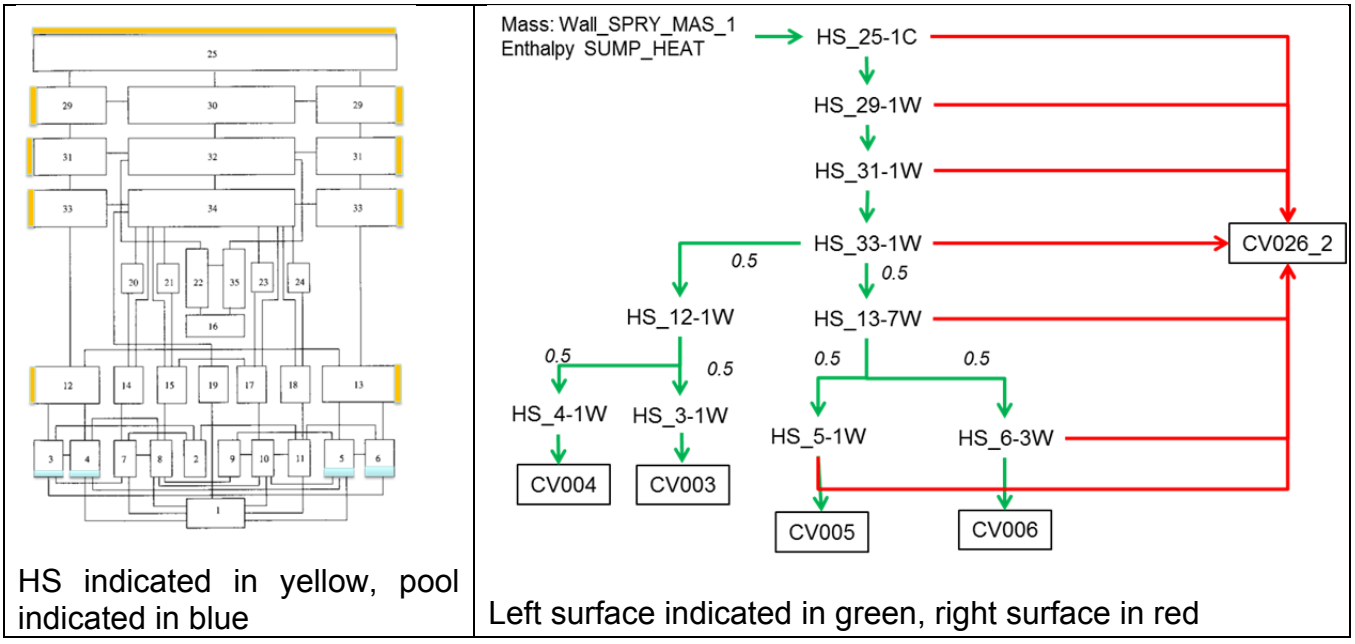

Figure 3.15-5. Film Network for HS_25-1C

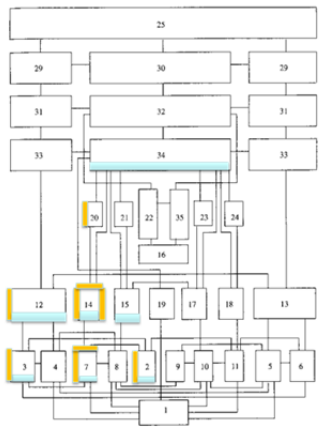

HS indicated in yellow, pool indicated in blue

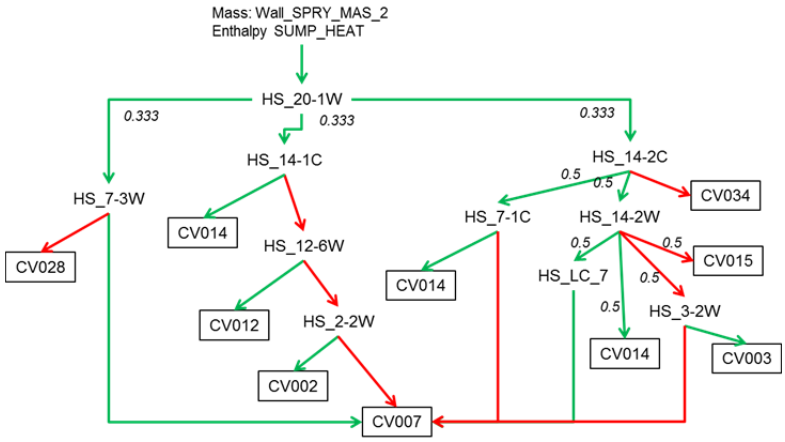

Left surface indicated in green, right surface in red

Figure 3.15-6. Film Network for HS_20-1W

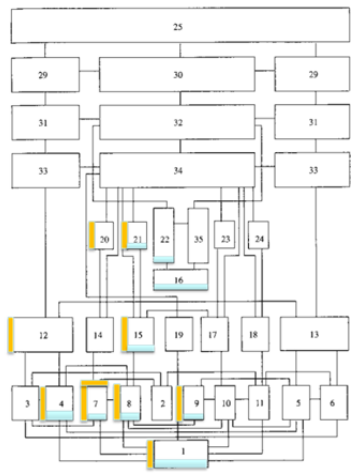

HS indicated in yellow, pool indicated in blue

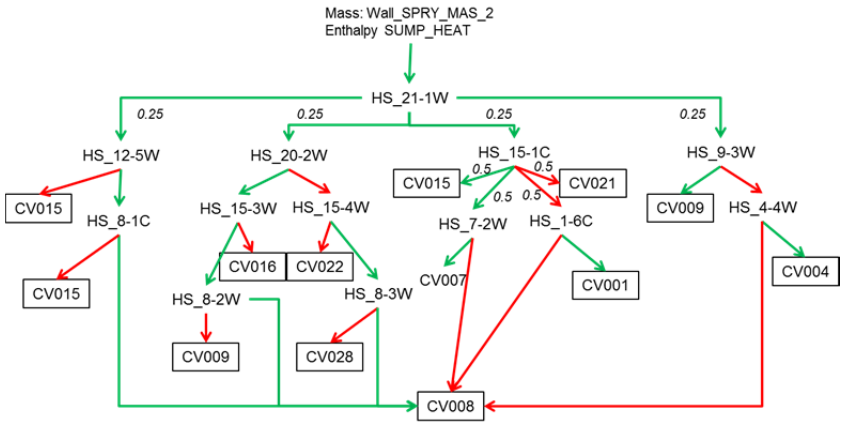

Left surface indicated in green, right surface in red

Figure 3.15-7. Film Network for HS_21-1W

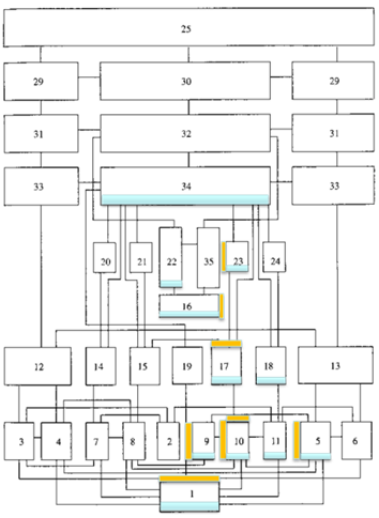

HS indicated in yellow, pool indicated in blue

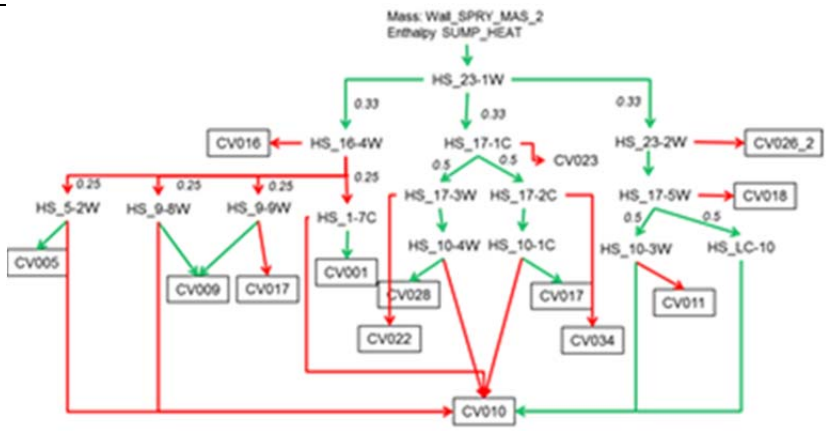

Left surface indicated in green, right surface in red

Figure 3.15-8. Film Network for HS_23-1W

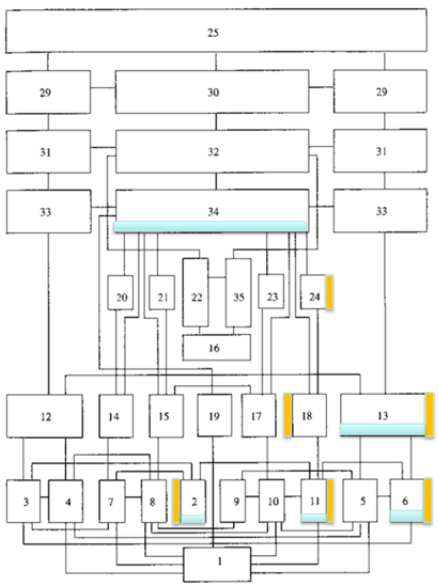

HS indicated in yellow, pool indicated in blue

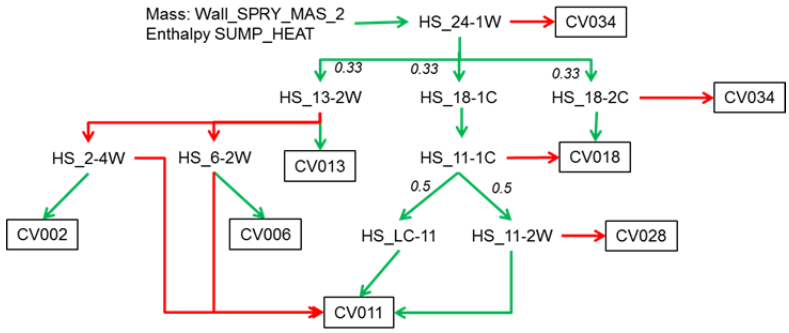

Left surface indicated in green, right surface in red

Figure 3.15-9. Film Network for HS_24-1W

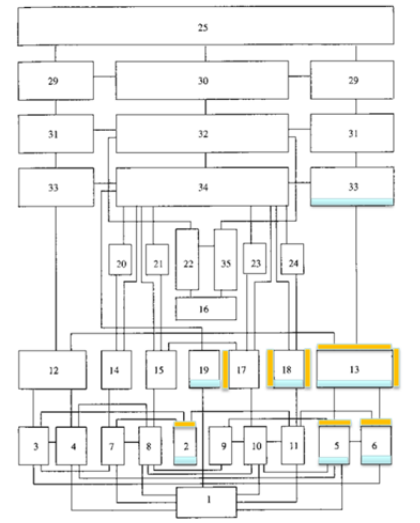

HS indicated in yellow, pool indicated in blue

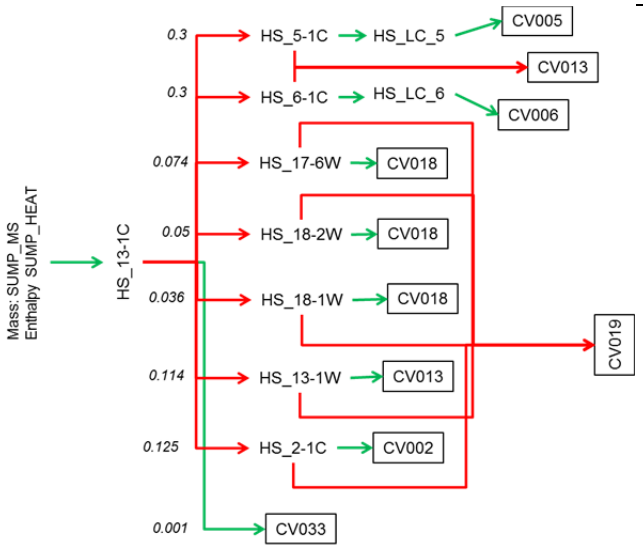

Left surface indicated in green, right surface in red

Figure 3.15-10. Film Network for HS_13-1C

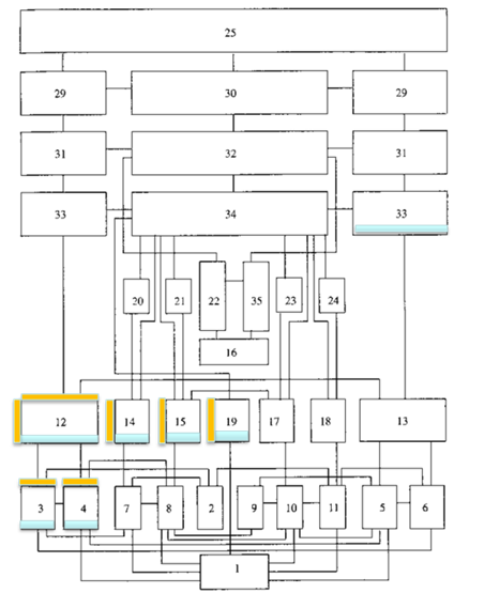

HS indicated in yellow, pool indicated in blue

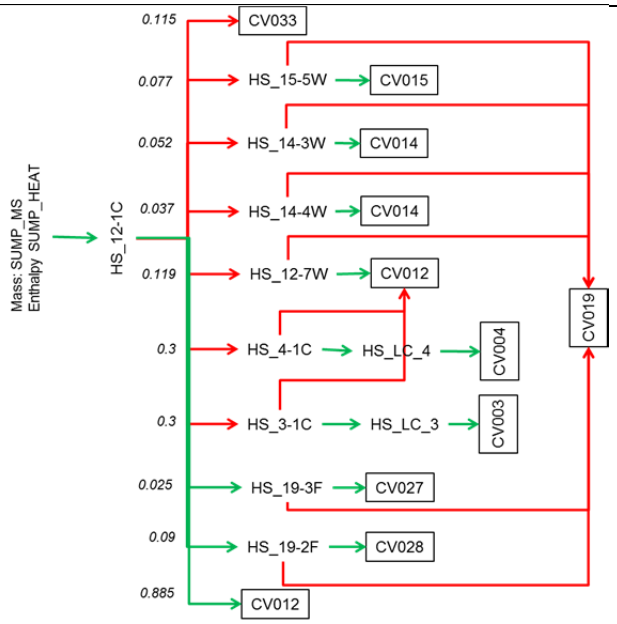

Left surface indicated in green, right surface in red

Figure 3.15-11. Film Network for HS_12-1C

3.15.5 Results of Analysis

The temperature and helium distributions are displayed for M-8-1 and M-8-2 in Figure 3.15-12 through Figure 3.15-15 at select moments in time. Note that the initial temperatures for M-8-1 were higher than for M-8-2 (and M-7-1). These figures show the temperature stratification that occurs for M-8-1, where sprays were not activated and the enhanced mixing that was observed for M-8-2, where sprays cooled the upper volumes of the containment. Consequently, the stratification of helium in the upper dome is much more significant for M-8-1 than M-8-2, as shown in Figure 3.15-15. It also shows that mixing is greater for those central compartments where the spray is active and is less effective in outer, lower compartments such as CV-12.

Figure 3.15-16 shows containment pressure for all three tests along with comparisons with previous code versions (M186 and M185). Temperature stratification is depicted in Figure 3.15-17 where temperature trends at various elevations are plotted for all three tests. Figure 3.15-18 through Figure 3.15-21 provide trend plots showing helium concentrations as a function of time for various distributions of control volumes. Figure 3.15-18 through Figure 3.15-20 show vertical distributions of the He concentration through the center compartments, the steam generator D loop, and the outer compartments, respectively; whereas Figure 3.15-21 shows horizontal distribution on the first floor. General trends show adequate comparison to test data.

MELCOR 2.1 results are identified as MELCOR_2.1 in the plot legends, while MELCOR 1.8.5 and MELCOR 1.8.6 results are identified as MELCOR_QZ and MELCOR_YO respectively.

3.15.6 Discussion

The highlights from the MELCOR simulations are summarized below.

3.15.6.1 Pressure response

For all three tests, the containment pressure response was reasonably well predicted by MELCOR. MELCOR slightly over-predicts the dome pressure in all cases, though the predicted pressure was within 10% of the data measurements. For M-7-1 and M-8-2, the pressure response is highly dependent on the condensation of steam onto heat structures. The film-tracking model provides for draining of condensation from surfaces and continued condensation on structural surfaces, thereby reducing containment pressure.

3.15.6.2 Gas Temperature Response

Without active sprays (M-8-1), MELCOR tends to over-predict stratification leading to higher temperatures in the dome; although, the MELCOR-predicted temperature change in the dome, the pressurizer compartments, and the majority of the lower compartments was within 10% of the data.

For the case of sprays (M-7-1 and M-8-2), the MELCOR model over-predicts the cooling effect of the sprays in the dome, leading to lower temperatures there.

3.15.6.3 Helium Concentrations

- For all three tests, the helium concentration stratification tendency in the dome was well predicted by MELCOR. However, for control volumes near the source (CV22 and CV35 for the M-8 tests and CV08 for M-7), the error in concentration is most significant. In particular, the M-8 models have some difficulty in modeling the flow into the neighboring dead volume (CV06), as might be expected with a control volume code. Notice though for M-7-1, the dead volume is reasonably predicted.

- Without the sprays (M-8-1), the helium concentrations in the lower region were slightly over-predicted by MELCOR. Both the MELCOR calculation and the data show extreme stratification of helium to the dome. For the cases with sprays enabled, the presence of the film network reduced the overall mixing to the lower locations of the containment. When the helium source rate decreased after 15 minutes, the calculated amount of mixing to the lower cells decreased. In contrast, the data shows steady mixing throughout the calculation. An under-prediction in the mixing during the containment spray tests may be attributed to the lack of any momentum transfer between the spray droplets and the vapor in the containment spray model [3.15.2].

- The M-7-1 test provides a comparison of first floor compartments to assess the horizontal distribution of the helium. The MELCOR model (including modeling assumptions) tends to over-predict the lateral movement of helium from the source compartment into adjacent compartments, though the agreement in hydrogen concentration in the adjacent compartments is remarkably good.

*Co*de Versions

As expected, there are no discernible differences between MELCOR 2.1 and MELCOR 1.8.5 or MELCOR 1.8.6 calculated results since this analysis was not greatly affected by improvements added to Version 2.1.

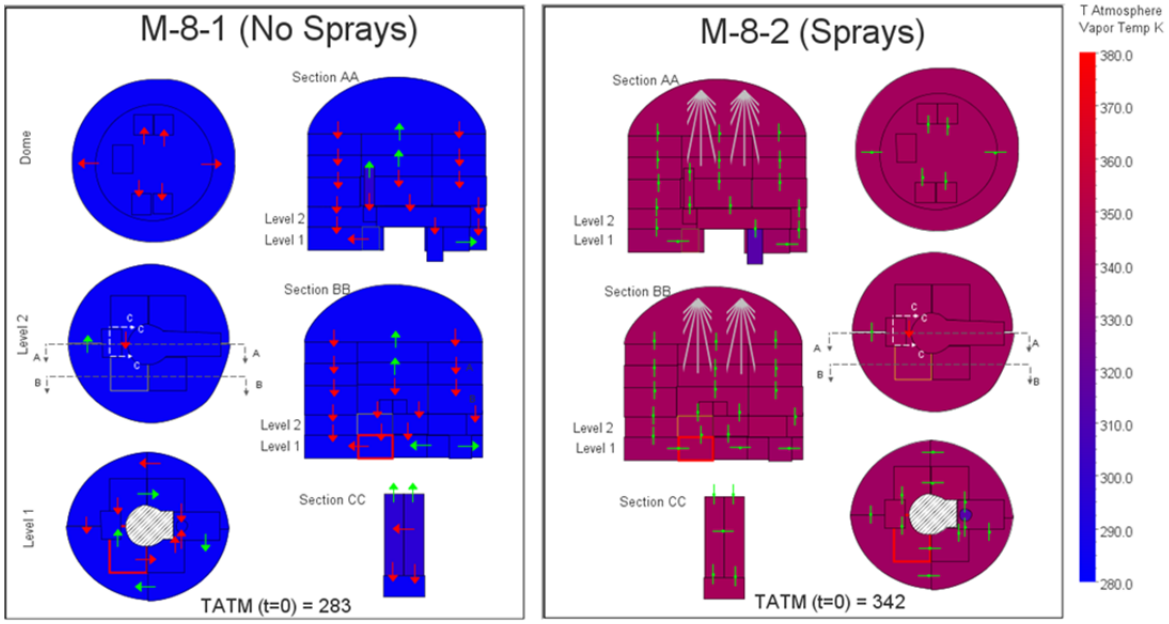

Figure 3.15-12. Initial Temperatures [K] M-8-1 & M-8-2 (Sprays)

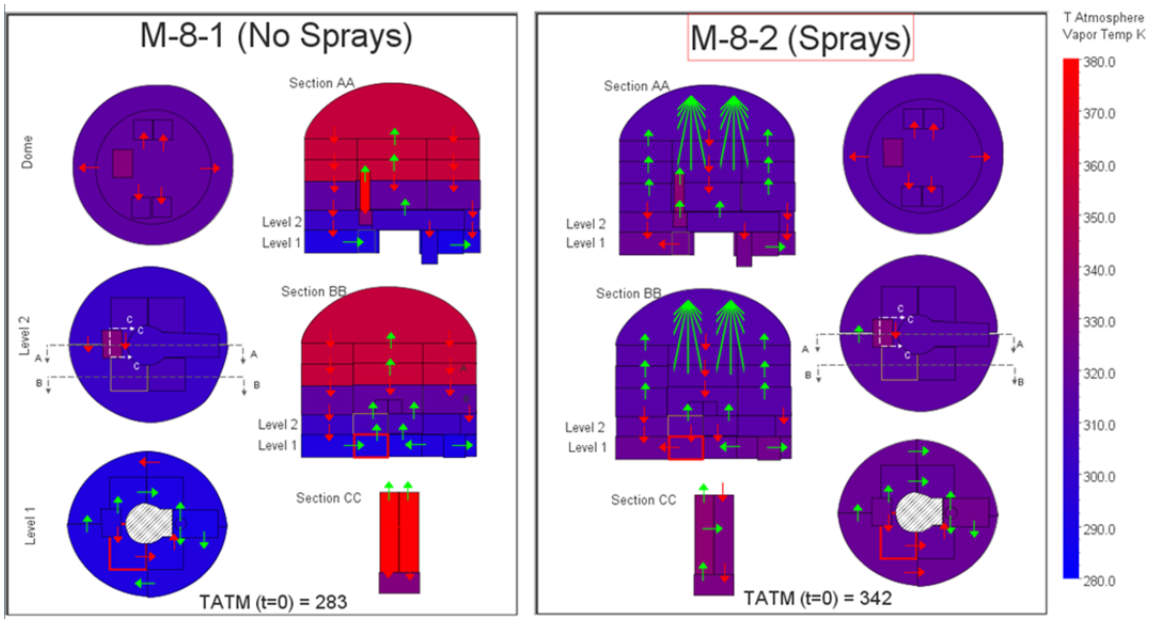

Figure 3.15-13. Final Temperatures [K] M-8-1 & M-8-2

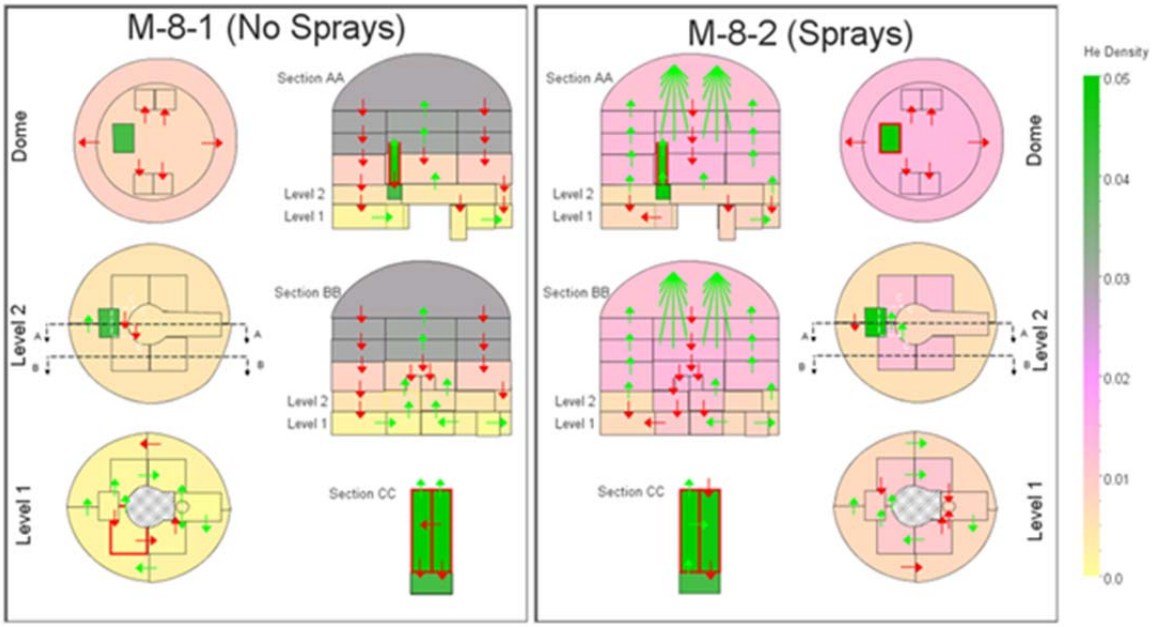

Figure 3.15-14. He Density Distribution (kg/m^3) for M-8-1 & M-8-2 (900 sec)

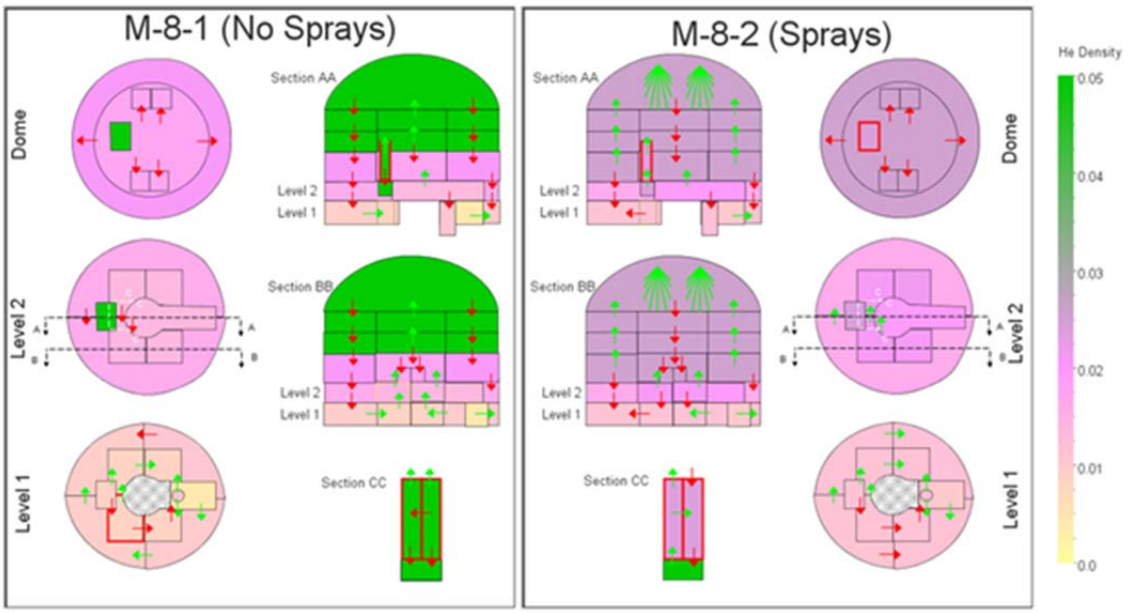

Figure 3.15-15. He Density Distribution (kg/m^3) for M-8-1 & M-8-2 (1800 sec)

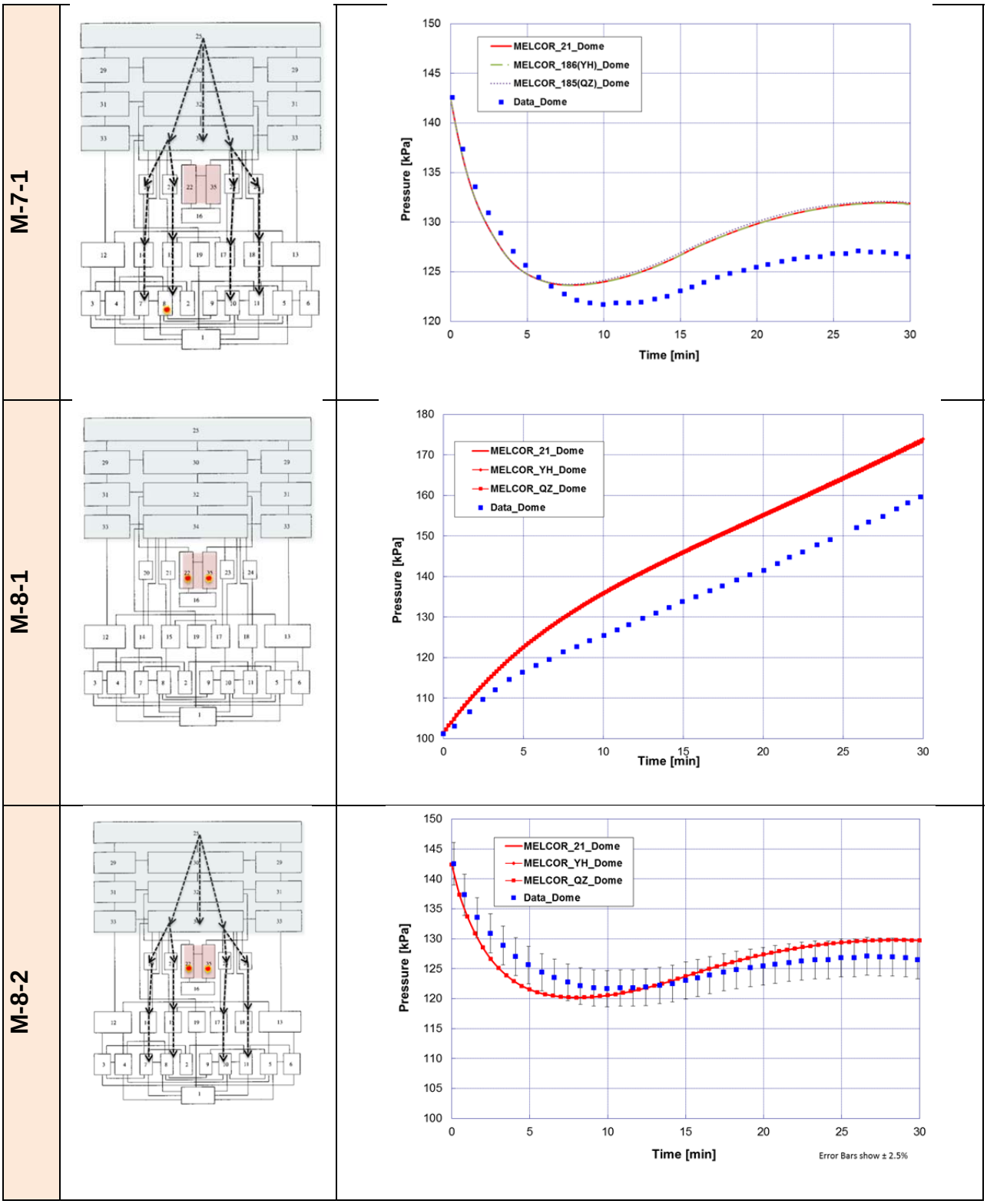

Figure 3.15-16. Containment Pressure Response
(color: control volume, line: MELCOR calculation, symbol: data)

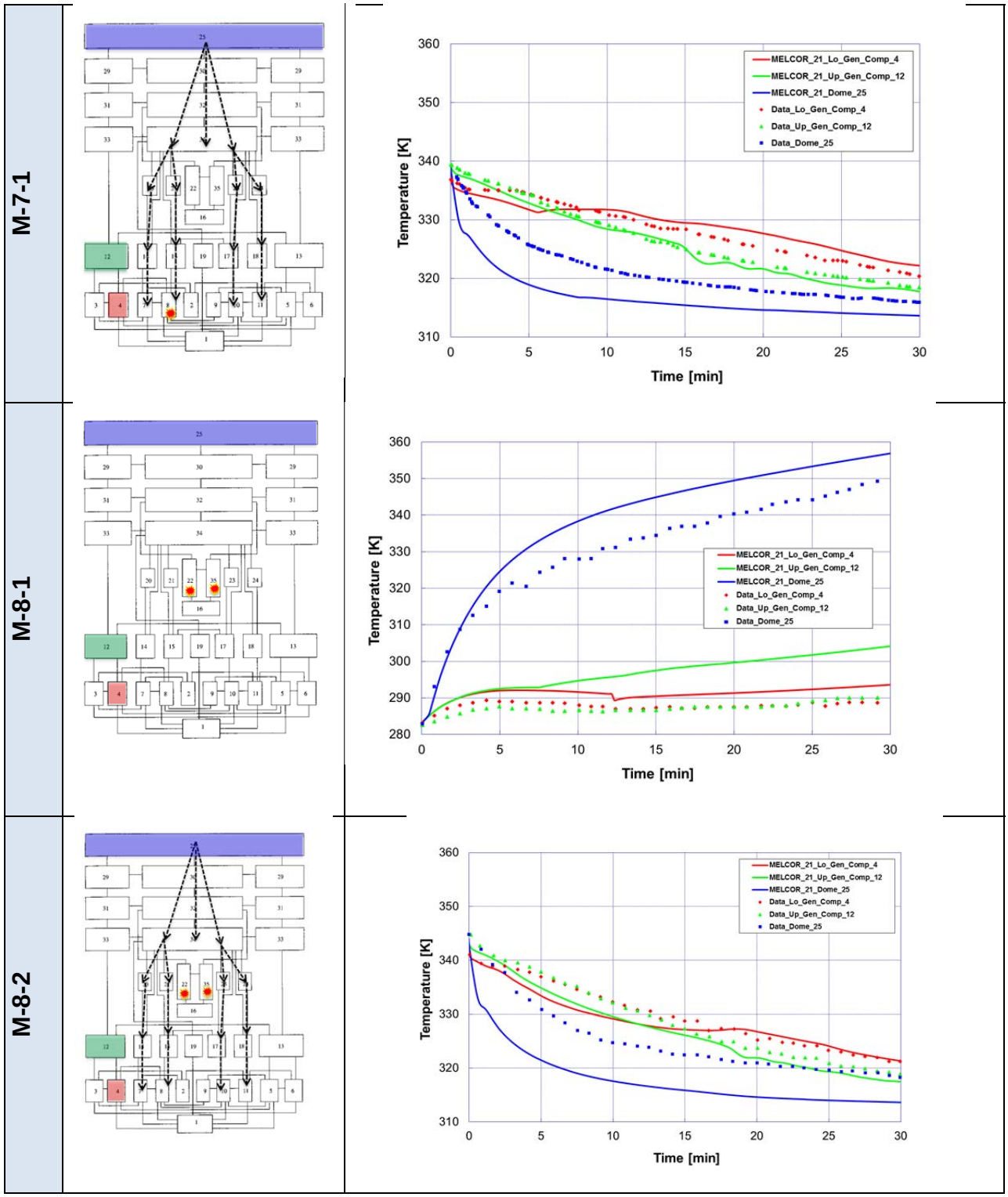

Figure 3.15-17. Temperature Stratification Calculated for NUPEC Mixing Tests (color: control volume, line: MELCOR calculation, symbol: data)

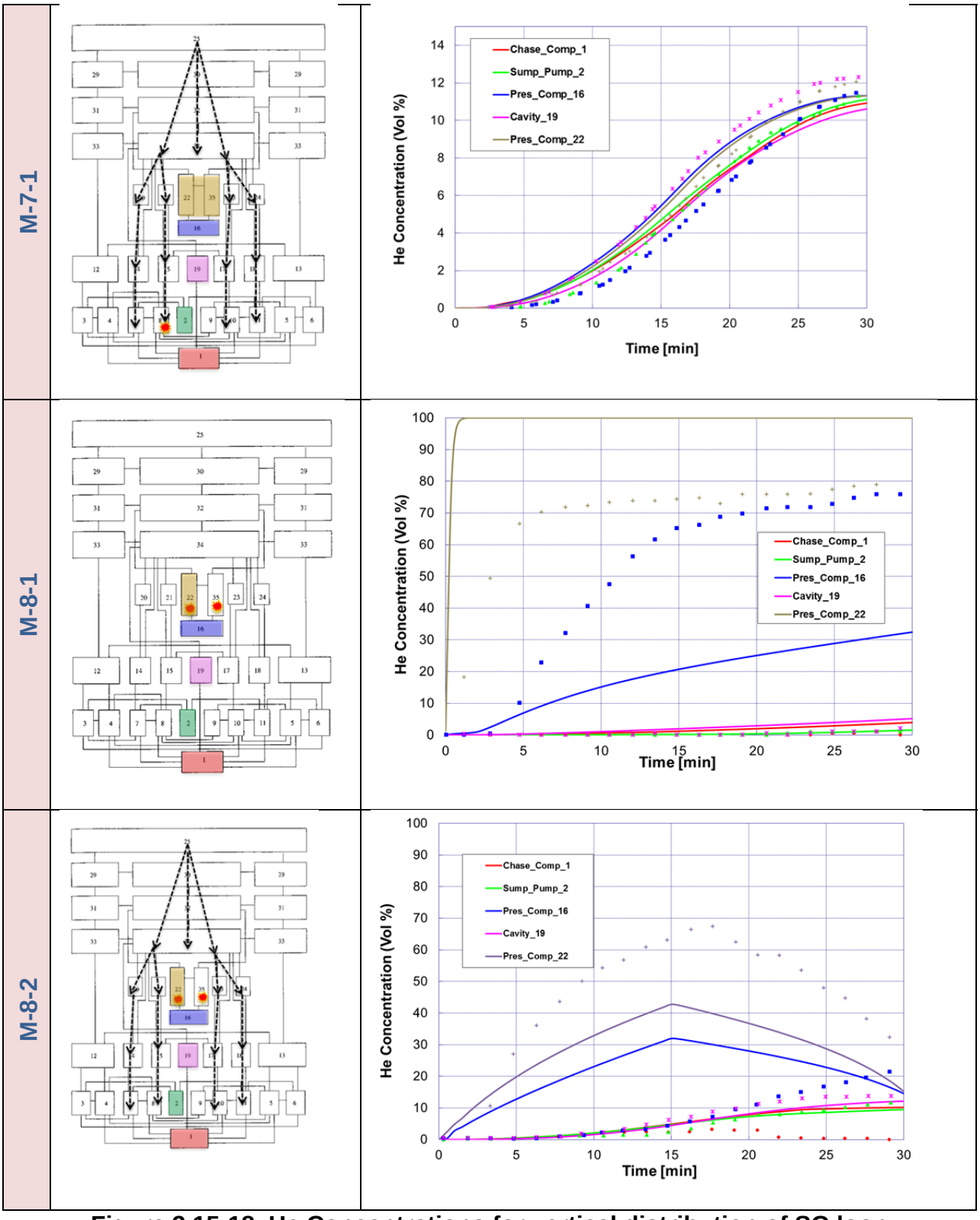

Figure 3.15-18. He Concentrations for vertical distribution of SG loop (color: control volume, line: MELCOR calculation, symbol: data)

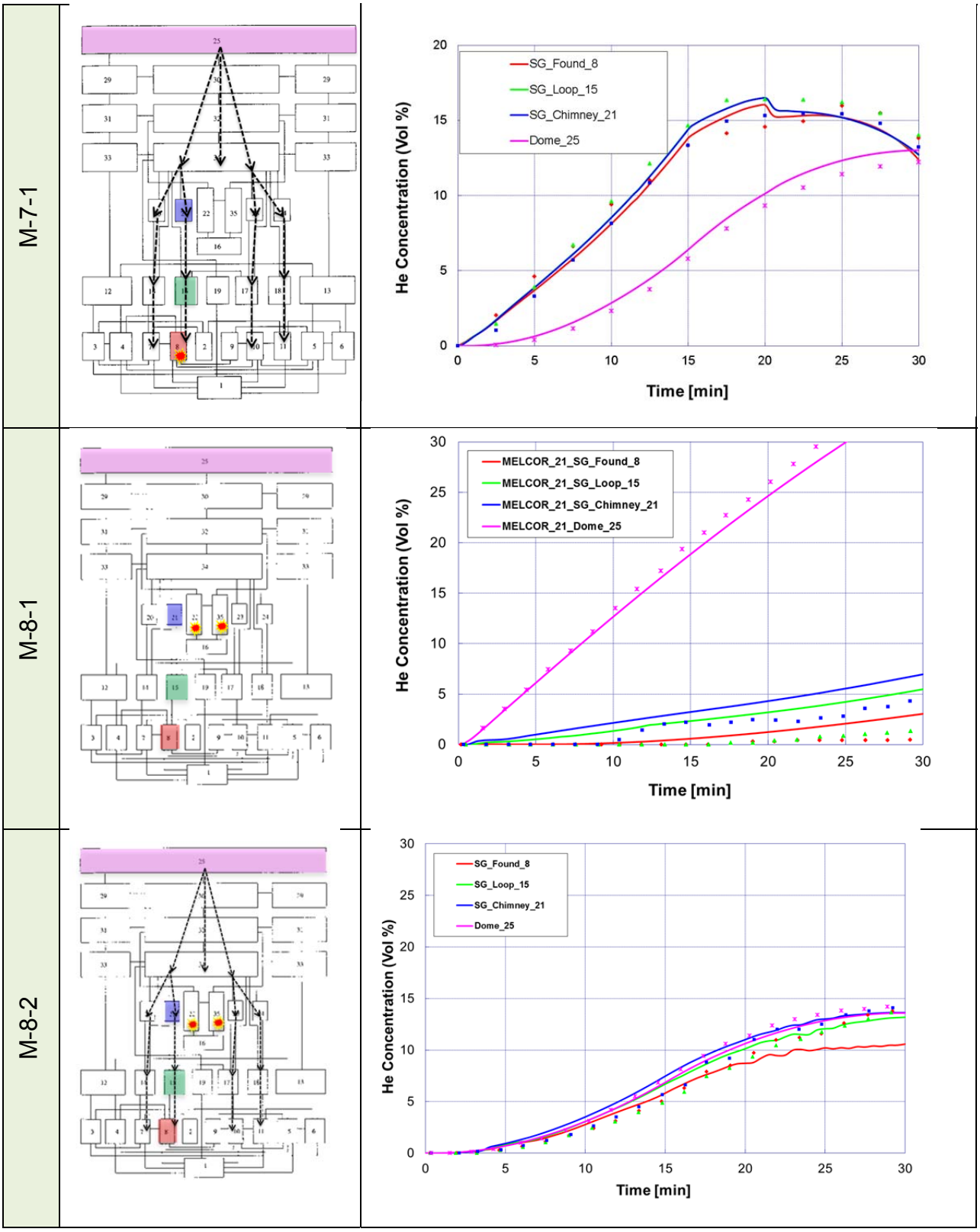

Figure 3.15-19. He Concentrations for vertical distribution of SG loop D (color: control volume, line: MELCOR calculation, symbol: data)

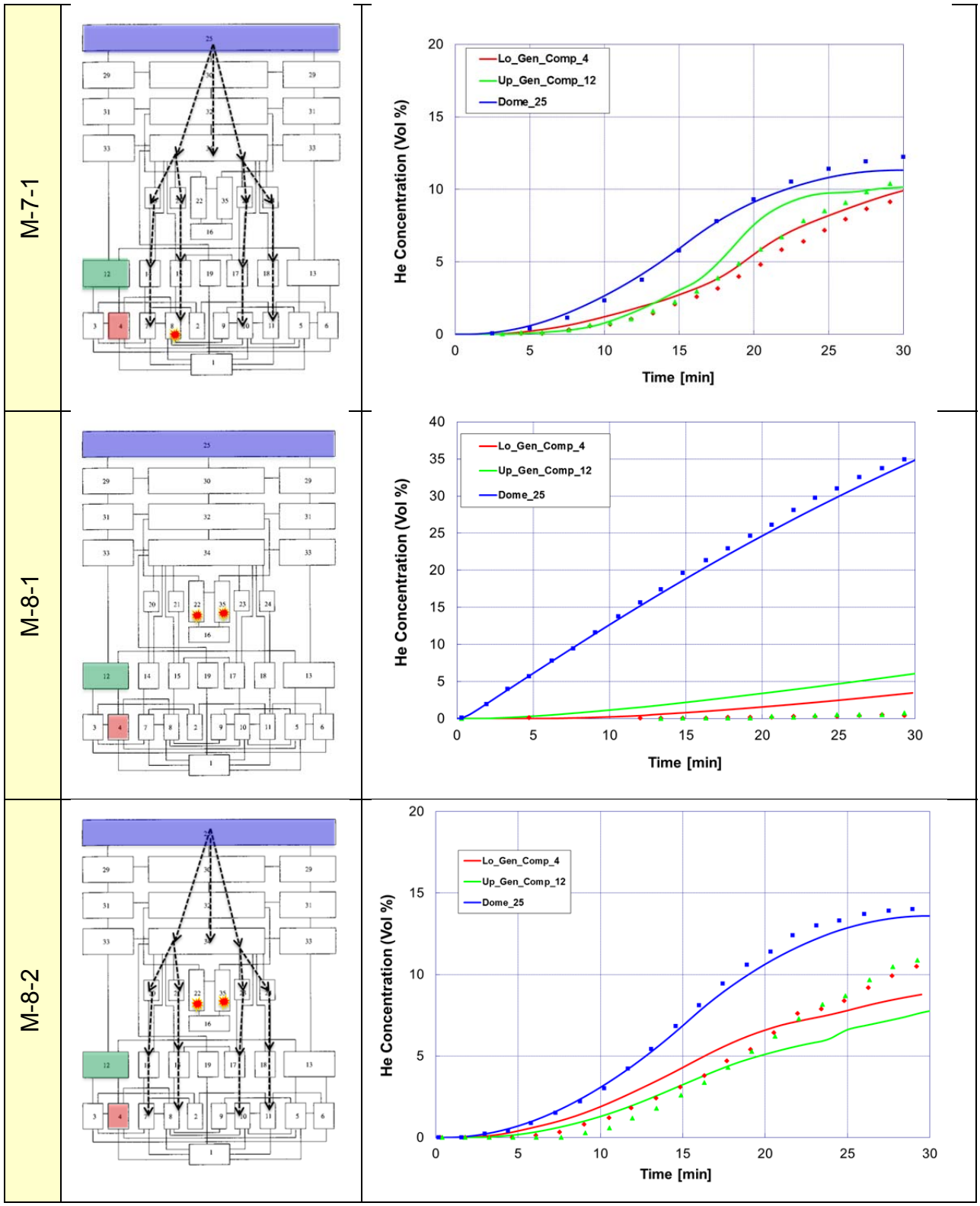

Figure 3.15-20. He Concentrations for vert. distribution of general region (color: control volume, line: MELCOR calculation, symbol: data)

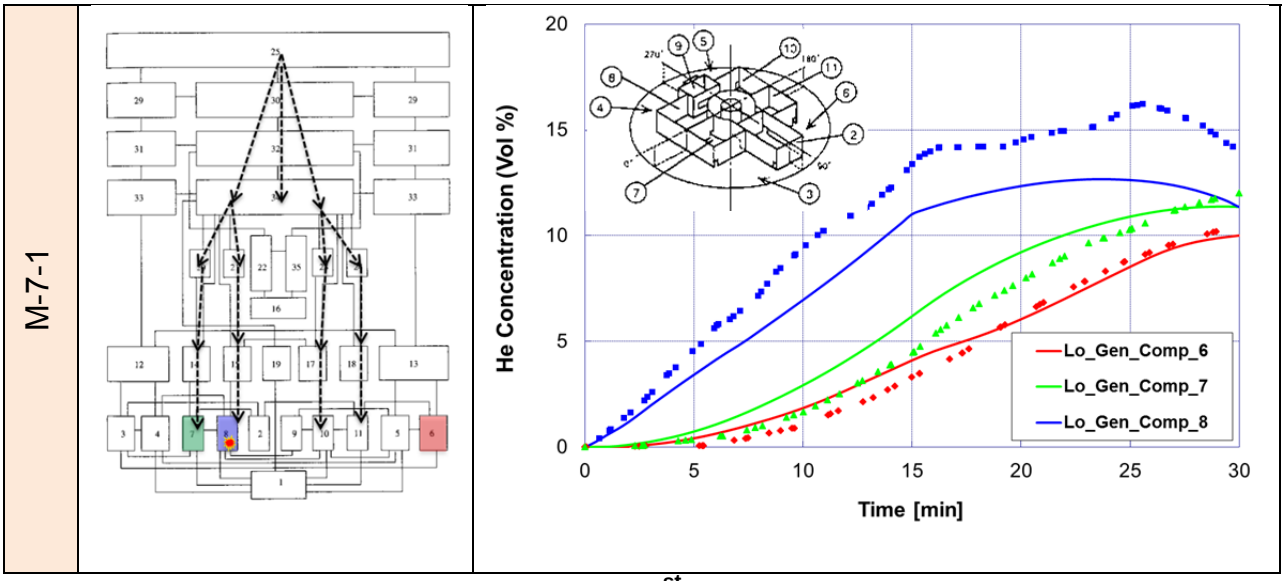

Figure 3.15-21. He Concentrations for 1st floor horizontal distribution (color: control volume, line: MELCOR calculation, symbol: data)

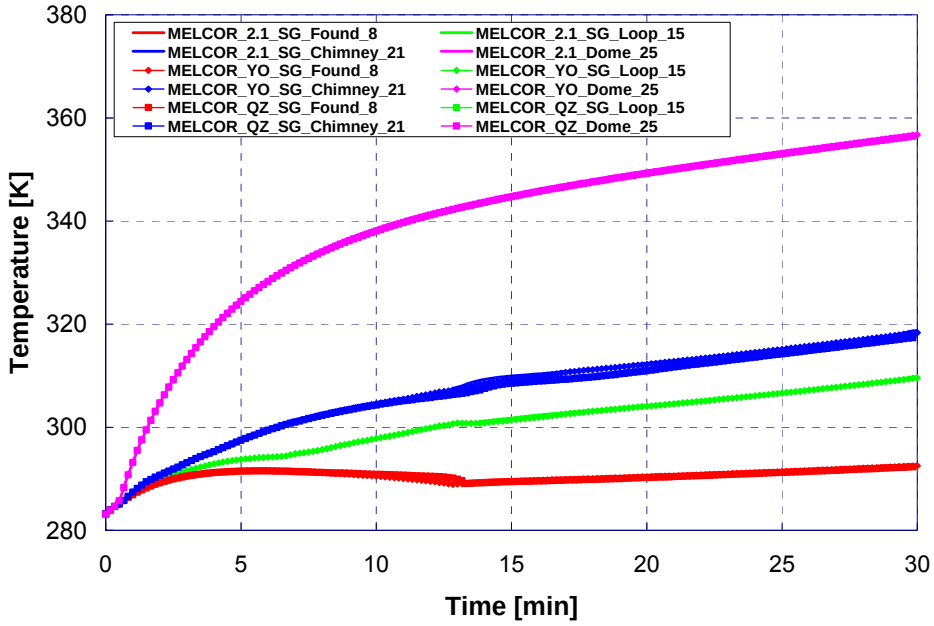

Figure 3.15-22. Selected Containment Gas Temperatures (comparison to MELCOR 1.8.5 QZ and MELCOR1.8.6 YO)

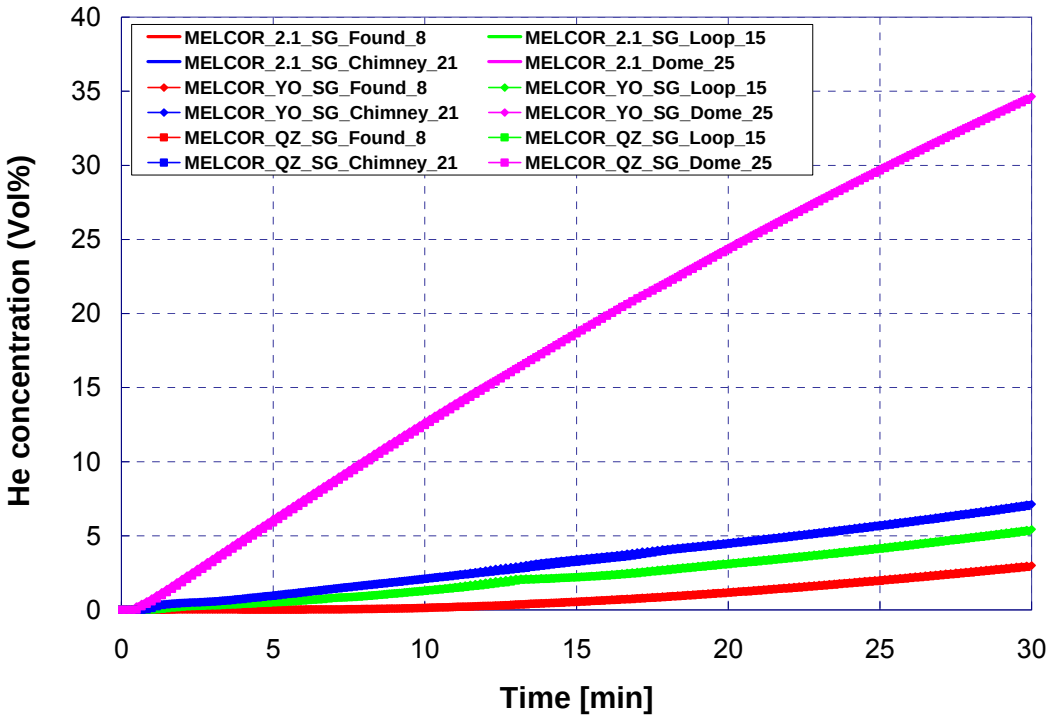

Figure 3.15-23. Containment He Concentrations (comparison to MELCOR 1.8.5 and MELCOR 1.8.6)

3.15.7 Reference

[3.15.1] Nuclear Power Engineering Corporation (NUPEC), System Safety Department, “Specification of ISP 35—NUPEC’s Hydrogen Mixing and Distribution Test—Test M 5 5”, ISP35 027, Revision 1, NUPEC, November 3 4, 1993.

[3.15.2] Dittus, P.W. and Boelter, L.M., Univ. Calif. Pub. Eng., Vol. 1, No. 13, pp 443-461 (reprinted in Int. Comm. Heat Mass Transfer, Vol. 12, pp 3-22, 1985).

[3.15.3] Stamps, D. W., “CONTAIN Assessment of the NUPEC Mixing Experiments,” SAND94 2880, August 1995.

[3.15.4] Stamps, D. W., Murata, K. K., “CONTAIN Assessment of the NUPEC Mixing Experiments—Supplement 1,” SAND94 2880, August 1995.

3.16 Analysis of the PHEBUS FPT-1 Experiment

3.16.1 Background

The FPT-1 experiment was an in-pile, irradiated fuel experiment conducted in the PHEBUS Fission Product Facility by the Nuclear Safety and Protection Institute (IPSN) at Cadarache, France, on July 26, 1996 [3.16.1] - [3.16.2]. This test was the second in a series of six in-pile source term experiments [3.16.3]. The FPT-1 system consisted of an in-pile fuel bundle assembly and upper plenum region, an external circuit including a steam generator U-tube and connecting lines, and a containment section. Figure 3.16-1 describes the PHEBUS facility including various components and systems within that facility.

The objective of the fuel bundle assembly was to assess fuel degradation and fission product release from a degraded fuel assembly. In the circuit, the objective was to determine fission product transport and deposition in steam generator tubes.

The key models exercised in the MELCOR analysis of this test include those for cladding oxidation, thermal modeling, core material relocation, and for the release, transport, and deposition of fission products in a LWR-type reactor coolant system. For purposes of model verification, the following measured parameters were available from the test database:

- Global-cladding oxidation was assessed from thermocouple responses and from measurements of hydrogen generation rates.

- Thermal modeling was assessed from thermocouple responses and temperature profiles.

- Material relocation was assessed from thermocouple responses (both time responses and axial profiles) caused by downward relocation of fuel material. In addition, radiography and transmission tomography provided information about the distribution of materials in the end state.

- Emission tomography of the fuel bundle and steam generator, as well as measurements of activity along the external line to the containment, provided data for fission product release, transport, and deposition comparison.

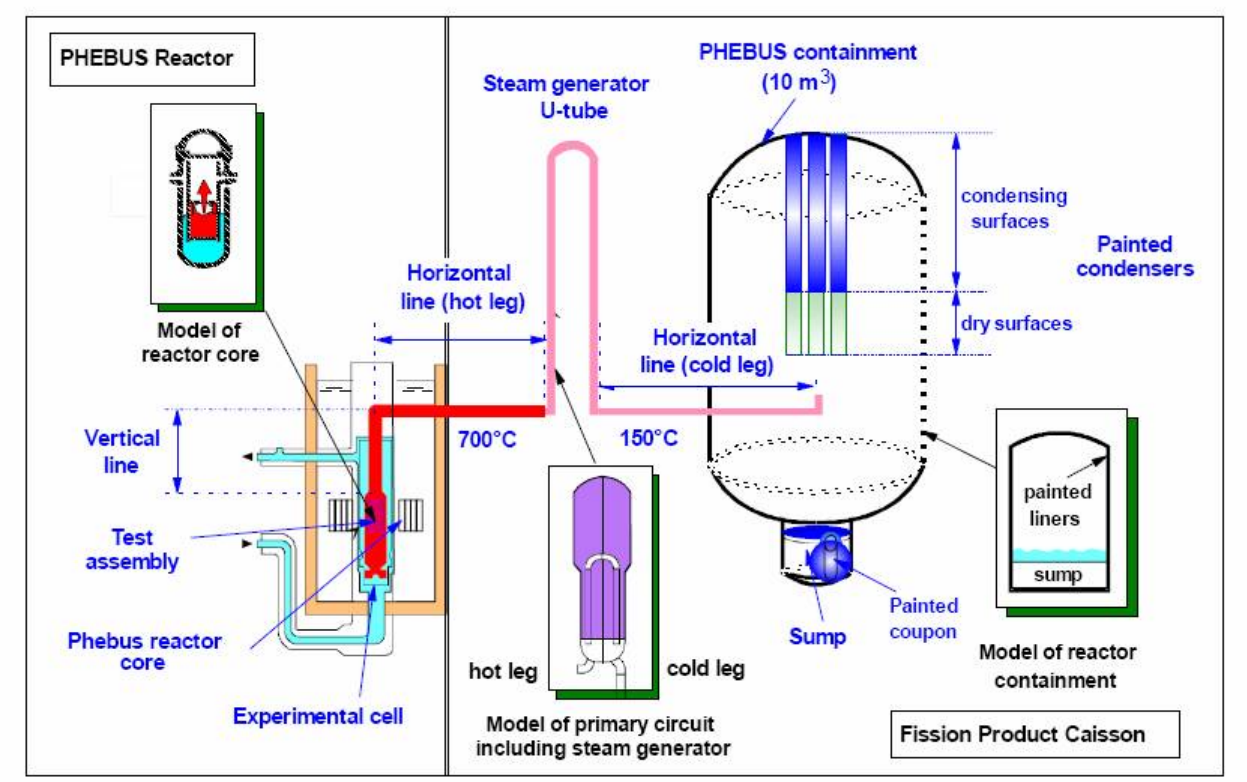

Figure 3.16-1 PHEBUS fission product facility [3.16.6].

3.16.2 Nodalization

Originally, MELCOR 1.8.6 and 1.8.5 input decks were developed to model the geometry and imposed test conditions of the FPT-1 experiment (i.e., bundle, vertical and horizontal line, steam generator, and containment). Due to different input format requirements for MELCOR 2.1, the 1.8.6 input deck has been directly converted to the 2.1 version format using a converter utility.

All three input decks incorporate data from the *Specification of ISP-46*, the *FPT-1 Data Book* and the *FPT-1 Final Repor*t [3.16.4] - [3.16.6], and they all use the same nodalization scheme described below. Differences between different versions of the PHEBUS FPT-1 input deck (i.e., MELCOR 1.8.5, MELCOR 1.8.6, and MELCOR 2.1) are noted in Section 3.16.3.

Overall, there are 30 control volumes, 29 flow paths, and 70 heat structures, describing the test-section and down-stream circuit, as shown in Figure 3.16-2. Note that, due to different input format requirements, control volume numbers and flow path numbers shown in Figure 3.16-2 do not represent the actual names of the control volumes and flow paths in MELCOR 2.1 input. Instead, they are recognized as sequence numbers for consistency.

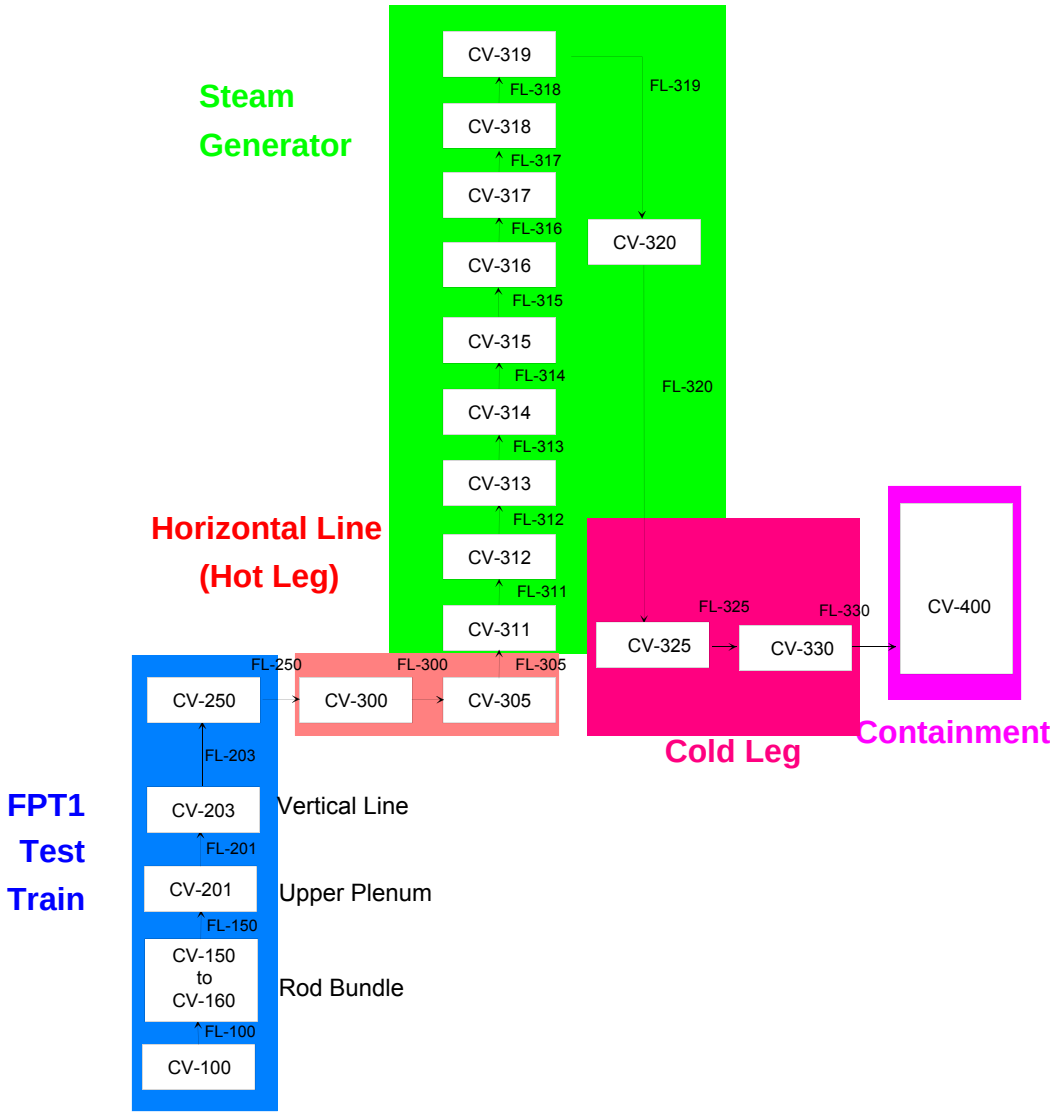

Figure 3.16-2. MELCOR representation of FPT-1 flow paths and control volumes

The fuel bundle region is axially subdivided into eleven control volumes, CV150-CV160, each control volume spanning both the inner and outer rings, i.e., single channel flow. The vertical line above the bundle is subdivided into three regions corresponding to the upper plenum, the lower vertical line, and the upper vertical line (see Figure 3.16-1). Two control volumes describe the horizontal line and riser that leads from the vertical line to the hot leg of the steam generator. The steam generator has 9 control volumes in the hot leg and one control volume in the cold leg. Finally, there are two control volumes connecting the steam generator to the containment, which is modeled with one control volume.

There are 33 heat structures that serve as the radial boundary for the outer ring of each core elevation (including lower plenum), 11 heat structures for the vertical line above the

bundle, 3 for the horizontal line and riser leading to the steam generator, 9 in the hot leg of the steam generator, 2 in the cold leg, 2 in the line to the containment, and 10 in the containment. There are a total of 21 radial nodes in heat structures that surround the bundle: 4 in the inner thoria liner, 1 in the steam gap between the liner and the inner shroud, 7 in the zirconia shroud, 1 in the steam gap outside the zirconia shroud, 2 in the ceramic spray coating on the pressure tube, and 6 nodes in the inconel pressure tube. In the upper plenum, the heat structures consist of an inner inconel tube surrounded by ZrO_2 beads inside an AISI-304-L steel tube, or zirconia shroud material, depending on the elevation. The steam generator tubing and piping is modeled as inconel-600 cylindrical heat structures with 4 radial nodes. Cooling and heater temperatures were taken from various system setpoints. In the vertical section above the upper plenum and the horizontal line feeding into the hot leg of the steam generator this temperature was 700 °C. The cold leg leaving the steam generator was heated to 150 °C, and the containment was held at 110 °C (93 °C in the sump). The steam generator temperature was 150 °C.

The FPT-1 MELCOR input model has 2 radial rings and 31 axial elevations defined for the MELCOR "COR" region that describes the FPT-1 test section. The lower axial elevation is an open geometry with no fuel rods representing the core inlet below the fuel bundle. The second axial elevation describes the core support plate composed of Zircaloy that is associated with the support structures component. Zircaloy spacer grids are present and provide axial support for relocating materials at axial levels 12 and 24. The control rod guide tubes, stiffeners and grid spacers were modeled as non-supporting structure (NS), and the core support plate was modeled as an edge-supported type structure.

The fuel bundle was modeled as a central ring surrounded by one outer radial ring. The center ring has a radius of 21.33 mm and comprises the central control rod, the control rod guide tube and 8 fuel rods (see data report [3.16.4]). The outer ring has a radius of 36.5 mm and comprises the remaining 12 fuel rods [3.16.4]. The initial flow area in a region without spacer grids is .00747 m^2 for the inner ring and 0.00186 m^2 for the outer ring.

3.16.3 MELCOR Input Specifications

Generally, material properties were obtained from the ISP specification [3.16.4]. However, to capture the effect of a reduced melting temperature of a eutectic mixture of UO_2 and ZrO_2, the default UO_2 and ZrO_2 enthalpy tables were overridden to allow UO_2 and ZrO_2 to melt at 2500 K (Figure 3.16-3). This was done to match the observed failure behavior in this experiment, apparently due to a reduced eutectic temperature of irradiated UO_2 and ZrO_2. Normally, the UO_2/ZrO_2 eutectic temperature for the PWR composition is about 2800 K. Further, the thermal conductivity of the shroud gaps were modeled to allow for closure of the gaps as temperatures exceeding 900 K (Figure 3.16-4).

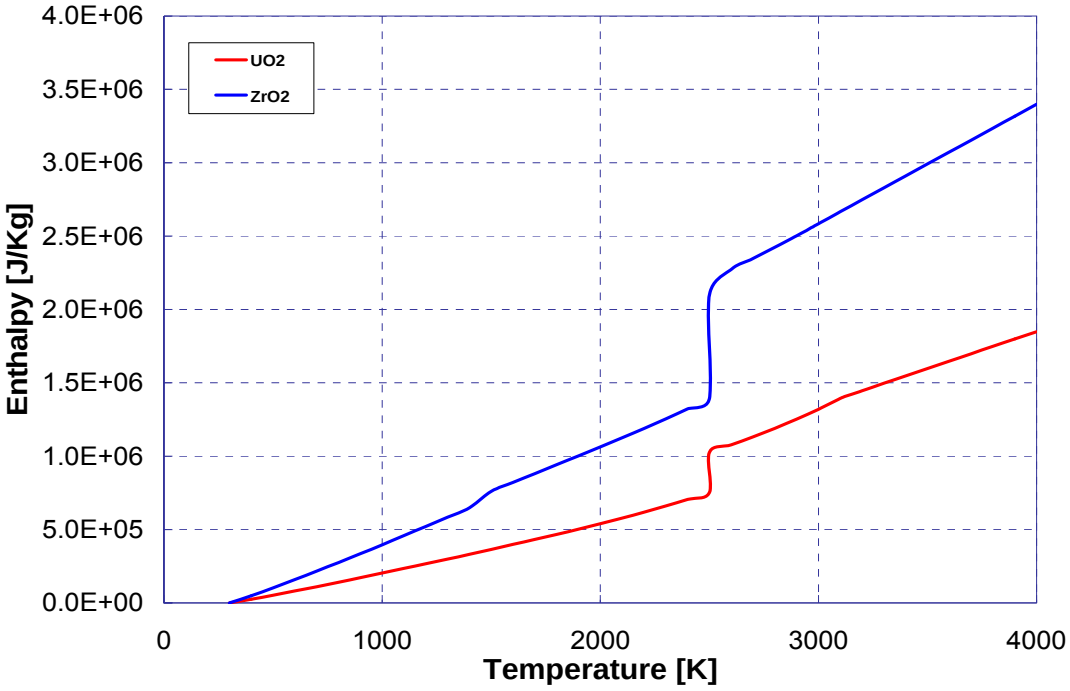

Figure 3.16-3. UO2 and ZrO2 Enthalpy Curves

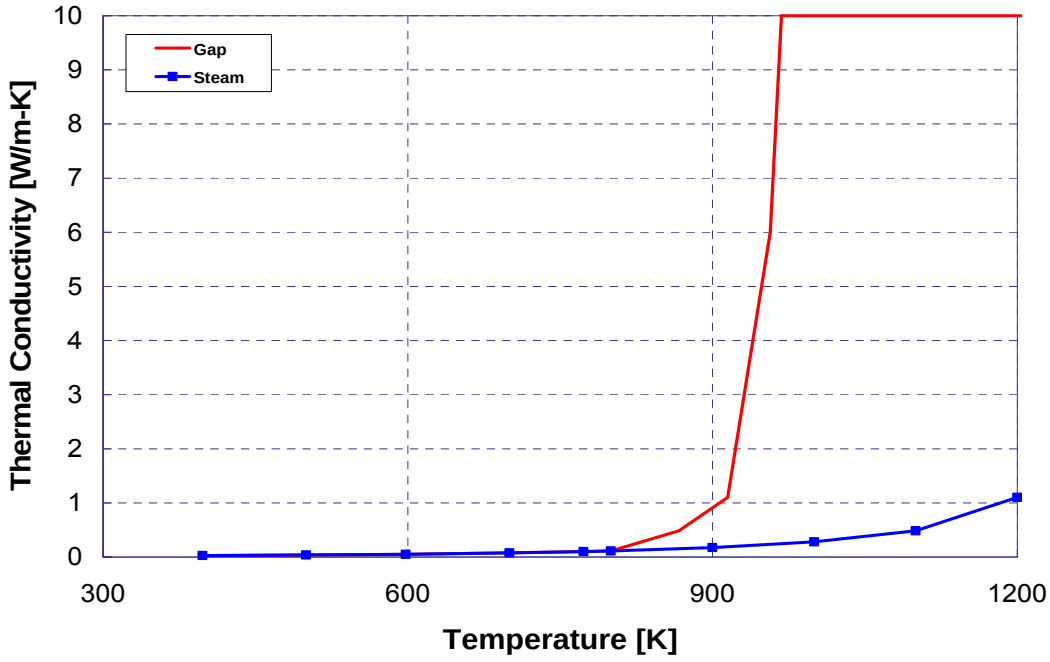

Figure 3.16-4. Gap Closure model

The radial radiation view factor, FCELR, was increased to 0.75, above the default value of 0.25. Because of the sparse two-ring fuel rod geometry, enhanced radiation from inner fuel rods to the shroud is justified.

The peak power used in these calculations (Figure 3.16-5) is 95% of the fission power heating suggested in the ISP specification and the fission product inventory is taken from the preliminary report [3.16.4]. Initial total masses for these groups were obtained from the FPT-1 Data book and are presented in Table 3.16-1 [3.16.1]. Note that MELCOR does not distinguish between certain elements of interest required for the ISP, but rather combines those elements into a single class. Deposition masses for individual elements are obtained by considering the fraction of the initial class inventory for a given element. Finally, in addition to these groups, CsI, produced as cesium and Iodine are released in the calculation, has been added as class 16, and was taken into account in determining deposition. No decay heat was associated with fission product classes.

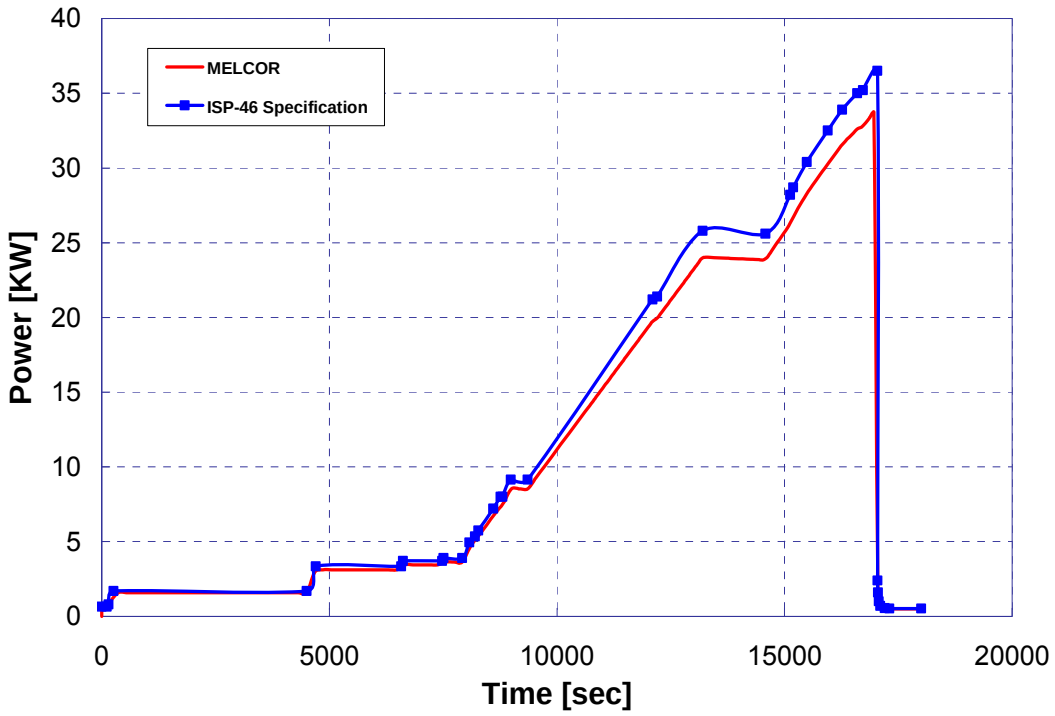

Figure 3.16-5. Fission power history

Table 3.16-1. Initial RN Mass Inventories

Element	Class	FPT1 Mass Inventory (g)	Initial RN class inventory in MELCOR model (g)	FPT1 Inventory Combined into MELCOR Classes (g)	Multiplier
Kr	RN 1	2.55	35.49	32.13	0.07185
Xe		29.58			0.83347
Rb	RN 2	2.53	18.37	18.39	0.13772
Cs		15.86			0.86336
Ba	RN 3	10.06	15.4	15.62	0.65325
Sr		5.56			0.36104
I	RN 4	1.12	1.98	1.12	0.56566
Te	RN 5	2.54	2.63	2.54	0.96578
Ru	RN 6	11.19	17.29	11.19	0.64719
Mo	RN 7	20.17	25	24.97	0.8068
Tc		4.8			0.192
Pu	RN 8	37.65	38.5	63.54	0.97792
Np		1.56			0.04052
Zr		24.33			0.63195
U	RN 10	9163	8967	9163	1.02186
Sb	RN 11	0.05	0.23	0.05	0.2174

Other non-default input that was required to simulate the bundle degradation characteristics included the fuel rod collapse temperature (SC1132) and the heat transfer coefficients between debris components and its associated conglomerate fuel mass (COR_CHT). The rod collapse temperature was selected as 2505 K to correspond to observed temperatures for which fuel rod relocation was important. (Note:

this was done in the original problem setup. It is not obvious why a collapse temperature of 2505 K would have any effect when the melt temperature of UO_2 and ZrO_2 have been set to 2500 K, and this should be checked in future assessments). The candling heat transfer coefficients for UO_2 and ZrO_2 were increased from 1000 W/m²-K to 30,000 and 20000 W/m^2-K respectively to improve heat transfer from conglomerate material to the particulate debris.

In the MELCOR 2.1 input model, the Modified CORSOR-BOOTH model was used to predict radionuclide release. In MELCOR 1.8.6 and 1.8.5, the CORSOR-BOOTH model was used. The model parameters as well as scaling factors were modified to reflect the ORNL Booth model as specified in reference [3.16.5].

The key difference between the MELCOR 1.8.6 and the MELCOR 1.8.5 input model is the addition of a new silver-indium-cadmium (Ag-In-Cd) control poison release model. FPT-1 experimental results show that the creation of aerosols by vaporization of Ag-In-Cd control poison could have a significant effect on overall aerosol behavior [3.16.6]. A new model for this release has been added to MELCOR 1.8.6 and was utilized in the 1.8.6 input model as well as in MELCOR 2.1 input. In conjunction with this model, three classes, “Ag-CR”, “In-CR”, and “Cd-CR”, were defined as class 17, 18, and 19, respectively. No decay power was associated with these classes.

Several other modifications to the MELCOR 1.8.6 input model were also required, due to many changes and modeling enhancements added to MELCOR 1.8.6. As a result, some of the COR records in the MELCOR 1.8.6 input model were modified, deleted, and added as necessary (see COR Package User’s Guide). Since MELCOR 2.1 input is created by directly converting MELCOR 1.8.6 input, no differences should exist between the two versions of input other than input format as required by each version of the code.

3.16.4 Results of Analysis

Although marginally higher, the heat-up of the bundle was generally well predicted by all three versions of MELCOR at all elevations. Selected temperatures calculated at the 200 mm, 400 mm, and 600 mm elevations are shown in Figure 3.16-6 through Figure 3.16-8, which closely follow the measured temperature thermocouple histories for the test (until thermocouple failures near 12,000 seconds). Between MELCOR versions 1.8.5, 1.8.6, and 2.1, there were no significant differences in the calculated temperatures. Fuel failure was not predicted to occur in the outer ring by all three versions of MELCOR calculations, although conditions were very close to failure. In fact, Figure 3.16-7 shows fuel temperatures close to 2500K at the time when power was reduced at 17,000 seconds, but the fuel failure criterion is applied to the clad temperature, which lags slightly behind the fuel temperature.

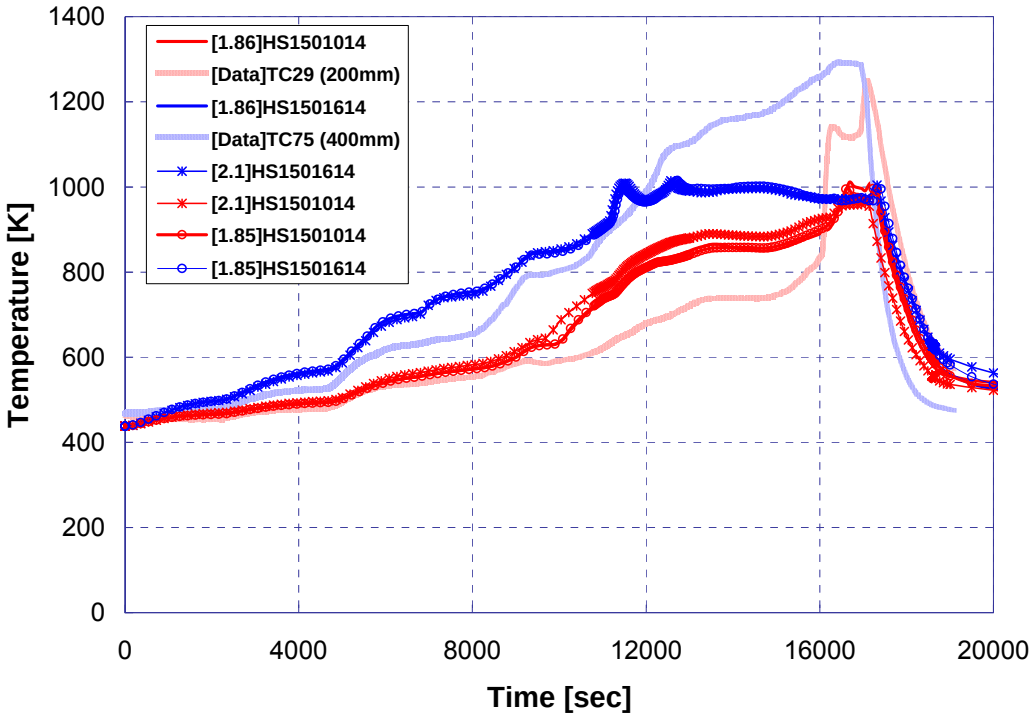

Figure 3.16-6. Outer shroud temperature at level 200 and 400 mm

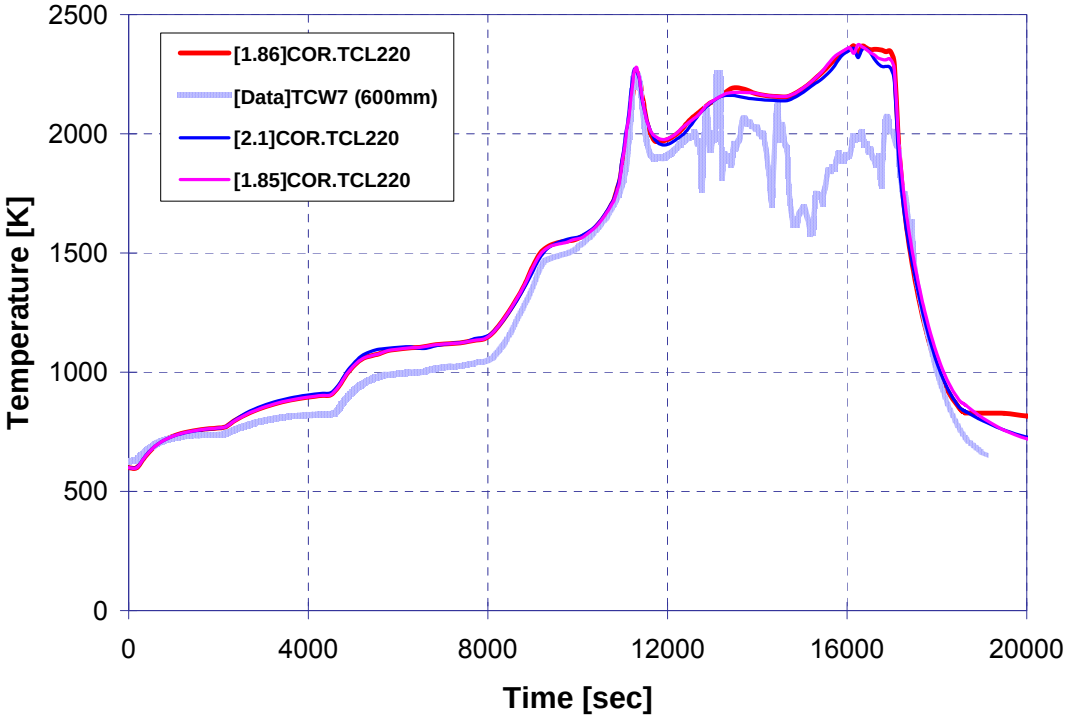

Figure 3.16-7. Fuel temperature in outer ring at level 400 mm

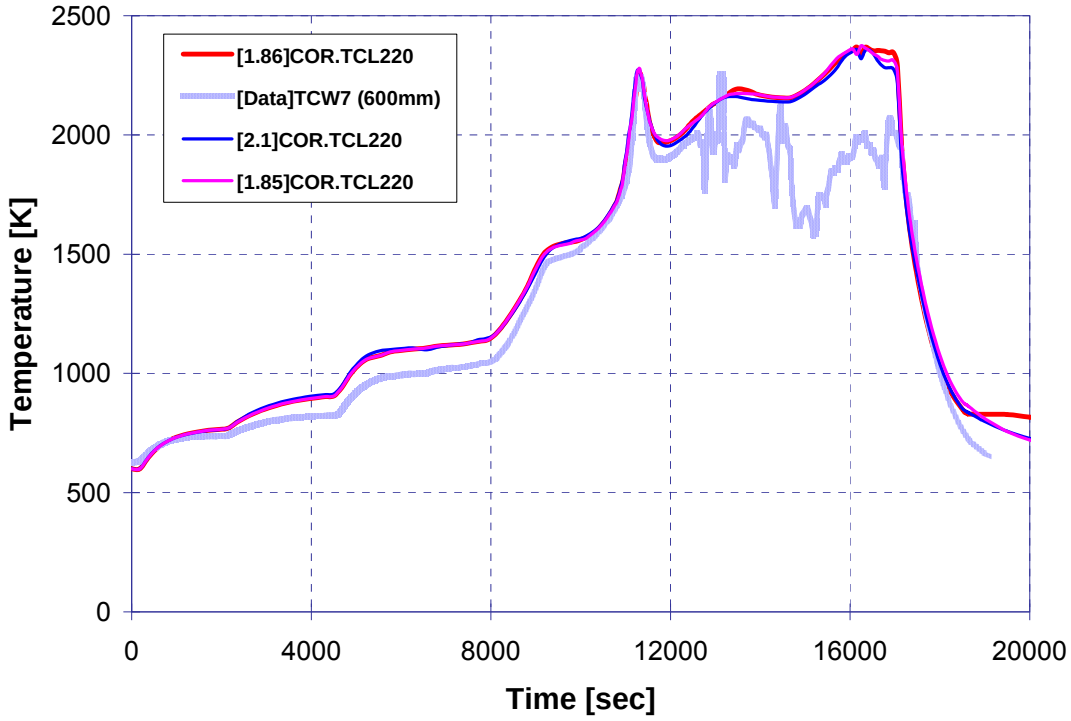

Figure 3.16-8. Clad temperature in outer ring at level 600 m

Figure 3.16-9 and Figure 3.16-10 show the hydrogen mass flow rate and the total accumulated hydrogen as compared to the measured data. The timing and the extent of the peak oxidation event were well predicted by all three versions of MELCOR. As shown in Figure 3.16-10, MELCOR 1.8.5 predicted slightly higher hydrogen production than MELCOR 2.1, MELCOR 1.8.6, and measured data, mostly reflecting higher peak fuel temperatures. Core degradation was reasonably well predicted by assuming a UO2/ZrO2 eutectic temperature of 2500 K and a rod failure temperature of 2505 K.

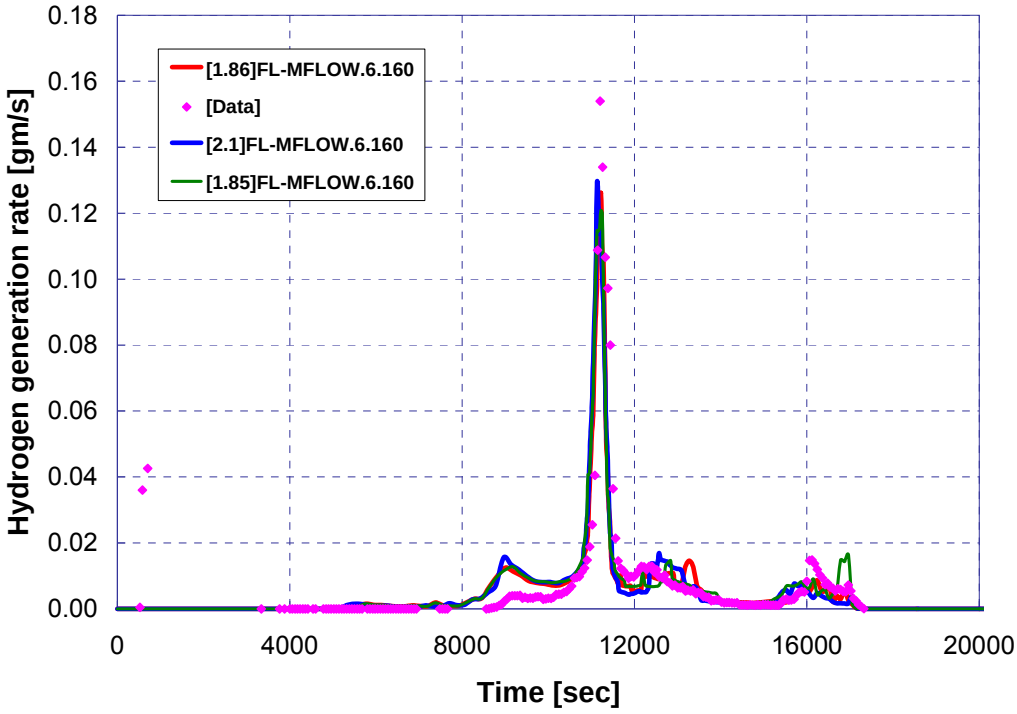

Figure 3.16-9. Hydrogen mass flow rate at core exit

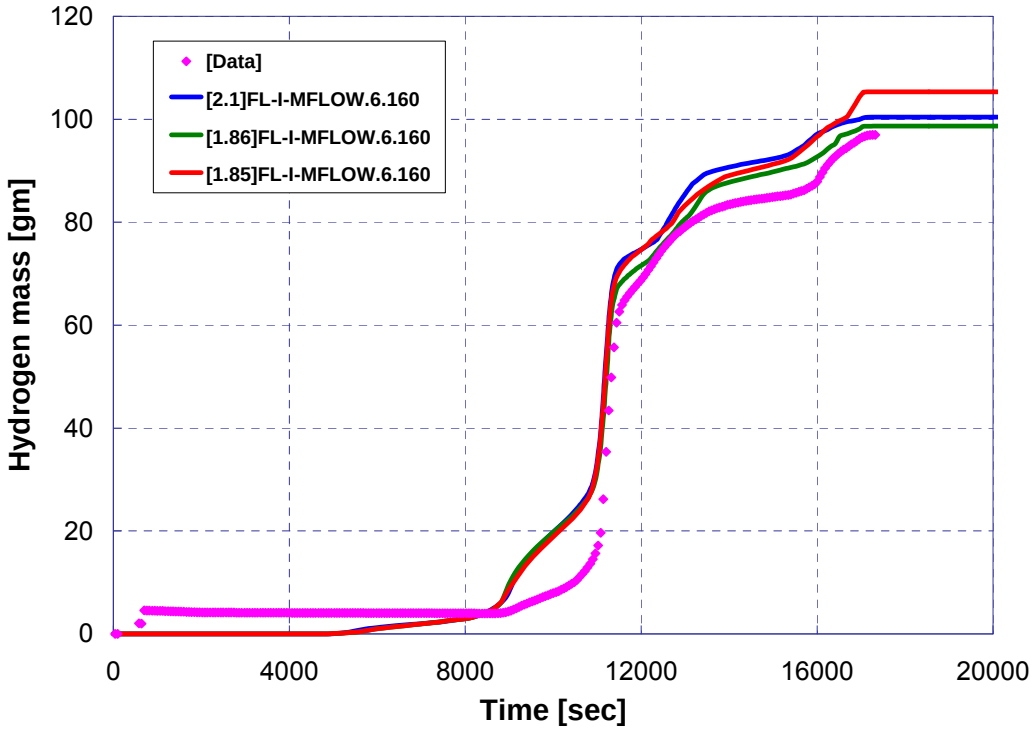

Figure 3.16-10. Accumulated hydrogen mass

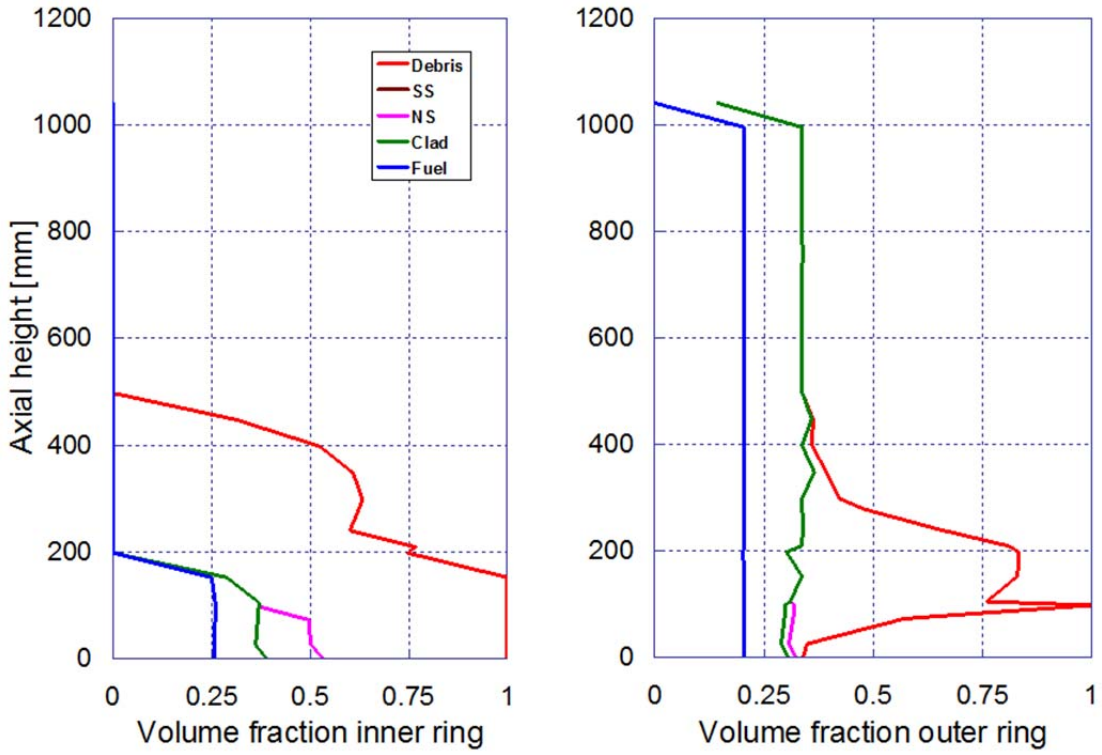

Figure 3.16-11. MELCOR 1.8.5 end state of bundle (18600 sec)

Figure 3.16-11, Figure 3.16-12, and

Figure 3.16-13 show volume fractions (cumulative stacked line plots) for various components in both inner and outer rings at the end state of the test bundle for MELCOR 1.8.5, 1.8.6 and 2.1, respectively. Note that all versions of MELCOR calculations predict that at termination the inner rods have failed and debris has relocated to the bottom of the bundle whereas the outer rods remained intact. This was the same behavior that was observed in the experiment.

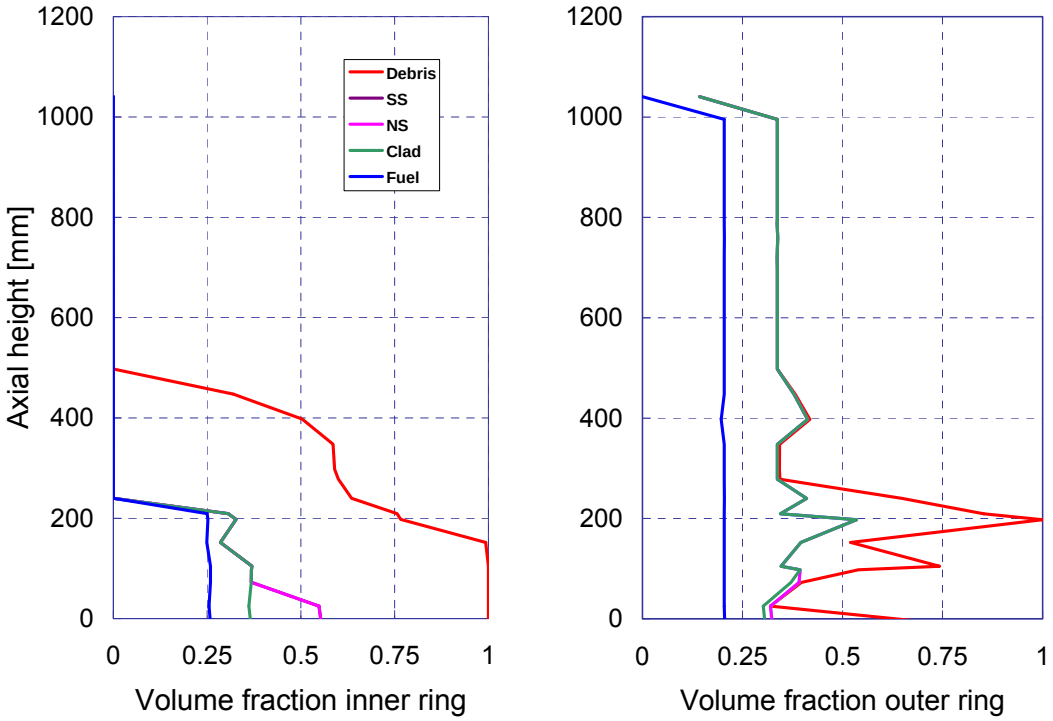

Figure 3.16-12. MELCOR 1.8.6 end state of bundle (18600 sec)

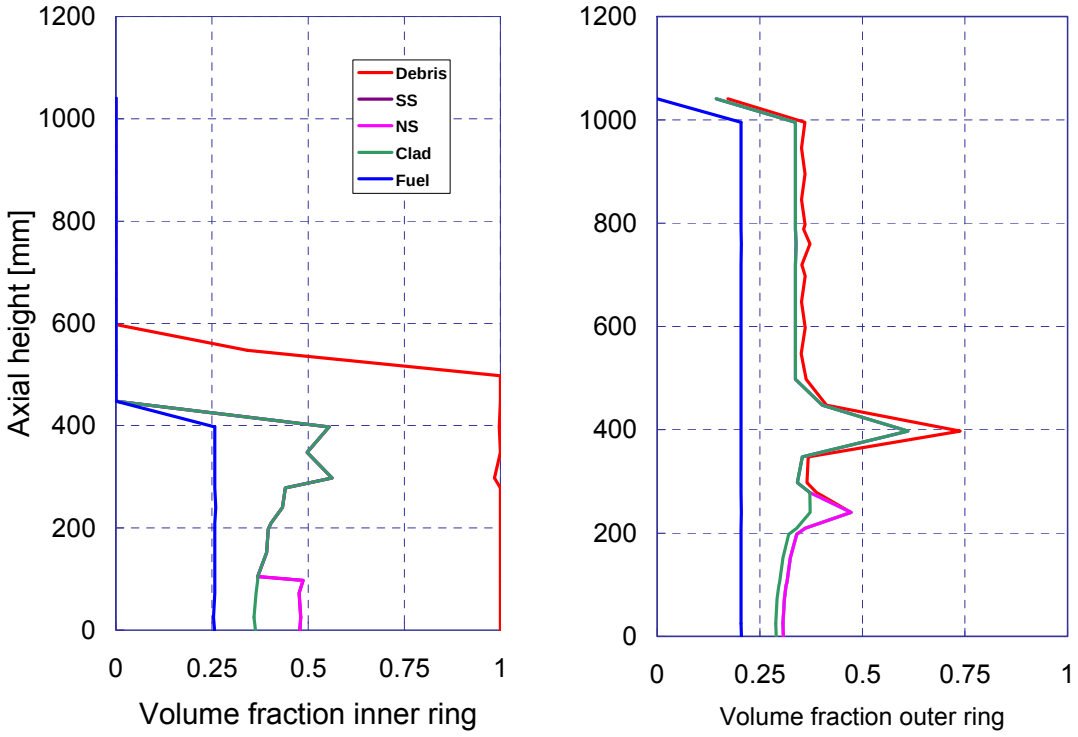

Figure 3.16-13. MELCOR 2.1 end state of bundle (18600 sec)

The composition of the debris at the bottom of the inner ring is shown in Figure 3.16-14,

Figure 3.16-15, and Figure 3.16-16 for MELCOR 1.8.5, 1.8.6 and 2.1, respectively. These plots all show that a significant mass of molten UO_2 present in the conglomerate particulate debris (PD) component relocated to the 200 mm elevation (axial levels 10 and 11) as was observed in the experiment. The complete voiding of the inner ring above a certain elevation in all calculations can be explained by the fact that the rod support model for all versions of MELCOR leads to total collapse of all fuel rod components in a ring extending above the point of failure, i.e., the elevation for which the rod exceeds the failure criterion (2500 K).

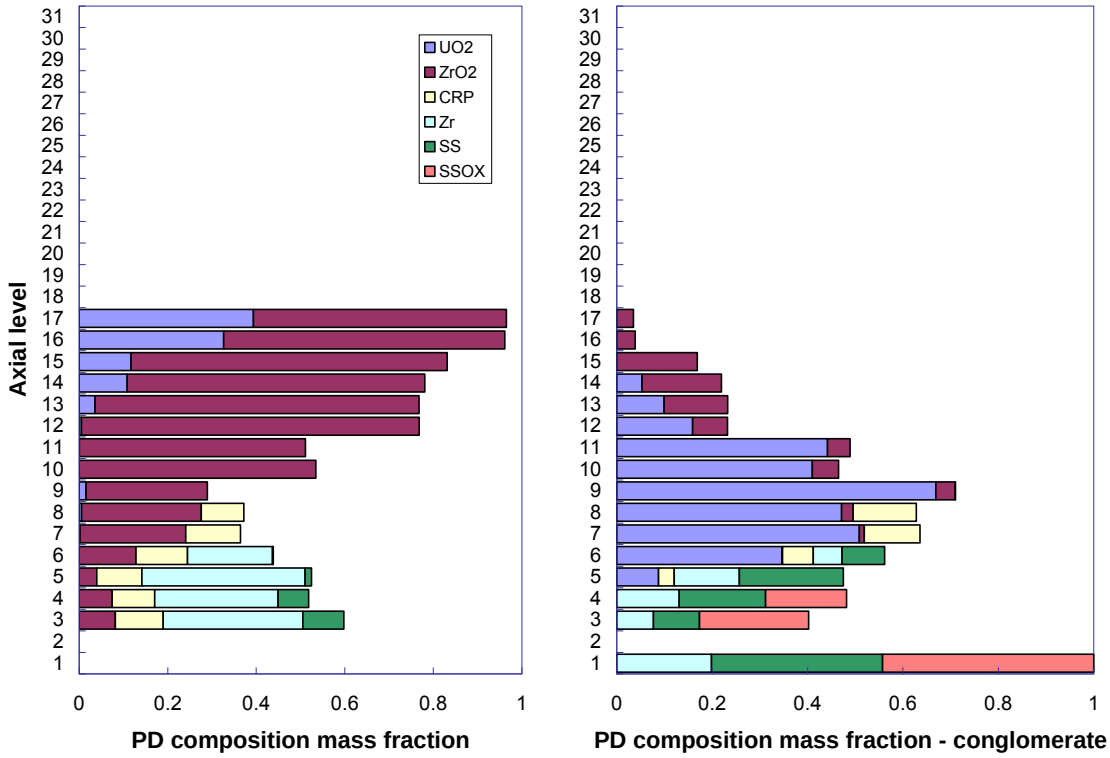

Figure 3.16-14. MELCOR 1.8.5 Inner ring composition of debris at end state

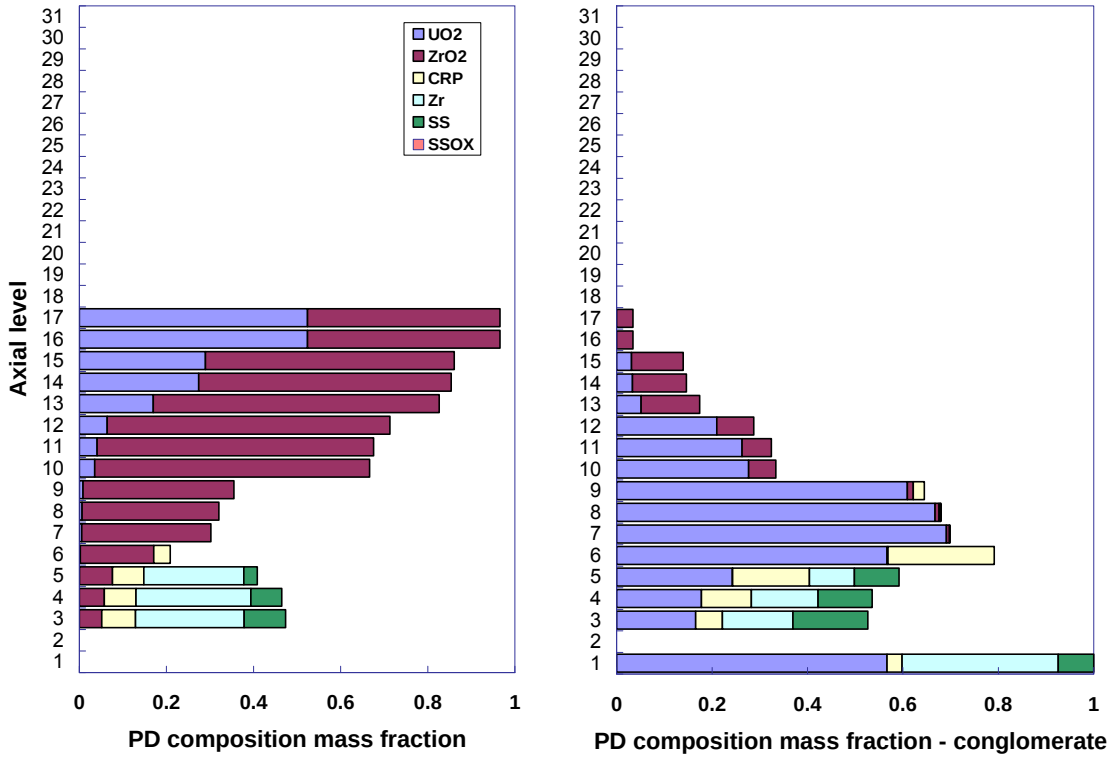

Figure 3.16-15. MELCOR 1.8.6 Inner ring composition of debris at end state

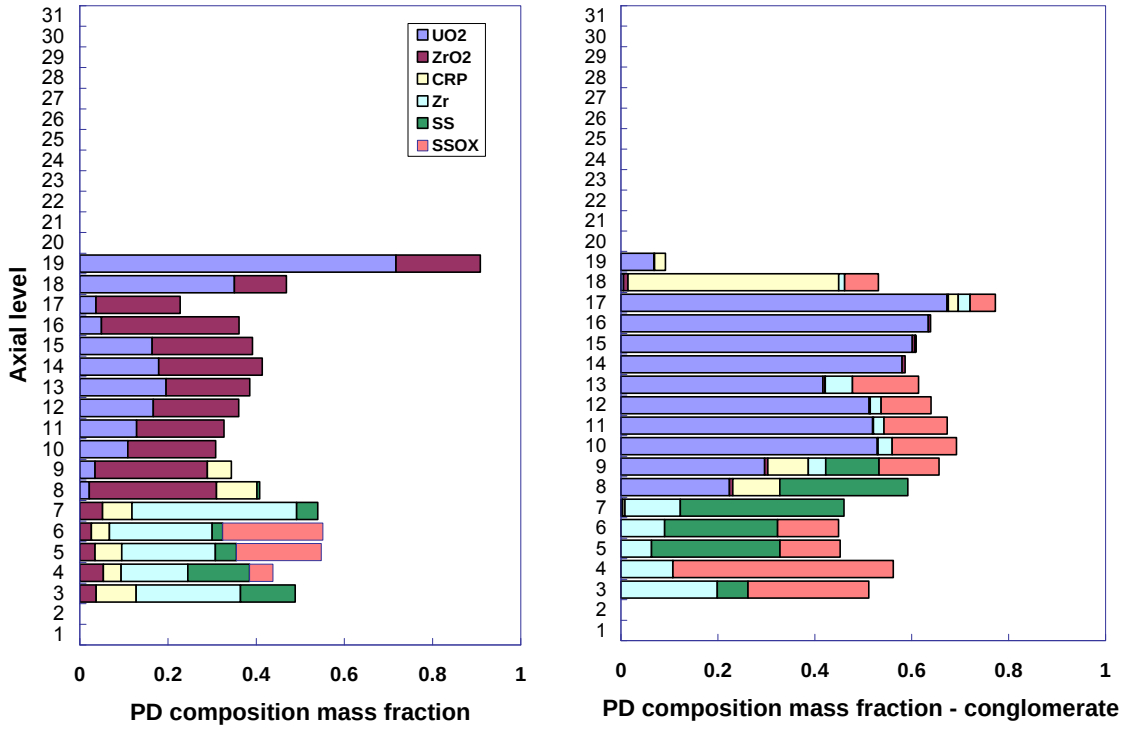

Figure 3.16-16. MELCOR 2.1 Inner ring composition of debris at end state

As shown in Figure 3.16-17, fluid temperatures along the hot leg of the steam generator are well predicted early in the calculation, though predicted heat losses to the tube are somewhat large late in the calculation, 11,000 sec to 15,000 sec, when fission product release is greatest. The results are essentially the same for all three versions of MELCOR, so only the results for MELCOR 2.1 are shown.

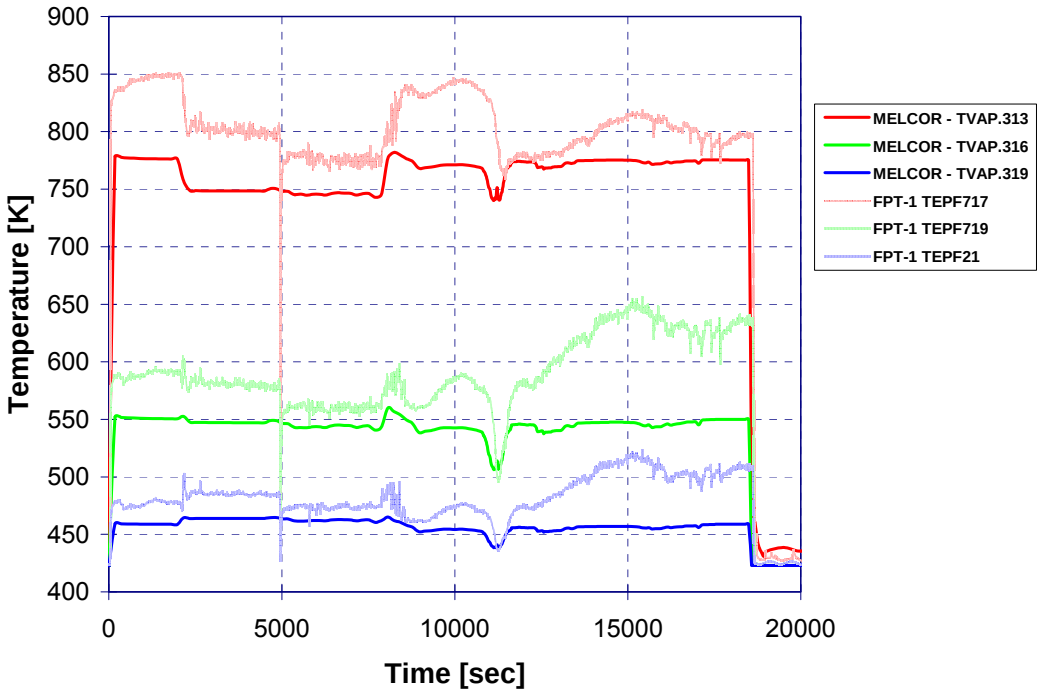

Figure 3.16-17. MELCOR 2.1 Steam generator temperatures

3.16.5 Discussion

The overall thermal assessment of the FPT-1 experiment by MELCOR 2.1, MELCOR 1.8.6, and MELCOR 1.8.5 simulations is generally good. All three versions of the code, however, still predict bundle and shroud temperatures higher than those measured in the test. Improvements in the predicted shroud temperatures may be possible by improving the gap closure model. Gap closure dependency was calculated as a function of the local gap temperature and not a function of the bulk shroud temperature, which is more likely responsible for thermal expansion of the insulator and ultimately gap closure.

3.16.6 References

[3.16.1] Berthet, B., et al., FPT-1 Quick Look Report, PHEBUS Document PF IP/96/310, Note Technique Leres n 55/96, (Restricted Distribution) September 1996.
[3.16.2] Vol 3: MELCOR Assessment Problems
[3.16.3] Schwarz, M., et al., “The PHEBUS PF International Research Program on Severe Accident: Status and Main Findings,” 26th Water Reactor Safety Information Meeting, Bethesda, Maryland, October 26-28, 1998.
[3.16.4] Schwarz, M., B. Clement and A.V. Jones, “Applicability of PHEBUS FP Results to Severe Accident Safety Evaluations and Management Measures,” FISA 99 EU Research in Reactor Safety, EUR 19532 EN, ISBN 92-828-9588-2.
[3.16.5] Haste, T., et al., Specification of International Standard Problem ISP-46 (PHEBUS FPT-1) Rev.1, Note Technique Semar 2002/05 le 30/01/02, Cadarache, France.
[3.16.6] Lorenz, R.A., M.F.Osborne, “A summary of ORNL Fission Product Release Test with Recommended Release Rates and Diffusion Coefficients,” NUREG/CR-6261, 1995.
[3.16.7] Jacquemain D., Bourdon S., de Braemaeker A., Barrachin M., “PHEBUS FPT1 Final Report,” Institut de protection et de sureté nucléaire, IPSN/DRS/SEA/PEPF Report SEA1/00, IP/00/479, Cadarache, France, 2000.

3.17 Analysis of the PHEBUS FPT3 Experiment

3.17.1 Background

The PHEBUS Fission Product Test (FPT) is an international integral experimental program that provides experimental data for validating computer codes used for severe reactor accident analysis. The program is conducted by the Institut de Radioprotection et de Sûreté Nucléaire (IRSN). The program provides information on core meltdown kinetics as well as the release, transport, and retention of fission products through a series of tests in an in-pile facility located in Cadarache, France. In that facility, an irradiated fuel rod bundle with a control rod or a debris bed is subjected to extensive degradation in a steam-rich or poor environment. Transport and behavior of the fission products, actinides and structural materials are investigated in a circuit representative of the reactor coolant system including a steam generator and a model containment building. The major elements of the test facility are illustrated in Figure 3.17-1. Also shown in the illustration are the corresponding elements of a pressurized water reactor.

The specific conditions of the FPT-3 test included an irradiated fuel bundle, a steam-poor environment, and B_4C control rod. The axial and radial cross sections of the test section containing the fuel bundle are also seen in Figure 3.17-1. There are a total of 20 fuel rods, along with the control rod, surrounded by a multi-layer shroud.

There are a number of phases to the experiment. First, there are two powered phases, fuel irradiation to create an initial fission product inventory, and the transition phase, which establishes initial conditions for the degradation phase. Power is provided by a driver core, and steam is also injected. Following core degradation, fission products are tracked through the primary circuit and into containment.

This is an integral test containing all portions of a real reactor accident, including water inventory loss, fuel heat up and failure, and fission product release. As such, it provides an extensive basis for the validation of many MELCOR models. In the past, modeling of Phebus tests with older MELCOR code versions have resulted in the implementation of new models, such as control rod silver release, and the modification of other models, such as the ONRL-Booth fission product release model.

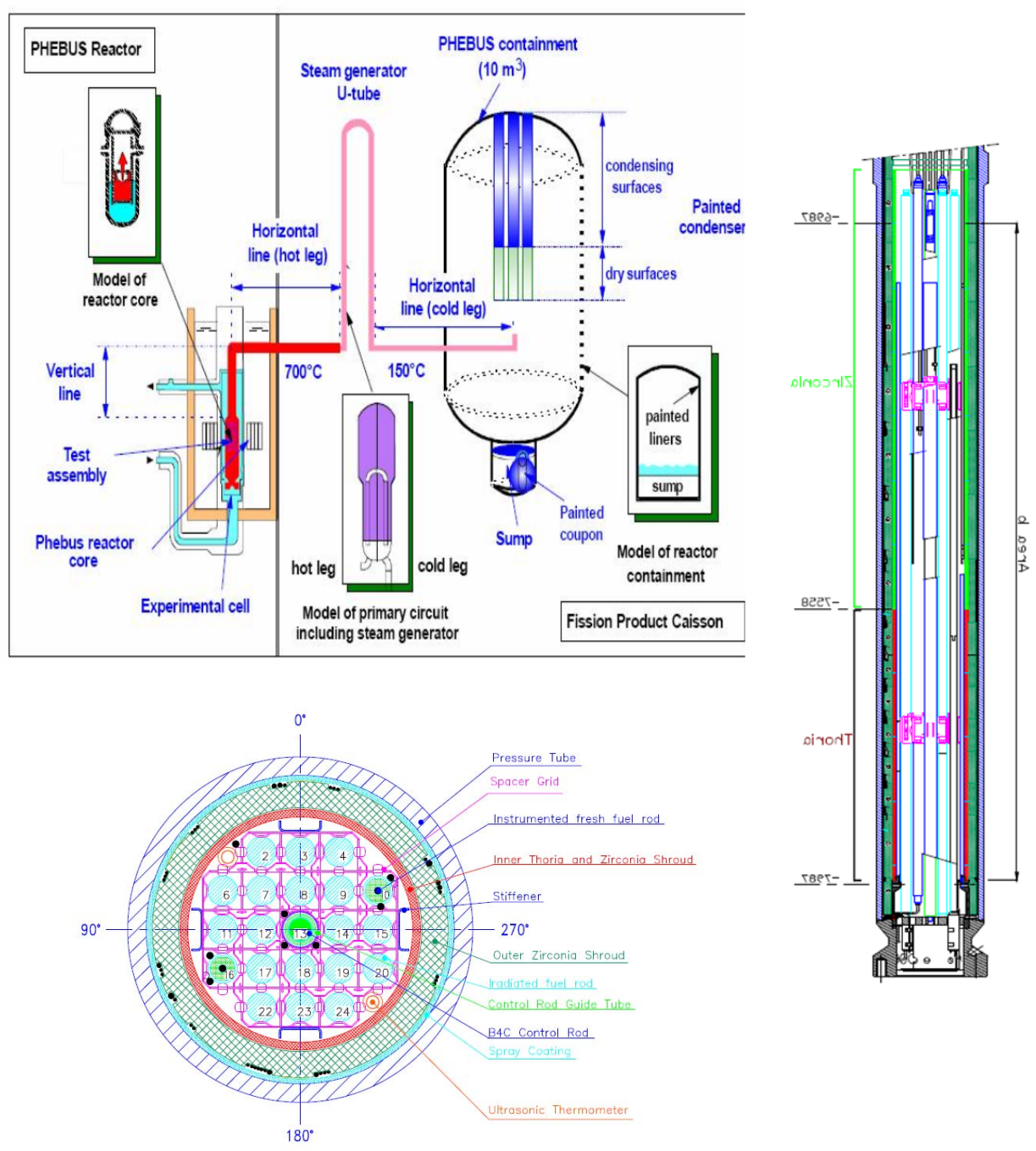

Figure 3.17-1. Phebus Facility and Cross Sections of the Test Bundle [3.17.1] and [3.17.2]

3.17.2 FPT 3 Experiment

3.17.2.1 Nodalization

The MELCOR nodalization was based on a 1.8.6 model originally developed for the FPT-1 test. This original model was modified for the FPT3 test using the FPT3 data book [3.17.2] and the benchmark guidelines [3.17.4]. The geometry and boundary conditions are specified for the test bundle, hot leg, steam generator, cold leg, and containment using control volumes and flow paths as shown in Figure 3.17-2. There are also heat structures associated with each CV and a number of additional deposition surfaces within containment. The figure shows a single CV for the containment, but in the final runs before benchmark submittal, this was re-nodalized to be represented by 5 CVs. The core is nodalized similarly to a full size LWR, except that there are only two rings, as shown in Figure 3.17-2. Control material for FPT3 was a single B4C control rod, surrounded by a guide tube, both of which were modeled explicitly, as is the insulating shroud surrounding the test bundle.

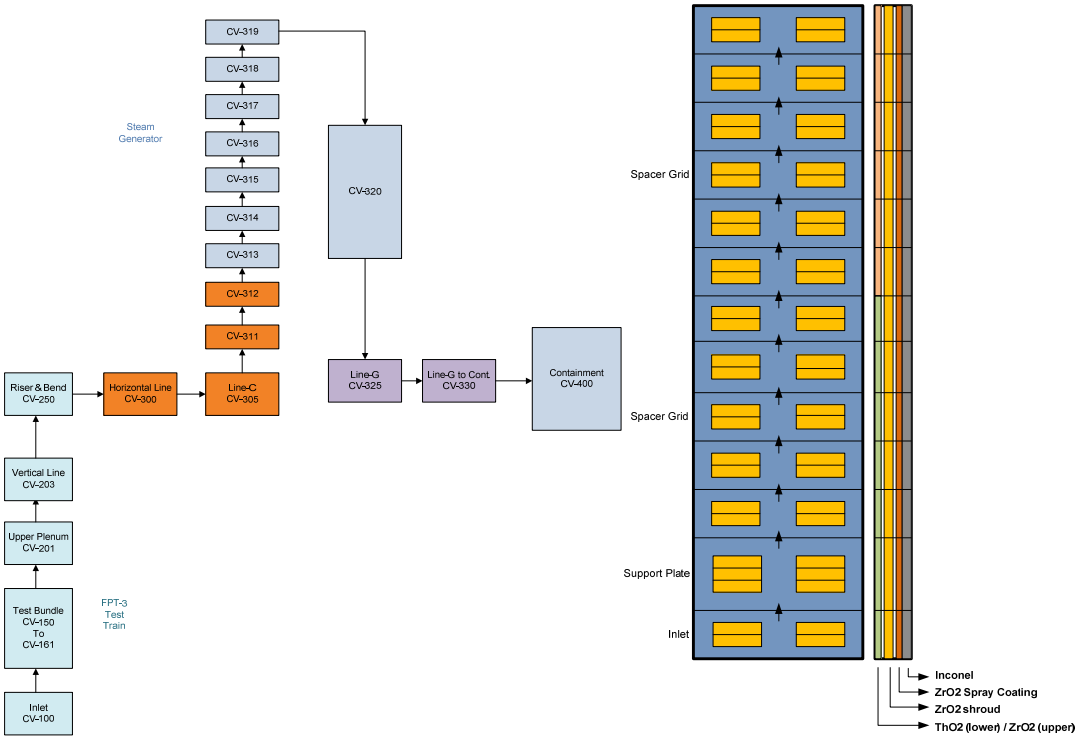

Figure 3.17-2. MELCOR Nodalization Scheme

To reflect test conditions, the vertical section above the upper plenum and the horizontal line feeding into the hot leg of the steam generator is set at 700 °C. The cold leg leaving

the steam generator is heated to 150 °C, and the containment is held at 110 °C (93 °C in the sump).

3.17.2.2 MELCOR Input Specifications

Whenever possible, MELCOR specifications were taken directly from the benchmark guidelines [3.17.4] and the FPT3 data book [3.17.2]. These inputs include core power, axial and radial power profiles, initial RN inventories, and most material properties. The exceptions for material properties are the melting temperature and enthalpy tables for UO_2 and ZrO_2 to allow eutectic liquefaction at 2500 K as observed in the experiment and the increase of the thermal conductivity of the shroud gap at 900 K, compared to steam, to represent gap closure due to thermal expansion of the inner and outer shroud.

Other MELCOR parameters were modified to more closely reflect experimental observations. These include setting cladding failure temperature to 1088 K, fuel collapse temperature to 2500K (2.1 default), B_4C liquefaction and oxidation temperatures to 1900K and 1550K, respectively, increasing the global failure temperature of NS to 1900K and increasing the candling heat transfer coefficients for UO_2 and ZrO_2 to 30,000 and 20,000 W/m^2-K, respectively. Also in the B_4C model, the "ROD" option was used and the limit on the fraction of B_4C mass available for oxidation is increased to 0.9999 from 0.02; this uses the PWR rod geometry but allows the B_4C to oxidize as long as it is within the heated core region.

The radial and axial radiation view factors, FCELR and FCELA, were increased to 0.75 and 0.25, respectively, from the MELCOR default value of 0.1 for each. This is due to the enhanced radiation from inner fuel rods to the shroud because of the sparse two-ring fuel geometry.

In addition to the SC modification described above, several other SCs were modified in the original deck. These included an increase in the minimum hydrodynamic volume fraction, a switch to the new default Zr breakout flow rate, and the modification of a large number of RN class defaults and diffusion parameters. Rather than attempt to justify each SC change individually, a sensitivity case was run with all SC records in the deck commented out to compare the difference.

3.17.2.3 Results of Analysis

Key events for the MELCOR FPT-3 base case calculation during the bundle degradation period are summarized in Table 3.17-1. The MELCOR calculated event timings are compared to those provided in the experimental data reports or estimated from the experimental results [3.17.5][3.17.6]. These MELCOR predictions compare very well with the experiment. Even the time to control rod rupture, which has the largest variation from the experimental observation, is within about 10 minutes of the observed timing.

Table 3.17-1– FPT3 Timing of Key Events

Event Description	MELCOR 2.1 Timing (sec)	Observed Timing (sec)
Clad failure	4632	4870
Beginning of H2 generation	8500	8440
Control rod rupture	9003	9680
First melt relocation	17000	16620

3.17.2.3.1 Thermal Response

In the FPT-3 results, some fuel temperatures were measured at the interior of a fuel rod and at the outer surface for others. These results are compared to fuel and cladding MELCOR temperatures as appropriate. The shroud temperature is measured between two HS nodes, so both temperatures are compared. Results are available at all elevations; sample results are shown for temperatures at the 300 mm and 800 mm elevations in Figure 3.17-3, representing the lower and upper elevations of the test bundle. The noise in the fuel temperature at 800 mm after 10,000 seconds indicates a broken thermocouple and should not be considered accurate.

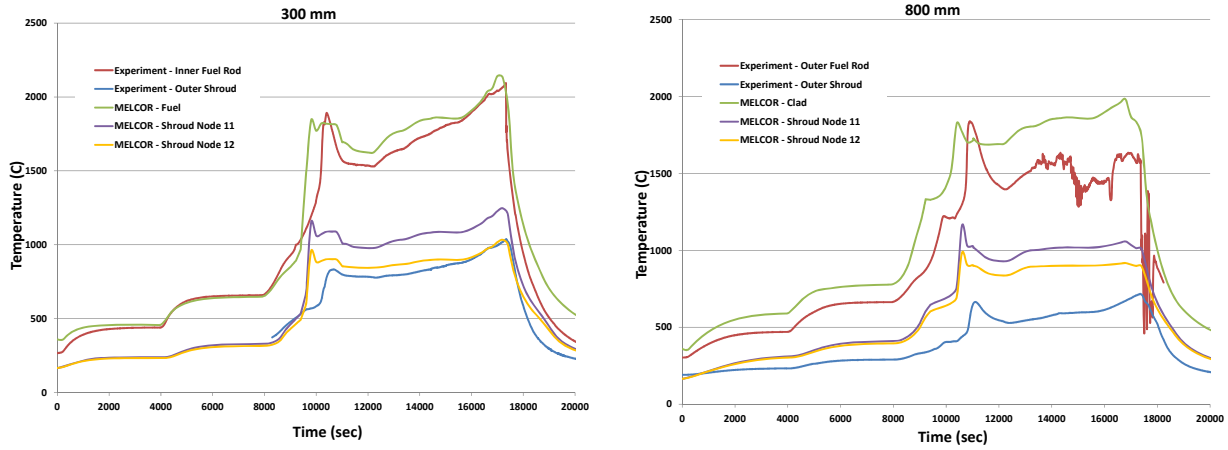

Figure 3.17-3 MELCOR Calculated Fuel Temperature Compared to Experiment

MELCOR predicts fuel temperatures accurately at lower elevations, but tends to over-predict the temperature at high elevations. Additionally, MELCOR predicts the onset of

steam oxidation (~10,000 seconds) slightly earlier than indicated by the experimental results leading to a large increase in temperature. This large increase causes the first core components to fail, temporarily leading to steady or lowering temperatures, even though cladding oxidation continues. However, the experimental power continues to increase and so all temperatures again begin to rise until all power is shut off at 17,400 seconds. Although temperature magnitudes differ, trends are well matched between MELCOR and the experiment following the oxidation peak.

Temperature in the shroud, which also matched the experiment until the first oxidation peak, is significantly over-predicted after this point. In fact, at high elevations, MELCOR is showing temperatures about 400^{o}C over experimental values. Since this difference is not closely observed in fuel temperatures, this signifies that there is a significant heat loss through the shroud in the experiment that in not being captured by MELCOR. This may result in generally higher core temperatures and lead to the quicker onset of oxidation.

3.17.2.3.2 Hydrogen Generation

In FPT-3, hydrogen is generated by oxidation, mainly from the zircaloy cladding but also from the B_4C in the central control rod. The mass flow rate of hydrogen leaving the RPV, which is a surrogate for hydrogen generation rate, and the total mass of hydrogen generated are shown in Figure 3.17-4. The major difference between current MELCOR results, the experiment, and other modeling results is the onset of oxidation, which for MELCOR occurs at least 500 seconds before any other. This reinforces the results shown with temperature, where the oxidation peak occurred earlier. The peak in oxidation at late times corresponds to fuel collapse.

There are large unexpected fluctuations in the mass flow rate but during the main oxidation phase (~10,000-11,000 seconds), the mass flow rates are very similar. This is shown also in the total mass, where the slope looks very similar. As shown with temperature results, the onset of fuel failure and relocation, indicated here by the ceasing of oxidation, occurs at the same general time. There is also a late spike in hydrogen indicated by experimental results, which is also predicted by MELCOR, although the timing does not quite line up.

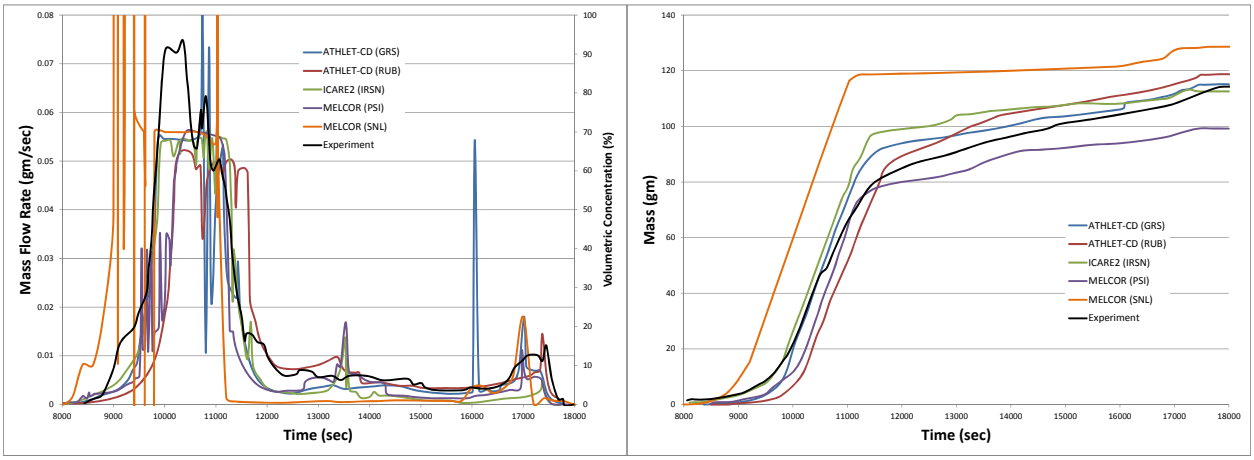

Figure 3.17-4. MELCOR Hydrogen Mass Flow and Total Mass Compared to Experiment

Control rod failure was investigated separately. It was discovered that the rod was failing much earlier with the base case model than the experiment indicated. It seems that NS failure logic is being applied, as opposed to the control rod specific logic. However, even when the NS failure logic was changed, the rod still failed earlier than the set points. This bug was reported, but at the time of this writing, has not been addressed. Since there are many chemical reactions that occur with the B4C, the earlier failure changes the oxidizing environment, which could be impacting the total hydrogen generation. However, it is unlikely that this is the cause of the earlier start to oxidation. It is possible that the missing heat loss from the shroud is the primary cause.

3.17.2.3.3 Radionuclide Release and Transport

Simultaneously with fuel damage and relocation, fission products are released from the fuel. Some of these fission products are retained in the pressure vessel, some deposit in the primary circuit (hot leg, steam generator, and cold leg), and some fraction reaches containment. Experimental data are available for a number of fission product classes in multiple locations in the Phebus system. An example of this data, compared to MELCOR is found in Figure 3.17-5. This shows the percentage of iodine that is released from the test bundle and the percentage that reaches point G, which is on the cold leg past the steam generator.

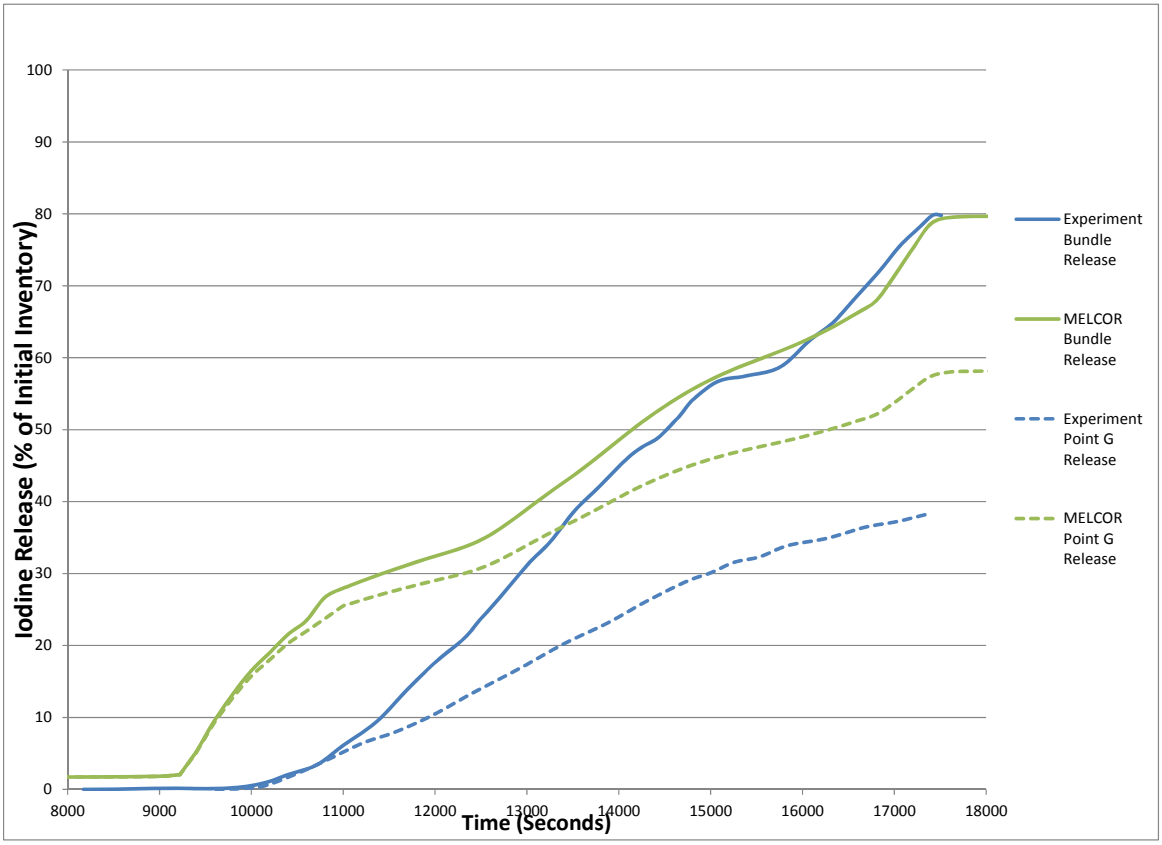

Figure 3.17-5. MELCOR Iodine Release Percentages Compared to Experiment

It can be seen that iodine release starts much earlier for MELCOR compared to the experiment. This is not a surprise as all previous MELCOR results have been predicting earlier iodine release as well. It is encouraging to note that when power is turned off, the release from the bundle is almost exactly predicted. MELCOR predicts that much more iodine reaches the cold leg than what is measured by the experiment. However, the slopes of the two lines are similar, indicating that deposition after the early releases happens at about the same rate.

Generally speaking, MELCOR does a good job of calculating the fission product releases from fuel as compared to the experiment (although all releases start earlier for MELCOR). MELCOR typically under-predicts the amount of deposition in the primary circuit. However, there are exceptions for individual RN classes for both bundle release and circuit deposition. It should also be noted that there were observed large deposits in the FPT-3 steam generator leading to flow blockages, which MELCOR would not predict.

3.17.2.3.4 SC Sensitivity

As described above, there were a large number of sensitivity coefficient modifications in the original deck. To see the impact of these modifications, the deck was run again with no SCs included. All other deck modifications were retained.

Core temperatures were generally similar, both in magnitude and timing. Total hydrogen production was also similar, although it started early, likely due to not having increased the temperature used by MELCOR to initiate oxidation. There was slightly less total hydrogen mass, but it was not a significant difference. Since both of these key results are similar, no figures are shown.

Fission product release from the fuel was significantly different (see Figure 3.17-6). The timing of the start of releases, and the increase in release with the onset of the first oxidation, are similar. However, the shape of the release curves, and the total release when core power is shut off, differ greatly. Without any sensitivity coefficients, releases occur more quickly and the total release is higher.

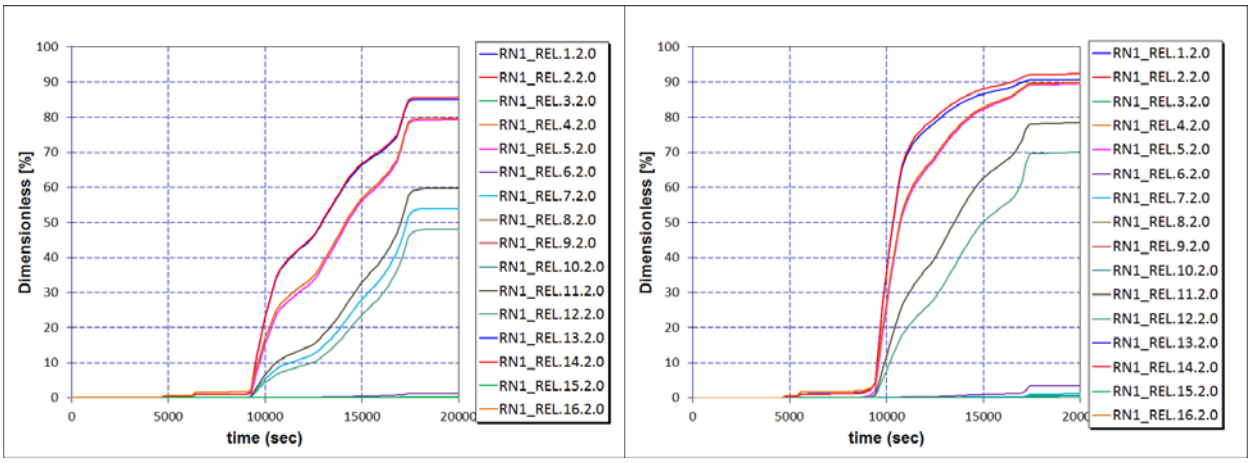

Figure 3.17-6. RN Class Releases from Fuel – Base Case (Left) vs. No SC Case (Right)

3.17.3 Discussion

Analysis of the FPT-3 experiment shows that MELCOR is capable of modeling a full system, integral experiment. Generally speaking, MELCOR predicts thermodynamic trends well, such as fuel heat-up and oxidation. This experiment provides a good example of how a small change in an initial event, in this case the onset of oxidation, can have a large impact on later results. It seems likely that the earlier onset of oxidation was due at least in part to the early failure of the B_4C control rod and the lack of heat loss from the shroud.

MELCOR only did a moderately successful job at predicting fission product release and transport. Typically MELCOR results were better for releases from fuel, but under-predicted deposition in the primary circuit. However, the sensitivity case with no SCs showed that releases from fuel differ from the experiment more than originally thought.

3.17.4 References

[3.17.1] Jacquemain D., Bourdon S., de Braemaeker A., Barrachin M., *PHEBUS FPT1 Final Report*, Institut de protection et de sureté nucléaire, IPSN/DRS/SEA/PEPF Report SEA1/00, IP/00/479, Cadarache, France, 2000.

[3.17.2] *Data Book FPT3,* Document PHEBUS FP: IP 07/575, IRSN, August 2007

[3.17.3] Gauntt, R.O., Cash, J.E., Cole, R.K., Erickson, C.M., Humphries, L.L., Rodriguez, S.B., Young, M.F., 2005, *MELCOR Computer Code Manuals, Vol.1: Primer and User's Guide, Version 1.8.6,* NUREG/CR 6119, Vol. 1, Rev. 3., U.S. Nuclear Regulatory Commission, Washington D.C.

[3.17.4] Bieliauskas A., Haste T., *Specifications of SARNET2 PHEBUS FPT3 Benchmark,* Institut de protection et de sureté nucléaire, DPAM-SEMIC-2011-057, Cadarache, France, 2011.

[3.17.5] Payot, F., et al., *PHEBUS FP FPT3 Final Report,* Document PHEBUS PF IP/11/589, IRSN, May 2011

[3.17.6] Repetto, G., et al., *Preliminary Analyses of the PHEBUS FPT3 Experiment using Severe Accident Codes (ATHLET-CD, ICARE/CATHARE, MELCOR)*, The 2nd European Review Meeting on Severe Accident Research (ERMSAR-2007), Forschungszentrum Karlsruhe Gmbh (FZK), Germany, 12-14 June 2007

3.18 Analysis of the POSEIDON Integral Experiments under Hot Pool Conditions

3.18.1 Background

In most light water reactor severe accident scenarios, fission product aerosols may encounter stagnant pools of water on the path to release. In boiling water reactors for instance, a steam-gas-fission product mixture may be discharged to the pressure suppression pool in the wetwell. In pressurized water reactors, a steam-gas-fission product mixture could pass through the pressurizer quench tank before entering containment. Steam generator tube rupture could also bring a steam-gas-fission product mixture in contact with a pool. These few examples highlight the importance of pool aerosol scrubbing phenomena to severe accident analysis.

The POSEIDON experiments were meant to provide insight into pool scrubbing phenomena and to help identify and correct any existing deficiencies in theoretical models. The first phase of the experiments consisted of 17 integral tests wherein the effects of all aerosol removal mechanisms were observed. The second phase was dedicated to separate effects testing wherein individual aerosol removal mechanisms were isolated

Integral experiments were designed to ascertain the dependence of hot pool decontamination factor (DF) on water height at different carrier gas steam mass fractions with a relatively constant inlet aerosol diameter. In this instance, DF is defined as the ratio of material introduced to the pool to material escaping from the pool..

3.18.2 Description of the POSEIDON Facility

The POSEIDON loop and associated aerosol generation system DRAGON are shown in Figure 3.18-1. The process of aerosol generation is described in section 3A of reference [3.18.1] as is the DRAGON system. A schematic of the POSEIDON facility is shown in Figure 3.18-2. The test section consists of four parts:

1. The aerosol laden gas injection system
2. The POSEIDON tank
3. The water heating and wall temperature control system
4. The collector system
5.

Each component is described more fully in section 3B of reference [3.18.1]. The test section design allows for aerosol/gas injection to a temperature-controlled tank containing the scrubbing pool. The collector system is designed such that aerosol/gas flow emerging from the pool surface is reliably captured and measured.

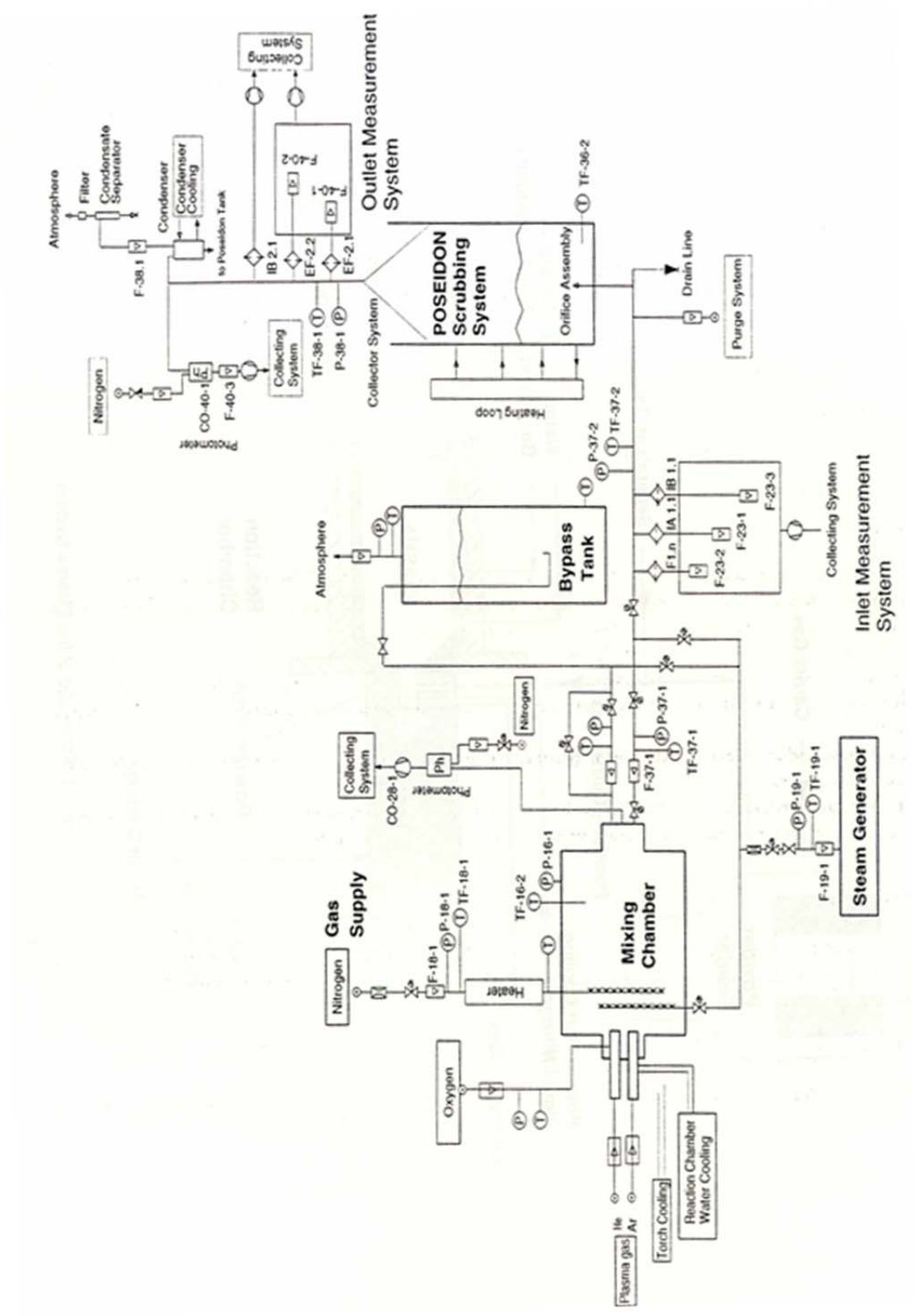

Figure 3.18-1 POSEIDON Facility and Instrumentation [3.18.1]

3.18.3 Description of the POSEIDON MELCOR Model

MELCOR 2.1 (revision 6110) and MELCOR 1.86 (revision 4073) were both used to model the POSEIDON facility. The nodalization diagram (for both code versions) is shown in Figure 3.18-3.

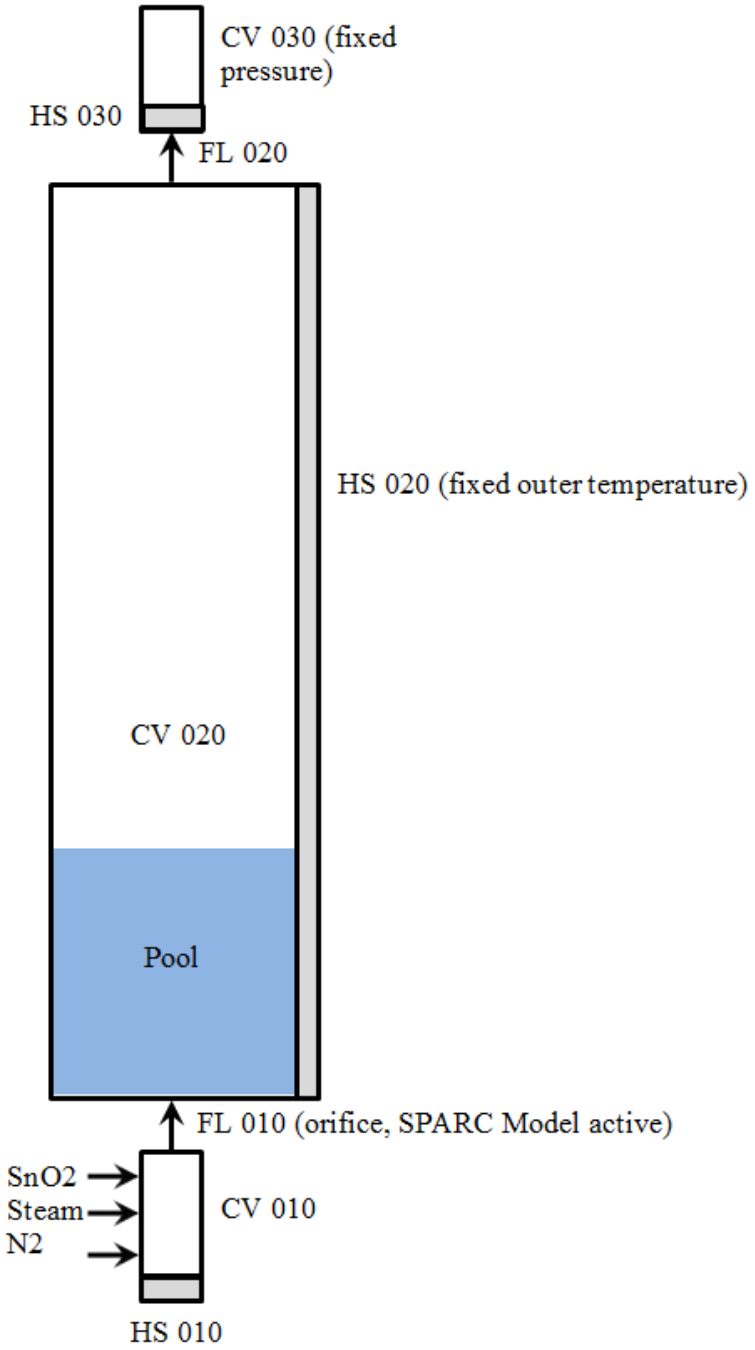

Figure 3.18-2 POSEIDON MELCOR Model Nodalization

Noteworthy specifics of the MELCOR modeling are discussed below.

Boundary conditions

Several boundary conditions were imposed on the MELCOR model to simulate the POSEIDON experimental configurations. The experiment-specific conditions were:

- Tank temperature
- Tank water level
- Nitrogen flow rate
- Steam flow rate
- Nitrogen and steam delivery temperature
- Outlet pressure
- Orifice size
- Aerosol generation rate
- Aerosol size distribution

The particular values applied in the different MELCOR calculations are noted below or presented in Table 3.18-1.

Pressure boundary condition

Consistent with outlet pressure reported in the POSEIDON experiments, a constant pressure was imposed in CV 30 of the MELCOR model unique for each calculation. Pressures elsewhere in the model developed in response to this constant pressure and the imposed flow rate of the carrier gas.

POSEIDON tank wall temperature

The heat structure representing the wall of the POSEIDON tank was held constant at the pool temperature reported in reference [3.18.1]. This temperature was experiment-specific.

SPARC model

MELCOR's SPARC model was activated in the flow path representing the orifice in the inlet at the base of the POSEIDON tank. Bubble-rise thermodynamic interactions and aerosol scrubbing were enabled.

Orifice size

The size of the orifice in the inlet to the POSEIDON tank utilized in the different experiments is not reported in reference [3.18.1]. The size, therefore, was calculated with successive trial and error MELCOR runs that identified the size consistent with the carrier gas flow rate and pressure drop from inlet to outlet. This resulted in an orifice diameter of 17.75 mm in Experiments PA06, PA07, PA08, and PA12 and a diameter of 17.2 mm in Experiment PA17.

Inlet aerosol size distribution

The size distribution of the SnO_2 particles introduced to the MELCOR calculation was characterized as lognormal with AMMD 0.3 μm and GSD 1.35 for calculations PA06, PA07, PA08 and PA12 consistent with the inlet aerosol flow rate in these calculations relative to the information in Table 3 of reference [3.18.1]. Similarly, the size distribution for calculation PA17 was characterized as lognormal with AMMD 0.43 μm and GSD 1.55. Minimum and maximum diameters were specified as 0.01 μm and 7 μm, respectively, from consideration of Figure 3.18-4, to Figure 3.18-6 [3.18.1].

Aerosol density

Aerosol density was specified to be the default MELCOR value of 1,000 kg/m^3.

Hygroscopic model

MELCOR's hygroscopic model was left inactive consistent with SnO_2 being non-hygroscopic.

Definition of SnO_2 aerosol as radioactive

The SnO_2 aerosol introduced to the MELCOR calculation was characterized as radioactive so that a MACCS flow path could be used to report outlet aerosol size distribution. The SnO_2 in the POSEIDON tests was not radioactive.

3.18.4 Results of the POSEIDON MELCOR 2.1 Analysis

MELCOR 2.1 simulations were accomplished for 5 of the experiments documented in reference [3.18.1]. The experiments were PA06, PA07, PA08, PA12 and PA17. PA06 was taken to be a base configuration from which parameters such as pool depth and steam fraction varied in the other experiments. Specifically:

- PA07 investigated a shallower pool
- PA08 investigated a deeper pool
- PA12 looked at the effect of introducing zero steam
- PA17 looked at the effects of higher steam fraction and larger particles

Table 3.18-1 and Table 3.18-2 summarize the results of the MELCOR POSEIDON calculations relative to data from POSEIDON experiments. Table 3.18-1 addresses conditions imposed in the experiments and calculations while Table 3.18-2 addresses the results obtained. Figure 3.18-3 through Figure 3.18-10 show the time histories of various parameters in the PA06 MELCOR calculation. Figure 3.18-11 and Figure 3.18-12 show size distributions of the SnO_2 particles exiting the top of the tank in the PA06 calculation. For comparison, analogous figures presenting data from the PA06 experiment are included as the attachment.

Considering the statistics presented in Table 3.18-2 on outlet particle size, i.e., aerodynamic mass median diameter (AMMD) and geometric standard deviation (GSD), realize that the lognormal distributions reported by MELCOR and presumably observed

in the tests have necessarily been transformed to normal distributions for which the mean (μ) and standard deviation (σ) could be determined. AMMD and GSD of the lognormal distributions were then calculated from μ and σ. The relations employed were:

$$\mu = \sum_{i=1}^{n} \ln(d_i) f(d_i)$$ Equation 3.18-1

$$V = \sum_{i=1}^{n} (\ln(d_i) - \mu)^2 f(d_i)$$ Equation 3.18-2

$$\sigma = \sqrt{V}$$ Equation 3.18-3

where;

- μ is the mean of the normal distribution of the natural logarithm of particle diameter
- V is the variance of the normal distribution of the natural logarithm of particle diameter
- σ is the standard deviation of the normal distribution of the natural logarithm of particle diameter
- d_i is the particle diameter associated with bin i
- $f(d_i)$ is the probability density function of particle diameter evaluated for bin i, i.e., the mass of particles in bin i normalized to the total mass of particles in all bins
- n is the number of particle size bins

With μ and σ known, the mean (AMMD in this case) and the GSD of the lognormal distribution of particle diameter are given by:

$$AMMD = e^{\mu + \sigma^2/2}$$ Equation 3.18-4

$$GSD = e^{\sigma}$$ Equation 3.18-5

Table 3.18-1: Average Experimental Parameters and Corresponding Average MELCOR (Calc) Conditions

Test	Inlet gas flow rate (kg/hr)		Inlet steam mass fraction		Inlet pressure (bar)		Inlet gas temperature (°C)		Inlet gas density (kg/m^3)		Pool temperature (°C)		Pool height (m)		Inlet aerosol flow rate (g/s)		Outlet gas pressure (bar)	
	Test	Calc	Test	Calc	Test	Calc	Test	Calc	Test	Calc	Test	Calc	Test	Calc	Test	Calc	Test	Calc
PA06	142.5	142.5	0.553	0.553	1.45	1.45	243.0	242.6	0.714	0.727	86.9	90.6	1.0	0.997	0.0118	0.0118	1.04	1.04
PA07	142.5	142.5	0.553	0.553	1.42	1.42	267.7	267.3	0.667	0.677	86.3	91.5	0.3	0.293	0.0119	0.0119	1.05	1.05
PA08	145.1	145.1	0.563	0.563	1.63	1.68	212.9	212.8	0.849	0.890	86.8	89.3	4.0	4.0	0.0096	0.0096	1.03	1.03
PA09	146.5		0.567		1.51		246.7		0.738		87.1		2.0		0.0117		1.04	
PA10	137.9		0.045		1.60		222.6		1.050		79.8		4.0		0.0117		1.03	
PA11	137.9		0.043		1.46		256.1		1.030		75.3		2.0		0.0152		1.04	
PA12	124.9	124.9	0.000	0.000	1.36	1.33	237.7	237.9	0.678	0.880	71.8	64.33	1.0	0.964	0.0161	0.0161	1.04	1.04
PA13	125.3		0.000		1.34		270.1		0.810		62.9		0.3		0.0149		1.04	
PA14	94.3		0.721		1.55		266.8		0.674		88.0		4.0		0.0081		1.04	
PA15	94.3		0.719		1.30		305.2		0.531		85.4		1.0		0.0091		1.04	
PA16	91.8	91.8	0.750	0.750	1.54	1.58	283.8	283.7	0.639	0.679	86.6	93.5	4.0	4.1	0.0386	0.0386	1.04	1.04
PA17	91.8	91.8	0.747	0.747	1.30	1.30	310.8	310.4	0.511	0.531	88.0	94.7	1.0	1.022	0.0571	0.0571	1.00	1.00
PA20	91.1	91.1	0.720	0.720	1.35	1.39	229.3	229.1	0.621	0.667	84.2	93.0	2.0	2.1	0.0063	0.0063	1.04	1.04
PA21	87.1		0.705		1.16		256.8		0.493		82.7		0.3		0.0076		0.99	

Table 3.18-2: Average Results Data From the POSEIDON Tests and Corresponding Average MELCOR (Calc) Results

Test	Outlet gas flowrate (kg/hr)		Outlet steam mass fraction		Outlet gas density (kg/m^3)		Outlet AMMD (μm)		Outlet GSD		DF	
	Test	Calc	Test	Calc	Test	Calc	Test	Calc	Test	Calc	Test	Calc
PA06	132.5	146.6	0.518	0.566	0.734	0.740	0.36	0.23	1.64	1.31	7.30±1.42	9.85
PA07	129.6	147.3	0.506	0.568	0.755	0.747	0.36	0.32	1.50	1.44	6.61±2.25	1.95
PA08	133.2	144.3	0.525	0.561	0.734	0.741	0.28	0.19	1.34	1.24	21.4±6.70	168.95
PA09	118.8		0.465		0.765		0.35		1.48		9.72±3.50	
PA10	205.9		0.360		0.800		0.26		1.45		10.6±2.38	
PA11	173.2		0.237		0.856		0.24		1.60		5.35±1.40	
PA12	166.6	146.4	0.249	0.147	0.843	0.950	0.30	0.29	1.55	1.42	3.42±0.62	3.43
PA13	147.6		0.152		0.895		0.26		1.55		2.59±0.65	
PA14	61.6		0.572		0.696		0.29		1.42		14.6±3.10	
PA15	50.4		0.475		0.722		0.31		1.59		4.86±1.04	
PA20	40.7		0.434		0.720		NA		NA		5.11±1.21	
PA21	51.5		0.527		0.655		0.32		1.50		2.45±0.58	
PA16	50.0		0.542		0.691		0.38		1.42		38.9±10.6	
PA17	50.8	78.6	0.539	0.704	0.695	0.668	0.46	0.29	1.62	1.47	12.3±6.17	31.52

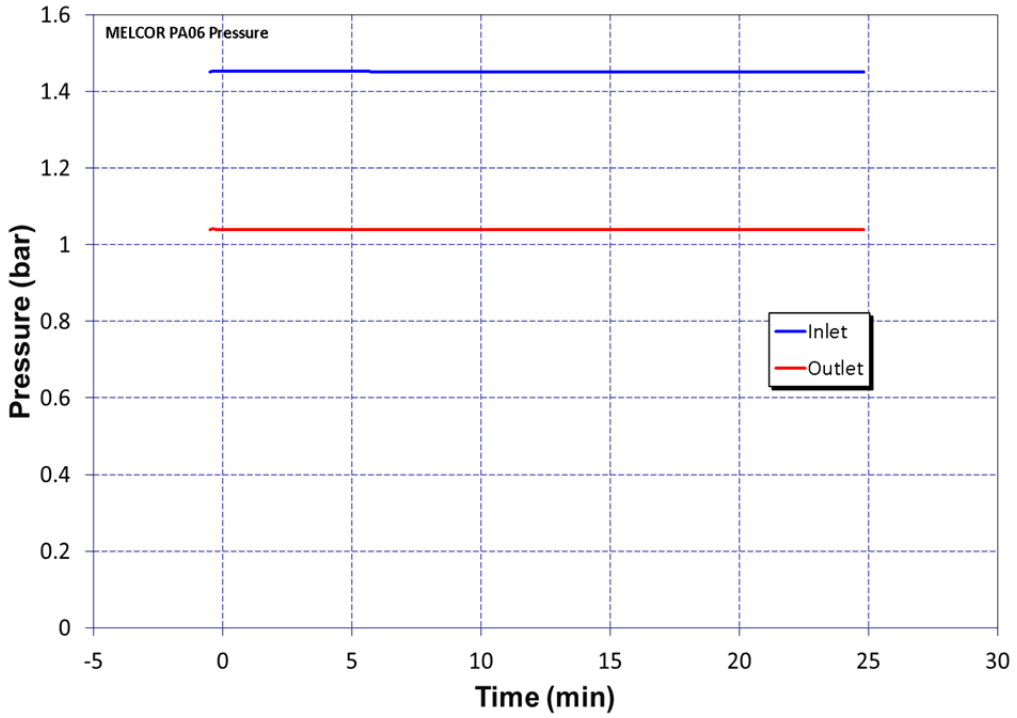

Figure 3.18-3 MELCOR PA06 Pressure

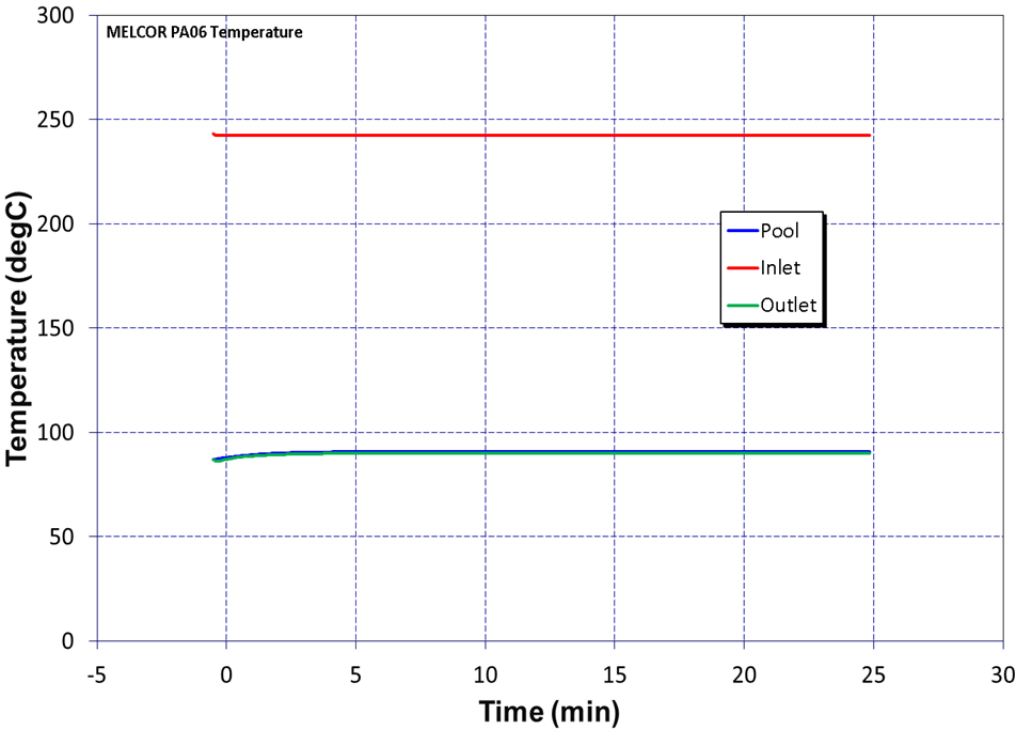

Figure 3.18-4 MELCOR PA06 Temperature

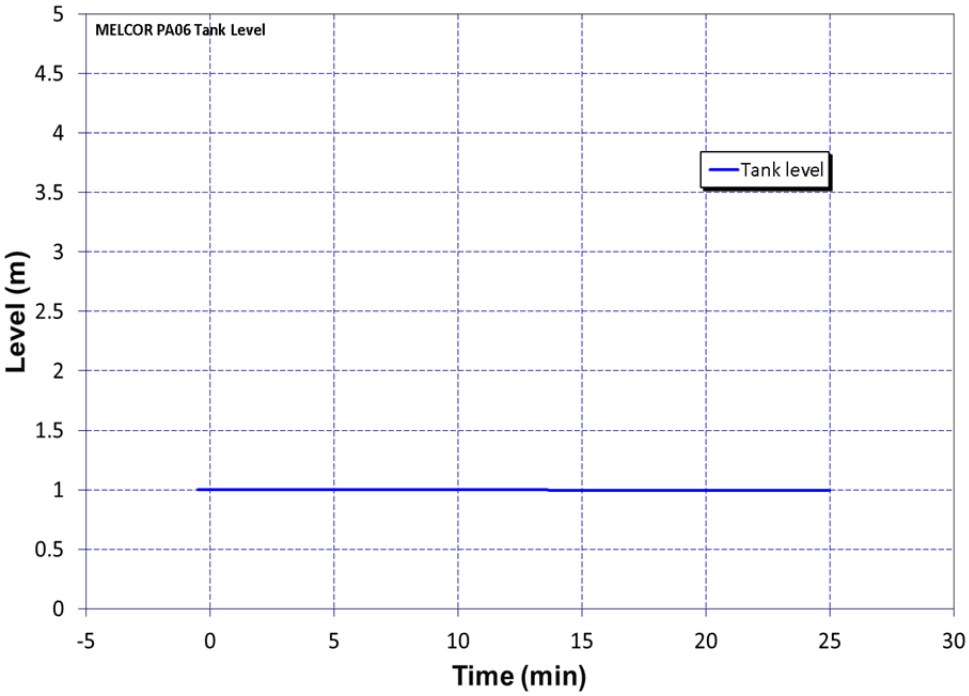

Figure 3.18-5 MELCOR PA06 Tank Level

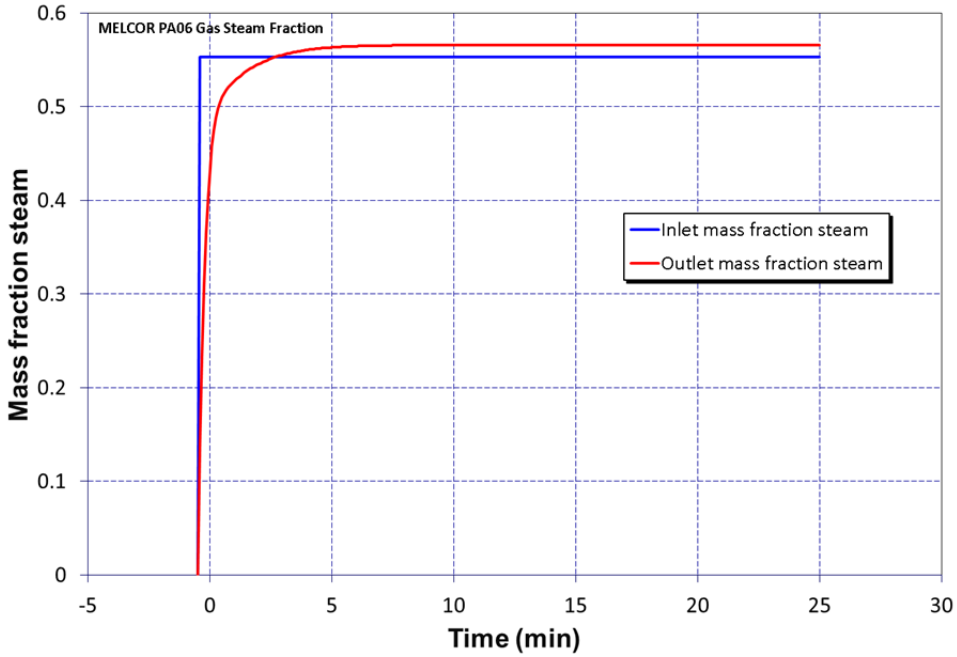

Figure 3.18-6 MELCOR PA06 Steam Fraction

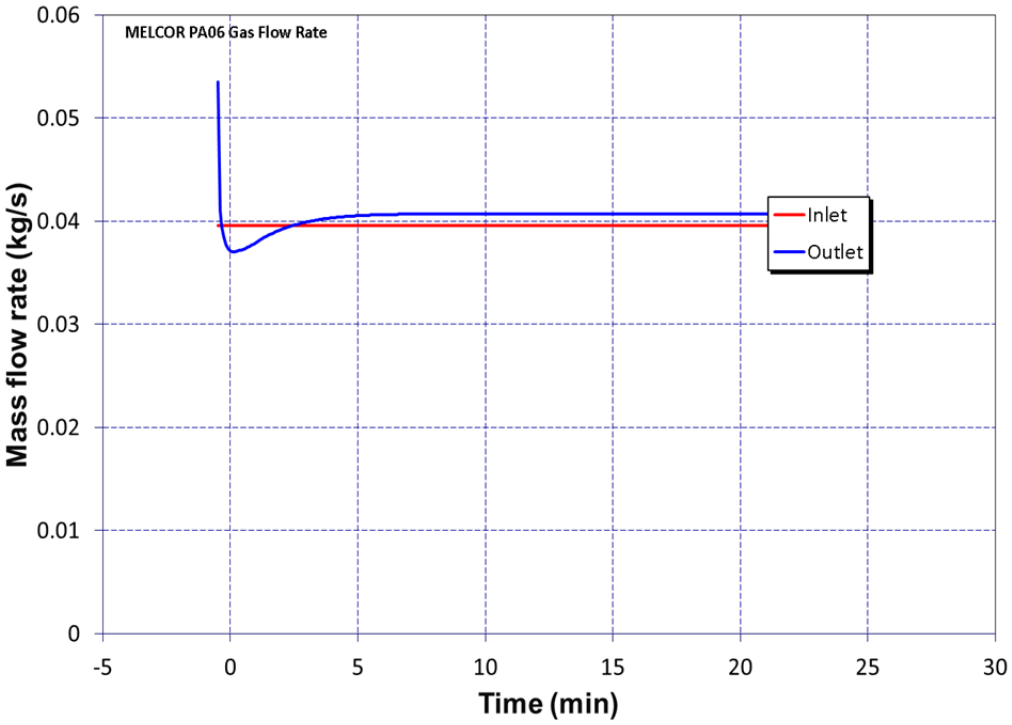

Figure 3.18-7 MELCOR PA06 Gas Flow Rate

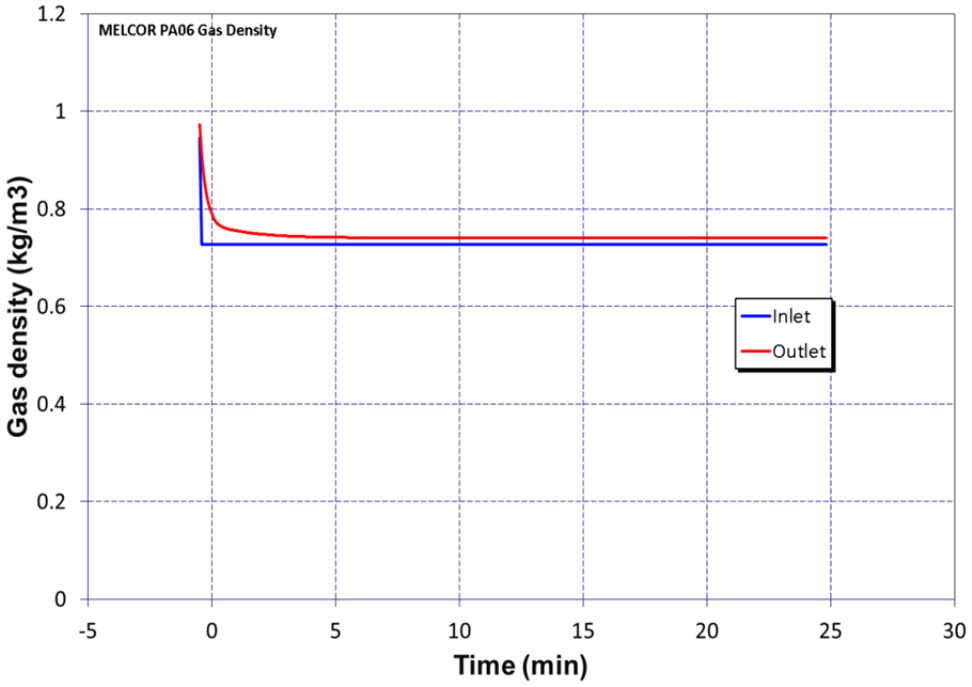

Figure 3.18-8 MELCOR PA06 Gas Density

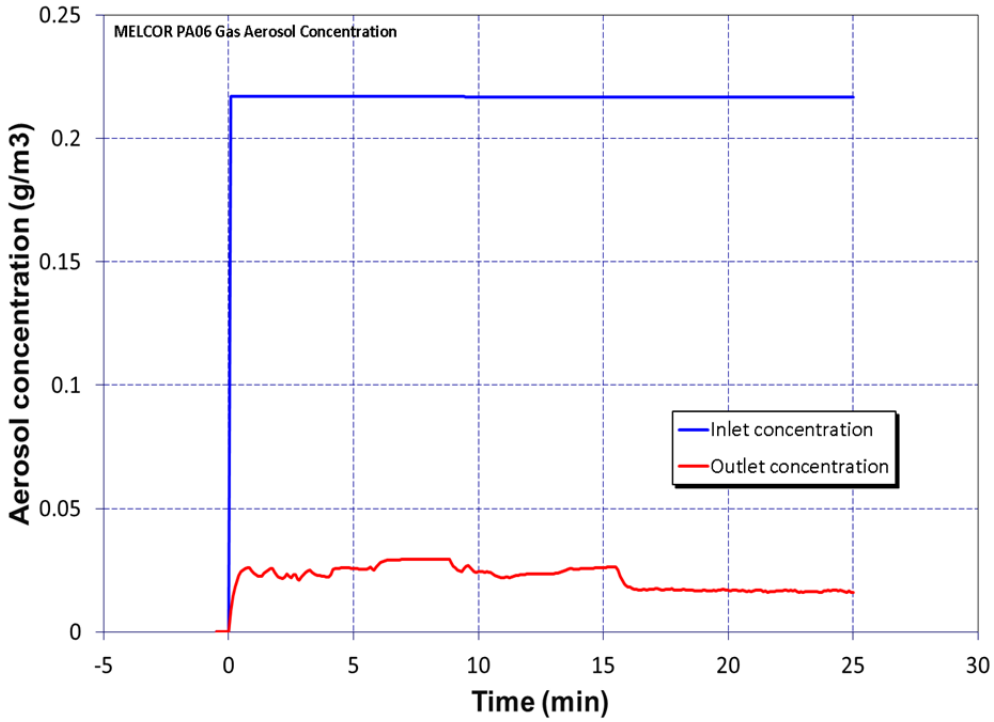

Figure 3.18-9 MELCOR PA06 Gas Aerosol Concentration

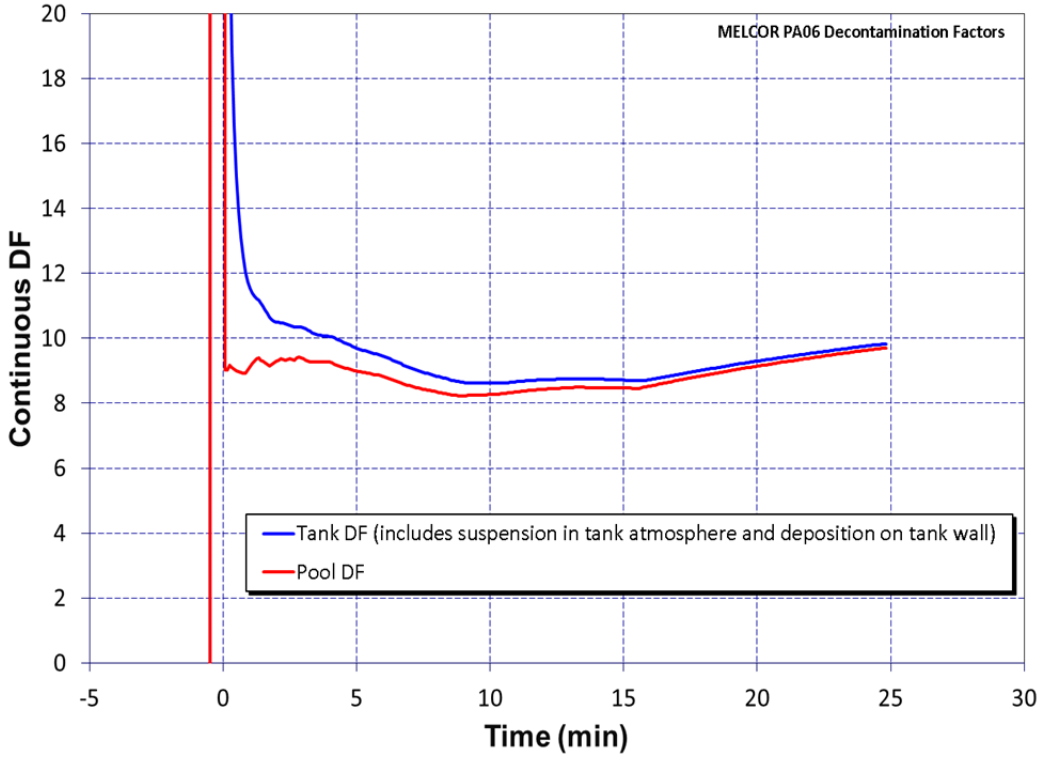

Figure 3.18-10 MELCOR PA06 Decontamination Factor

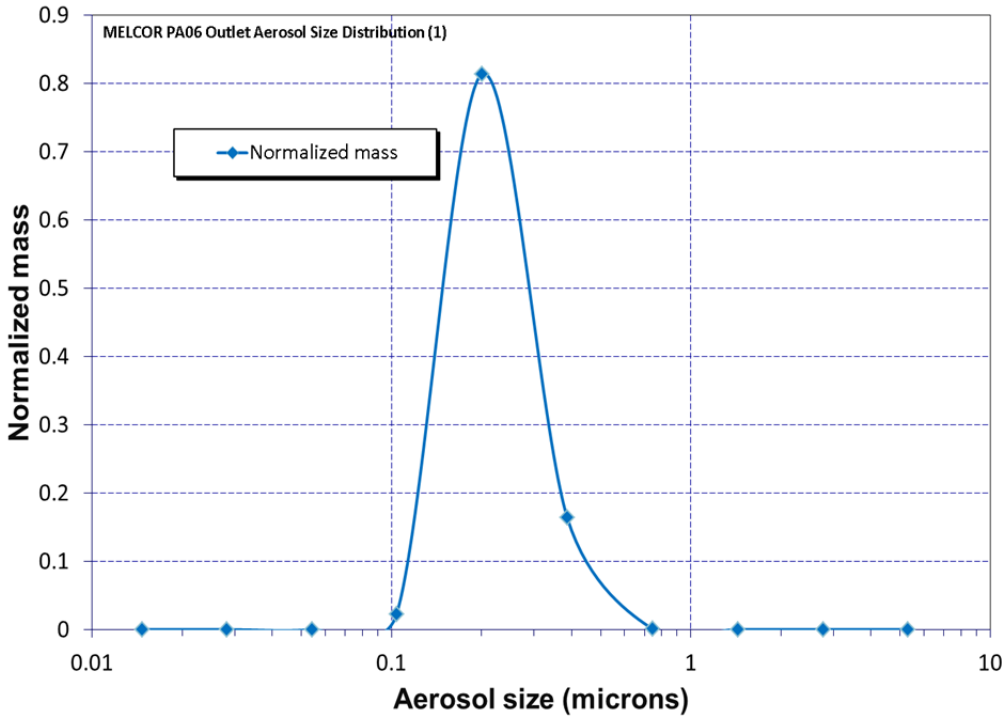

Figure 3.18-11 MELCOR PA06 Outlet Aerosol Size Distribution

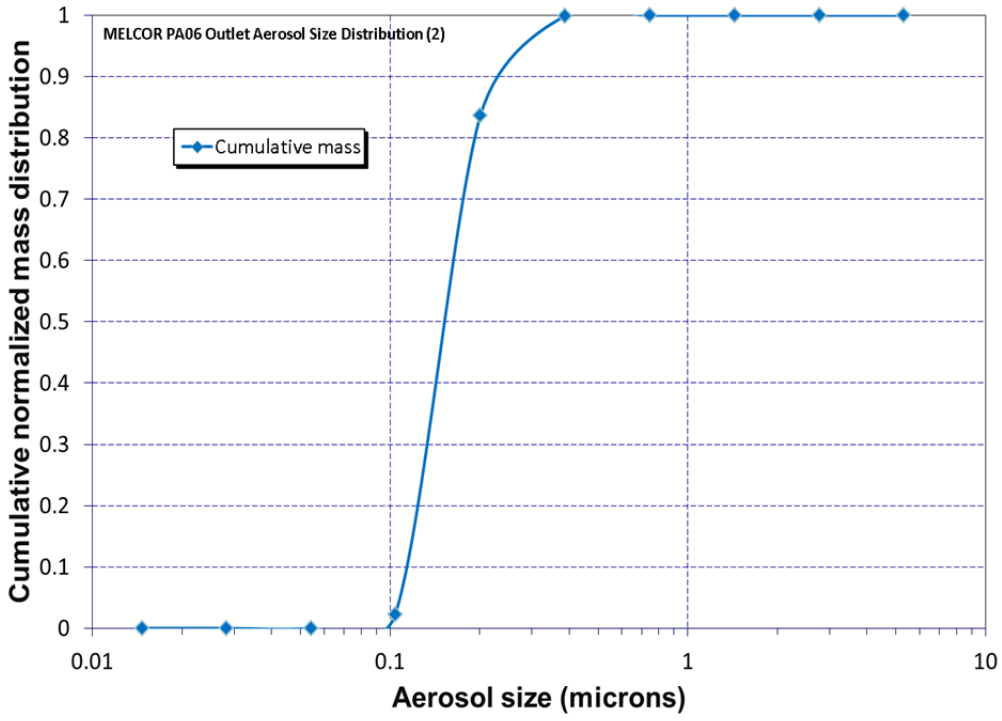

Figure 3.18-12 MELCOR PA06 Outlet Cumulative Aerosol Size Distribution

3.18.5 MELCOR 1.8.6 comparisons

To investigate the degree of agreement between MELCOR 2.1 and MELCOR 1.8.6 in simulating the POSEIDON experiments, a MELCOR 1.8.6 calculation was performed of Experiment PA06.While the thermal hydraulic results of the two code versions were virtually identical, the calculated DFs varied significantly, and the AMMD and GSD of the outlet particle size distributions varied slightly as presented in Table 3.18-3.

Table 3.18-3 Results comparison between MELCOR 2.1 and MELCOR 1.8.6 for PA06

	MELCOR 2.1	MELCOR 1.8.6
DF	9.85	27.75
AMMD	0.23	0.21
GSD	1.31	1.24

3.18.6 Results discussion

The trends in the MELCOR POSEIDON calculations correspond well with the trends in the POSEIDON experiments and are predictable. Specifically, in both the calculations and the experiments:

- A deeper pool resulted in more aerosol capture and a larger DF
- Having zero steam in the carrier gas led to less capture and a smaller DF
- Larger particles combined with greater steam content in the carrier gas led to more capture and a larger DF

The DF calculated by MELCOR for the deepest POSEIDON pool, i.e., 4 m, is considerably overestimated (169.0 compared to 21.4).

The DF calculated by MELCOR for a large particle size (relative to the other POSEIDON integral experiments) and a high fraction of steam in the carrier gas was significantly overestimated (31.5 compared to 12.3).

AMMD and GSD of the distributions of outlet particle size were consistently smaller in the MELCOR calculations than in the experiments.

There appear to be meaningful differences between DFs calculated by the 2.1 and 1.8.6 versions of MELCOR for the POSEIDON experiments, with Version 1.8.6 DFs generally greater. For PA06 this results in relatively poorer agreement, as the experimental DF of 7.3 +/- 1.42 (Table 3.18-2.) compares more favorably with the MELCOR 2.1 DF of 9.85 than the MELCOR 1.8.6 DF of 27.75.

A comment arising from the SNL independent review conducted of this MELCOR assessment was that deposition mechanisms addressed by the code other than gravitational would be better represented if physical density and diameter were defined (on input) rather than 1,000 kg/m3 and aerodynamic diameter. Brownian diffusion for example would be better represented. (Gravitational deposition will proceed identically whether physical density and diameter or 1,000 kg/m3 and aerodynamic diameter are defined). The potential differences in overall deposition that could result from changing the aerosol definition in the subject calculations were, however, judged to be small. Accordingly, the calculations were allowed to stand as presented here.

3.18.7 References

[3.18.1]A. Dehbi, D. Suckow, S. Guentay, “POSEIDON Integral Experiments Under Hot Pool Conditions”, Paul Scherrer Institute, TM-49-POS-1-97, March 1997.

Attachment: Selected Figures from Reference [3.18.1]

Figure 8: Gas pressures

Figure 9: Fluid temperatures

Figure 10: Gas steam mass fraction

Figure 11: Gas total flow rate

Experiment PA06

Figure 12: Gas density

Figure 13: Aerosol concentration

Figure 14: Pool decontamination factor

Figure 15: Outlet aerosol size distribution

3.19 Analysis of STORM Aerosol Mechanical Deposition Tests

3.19.1 Background

The International Standard Problem (ISP) No. 40 exercise was intended for examining the aerosol deposition and resuspension in pipes. The exercise was based on the STORM test SR-11 that took place in April 1977 and included two distinct phases: (1) aerosol deposition by thermophoresis and eddy impaction, and (2) aerosol resuspension under a stepwise increasing gas flow [3.19.1].

3.19.2 Experiment

The selection of the experimental conditions in the STORM tests was based on a detailed examination of a number of severe accident calculations for full light water reactor plants. The conditions selected corresponded broadly to those, particularly, that can be expected in the relief lines of a pressurized water reactor in a station blackout sequence.

As shown in Figure 3.19-1, the STORM test facility consists of gas and aerosol generators, a mixing vessel, a test section, and a wash and filtering system. Carrier gas and aerosol pass through the test section, which is a straight pipe that is 5.0 m long with a 6.3 cm inner diameter [3.19.1]. Because the STORM tests consist of two parts – deposition and resuspension – the sampling of the aerosols for both parts is also shown in this figure. The aerosol size distribution and concentration are measured upstream and downstream of the test section. To ensure resuspension, the test section is enclosed in an oven. The oven is open during the deposition phase to maximize the thermophoresis deposition and then it is closed and heated immediately at the beginning of the resuspension phase.

The deposition phase of test was done using a plasma torch, to generate aerosol while the carrier gas and steam/nitrogen mixture is fed through it to oxidize the tin vapor to form tin oxide (SnO_2) (see Table 3.19-1).

The flow rate of the aerosol (~3.83×10^{-4} kg/s) at the entrance of the test section is practically constant during the entire deposition phase of the experiment [3.19.1]. The particle size distribution is assumed log-normal with a 0.43 μm geometric mean diameter and a 1.7 geometric standard deviation [3.19.1]. An aerosol material density of 4000 kg/m^3 is used [3.19.1].

Since MELCOR does not model particle resuspension, the resuspension phase in the experiment is not described further.

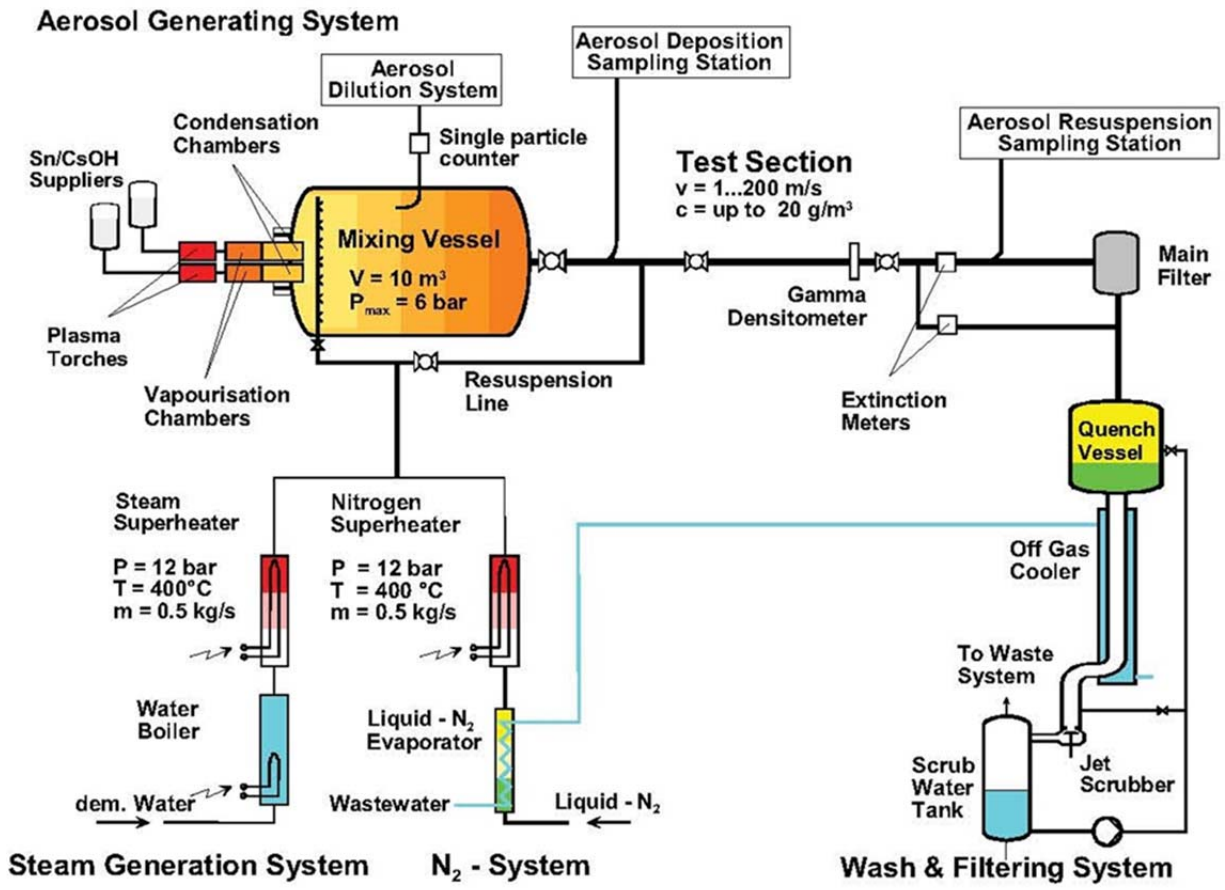

Figure 3.19-1 STORM Experimental Facility Setup [3.19.1]

Table 3.19-1 Carrier Gas Mass Flow Rate for the Deposition Phase [3.19.1]

Gas	Mass Flow Rate (kg/s)
Steam	1.1060×10^{-2}
Nitrogen	0.5467×10^{-2}
Air	0.5728×10^{-2}
Argon	0.7194×10^{-2}
Helium	0.0119×10^{-2}

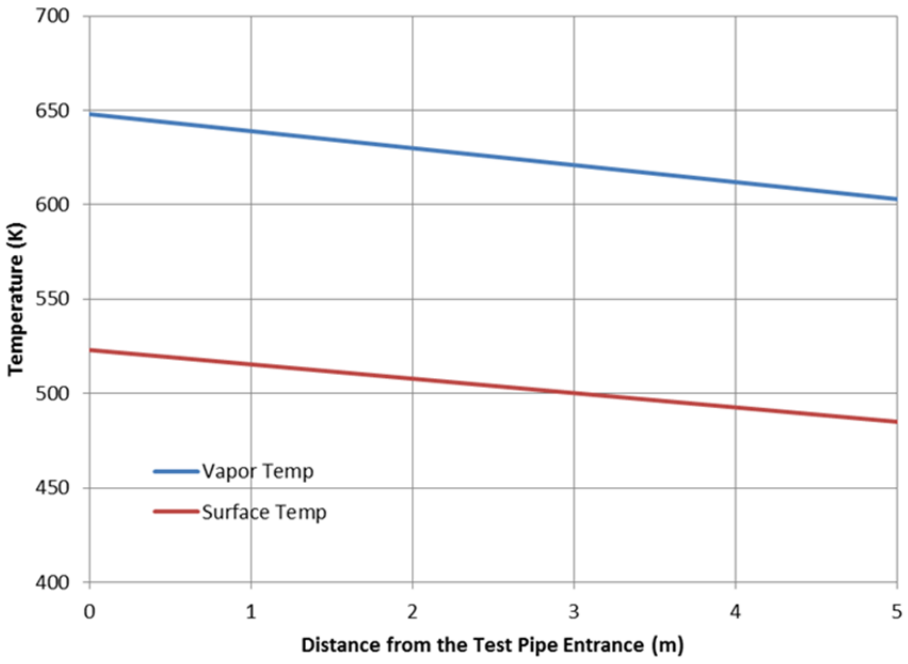

Figure 3.19-2 Experimental Temperature Profile along the Test Section [3.19.1].

3.19.3 MELCOR Model

The MELCOR nodalization was developed to model the test section into 5 equal-sized regions. Each is 1-meter long. An environment volume is connected to the last region of the test section. All sources are injected into first region of the test section. Cylindrical heat structures are used to model the wall of the test sections. A tabular function specifying the surface temperature is input for the right hand side of the heat structure (see Figure 3.19-2 for the surface temperature used). The initial atmospheric pressure of $1x10^5$ Pa is used for the test sections. A time-dependent heat transfer coefficient is applied to the left hand side of the heat structure. Two sensitivity studies are carried out: (1) varying heat transfer coefficients (HTCs), and (2) turbulent deposition model. Table 3.19-2 shows sensitivity studies done for this experiment. Note that the default option of 2.0 is used for both MELCOR 1.8.6 and 2.1 decks. Case 0 is the base case, which only invokes the default option of 2.0. The descriptions of the subsequent cases are also shown in this table. For Case 2 as shown in this table, the turbulent deposition model is invoked, which includes options: IMODEL=0 which is default; ITURB=2 for using Wood's model for rough pipes for this experiment; and ITRANS=0 which is also default.

Table 3.19-2 Sensitivity Runs Conducted

Case #	MELCOR 2.1 (v6110)	MELCOR 1.8.6 (v3964)
0	Default, aerosol GSD = 4.3E-7 m, DMIN=1E-7 m	Same as 2.1
1	Apply constant HTC of 30 W/m^2-K to the LHS of HS	Same as 2.1
2	Same as 1, except adding turbulent deposition in a straight pipe model with a pipe roughness of 5x10^{-5} m, Turbulent model options: IMODEL=0,ITURB=2, and ITRANS=0	Same as 2.1
3	Same as 1, except apply a constant HTC of 50 W/m^2-K to the LHS of HS	
4	Same as 1, except apply gradual increases of HTC from the entrance of the test sections from 30 to 44 W/m^2-K.	
5	Same as 1, except apply constant HTC of 60 W/m^2-K to the LHS of HS	

3.19.4 Discussions and Results

A number of runs are conducted for both MELCOR 1.8.6 and 2.1 (see Table 3.19-2). As shown in this table, the use of the HTC input is to enable the SnO_2 deposition for the inner pipe wall via thermophoresis. Without this input, the gas temperature did not change significantly along the pipe sections, which yields very minimal aerosol deposition. By adding this HTC input, the gas temperature drops along the pipe sections (see Figure 3.19-3). As shown in Figure 3.19-4 for MELCOR 2.1, by increasing the HTC values to the pipe wall, the gas temperature in the pipe sections drops more significantly (see the definition of each Case in this figure within Table 3.19-2). Note that all cases modeled with MELCOR had gas temperatures below the experimental values. The closest calculated gas temperature is the default case (Case 0), where no HTC is imposed. The next closest cases are Case 1 and Case 2 with a constant HTC of 30 W/m^2-K. The largest disagreement of MELCOR with the data for the gas temperature is for a constant HTC of 60 W/m^2-K (Case 5). The resulting aerosol deposition is opposite to that of Figure 3.19-5. As shown in this figure, the closest calculated deposition mass to the experiment's value is Case 5, and the furthest is Case 1. Case 4 shows variable HTC along the pipe. The deposition in this case falls further away from the data values, as the HTC increases along the pipe. The maximum HTC is 44 W/m^2-K, which is still smaller than the constant HTC cases of Case 3 and Case 4. Because the flow velocity through the pipe is relatively high, on the order of 10 m/s,

turbulent aerosol deposition should be included for the straight pipe. Therefore, the activation of the turbulent deposition for Case 1 is included as Case 2. As shown in Figure 3.19-6, the inclusion of the turbulent deposition yields a higher deposition mass. Note there should be no gas temperature difference between Case 1 and Case 2, because the HTC values are the same for both cases.

For Case 2, the contribution of each settling deposition model for MELCOR 2.1 is provided in Figure 3.19-7. As shown in this figure, the contribution from thermophoresis is highest, as expected, followed by turbulent deposition and gravitational contributions. At about 2 m from the entrance, turbulent deposition surpasses gravitational deposition. The smallest contribution to the overall deposition is due to diffusive deposition. The dominance of thermophoresis deposition is consistent with Reference 1.

In comparison with MELCOR 1.8.6, Figure 3.19-8 and Figure 3.19-9 show the gas temperature and cumulative deposition results for Case 2, respectively As shown in these figures, there are virtually no differences between MELCOR 1.8.6 and 2.1.

3.19.5 Conclusions

The use of the fixed heat transfer boundary at the pipe walls increases thermophoresis deposition. By doing so, the aerosol deposition calculated by MELCOR agrees well with the experimental data. However, this modeling would reduce agreement with the measured gas temperature. There are no differences in the calculation results between MELCOR 1.8.6 and 2.1 for any given case. Note that only the deposition phase of the experiment was simulated. Once the physics model for aerosol resuspension is added to MELCOR, the resuspension phase of the experiment can be assessed.

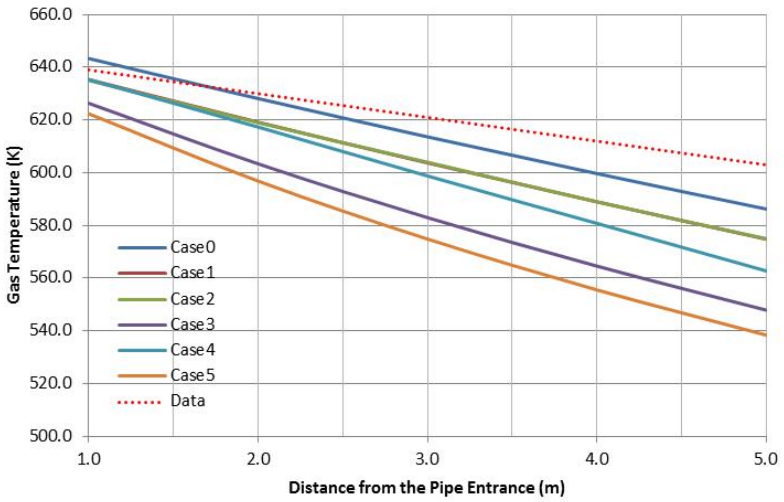

Figure 3.19-10 Gas Temperature for Various Cases in MELCOR 2.1

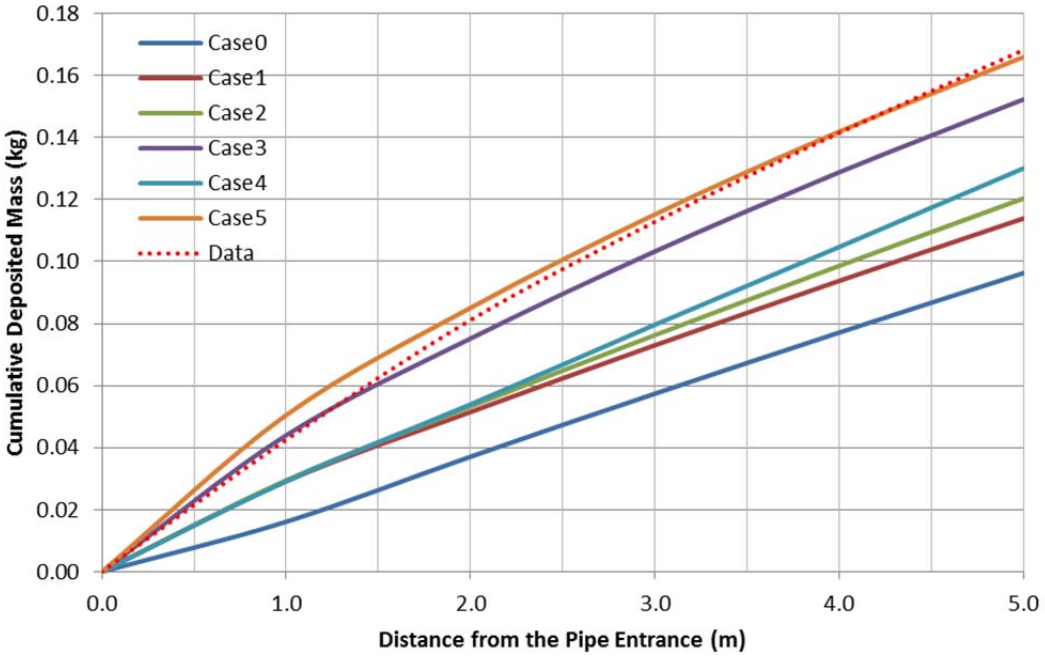

Figure 3.19-11 Cumulative Deposited Mass for Various Cases in MELCOR 2.1

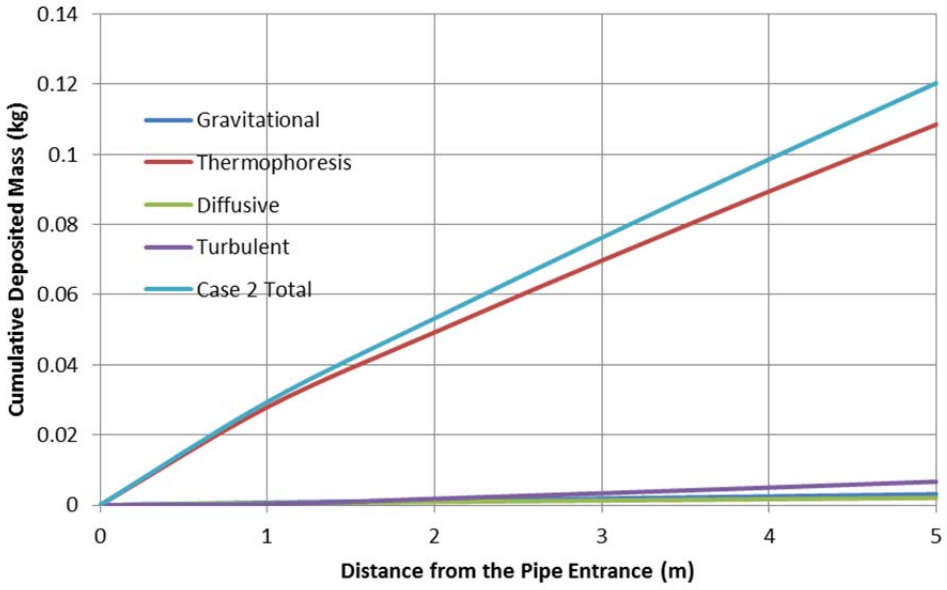

Figure 3.19-12 MELCOR 2.1 Case 2 Results with Individual Deposition Process Contribution

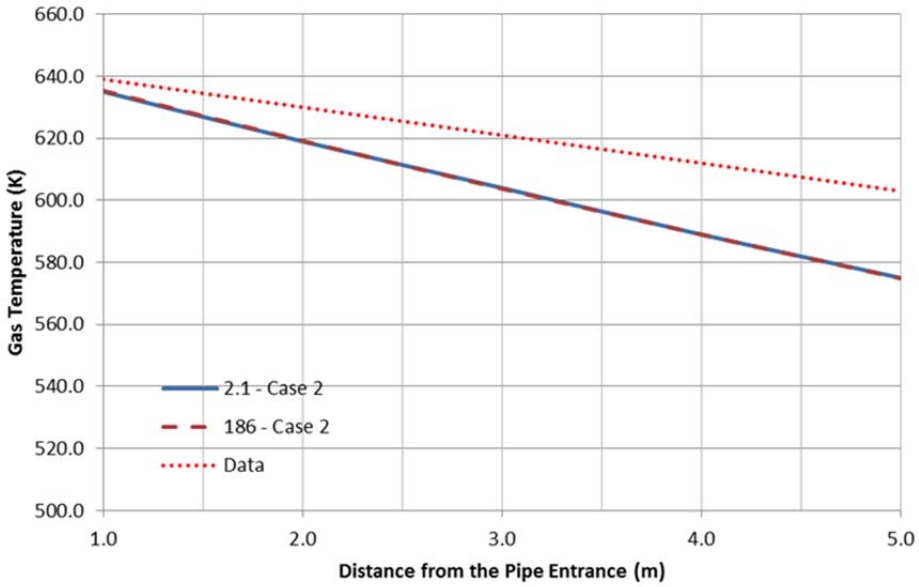

Figure 3.19-13 Comparison of MELCOR 1.8.6 and MELCOR 2.1 for Gas Temperature for Case 2

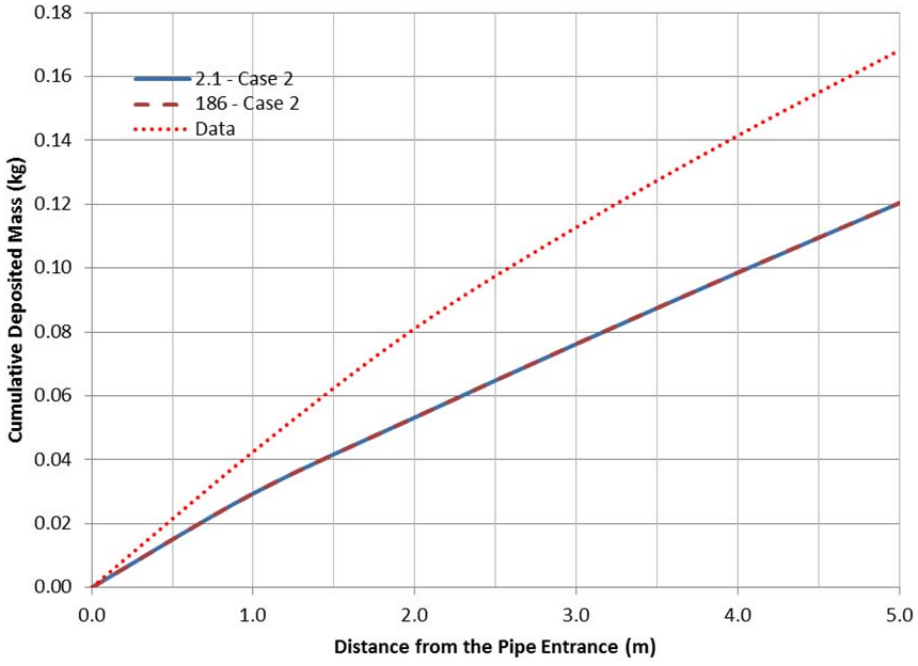

Figure 3.19-14 Comparison of MELCOR 1.8.6 and 2.1 for Cumulative Deposited Mass for Case 2

3.19.6 References

[3.19.1] International Standard Problem 40 - Aerosol Deposition and Resuspension, Final Comparison Report, NEA/CSNI/R(99)4, Joint Research Centre European Commission, February 1999.

[3.19.2] N.E. Bixler, et.al, “Recent MELCOR and VICTORIA Fission Product Research at NRC,” SAND99-0179C, Sandia National Laboratories, December 1998.

3.20 Melt Coolability and Concrete Interaction Experiments CCI-1, CCI-2 and CCI-3

3.20.1 Background

The OECD-sponsored Melt Coolability and Concrete Interaction (MCCI) program was conducted to resolve ex-vessel debris coolability issues, and to investigate molten core-concrete interaction phenomena. Particular areas of interest were the rates of concrete lateral and axial erosion, gas/aerosol generation, top crust formation and strength, and melt cooling via eruption through the top surface. CCI-1, CCI-2 and CCI-3 are part of the first phase of the CCI tests. This first phase was mostly intended to investigate erosion with different concretes. The second phase of three tests was intended to investigate effects of scale and bottom coolability. The MCCI program was a follow-on to the EPRI-sponsored Melt Attack and Coolability Experiments (MACE) and included other test series such as the Melt Eruption Tests (MET) and Small-Scale Water Ingression and Crust Strength (SSWICS).

3.20.2 MCCI experiments

3.20.2.1 General

The MCCI experiments were conducted in a facility developed for the MACE tests. The experimental rig consisted of a rectangular model of a concrete cavity with two of the walls containing tungsten electrodes to directly heat the melt via direct electric heating (DEH). However, although MACE developed a “circular” cross-section as a result of erosion of the concrete in the electrode walls, CCI used MgO walls and was a two-dimensional (2D) experiment with side erosion only in one direction.

The experiments used fully oxidized PWR melt simulant with 2D concrete test sections. The melt was initially formed using a thermite burn, then heated using by DEH. The power level was chosen to represent a range of expected heat fluxes in the early stages of an ex-vessel reactor accident.

3.20.2.2 Experiment Setup

The test apparatus is shown in Figure 3.20-1. It consists of the test chamber, the lower part of which is the concrete/MgO walls and bottom, provision for flooding the melt, a penetration lance to test the crust strength, and plumbing to condense/collect steam. The internal atmosphere of the apparatus is initially helium. No attempt was made to analyze evolved gas/aerosols; they were filtered out in the outlet from the rig. Top and side cross-sections of the test chamber are shown in Figure 3.20-2 and Figure 3.20-3.

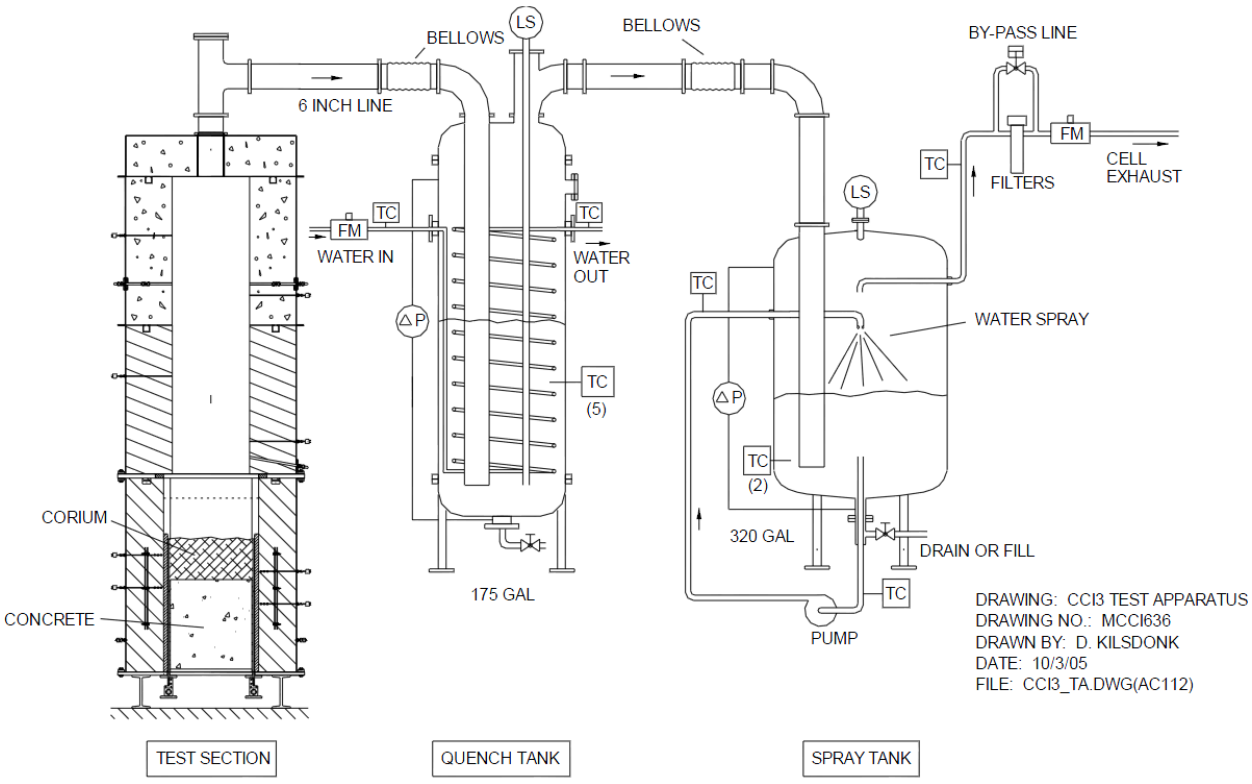

Figure 3.20-1. MCCI experimental setup

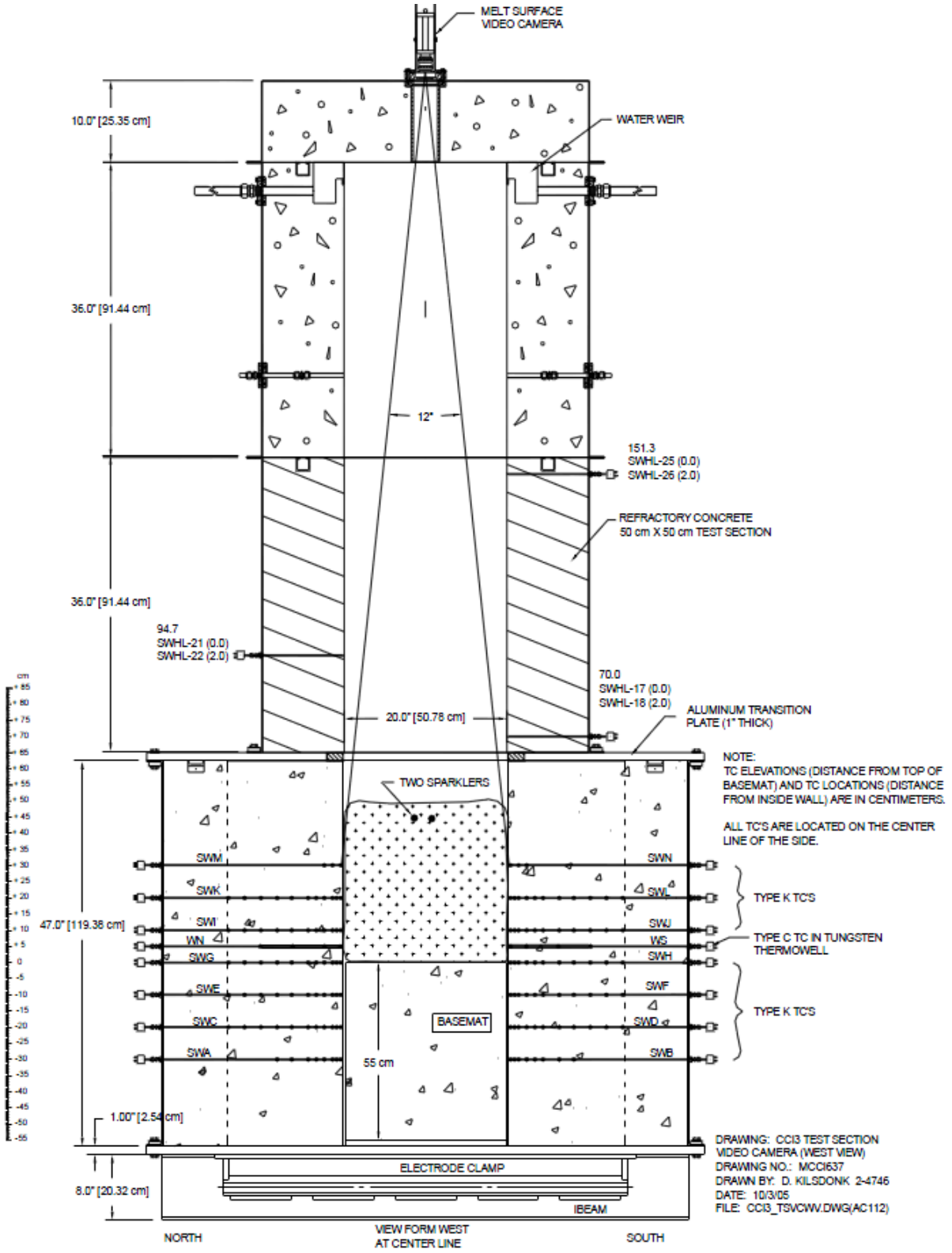

Figure 3.20-2. Details of the test section

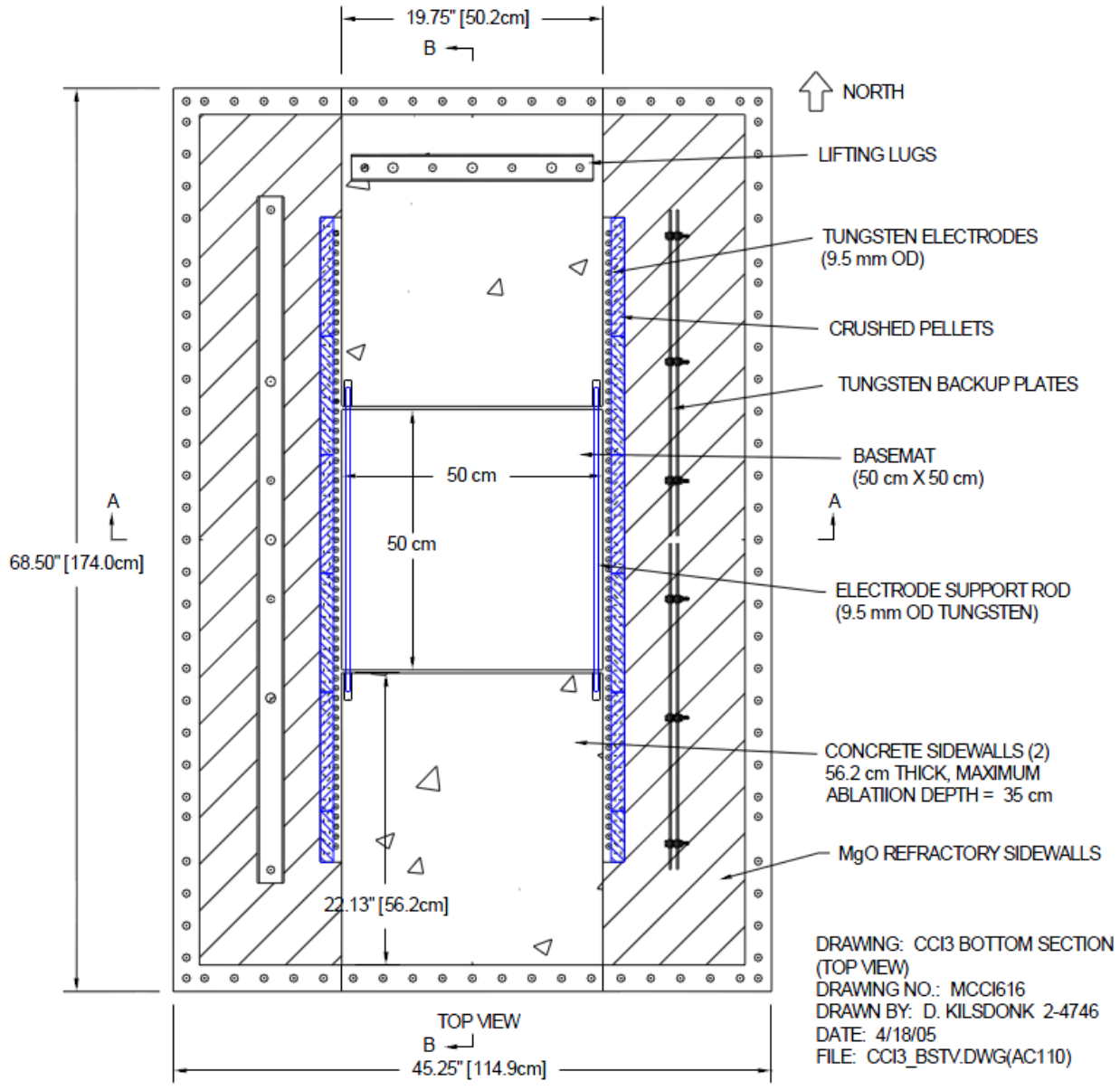

Figure 3.20-3. Top view of lower test section

The experiments chosen for analysis with MELCOR, CCI-1, CCI-2, and CCI-3 (similar to CCI-1) differ mainly in the choice of concrete (limestone/sand and siliceous). CCI-1 can be compared to CCI-3, which was the same setup but exhibited uniform lateral ablation, versus CCI-1, which was highly non-uniform.

The specifications for the CCI-1/CCI-3 and CCI-2 tests are given in Table 3.20-1.

Table 3.20-1. CCI series test specifications

Parameter	Specification for Test:	
	CCI-1/CCI-3	**CCI-2**
Corium	PWR + 8 wt% SIL	PWR + 8 wt% LCS
Concrete type[a]	SIL (US type)	LCS
Basemat cross-section	50 cm x 50 cm	50 cm x 50 cm
Initial melt mass (depth)	400 kg (25 cm)	400 kg (25 cm)
Lateral/Axial ablation limit	35/35 cm	35/35 cm
System pressure	Atmospheric	Atmospheric
Initial melt temperature	1950 °C	1880 °C
Power supply	150 kW	120 kW
Criteria for water addition	5.5 h of operation, or lateral/axial ablation reaches 30 cm	5.5 h of operation, or lateral/axial ablation reaches 30 cm
Inlet water flow rate	2 liter/s at 20 °C	2 liter/s at 20 °C
Water depth over melt	50 ± 5 cm	50 ± 5 cm
Test termination criteria	Melt temperature < concrete liquidus, ablation halted, 35 cm ablation limit reached	Melt temperature < concrete liquidus, ablation halted, 35 cm ablation limit reached
[a]SIL is siliceous, LCS is Limestone/Common Sand concrete		

3.20.2.3 CCI-1

The actual sequence of events in CCI-1 is given in Table 3.20-2.

Table 3.20-2. CCI-1 experiment events

Time (minutes)	Event
0.00	Thermite burn completed, results in initial melt temperature is 2050 °C
0.36-0.46	Onset of ablation
2.80	Full DEH power reached
65.83	Crust lance probe used to break crust
67.65	Water addition started (29.2 cm ablation)
78.55	DEH power terminated, nearing max ablation limit of 35 cm
119.72	Data acquisition terminated

As can be seen, the experiment was terminated early due to the ablation limit being reached in one sidewall. This test had a very asymmetric lateral ablation. Also, there is a slight delay in the onset of ablation due to initial formation of a crust on the sidewalls.

3.20.2.4 CCI-2

The actual sequence of events in CCI-2 is given in Table 3.20-3.

Table 3.20-3. CCI-2 experiment events

Time (minutes)	Event
0.00	Thermite burn completed, results in initial melt temperature 2000 °C
0.10-0.38	Onset of ablation
1.56	Full DEH power reached
5.0-23.0	Quiescent melt, then eruptions and churning
298.9	Crust lance tried to break crust
300.79	Water addition started
312.6	DEH power switched to constant voltage (power falls)
423.1	Data acquisition terminated

3.20.2.5 CCI-3

The actual sequence of events in CCI-3 is given in Table 3.20-4.

Table 3.20-4. CCI-3 experiment events

Time (minutes)	Event
0.00	Thermite burn completed, results in initial melt temperature is 1950 °C
0.0-0.8	Onset of ablation
1.6	Full DEH power reached
104.7	Crust lance probe used to break crust
107.6	Water addition started (29.2 cm ablation)
146.4	DEH power terminated, nearing max ablation limit of 35 cm
173.3	Data acquisition terminated

3.20.2.6 MELCOR input specifications

The problems were set up generally following the approach in a scoping study done using MELCOR 1.8.5. [3.20.1]. The problems have 1 CV representing the test section and 1 CV as the environment. The CAVITY model was initialized as per the experiment specifications in Table 3.20-1, with the test section dimensions and concrete compositions taken from reference [3.20.2]. The rectangular lower test section was approximated as a circular cylinder in MELCOR with the cylinder cross-section the same area as the 50x50 cm test section, 1.2 m high. One melt layer was used in the CAVITY model, with 400 kg melt mass. The ablation temperature for the concrete is taken as the concrete liquidus temperature [3.20.3]. The flooding was modeled as a water source into the test section CV started at the time given in the experiment events

tables, and the water height maintained at 50 cm depth, as per the experimental specification, using a CF that monitored the collapsed liquid level CLIQLEV in the CV.

For these tests, the user input parameter HTRINT (enabled using CAV_SC 2309(10)) was set to 5.0 to enhance the heat transfer to the top of the melt, and COND.CRUST was set to 3.0 (increases the conductivity of the top crust). Using these parameters requires MELCOR 2.1 Revision 4909 or greater. Note that MELCOR 2.1 revision 6110 was used to generate the following results and that MELCOR 1.8.6 was not used to model the CCI experiments.

3.20.3 Results

3.20.3.1 CCI-1

The experimental results were, as mentioned, a very non-uniform sidewall ablation. A large difference was also observed in the lateral/axial ablation rates, which was also seen in CCI-3. The lateral was 10 cm/hr during the last hour, whereas the axial was 2.5 cm/hr. The corresponding heat fluxes into the walls were 97 and 25 kW/m^2 respectively. These results are given in Table 3.20-5 along with the MELCOR calculation results. The radial ablation depth compares fairly well, and the axial ablation is a factor of 1.5 too high. A second MELCOR run done with the cavity sidewall and bottom film models set to 'SLAG' yielded almost identical results. The initial delay in ablation caused by the formation of crusts on the walls is not seen in the MELCOR simulation.

Table 3.20-5. CCI-1 Comparison with MELCOR

Parameter	CCI-1 Experiment	MELCOR 2.1 (rev 6110)
Sidewall ablation depth (cm)	7.6 and 34.3	15.1
Basemat ablation (cm)	7.6	10.5
Lateral rate (cm/h)	10	4.0
Axial rate (cm/h)	2.5	4.3

A sketch of the experiment end-state is seen in Figure 3.20-4 [3.20.4], and the result of the MELCOR calculation is seen in Figure 3.20-5.

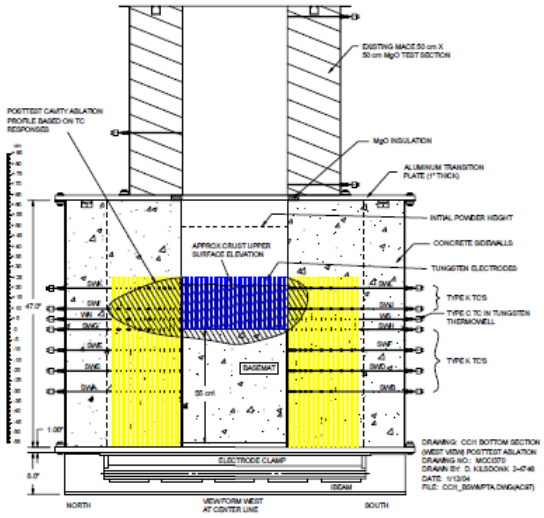

Figure 3.20-4. CCI-1 final state

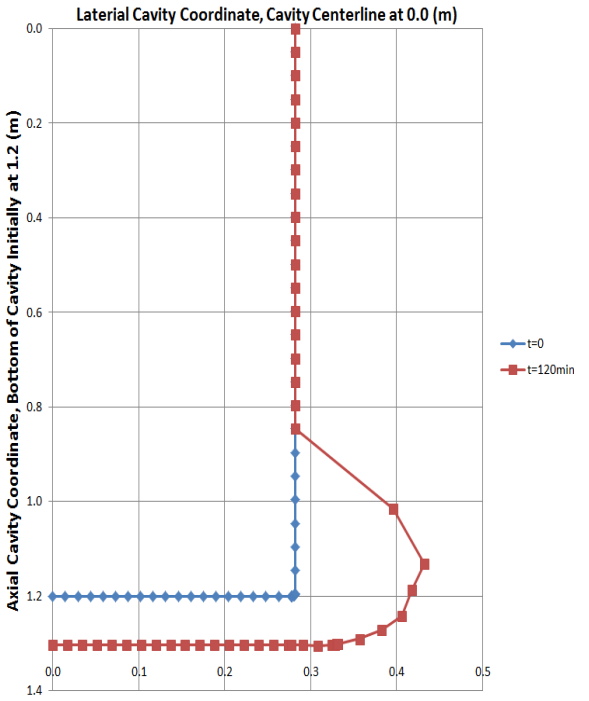

Figure 3.20-5. MELCOR CCI-1 cavity shape

3.20.3.2 CCI-2

In CCI-2, the lateral/axial ablation rates were about the same, 4 cm/h, with a corresponding heat flux of 60 kW/m^2. This difference from CCI-1 is probably due to the much higher gas release from the limestone/sand concrete in CCI-2 compared to the siliceous in CCI-1. These results are given in Table 3.20-6 along with the MELCOR calculation results. The MELCOR results compare well, except for a smaller axial ablation depth.

Table 3.20-6. CCI-2 Comparison with MELCOR

Parameter	CCI-1 Experiment	MELCOR 2.1 (rev 6110)
Sidewall ablation depth (cm)	30	28.1
Basemat ablation (cm)	30	19.6
Lateral rate (cm/h)	4	3.5
Axial rate (cm/h)	4	1.9

A sketch of the experiment end-state is seen in Figure 3.20-6 [3.20.5], and the result from MELCOR is seen in Figure 3.20-7.

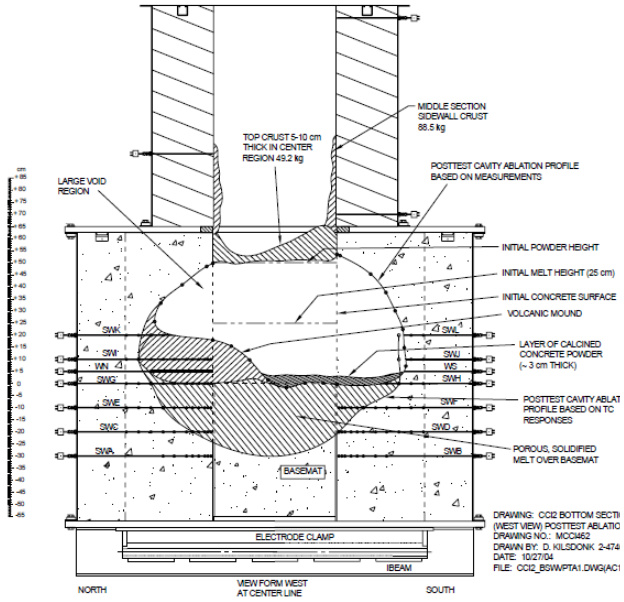

Figure 3.20-6. CCI-2 final state

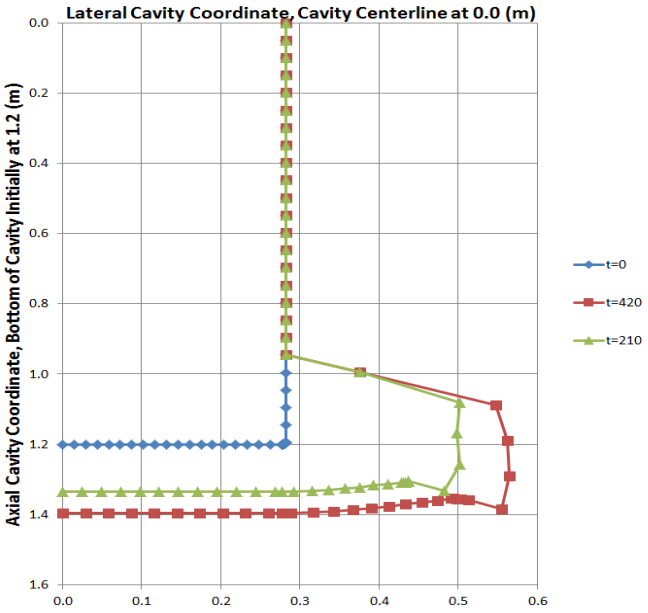

Figure 3.20-7. MELCOR CCI-2 cavity shape

3.20.3.3 CCI-3

A 4x difference was observed in the lateral/axial ablation rates, which was also seen in CCI-1. The lateral was 10 cm/h during the last hour, whereas the axial was 2.5 cm/h. The corresponding heat fluxes into the walls were 97 and 25 kW/m^2 respectively. These results are given in Table 3.20-7 along with the MELCOR calculation results. The radial ablation depth is somewhat low, and the axial ablation is a factor of 2 too high.

Table 3.20-7. CCI-3 Comparison with MELCOR

Parameter	CCI-3 Experiment	MELCOR 2.1 (rev 6110)
Sidewall ablation depth (cm)	34/27	17.1
Basemat ablation (cm)	5	11.2
Lateral rate (cm/h)	10	3.5
Axial rate (cm/h)	2.5	3.2

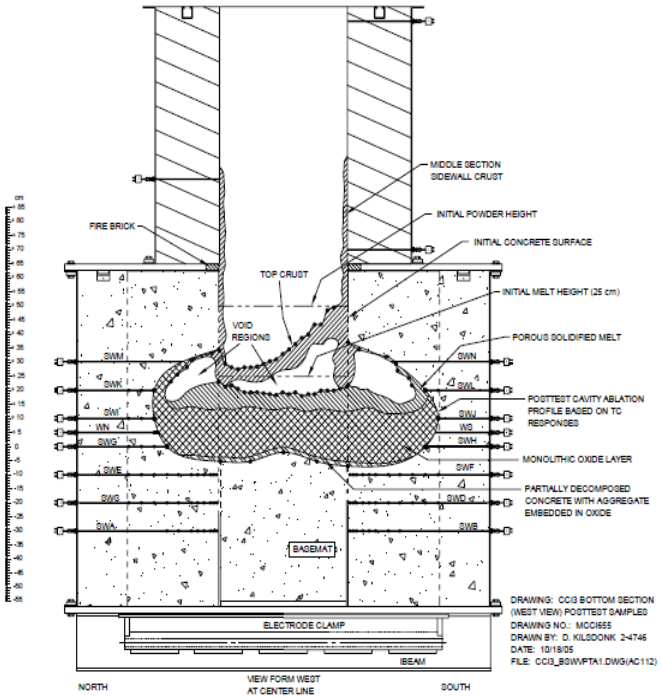

Figure 3.20-8. CCI-3 final state

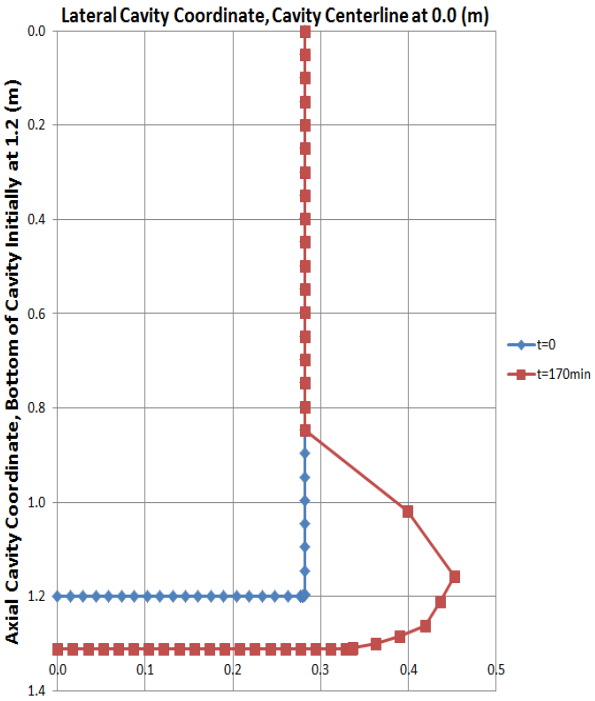

Figure 3.20-9. MELCOR CCI-3 cavity shape

3.20.4 Comparison to CAV 1.86 Defaults

Comparison runs were done using MELCOR 2.1 (rev 6110) with CAV 1.8.6 defaults. The ablation depths are shown in Table 3.20-8. In general, the peak top heat fluxes were less for the 1.86 defaults.

Table 3.20-8. Comparison of results with CAV 1.86 defaults vs 2.1

	MELCOR 2.1		MELCOR 2.1 with CAV 1.8.6 Defaults	
Parameter	**Sidewall ablation depth (cm)**	**Basemat ablation (cm)**	**Sidewall ablation depth (cm)**	**Basemat ablation (cm)**
CCI-1	15.1	10.5	16.4	9.3
CCI-2	28.1	19.6	29.7	20.0
CCI-3	17.1	11.3	18.8	10.4

3.20.5 Discussion

Generally, the MELCOR results compare fairly well with the experiments, as far as the rates are concerned. The axial ablation distance in CCI-1 and CCI-3, however, are not such a good match, most likely because of the difference in geometry – MELCOR does a radial ablation, causing the melt to spread quite a bit, whereas in the CCI experiments, the lateral ablation is in one direction only, resulting in less spreading. There is no treatment in MELCOR of the top cooling caused by melt eruptions, and although the increased heat loss was simulated by increasing the top heat transfer parameters, this is not a complete solution and of course is not phenomenological. Some of these issues should be addressed with the addition of the water ingression and melt eruption models adapted from CORQUENCH.[3.20.6]

3.20.6 References

[3.20.1] H. Ley, “MELCOR Parameter Studies for 2-D Molten Core Concrete Interaction Experiments,” (2002).

[3.20.2] M.T. Farmer, et al., “OECD MCCI Project 2-D Core Concrete Interaction (CCI) Tests: Final Report,” OECD/MCCI-2005-TR05, Argonne Nation Laboratory, Argonne, IL (2006).

[3.20.3] M.F. Roche et al., “Solidus and Liquidus Temperatures of Core-Concrete Mixtures,” NUREG/CR-6032, ANL-93/9, Argonne National Laboratory, Argonne, IL (1993).

[3.20.4] M.T. Farmer et al., “OECD MCCI Project 2-D Core Concrete Interaction (CCI) Tests: CCI-1 Test Data Report-Thermalhydraulic Results,” OECD/MCCI-2004-TR01, Argonne National Laboratory, Argonne, IL (2004).

[3.20.5] M.T. Farmer et al., “OECD MCCI Project 2-D Core Concrete Interaction (CCI) Tests: CCI-2 Test Data Report-Thermalhydraulic Results,” OECD/MCCI-2004-TR05, Argonne National Laboratory, Argonne, IL (2004).

[3.20.6] M.T. Farmer, “OECD MCCI Project The CORQUENCH Code for Modeling of Ex-Vessel Corium Coolability under Top Flooding Conditions”, OECD/MCCI-2010-TR03, Argonne National Laboratory, Argonne, IL (2011).

4. Comparisons of Code Versions

Many of the validation analyses referenced in this report were performed with earlier versions of the MELCOR code, since a completed publication of the MELCOR 1.8.6 validation is not available [4.1] through [4.14]. However, given the level of maturity in many of the existing MELCOR physics models, essential validation exercises for the most part are not strongly dependent on the code version. Even so, small modeling changes and coding errors can impact results. Therefore a discussion of code version and the impact on validation is in presented here.

SNL is currently updating the validation report for MELCOR Version 2.1. MELCOR Version 2.1 is largely identical to Version 1.8.6 with respect to model pedigree, the main difference being conversion of the source code to FORTRAN 95. Changes made to 2.0 subsequent to its release have mainly affected new modeling for high temperature gas reactors. Significant code corrections made to 2.x were also made in the 1.8.6 version and made available to the SOARCA analysis team. In any event, the 2.1 validation report will also present validation results using MELCOR 1.8.6 for many of these analyses, since a comprehensive validation report was never published for that code version.

In order to better appreciate the significance of the historical validation analyses, an evolution of code development with code versions is required. Appendix B provides a list of major code modifications that were made to the code during the development cycle. Note that this list only considers those physics models that may be directly related to these assessments and the SOARCA project. It does not contain many usability features and physical models that were not used in the SOARCA project, such as the point kinetics and the intermediate heat exchanger models. It also does not catalogue model corrections and other bugs that were addressed.

Finally, since many of the historical validation cases have already been updated with Version 2.1, the following sections provide comparisons of select computational results with the historic code assessment analysis. However, it is not the intention of this report to reproduce the details of the validation report here. Instead, the following discussions focus on a few physical models assessed.

4.1 Airborne Physics

MAEROS is a multisectional, multicomponent aerosol dynamics code that evaluates the size distribution of each type of aerosol mass, or component, as a function of time. MELCOR uses the MAEROS code for modeling aerosol agglomeration and deposition processes of nonhygroscopic aerosols. The MAEROS models have been in the code since MELCOR Version 1.8.0 with only error corrections and extension since. Hygroscopic models were added to the code in Version 1.8.4.

Agglomeration of non-hygroscopic aerosols from condensation of water vapor is assessed in the ABCOVE [4.2] and DEMONA experiments. Figure 4-1 shows the non-hygroscopic aerosol mass calculated for 1.8.2, 1.8.6, and 2.x, together with data from the AB-5 test. Note for this simple one volume calculation, the results have not changed noticeably since the early versions of the code. Similarly, the DEMONA test shows depletion of SnO_2 due to condensation on the non-hygroscopic aerosol (see Figure 4-2. These examples demonstrate the version independence of such calculations.

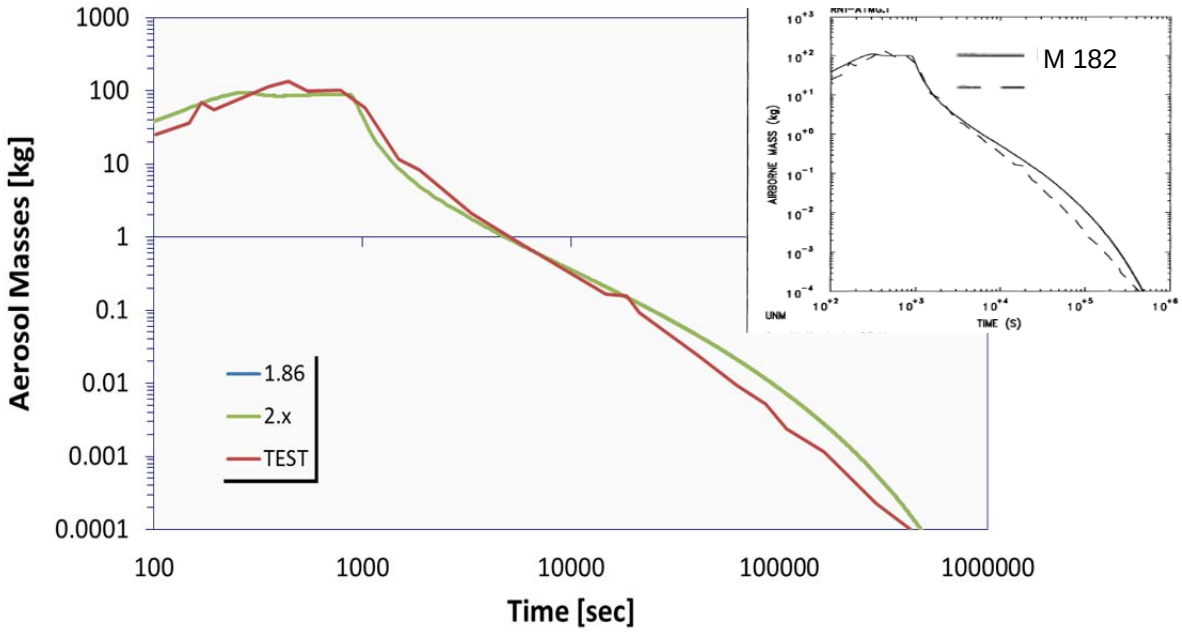

Figure 4-1 CSTF Airborne Mass Test AB5

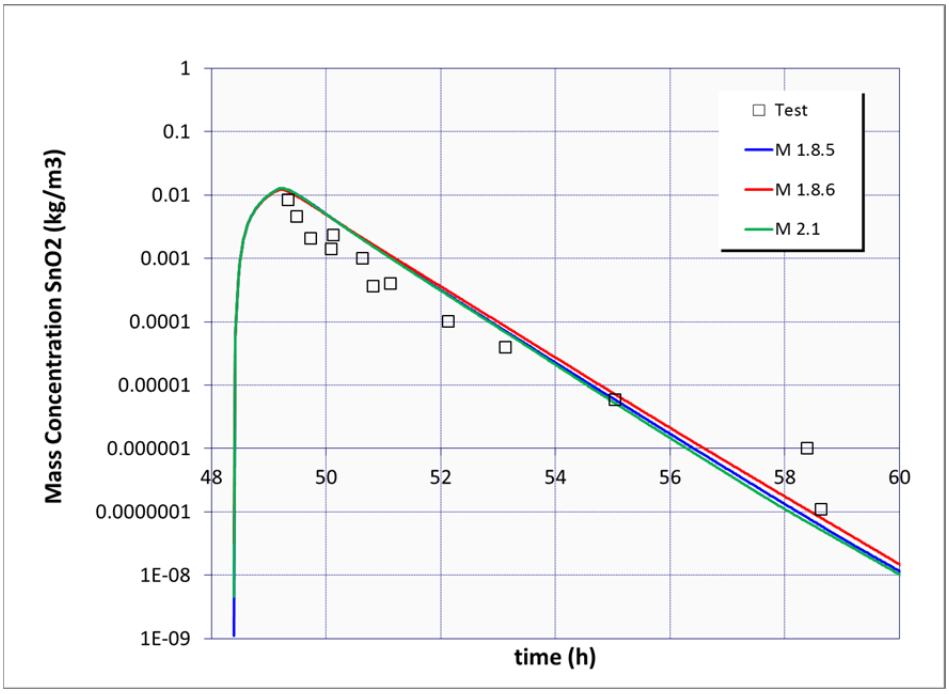

Figure 4-2 Depletion of SnO2 in DEMONA-B3 experiment

4.2 Oxidation

Metal oxidation is calculated using standard parabolic kinetics, with appropriate rate constant expressions for Zircaloy and steel, limited by gaseous diffusion considerations if necessary. For the Zircaloy-H2O reaction, the rate constant is evaluated using the Urbanic-Heidrich constants. Though these constants and equations have not changed since they were first implemented into the code, other changes to the code can lead to changes in clad temperature, surface areas, and oxidation thickness histories. Therefore, changes in results are not so much indicative of changes to the oxidation models as they are changes in the core heatup and degradation modeling. **Figure 4-3** and **Figure 4-4** show the hydrogen generation calculated for the Phebus-B9+ and FPT-1 assessment cases respectively, using MELCOR Versions 1.8.5, 1.8.6, and 2.1. Note that only minor differences are observed for these three code versions. There is a slight trend in the data showing that MELCOR 1.8.5 predicted higher hydrogen generation than MELCOR 2.1 and MELCOR 1.8.6 and that all three versions slightly overpredict the cumulative hydrogen generation.

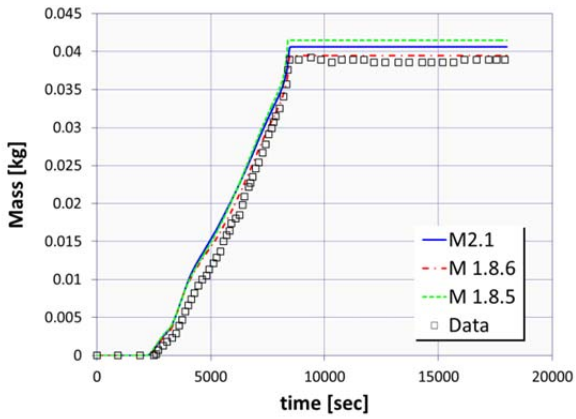

Figure 4-3 PHEBUS-B9+ hydrogen generation

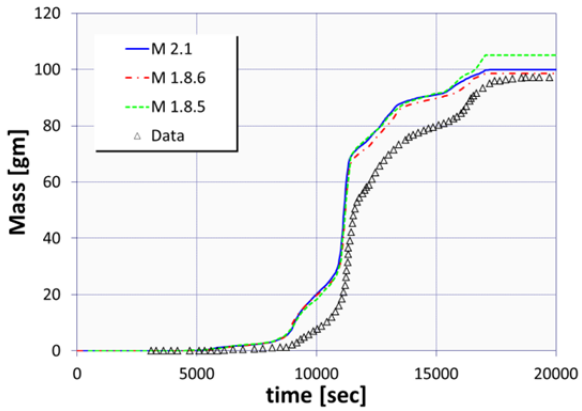

Figure 4-4 FPT-1 hydrogen generation

4.3 Hydrogen Stratification in Containment

Because of its lower density than surrounding air, hydrogen in a containment would concentrate in higher regions of the containment. It is important to be able to capture this stratification to predict local regions of flammability. The NUPEC 8-8-1 mixing test provides an excellent validation of MELCOR's capabilities for calculating stratification of helium in a large, compartmentalized containment. The M 1.8.5 input deck was converted to M1.8.6 and then to M 2.x, using SNAP as the converter. Though there are noticeable discrepancies between calculations and test data, it is important to observe that all three code versions give identical results (see Figure 4-5 and Figure 4-6). Overall, MELCOR does a reasonable job of capturing helium stratification for these tests.

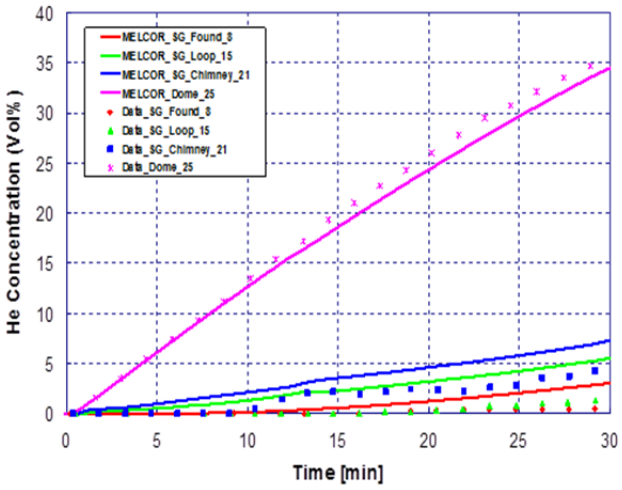

Figure 4-5 Helium stratification calculated for NUPEC M-8-1 for MELCOR 2.x

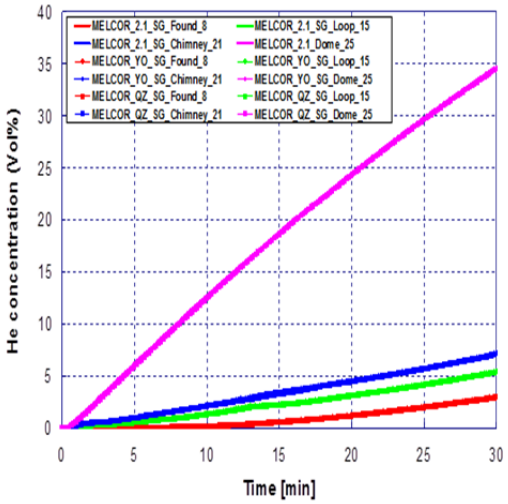

Figure 4-6 Helium stratification calculated for NUPEC M-8-1 for three MELCOR code versions

4.3.1 Combustion Modeling

MELCOR uses relatively simple models for burning of premixed gases without modeling the actual reaction kinetics or tracking the actual flame front propagation based on the HECTR 1.5 code and was implemented in the code before MELCOR 1.8.0. These models have a high level of maturity and only minor code corrections have been made to these models in recent code versions.

Table 4-1 through Table 4-3 show burn characteristics calculated for the NTS hydrogen burn tests. These tests were performed by the NRC and the EPRI and were used as part of the MELCOR - CONTAIN parity study. No significant changes are observed among those tests included in the assessment study.

Table 4-1 Hydrogen burn characteristics from experiment and MELCOR.

Test	Experiment	M 1.8.5	M 1.8.6	M 2.1
NTSP01	32.0	36	35.67	35.67
NTSP12	58.0	74	72.94	72.94
NTSP15	100.0	100	100.0	100.0
NTSP20	100.0	100	100.0	100.0

Table 4-2 Hydrogen burn characteristics from experiment and MELCOR.

Test	Experiment	M 1.8.5	M 1.8.6	M 2.1
NTSP01	68.5	2.0	1.9	1.9
NTSP12	27.0	9.0	9.2	9.2
NTSP15	6.0	1.7	1.2	1.2
NTSP20	2.0	6.0	4.0	4.0

Table 4-3 Pressure ratio calculated with recent MELCOR code versions compared to test results.

Test ID & InitialH2 & H2O Concentrations			P(max)/P(initial)			
Test ID	**H_2, v/o**	**H_2O, v/o**	**M 1.8.5**	**M1.8.6**	**M2.1**	**Test**
Standard Tests						
NTSP01	5.3	4.2	1.71	1.70	1.70	1.48
NTSP15	9.9	4.2	4.11	4.08	4.08	3.61
Steam-Laden Tests						

NTSP12	6.9	28.3	2.37	2.36	2.36	1.831
NTSP20	12.9	27.8	3.97	3.95	3.95	3.87

4.4 Containment Pressure Response to Sprays

A series of experiments were conducted in the CSE vessel to evaluate the performance of aqueous sprays as a means of decontaminating containment atmospheres [4.4]. Measurements were obtained which provide a suitable basis for judging the ability of various mathematical models to predict spray performance in large nuclear power plant buildings. Assessments have been performed with M 1.8.3, M 1.8.6, and MELCOR 2.x models for the A9 experiment.

The containment pressure response is shown in Figure 4-7 and Figure 4-8 for all modern code versions. These calculations indicate that the modeling of heat removal from sprays has not significantly changed in these recent code versions.

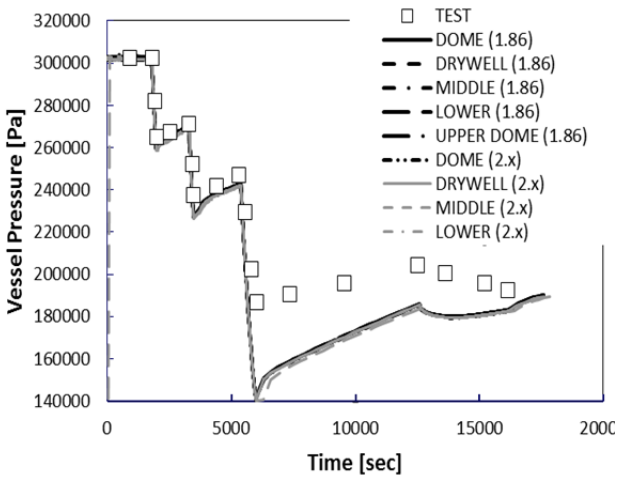

Figure 4-7 MELCOR 1.8.6 & 2.x assessments of CSE A9

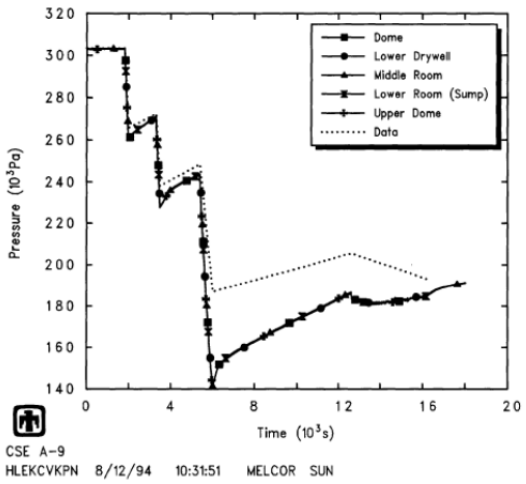

Figure 4-8 MELCOR 1.8.3 assessments of CSE A9

4.5 Fission Product Release

Fission product release rates are validated by comparison to several experimental series, principally the ORNL VI tests, Phebus FPT-1, and VERCORS-2 and 4. The release rates are set relative to Cs based on the VI tests. The releases were then adjusted based on FPT-1, which has the most complete data for the various fission products. The resulting release coefficients, termed modified ORNL-Booth, were then compared to the VERCORS tests. VERCORS-2 has data only on Cs release, and VERCORS-4 has some others also. The last comparisons to VI and VERCORS were done with MELCOR 1.8.5 and 1.8.6; comparisons to FPT-1 have been done with 1.8.5, 1.8.6 and 2.1. In general, differences observed were due to the switch to the modified ORNL-Booth release coefficients in 1.8.5 rather than to any version differences.

4.5.1 Molten Core-Concrete Interaction

The source term during the late phase of a severe accident is dominated by the molten debris – concrete interactions that occur in the reactor cavity. CORCON-MOD3 was implemented into MELCOR 1.8.3 and, aside from a few changes in default sensitivity coefficients, has largely remained unchanged. The SURC-1 test examines the one-dimensional ablation front from an overlying core debris. Results of simulations for MELCOR 1.8.6 and MELCOR 2.1 are shown in Figure 4-9. These results that the CORCON models continue to give good results in predicting the ablation front for these tests. The MELCOR 2.1 assessment report will investigate more recent tests such as the OECD MCCI tests.

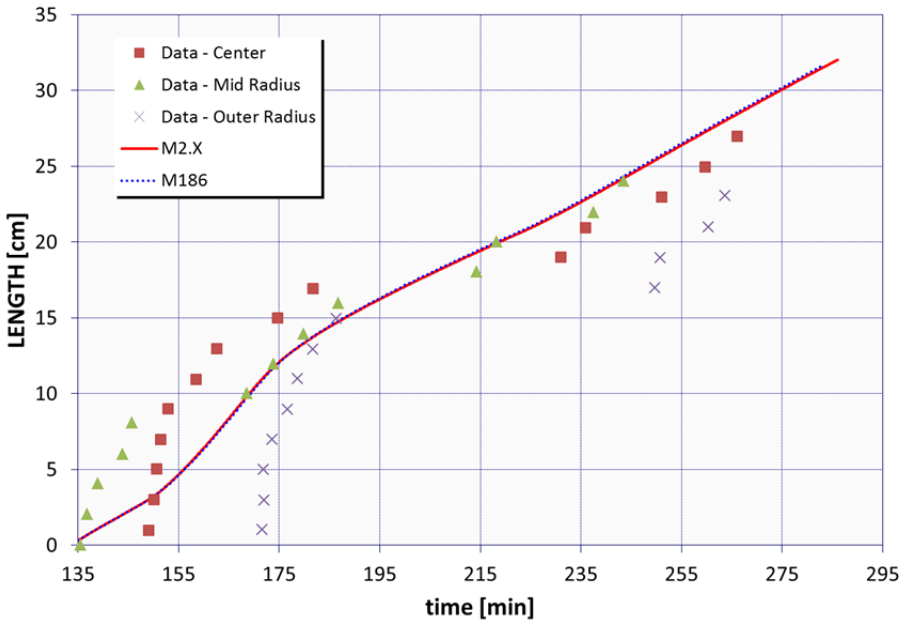

Figure 4-9 MELCOR 1.8.6 & 2.x assessments of ablation depth in SURC-1 Test

4.6 REFERENCES

[4.1] Gauntt, R. O., Cash, J.E., Cole, R. K., Erickson, C. M, Humphries, L.L., Rodriguez, S. B., Young, M. F., 2005, "MELCOR Computer Code Manuals, Vol. 1: Primer and User's Guide, Version 1.8.6," NUREG/CR-6119, Vol. 1, Rev. 3, U.S. Nuclear Regulatory Commission, Washington, DC.

[4.2] Souto, F.J., Haskin, F.E., Kmetyk, L.N., "MELCOR 1.8.2 Assessment: Aerosol Experiments ABCOVE AB5, AB6, AB7, and LACE LA2," SAND94-2166 (1994)

[4.3] Tautges, T.J., "MELCOR 1.8.2 Assessment: The MP-1 and MP-2 Late Phase Melt Progression Experiments," SAND94-0133 (1994).

[4.4] Kmetyk, L.N., "MELCOR 1.8.3 Assessment: CSE Containment Spray Experiments," SAND94-2316 (1994).

[4.5] Tills, J., Notafrancesco, A, Longmire, P., "An Assessment of MELCOR 1.8.6: Design Basis Accident Tests of the Carolinas Virginia Tube Reactor (CVTR) Containment (Including Selected Separate Effects Tests)," SAND2008-1224 (2008).

[4.6] Tautges, T., "MELCOR 1.8.2 Assessment: The DFI-4 BWR Damaged Fuel Experiment," SAND93-1377 (1993).

[4.7] Tautges, T., “MELCOR 1.8.3 Assessment: GE Large Vessel Blowdown and Level Swell Experiments,” SAND94-0361 (1994).

[4.8] Kmetyk, L.N., “MELCOR 1.8.2 Assessment: IET Direct Containment Heating Tests,” SAND93–1475 (1993).

[4.9] Kmetyk, L.N., “MELCOR 1.8.1 Assessment: LACE Aerosol Experiment LA4,” SAND91–1532 (1991).

[4.10] Kmetyk, L.N., “MELCOR 1.8.1 Assessment: LOFT Integral Experiment LP-FP-2,” SAND92–1373 (1992).

[4.11] Kmetyk, L.N., “MELCOR 1.8.1 Assessment: Marviken-V Aerosol Transport Tests ATT-2b/ATT-4,” SAND92–2243 (1993).

[4.12] Gross, R.J., “PNL Ice Condenser Aerosol Experiments,” SAND92–2165 (1993).

[4.13] Kmetyk, L.N., “MELCOR 1.8.1 Assessment: FLECHT SEASET Natural Circulation Experiments,” SAND91-2218 (1991).

[4.14] Kmetyk, L.N., “MELCOR 1.8.1 Assessment: ACRR Source Term Experiments ST-1/ST- 2", SAND91-2833 (1992).

Appendix A Updated Default Parameters

Table A-1 Summary of Updated Default Parameters.

#	Description	Parameter(s)	Field(s)	Value(s) used in SOARCA	Current Default Value(s)
1	COR package candling heat transfer coefficient.	COR00005	HFRZUO HFRZZR HFRZSS HFRZZX HFRZSX HFRZCP	7500 W/m^2-K 7500 W/m^2-K 2500 W/m^2-K 7500 W/m^2-K 2500 W/m^2-K 2500 W/m^2-K	1000 W/m^2-K 1000 W/m^2-K 1000 W/m^2-K 1000 W/m^2-K 1000 W/m^2-K 1000 W/m^2-K
2	COR package radiation heat transfer parameters	COR00003	FCELR FCELA	0.1 0.1	0.25 0.25
3	COR package min. porosity for flow and heat transfer	SC1505	(1) (2)	0.05 0.05	0.001 0.001
4	COR package min. CVH volume fraction	SC4414	(1)	0.01	0.001
5	COR package 1-dim. stress/strain distribution	SC1600	(1)	1.0	0.0
6	COR package min yield stress temperature	SC1603	(2)	1700.0 K	1800.0 K
7	COR package temp. for enhanced debris to lower head conduction	SC1250	(1)	2800.0 K	3200.0 K
8	CVH/FL direct versus iterative solution algorithm	SC4415	(1)	1.0	0.5

#	Description	Parameter(s)	Field(s)	Value(s) used in SOARCA	Current Default Value(s)
9	HS temperature convergence criterion	SC4055	(2)	0.5	5.0×10^{-4}
10	CAV package emissivity of oxide, metallic, and surrounding materials	CAVnnak	EMISS.OX EMISS.MET EMISS.SUR	0.9 0.9 0.9	0.6 0.6 0.6
11	Multipliers for surface boiling heat transfer and material (oxide/metallic) conductivity	CAVnnak	BOILING COND.OX COND.MET	10.0 (multiplier) 5.0 5.0	CORCON-Mod3 1.0 1.0
12	DCH package default classes – new default class 17 (Cs_2MoO_4)			* arrays initialized with 17 classes	* arrays initialized with 16 classes
13	RN class 17 physical properties	SC7120 SC7120 SC7170 SC7170 SC7170	(1,17) (2,17) (3,17) (4,17) (9,17)	351.75 kg/kg-mole 425.75 kg/kg-mole 0.67 kg/kg-H_2O 0.67 kg/kg-H_2O 4030.0 kg/m^3	28.97 kg/kg-mole 28.97 kg/kg-mole 0.0 kg/kg-H_2O 0.0 kg/kg-H_2O 1000.0 kg/m^3

Appendix B MELCOR Code Version Progression Overview

MELCOR 1.8.3

- CORCON-MOD3 (including VANESA) was added to MELCOR to replace the separate CORCON-MOD2 and VANESA models.

MELCOR 1.8.4

- Previous versions of MELCOR were known to predict too-early collapse of reactor cores. A model for retention of molten metals behind oxide shells (particularly, molten Zircaloy on fuel rods), with ultimate failure by another mechanism was added to correct that behavior.

- A creep rupture model was added for the lower head, together with the capability to model external cooling of the lower head in a flooded cavity.

- A “flow blockage” model was added to account for redistribution of flow through a reactor core as a result of changed flow resistance when intact geometry is lost and a debris bed or pool forms.

- A capability was added to calculate radiative heat transfer between pairs of heat structure surfaces.

- Models were added for the behavior of hygroscopic aerosols and for the chemisorption of Cs onto the surfaces of heat structures.

- The SPARC 90 pool decontamination model replaced a previous “preliminary” version of SPARC (SPARC 87). In addition to other improvements, the new model includes removal of iodine vapor.

MELCOR 1.8.5

- A diffusion flame model was added to calculate the combustion of hydrogen flowing through flow paths during direct containment heating.

- Previous versions of MELCOR required the use of a single component (called “Other Structure”, OS) to represent all support structures, control structures, and miscellaneous structures in the core in addition to fuel rods and BWR canisters. This approach had serious deficiencies, and none of the structures could be realistically represented. New components referred to as “Supporting Structure” (SS) and “Non-supporting Structure” (NS) were introduced. Both parametric and mechanistic, load-based, failure models were added for SS, which can support other core components. NS is subject to simpler failure models, but these have

sufficient flexibility to represent BWR control blades, PWR control rods, and structures such as filler rods in experiments.

- Optional models were added for convective heat transfer to water pools from the top and bottom surfaces of SS plates, and for radiative heat transfer between the bottom of such a plate and the water pool or lower head below it.

- Previous versions of MELCOR did not properly differentiate between debris in the channel and debris in the bypass of a BWR. This was resolved by introduction of a “Particulate debris in the Bypass” (PB) component. After failure of the fuel canisters in a BWR that separate PD from PB, the two debris fields were allowed to mix and equilibrate. A debris exclusion model (with flexible user control) was implemented to control the relocation of particulate debris (PD and/or PB) based on the presence or absence of intact structures that could prevent it (for example, solid debris cannot, as a general rule, enter the small spaces between fuel rods.)

- The flow blockage model was much improved as a result of the ability to distinguish particulate debris in the channel of a BWR from that in the bypass, and a model was added to allow the opening of a flow path on failure of a channel box (canister).

- Improvements were made to the implementation of candling and debris slumping models and to those for conductive, radiative, and candling heat transfer.

- Cesium iodide was added as a default class.

- Substantial improvements were made in the model for hygroscopic aerosols.

- A model for the chemical behavior of iodine in water pools was added to MELCOR. It includes models for pH, including transport of nitric and hydrochloric acid formed by radiolysis off air and plastic in cables, respectively. The effects of different surface coatings on containment structures are also modeled.

MELCOR 1.8.6

- Flexibility was added to allow the user to enhance quenching of ejected debris through conductivity multipliers.

- New LM-CREEP and PIPE-STR CF types were added to make it far less difficult for users to model pipe ruptures.

- Modeling of the lower plenum and head was heavily revised. The curvature of the head and its effect on lower plenum volumes can now be consistently modeled (this was not possible in previous versions). The head can take the form of a cylinder, hemisphere, or hemispherical segment. Heat transfer and failure

models were improved. Because the new model contains all of the capabilities of the separate BH package, this package was eliminated.

- Models were added for formation of stratified molten debris pools, both in the core and in the lower plenum. These include circulation-driven convective heat transfer in the case of coherent pools.

- A core periphery model was introduced for PWRs to allow proper modeling of the core baffle (shroud) and core formers, and the bypass region between the baffle and the core support barrel. Such modeling was impossible in previous versions of MELCOR.

- A model was added for quenching of core structures by reflood of water from below. A model was also added to evaluate oxidation of the submerged but unquenched surfaces that could be predicted by this model.

- More realistic models were added for behavior of control poison in a PWR. One involves oxidation of B4C control poison, the other models release of AgInCd control poison, including formation of aerosols.

- The local fluid temperature model (also known as “dT/dz” was improved to reduce problems with small stagnant volumes that had forced falsification of geometry in some previous input decks.

- Treatment of support structures modeling columns was modified to allow better representation of the support in a typical PWR. The package now allows user-defined “flavors” of support structures, allowing further flexibility.

- A model was added to calculate breakaway oxidation of Zircaloy in air.

- The default modeling of collapse of BWR canisters was modified; previous code versions predicted survival to unreasonably high temperatures.

- The previous approach to specification of the inner and outer areas of BWR canisters did not always allow a correct representation; these areas may now be directly input.

- Current best practices for modeling reactor cores involve reducing the melt temperatures used for ZrO2, UO2, and B4C from handbook values to account for the fact that they do not typically appear as pure materials. Redefinition of all the tables and other MP input is tedious and time consuming, particularly if one is interested in the effects of changes in these reductions. So-called “interacting materials”, ZRO2-INT, UO2-INT, and B4C-INT were added to the MP package. Their properties differ from those of the pure materials only in the melt temperatures. Initialization in MELGEN uses the modified melt temperature to

generate complete and consistent properties tables from those of the pure materials; the melt temperature of any of these materials can be modified from its default value with a single input record.

- Creep data have been added to the MP package.

- The user can now specify (via Control Functions) the failure criteria for COR components and add arbitrary heat sources in and heat transfer paths between them.

- A new fuel collapse model was added to allow a user to supply a time at temperature lifetime failure table to determine rod collapse. Fuel collapse was previously specified by a failure temperature.

- The user has more control over the flow resistance calculated from the Ergun equation in the flow blockage model to account for phenomena such as fuel swelling.

- New sensitivity coefficients are available to modify the surface emissivities used in the radiation model.

- A new, optional model was added to treat flashing of superheated water entering a volume, either through a flow path or from a volume source. It improves the partition of mass and enthalpy of the water between the volume pool and atmosphere, and includes the formation of water aerosols.

- Previous versions of MELCOR could exhibit unphysical behavior if the volume of either hydrodynamic field (pool or atmosphere) in a volume became very small or was absent. A new thermodynamic model has been added to better model these situations.

- Heat structure surfaces may be partially covered by a water pool. In previous code versions, a rising pool surface acted as a “squeegee”, increasing the film thickness by maintaining its total mass rather than subsuming the covered portion of the film. This was corrected in MELCOR 1.8.6.

- Mechanistic models are used for draining of thick films from surfaces that are involved in a “film tracking network”, but previous versions of MELCOR used a simple maximum film thickness to remove water from too-thick films on other surfaces. The mechanistic treatment is now used universally, replacing the maximum limit on isolated structure surfaces. In effect, an isolated structure surface is treated as if it form a film tracking network of length one.

- A new version of the CORSOR Booth release model corrects an obvious error in the previous implementation based on published material from Battelle Columbus.

- The algorithm previously used to interpolate aerosol agglomeration and deposition kernels could lead to significant errors if a calculation spanned a wide range of temperatures and/or pressures. A much-improved interpolation algorithm has been implemented.

- The aerosol filter model was extended to allow specification of decontamination factor by particle size as well as by class. Each decontamination factor may now be defined by either a constant or a control function.

- A model was added to calculate deposition of water from a jet impacting on the surface of a heat structure.

- New turbulent deposition models were added along with bend impaction model.